

**A QUADRATIC CUMULATIVE PRODUCTION MODEL FOR THE
MATERIAL BALANCE OF AN ABNORMALLY PRESSURED
GAS RESERVOIR**

A Thesis

by

FELIX E. GONZALEZ ROMERO

Submitted to the Office of Graduate Studies of
Texas A&M University
in partial fulfillment of the requirements for the degree of
MASTER OF SCIENCE

December 2003

Major Subject: Petroleum Engineering

**A QUADRATIC CUMULATIVE PRODUCTION MODEL FOR THE
MATERIAL BALANCE OF AN ABNORMALLY PRESSURED
GAS RESERVOIR**

A Thesis

by

FELIX E. GONZALEZ ROMERO

Submitted to the Office of Graduate Studies of
Texas A&M University
in partial fulfillment of the requirements for the degree of

MASTER OF SCIENCE

Approved as to style and content by:

Thomas A. Blasingame
(Chair of Committee)

W. John Lee
(Member)

Robert R. Berg
(Member)

Stephen A. Holditch
(Head of Department)

December 2003

Major Subject: Petroleum Engineering

ABSTRACT

A Quadratic Cumulative Production Model for the Material Balance of
an Abnormally Pressured Gas Reservoir. (December 2003)

Felix E. Gonzalez Romero,

B.S., Universidad Central de Venezuela;

M.Eng., Universidad Simon Bolivar

Chair of Advisory Committee: Dr. Thomas A. Blasingame

The premise of this research is the concept, development, and application of an approximate relation for the material balance of abnormally pressured gas reservoirs. The approximation is formulated directly from the rigorous material balance for the case of an abnormally pressured gas reservoir. This result is given by:

$$\frac{p}{z} \approx \frac{p_i}{z_i} \left[1 - \frac{G_p}{G} \right] (1 + \omega G_p) \quad \text{where } \omega G_p \equiv \bar{c}_e(p)(p_i - p)$$

We note that the primary assumption in this derivation is that ωG_p (or $\bar{c}_e(p)(p_i - p)$) < 1 . Further, we can proceed by assuming that ω is either constant or some arbitrary function. If we assume $\omega = \text{constant}$, then the following form results:

$$\frac{p}{z} \approx \frac{p_i}{z_i} - \alpha G_p - \beta G_p^2$$

At first glance there may be concern that this approximation is not sufficiently valid for field applications — however, we have shown this relation to be an extraordinarily accurate approximation of the rigorous material balance. This result is suited not only for use as a characteristic model, but also for use as a data analysis mechanism (*i.e.*, this result is used to develop a suite of analysis plots, plotting functions, a type curve, etc.). We note that we also address the case of ω being a linear function of G_p , and we note that this result is typically identical (or essentially identical) to the case of ω being assumed to be constant.

In this work we provide the following new results:

- A suite of 6 (six) plotting functions based on the $p/z-G_p^2$ material balance model.
- A suite of 4 (four) $\omega-G_p$ performance plots which are used to calibrate analysis.
- A new type curve in terms of a dimensionless pressure function ($p_D = (p_i/z_i - p/z)/p_i/z_i$) versus a dimensionless cumulative production function ($G_{pD} = G_p/G$), where the type curve solution is based on the new $p/z-G_p^2$ material balance model.

We also use the "Gan" analysis approach (3 (three) specialized plots), where this analysis is based on the observation of 2-straight line trends on a $p/z-G_p$ plot for an abnormally pressured reservoir. The Gan analysis is used primarily for orientation, particularly with regard to the 4 new $\omega-G_p$ performance plots.

In order to establish a comprehensive validation of the new method for applications to performance data from abnormally pressured reservoirs, we provide a complete analysis suite for the following cases.

- 4 (four) numerical simulation cases (3 "dry gas" cases, 1 "gas condensate" case).
- 20 (twenty) field cases taken from the petroleum literature, or acquired from industry sources.

It is relevant to note that all validation cases have been successfully evaluated using the new methodology and we propose that this new technique will become a standard practice for the analysis of reservoir performance data obtained from abnormally pressured gas reservoirs.

DEDICATION

This work is dedicated:

To my parents, Maria and Ramon, for their unlimited love — and for all they have done for me;

*To my wife, Siomara, and to our children, Stefanny and Santiago,
for their love, support, and prayers.*

*To my siblings, Rosalba and David, for they have always have been with me
— in good times as well as bad ...*

ACKNOWLEDGEMENTS

I want to express my gratitude and appreciation to:

Dr. Tom Blasingame, chair of my advisory committee, for his valuable guidance, intellectual contributions, and his patience in helping me bring this research to its completion.

Drs. John Lee and Bob Berg for serving as members of my advisory committee.

My country, Venezuela, and my company, PDVSA-INTEVEP, for sponsoring my graduate studies in Petroleum Engineering at Texas A&M University.

I thank my wife, Siomara, for her love, her prayers, and her patience with me throughout the many years we have been together. I also thank , Siomara, for our children, Stefanny and Santiago, for they are the center of our lives and our reason for being alive — without them, life would only be existence.

Finally, I thank my parents — my mother Maria and my father Ramon, to whom I owe all that I am, or will become.

TABLE OF CONTENTS

	Page
CHAPTER I INTRODUCTION.....	1
1.1 Introduction	1
1.2 Objectives.....	1
1.3 Statement of the Problem.....	2
1.4 Plotting Functions.....	4
1.5 Validation and Application.....	5
1.6 Summary and Conclusions	5
1.7 Future Efforts.....	7
1.8 Organization of the Thesis.....	7
CHAPTER II LITERATURE REVIEW — MATERIAL BALANCE FOR ABNORMALLY PRESSURED GAS RESERVOIRS	9
2.1 Specialized Results and Material Balance Relations	9
2.2 Methods Which Require Knowledge of Formation Compressibility	19
2.3 Methods Which Do Not Require Knowledge of Formation Compressibility.....	21
2.4 Field Cases — Abnormally Pressured Gas Reservoirs.....	21
2.5 Issues Related to Abnormally Pressured Gas Reservoirs	21
CHAPTER III A SIMPLIFIED MODEL FOR THE MATERIAL BALANCE OF ABNORMALLY PRESSURED GAS RESERVOIRS (THE "QUADRATIC CUMULATIVE PRODUCTION" MODEL).....	25
3.1 Model Development	25
3.2 Plotting Functions for Data Analysis	30
3.3 New Type Curve for Material Balance Analysis.....	36
3.4 Discussion of Application Procedure	38
3.5 Example Analysis of Field Data — Anderson L Reservoir (Case 3)	39
CHAPTER IV SUMMARY, CONCLUSIONS, AND RECOMMENDATIONS FOR FUTURE WORK	50
4.1 Summary.....	50
4.2 Conclusions	50
4.3 Recommendations for Future Work	53
NOMENCLATURE	54
REFERENCES	56

	Page
APPENDIX A — DEVELOPMENT AND VALIDATION OF A SIMPLIFIED MODEL FOR THE MATERIAL BALANCE OF ABNORMALLY PRESSURED GAS RESERVOIRS ("QUADRATIC CUMULATIVE PRODUCTION" MODEL)	59
APPENDIX B — DEVELOPMENT OF PLOTTING FUNCTIONS FOR THE "QUADRATIC CUMULATIVE PRODUCTION" FORM OF THE MATERIAL BALANCE RELATION FOR ABNORMALLY PRESSURED GAS RESERVOIRS.....	71
APPENDIX C — DEVELOPMENT OF A TYPE CURVE SOLUTION FOR THE ANALYSIS OF $p/z—G_p$ DATA FOR THE CASE OF AN ABNORMALLY PRESSURED GAS RESERVOIR USING THE "QUADRATIC CUMULATIVE PRODUCTION" FORM OF THE MATERIAL BALANCE RELATION.....	74
APPENDIX C — FIELD VALIDATION OF THE "QUADRATIC CUMULATIVE PRODUCTION" FORM OF THE GAS MATERIAL BALANCE RELATION	78
VITA.....	273

LIST OF FIGURES

FIGURE	Page
2.1	Schematic behavior of p/z versus G_p for an abnormally pressured gas reservoir — note the influence of the abnormal and normal pressure periods (adapted from ref. 2)..... 12
2.2	Schematic behavior of the $\bar{c}_e(p)(p_i - p)$ function versus $(p/z)/(p_i/z_i)$ on "Gan Plot 1" (ref. 2). Note the influence of the "inflection point." 13
2.3	Schematic behavior of p/z versus G_p for an abnormally pressured gas reservoir illustrating the influence of the "inflection point" (ref. 2). 14
2.4	Example p/z versus G_p plot for the case of an abnormally pressured gas reservoir illustrating a secondary trend starting at an inflection point defined by the hydrostatic (or normal) pressure (Reservoir 33) (ref. 4). 15
2.5	Example p/z versus G_p plot for the case of an abnormally pressured gas reservoir illustrating a secondary trend starting at an inflection point defined by the hydrostatic (or normal) pressure (Reservoir 117) (ref. 4)..... 15
2.6	Schematic $d(p/z)/dG_p$ versus G_p profiles for various reservoir cases (ref. 3). 16
2.7	p/z versus G_p for North Ossun Field (South Louisiana), data fitted and extrapolated using the model proposed by Bourgoyne, <i>et al.</i> (ref. 5). 17
2.8	"Type curve" of formation compressibility versus pressure — Yale, <i>et al.</i> correlation (ref. 6). 18
2.9	Effect of effective compressibility on the estimation of gas-in-place — North Ossun Field (South Louisiana) (ref. 10). 20
2.10	Influence of abnormal pressure effects on typical well log responses (ref. 24). 22
2.11	Correlation of pore pressure gradient with temperature and reservoir fluid types (ref. 29). .. 24
2.12	Comparison of instantaneous and cumulative formation compressibility functions (ref. 1). 24
3.1	Behavior of the ω -parameter versus G_p/G for a simulated dry gas reservoir case. Note that in this case the maximum depletion of the model is approximately 70 percent — which justifies the (relatively) poor agreement of the constant model with the data trend. ... 27
3.2	Behavior of the ω -parameter versus G_p/G for the "Anderson L" field case example ²¹ (South Texas, USA). Note that this case shows an apparent depletion of about 50 percent — this is a possible explanation for the reasonably good correlation of data with both the constant and linear models. 28
3.3	p/z versus G_p plot for the simulated performance of an abnormally pressured gas reservoir (variable compressibility only) (dry gas reservoir case). 29

FIGURE	Page
3.4 p/z versus G_p plot for the "Anderson L" field case example ²¹ (South Texas, USA) (a suspected abnormally pressured gas reservoir case).	29
3.5 Plot of $\Delta(p/z)$ vs. G_p — Case 1.	33
3.6 Plot of $\Delta(p/z)/G_p$ vs. G_p — Case 1.	33
3.7 Plot of $\frac{1}{G_p} \int_0^{G_p} \Delta(p/z) dG_p$ vs. G_p — Case 1.	34
3.8 Plot of $\frac{1}{G_p^2} \int_0^{G_p} \Delta(p/z) dG_p$ vs. G_p — Case 1.	34
3.9 Plot of $\Delta(p/z) - \frac{1}{G_p} \int_0^{G_p} \Delta(p/z) dG_p$ vs. G_p — Case 1.	35
3.10 Plot of $\frac{1}{G_p} \left[\Delta(p/z) - \frac{1}{G_p} \int_0^{G_p} \Delta(p/z) dG_p \right]$ vs. G_p — Case 1.	35
3.11 p_D and p_{Di} versus G_{pD} "type curve" plot for the "quadratic cumulative production" material balance relation for an abnormally pressured gas reservoir.	37
3.12 Screen capture of the proposed analysis sequence in MS Excel.	38
3.13 Base plot of p/z vs. G_p — Case 3.	41
3.14 Plot of $\Delta(p/z)$ vs. G_p — Case 3.	41
3.15 Plot of $\Delta(p/z)/G_p$ vs. G_p — Case 3.	42
3.16 Plot of $\frac{1}{G_p} \int_0^{G_p} \Delta(p/z) dG_p$ vs. G_p — Case 3.	42
3.17 Plot of $\frac{1}{G_p^2} \int_0^{G_p} \Delta(p/z) dG_p$ vs. G_p — Case 3.	43
3.18 Plot of $\Delta(p/z) - \frac{1}{G_p} \int_0^{G_p} \Delta(p/z) dG_p$ vs. G_p — Case 3.	43
3.19 Plot of $\frac{1}{G_p} \left[\Delta(p/z) - \frac{1}{G_p} \int_0^{G_p} \Delta(p/z) dG_p \right]$ vs. G_p — Case 3.	44
3.20 Plot of $\bar{c}_e(p)(p_i - p)$ vs. G_p/G — Case 3.	44
3.21 Plot of $1/[1 - \bar{c}_e(p)(p_i - p)]$ vs. G_p/G — Case 3.	45
3.22 Plot of ω vs. G_p — Case 3.	45

FIGURE	Page
3.23 Plot of ω vs. G_p/G — Case 3.	46
3.24 Comparison plot of p/z vs. G_p — Case 3.	46
3.25 Plot of dimensionless p/z functions vs. G_{pD} — Case 3.	47
3.26 Plot of $\bar{c}_e(p)(p_i - p)$ vs. $(p/z)/(p_i/z_i)$ — Case 3.	47
3.27 Plot of $(p/z)/(p_i/z_i)$ vs. G_p/G — Case 3.	48
3.28 Summary plot of p/z vs. G_p — Case 3.	48
3.29 Plot of pore volume compressibility computed using Fetkovich, <i>et al.</i> approach and compared to laboratory data — Case 3 (Anderson L Reservoir (assumed $S_{wi}=0.25$)).	49

LIST OF TABLES

TABLE	Page
2.1 Categorization of literature for this work.	10
2.2 Geopressured aquifers in southern Louisiana and adjacent areas of the continental shelf (ref. 23).	23
2.3 Geopressure ratio (geostatic ratio) and composition of formation water in geopressured aquifers of Texas and Louisiana, Northern Gulf of Mexico Basin. (ref. 23).	23
3.1 Summary of plotting functions used to implement the quadratic cumulative production material balance relation for abnormal pressure effects (applied to Case 1 (numerical simulation case)).	31
3.2 Summary of plots and plotting functions for the example analysis of the Anderson L Reservoir (South Texas, USA) (Case 3, Appendix D).	40

CHAPTER I

INTRODUCTION

1.1 Introduction

In this work we establish the validity of an approximation to the rigorous gas material balance equation for the specific case of an abnormally pressured gas reservoir. The genesis of this work is both the wide variety of solutions for this case (*i.e.*, our desire to develop an accurate and practical general solution for the case of an abnormally pressured gas reservoir) as well as the need for a methodology that can be considered essentially rigorous. Our approach does utilize an approximation, but we will show that this approximation is the minimum expansion of a binomial series that results in a very consistent and accurate model for the material balance of abnormally pressured gas reservoirs.

1.2 Objectives

The primary objectives of this work are:

- To develop a quadratic formulation of the rigorous material balance for the case of an abnormally pressured gas reservoir in terms of cumulative gas production. This result is given as: (the derivation is given in Appendix A)

$$\frac{P}{z} \approx \frac{P_i}{z_i} - \alpha G_p - \beta G_p^2 \dots\dots\dots(1.1)$$

- To develop plotting functions for the analysis of reservoir performance behavior based on the quadratic cumulative production formulation of the rigorous material balance for the case of an abnormally pressured gas reservoir. We note that we use 10 (ten) specific data plotting functions as part of this work — others are available, but we favor the 10 functions used due to consistency and data representation/visualization. These functions are derived in Appendix B.
- To develop and validate a dimensionless "type curve" solution based on Eq. 1.1 and an auxiliary functions (*i.e.*, the "pressure integral" of Eq. 1.1 based on G_p) (Appendix C).
- To validate and demonstrate the plotting functions and analysis relations (based on the plotting functions) using simulated reservoir performance cases (4) and various field performance cases (20). While our validation efforts may not be "exhaustive," we would define our validate procedure as conclusive and sufficient. In short, all cases (simulation and field data) were successfully analyzed using this new analysis methodology.

This thesis follows the style and format of the *SPE Journal*.

- To provide a comprehensive analysis/interpretation methodology using a dynamic (or linked) analysis approach where all model functions are tied to a common set of control parameters. As such, we implemented the analysis module as a spreadsheet in MS Excel.

1.3 Statement of the Problem

The rigorous material balance for the case of an abnormally pressured gas reservoir was developed by Fetkovich, *et al.*,¹ and is given as:

$$\frac{p}{z} [1 - \bar{c}_e(p)(p_i - p)] = \frac{p_i}{z_i} - \frac{p_i}{z_i} \frac{1}{G} \left[G_p - G_{inj} + W_p R_{sw} + \frac{5.615}{B_g} (W_p B_w - W_{inj} B_w - W_e) \right] \quad (1.2)$$

Where Fetkovich, *et al.* define the "effective compressibility" function, $\bar{c}_e(p)$, as:

$$\bar{c}_e(p) = \frac{1}{(1 - S_{wi})} [S_{wi} \bar{c}_w + \bar{c}_f + M(\bar{c}_w + \bar{c}_f)] \quad (1.3)$$

Considering the case where $G_{inj} = W_{inj} = W_p = W_e = 0$, we obtain the common form of the gas material balance relation for the case of "abnormal pressure" effects. This result is given as:

$$\frac{p}{z} [1 - \bar{c}_e(p)(p_i - p)] = \frac{p_i}{z_i} \left[1 - \frac{G_p}{G} \right] \quad (1.4)$$

Gan and Blasingame² utilized Eq. 3 to develop a sequence of spreadsheet-based analyses for estimating the gas-in-place, G , as well as the pore volume compressibility function, c_f . The premise of the Gan and Blasingame approach is that two linear trends are often observed on a plot of p/z versus G_p for the case of an abnormally pressured gas reservoir — the first trend is the "abnormal" pressure trend, and the second is the "normal" pressure (or depletion) trend. The "abnormal" pressure trend is given by:

$$\frac{p/z}{p_i/z_i} = \left[1 - \frac{G_p}{G_{app}} \right] \quad (1.5)$$

The "normal" (or depletion) pressure trend is given by:

$$p/z = \frac{(p/z)_A}{(1 - G_{pA}/G)} \left[1 - \frac{G_p}{G} \right] \quad (1.6)$$

Gan and Blasingame applied this methodology to several cases of simulated reservoir performance, and as many field cases that could be found in the literature or from industry sources. The proposed methodology was shown to be robust and accurate for virtually all cases. This limitation of this approach (and of all existing analyses for abnormally pressured gas reservoirs) is that the only indication of "abnormal pressure" behavior is the decline in the p/z versus G_p performance from an apparent linear trend. In other words, no methodology exists in practice which can be used to verify the influence of abnormal pressure

prior to some indication in p/z versus G_p performance. We do note that the Moran and Samaniego³ approach — *i.e.*, the use of the $d(p/z)/dG_p$ function does hold some utility in being able to distinguish "normal" and "abnormal" pressure behavior uniquely — however, this method is not well suited to field use due to the behavior of the $d(p/z)/dG_p$ function derived from field performance data.

It can be argued that the magnitude of reservoir pressure compared to the hydrostatic gradient can indicate abnormal pressure behavior⁴ — however, predicting the onset of "normal pressure" behavior is not possible based solely on p/z versus G_p performance. Gan and Blasingame did propose a series of diagnostic checks to establish the existence of abnormal pressure effects, as well as provide an approximate correlation for the onset of "normal pressure" behavior. However, these are simply supplemental mechanisms to assist with the proposed "two straight line p/z analysis. "

As noted above, Moran and Samaniego³ provide an innovative and rigorous approach for the analysis of $p/z—G_p$ performance which utilizes the concept of $d(p/z)/dG_p$ (and other derivative functions). This work could (and probably should) be seen as a breakthrough analysis technique — it is proposed as an analog to derivative analyses used in well testing and the theoretical aspects of this approach are well-founded. *Unfortunately*, the quality of p/z data are almost always inadequate for such analysis — and added to this issue that of data quantity (typically less than 10 $p/z—G_p$ points are available for a given reservoir), and the Moran and Samaniego method becomes an approach that is theoretically sound, but impractical for most field applications.

The motivation for the present work was the recognition that the Moran and Samaniego approach has the ability to provide "early" insight into "abnormal pressure" effects. We note that the Gan and Blasingame approach, while useful in concept and application, could be improved upon given a single (simple) model function (as opposed to using two models (*i.e.*, the abnormal and normal pressure straight-line p/z versus G_p trends)). Gan and Blasingame do provide a single model which uses the unit-step function as switch (triggered by the p/z inflection value $(p/z)_{infl}$) — however, this model is empirical in development and application and we only reference its existence for completeness).

Given these motivations, we proceeded to develop the general $p/z—G_p$ approximation as well as the "quadratic" ($p/z—G_p^2$) and "cubic" ($p/z—G_p^3$) approximations. The major results of this development are summarized below, and the details of this development are provided in Appendix A. We provide the development of an approximate formulation of the rigorous material balance for the case of an abnormally-pressured gas reservoir in terms of cumulative gas production and an auxiliary function (ω).

Specifically, the general result (derived in Appendix A) is given by:

$$\frac{p}{z} \approx \frac{p_i}{z_i} \left[1 - \frac{G_p}{G} \right] (1 + \omega G_p) \dots\dots\dots(1.7)$$

where the ω -function is defined by:

$$\omega G_p \equiv \bar{c}_e(p)(p_i - p) \dots\dots\dots(1.8)$$

Eq. 1.7 is approximate in the sense that the $(1 + \omega G_p)$ term is actually comprised of the first two terms in the binomial (or geometric) series expansion for $1/(1 - \omega G_p)$ (recall that the binomial series is defined for this case as $1/(1 - x) = 1 + x + x^2 + x^3 + \dots$).

Expanding Eq. 1.7, we have:

$$\frac{p}{z} \approx \frac{p_i}{z_i} \left[1 - \left(\frac{1}{G} - \omega \right) G_p - \frac{\omega}{G} G_p^2 \right] \dots\dots\dots(1.9)$$

Assuming that the ω -function is constant (hence, we refer to this as the " ω -parameter"), we can simplify Eq. 1.9 to yield the following form:

$$\frac{p}{z} \approx \frac{p_i}{z_i} - \alpha G_p - \beta G_p^2 \dots\dots\dots(1.1)$$

Where the α and β coefficients are defined by:

$$\alpha \equiv \left(\frac{1}{G} - \omega \right) \frac{p_i}{z_i} \dots\dots\dots(1.10)$$

$$\beta \equiv \frac{\omega}{G} \frac{p_i}{z_i} \dots\dots\dots(1.11)$$

As noted earlier in this work, we use Eq. 1.1 (*i.e.*, the quadratic cumulative production model) a basis to develop plotting functions which are used for the analysis of p/z versus G_p data. The development of these plotting functions is discussed in the next section.

1.4 Plotting Functions

The plotting functions for the analysis of a given p/z — G_p data are derived in Appendix B. In this work we use a "multiplot spreadsheet" approach for the analysis of p/z — G_p data, where this approach incorporates each plotting function as well as the appropriate model relation. This approach allows us to simultaneously "match" multiple data functions with the appropriate model response using a dynamic trial and error approach. This approach may seem tedious, but it is actually straightforward and concise. Interested readers should not presume that statistical regression analysis will provide superior results as compared to the proposed "hand" analysis. In fact, our proposed approach should be superior to statistical methods in most cases due to data quality/quantity issues.

As noted, the plotting functions for the analysis of p/z versus G_p data are derived and summarized in Appendix B of this proposal.

1.5 Validation and Application

We provide a comprehensive validation process that utilizes synthetic reservoir performance (*i.e.*, cases where we know the input and output responses), as well as field data obtained from the petroleum literature. We consider the case of "abnormal pressure" effects which originate from a pressure-dependent formation (or pore volume) compressibility function.

As noted earlier, as part of the validation sequence we utilize 24 separate cases of performance data for abnormally pressured gas reservoirs — 4 (four) cases were derived using numerical simulation, and 20 (twenty) cases were obtained from the petroleum literature or industry sources. The analysis for all 24 (twenty-four) cases are documented in complete detail in Appendix D.

1.6 Summary and Conclusions

1. Quadratic Cumulative Production Model: We have successfully derived an approximate general model in terms of cumulative gas production for the case of an abnormally pressured gas reservoir. The general form of this result is given as:

$$\frac{p}{z} \approx \frac{p_i}{z_i} - \left(\frac{1}{G} - \omega\right) \frac{p_i}{z_i} G_p - \frac{\omega}{G} \frac{p_i}{z_i} G_p^2 \left[\text{where } \omega \equiv \frac{1}{G_p} \bar{c}_e(p)(p_i - p) \right]$$

This model has a mathematical limitation imposed by the expansion of the compressibility-pressure drop term using a binomial series. In addition to this general result, we have also derived specific results using the cumulative gas production in "quadratic" and "cubic" formulations (respectively):

$$\frac{p}{z} \approx \frac{p_i}{z_i} \left[1 - \left(\frac{1}{G} - \omega\right) G_p - \frac{\omega}{G} G_p^2 \right] \quad (\text{where } \omega = \text{constant}) \dots\dots\dots(\text{quadratic form})$$

$$\frac{p}{z} \approx \frac{p_i}{z_i} - \left(\frac{1}{G} - a\right) \frac{p_i}{z_i} G_p - \left(\frac{a}{G} + b\right) \frac{p_i}{z_i} G_p^2 + \frac{b}{G} \frac{p_i}{z_i} G_p^3 \quad (\text{where } \omega \equiv a - bG_p) \dots\dots\dots(\text{cubic form})$$

Eq. 1 (the "quadratic" formulation) is the basis for most of the plotting/analysis relations provided in this work.

2. Plotting Functions derived from the Quadratic Cumulative Production Model: Using Eq. 1.1 (*i.e.*, the "quadratic" cumulative production formulation), we have derived a sequence of plotting functions (for use in plots where the specified plotting function is plotted versus the cumulative gas production) (all plotting functions are developed and presented in Appendix B). These plotting functions have been shown to be extraordinarily effective for identifying the appropriate linear, quadratic, or even cubic data trends. Each function is formulated to accentuate a particular aspect of the model (Eq. 1.1) and

the entire sequence of plotting functions is typically used to ensure uniformity in the analysis/interpretation of the data.

3. Auxiliary Analysis: (ω - G_p performance plots) We have proposed and validated 4 (four) auxiliary plots which illustrate the performance of the ω variable (or the $\bar{c}_e(p)(p_i - p)$ function). Our goal is to establish these "auxiliary analysis" plots as a basis for relating the ω variable with the estimate of gas-in-place. The primary function of these plots is the utility of establishing the ω - G_p behavior for a particular case — the most common use of these plots is as the "watch" plots during the interactive analysis (these plots clearly illustrate the influence of G_p during the interactive analysis)
4. Type Curve Solution: As part of our strategy to establish the new p/z - G_p^2 model as the preferred mechanism for the analysis of reservoir performance data for the case of an abnormally pressured gas reservoir, we developed a new "type curve" solution using the dimensionless form of the new quadratic cumulative production model. The governing relations for this development are:

$$p_D = (1 - \omega_D)G_{pD} + \omega_D G_{pD}^2 \left[\text{where } p_D = \left[1 - \frac{p/z}{p_i/z_i} \right] = \left[\frac{p_i/z_i - p/z}{p_i/z_i} \right], G_{pD} = \frac{G_p}{G}, \text{ and } \omega_D = \omega G \right]$$

$$p_{Di} = \frac{1}{G_{pD}} \int_0^{G_{pD}} p_D dG_{pD} = (1 - \omega_D) \frac{1}{2} G_{pD} + \omega_D \frac{1}{3} G_{pD}^2$$

We note that we did not utilize the new type curve as a "standalone" analysis plot, but rather, we used this plot as another component of our dynamic analysis methodology. In particular, the plot was useful in establishing the "goodness-of-fit" for a given set of parameters.

5. Gan Analysis: Our goal in this work was to use the Gan-Blasingame analysis (ref. 2) to orient our "matching" process in selecting values of the control parameters. While we recognize that the Gan-Blasingame analysis may not be as thorough the proposed methodology, we were able to use the Gan-Blasingame analysis to guide and refine our other analyses. In particular, the use of the 2 separate straight-line p/z - G_p trends (*i.e.*, a high (or "abnormal") pressure trend (early) and a low (or "normal") pressure trend (late)) is essentially independent of other methods, and provides balance in the analysis. The most sensitive tool in the Gan-Blasingame analysis sequence, the $\bar{c}_e(p)(p_i - p)$ versus $(p/z)/(p_i/z_i)$ plot, is a particularly in the proposed interactive analysis.

1.7 Future Efforts

The following future efforts are recommended:

1. External Drive Energy: Extend this methodology for cases of external drive energy.
2. Additional Validation: Continue the validation using additional field and numerical simulation performance cases. Focus on estimating the $c_f(p)$ profiles for a given case.
3. Software: Implement the entire analysis sequence into a standalone software package.

1.8 Organization of the Thesis

The outline of the proposed research thesis is as follows:

- Chapter I — Introduction
 - Research Problem
 - Research Objectives
 - Summary
- Chapter II — Literature Review — Material Balance for Abnormally Pressured Gas Reservoirs
 - Specialized Results and Material Balance Relations
 - Methods which Require Knowledge of Formation Compressibility
 - Methods which Do Not Require Knowledge of Formation Compressibility
 - Field Cases — Abnormally Pressured Gas Reservoirs
 - Issues Related to Abnormally Pressured Gas Reservoirs
- Chapter III — A Simplified Model for the Material Balance of Abnormally Pressured Gas Reservoirs (the "Quadratic Cumulative Production" Model)
 - Model Development
 - Plotting Functions for Data Analysis
 - Application Procedure
 - Example Analysis of Field Data — Anderson L Reservoir
- Chapter IV — Summary, Conclusions, and Recommendations for Future Work
 - Summary
 - Conclusions
 - Recommendations for future work
- Nomenclature
- References
- Appendices
 - Appendix A — Development and Validation of a Simplified Model for the Material Balance of Abnormally Pressured Gas Reservoirs ("Quadratic Cumulative Production" Model)
 - Appendix B — Development of Plotting Functions for the "Quadratic Cumulative Production" Form of the Material Balance Relation for Abnormally Pressured Gas Reservoirs

- Appendix C — Development of a Type Curve Solution for the Analysis of $p/z—G_p$ Data for the Case of an Abnormally Pressured Gas Reservoir Using the "Quadratic Cumulative Production" Form of the Material Balance Relation
- Appendix D — Field Validation of the "Quadratic Cumulative Production" Form of the Gas Material Balance Relation
- Vita

CHAPTER II

LITERATURE REVIEW — MATERIAL BALANCE FOR ABNORMALLY PRESSURED GAS RESERVOIRS

In this chapter we present a sample of the literature sufficient to support our proposed work as well as ensure that we have not embarked on a previously pursued path. We believe that our concepts and developments are original, and we have found no evidence that any analogous developments have been proposed or investigated. Our goal is to provide a basis for our new approach relative to the existing material balance relations, as well as provide access to a wide variety of field data cases which can be used for validation purposes.

As we begin our literature review, we will first categorize the various topics and references related to this subject as this will aid in our review and discussion of existing methodologies. The categorization of literature for this work is given in **Table 2.1**. We have assembled the data in the following categories for reference:

- Specialized Results and Material Balance Relations
- Methods which Require Knowledge of Formation Compressibility
- Methods which Do Not Require Knowledge of Formation Compressibility
- Field Cases — Abnormally Pressured Gas Reservoirs
- Issues Related to Abnormally Pressured Gas Reservoirs

2.1 Specialized Results and Material Balance Relations

The material balance proposed by Fetkovich, *et al.*¹ in 1991 (published in 1998) is one of the most significant works in gas reservoir engineering developed over the last 30 years. This result is given as:

$$\frac{p}{z} [1 - \bar{c}_e(p)(p_i - p)] = \frac{p_i}{z_i} - \frac{p_i}{z_i} \frac{1}{G} \left[G_p - G_{inj} + W_p R_{sw} + \frac{5.615}{B_g} (W_p B_w - W_{inj} B_w - W_e) \right] \dots\dots\dots (2.1)$$

Where Fetkovich, *et al.* define the "effective compressibility" function, $\bar{c}_e(p)$, as follows:

$$\bar{c}_e(p) = \frac{1}{(1 - S_{wi})} [S_{wi} \bar{c}_w + \bar{c}_f + M(\bar{c}_w + \bar{c}_f)] \dots\dots\dots (2.2)$$

For our purposes (*i.e.*, focusing on "abnormal pressure" effects), we set $G_{inj} = W_{inj} = W_p = W_e = 0$, which yields:

$$\frac{p}{z} [1 - \bar{c}_e(p)(p_i - p)] = \frac{p_i}{z_i} \left[1 - \frac{G_p}{G} \right] \dots\dots\dots (2.3)$$

Table 2.1 – Categorization of literature for this work.

Reference	Author	Topic
Specialized Results and Material Balance Relations		
1	Fetkovich, <i>et al.</i>	Generalized Gas Material Balance for High Pressures
2	Gan and Blasingame	Semi-Analytical p/z Technique for Abnormally Pressured Gas Reservoirs
3	Moran and Samaniego	$d(p/z)/dG_p$ Technique for Material Balance Analysis
4	Prasad and Rogers	Generalized Tank Model (notes hydrostatic p/z point)
5	Bourgoyne	Shale Water as a Pressure Support Mechanism in Superpressure Reservoirs
6	Yale, <i>et al.</i>	Application of Variable c_f for Improved Reservoir Analysis
7	Ambastha	Material Balance Analysis for Volumetric/Abnormally Pressured Reservoirs
8	Chu, <i>et al.</i>	Gas Reservoir Performance in Abnormally High Pressure Carbonates
9	Wang	General Material Balance for Normally/Abnormally Pressured Reservoirs
Methods which Require Knowledge of Formation Compressibility		
10	Hammerlindl	Predicting Gas Reservoir in Abnormally Pressured Reservoirs
11	Ramagost and Farshad	p/z Abnormally Pressured Gas Reservoirs
12	Begland and Whitehead	Depletion Performance of Volumetric High-Pressured Gas Reservoirs
13	Elsharkawy	Estimating Gas In-Place for Abnormal Pressured Gas Reservoirs
14	Wang, <i>et al.</i>	Analysis of Overpressured Reservoirs with A New Material Balance Method
Methods which Do Not Require Knowledge of Formation Compressibility		
15	Roach	Analyzing Geopressured Reservoirs-A Material Balance Technique
16	Bernard	Gulf Coast Geopressured Gas Reservoirs: Drive Mechanism/Perf. Prediction
17	Poston and Chen	Simultaneous Determination of c_f and G in Abnormally Pressured Reservoirs
18	Poston and Chen	Case History Studies: Abnormal Pressured Gas Reservoirs
19	Guehria	A New Approach to p/z Analysis in Abnormally Pressured Reservoirs
Field Cases — Abnormally Pressured Gas Reservoirs		
20	Harville and Hawkins	Rock Compressibility and Failure in Geopressured Gas Reservoirs
21	Duggan	The Anderson "L" – An Abnormally Pressured Gas Reservoir in South Texas
22	Bourgoyne	Shale Water/Pressure Support Mechanism — Abnormal Formation Pressure
Issues Related to Abnormally Pressured Gas Reservoirs		
23	Jones	Hydrodynamics of Geopressure in the Northern Gulf of Mexico Basin
24	Fertl and Timko	Parameters for Identification of Overpressure Formations
25	Fertl	A look at Abnormally Pressured Formations in the U.S.S.R
26	Gill	Shale Mineralogy and Overpressure: Case Histories of Pressure Detection
27	Quitza and Bassiouni	The Possible Impact of the Geopressure Resource on Oil and Gas Exploration
28	Engineer	Cal Canal Field: A Tight/Abnormally Pressured Gas Condensate Reservoir
29	Pilkington	Pressure and Temperature Data — Exploration/Overpressure Detection
30	Harari, <i>et al.</i>	Pore Compressibility Study of Arabian Carbonate Reservoir Rocks
31	Yassir and Bell	Abnormally High Fluid Pressures/Associated Porosities and Stress Regimes

We also require the various definitions that Fetkovich, *et al.* employed in this derivation, specifically, we need the definitions of \bar{c}_f and \bar{c}_w . These definitions are given as:

$$\bar{c}_f = \frac{1}{V_{pi}} \frac{(V_{pi} - V_p)}{(p_i - p)} \dots\dots\dots(2.4)$$

$$\bar{c}_w = \frac{1}{B_{tw}(p_i)} \frac{(B_{tw} - B_{twi})}{(p_i - p)} \dots\dots\dots(2.5)$$

and the "total water formation volume factor," B_{tw} is defined as:

$$B_{tw} = B_w \frac{1}{5.615} [R_{swi} - R_{sw}] B_g \dots\dots\dots(2.6)$$

and the *instantaneous* formation and water compressibility terms are defined by:

$$c_f = \frac{1}{V_p} \left[\frac{\partial V_p}{\partial p} \right]_T \dots\dots\dots(2.7)$$

$$c_w = \frac{1}{B_w} \left[\frac{\partial B_w}{\partial p} \right]_T \dots\dots\dots(2.8)$$

and, finally, the "nonpay/aquifer contribution ratio" (M) is defined by:

$$M = \frac{V_{pNNP} + V_{pAQ}}{V_{pR}} \dots\dots\dots(2.9)$$

For our work (and in general for the case of an abnormally pressured gas reservoir), M is assumed to be negligible. We recommend that formulations which include the M -parameter should be developed and applied only for the case where it is strongly believed that a "nonpay" or aquifer contribution of energy exists. We also note that we will generally assume the cumulative water compressibility term (\bar{c}_w) to be constant, but we also acknowledge that there is no real loss of generality to retain a pressure-dependent relation for the cumulative water compressibility term. In contrast, we will generally consider that the cumulative formation compressibility (\bar{c}_f) is pressure-dependent and we will attempt to estimate (\bar{c}_f) using Eq. 2.2. Rearranging Eq. 2.2, and solving for the cumulative formation compressibility term (\bar{c}_f), we have:

$$\bar{c}_f = \frac{1}{(1+M)} [(1 - S_{wi}) \bar{c}_e - (S_{wi} + M) \bar{c}_w] \dots\dots\dots(2.10)$$

Although it is useful to have an estimate of the (\bar{c}_f) function (which is obviously pressure dependent), it is more practical (and valuable) to estimate the instantaneous formation compressibility function, c_f . In order to develop an identity, we equate Eqs. 2.2 and 2.7, and solve for c_f — this gives:

$$c_f = \frac{V_{pi}}{V_p} \frac{(p_i - p)}{(V_{pi} - V_p)} \left[\frac{\partial V_p}{\partial p} \right]_T \bar{c}_f \dots\dots\dots(2.11)$$

Using a backwards difference to estimate the $\left[\frac{\partial V_p}{\partial p} \right]_T$ term in Eq. 2.11, we obtain:

$$c_f(p_j) = \frac{V_{pi}}{V_p(p_j)} \frac{(p_i - p_j)}{[V_{pi} - V_p(p_j)]} \frac{[V_p(p_j) - V_p(p_{j-1})]}{(p_j - p_{j-1})} \bar{c}_f(p_j) \dots\dots\dots(2.12)$$

Although an approximate formulation, we will next discuss the Gan and Blasingame² methodology which utilizes the Fetkovich, *et al.*¹ material balance formulation as a basis for "correlating" the abnormal and normal pressure behavior of a gas reservoir (via the $\bar{c}_e(p)(p_i - p)$ function).

Gan and Blasingame proposed the following relations for the "2 straight lines" that are typically observed on a p/z versus G_p plot for the case of an abnormally pressured gas reservoir:

$$p/z = p_i / z_i \left[1 - \frac{G_p}{G_{app}} \right] \quad \text{(first straight-line (abnormal pressure trend))} \dots\dots\dots (2.13a)$$

$$p/z = \frac{(p/z)_A}{(1 - G_{pA} / G)} \left[1 - \frac{G_p}{G} \right] \quad \text{(second straight-line (normal pressure trend))} \dots\dots\dots (2.13b)$$

A schematic plot of p/z versus G_p for the case of an abnormally pressured gas reservoir is shown in **Fig. 2.1**.

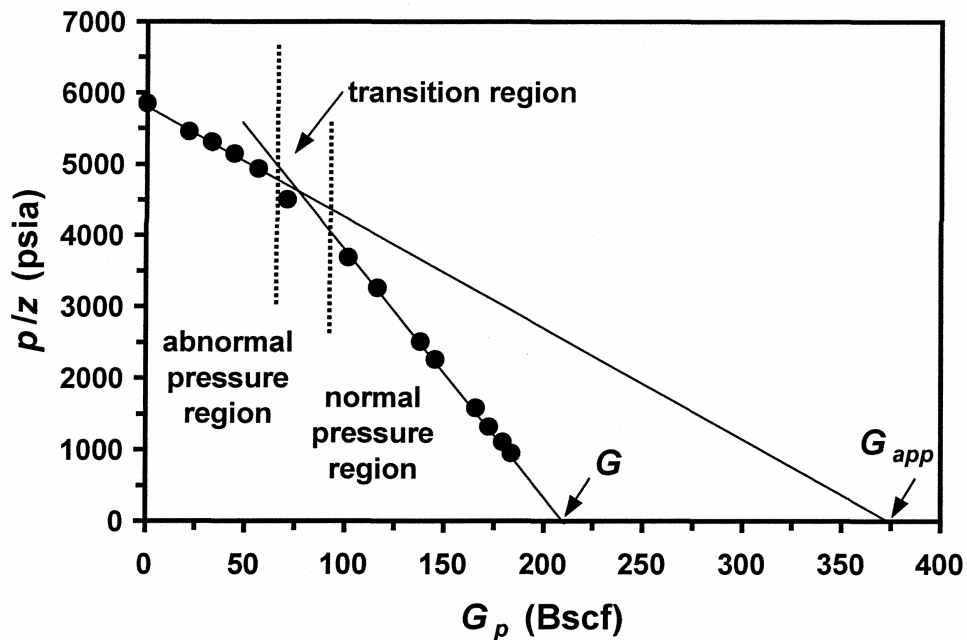


Figure 2.1 – Schematic behavior of p/z versus G_p for an abnormally pressured gas reservoir — note the influence of the abnormal and normal pressure production sequences (adapted from ref. 2).

Gan and Blasingame developed the following relations for the $\bar{c}_e(p)(p_i - p)$ function based on the "2 straight lines" that are typically observed on a p/z versus G_p plot for the case of an abnormally pressured gas reservoir:

$$[\bar{c}_e(p_i - p)]_1 = 1 - \frac{\left[\frac{p_i}{z_i}\right]}{\left[\frac{p}{z}\right]} + \frac{\left[\frac{p_i}{z_i}\right]}{\left[\frac{p}{z}\right]} \frac{G_{app}}{G} - \frac{G_{app}}{G} \quad \text{(abnormal pressure trend (first line)).....(2.14a)}$$

$$[\bar{c}_e(p_i - p)]_2 = 1 - \frac{\left[\frac{p_i}{z_i}\right]}{\left[\frac{p}{z}\right]_A} \left[1 - \frac{G_{pA}}{G}\right] \quad \text{(normal pressure trend (second line)).....(2.14b)}$$

A schematic plot of the $\bar{c}_e(p)(p_i - p)$ function versus $(p/z)/(p_i/z_i)$ for the case of an abnormally pressured gas reservoir is shown in **Fig. 2.2**.

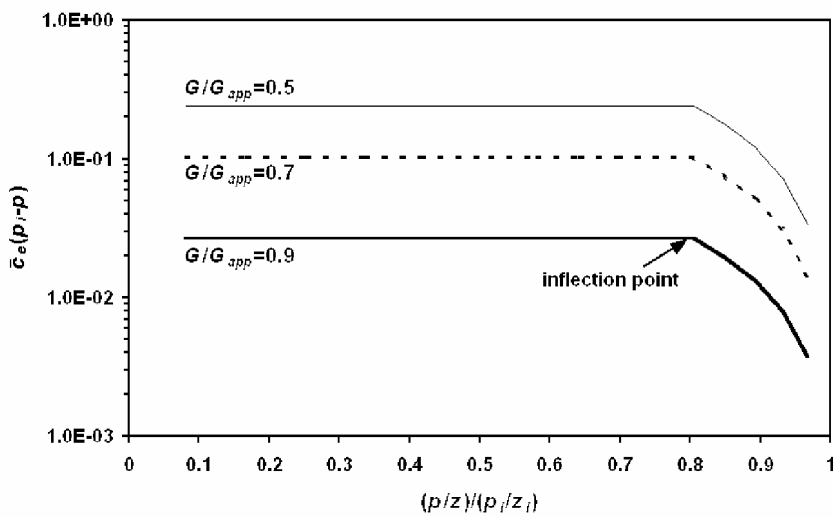


Figure 2.2 – Schematic behavior of the $\bar{c}_e(p)(p_i - p)$ function versus $(p/z)/(p_i/z_i)$ on "Gan Plot 1" (ref. 2). Note the influence of the "inflection point."

Analysis is performed using the Gan-Blasingame methodology by adjusting the location of the "inflection point" and the gas-in-place, G . The primary weakness of this methodology is that it requires a clear and distinct "normal pressure" trend to be observed on the p/z versus G_p plot, which is typically the case in practice — however, because this methodology cannot be used until the second trend is observed, this is a major limitation. Another limitation is more theoretical — the use of a second linear p/z — G_p trend for the

normal pressure behavior in an abnormally pressured gas reservoir is an empirical hypothesis, based on observation, there is no direct mechanism (to our knowledge) to rigorously derive a second, normal pressure $p/z—G_p$ trend. In **Fig. 2.3** we present schematic p/z versus G_p plot to illustrate the influence of the "inflection point" (*i.e.*, the changeover point for the abnormal and normal pressure systems). We will comment that the selection of the inflection point is somewhat subjective — and balancing this selection with an estimate of the gas-in-place was noted by Gan and Blasingame² to be problematic in some cases (particularly field cases with limited data).

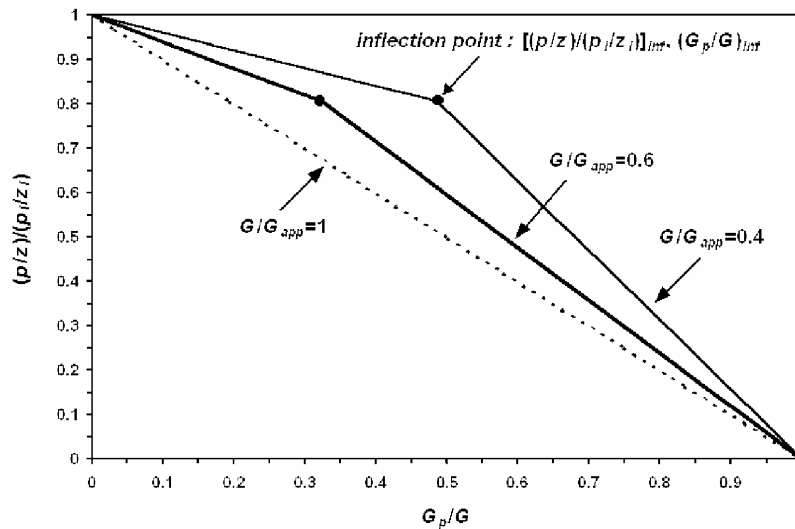


Figure 2.3 – Schematic behavior of p/z versus G_p for an abnormally pressured gas reservoir illustrating the influence of the "inflection point" (ref. 2).

As a final comment, we note that Prasad and Rogers⁴ proposed a similar 2 straight line $p/z—G_p$ methodology as Gan and Blasingame, but Prasad and Rogers made no attempt to develop a systematic analysis methodology. We note this as point of clarification between the two works. We also note that Prasad and Rogers provided a large database of $p/z—G_p$ data in their work, this data has been utilized systematically by other researchers (as well as ourselves) to provide validation examples for the case of a reservoir exhibiting abnormal pressure behavior (see **Figs. 2.4** and **2.5** for examples from Prasad and Rogers).

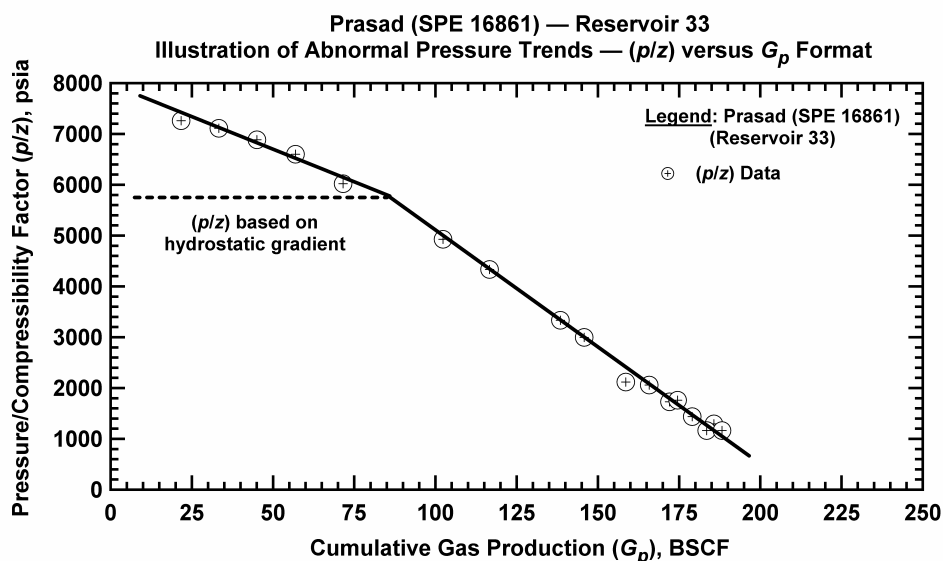


Figure 2.4 – Example p/z versus G_p plot for the case of an abnormally pressured gas reservoir illustrating a secondary trend starting at an inflection point defined by the hydrostatic (or normal) pressure (Reservoir 33) (ref. 4).

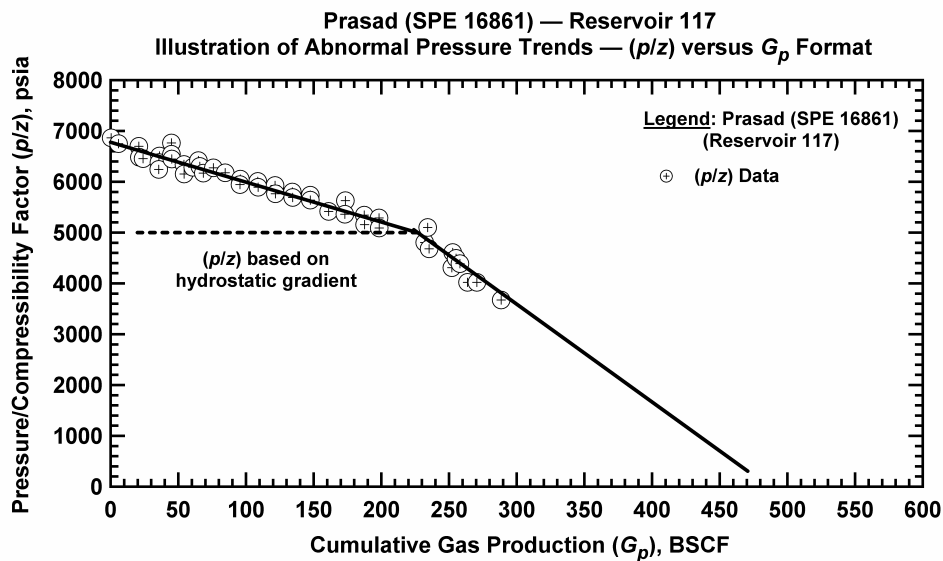


Figure 2.5 – Example p/z versus G_p plot for the case of an abnormally pressured gas reservoir illustrating a secondary trend starting at an inflection point defined by the hydrostatic (or normal) pressure (Reservoir 117) (ref. 4).

We next discuss the method of Moran and Samaniego³ — where this approach utilizes the $d(p/z)/dG_p$ function. At first glance this is both intuitive and potentially very useful — particularly for the interpretation of data from an abnormally pressured gas reservoir. Unfortunately, the reality of reservoir performance data is that these data simply contain too much noise and/or too little accuracy for the $d(p/z)/dG_p$ function to be of much value. We recommend the consideration of this approach, but we also recognize that very serious practical limitations exist. A schematic plot of the $d(p/z)/dG_p$ versus G_p for various reservoir conditions is shown in **Fig. 2.6**.

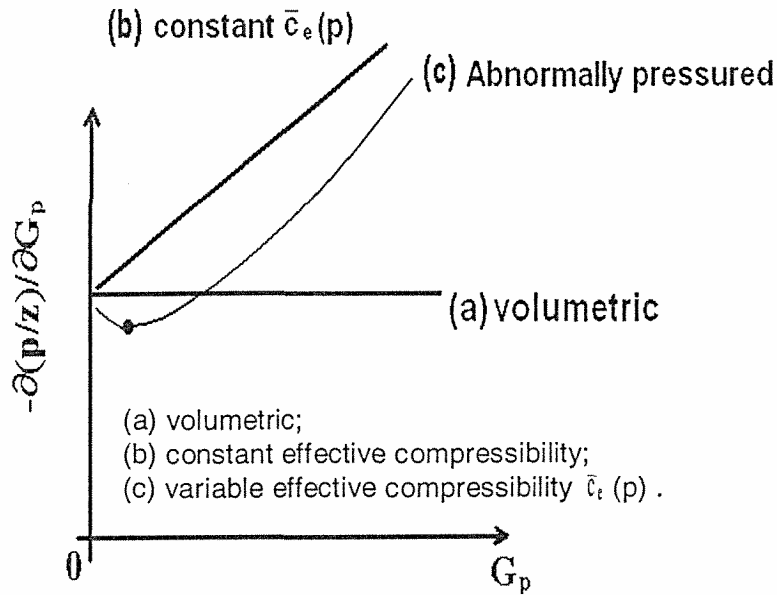


Figure 2.6 – Schematic $d(p/z)/dG_p$ versus G_p profiles for various reservoir cases (ref. 3).

The next material balance model to be addressed is that of Bourgoyne, *et al.*⁵ — where these authors proposed and developed a completely new material balance model for the case of a "superpressure" gas reservoir. We will note that this model appears to function very well for the cases that Bourgoyne, *et al.* provide — and we are aware of some use of this technique in the petroleum industry. However, the methodology has not become a mainstream technique, and further, it is not likely to supplant recent developments such as the Fetkovich, *et al.* material balance relation (ref. 1). For the sake of completeness, we document the solution of Bourgoyne, *et al.*⁵ below.

$$G_p = G - m \frac{p}{z} - a \frac{p^2}{z} \dots\dots\dots(2.15)$$

$$m = \frac{z_i}{p_i} G(1 - c_e p_i) \dots\dots\dots(2.16)$$

$$a = G \frac{z_i}{p_i} c_e \dots\dots\dots(2.17)$$

$$c_e = \frac{1}{(1 - S_{wi})} \left[(S_{wi} + M)c_w + (1 + M)c_f + (1 + M) \frac{V_{sh}}{\phi} c_s \right] \dots\dots\dots(2.18)$$

where:

- M = Ratio of aquifer volume to reservoir volume, fraction
- c_s = Shale compressibility, 1/psi
- V_{sh} = Shale fraction of the reservoir and aquifer volume, fraction

In **Fig. 2.7** we present the analysis of Bourgoyne, *et al.* for the case of "North Ossun" Field in South Louisiana. The model trend shown on **Fig. 2.7** is that of Eq. 2.15, fitted by Bourgoyne, *et al.* We believe that Bourgoyne, *et al.* have provided a reasonable estimate of gas-in-place using this method (114 BSCF) (our work yielded an estimate of 86.5 BSCF (see Appendix D)). We conclude that the Bourgoyne, *et al.* model (*i.e.*, Eq. 2.15) appears to be a feasible model for the analysis of reservoir performance data from an abnormally pressured gas reservoir, although we would recommend this technique only as a component in a suite of other analyses.

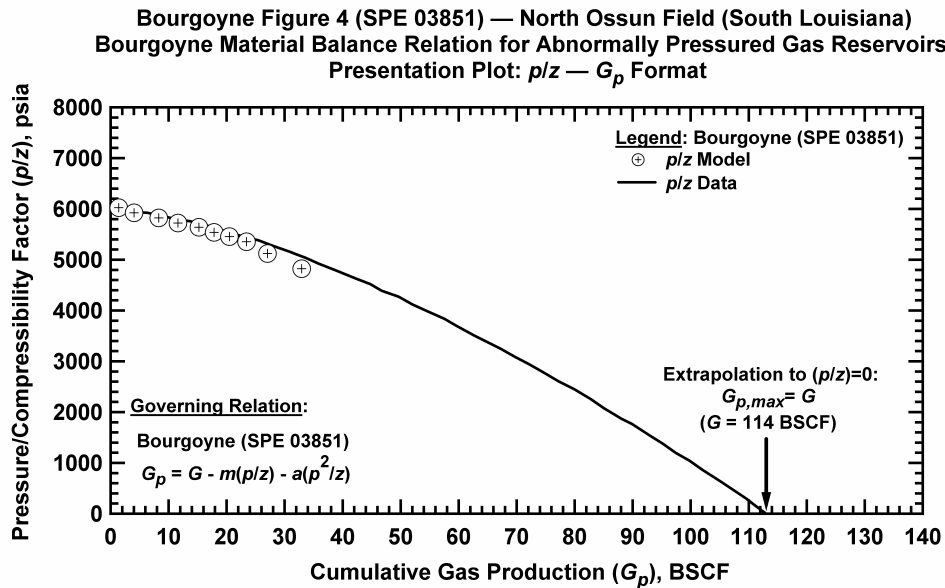


Figure 2.7 – p/z versus G_p for North Ossun Field (South Louisiana), data fitted and extrapolated using the model proposed by Bourgoyne, *et al.* (ref. 5).

Our remaining discussions of material balance models will simply address other models that have been proposed in recent times, and give a brief perspective on the utility of such models. Yale, *et al.*⁶ proposed a modified formulation of a material balance that is analogous in approach to that of Fetkovich, *et al.*¹ — although Yale, *et al.* used a formulation in terms of formation volume factors to represent the various energy components, whereas Fetkovich, *et al.* use the "cumulative compressibility" approach. We recommend the Fetkovich, *et al.* formulation — but we note that Yale, *et al.* also provide a significant body of data concerning the estimation (and correlation) of the instantaneous formation compressibility, c_f . This is a major contribution and this work should not be overlooked. Yale, *et al.* produced a "type curve" for formation compressibility that is shown in **Fig. 2.8** — this work could help to orient analysis in the case of abnormally pressured gas reservoirs.

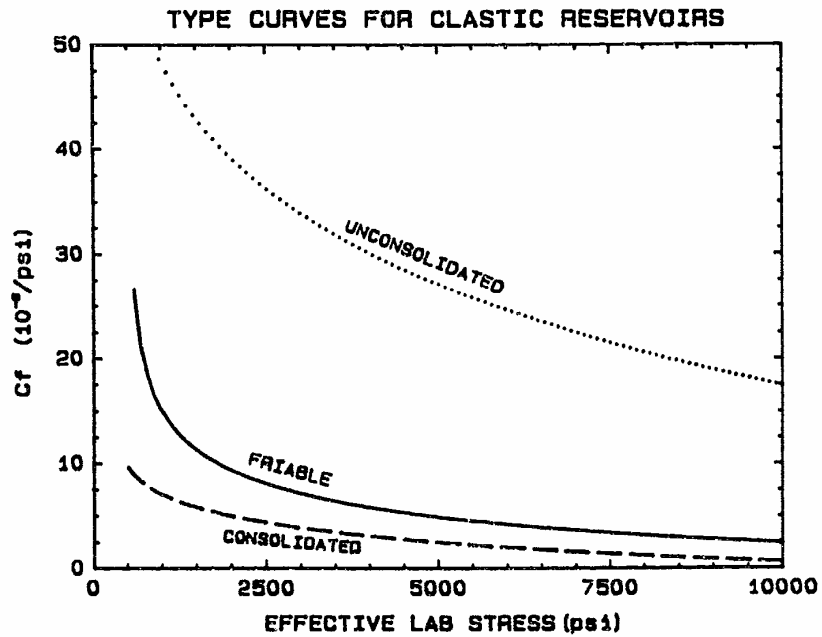


Figure 2.8 — "Type curve" of formation compressibility versus pressure — Yale, *et al.* correlation (ref. 6).

In reference 7, Ambastha proposes and validates a "type curve" concept for a p_D (dimensionless p/z function) versus G_{pD} (dimensionless G_p function) for the case of an abnormally pressured gas reservoir. This is a significant innovation — unfortunately, the format of the type curves cause the data to be skewed to a relatively small view field. We have proposed an alternative type curve in this present work, and we recommend our format as it provides more resolution of the model and data functions.

Chu, *et al.*⁸ propose a modification of the Fetkovich, *et al.*¹ approach, and we note this work due to its consideration of the cumulative compressibility function in a different manner than Fetkovich, *et al.* Given the level of detail presented by Chu, *et al.*, we are uncertain as to any advantage of their proposed approach over that of Fetkovich, *et al.*

We also note the new material balance relations proposed by Wang⁹ for various cases including the case of an abnormally pressured gas well. Wang provides a similar argument to Chu, *et al.*⁸ that Fetkovich, *et al.*¹ provide "no mathematical derivation to validate their treatment of overpressure effect." Wang then proposed an alternate development of the "overpressure effect" (as did Chu, *et al.*) — in particular, Wang used a mathematical expansion for the formation compressibility function. We will not dispute that the Fetkovich, *et al.* approach does not directly incorporate a specific *mechanism* for abnormal pressure effects — however, we do note that the Fetkovich, *et al.* approach does provide a "lumped" variable approach (via the effective cumulative compressibility function) to *address* the abnormal pressure issue. At this time, we are satisfied that the Fetkovich, *et al.* approach is the most reasonable basis for our work.

2.2 Methods Which Require Knowledge of Formation Compressibility

In this section we consider the material balance methods for abnormally pressured gas reservoirs which do require prior knowledge of the formation compressibility. In simple terms, each of these methods (refs. 10-14) all require formation compressibility as an input variable — formation compressibility (or effective compressibility) is not estimated simultaneously, but is used as a fixed parameter in the proposed analysis.

Hammerlindl¹⁰ is credited with recognizing and quantifying the influence of abnormal pressure effects on the estimation of gas-in-place (see **Fig. 2.9**). Ramagost and Farshad¹¹ developed the "correction" of the *p/z* versus *G_p* plot that became the most common method of analysis for abnormally pressured gas reservoirs. The pertinent equations for this methodology are provided below.

$$\frac{p}{z} [1 - c_e(p_i - p)] = \frac{p_i}{z_i} \left[1 - \frac{G_p}{G} \right] \dots\dots\dots(2.19)$$

Where the effective compressibility function, *c_e*, is given by:

$$c_e = \frac{1}{(1 - S_{wi})} (S_{wi}c_w + c_f) \dots\dots\dots(2.20)$$

Recalling the definition of the "cumulative effective compressibility" function, *c̄_e(p)*, given by Fetkovich, *et al.*,¹ we have:

$$\bar{c}_e(p) = \frac{1}{(1 - S_{wi})} [S_{wi}\bar{c}_w + \bar{c}_f + M(\bar{c}_w + \bar{c}_f)] \dots\dots\dots(2.2)$$

The definitions of the effective compressibility function, c_e , and the "cumulative effective compressibility" function, $\bar{c}_e(p)$, are similar by design — and we could simply imply that whether constant or a function of pressure such a "lumped" variable is necessary for providing an analysis using conventional $p/z-G_p$ data. Ramagost and Farshad propose a "corrected" p/z plot of $p/z [1 - c_e(p_i - p)]$ versus G_p — and we note that this has easily been the most popular technique for the analysis of reservoir performance data obtained from abnormally pressured gas reservoirs. The limitation is that the c_e variable (whether constant, or treated as a variable) must be known in advance. This is a serious limitation and is the motivation for a variety of developments which pursued the simultaneous determination of c_e and the gas-in-place.

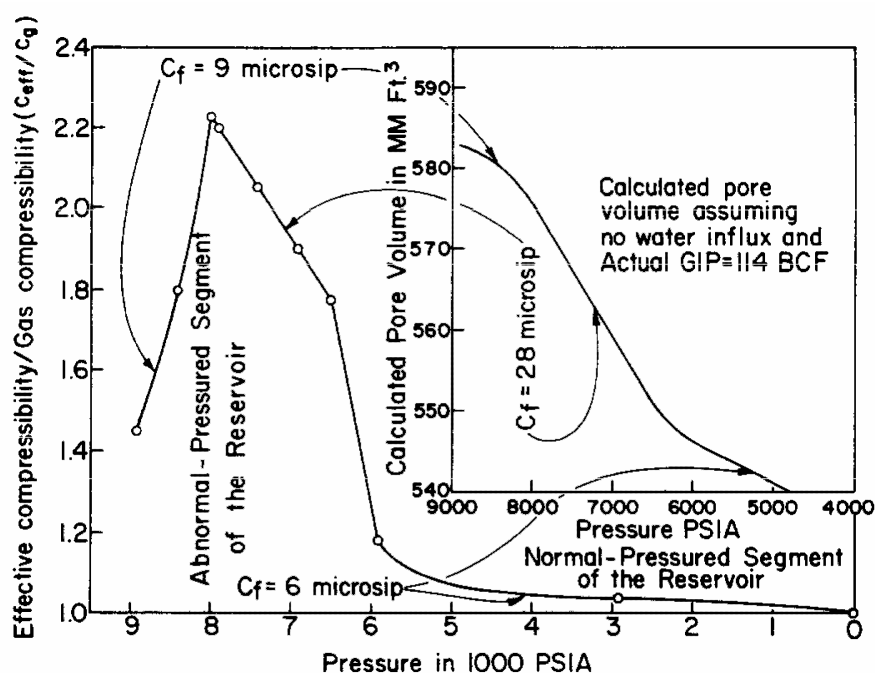


Figure 2.9 – Effect of effective compressibility on the estimation of gas-in-place — North Ossun Field (South Louisiana) (ref. 10).

We note that the other references in this section (Begland and Whitehead¹², Elsharkawy¹³, and Wang, *et al.*¹⁴) have the same limitation of requiring knowledge of the various compressibility functions and saturations prior to analysis. We next review the methods proposed for analysis without direct knowledge of these compressibility functions and saturations prior to analysis. We will note in advance that several of these methods are based on the construction of a linearized plotting function — which we will also note sometimes does not evolve.

2.3 Methods Which Do Not Require Knowledge of Formation Compressibility

In this section we address solutions which do not require knowledge of formation compressibility prior to analysis. As noted in the previous section, this issue motivated the development of a simultaneous solution for the determination of c_e and the gas-in-place — of which virtually all developments can be traced to Roach,¹⁵ where Eq. 2.19 was rearranged to yield a linear plotting function. This process yields the following results:

$$y = \frac{1}{G}x - c_e \dots\dots\dots(2.21)$$

Where the x and y variables are defined as:

$$y = \frac{[(p_i / z_i)/(p / z)] - 1}{(p_i - p)} \dots\dots\dots(2.22)$$

$$x = \frac{[(p_i / z_i)/(p / z)] G_p}{(p_i - p)} \dots\dots\dots(2.23)$$

References 15-16 all use Eq. 2.21 as a basis for estimating c_e and G . Guehria¹⁹ used an automated regression algorithm to estimate the formation compressibility function required in the material balance relation that was proposed in that work. Reference 19 is included in this section because it represents a case where the formation compressibility profile is estimated simultaneously (albeit using a regression algorithm). The issue of using regression in material balance calculations is relevant — Fetkovich, *et al.*¹ note that direct analysis techniques are preferred to "a pure statistical best fit that may lead to unrealistic solutions" — in this case a possibly negative c_f profile. We recognize that the case of a negative c_f profile can be safeguarded, but the point that a direct solution is preferred should not be diminished or ignored — such solutions will always be more consistent than a statistically-derived regression of the data and model.

2.4 Field Cases — Abnormally Pressured Gas Reservoirs

In this section we briefly address the 20 (twenty) "data cases" used in this work (refs. 2, 4, 11, and 18-22). The most important issue is that we have tried to limit our "data cases" to those field case histories which can be effectively documented (*i.e.*, we have focused on cases which have been analyzed in the literature) and we have limited our own industry cases to a minimum (2 cases from ref. 2). We also note that it is not our intention to reproduce the results of previous investigations — but rather, our goal is an independent analysis and interpretation of the data using our proposed methodology.

2.5 Issues Related to Abnormally Pressured Gas Reservoirs

This section addresses the various issues related to abnormally pressured gas reservoirs — in particular, the mechanisms which cause abnormal pressure effects and the pressure-dependent compressibility behavior. References 23-26, 29 and 31 address the origin and distribution of abnormal pressure effects,

while refs.27-28 address the economic and operational issues related to abnormal reservoir pressures, and refs. 6, 20, and 30 consider the pressure dependence of formation compressibility.

The issue of the *identification* of abnormal pressure effects was addressed much earlier than the any proposals for reservoir engineering solutions that would incorporate such effects. Obviously, abnormal pressure effects have a much more immediate impact on drilling and well completion operations. As such, inductive methods using well log and formation pressure and temperature data were developed to address the identification of abnormal pressures. Fertl and Timk²⁴ developed a series of schematic plots illustrating the effect of abnormal pressures on well log responses as shown in **Fig. 2.10**. Jones²³ provided the data in **Tables 2.2** and **2.3** as evidence of abnormal pressure for various locations in the U.S. Gulf Coast region. Pilkington²⁹ established a graphical correlation of abnormal pressure gradients as a function of temperature and reservoir fluids (see **Fig. 2.11**). All of this information helps to orient the analyst on what constitutes abnormal formation pressures and what factors are likely to produce abnormal pressures (at least in the U.S. Gulf Coast region).

Our final discussion point in this chapter is devoted to the comparison of instantaneous and cumulative formation compressibility. Fetkovich, *et al.*¹ present a comparison of a specific case of instantaneous and cumulative formation compressibility, and we have reproduced their work in **Fig. 2.12**. We recognize that these functions have different definitions, and we concede that the definition (and use) of "cumulative formation compressibility" is somewhat idealized. However, we believe that efforts should be made to assess the instantaneous formation compressibility prior to analysis — if for no other reason than this data may help orient the analysis/interpretation.

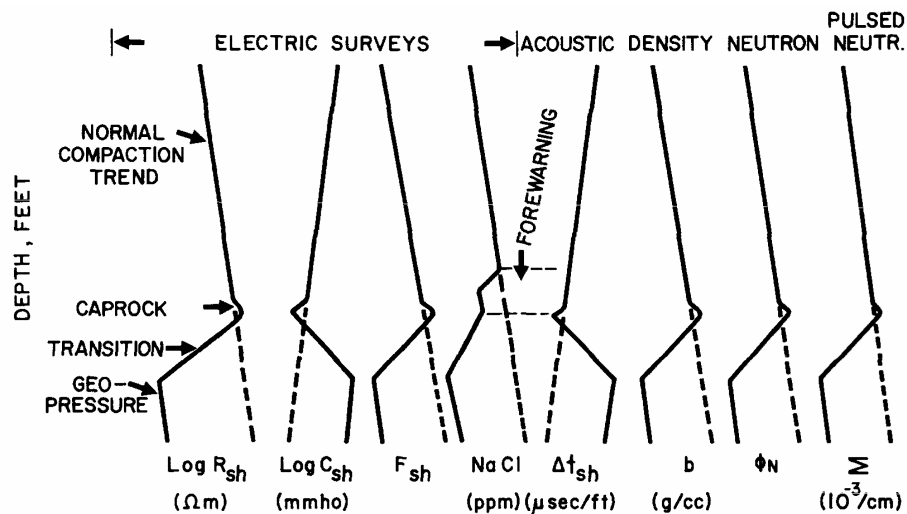


Figure 2.10– Influence of abnormal pressure effects on typical well log responses (ref. 24).

Table 2.2 – Geopressured aquifers in southern Louisiana and adjacent areas of the continental shelf (ref. 23).

Dcpth (feet)	Field Name	Temperature (degrees F.)	Pressure (psi)	Geostatic Ratio	Depth (feet)	Field Name	Temperature (degrees F.)	Pressure (psi)	Geostatic Ratio
1355-1430	Bay Marchand	91	680	0.502	12693-12757	Vermilion	235	8,276	0.652
2674- ?	Southeast Pass	106	1,390	.520	12900-12935	Bastian Bay	224	8,859	.687
5405-5433	Ship Shoal	140	3,132	.579	12942-12949	Bayou Chevrul	246	11,067	.855
6268-6311	West Cameron	163	3,205	.511	13200-13228	Lake Chicot	232	11,522	.873
7080-7090	Do.	173	3,712	.524	13265-13275	West Cameron	280	11,664	.879
7483-7507	Do.	179	3,993	.533	13617-13640	Thibodaux	237	10,418	.765
7996-8013	Do.	187	4,370	.546	13700-13735	Thornwell	272	12,282	.896
8400-8413	Vermilion Bay	208	4,580	.545	13708-13761	West Delta	239	10,782	.787
8700-8831	Do.	211	4,680	.538	13753- ?	Caillou Island	270	7,113	.517
9012-9047	Eugene Island	182	4,715	.523	13937-13950	Rousseau	241	10,635	.763
9033-9061	South Pelto	219	4,938	.547	14145-14178	Ship Shoal	261	7,109	.503
9401-9422	Church Point	201	6,417	.683	14150-14225	Houma	253	10,790	.763
9464-9533	South Pelto	225	5,416	.572	14300-14341	Lake Sand	263	10,975	.767
9824-9877	East Cameron	213	6,025	.613	14344-14376	Garden City	259	12,096	.843
9879-9906	Do.	213	6,001	.607	14594-14606	Do.	263	12,295	.842
10005-10047	Iowa	246	7,169	.717	14602-14628	Constance Bayou	278	7,340	.503
10025-10039	Jefferson Island	194	5,379	.537	14600-14650	Lapeyrouse	264	9,075	.622
10410-10418	High Island	209	7,802	.749	14700-14731	Do.	266	10,020	.682
10500-10517	English Bayou	233	8,154	.777	14900-14940	Lake Washington	266	10,180	.683
10585-10630	West Cameron	223	6,325	.598	15050-15084	Garden City	260	14,210	.944
10790-10816	Raceland	208	6,792	.629	15150-15160	Deep Lake	332	9,390	.620
10800-10906	Mud Lake	231	5,724	.530	15249-15289	Lake Pagle	268	10,819	.709
10950-10974	Churchpoint	243	7,686	.702	15318-15375	Thornwell	315	11,376	.743
11200-11389	Mud Lake	246	6,272	.560	15336-15407	Lake Arthur	329	13,933	.909
11330-11356	Rayne	217	6,900	.609	15580-15595	Leleux	277	13,570	.871
11650-11679	Chalkley	233	9,345	.802	15600-15800	Deep Lake	366	9,885	.634
11933-11943	Erath	231	6,602	.553	15871-15880	Lake Sand	296	12,505	.788
11950-11995	Bayou Penchant	230	9,031	.756	16000-16018	Lacassine	275	14,625	.914
12200-12246	Lake Arthur	262	10,100	.828	16450-16495	Hollywood	280	14,540	.884
12295-12328	Thornwell	303	11,800	.960	16570-16585	Weeks Island	266	9,495	.573
12450-12493	Belle Isle	231	6,690	.537	17300-17340	Belle Isle	316	11,420	.660
12550-12562	Grand Isle	263	8,745	.697	17395-17429	Lake Sand	318	13,477	.775

Table 2.3 – Geopressure ratio (geostatic ratio) and composition of formation water in geopressured aquifers of Texas and Louisiana, Northern Gulf of Mexico Basin. (ref. 23).

Dcpth (feet)	Field Name	Temperature (degrees F.)	Pressure (psi)	Geostatic Ratio	Depth (feet)	Field Name	Temperature (degrees F.)	Pressure (psi)	Geostatic Ratio
1355-1430	Bay Marchand	91	680	0.502	12693-12757	Vermilion	235	8,276	0.652
2674- ?	Southeast Pass	106	1,390	.520	12900-12935	Bastian Bay	224	8,859	.687
5405-5433	Ship Shoal	140	3,132	.579	12942-12949	Bayou Chevrul	246	11,067	.855
6268-6311	West Cameron	163	3,205	.511	13200-13228	Lake Chicot	232	11,522	.873
7080-7090	Do.	173	3,712	.524	13265-13275	West Cameron	280	11,664	.879
7483-7507	Do.	179	3,993	.533	13617-13640	Thibodaux	237	10,418	.765
7996-8013	Do.	187	4,370	.546	13700-13735	Thornwell	272	12,282	.896
8400-8413	Vermilion Bay	208	4,580	.545	13708-13761	West Delta	239	10,782	.787
8700-8831	Do.	211	4,680	.538	13753- ?	Caillou Island	270	7,113	.517
9012-9047	Eugene Island	182	4,715	.523	13937-13950	Rousseau	241	10,635	.763
9033-9061	South Pelto	219	4,938	.547	14145-14178	Ship Shoal	261	7,109	.503
9401-9422	Church Point	201	6,417	.683	14150-14225	Houma	253	10,790	.763
9464-9533	South Pelto	225	5,416	.572	14300-14341	Lake Sand	263	10,975	.767
9824-9877	East Cameron	213	6,025	.613	14344-14376	Garden City	259	12,096	.843
9879-9906	Do.	213	6,001	.607	14594-14606	Do.	263	12,295	.842
10005-10047	Iowa	246	7,169	.717	14602-14628	Constance Bayou	278	7,340	.503
10025-10039	Jefferson Island	194	5,379	.537	14600-14650	Lapeyrouse	264	9,075	.622
10410-10418	High Island	209	7,802	.749	14700-14731	Do.	266	10,020	.682
10500-10517	English Bayou	233	8,154	.777	14900-14940	Lake Washington	266	10,180	.683
10585-10630	West Cameron	223	6,325	.598	15050-15084	Garden City	260	14,210	.944
10790-10816	Raceland	208	6,792	.629	15150-15160	Deep Lake	332	9,390	.620
10800-10906	Mud Lake	231	5,724	.530	15249-15289	Lake Pagle	268	10,819	.709
10950-10974	Churchpoint	243	7,686	.702	15318-15375	Thornwell	315	11,376	.743
11200-11389	Mud Lake	246	6,272	.560	15336-15407	Lake Arthur	329	13,933	.909
11330-11356	Rayne	217	6,900	.609	15580-15595	Leleux	277	13,570	.871
11650-11679	Chalkley	233	9,345	.802	15600-15800	Deep Lake	366	9,885	.634
11933-11943	Erath	231	6,602	.553	15871-15880	Lake Sand	296	12,505	.788
11950-11995	Bayou Penchant	230	9,031	.756	16000-16018	Lacassine	275	14,625	.914
12200-12246	Lake Arthur	262	10,100	.828	16450-16495	Hollywood	280	14,540	.884
12295-12328	Thornwell	303	11,800	.960	16570-16585	Weeks Island	266	9,495	.573
12450-12493	Belle Isle	231	6,690	.537	17300-17340	Belle Isle	316	11,420	.660
12550-12562	Grand Isle	263	8,745	.697	17395-17429	Lake Sand	318	13,477	.775

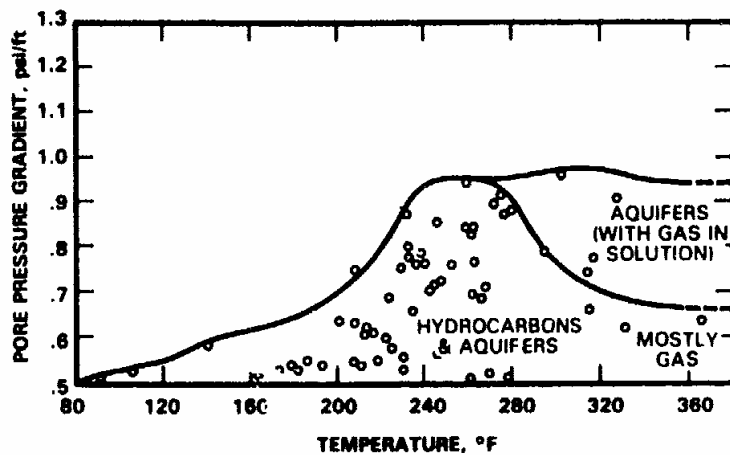


Figure 2.11– Correlation of pore pressure gradient with temperature and reservoir fluid types (ref. 29).

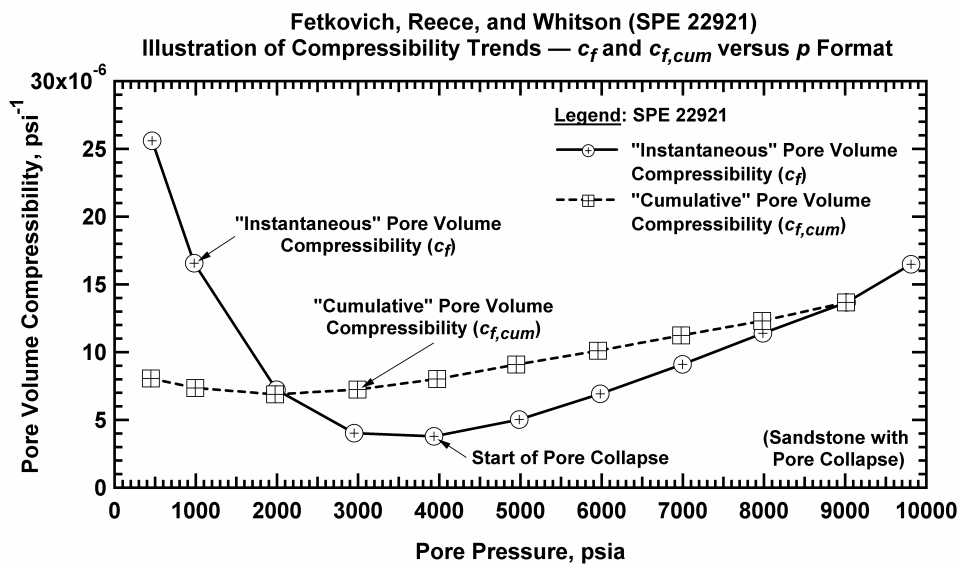


Figure 2.12– Comparison of instantaneous and cumulative formation compressibility functions (ref. 1).

CHAPTER III
A SIMPLIFIED MODEL FOR THE MATERIAL BALANCE OF
ABNORMALLY PRESSURED GAS RESERVOIRS
(THE "QUADRATIC CUMULATIVE PRODUCTION" MODEL)

3.1 Model Development

The most relevant issue to consider regarding the validity of this work is that we have utilized the Fetkovich, *et al.*¹ material balance formulation and we have established an approximating condition that permits us to formulate an explicit, closed form approximation to the Fetkovich, *et al.* material balance in terms of p/z and G_p . We have systematically established the stated approximating condition, and while our simplified material balance model may not be considered exact, we will show that the approximating condition is essentially universal (*i.e.*, it was shown to be valid for every case we considered). Equally important is the observation that our new simplified material balance relation yielded correct estimates of gas-in-place for every case considered — and the model was shown to be tuned to performance data using at stages as small as 5-10 percent depletion (*i.e.*, $G_p/G < 0.10$).

Our starting point is the Fetkovich, *et al.*¹ material balance formulation where $G_{inj}=W_{inj}=W_p=W_e=0$, and we only consider the effect of the cumulative effective compressibility function, $\bar{c}_e(p)$. This form is:

$$\frac{p}{z} [1 - \bar{c}_e(p)(p_i - p)] = \frac{p_i}{z_i} \left[1 - \frac{G_p}{G} \right] \dots\dots\dots(3.1)$$

Defining the ω -function, we have

$$\omega G_p \equiv \bar{c}_e(p)(p_i - p) \dots\dots\dots(3.2)$$

Defining the ω -function, we have

$$\omega \equiv \frac{1}{G_p} \bar{c}_e(p)(p_i - p) \dots\dots\dots(3.3)$$

Alternatively, we can also define the ω -function using the p/z , p_i/z_i , G , and G_p terms in Eq. 3.1, this effort gives

$$\omega \equiv \frac{1}{G_p} - \frac{p_i/z_i}{p/z} \left[\frac{1}{G_p} - \frac{1}{G} \right] \dots\dots\dots(3.4)$$

We have defined the ω -function as a mechanism to assess the abnormal pressure behavior if the reservoir system — we correlate ω with the cumulative gas production, G_p in order to establish a correlation. Substituting Eq. 3.2 into Eq. 3.1 and rearranging, we obtain the following result:

$$\frac{p}{z} = \frac{p_i}{z_i} \frac{1}{1 - \omega G_p} \left[1 - \frac{G_p}{G} \right] \dots\dots\dots(3.5)$$

At this point Eq. 3.5 is completely identical to Eq. 3.1, we have only used the ω -function as a variable of substitution for the $\bar{c}_e(p)(p_i - p)$ term in Eq. 3.1. Our next step is to attempt to obtain an alternate form of Eq. 3.5 that will directly (and uniquely) relate p/z and G_p — in its current form, Eq. 3.5 has some utility, but we would like a more useful form, perhaps a polynomial. As an aside, we can rearrange Eq. 3.5 directly to obtain the following form:

$$\frac{(p/z)}{(p_i/z_i)} = \frac{1 - \theta G_p}{1 - \omega G_p} \quad (\text{where } \theta = 1/G) \dots\dots\dots(3.6)$$

The rational formulation given by Eq. 3.6 can not be reduced further, and is not practical as an analysis relation. The question remains as to the character ω -function — we will proceed considering three possibilities — ω is constant, ω is linear with G_p , or ω is simply a generic function of G_p (no functional form is implied). From the developments presented so far, these are bold claims — however, using 24 (twenty-four) validation cases in Appendix D, we provide substantial evidence that ω can either be assumed constant or assumed to be a simple linear function of G_p .

Another assumption that can be made is regarding the behavior of the ωG_p product — we will state that we believe $\omega G_p < 1$. Therefore, we can use a binomial (or geometric) series expansion for $1/(1 - \omega G_p)$ (recall that the binomial series is defined for this case as $1/(1-x) = 1 + x + x^2 + x^3 + \dots$), and we will only use a single term expansion (*i.e.*, $1/(1 - \omega G_p) \approx 1 + \omega G_p$). Making this substitution in Eq. 3.5, we have:

$$\frac{p}{z} \approx \frac{p_i}{z_i} \left[1 - \frac{G_p}{G} \right] (1 + \omega G_p) \dots\dots\dots(3.7)$$

Now, if we assume that the ω -function is constant (hence, we refer to this as the " ω -parameter"), Eq. 3.7 can be expanded to yield:

$$\frac{p}{z} \approx \frac{p_i}{z_i} - \alpha G_p - \beta G_p^2 \dots\dots\dots(3.8)$$

Where the α and β coefficients are defined by:

$$\alpha \equiv \left(\frac{1}{G} - \omega \right) \frac{p_i}{z_i} \dots\dots\dots(3.9)$$

$$\beta \equiv \frac{\omega}{G} \frac{p_i}{z_i} \dots\dots\dots(3.10)$$

The obvious question at this point is what does the ω -function look like? Is there any reason to believe that the ω -function will be constant or even a simple function of G_p ? In Appendix A we provide a complete development and discussion of the rationale we use to establish the character of the ω -function and the $\bar{c}_e(p)(p_i - p)$ product. In this chapter we will only focus on the behavior of the ω -function relative to the validation of Eq. 3.8. As such, we present plots of ω versus G_p/G for two sample cases (see

Appendix D for all analyses). We have chosen to plot ω versus G_p/G (rather than G) so that we can establish the validity of the ω profile as a function of the depletion in the reservoir (*i.e.*, G_p/G).

The first case is "Case 1," a numerical simulation case using an input c_f profile obtained from the Fetkovich, *et al.*¹ reference. The second case is "Case 3," the classic literature example for an abnormally pressured gas reservoir — the "Anderson L" case presented in ref. 21. In **Fig. 3.1** we present a plot of the ω versus G_p/G profile for "Case 1," the numerical simulation case. We note development of a clear linear trend in the ω versus G_p/G data function — validating our hypothesis to some degree. We have constructed model trends for the ω constant and linear cases — and both model trends appear to be relevant. We have elected to place the model trend for the ω =constant case in the middle of the ω versus G_p/G trend. This appears to be a good balance and suggests that our concept (*i.e.*, $\omega \approx$ constant) is reasonable — particularly considering the applications to field data.

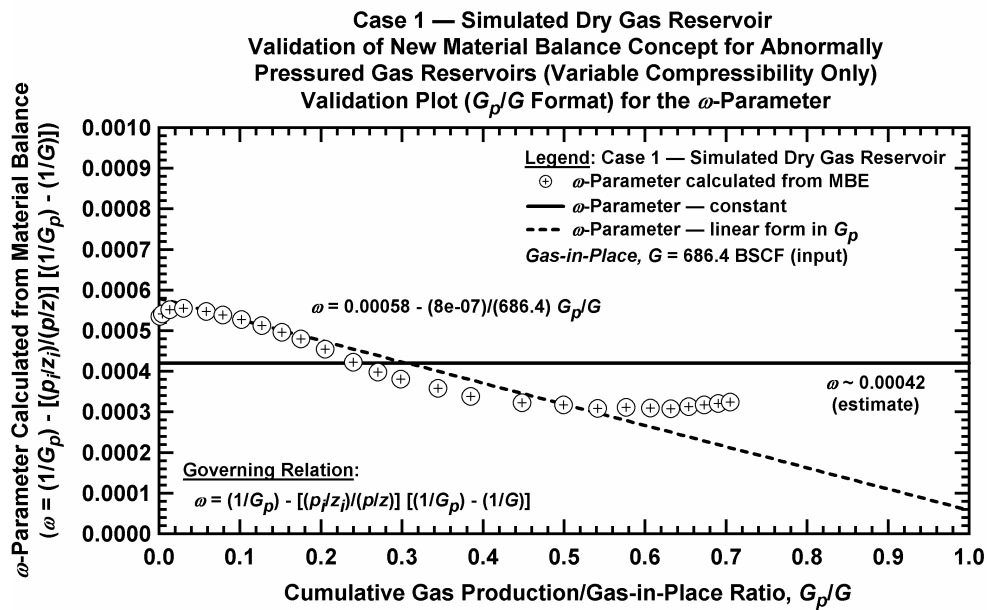


Figure 3.1 — Behavior of the ω -parameter versus G_p/G for a simulated dry gas reservoir case. Note that in this case the maximum depletion of the model is approximately 70 percent — which justifies the (relatively) poor agreement of the constant model with the data trend.

The second case is "Case 3," the Anderson L field data case (South Texas, USA) (from ref. 21). For this case, we present the plot of the ω versus G_p/G in **Fig. 3.2**. In this case we prefer to place the constant ω trend towards the top of the ω versus G_p/G data distribution, this placement represents a balance of the analysis on this particular plot, as well as the match of the various data functions for this case using the

other data plots which are being simultaneously matched. We also note that the apparent linear trend of ω versus G_p/G is both reasonable and consistent. Our primary concern is the viability of this analysis plot for field data, and, at least in this particular case, we would say that the ω — G_p/G methodology is both sound and accurate.

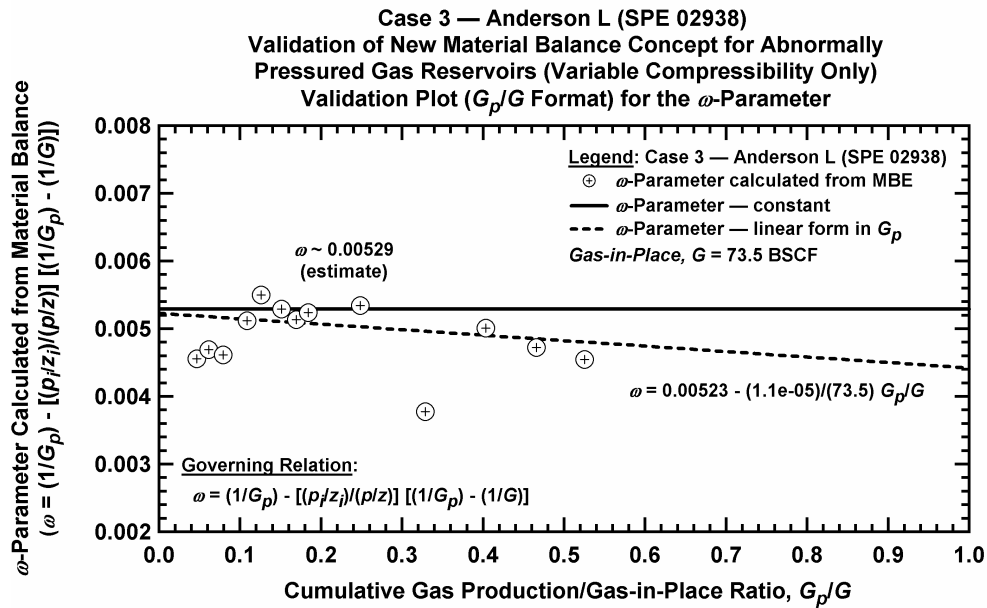


Figure 3.2 – Behavior of the ω -parameter versus G_p/G for the "Anderson L" field case example²¹ (South Texas, USA). Note that this case shows an apparent depletion of about 50 percent — this is a possible explanation for the reasonably good correlation of data with both the constant and linear models.

The "proof" of Eq. 3.8 (*i.e.*, the quadratic cumulative production model) lies in the validity of the constant ω -parameter determined from the previous analysis (*i.e.*, **Figs. 3.1 and 3.2**). Substituting $\omega = 0.00042$ 1/BSCF for "Case 1" into Eq. 3.8, we obtain the p/z versus G_p profile shown in **Fig. 3.3**. Similarly, for "Case 3" (Anderson L Field) we substitute $\omega = 0.00529$ 1/BSCF into Eq. 3.8 and generate the profile shown in **Fig. 3.4**. We note an extraordinarily accurate fit of the data trends in both **Figs. 3.3 and 3.4**, which we believe validates our concept for the p/z — G_p^2 material balance relation (*i.e.*, Eq. 3.8).

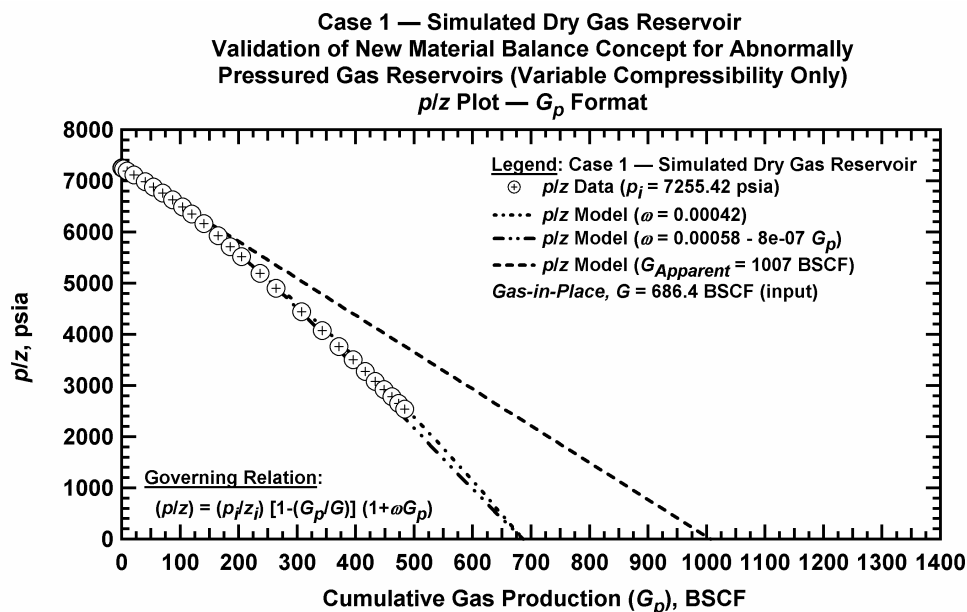


Figure 3.3 – p/z versus G_p plot for the simulated performance of an abnormally pressured gas reservoir (variable compressibility only) (dry gas reservoir case).

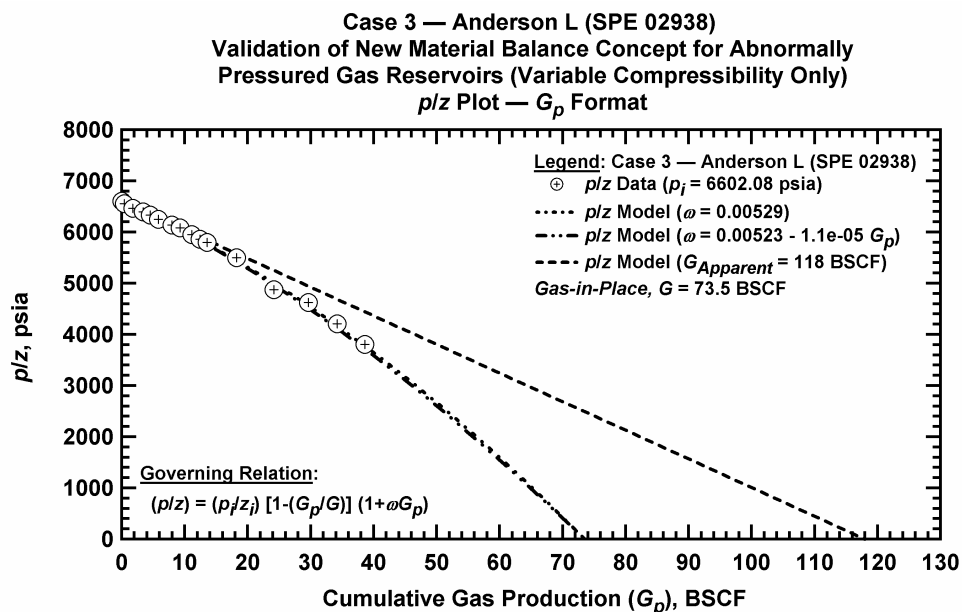


Figure 3.4 – p/z versus G_p plot for the "Anderson L" field case example²¹ (South Texas, USA) (a suspected abnormally pressured gas reservoir case).

In summary, we have established a group of diagnostic plots based on the characteristics of the effective compressibility-pressure drop term, $\bar{c}_e(p)(p_i - p)$ (defined using Eq. 3.1), as well as the ω -function (defined using Eq. 3.4). We recognize that there may be a slight bit of confusion between the new ω -function and the $\bar{c}_e(p)(p_i - p)$ function (recall that $\omega \equiv (1/G_p) \bar{c}_e(p)(p_i - p)$) — however, we believe it is necessary to maintain the original Fetkovich, *et al.*¹ variable (*i.e.*, $\bar{c}_e(p)(p_i - p)$) for the purpose of establishing the validity of Eq. 3.8 (see Appendix A for specific details). Further, we also believe it is necessary to establish the ω -function as an independent variable for the purpose of our approximate material balance relations for the case of a reservoir exhibiting abnormal pressure effects.

For reference, we present the following itemized list of new diagnostic plots developed in this work: (again, the specific details are given in Appendix A)

- Log-log plot of $\bar{c}_e(p)(p_i - p)$ vs. G_p/G (yields a power law trend).
- Cartesian plot of $1/[1 - \bar{c}_e(p)(p_i - p)]$ vs. G_p/G (yields a linear trend).
- Cartesian plot of ω vs. G_p (user selects a constant ω value or a linear ω versus G_p trend).
- Cartesian plot of ω vs. G_p/G (user selects a constant ω value or a linear ω versus G_p trend).

3.2 Plotting Functions for Data Analysis

In this section we focus on the presentation and implementation of plotting functions developed using Eq. 3.8 (the specific plotting functions are developed in Appendix B, in full detail). We present an inventory of the plotting functions we have selected to use in this work as follows:

$$\text{Plotting Function 1 (PF}_1\text{): } \Delta(p/z) \text{ versus } G_p \text{ (quadratic).....(3.11)}$$

$$\text{Plotting Function 2 (PF}_2\text{): } \Delta(p/z)/G_p \text{ versus } G_p \text{ (linear).....(3.12)}$$

$$\text{Plotting Function 3 (PF}_3\text{): } \frac{1}{G_p} \int_0^{G_p} \Delta(p/z) dG_p \text{ versus } G_p \text{ (quadratic).....(3.13)}$$

$$\text{Plotting Function 4 (PF}_4\text{): } \frac{1}{G_p^2} \int_0^{G_p} \Delta(p/z) dG_p \text{ versus } G_p \text{ (linear).....(3.14)}$$

$$\text{Plotting Function 5 (PF}_5\text{): } \Delta(p/z) - \frac{1}{G_p} \int_0^{G_p} \Delta(p/z) dG_p \text{ versus } G_p \text{ (quadratic).....(3.15)}$$

$$\text{Plotting Function 6 (PF}_6\text{): } \frac{1}{G_p} \left[\Delta(p/z) - \frac{1}{G_p} \int_0^{G_p} \Delta(p/z) dG_p \right] \text{ versus } G_p \text{ (linear).....(3.16)}$$

Each of these 6 (six) plotting functions (PF_1 - PF_6) is used to provide unique insight into the character of the basis function (Eq. 3.8) — we will present an illustrative example of these functions next.

As an illustrative example, in **Table 3.1** we present the plotting functions for "Case 1" (our base numerical simulation case — a dry gas reservoir with $c_f(p)$ obtained from ref. 1).

Table 3.1 – Summary of plotting functions used to implement the quadratic cumulative production material balance relation for abnormal pressure effects (applied to Case 1 (numerical simulation case)).

Base Relation	Name	Plotting Functions	Character	Fig.
Eq. 3.11	(PF ₁)	$\Delta(p/z)$ versus G_p	Quadratic	3.5
Eq. 3.12	(PF ₂)	$\Delta(p/z)/G_p$ versus G_p	Linear	3.6
Eq. 3.13	(PF ₃)	$\frac{1}{G_p} \int_0^{G_p} \Delta(p/z) dG_p$ vs. G_p	Quadratic	3.7
Eq. 3.14	(PF ₄)	$\frac{1}{G_p^2} \int_0^{G_p} \Delta(p/z) dG_p$ vs. G_p	Linear	3.8
Eq. 3.15	(PF ₅)	$\Delta(p/z) - \frac{1}{G_p} \int_0^{G_p} \Delta(p/z) dG_p$ vs. G_p	Quadratic	3.9
Eq. 3.16	(PF ₆)	$\frac{1}{G_p} \left[\Delta(p/z) - \frac{1}{G_p} \int_0^{G_p} \Delta(p/z) dG_p \right]$ vs. G_p	Linear	3.10

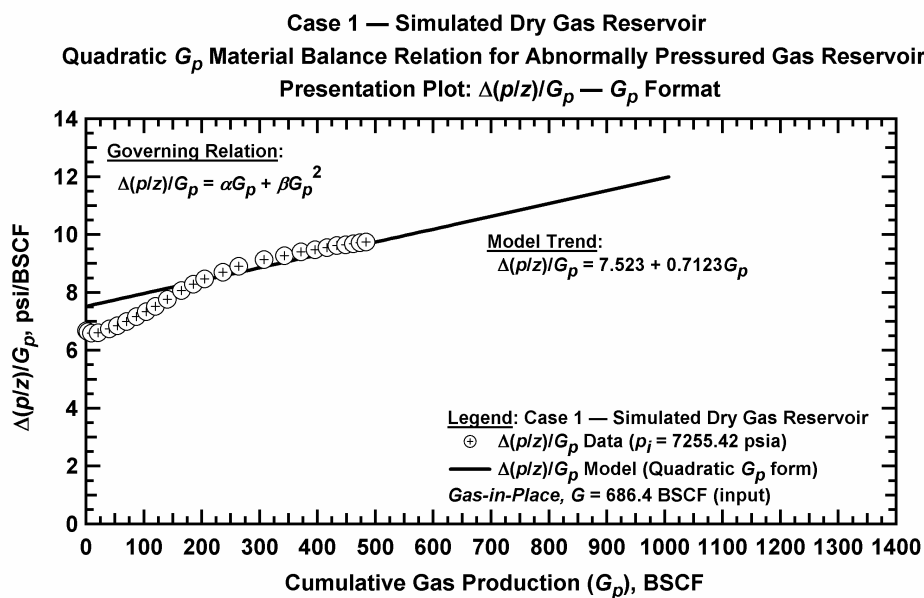
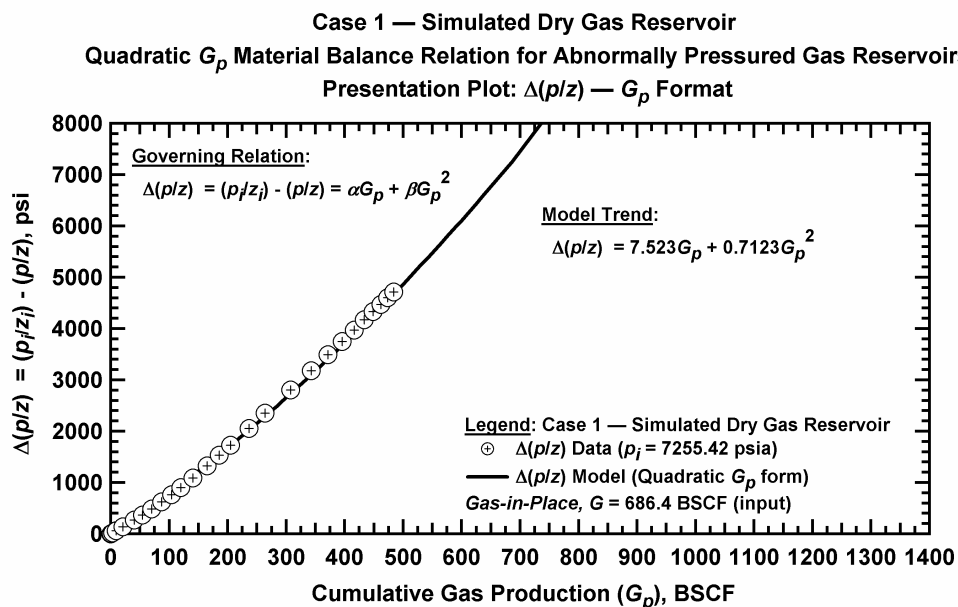
It is tempting to presume that we could extend the "quadratic" plotting functions (PF₁, PF₃, and PF₅) to some other format and that these functions could yield independent estimates of gas-in-place. We have not pursued this effort (nor have we pursued independent analysis of the "linear" plotting function (PF₂, PF₄, and PF₆)) — primarily because our "analysis" goal is to achieve a consistent estimate of gas-in-place across all data functions (including the diagnostic plots, the Gan-Blasingame plots (ref. 2), the new p_D - G_{pD} type curve, and the p/z - G_p summary plots). We achieve this goal by performing a dynamic, *simultaneous match* of all data functions in a spreadsheet program — using a single set of control parameters.

In **Fig 3.5** (PF₁) we note that the "quadratic" characteristic behavior of PF₁ is clearly evident — we also note excellent agreement in the data and model functions. Similarly, in **Fig 3.6** (PF₂) we find that PF₂ does exhibit the expected linear trend against G_p — however, we also note a characteristic oscillation of the data about the linear model trend. We will comment that this oscillation in the data function is likely a legitimate feature of this numerical simulation data — we do not believe this behavior to be an artifact.

Recall that our base model (Eq. 3.8) is approximate, and this oscillation merely proves that our model (and its related plotting functions) is approximate.

On the other hand, based on extensive application to field data (presented in Appendix D), we can state that essentially none of the field data cases exhibit such oscillations (we only observe random variations about the trend as one might expect from field data). We will also comment that of the other 2 simulation cases (*i.e.*, Case 2 and Case 23 (see Appendix D)) only Case 23 exhibits an "oscillation" feature (we will note that for Case 2, only a few data exist). We propose that this feature is due to the character of the $c_j(p)$ function input into the simulation (see Appendix D (Fig. D.1.q)), and we also note that the $c_j(p)$ function (obtained from ref. 1) could be considered an extreme case.

We present (PF_3) in **Fig. 3.7** and we note very good agreement of the data and model functions. Similarly, we note in **Fig. 3.8** (PF_4) the same behavior that we observed in **Fig. 3.6** (*i.e.*, oscillation of the data functions about a linear model trend). In **Fig. 3.9** (PF_5) we note a good agreement of the model and data, and we will comment that this is a "difference function," as such we would expect that any minor deviations observed in previous plotting functions may be exaggerated (as we note in the middle of the quadratic trend). Likewise, in **Fig. 3.10** (PF_6) we find a reasonable match of the (oscillating) data function about the linear model trend — as in **Fig. 3.9**, (PF_6) is also a "difference function" and we would expect some exaggeration of features observed on the plotting functions presented earlier. We again comment that all of the analyses shown in this sequence (*i.e.*, the generation of the model function) were performed as a simultaneous match of all plots using control values of the gas-in-place and other parameters (we note that the gas-in-place parameter dominates the analysis).



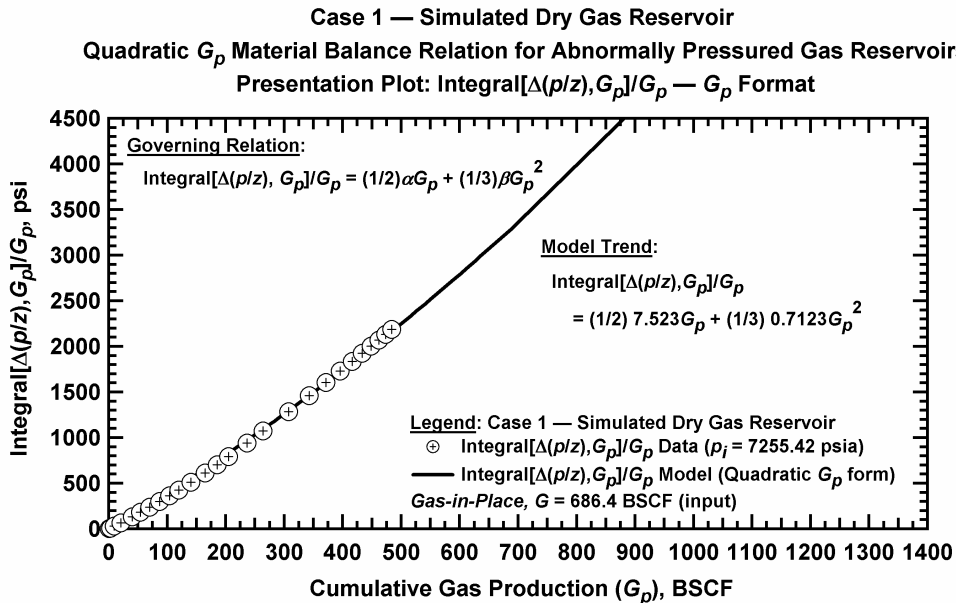


Figure 3.7 – Plot of $\frac{1}{G_p} \int_0^{G_p} \Delta(p/z) dG_p$ vs. G_p — Case 1.

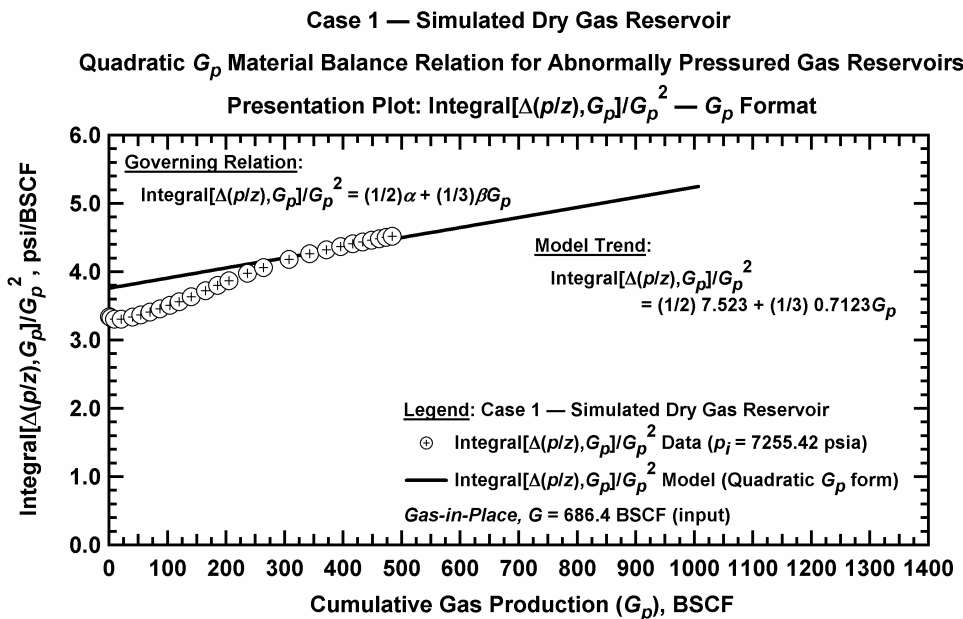


Figure 3.8 – Plot of $\frac{1}{G_p^2} \int_0^{G_p} \Delta(p/z) dG_p$ vs. G_p — Case 1.

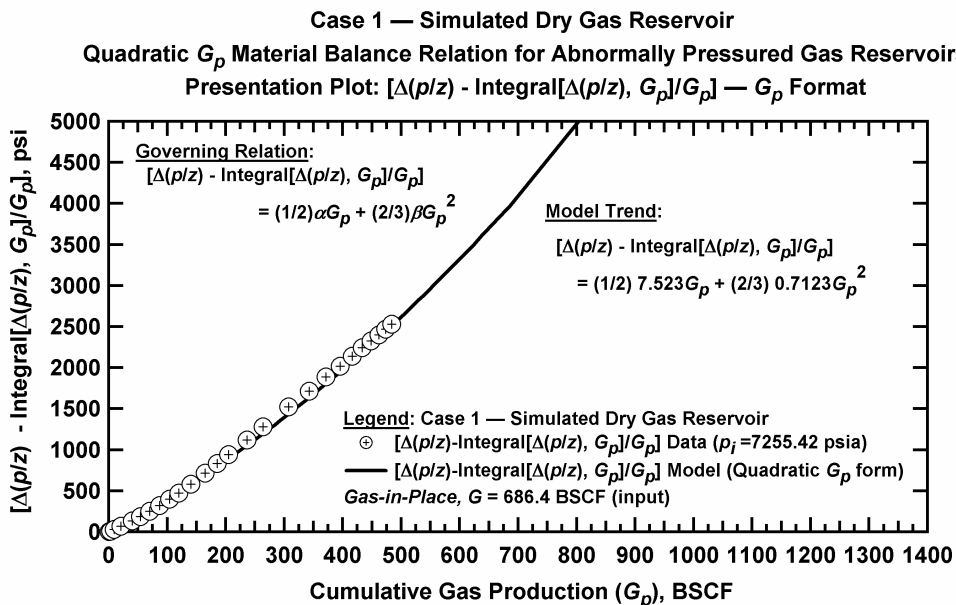


Figure 3.9 – Plot of $\Delta(p/z) - \frac{1}{G_p} \int_0^{G_p} \Delta(p/z) dG_p$ vs. G_p — Case 1.

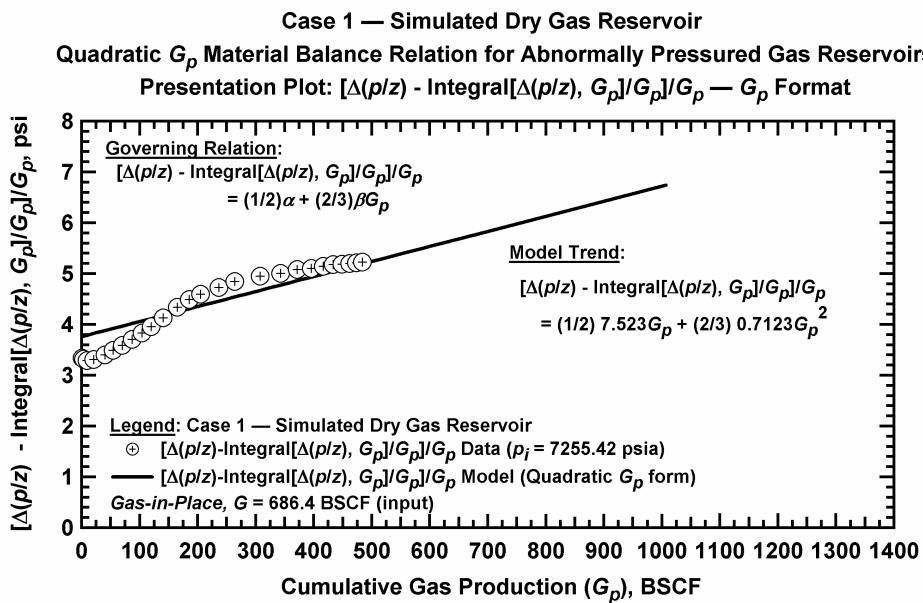


Figure 3.10 – Plot of $\frac{1}{G_p} \left[\Delta(p/z) - \frac{1}{G_p} \int_0^{G_p} \Delta(p/z) dG_p \right]$ vs. G_p — Case 1.

3.3 New Type Curve for Material Balance Analysis

In Appendix C we develop and present a new type curve solution that includes the dry gas material balance (no abnormal pressure effects), as well as the case of a gas reservoir with abnormal pressure effects as represented by Eq. 3.8. We note that Eq. 3.8 is also valid for the case of no abnormal pressure effects (*i.e.*, $\omega=0$).

Beginning with an alternate form of Eq. 3.8, we have

$$\frac{p}{z} = \frac{p_i}{z_i} \left[1 - \left(\frac{1}{G} - \omega \right) G_p - \frac{\omega}{G} G_p^2 \right] \dots\dots\dots (3.17)$$

In developing a "type curve" solution we must resort to "dimensionless" variables — therefore, we employ the following dimensionless variables in this effort:

$$\omega_D = \omega G \dots\dots\dots (3.18)$$

$$p_D = \left[1 - \frac{p/z}{p_i/z_i} \right] = \left[\frac{p_i/z_i - p/z}{p_i/z_i} \right] \dots\dots\dots (3.19)$$

$$G_{pD} = \frac{G_p}{G} \dots\dots\dots (3.20)$$

Substituting Eqs. 3.18, 3.19, and 3.20 into Eq. 3.17, we obtain the "dimensionless" form of the "quadratic cumulative production" material balance relation for an abnormally pressured gas reservoir:

$$p_D = (1 - \omega_D) G_{pD} + \omega_D G_{pD}^2 \dots\dots\dots (3.21)$$

Defining the "dimensionless pressure integral" function $p_{Di} = \frac{1}{G_{pD}} \int_0^{G_{pD}} p_D dG_{pD}$ — and substituting Eq. 3.21 into this definition yields:

$$p_{Di} = (1 - \omega_D) \frac{1}{2} G_{pD} + \omega_D \frac{1}{3} G_{pD}^2 \dots\dots\dots (3.22)$$

We present the "gas material balance type curve" in **Fig. 3.11**, where we note that we have used *both* the "dimensionless" pressure and pressure integral functions, p_D and p_{Di} (respectively) on this type curve.

Reviewing **Fig. 3.11** we note that our definition of p_D (and p_{Di}) has yielded very good model trends — where it should be both straightforward and consistent as a data analysis tool. In this work we have not employed Fig. 3.2 as an independent data analysis tool, but rather, as a component in the dynamic matching methodology we implemented in MS Excel. It is worth noting that we did use the type curve as a "start-up" analysis mechanism in our implementation (*i.e.*, we used this plot to start or orient our analysis), and we also used **Fig. 3.11** routinely as a "check" for our other analysis (ω_D is estimated independently on this plot (regardless of how the plot is implemented for analysis)). In summary, the type curve plot has shown to be extremely valuable in the analysis sequence for our analysis and interpretation of abnormally pressured gas reservoirs.

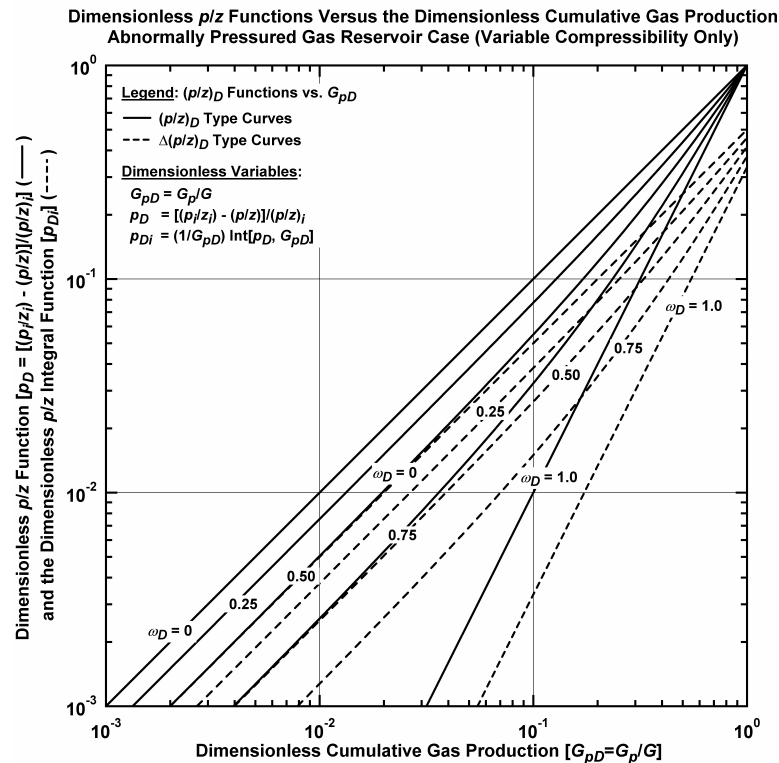


Figure 3.11— p_D and p_{Di} versus G_{pD} "type curve" plot for the "quadratic cumulative production" material balance relation for an abnormally pressured gas reservoir.

As a final comment, we will note that on occasion, the p_D (and p_{Di}) data function at small values of G_{pD} (maybe the first 1-2 points) appears to "curl" slightly (generally upwards). Based on our definition of the p_D variable (Eq. 3.19), this feature appears to be related to an incorrect estimate of initial reservoir pressure (p_i), which yields an incorrect estimate of p_i/z_i . This was seldom an issue, and the remainder of the data tended to match the type curve extremely well.

The analysis methodology illustrated in **Fig. 3.12** is referenced to all of the model functions, as well as the relevant data functions (*e.g.*, ω and $\bar{c}_e(p)(p_i - p)$) where the affected functions are updated as the control parameters are adjusted. We note that we generally focus on the Gan-Blasingame² plots (Row 1: 3 topmost plots) as "watch" plots, and we use the $\omega-G_p$ and the $\bar{c}_e(p)(p_i - p) - G_p$ function plots (Row 4: 5 bottommost plots) as our dominant "control" plots. The plotting functions (Rows 2 and 3 (7 plots total)) are used primarily for orientation and assessment of data quality, as is also the type curve plot (the rightmost plot, lying across Rows 1-3).

The control parameters are located at the topmost portion of the module (note that the control parameters are varied using "slide bars," where a particular slide bar can be overwritten using an input value). We believe that our approach is consistent and robust — and we particularly appreciate that this approach controls the entire analysis process dynamically — any parameter change is reflected globally throughout all of the data and model functions.

3.5 Example Analysis of Field Data — Anderson L Reservoir (Case 3)

In **Table 3.2** we present the inventory of the data analysis plots developed for the Anderson L Reservoir (our "Case 3" in Appendix D). We simply present these results for the consideration of the reader. We note that all analyses were performed exactly as described above — a set of parameters was optimized using a dynamic/simultaneous analysis of all data in MS Excel. As we stated earlier in this work, *we do not recommend that this analysis sequence be automated in any fashion* — user input and control are critical as a regression algorithm may pursue solutions which are non-optimal at best, or physically inconsistent at worst.

Our primary goal in this presentation of results for the Anderson L Reservoir case is to demonstrate conclusively that underlying "quadratic cumulative production" material balance approximation is accurate and robust — we believe this is clearly proven by the evidence presented for this case as well as the cases presented in Appendix D.

Table 3.2– Summary of plots and plotting functions for the example analysis of the Anderson L Reservoir (South Texas, USA) (Case 3, Appendix D).

Base Relation	Plotting Functions	Fig.
Eq. 3.17	p/z versus G_p (base plot)	3.13
Eq. 3.11	$\Delta(p/z)$ versus G_p	3.14
Eq. 3.12	$\Delta(p/z)/G_p$ versus G_p	3.15
Eq. 3.13	$\frac{1}{G_p} \int_0^{G_p} \Delta(p/z) dG_p$ vs. G_p	3.16
Eq. 3.14	$\frac{1}{G_p^2} \int_0^{G_p} \Delta(p/z) dG_p$ vs. G_p	3.17
Eq. 3.15	$\Delta(p/z) - \frac{1}{G_p} \int_0^{G_p} \Delta(p/z) dG_p$ vs. G_p	3.18
Eq. 3.16	$\frac{1}{G_p} \left[\Delta(p/z) - \frac{1}{G_p} \int_0^{G_p} \Delta(p/z) dG_p \right]$ vs. G_p	3.19
Eq. 3.1	$\bar{c}_e(p)(p_i - p)$ vs. G_p/G	3.20
Eq. 3.1	$1/[1 - \bar{c}_e(p)(p_i - p)]$ vs. G_p/G	3.21
Eq. 3.4	ω vs. G_p	3.22
Eq. 3.4	ω vs. G_p/G	3.23
Eq. 3.17	p/z vs. G_p (results plot for ω — G_p analysis)	3.24
Eq. 3.21/22	p_D and p_{Di} vs. G_{pD}	3.25
"Gan Plot 1"	$\bar{c}_e(p)(p_i - p)$ vs. $(p/z)/(p_i/z_i)$	3.26
"Gan Plot 2"	$(p/z)/(p_i/z_i)$ vs. G_p/G	3.27
"Gan Plot 3"	p/z vs. G_p (results plot for Gan analysis)	3.28
(various)	$c_f(p)$ vs. G (results/comparison plot)	3.29

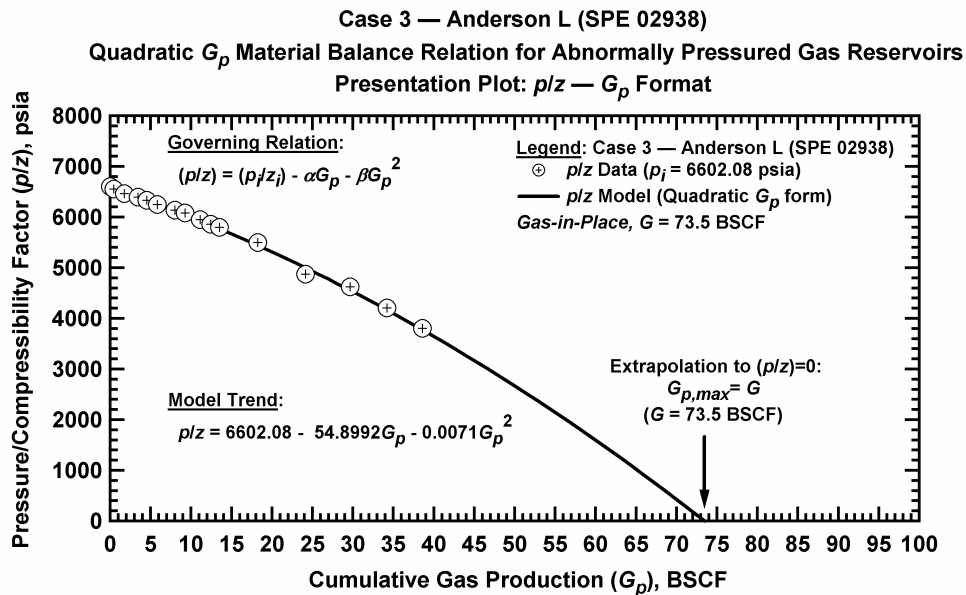


Figure 3.13— Base plot of p/z vs. G_p — Case 3.

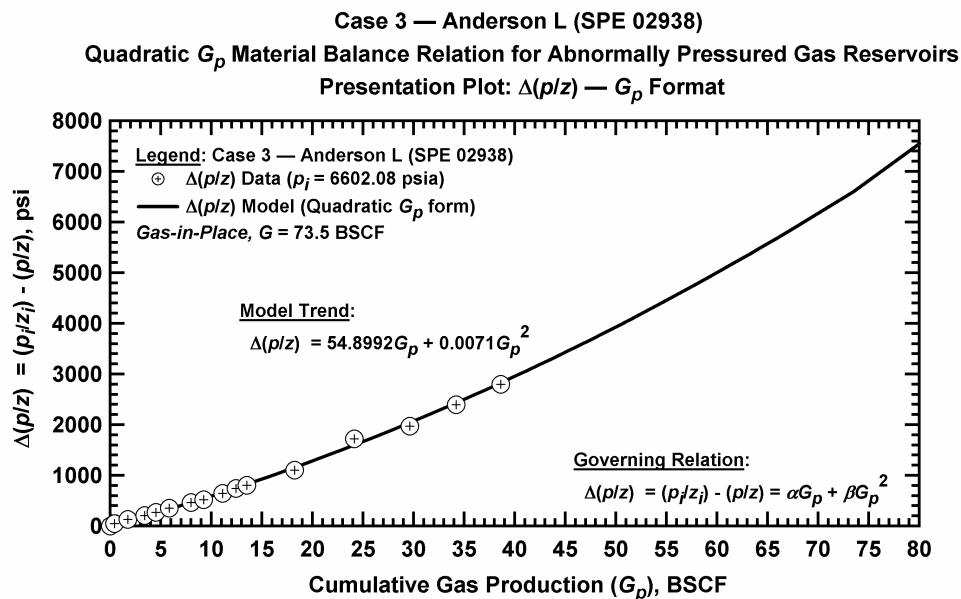


Figure 3.14— Plot of $\Delta(p/z)$ vs. G_p — Case 3.

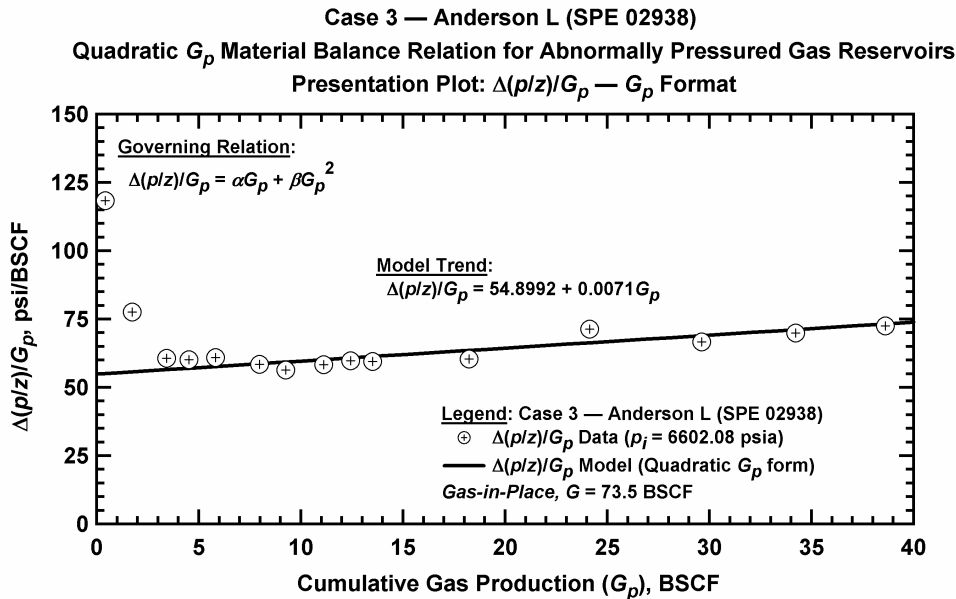


Figure 3.15– Plot of $\Delta(p/z)/G_p$ vs. G_p — Case 3.

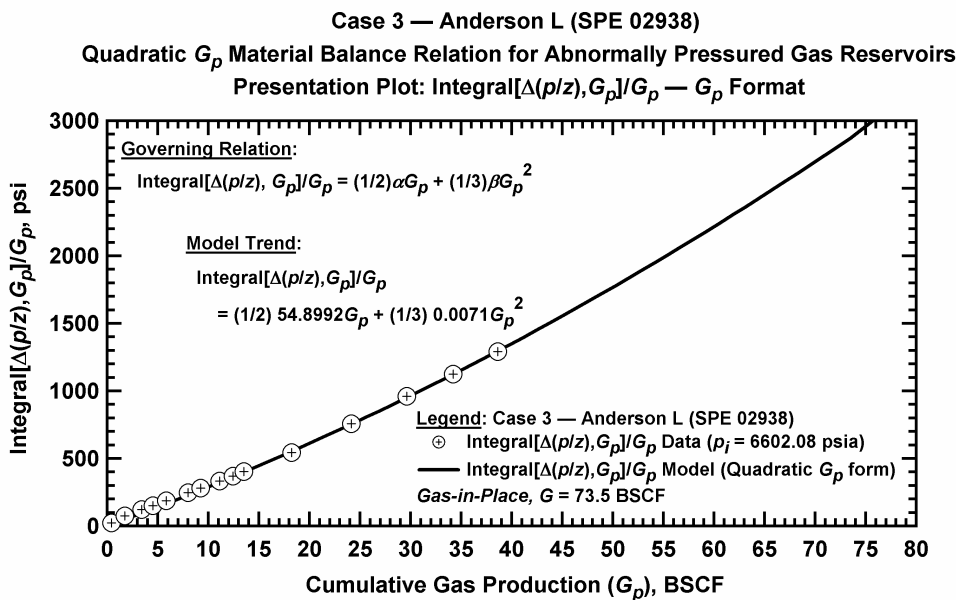


Figure 3.16– Plot of $\frac{1}{G_p} \int_0^{G_p} \Delta(p/z) dG_p$ vs. G_p — Case 3.

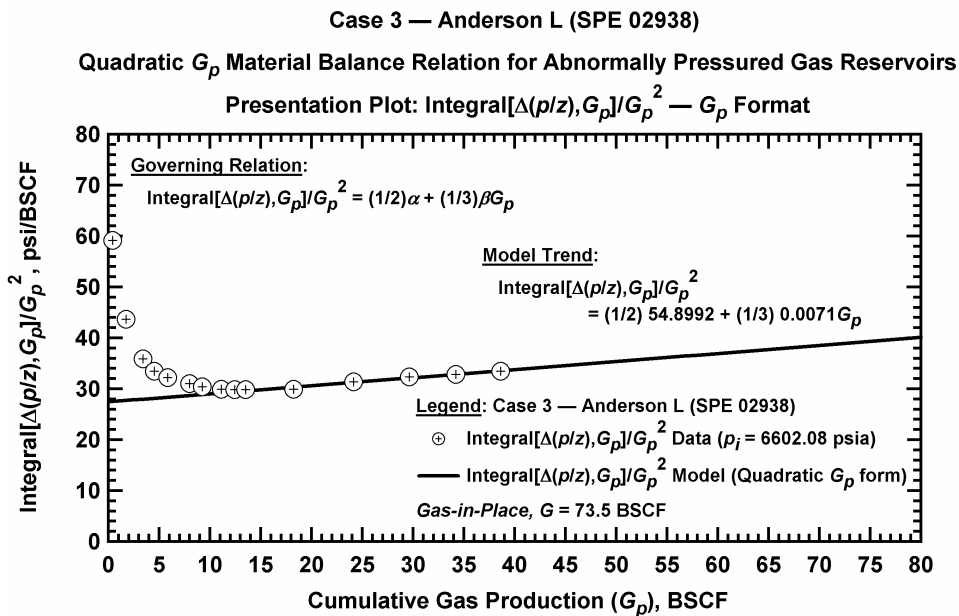


Figure 3.17 – Plot of $\frac{1}{G_p^2} \int_0^{G_p} \Delta(p/z) dG_p$ vs. G_p — Case 3.

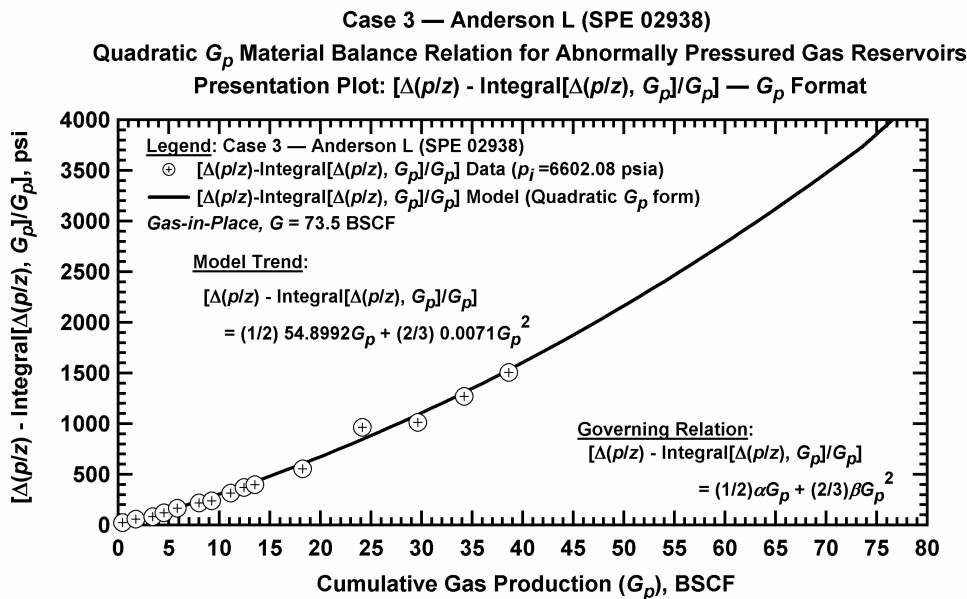


Figure 3.18 – Plot of $\Delta(p/z) - \frac{1}{G_p} \int_0^{G_p} \Delta(p/z) dG_p$ vs. G_p — Case 3.

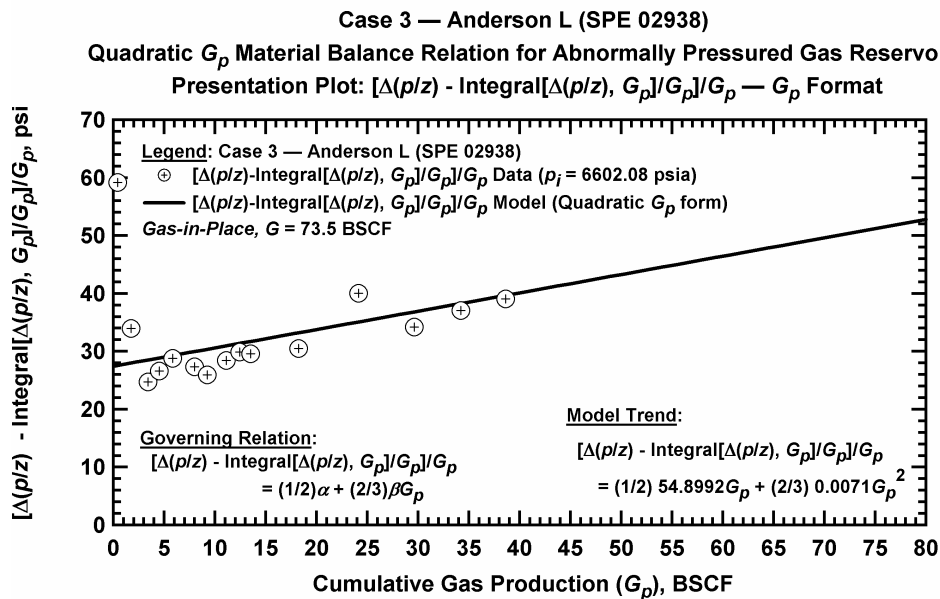


Figure 3.19– Plot of $\frac{1}{G_p} \left[\Delta(p/z) - \frac{1}{G_p} \int_0^{G_p} \Delta(p/z) dG_p \right]$ vs. G_p — Case 3.

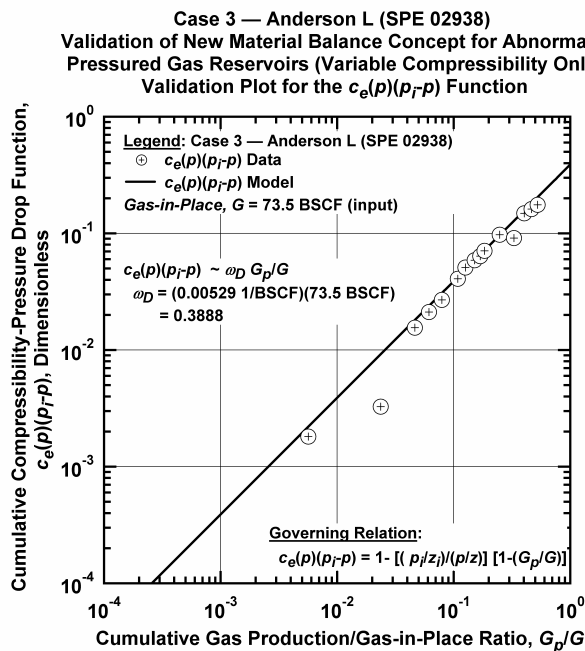


Figure 3.20– Plot of $\bar{c}_e(p)(p_i - p)$ vs. G_p/G — Case 3.

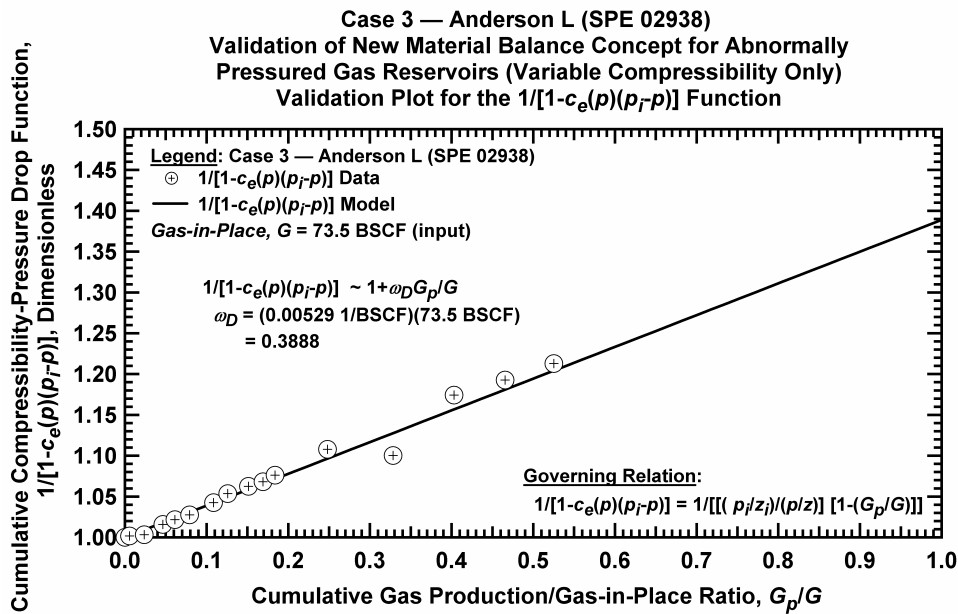


Figure 3.21 – Plot of $1/[1-\bar{c}_e(p)(p_i - p)]$ vs. G_p/G — Case 3.

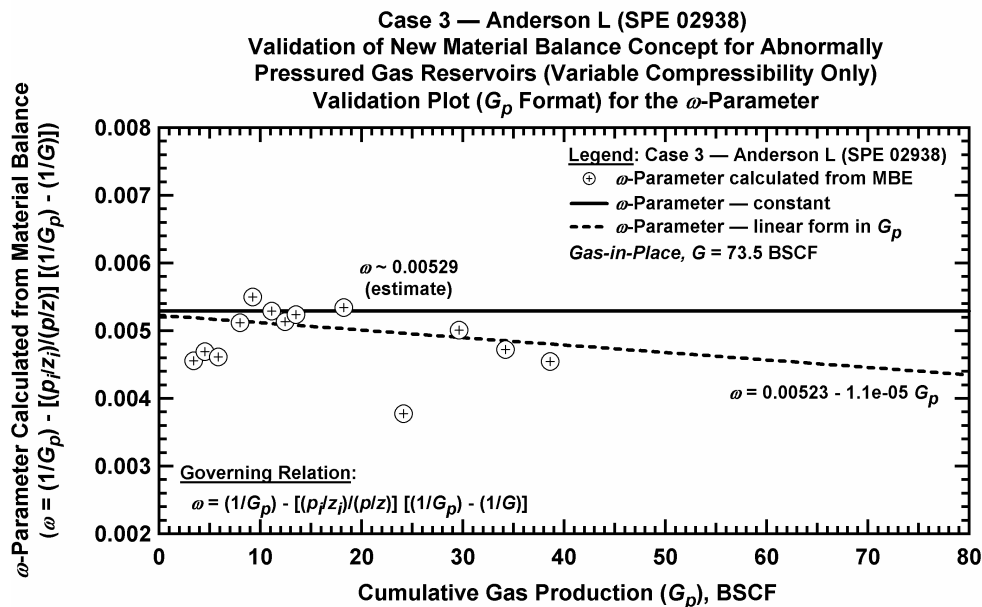


Figure 3.22 – Plot of ω vs. G_p — Case 3.

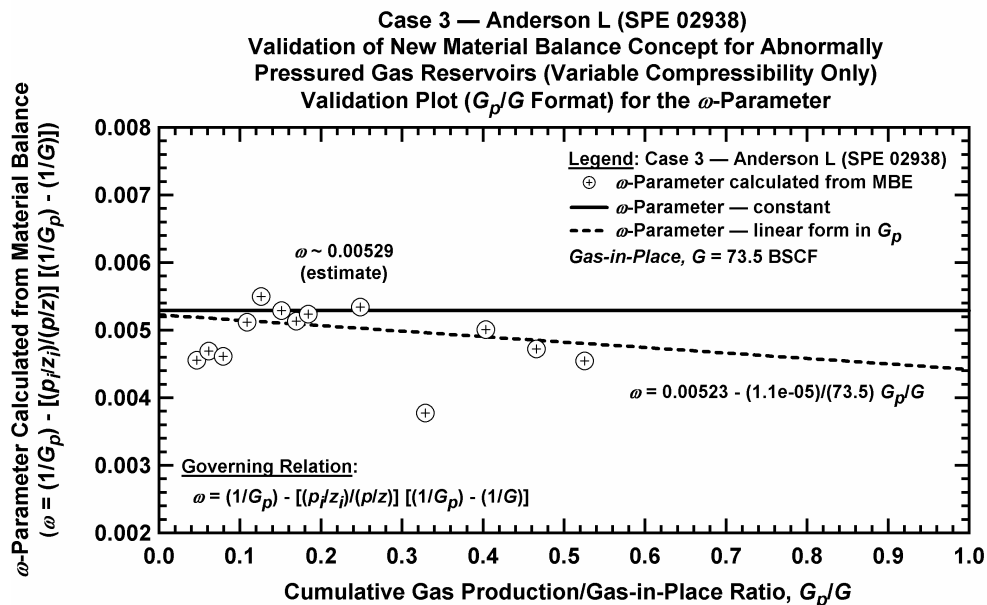


Figure 3.23— Plot of ω vs. G_p/G — Case 3.

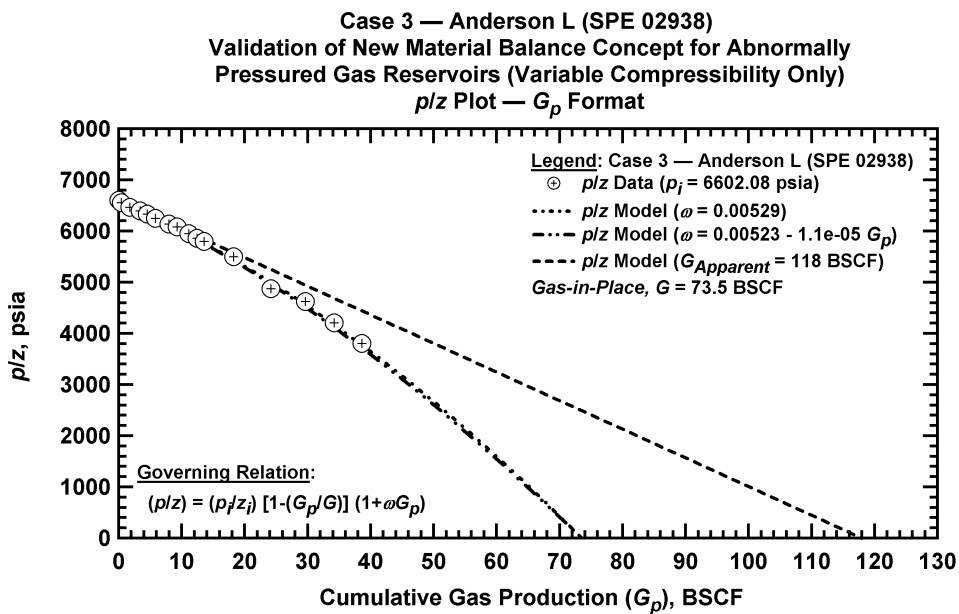


Figure 3.24— Comparison plot of p/z vs. G_p — Case 3.

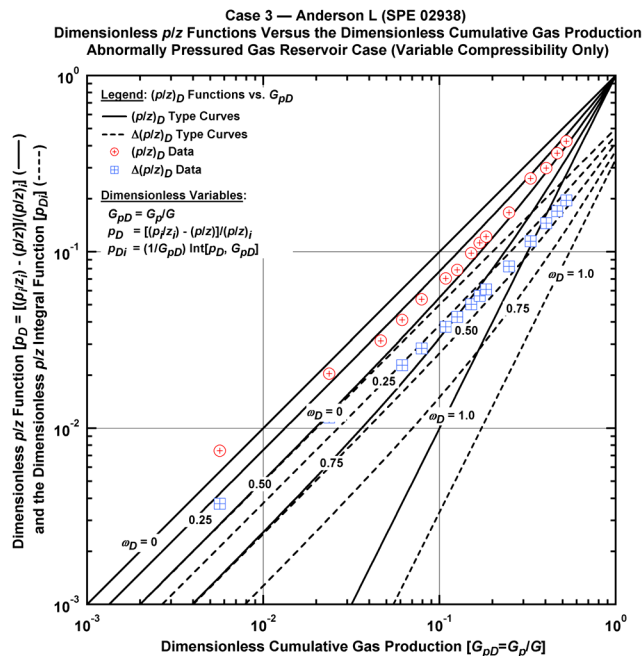


Figure 3.25— Plot of dimensionless p/z functions vs. G_{pD} — Case 3.

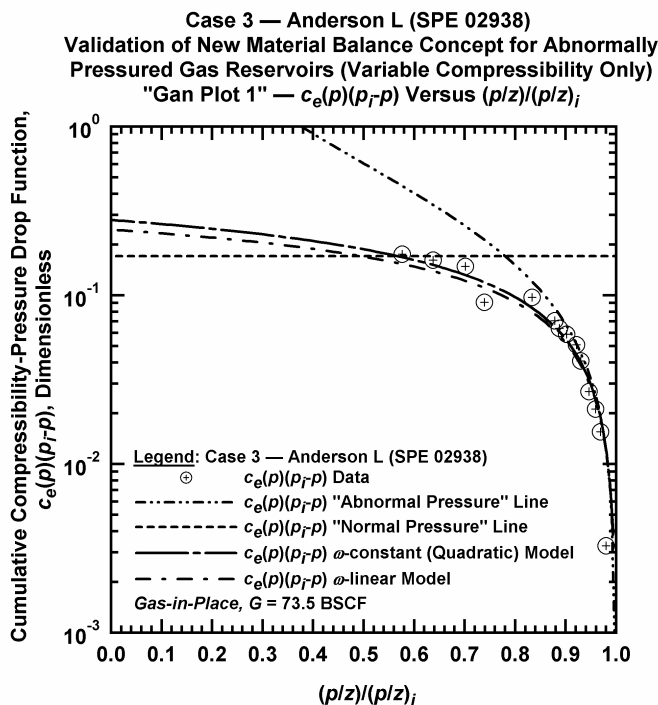


Figure 3.26— Plot of $\bar{c}_e(p)(p_i - p)$ vs. $(p/z)/(p/z)_i$ — Case 3.

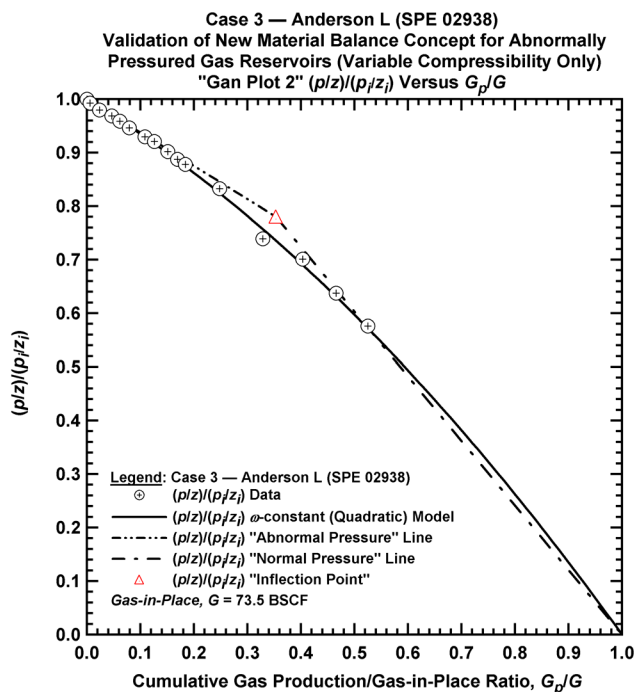


Figure 3.27 – Plot of $(p/z)/(p/z_i)$ vs. G_p/G — Case 3.

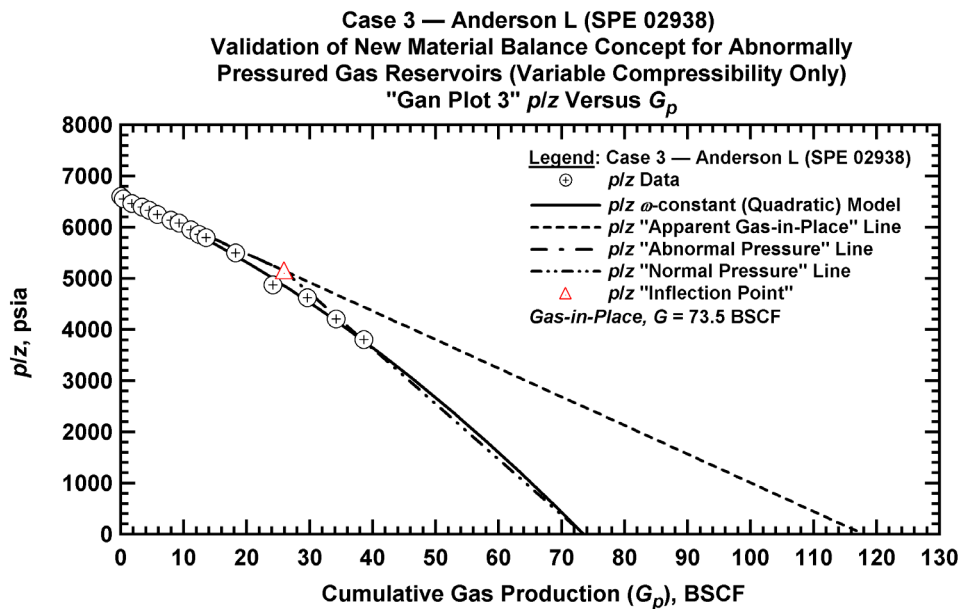


Figure 3.28 – Summary plot of p/z vs. G_p — Case 3.

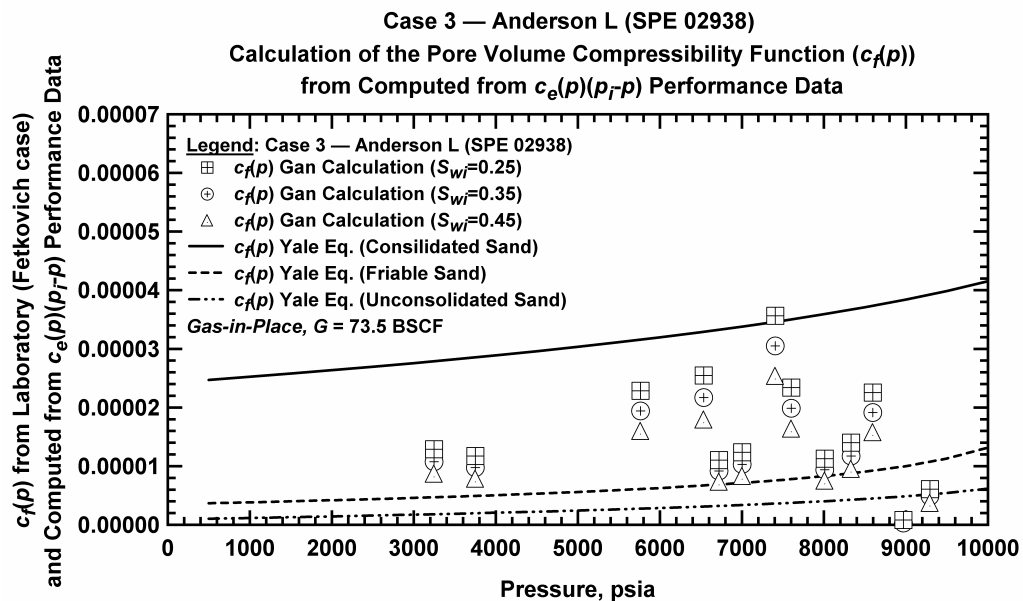


Figure 3.29— Plot of pore volume compressibility computed using Fetkovich, *et al.* approach and compared to laboratory data — Case 3 (Anderson L Reservoir (assumed $S_{wi}=0.25$)).

CHAPTER IV

SUMMARY, CONCLUSIONS, AND RECOMMENDATIONS FOR FUTURE WORK

4.1 Summary

The most important summary comment that can be made regarding this work is that we believe that the quadratic cumulative production model (*i.e.*, the $p/z-G_p^2$ material balance model) derived in this work is the most appropriate approximation developed to date for the case of an abnormally pressured gas reservoir. Our efforts have derived the $p/z-G_p^2$ approximation (as well as another more general approximation) directly from the rigorous gas material for the case of an abnormally pressured gas reservoir.

Our analysis methodology includes 10 (ten) new specialized plots (6 (six) new data plotting functions and 4 (four) new diagnostic plots), as well as a new type curve solution and the utilization of the Gan-Blasingame approach² (which includes 3 (three) additional specialized plots). We have implemented all of these plots in a simultaneous analysis sequence using a spreadsheet program module in MS Excel. For validation, we have used 4 (four) numerical simulation cases and 20 (twenty) field data cases (see Appendix D for a complete inventory of cases) — where we note that all of these cases were successfully analyzed using our new analysis methodology.

4.2 Conclusions

The following conclusions are made based on the results obtained from this work

1. Quadratic Cumulative Production Model: (*i.e.*, the $p/z-G_p^2$ material balance model) The $p/z-G_p^2$ material balance model for an abnormally pressured gas reservoir is derived from the rigorous gas material balance in Appendix A. This result is given as:

$$\frac{p}{z} \approx \frac{p_i}{z_i} - \left(\frac{1}{G} - \omega\right) \frac{p_i}{z_i} G_p - \frac{\omega}{G} \frac{p_i}{z_i} G_p^2 \left[\text{where } \omega \equiv \frac{1}{G_p} \bar{c}_e(p)(p_i - p) \right] \dots\dots\dots(4.1)$$

The primary assumption in this derivation is that ωG_p (or $\bar{c}_e(p)(p_i - p)$) < 1 . Further, we can proceed to develop a variety of relations by assuming that ω is either constant or is defined by some arbitrary function of G_p (*e.g.*, a linear trend of ω versus G_p). For the case of ω =constant, we have:

$$\frac{p}{z} \approx \frac{p_i}{z_i} - \alpha G_p - \beta G_p^2 \dots\dots\dots(4.2)$$

Where α and β could be defined arbitrarily — however, we prefer the following identities established using the assumption that ω =constant:

$$\alpha \equiv \left(\frac{1}{G} - \omega\right) \frac{p_i}{z_i} \dots\dots\dots(4.3)$$

$$\beta \equiv \frac{\omega}{G} \frac{P_i}{z_i} \dots\dots\dots(4.4)$$

2. Plotting Functions derived from the Quadratic Cumulative Production Model: In this work we derived the following plotting functions based on the quadratic cumulative production model (*i.e.*, Eq. 1.x):

Plotting Function 1 (PF_1): $\Delta(p/z)$ versus G_p (quadratic).....(4.5)

Plotting Function 2 (PF_2): $\Delta(p/z)/G_p$ versus G_p (linear).....(4.6)

Plotting Function 3 (PF_3): $\frac{1}{G_p} \int_0^{G_p} \Delta(p/z) dG_p$ vs. G_p (quadratic).....(4.7)

Plotting Function 4 (PF_4): $\frac{1}{G_p^2} \int_0^{G_p} \Delta(p/z) dG_p$ vs. G_p (linear).....(4.8)

Plotting Function 5 (PF_5): $\Delta(p/z) - \frac{1}{G_p} \int_0^{G_p} \Delta(p/z) dG_p$ vs. G_p (quadratic).....(4.9)

Plotting Function 6 (PF_6): $\frac{1}{G_p} \left[\Delta(p/z) - \frac{1}{G_p} \int_0^{G_p} \Delta(p/z) dG_p \right]$ vs. G_p (linear).....(4.10)

The utility of these 6 (six) plotting functions (PF_1 - PF_6) is that we can like the analysis (*i.e.*, we tie the model function(s) to a common estimate of gas-in-place (G) for the purpose of consistency using a spreadsheet type of program). If we wanted to use a plotting function to estimate a particular property, we would only employ the "linear" cases (*i.e.*, PF_2 , PF_4 , and PF_6). However, we prefer the "unified" analysis approach where we use a common set of results and observe the performance of the model functions relative to the data functions for each particular plot.

3. Auxiliary Analysis: (ω - G_p performance plots) We have proposed 4 (four) auxiliary plots which consider the performance of the ω variable (or the $\bar{c}_e(p)(p_i - p)$ function) as a mechanism to "calibrate" the estimation of the ω variable with the estimate of gas-in-place. In our experience, these plots have become the "driver" in the analysis process as we tend to use these plots to gauge changes in various properties (particularly the gas-in-place).

For reference, the four ω - G_p performance plots are as follows: (recall that $\omega G_p \equiv \bar{c}_e(p)(p_i - p)$)

- Log-log plot of $\bar{c}_e(p)(p_i - p)$ vs. G_p/G (yields a power law trend).
- Cartesian plot of $1/[1 - \bar{c}_e(p)(p_i - p)]$ vs. G_p/G (yields a linear trend).
- Cartesian plot of ω vs. G_p (user selects a constant ω value or a linear ω versus G_p trend).
- Cartesian plot of ω vs. G_p/G (user selects a constant ω value or a linear ω versus G_p trend).

4. Type Curve Solution: We have developed a new "type curve" solution using the new quadratic cumulative production model as the basis function for this plot (we note that, for generality, the model is written in a dimensionless form). The type curve model is given by the following dimensionless pressure and pressure integral relations:

$$p_D = (1 - \omega_D)G_{pD} + \omega_D G_{pD}^2 \dots\dots\dots(4.11)$$

$$p_{Di} = \frac{1}{G_{pD}} \int_0^{G_{pD}} p_D dG_{pD} = (1 - \omega_D) \frac{1}{2} G_{pD} + \omega_D \frac{1}{3} G_{pD}^2 \dots\dots\dots(4.12)$$

where the following dimensionless definitions are used:

$$\omega_D = \omega G \dots\dots\dots(4.13)$$

$$p_D = \left[1 - \frac{p/z}{p_i/z_i} \right] = \left[\frac{p_i/z_i - p/z}{p_i/z_i} \right] \dots\dots\dots(4.14)$$

$$G_{pD} = \frac{G_p}{G} \dots\dots\dots(4.15)$$

As were all of the other plots, the type curve solution was implemented as a dynamic plot in our analysis spreadsheet. This plot is useful for a visualization of the data/model match, where the model remains fixed. Determination of the ω_D parameter from the type curve match is useful for validating the global estimate of gas-in-place being used to control the entire analysis module.

5. Gan Analysis: The Gan analysis (ref. 2) consists of 3 (three) separate plots which utilize the hypothesis that, for an abnormally pressured gas reservoir, we should expect to observe 2 separate straight-line trends (*i.e.*, a high (or "abnormal") pressure trend early in the life of the reservoir, and a low (or "normal") pressure trend late in the life of the reservoir). While the Gan method is an approximation, it is very useful for orienting our analysis sequence (similar to the ω - G_p performance plots). In analyzing field data, we found the Gan "Plot 1" (*i.e.*, $\bar{c}_e(p)(p_i - p)$ versus $(p/z)/(p_i/z_i)$) particularly useful for identifying characteristic behavior (*i.e.*, abnormal pressure effects).

4.3 Recommendations for Future Work

We put forth the following recommendations as mechanisms to extend this research work

1. External Drive Energy: Consider the extension of this methodology for cases of external drive energy (*e.g.*, water influx, gas injection, etc.).
2. Additional Validation: Continue the validation of this approach by applying the methodology to additional field cases as well as provide an exhaustive effort using numerical simulation. In this work we chose a "typical" $c_f(p)$ profile from Fetkovich, *et al.*¹ — there are a wide variety of laboratory derived $c_f(p)$ profiles in the literature, and we recommend that these profiles should also be considered.
3. Software: Implement the entire analysis sequence into a standalone software package (as opposed to performing the analysis in a spreadsheet program).

NOMENCLATURE

Field Variables: (Pressure, Formation, and Fluid Properties)

B_w	= Water formation volume factor, RB/STB
B_g	= Gas formation volume factor, RB/MSCF
B_{gi}	= Initial gas formation volume factor, RB/MSCF
c_e	= Instantaneous effective compressibility, 1/psi
\bar{c}_e	= Cumulative effective compressibility, 1/psi
c_t	= Instantaneous pore volume compressibility, 1/psi
\bar{c}_f	= Cumulative pore volume compressibility, 1/psi
c_f	= Instantaneous pore volume compressibility, 1/psi
c_w	= Instantaneous water compressibility, 1/psi
\bar{c}_w	= Cumulative total water compressibility, 1/psi
G	= Gas-in-place, MSCF (or BSCF)
G_{app}	= Apparent gas-in-place, MSCF (or BSCF)
G_{inj}	= Injected gas volume, MSCF (or BSCF)
G_p	= Cumulative gas production, MSCF (or BSCF)
M	= Ratio of aquifer to reservoir volume, dimensionless
p	= Average reservoir pressure, psia
p_i	= Initial reservoir pressure, psia
R_{sw}	= Solution gas water ratio, SCF/STB
S_{wi}	= Irreducible water saturation, dimensionless
W_e	= Cumulative water influx, RB
W_{inj}	= Cumulative water injection, STB
W_p	= Cumulative water production, STB
z	= Gas compressibility factor, dimensionless
z_i	= Gas compressibility factor at p_i , dimensionless
Δp	= Pressure drop, psia
ω	= Abnormal pressure model parameter

Dimensionless Variables:

G_{pD} = Dimensionless cumulative gas production

p_D = Dimensionless p/z function

p_{Di} = Dimensionless p/z integral function

ω_D = Dimensionless abnormal pressure model parameter

Greek Symbols:

α = Parameter, 1/BSCF

β = Parameter, 1/BSCF²

ϕ = Porosity, fraction

ω = Parameter, 1/BSCF

Subscript:

e = Effective

i = Initial

REFERENCES

1. Fetkovich, M.J., Reese, D.E., and Whitson, C.H.: "Application of a General Material Balance for High-Pressure Gas Reservoirs," *SPE Journal* (March 1998) 3-13.
2. Gan, R.G., and Blasingame, T.A.: "A Semi-Analytical p/z Technique for the Analysis of Reservoir Performance from Abnormally Pressured Gas Reservoirs," paper SPE 71514 presented at the 2001 SPE Annual Technical Conference and Exhibition held in New Orleans, LA, 30 September-3 October.
3. Moran, O., and Samaniego, F.: "A Production Mechanism Diagnosis Approach to the Gas Material Balance," paper SPE 71522 presented at the 2001 SPE Annual Technical Convention and Exhibition, New Orleans, LA, 30 September-3 October.
4. Prasad, R.K and Rogers, L.A.: Superpressured Gas Reservoirs: Case Studies and a Generalized Tank Model," paper SPE 16881 presented at the 1987 SPE Annual Technical Conference and Exhibition, Dallas, TX, 27-30 September 1987.
5. Bourgoyne, A.T., Jr., Hawkins, M.F., Lavaquial, F.P., and Wickenhauser, T.L.: "Shale Water as a Pressure Support Mechanism in Superpressure Reservoirs," Paper SPE 3851 (Unsolicited Manuscript) (1970), available at SPE, Richardson, TX.
6. Yale, D.P., Nabor, G.W., Russell, J.A., Pham, H.D., and Yousef, M.: "Application of Variable Formation Compressibility for Improved Reservoir Analysis," paper SPE 26647 presented at the 1993 SPE Annual Technical Conference and Exhibition, Houston, TX, 3-6 October.
7. Ambastha, A. K.: "Evaluation of Material Balance Analysis for Volumetric, Abnormally Pressured Gas Reservoir," *Journal of Canadian Petroleum Technology*, (1993) **32**, No. 8, 19-24.
8. Chu, W.C., Kazemi, H., Buettner, R.E., and Stouffer, T.L. "Gas Reservoir Performance in Abnormally High Pressure Carbonates," Paper SPE 35591 presented at the 1996 Gas Technology Symposium held in Calgary, Alberta, Canada, 28 April-1 May.
9. Wang, S.W.: "A General Linear Material Balance Method for Normally and Abnormally Pressured Petroleum Reservoirs," paper SPE 48954 presented at the 1998 SPE Annual Technical Conference and Exhibition, New Orleans, LA, 27-30 September.
10. Hammerlindl, D.J.: "Predicting Gas Reservoir in Abnormally Pressured Reservoirs," Paper SPE 3479 presented at the 1971 Annual Fall Meeting of AIME, 3-6 October.

11. Ramagost, B.P., and Farshad, F.F.: "*p/z* Abnormally Pressured Gas Reservoirs," paper SPE 10125 presented at the 1981 SPE Annual Technical Conference and Exhibition, San Antonio, TX, 5-7 October.
12. Begland, T.F., and Whitehead W.R.: "Depletion Performance of Volumetric High-Pressured Gas Reservoirs," paper SPE 15523 presented at the 1986 SPE Annual Technical Conference and Exhibition, New Orleans, LA, 5-8 October.
13. Elsharkaky, A. M.: "Analytical and Numerical Solutions for Estimating the Gas In-Place for Abnormal Pressured," paper SPE 29934 presented at the 1995 International Meeting on Petroleum Engineering, Beijing, 14-17 November.
14. Wang, S.W., Stevenson, V.M., Ohaeri, C.U., and Wotring, D.H.: "Analysis of Overpressured Reservoirs with a New Material Balance Method," paper SPE 56690 presented at the 1999 SPE Annual Technical Conference and Exhibition, Houston, Texas, 3-6 October.
15. Roach, R.H.: "Analyzing Geopressured Reservoirs-A Material Balance Technique," paper SPE 9968 (Unsolicited Manuscript) (1981), available at SPE, Richardson, TX.
16. Bernard W.J.: "Gulf Coast Geopressured Gas Reservoirs Drive Mechanism and Prediction," paper SPE 14362 presented at the 1985 SPE Annual Technical Conference and Exhibition, Las Vegas, NV, 22-25 September.
17. Poston, S.W., and Chen H.Y.: "The Simultaneous Determination of Formation Compressibility and Gas-in-Place in Abnormally Pressured Reservoirs," paper SPE 16227 presented at the 1987 SPE Production Operations Symposium, Oklahoma City, OK, 8-10 March.
18. Poston, S.W., and Chen, H.Y.: "Case History Studies: Abnormal Pressured Gas Reservoirs," paper SPE 18857 presented at the 1989 SPE Production Operations Symposium, Oklahoma City, OK, 13-14 March.
19. Guehria, F.M.: "A New Approach to *p/z* Analysis in Abnormally Pressured Reservoirs," paper SPE 36703 presented at the 1996 SPE Annual Technical Conference and Exhibition, Denver, CO, 6-9 October.
20. Harville, D.W., and Hawkins, M.F., Jr.: "Rock Compressibility and Failure as Reservoir Mechanisms in Geopressured Gas Reservoirs," *JPT* (December 1969), 1528-1530.

21. Duggan, J.O.: "The Anderson "L" — An Abnormally Pressured Gas Reservoir in South Texas," *JPT* (February 1971) 132-138.
22. Bourgoyne, A.T., Jr.: "Shale Water as a Pressure Support Mechanism in Gas Reservoirs Having Abnormal Formation Pressure," *Journal of Petroleum Science* (1990) **3**, 305.
23. Jones, P.H.: "Hydrodynamics of Geopressure in the Northern Gulf of Mexico Basin," *JPT* (July 1969), 803-810.
24. Fertl, W.H, and Timko, D.J.: "Parameters for Identification of Overpressure Formations," paper SPE 3223 (Unsolicited Manuscript) (1971), available at SPE Richardson, TX.
25. Fertl, W.H.: "A look at Abnormally Pressured Formations in the U.S.S.R.," paper SPE 3616 presented at the 1971 Annual Fall Meeting of AIME, New Orleans, LA, 3-6 October.
26. Gill, J.A.: "Shale Mineralogy and Overpressure: Some Case Histories of Pressure Detection Worldwide Utilizing Consistent Shale Mineralogy Parameters," paper SPE 3890 was presented at the Abnormal Subsurface Pressure Symposium of AIME, Baton Rouge, LA, 15-16 May.
27. Quitzau, R., and Bassiouni Z.: "The Possible Impact of the Geopressure Resource on Conventional Oil and Gas Exploration," paper SPE 10281 presented at the 1981 SPE Annual Technical Conference and Exhibition, San Antonio, TX, 5-7 October.
28. Engineer R.: "Cal Canal Field, California: Case History of a Tight and Abnormally Pressured Gas Condensate Reservoir," paper SPE 13650 presented at the 1985 California Regional Meeting, Bakersfield, CA, 27-29 March.
29. Pilkington, P.E.: "Uses of Pressure and Temperature Data in Exploration and New Developments in Overpressure Detection," *JPT* (May 1988), 543-549.
30. Harari, Z., Wang, S., and Salih, S.: "Pore Compressibility Study of Arabian Carbonate Reservoir Rocks," paper SPE 27625 (Unsolicited Manuscript) (1993), available at SPE Richardson, TX.
31. Yassir, N.A., and Bell, J.S.: "Abnormally High Fluid Pressures and Associated Porosities and Stress Regimes in Sedimentary Basins," *SPE Formation Evaluation* (March 1996), 5-10.

APPENDIX A

DEVELOPMENT AND VALIDATION OF A SIMPLIFIED MODEL FOR THE MATERIAL BALANCE OF ABNORMALLY PRESSURED GAS RESERVOIRS ("QUADRATIC CUMULATIVE PRODUCTION" MODEL)

The general material balance relation for an abnormally pressured gas reservoir is given as follows by Fetkovich, *et al.*:¹

$$\frac{p}{z} [1 - \bar{c}_e(p)(p_i - p)] = \frac{p_i}{z_i} - \frac{p_i}{z_i} \frac{1}{G} \left[G_p - G_{inj} + W_p R_{sw} + \frac{5.615}{B_g} (W_p B_w - W_{inj} B_w - W_e) \right] \dots\dots\dots (A.1)$$

Where Fetkovich, *et al.* define the "effective compressibility" function, $\bar{c}_e(p)$, as follows:

$$\bar{c}_e = \frac{1}{(1 - S_{wi})} [S_{wi} \bar{c}_w + \bar{c}_f + M(\bar{c}_w + \bar{c}_f)] \dots\dots\dots (A.2)$$

Setting $G_{inj} = W_{inj} = W_p = W_e = 0$, we obtain the common form of the gas material balance relation (*i.e.*, we are simply interested in the issue of "abnormal pressure" effects):

$$\frac{p}{z} [1 - \bar{c}_e(p)(p_i - p)] = \frac{p_i}{z_i} \left[1 - \frac{G_p}{G} \right] \dots\dots\dots (A.3)$$

Fetkovich, *et al.* proposed Eq. A.1 (or Eq. A.3) based on the concept that the "cumulative compressibility" function (*i.e.*, $\bar{c}_e(p)$) provides a better representation of the "abnormal pressure" effects observed in gas reservoir behavior (caused primarily by pore and water compressibility). Eq. A.3 has become the generally accepted reference model for the behavior of abnormally pressured gas reservoirs, although we do note that the implementation proposed by Fetkovich, *et al.* is tedious and is over-constrained by data requirements. Our goal is to utilize Eq. A.3 and develop an appropriate (and accurate) approximation for $p/z - G_p$ behavior such that simplified performance models and plotting functions can be proposed and utilized.

The first step is to isolate the $\bar{c}_e(p)$ function in Eq. A.3 — solving for the $\bar{c}_e(p)(p_i - p)$ and $\bar{c}_e(p)$ terms in Eq. A.3 gives us the following forms:

$$\bar{c}_e(p)(p_i - p) = 1 - \frac{p_i/z_i}{p/z} \left[1 - \frac{G_p}{G} \right] \dots\dots\dots (A.4a)$$

$$\bar{c}_e(p) = \left[1 - \frac{p_i/z_i}{p/z} \left[1 - \frac{G_p}{G} \right] \right] \frac{1}{(p_i - p)} \dots\dots\dots (A.4b)$$

We note that Fetkovich, *et al.* use these results (in particular, Eq. A.4b) as a "matching" function for comparison with results generated using Eq. A.2. In contrast, we are interested in the behavior of the $\bar{c}_e(p)(p_i - p)$ function (Eq. A.4a) — and, in particular, isolating the behavior of $\bar{c}_e(p)(p_i - p)$ versus G_p . We propose that the following approximate model for the behavior of $\bar{c}_e(p)(p_i - p)$ versus G_p :

$$\bar{c}_e(p)(p_i - p) \approx \omega G_p \dots\dots\dots (A.5)$$

We can readily note from Eq. A.4a that G_p function exerts a strong influence on the $\bar{c}_e(p)(p_i - p)$ function — however, it is neither intuitive (nor obvious) that Eq. A.5 represents a valid model for the behavior of the $\bar{c}_e(p)(p_i - p)$ function. We must use synthetic and field data in order to validate our concept and establish Eq. A.5 as a viable model for the $\bar{c}_e(p)(p_i - p)$ function. We provide 2 validation cases in this Appendix — the first case is a dry gas reservoir case simulated using the $c_f(p)$ function provided in Fig. 3 of the Fetkovich, *et al.* work (ref. 1) and the second case is the "Anderson L" reservoir case (ref. 4) which is regarded as a literature standard for field cases of abnormally pressured gas reservoirs.

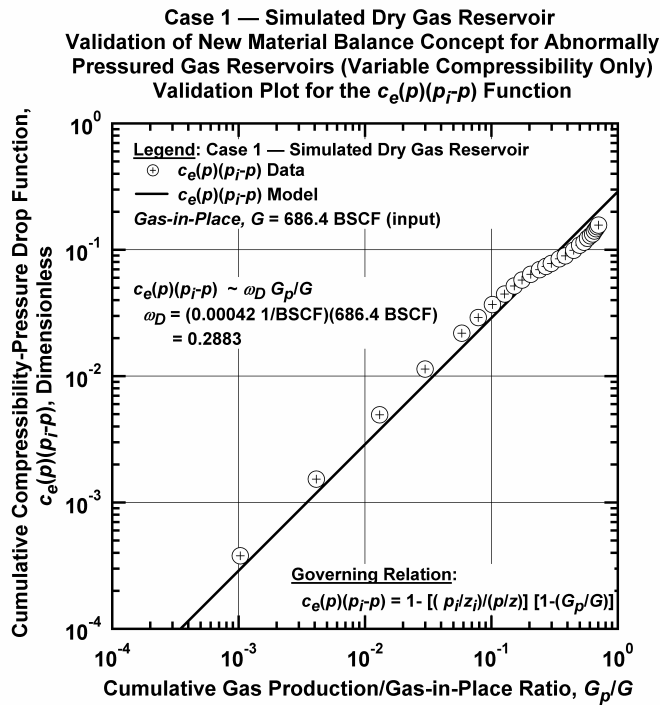


Figure A.1 – Behavior of the $\bar{c}_e(p)(p_i - p)$ function versus G_p/G for a simulated dry gas reservoir case. The $c_f(p)$ function (*i.e.*, the instantaneous pore volume compressibility) used in this case was obtained from **Fig. 3** of the Fetkovich, *et al.* work.¹

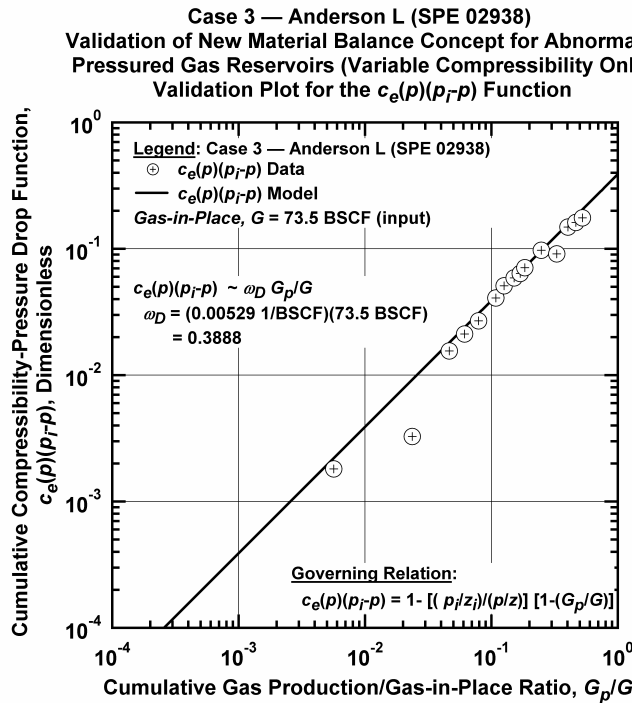


Figure A.2 – Behavior of the $\bar{c}_e(p)(p_i - p)$ function versus G_p/G for the "Anderson L" field case example²¹ (South Texas, USA).

In **Fig. A.1** we present the behavior of $\bar{c}_e(p)(p_i - p)$ versus G_p/G functions for the synthetic (dry gas) case on a log-log format and we note that a strong "power law" trend is evident up to large values of G_p (in particular, very large levels of depletion). We note a similar behavior of these functions for the "Anderson L" field data case in **Fig. A.2** — in fact, the match appears very strong considering the quantity and quality of the data. At this point we note that the concept model given by Eq. A.5 is an intermediate step — we are actually interested in the behavior of the function $1/[1 - \bar{c}_e(p)(p_i - p)]$ as this is the multiplier for the right-hand-side (RHS) of the material balance equation. Our proposed mode for the $1/[1 - \bar{c}_e(p)(p_i - p)]$ function is:

$$1/[1 - \bar{c}_e(p)(p_i - p)] \approx 1 + \xi G_p \dots\dots\dots (A.6)$$

We could have simply proceeded directly to the $1/[1 - \bar{c}_e(p)(p_i - p)]$ function, as opposed to investigating the $\bar{c}_e(p)(p_i - p)$ function — however, it is our contention that Eq. A.5 can be used to establish Eq. A.6 (via expansion of the $1/[1 - \bar{c}_e(p)(p_i - p)]$ term using a geometric series based on Eq. A.5). Recalling the definition of a geometric series, we have:

$$1/[1 - x] \approx 1 + x + x^2 + x^3 + \dots \quad (-1 < x < 1) \dots\dots\dots (A.7)$$

A single-term expansion of Eq. A.7 can be written as:

$$1/[1-x] \approx 1+x \quad (-1 < x < 1) \dots\dots\dots (A.8)$$

Substituting $x = \bar{c}_e(p)(p_i - p)$ into Eq. A.8 and function gives us:

$$1/[1 - \bar{c}_e(p)(p_i - p)] \approx 1 + \bar{c}_e(p)(p_i - p) \quad (\bar{c}_e(p)(p_i - p) < 1) \dots\dots\dots (A.9)$$

Substituting $\bar{c}_e(p)(p_i - p) \approx \omega G_p$ into the right-hand-side (RHS) of Eq. A.9 yields:

$$1/[1 - \bar{c}_e(p)(p_i - p)] \approx 1 + \omega G_p \quad (\omega G_p < 1) \dots\dots\dots (A.10)$$

Comparing Eqs. A.6 and A.10 we find that $\xi \approx \omega$ — which is not a rigorous proof of Eq. A.5, but does directionally confirm our concept model for the form given by Eq. A.6. In **Fig. A.3** we present the function $1/[1 - \bar{c}_e(p)(p_i - p)]$ versus G_p/G (on a Cartesian grid) for the simulated performance case — we note a very reasonable match of the data and model functions, where this comparison suggests that Eq. A.6 is a viable model for the behavior of the $1/[1 - \bar{c}_e(p)(p_i - p)]$ function. We present the results for the Anderson L field case in **Fig. A.4** and we confirm a very strong agreement of this data and the proposed model (Eq. A.6).

Recalling the original material balance (neglecting G_{inj} , W_{inj} , W_p , and W_e) we have Eq. A.3:

$$\frac{p}{z} [1 - \bar{c}_e(p)(p_i - p)] = \frac{p_i}{z_i} \left[1 - \frac{G_p}{G} \right] \dots\dots\dots (A.3)$$

For completeness, we need to establish the identity for the $1/[1 - \bar{c}_e(p)(p_i - p)]$ function — to do so we solve Eq. A.3 for the $1/[1 - \bar{c}_e(p)(p_i - p)]$ function. This gives:

$$1/[1 - \bar{c}_e(p)(p_i - p)] = \frac{1}{\frac{p_i/z_i}{p/z} \left[1 - \frac{G_p}{G} \right]} \dots\dots\dots (A.11)$$

As noted above, Eq. A.11 is given more for completeness than for application/validation.

We now present the development of the approximate material balance relation for dry gas reservoirs experiencing abnormal pressure effects which result from pressure-dependent pore volume compressibility (no water influx, water injection/production terms, etc. are considered in this development).

As a start, we divide through Eq. A.3 by the $[1 - \bar{c}_e(p)(p_i - p)]$ term to yield a more convenient form of the material balance equation for this case. This gives:

$$\frac{p}{z} = \frac{p_i}{z_i} \left[1 - \frac{G_p}{G} \right] \frac{1}{[1 - \bar{c}_e(p)(p_i - p)]} \dots\dots\dots (A.12)$$

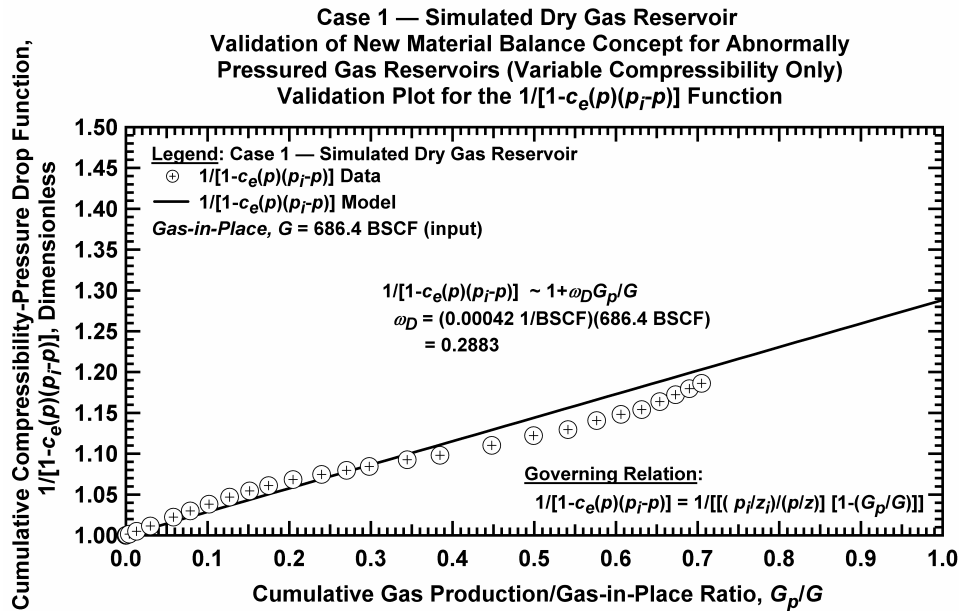


Figure A.3 – Behavior of the $1/[1-\bar{c}_e(p)(p_i-p)]$ function versus G_p/G for a simulated dry gas reservoir case. The $c_f(p)$ function (*i.e.*, the instantaneous pore volume compressibility) used in this case was obtained from **Fig. 3** of the Fetkovich, *et al.* work.¹ The purpose of this presentation is to establish the linearity of the $1/[1-\bar{c}_e(p)(p_i-p)]$ function versus G_p/G .

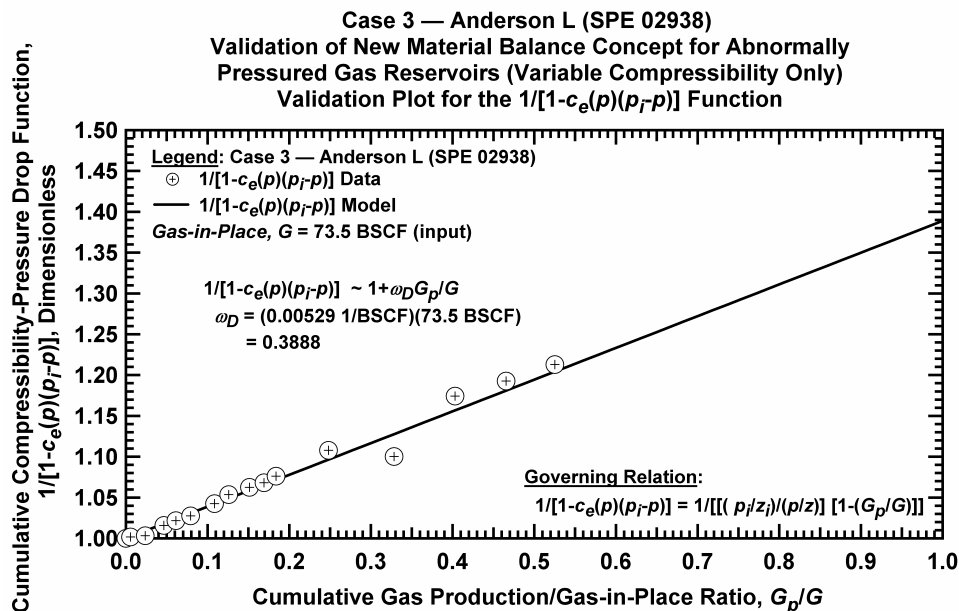


Figure A.4 – Behavior of the $1/[1-\bar{c}_e(p)(p_i-p)]$ function versus G_p/G for the "Anderson L" field case example²¹ (South Texas, USA). A strong linear trend is evident for this particular case.

Substituting Eq. A.10 into Eq. A.12 we have:

$$\frac{p}{z} \approx \frac{p_i}{z_i} \left[1 - \frac{G_p}{G} \right] (1 + \omega G_p) \dots\dots\dots (A.13)$$

Expanding terms in the right-hand-side (RHS) of Eq. A.13, we obtain:

$$\frac{p}{z} \approx \frac{p_i}{z_i} \left[1 - \left(\frac{1}{G} - \omega \right) G_p - \frac{\omega}{G} G_p^2 \right] \dots\dots\dots (A.14)$$

At this point we simply consider the ω -parameter to be an arbitrary constant required by the model. We have made no attempts to quantify the ω -parameter, other than to provide the definition of the ω -parameter (*i.e.*, $\omega G_p \equiv \bar{c}_e(p)(p_i - p)$) — where we note that we will generally consider ω to be a *function*, but the specific goal of this particular derivation is to establish the relevance ω as a *constant* (*i.e.*, a parameter). Substituting the definition of the ω -parameter (Eq. A.5) into the material balance relation (specifically, the form given by Eq. A.4a), we have the following definition of the ωG_p product:

$$\omega G_p \equiv 1 - \frac{p_i/z_i}{p/z} \left[1 - \frac{G_p}{G} \right] \dots\dots\dots (A.15)$$

Or, moving the G_p function to the right-hand-side (RHS), we have:

$$\omega \equiv \frac{1}{G_p} - \frac{p_i/z_i}{p/z} \left[\frac{1}{G_p} - \frac{1}{G} \right] \dots\dots\dots (A.16)$$

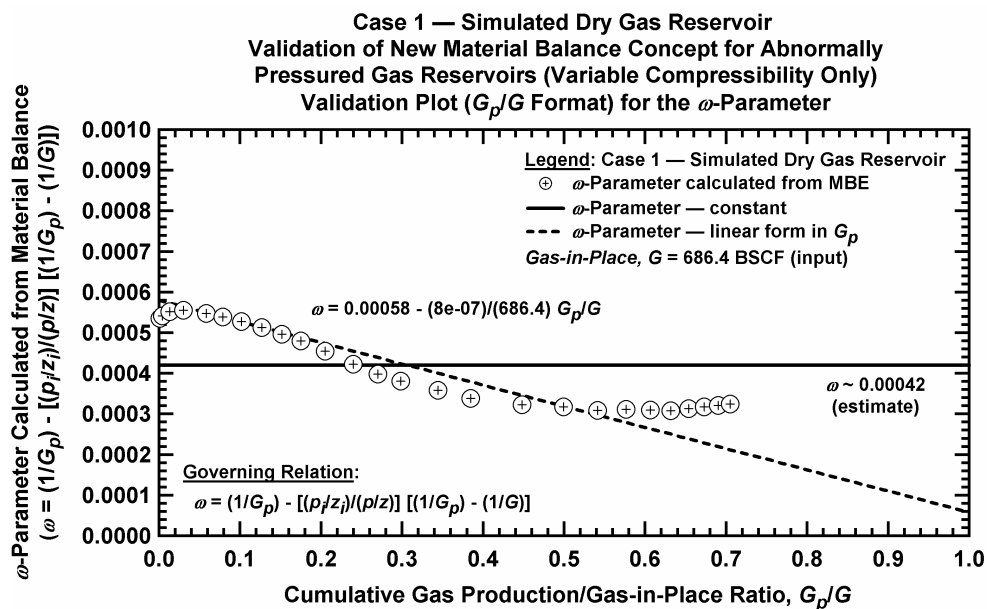
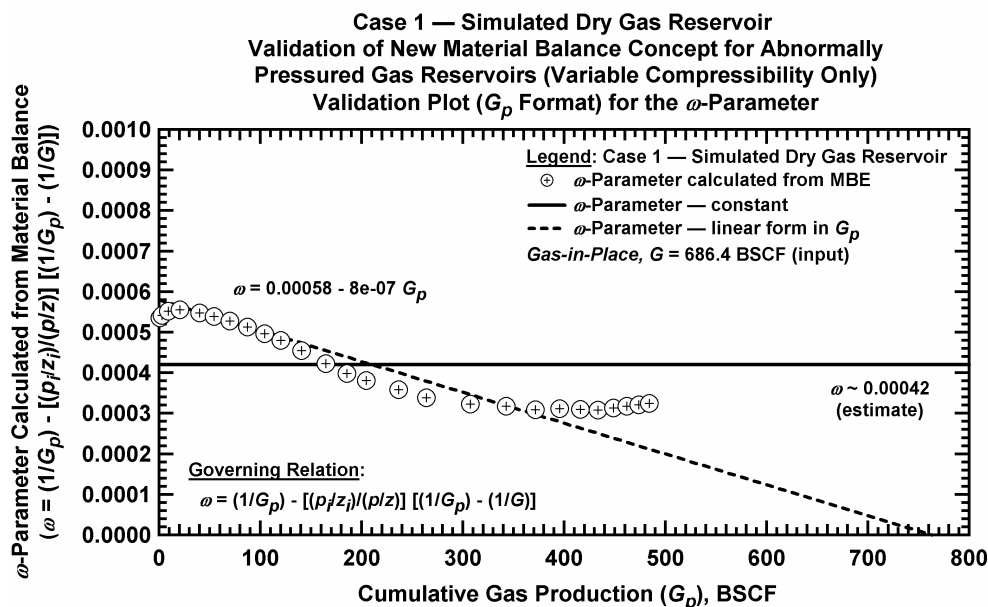
From inspection of Eq. A.16 we note that the ω -parameter actually a function (*i.e.*, there is no obvious indication that ω would be constant) — however, the only mechanism we can use to prove our contention that the ω -parameter is at least "approximately" constant is to consider synthetic and field data estimations of this parameter. As such, the ω -parameter is plotted against G_p in **Figs. A.5 and A.6** for the case of simulated gas reservoir performance and the Anderson L field case, respectively.

We note in **Fig. A.5** (the simulated data case where $G_{p,10}/G \approx 0.7$) that our estimate of $\omega=4.2 \times 10^{-4}$ is a reasonable average of the values for $0 < G_p < 500$ BSCF — although we acknowledge that this estimate is certainly open to other interpretations. For the Anderson L reservoir case (**Fig. A.6**) we find an extraordinary match of our estimate ($\omega=4.5 \times 10^{-3}$) compared to the data trend — in this case $G_{p,10}/G \approx 0.5$ — which probably accounts for the much better performance of the data for this case (as compared to the simulated data case). Revisiting Eq. A.14 and expanding the right-hand-side (RHS) term, we have:

$$\frac{p}{z} \approx \frac{p_i}{z_i} - \left(\frac{1}{G} - \omega \right) \frac{p_i}{z_i} G_p - \frac{\omega}{G} \frac{p_i}{z_i} G_p^2 \dots\dots\dots (A.17)$$

Or, using shorthand notation, Eq. A.17 becomes:

$$\frac{p}{z} \approx \frac{p_i}{z_i} - \alpha G_p - \beta G_p^2 \dots\dots\dots (A.18)$$



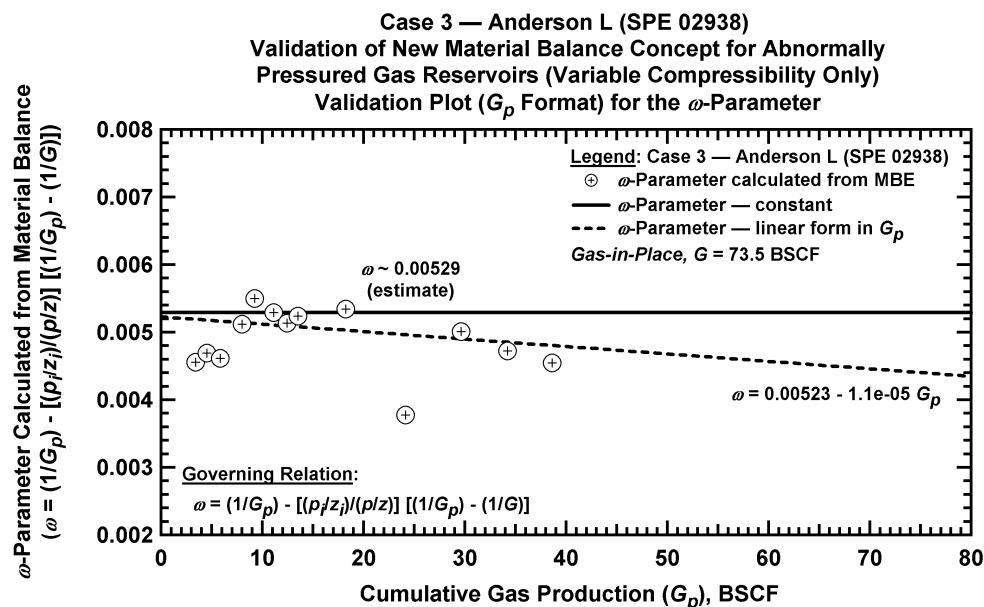


Figure A.6a – Behavior of the ω -parameter versus G_p for the "Anderson L" field case example⁴ (South Texas, USA). We note excellent agreement between the ω -parameter function and the prescribed value of ω for this case.

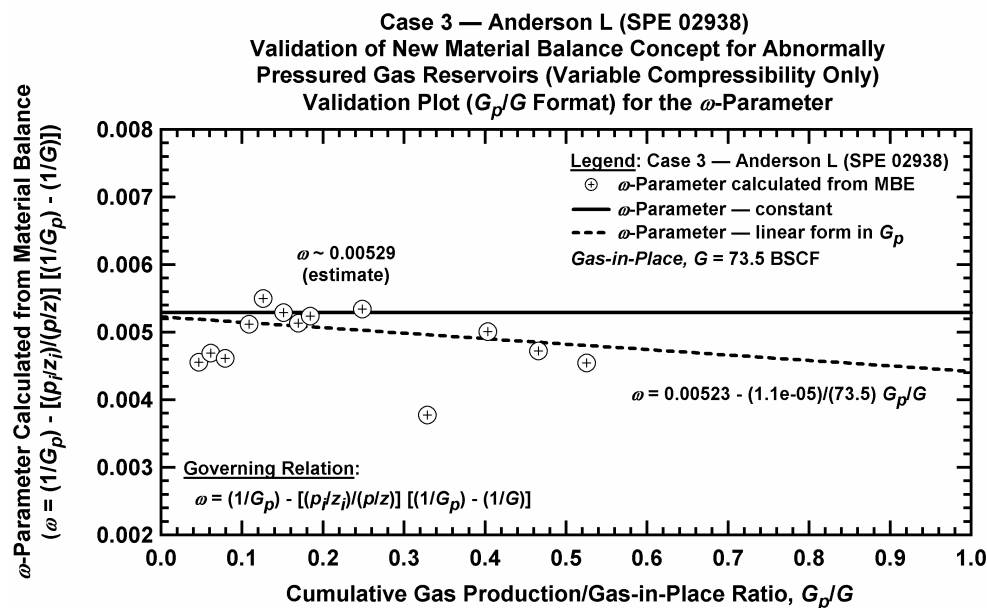


Figure A.6b – Behavior of the ω -parameter versus G_p/G for the "Anderson L" field case example²¹ (South Texas, USA). Note that this case shows an apparent depletion of about 50 percent — this is a possible explanation for the reasonably good correlation of data with both the constant and linear models.

Where the α and β coefficients are given by:

$$\alpha \equiv \left(\frac{1}{G} - \omega\right) \frac{P_i}{z_i} \dots\dots\dots (A.19)$$

$$\beta \equiv \frac{\omega}{G} \frac{P_i}{z_i} \dots\dots\dots (A.20)$$

Eq. A.18 is the most basic building block of this work — our goal is to utilize this model as an appropriate approximation for the rigorous gas material balance case for an abnormally pressured reservoir (*i.e.*, Eq. A.3). From this point forward we will consider Eq. A.18 to be valid as a material balance model — and, as such, we will use Eq. A.18 as the basis for plotting functions, reserve calculations, etc — specifically for the case of an abnormally pressured gas reservoir.

As an aside, we will note that the plots of the ω -parameter versus G_p (**Figs. A.5a and A.6a**) do indicate a slightly decaying linear trend for the behavior of the ω -parameter as a function of G_p (see trends shown on **Figs. A.5a and A.6a**). We have also prepared plots of the ω -parameter versus G_p/G in order to establish the influence of reservoir depletion on the ω -parameter (**Figs. A.5b and A.6b**). The most important conclusion that can be derived from **Figs. A.5 and A.6** (both formats) is that the behavior of the ω -parameter is unique and can be approximated as a constant or as a linear function of G_p (or G_p/G). This conclusion forms the basis for the development of the "quadratic" and "cubic" cumulative production relations for gas material balance (the quadratic relation is given by Eq. A.18 and the cubic relation is derived below).

Presuming a linear trend for the ω - G_p behavior we have:

$$\omega \equiv a - bG_p \dots\dots\dots (A.21)$$

Substitution of Eq. A.21 into Eq. A.13 gives us:

$$\frac{p}{z} \approx \frac{P_i}{z_i} \left[1 - \frac{G_p}{G} \right] \left[1 + (a - bG_p)G_p \right] \dots\dots\dots (A.22)$$

Expanding terms on the right-hand-side (RHS), we have:

$$\begin{aligned} \frac{p}{z} &\approx \frac{P_i}{z_i} \left[1 - \frac{G_p}{G} \right] \left[1 + aG_p - bG_p^2 \right] \\ &\approx \frac{P_i}{z_i} \left[(1 + aG_p - bG_p^2) - \left(\frac{G_p}{G} + \frac{a}{G}G_p^2 - \frac{b}{G}G_p^3 \right) \right] \\ &\approx \frac{P_i}{z_i} \left[1 - \left(\frac{1}{G} - a \right)G_p - \left(\frac{a}{G} + b \right)G_p^2 + \frac{b}{G}G_p^3 \right] \dots\dots\dots (A.23a) \end{aligned}$$

Presuming a linear trend for the ω - G_p behavior we have:

$$\frac{p}{z} \approx \frac{P_i}{z_i} - \left(\frac{1}{G} - a \right) \frac{P_i}{z_i} G_p - \left(\frac{a}{G} + b \right) \frac{P_i}{z_i} G_p^2 + \frac{b}{G} \frac{P_i}{z_i} G_p^3 \quad (\text{where } \omega \equiv a - bG_p) \dots\dots\dots (A.23b)$$

The general form of Eq. A.23 is given by:

$$\frac{p}{z} \approx \frac{p_i}{z_i} - \hat{a}G_p - \hat{b}G_p^2 + \hat{c}G_p^3 \dots\dots\dots (A.24)$$

Where the coefficients \hat{a} , \hat{b} , and \hat{c} are defined as:

$$\hat{a} \equiv \left(\frac{1}{G} - a\right) \frac{p_i}{z_i} \dots\dots\dots (A.25a)$$

$$\hat{b} \equiv \left(\frac{a}{G} + b\right) \frac{p_i}{z_i} \dots\dots\dots (A.25b)$$

$$\hat{c} \equiv \frac{b}{G} \frac{p_i}{z_i} \dots\dots\dots (A.25c)$$

We believe that the implementation of Eq. A.24 (the "cubic" cumulative production relation for gas material balance) would be problematic and generally less stable than the "quadratic" material balance model (*i.e.*, Eq. 18). Hence, our focus in this work will be the development of plotting functions and analysis relations for Eq. 18.

The practical application of the "quadratic" and "cubic" cumulative production relations for gas material balance (Eqs. A.18 and A.24) is the comparison of these models to p/z versus G_p data. As such, we will provide 2 example applications — a synthetic gas reservoir performance case and the "Anderson L" gas reservoir field case (see **Figs. A.7 and A.8**).

In **Fig. A.7** we provide data for the synthetic data case and we immediately note (as before) that this case has experienced significant reservoir depletion. The initial linear trend is that of the "apparent" gas-in-place model which has been the starting point of traditional analyses of material balance data from abnormally pressured gas reservoirs. We do not utilize the "apparent" gas-in-place trend and only note its presence for reference.

The specific trends of interest on **Fig. A.7** are those given by the constant " ω " model (Eq. A.18) and the linear " ω " model (Eq. A.24). We have previously referred to Eq. A.18 as the "quadratic" cumulative production relation for gas material balance (abnormally pressured reservoir case), and Eq. A.24 is the "cubic" G_p relation. For reference, the governing relation for the ω -parameter is given by Eq. A.16:

$$\omega \equiv \frac{1}{G_p} - \frac{p_i/z_i}{p/z} \left[\frac{1}{G_p} - \frac{1}{G} \right] \dots\dots\dots (A.16)$$

And the p/z — G_p model in terms of ω is given by Eq. A.13:

$$\frac{p}{z} \approx \frac{p_i}{z_i} \left[1 - \frac{G_p}{G} \right] (1 + \omega G_p) \dots\dots\dots (A.13)$$

Since these are validation cases and we have all of the relevant data, we note that the " ω " models shown in **Fig. 7** were "tuned" for this case using **Fig. A.5a** — *i.e.*, the constant or linear estimates of the ω -parameter are determined using data (shown on **Fig. A.5a**), as opposed to using Eqs. A.18 and A.24 as regression models. In practice we will use Eq. A.18 to derive plotting functions to estimate the relevant model parameters — however, in this case, our goal is to illustrate the connection between the " ω " models and the $p/z — G_p$ behavior.

In this particular case we note that using a constant value of ω is fairly straightforward — specifically the influence of a particular ω value can be established by sampling. In contrast, the "best fit" of the $\omega — G_p$ data (*i.e.*, the proposed straight-line trend on **Fig. A.5a**) yields a reasonable match of the $p/z — G_p$ data on **Fig. A.7**. On the other hand, the optimal match of the $p/z — G_p$ data on **Fig. A.7** using a generalized model for $\omega=a+bG_p$ yields a linear trend that lies substantially away from the $\omega — G_p$ data on **Fig. A.5a** (for clarity, this "optimal" trend is not included on **Fig. A.5a**).

Obviously, for practical applications we will not have the "answer" (*i.e.*, G) at our disposal and construction of **Figs. A.5a and A.5b** will not be possible (as a direct analysis technique), so this issue is more of a concept/ validation concern. We note that multiple optimizations of the linear $\omega — G_p$ trend are possible, and we must simply accept that Eqs. A.18 and A.24 (*i.e.*, the final forms using the constant and linear (G_p) models for the ω -parameter) are viable mechanisms for applications in material balance analysis.

Similar conclusions are made for the "Anderson L" (South Texas, USA) field case. In particular, we note the coordination between the analyses of the ω -parameter on **Fig. A.6a** and the corresponding $p/z — G_p$ plot, **Fig. A.8**. In fact, we can note that the data for the Anderson L case appear to perform better than the synthetic reservoir performance case (again, this could be a production of the lower level of reservoir depletion experienced by the Anderson L case. As with the synthetic reservoir performance case, we again note that the models presented in **Fig. A.8** are tied directly to the $\omega — G_p$ behavior presented in **Fig. A.6a**. Specifically, the " ω " models presented in **Fig. A.8** have not been tuned using statistical regression.

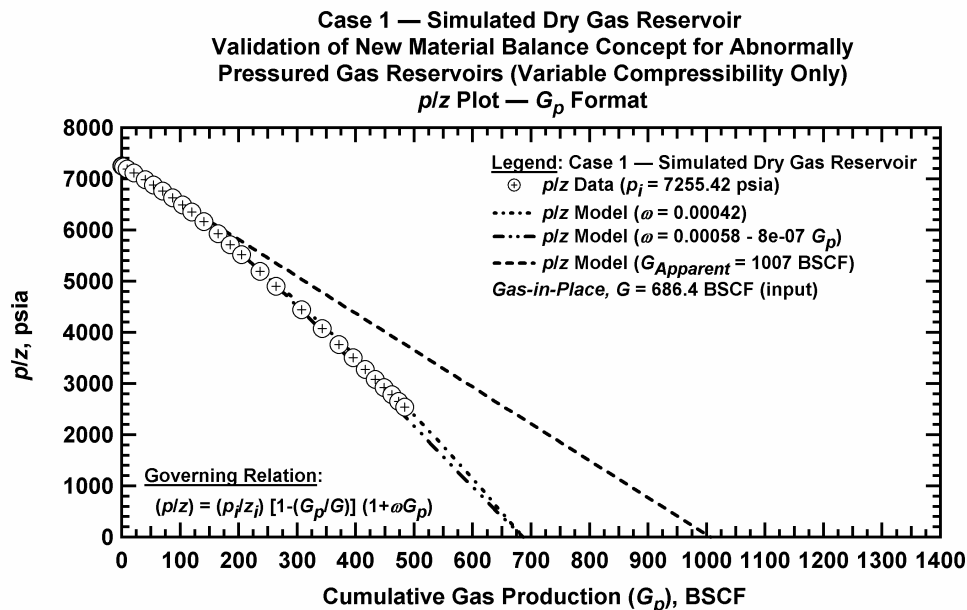


Figure A.7 — p/z versus G_p plot for the simulated performance of an abnormally pressured gas reservoir (variable compressibility only) (dry gas reservoir case).

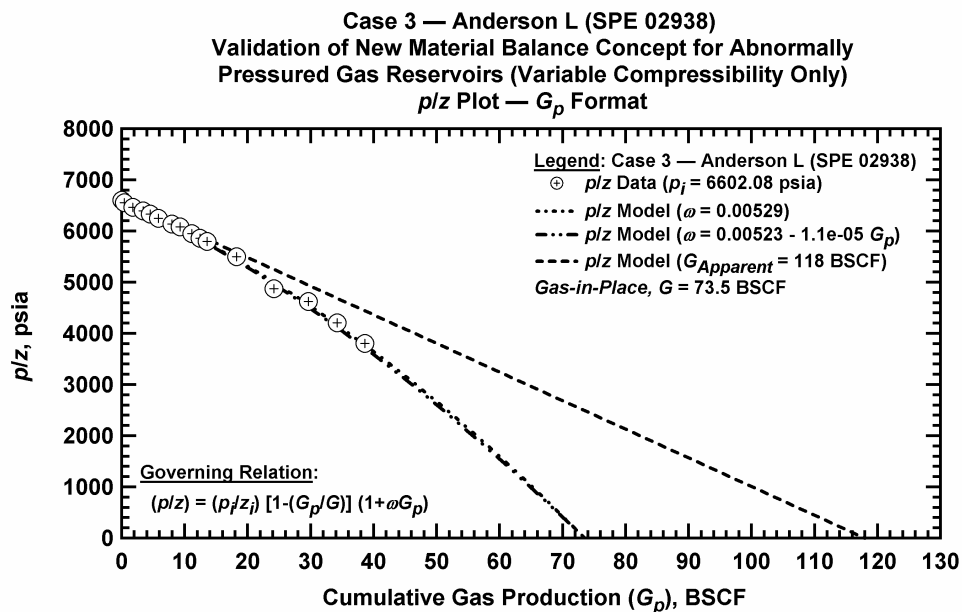


Figure A.8 — p/z versus G_p plot for the "Anderson L" field case example²¹ (South Texas, USA) (a suspected abnormally pressured gas reservoir case).

APPENDIX B

DEVELOPMENT OF PLOTTING FUNCTIONS FOR THE "QUADRATIC CUMULATIVE PRODUCTION" FORM OF THE MATERIAL BALANCE RELATION FOR ABNORMALLY PRESSURED GAS RESERVOIRS

The base relation for this work is the "quadratic cumulative production" relation for the material balance of abnormally pressured gas reservoirs (derived specifically for the pressure-dependent pore volume compressibility case). This result was derived in Appendix A and is given by:

$$\frac{P}{z} \approx \frac{P_i}{z_i} - \alpha G_p - \beta G_p^2 \dots\dots\dots (A.18)$$

(Data Plot: p/z versus G_p (quadratic trend))

Where the α and β coefficients are given by:

$$\alpha \equiv \left(\frac{1}{G} - \omega\right) \frac{P_i}{z_i} \dots\dots\dots (A.19)$$

$$\beta \equiv \frac{\omega}{G} \frac{P_i}{z_i} \dots\dots\dots (A.20)$$

For convenience, we define the " p/z difference function" as:

$$\Delta(p/z) = \frac{P_i}{z_i} - \frac{P}{z} = \alpha G_p + \beta G_p^2 \dots\dots\dots (B.1)$$

(Data Plot: $\Delta(p/z)$ versus G_p (quadratic trend))

Dividing through Eq. B.1 by the cumulative gas production (G_p), we have:

$$\frac{\Delta(p/z)}{G_p} = \alpha + \beta G_p \dots\dots\dots (B.2)$$

(Data Plot: $\Delta(p/z)/G_p$ versus G_p (linear trend))

While we are intrigued by the work of Moran and Sameniego³ which uses the derivation of the p/z behavior, we believe that application of this approach will always be limited due to data quality and quantity. However, we believe that the development of "auxiliary" " p/z " functions is a practical necessity for the analysis of reservoir performance data which are affected by abnormal pressure effects. Therefore, we propose a series of "integral" functions based on Eq. B.2 as auxiliary functions for the purpose of data analysis (specifically, data plotting functions).

Integrating Eq. B.2 with respect to G_p yields:

$$\begin{aligned} \int_0^{G_p} \Delta(p/z) dG_p &= \int_0^{G_p} [\alpha G_p + \beta G_p^2] dG_p \dots\dots\dots (B.3) \\ &= \frac{\alpha}{2} G_p^2 + \frac{\beta}{3} G_p^3 \\ &\quad \text{(Data Plot: } \int_0^{G_p} \Delta(p/z) dG_p \text{ versus } G_p \text{ (cubic trend))} \end{aligned}$$

Dividing Eq. B.3 by G_p yields the primary "integral" function of interest:

$$\begin{aligned} \frac{1}{G_p} \int_0^{G_p} \Delta(p/z) dG_p &= \frac{\alpha}{2} G_p + \frac{\beta}{3} G_p^2 \dots\dots\dots (B.4) \\ &\quad \text{(Data Plot: } \frac{1}{G_p} \int_0^{G_p} \Delta(p/z) dG_p \text{ vs. } G_p \text{ (quadratic trend))} \end{aligned}$$

Dividing Eq. B.3 by G_p^2 yields an auxiliary "integral" function:

$$\begin{aligned} \frac{1}{G_p^2} \int_0^{G_p} \Delta(p/z) dG_p &= \frac{\alpha}{2} + \frac{\beta}{3} G_p \dots\dots\dots (B.5) \\ &\quad \text{(Data Plot: } \frac{1}{G_p^2} \int_0^{G_p} \Delta(p/z) dG_p \text{ vs. } G_p \text{ (linear trend))} \end{aligned}$$

Subtracting Eq. B.4 from Eq. B.1 gives us:

$$\begin{aligned} \Delta(p/z) - \frac{1}{G_p} \int_0^{G_p} \Delta(p/z) dG_p &= [\alpha G_p + \beta G_p^2] - \left[\frac{\alpha}{2} G_p + \frac{\beta}{3} G_p^2 \right] \dots\dots\dots (B.6) \\ &= \frac{1}{2} \alpha G_p + \frac{2}{3} \beta G_p^2 \\ &\quad \text{(Data Plot: } \Delta(p/z) - \frac{1}{G_p} \int_0^{G_p} \Delta(p/z) dG_p \text{ vs. } G_p \text{ (quadratic trend))} \end{aligned}$$

Dividing Eq. B.6 by G_p yields the "integral-difference" formulation, that, at least in concept, is analogous to the "derivative" functions proposed by Moran and Sameniogo.³ This result is given as:

$$\begin{aligned} \frac{1}{G_p} \left[\Delta(p/z) - \frac{1}{G_p} \int_0^{G_p} \Delta(p/z) dG_p \right] &= \frac{1}{2} \alpha + \frac{2}{3} \beta G_p \dots\dots\dots (B.7) \\ &\quad \text{(Data Plot: } \frac{1}{G_p} \left[\Delta(p/z) - \frac{1}{G_p} \int_0^{G_p} \Delta(p/z) dG_p \right] \text{ vs. } G_p \text{ (linear trend))} \end{aligned}$$

Our analysis procedure will employ all of the plots are designated (*i.e.*, Eqs. A.18, B.1 to B.7). The procedure will be implemented using a spreadsheet approach where the coefficients p_i/z_i , α , and β are specified — p_i/z_i is typically known (or can be estimated) as the initial condition while α and β are estimated by trial and error. The α and β parameters can be tied to a single " ω " value (per Eqs. A.19 and

20) or these coefficients can be estimated *independently*. We recommend a spreadsheet approach using hand manipulation of the coefficients over the statistical optimization of the coefficients using regression methods. A visual analysis of multiple data functions simultaneously allows the user to constrain the analysis and avoid physically inconsistent parameter estimates (*e.g.*, negative values).

APPENDIX C

DEVELOPMENT OF A TYPE CURVE SOLUTION FOR THE ANALYSIS OF $p/z—G_p$ DATA FOR THE CASE OF AN ABNORMALLY PRESSURED GAS RESERVOIR USING THE "QUADRATIC CUMULATIVE PRODUCTION" FORM OF THE MATERIAL BALANCE RELATION

As with previous developments, the base relation for the work in this Appendix is the "quadratic cumulative production" relation for the material balance of abnormally pressured gas reservoirs (derived specifically for the pressure-dependent pore volume compressibility case (see Appendix A). The "quadratic cumulative production" relation is given by:

$$\frac{p}{z} \approx \frac{p_i}{z_i} - \alpha G_p - \beta G_p^2 \quad (\text{Data Plot: } p/z \text{ versus } G_p \text{ (quadratic trend)}) \dots\dots\dots (\text{A.18})$$

Where the α and β coefficients are given by:

$$\alpha \equiv \left(\frac{1}{G} - \omega\right) \frac{p_i}{z_i} \dots\dots\dots (\text{A.19})$$

$$\beta \equiv \frac{\omega}{G} \frac{p_i}{z_i} \dots\dots\dots (\text{A.20})$$

Substituting Eqs. A.19 and A.20 into Eq. A.18 gives us: (we presume that Eq. A.18 is valid and use (=) rather than (\approx))

$$\frac{p}{z} = \frac{p_i}{z_i} \left[1 - \left(\frac{1}{G} - \omega\right) G_p - \frac{\omega}{G} G_p^2 \right] \dots\dots\dots (\text{A.14})$$

Defining a dimensionless " ω_D " parameter, we have

$$\omega_D = \omega G \dots\dots\dots (\text{C.1})$$

Substituting Eq. C.1 Eq. A.14 yields:

$$\frac{p}{z} = \frac{p_i}{z_i} \left[1 - \frac{1}{G} (1 - \omega_D) G_p - \frac{\omega_D}{G^2} G_p^2 \right] \dots\dots\dots (\text{C.2})$$

Rearranging terms on the right-hand-side (RHS) of Eq. C.2 gives us:

$$\frac{p}{z} = \frac{p_i}{z_i} \left[1 - (1 - \omega_D) \frac{G_p}{G} - \omega_D \frac{G_p^2}{G^2} \right] \dots\dots\dots (\text{C.3})$$

Further rearranging terms Eq. C.3, we have:

$$\left[1 - \frac{p/z}{p_i/z_i} \right] = (1 - \omega_D) \frac{G_p}{G} + \omega_D \frac{G_p^2}{G^2} \dots\dots\dots (\text{C.4a})$$

or,

$$\left[\frac{p_i/z_i - p/z}{p_i/z_i} \right] = (1 - \omega_D) \frac{G_p}{G} + \omega_D \frac{G_p^2}{G^2} \dots\dots\dots (C.4b)$$

Carefully reviewing Eqs. C.4a and C.4b, we observe the following "intuitive" dimensionless variables:

$$p_D = \left[1 - \frac{p/z}{p_i/z_i} \right] = \left[\frac{p_i/z_i - p/z}{p_i/z_i} \right] \dots\dots\dots (C.5)$$

$$G_{pD} = \frac{G_p}{G} \dots\dots\dots (C.6)$$

Substituting Eqs. C.5 and C.6 into Eq. C.4a (or C.4b), we obtain the "dimensionless" form of the "quadratic cumulative production" material balance relation for an abnormally pressured gas reservoir:

$$p_D = (1 - \omega_D) G_{pD} + \omega_D G_{pD}^2 \dots\dots\dots (C.7)$$

In order to develop an "auxiliary" function to aid in this analysis, we define the "dimensionless pressure integral" function as follows for this case:

$$p_{Di} = \frac{1}{G_{pD}} \int_0^{G_{pD}} p_D dG_{pD} \dots\dots\dots (C.8)$$

Substituting Eq. C.7 into Eq. C.8, we have:

$$p_{Di} = \frac{1}{G_{pD}} \int_0^{G_{pD}} \left[(1 - \omega_D) G_{pD} + \omega_D G_{pD}^2 \right] dG_{pD} \dots\dots\dots (C.9)$$

Completing the integration in Eq. C.9 yields:

$$p_{Di} = \frac{1}{G_{pD}} \left[(1 - \omega_D) \frac{1}{2} G_{pD}^2 + \omega_D \frac{1}{3} G_{pD}^3 \right]$$

Multiplying through by the $1/G_{pD}$ term, we have:

$$p_{Di} = (1 - \omega_D) \frac{1}{2} G_{pD} + \omega_D \frac{1}{3} G_{pD}^2 \dots\dots\dots (C.10)$$

In **Fig. C.1** we present the "type curve" based on Eqs. C.7 and C.10 for the "dimensionless" pressure and pressure integral functions, p_D and p_{Di} , respectively.

In order to use **Fig. C.1**, we use the *data* function defined by Eq. C.5 for p_D :

$$(p_D)_{\text{data}} = 1 - \frac{p/z}{p_i/z_i} \dots\dots\dots (C.11)$$

We will use the definition of the "pressure integral" function (Eq. C.8) to develop an expression for computing the data function for p_{Di} . Recalling Eq. C.8, we have

$$p_{Di} = \frac{1}{G_{pD}} \int_0^{G_{pD}} p_D dG_{pD} \dots\dots\dots (C.8)$$

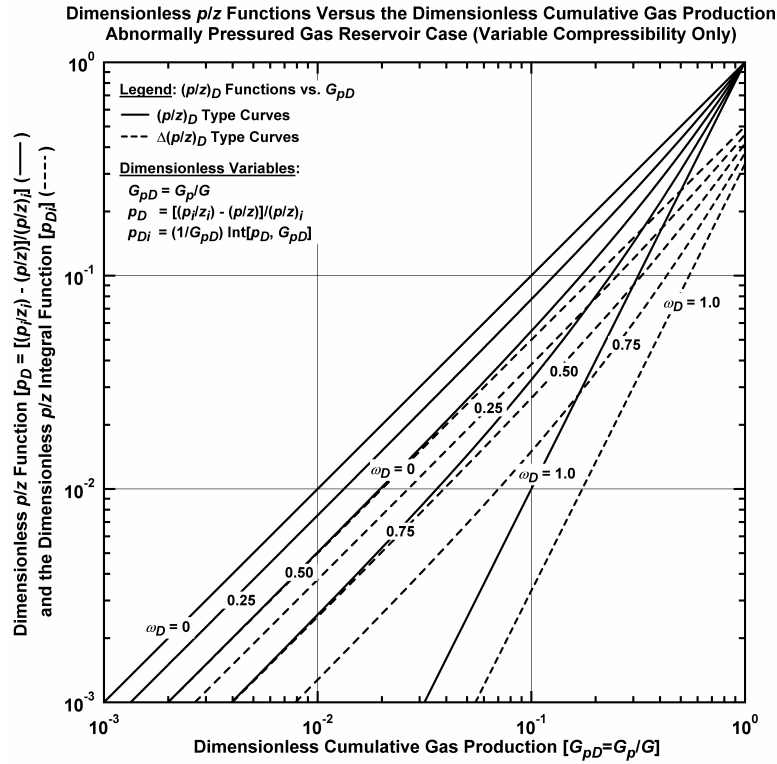


Figure C.1 – p_D and p_{Di} versus G_{pD} "type curve" plot for the "quadratic cumulative production" material balance relation for an abnormally pressured gas reservoir.

Defining a variable of substitution, $G_p = GG_{pD}$ (i.e., using Eq. C.6), we have

$$G_p = GG_{pD}$$

Taking the derivative of this variable of substitution, we obtain:

$$dG_p = G dG_{pD}$$

Or, solving for dG_{pD} , we have

$$dG_{pD} = \frac{1}{G} dG_p \dots\dots\dots (C.12)$$

Evaluating the limits of the new variable of substitution, G_p , we obtain:

$$\text{at } G_{pD} = 0; G_p = 0$$

$$\text{at } G_{pD} = G_{pD}; G_p = G_p$$

Substitution of Eq. C.13 into Eq. C.12, and using the new limits (in terms of G_{pD}), we obtain:

$$p_{Di} = \frac{G}{G_p} \int_0^{G_p} p_D \frac{1}{G} dG_p$$

Canceling the G terms, we have:

$$(p_{Di})_{\text{data}} = \frac{1}{G_p} \int_0^{G_p} (p_D)_{\text{data}} dG_p \dots\dots\dots (C.13)$$

Where Eq. C.13 is the "data formulation" for p_{Di} , and we note that $(p_{Di})_{\text{data}}$ is used as a variable in the type curve matching process.

APPENDIX D

FIELD VALIDATION OF THE

"QUADRATIC CUMULATIVE PRODUCTION" FORM

OF THE GAS MATERIAL BALANCE RELATION

In this Appendix we present the analysis and interpretation of an exhaustive library of field and numerical simulation cases of reservoir performance of "abnormally pressured" natural gas reservoirs. In particular, we apply our new analysis technique to each case, as well as the Gan and Blasingame technique (ref. #) and a few simplified plots (*e.g.*, the apparent gas-in-place plot). Our primary objective in this Appendix is to establish a definitive sequence of analysis and interpretation which successfully illustrates the application of our new methodology.

The summary table of results for the cases considered in this Appendix is shown in Table D.1.

Table D.1 — Analysis and interpretation results for the cases considered in this work.

Case	Reservoir Name	Reference	Pressure Gradient (psi/ft)	Reference G (BSCF)	Gan (ref. 8) G (BSCF)	This Work G (BSCF)
0	Base Simulation ($c_f(p)=0$)	This work	---	---	N/A	686.4
1	Dry Gas	This work	---	---	N/A	686.4
2	Gas Condensate	This work	---	---	N/A	20.5
3	Anderson L (South Texas)	Ref 21	0.843	72.0	75.5	73.5
4	Offshore Louisiana	Ref 11	0.85	470.0	497.5	441.6
5	Southeast Texas	Ref 19	0.83	211.0	268.0	262.6
6	North Ossun Field	Ref. 20	0.725	118.0	89.6	86.5
7	Stafford	Ref 2/unp	---	25.0	22.8	23.5
8	Reservoir 117	Ref 4	0.77	562.5	461.3	503.4
9	Reservoir 268	Ref 4	0.67	30.5	32.5	30.2
10	Cajun Reservoir	Ref 2	---	220.0	214.0	207.6
11	South La (Bourgoyne)	Ref 22	---	16.0	13.8	13.3
12	GOM Reservoir	Ref 2/unp	---	22.4	15.4	15.1
13	Reservoir 33	Ref 4	0.81	217.0	215.1	208.9
14	Reservoir 41	Ref 4	0.69	41.0	48.6	49.3
15	Example 4	Ref 14	0.749	48.1	36.3	53.8
16	Reservoir 70	Ref 4	0.68	11.0	12.1	11.8
17	Reservoir 195	Ref 4	0.64	53.1	51.7	50.2
18	Field 38	Ref 18	---	80.1	70.0	68.8
19	ROB 43-1	Ref 18	---	101.0	107.6	117.0
20	GOM Case 2	Ref 18	---	142.0	163.5	180.8
21	Reservoir 197	Ref 4	0.62	14.5	14.6	13.7
22	Louisiana Reservoir	Ref 19	---	109.0	128.5	137
23	Simulated Dry Gas	Ref 2	---	---	51.8	51.8

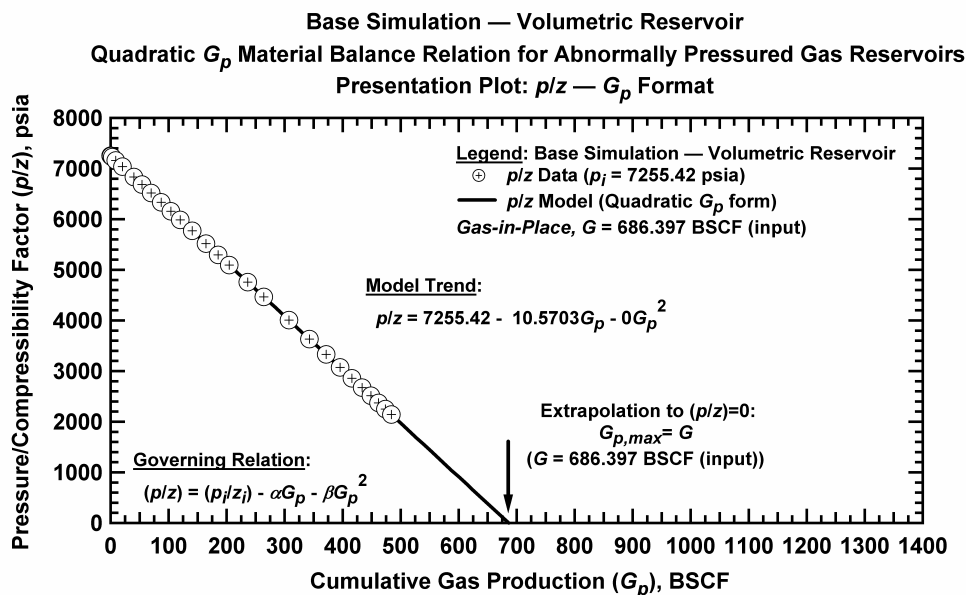


Figure D.1.a — Plot of p/z vs. G_p — Base Simulation Case (i.e., Case 0).

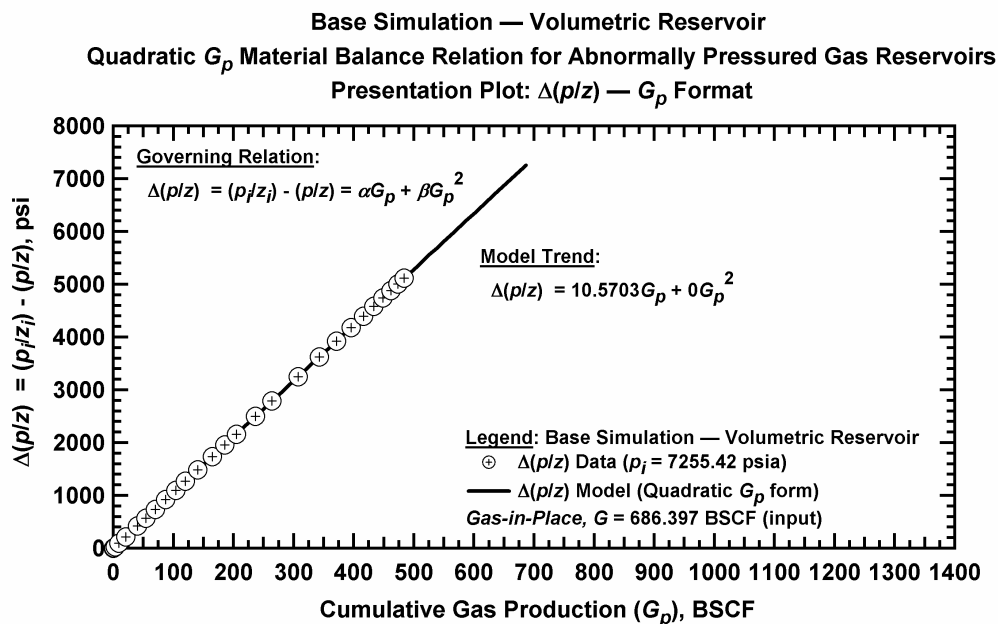


Figure D.1.b — Plot of $\Delta(p/z)$ vs. G_p — Base Simulation Case.

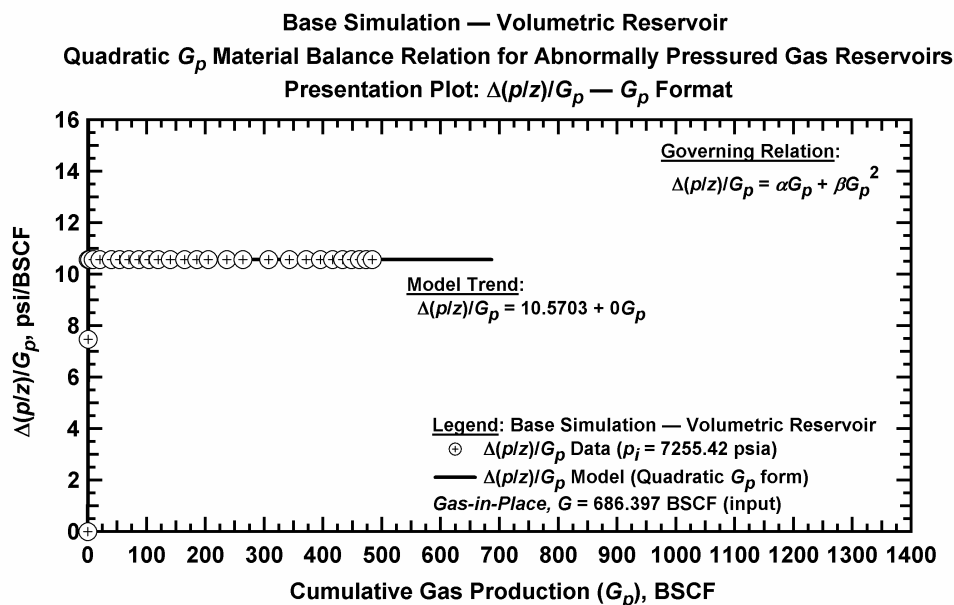


Figure D.1.c — Plot of $\Delta(p/z)/G_p$ vs. G_p — Base Simulation Case.

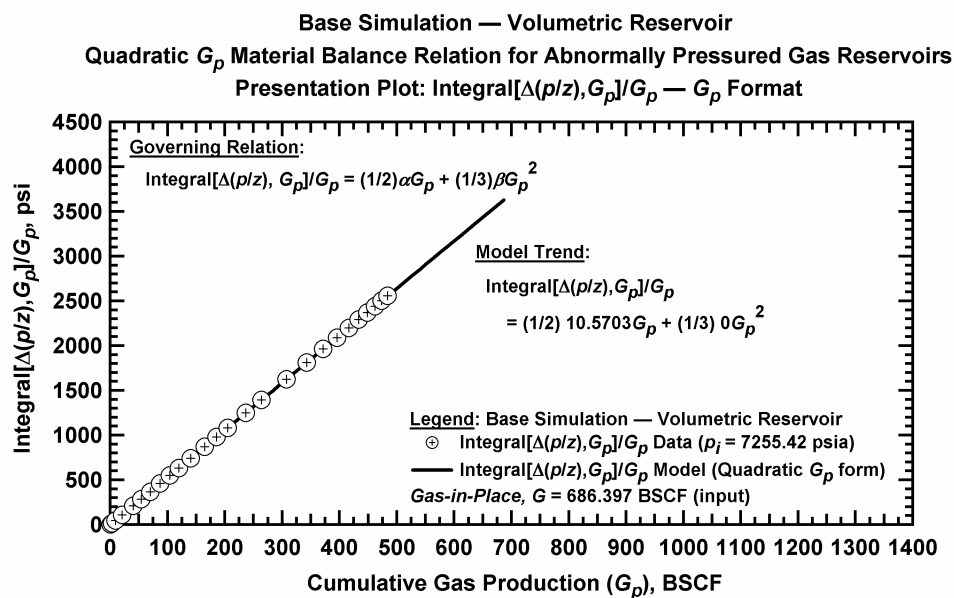


Figure D.1.d — Plot of $\frac{1}{G_p} \int_0^{G_p} \Delta(p/z) dG_p$ vs. G_p — Base Simulation Case.

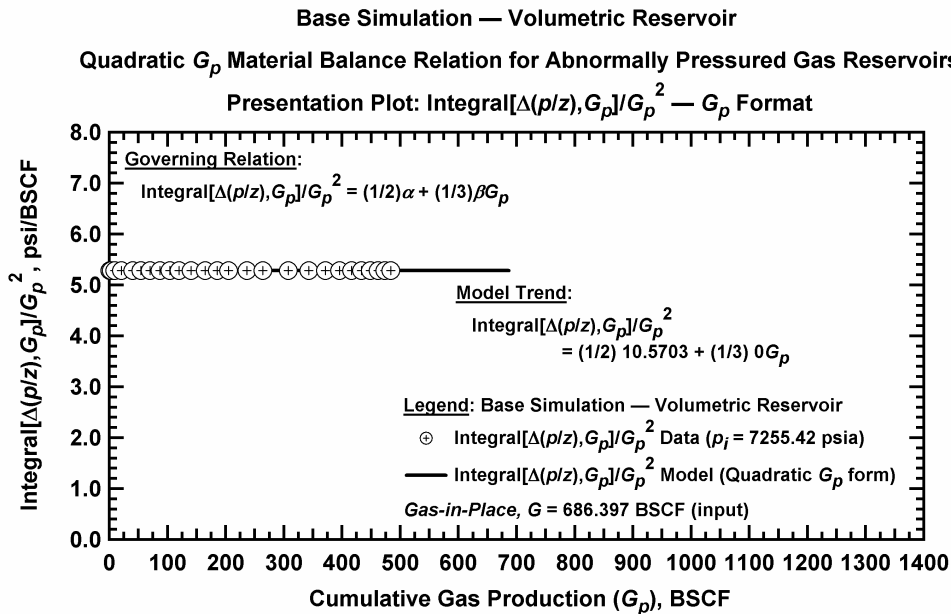


Figure D.1.e — Plot of $\frac{1}{G_p^2} \int_0^{G_p} \Delta(p/z) dG_p$ vs. G_p — Base Simulation Case.

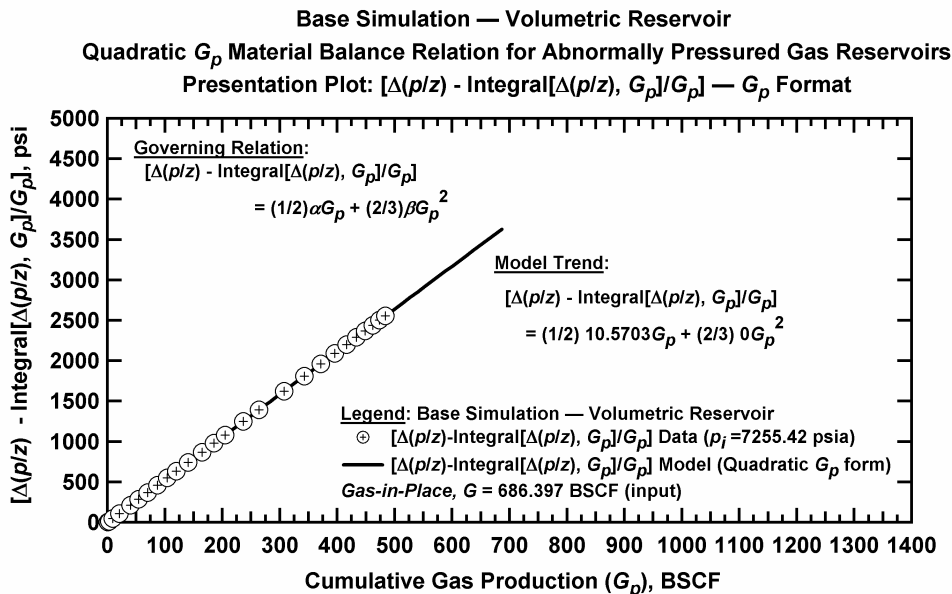


Figure D.1.f — Plot of $\Delta(p/z) - \frac{1}{G_p} \int_0^{G_p} \Delta(p/z) dG_p$ vs. G_p — Base Simulation Case.

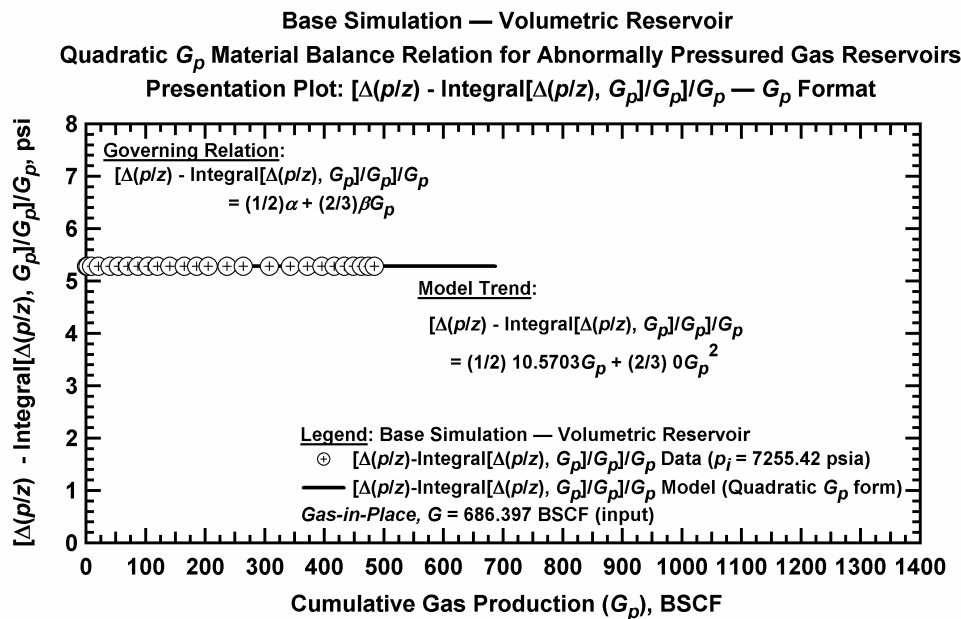


Figure D.1.g — Plot of $\frac{1}{G_p} \left[\Delta(p/z) - \frac{1}{G_p} \int_0^{G_p} \Delta(p/z) dG_p \right]$ vs. G_p — Base Simulation Case.

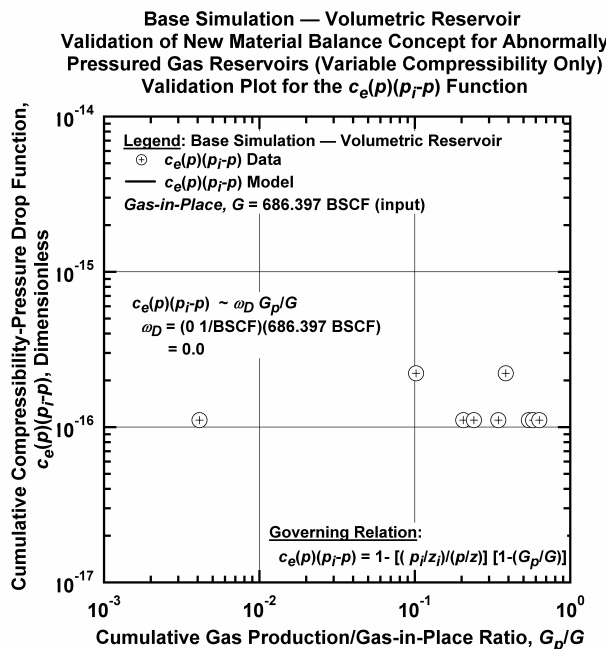


Figure D.1.h — Plot of $\bar{c}_e(p)(p_i - p)$ vs. G_p/G — Base Simulation Case.

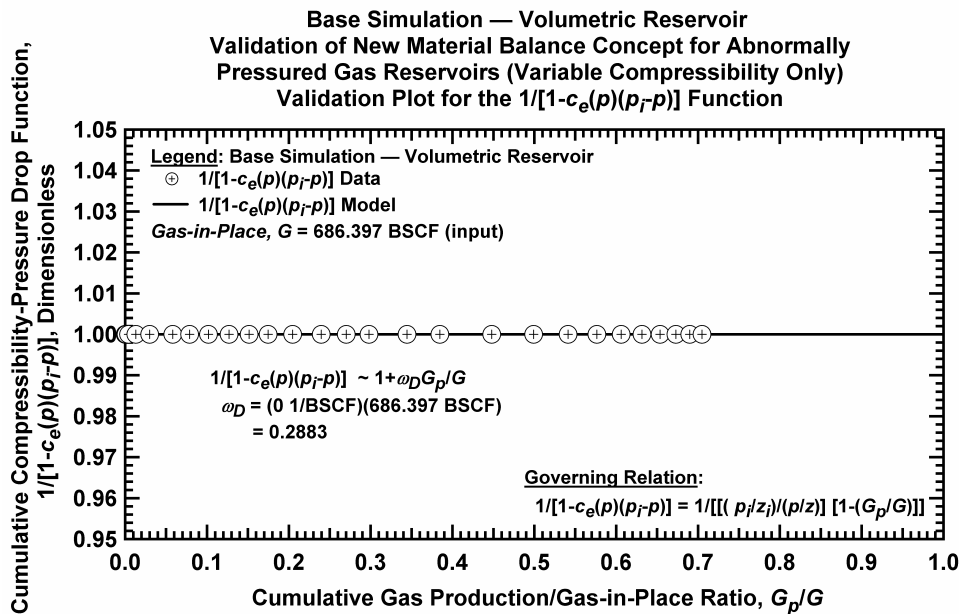


Figure D.1.i — Plot of $1/[1-\bar{c}_e(p)(p_i - p)]$ vs. G_p/G — Base Simulation Case.

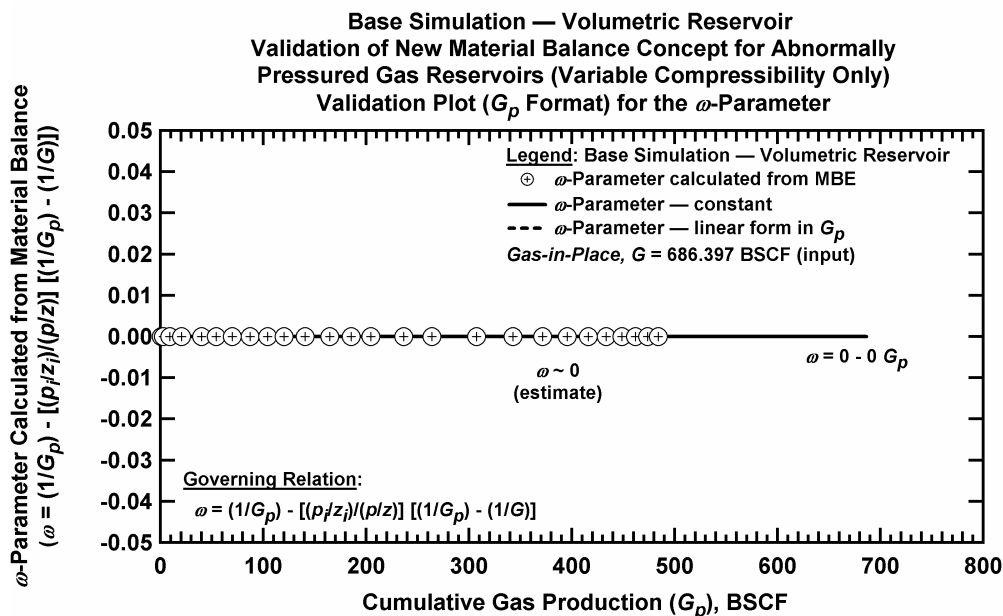


Figure D.1.j — Plot of ω vs. G_p — Base Simulation Case.

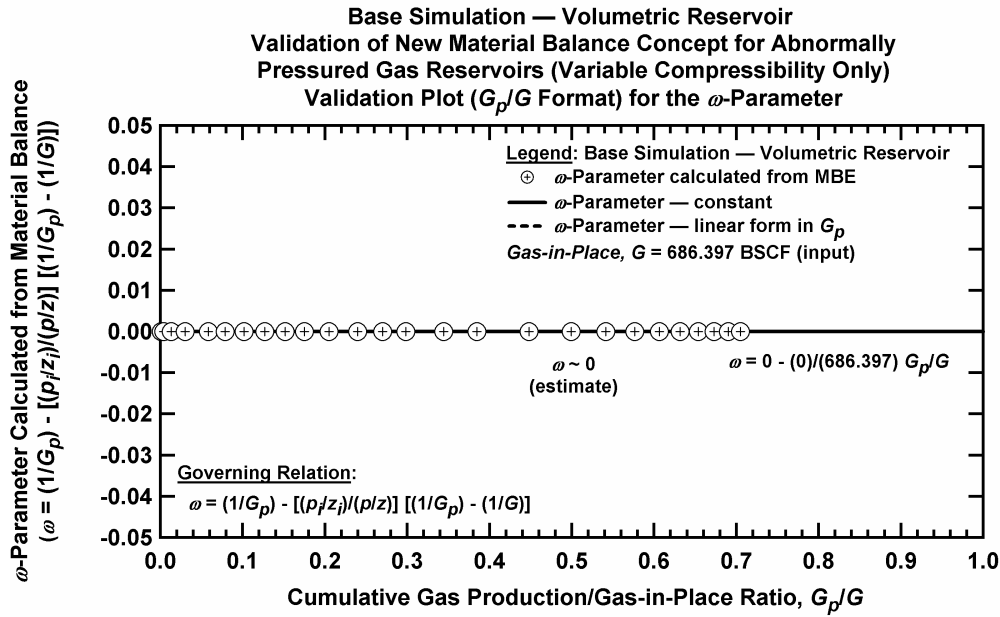


Figure D.1.k — Plot of ω vs. G_p/G — Base Simulation Case.

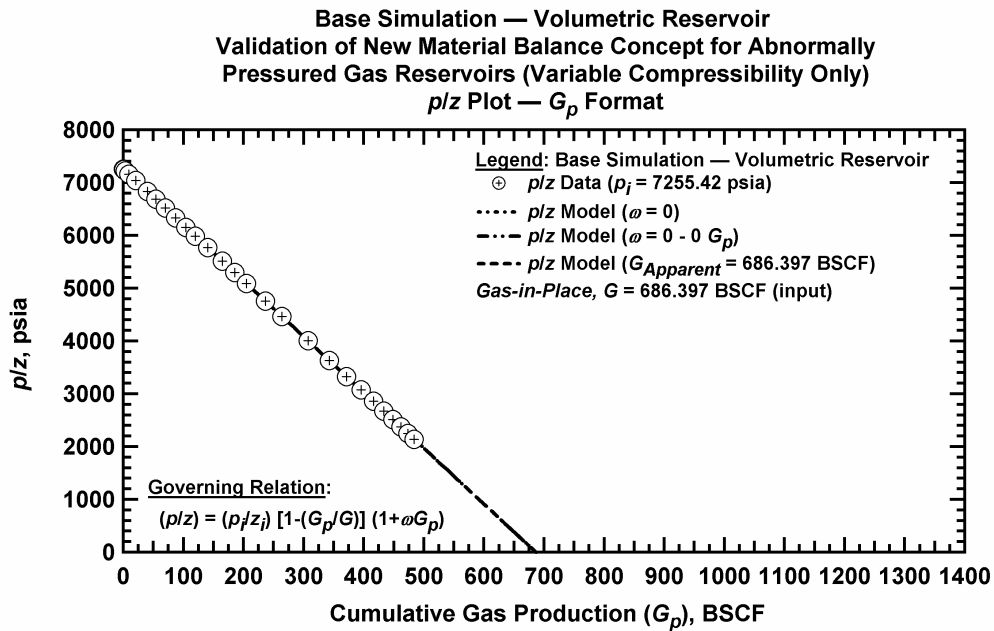


Figure D.1.l — Comparison plot of p/z vs. G_p — Base Simulation Case.

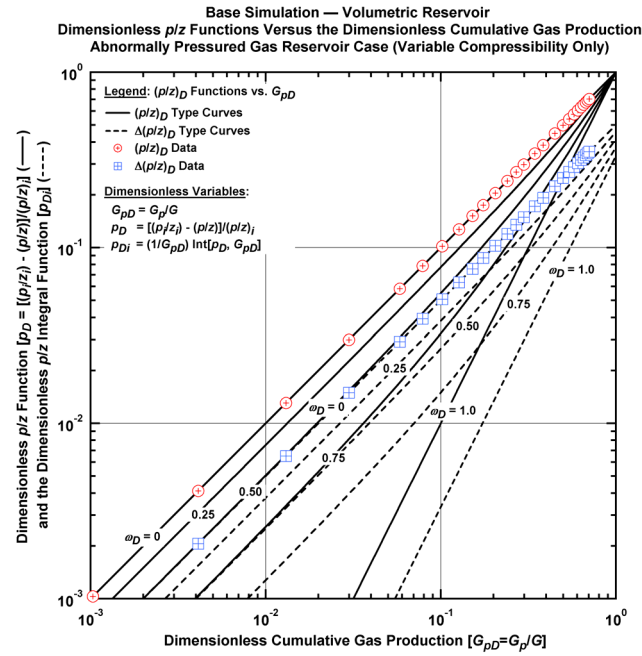


Figure D.1.m — Plot of dimensionless p/z functions vs. G_{pD} — Base Simulation Case.

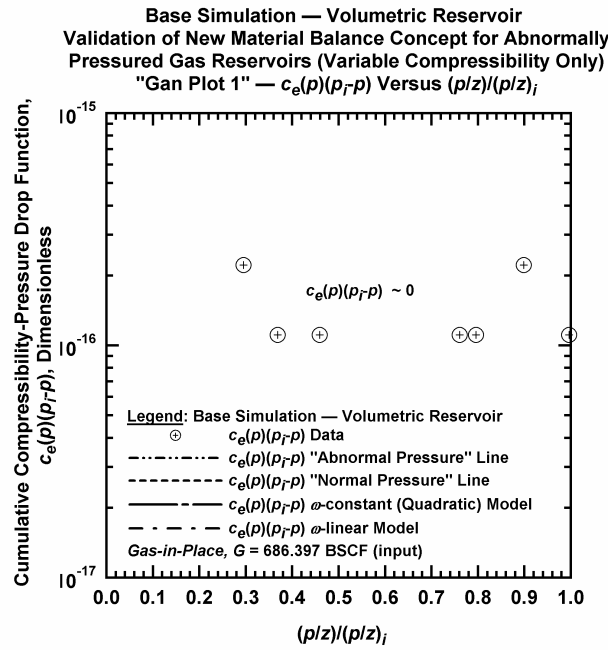


Figure D.1.n — Plot of $\bar{c}_e(p)(p_i - p)$ vs. $(p/z)/(p/z)_i$ — Base Simulation Case.

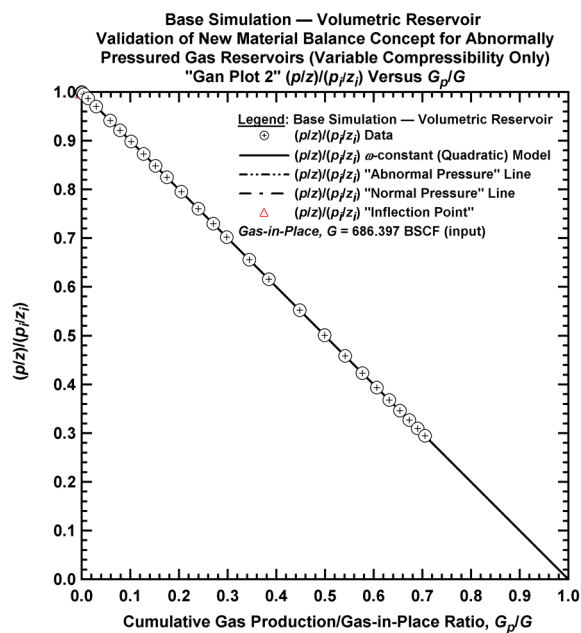


Figure D.1.o — Plot of $(p/z)/(p/z_i)$ vs. G_p/G — Base Simulation Case.

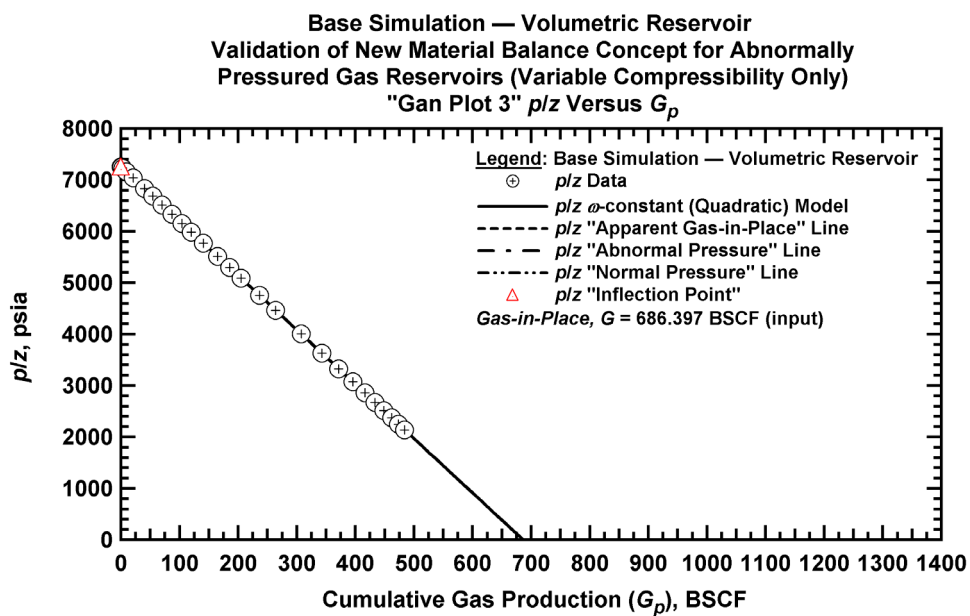


Figure D.1.p — Summary plot of p/z vs. G_p — Base Simulation Case.

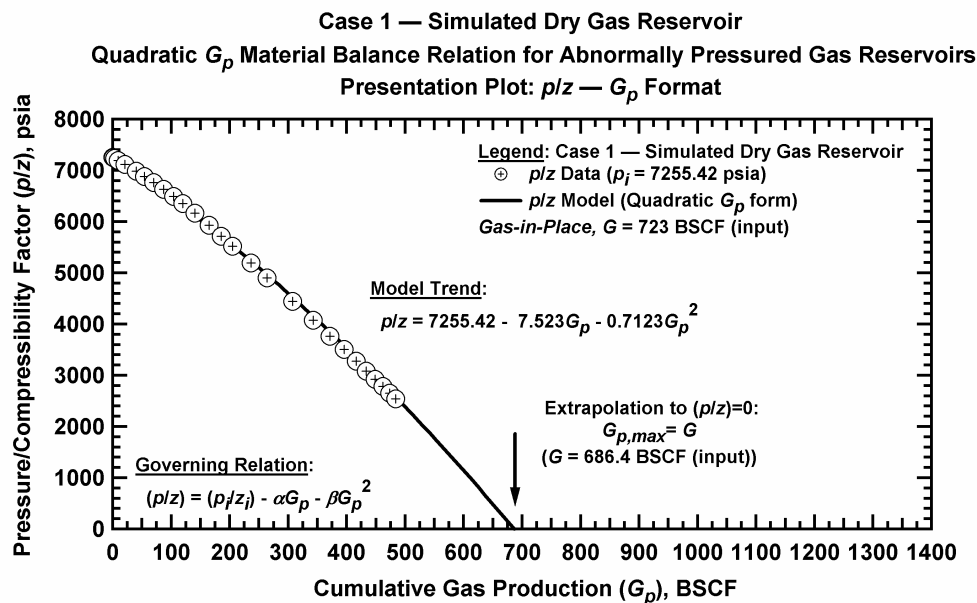


Figure D.2.a — Plot of p/z vs. G_p — Case1 (abnormal pressure effects are present in these data).

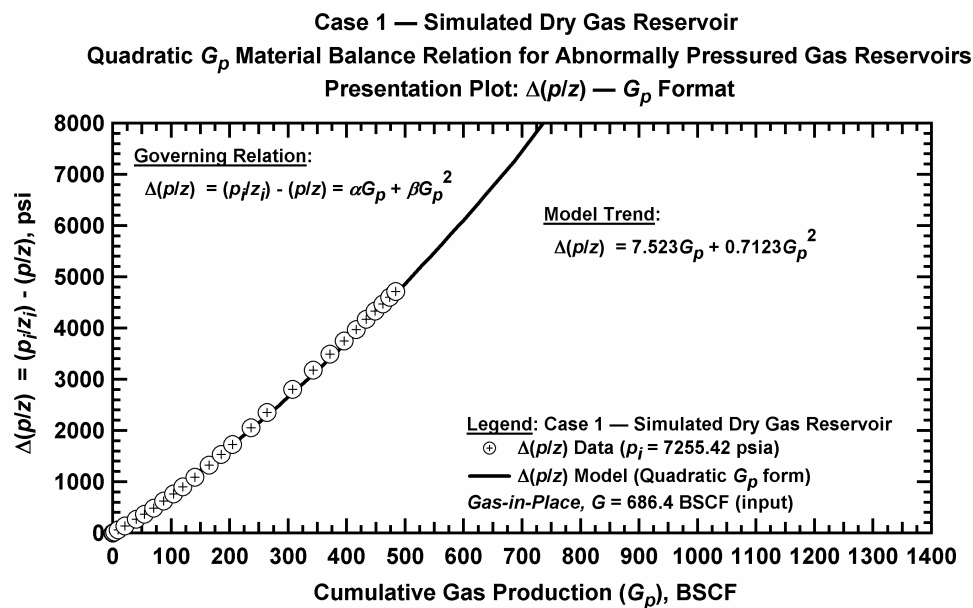


Figure D.2.b — Plot of $\Delta(p/z)$ vs. G_p — Case 1.

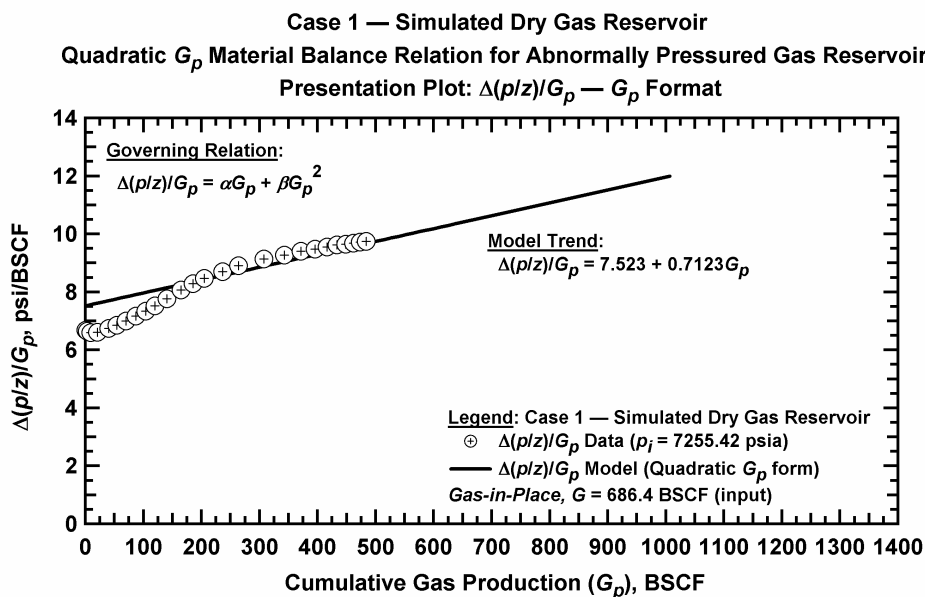


Figure D.2.c — Plot of $\Delta(p/z)/G_p$ vs. G_p — Case 1.

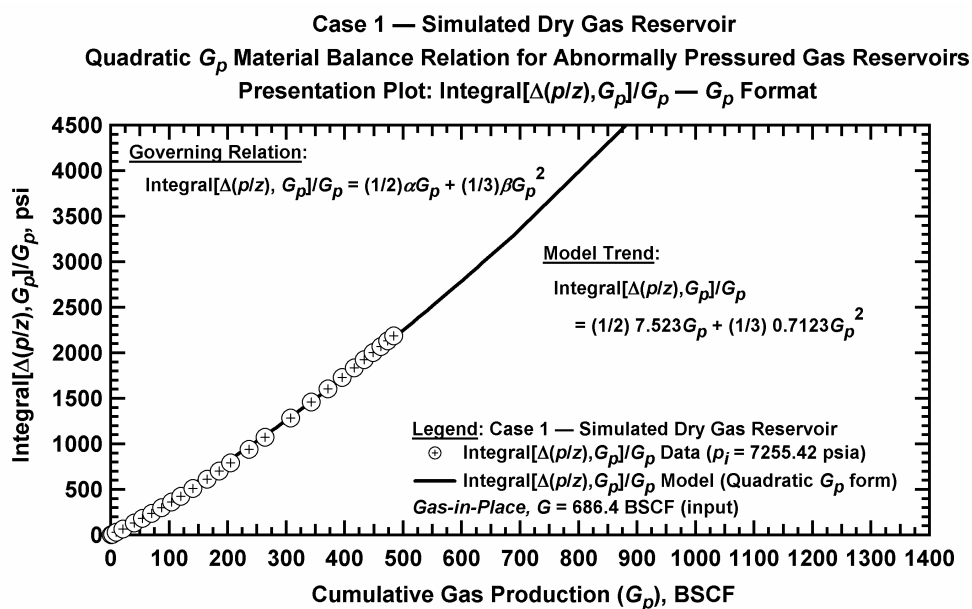


Figure D.2.d — Plot of $\frac{1}{G_p} \int_0^{G_p} \Delta(p/z) dG_p$ vs. G_p — Case 1.

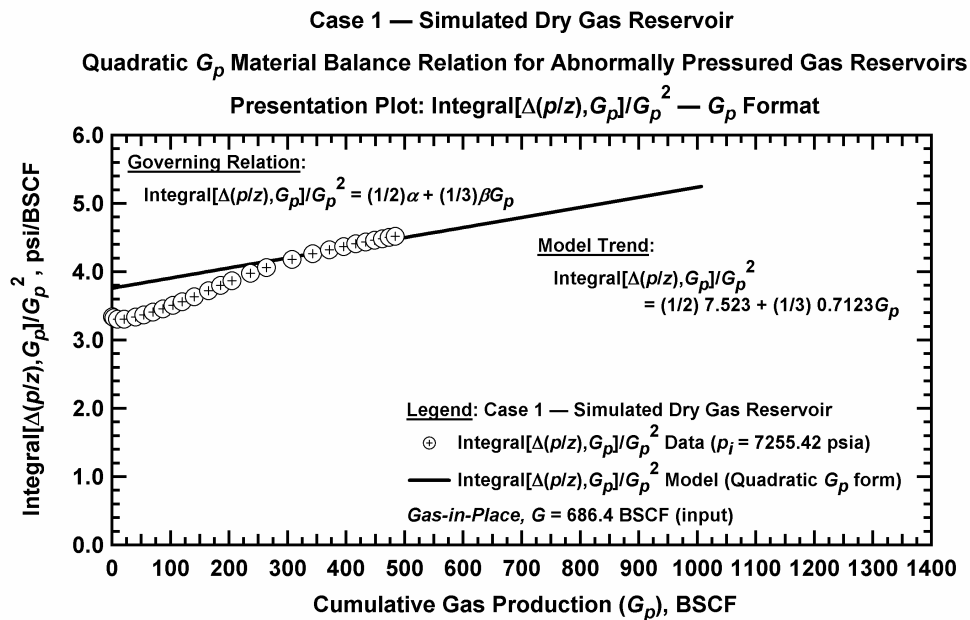


Figure D.2.e — Plot of $\frac{1}{G_p^2} \int_0^{G_p} \Delta(p/z) dG_p$ vs. G_p — Case 1.

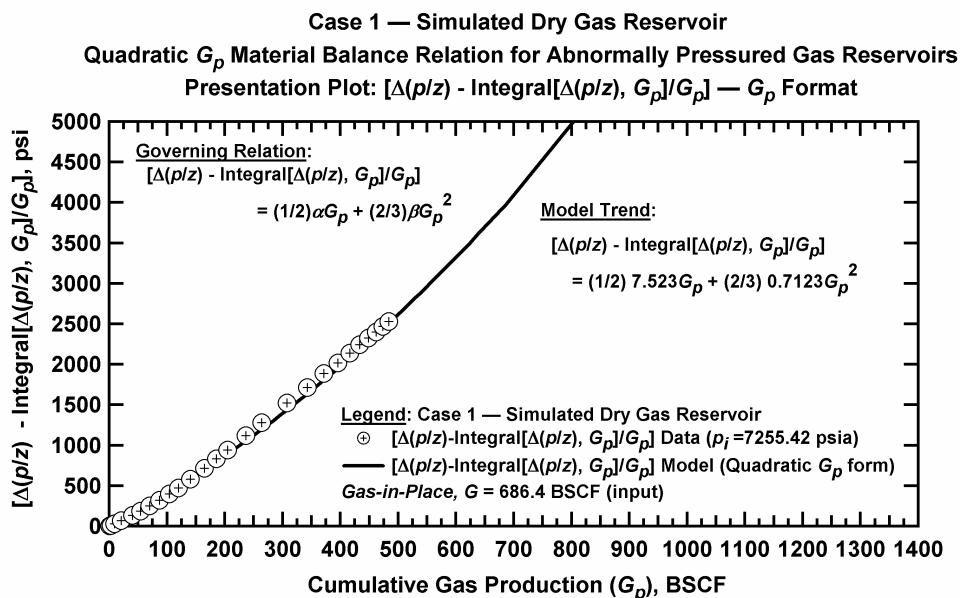


Figure D.2.f — Plot of $\Delta(p/z) - \frac{1}{G_p} \int_0^{G_p} \Delta(p/z) dG_p$ vs. G_p — Case 1.

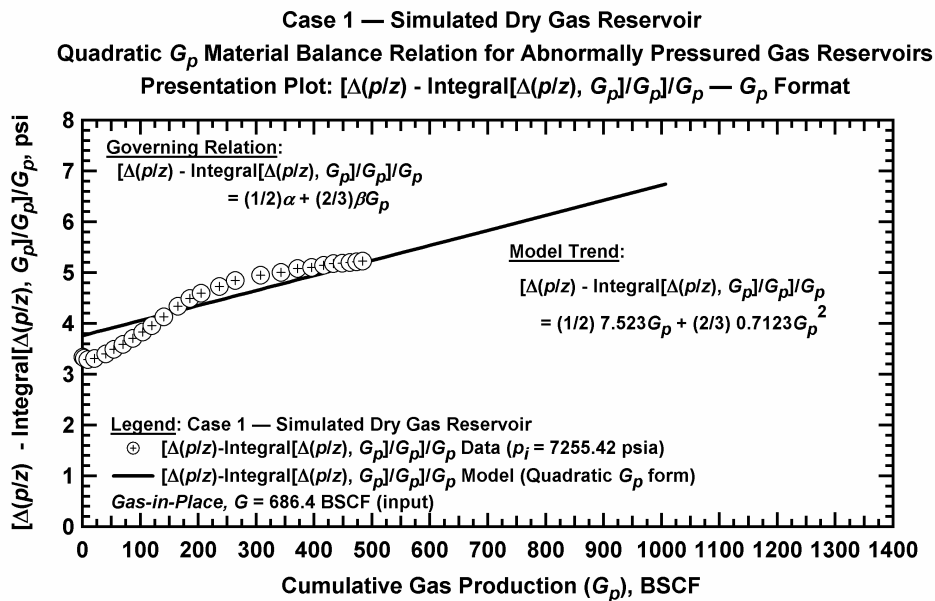


Figure D.2.g — Plot of $\frac{1}{G_p} \left[\Delta(p/z) - \frac{1}{G_p} \int_0^{G_p} \Delta(p/z) dG_p \right]$ vs. G_p — Case 1.

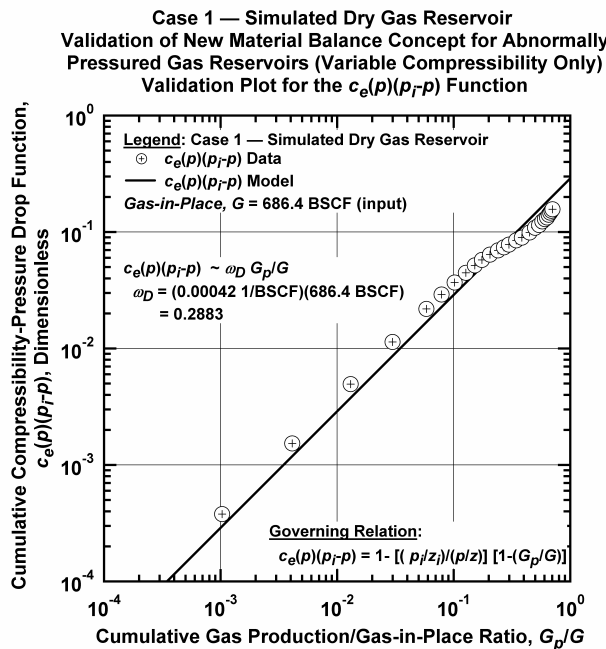


Figure D.2.h — Plot of $\bar{c}_e(p)(p_i - p)$ vs. G_p/G — Case 1.

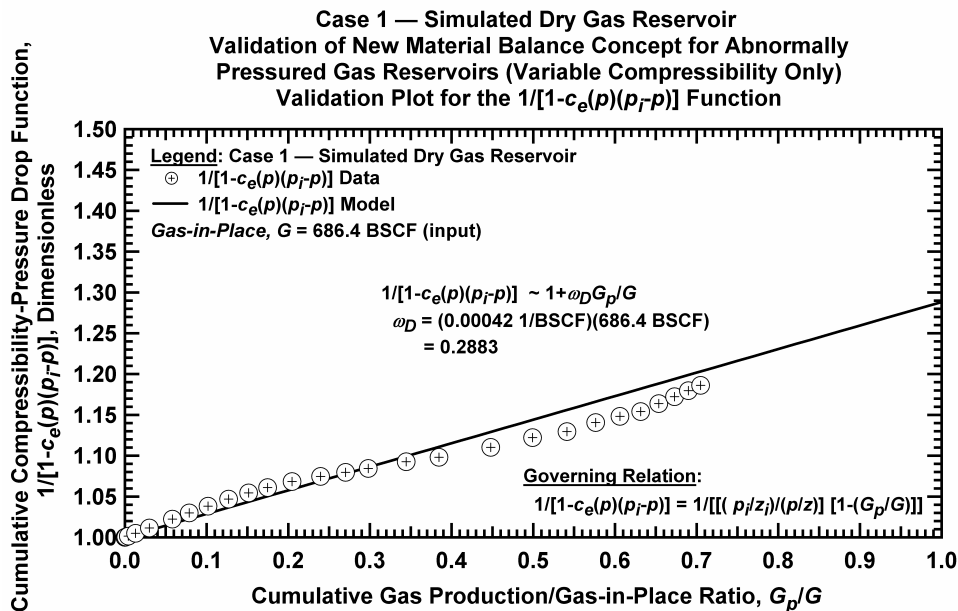


Figure D.1.i — Plot of $1/[1-\bar{c}_e(p)(p_i-p)]$ vs. G_p/G — Case 1.

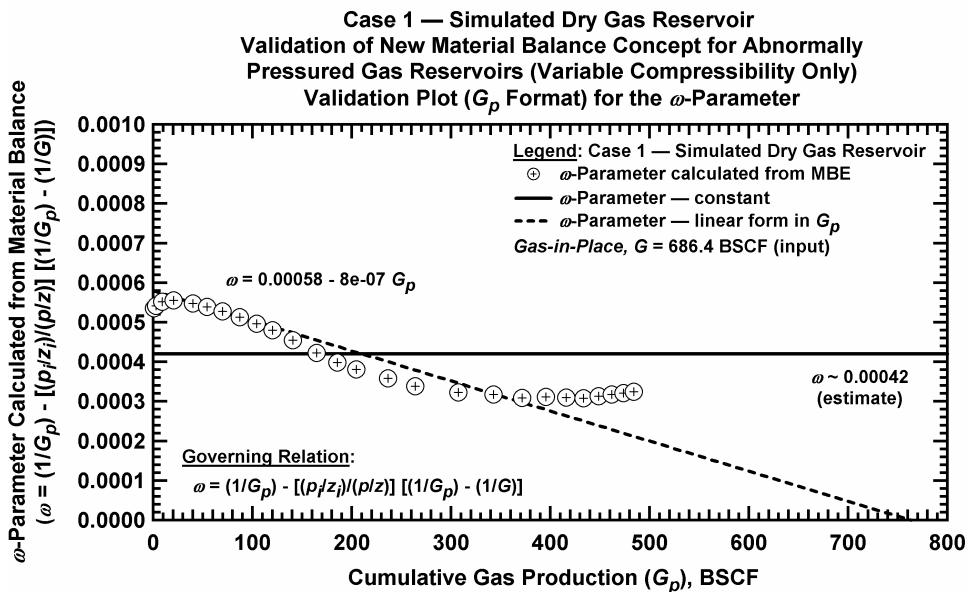


Figure D.2.j — Plot of ω vs. G_p — Case 1.

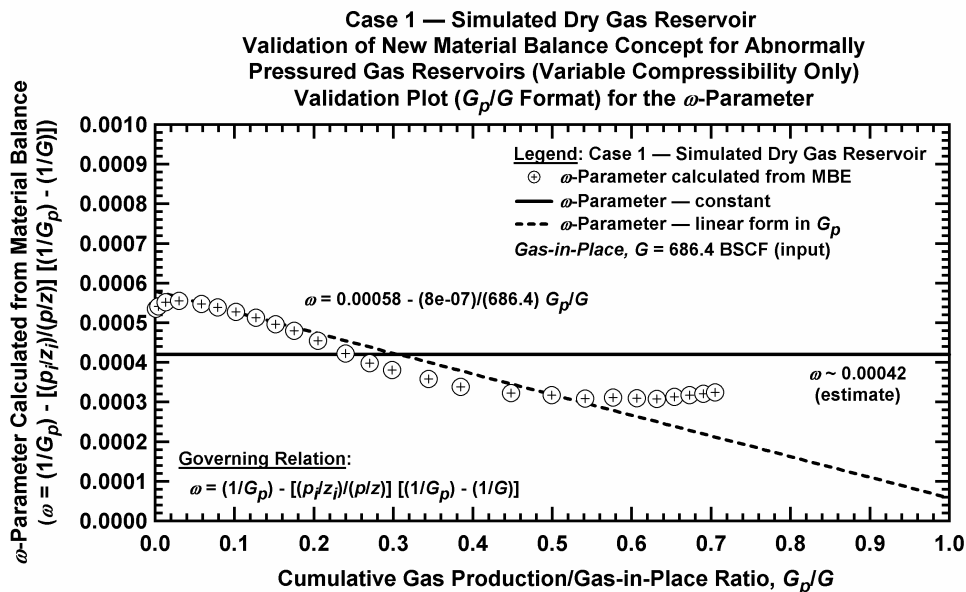


Figure D.2.k — Plot of ω vs. G_p/G — Case 1.

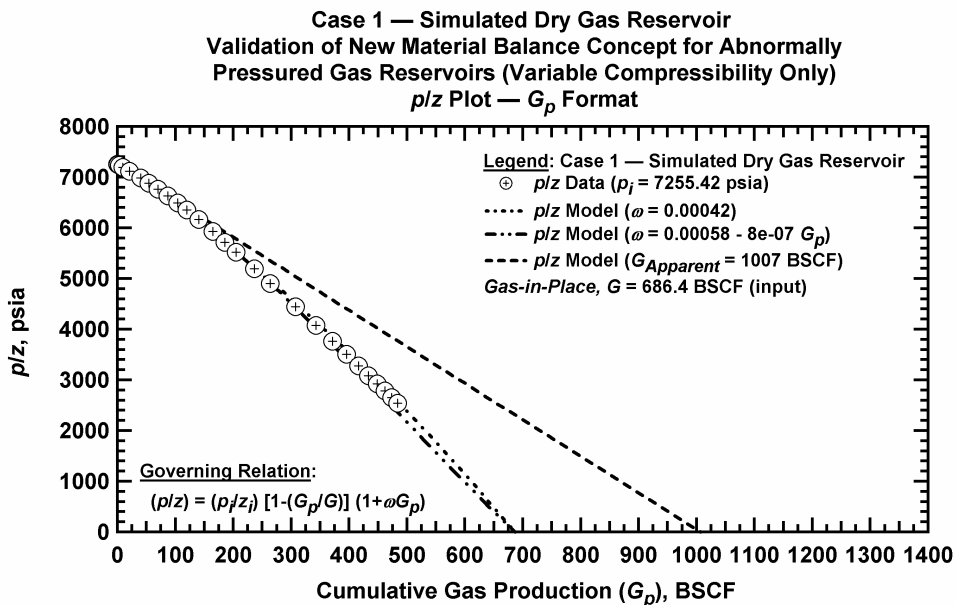


Figure D2.1 — Comparison plot of p/z vs. G_p — Case 1.

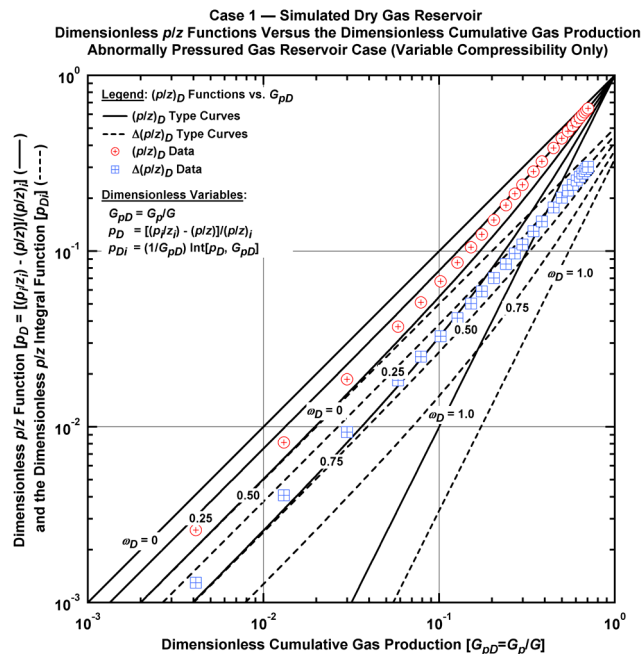


Figure D.2.m — Plot of dimensionless p/z functions vs. G_{pD} — Case 1.

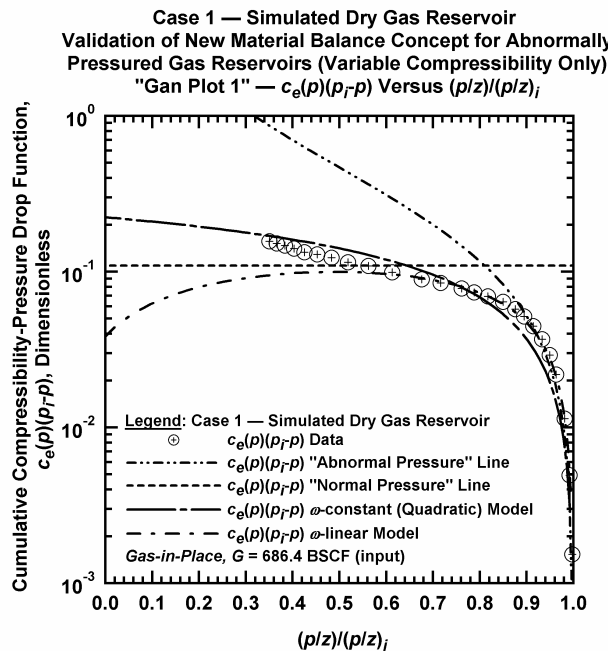


Figure D.2.n — Plot of $\bar{c}_e(p)(p_i - p)$ vs. $(p/z)/(p/z)_i$ — Case 1.

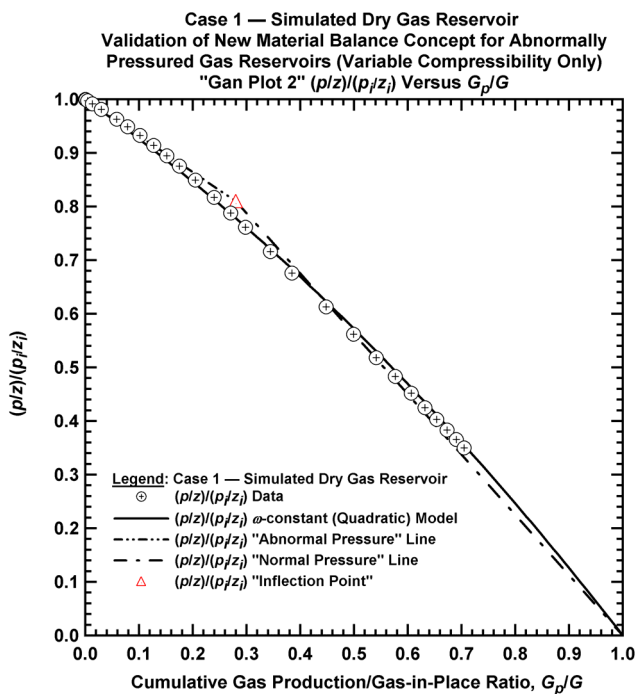


Figure D.2.o — Plot of $(p/z)/(p_i/z_i)$ vs. G_p/G — Case 1.

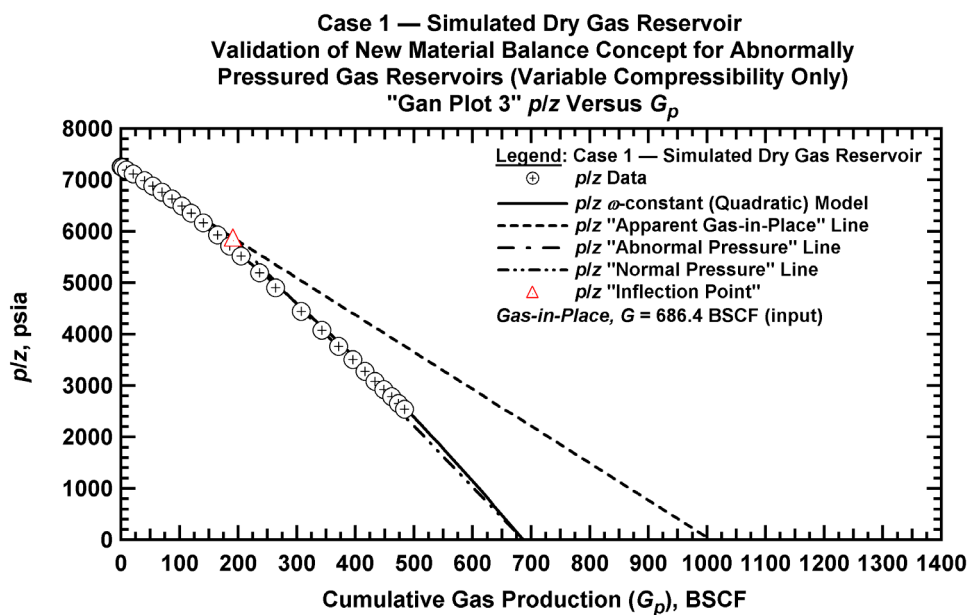


Figure D.2.p — Summary plot of p/z vs. G_p — Case 1.

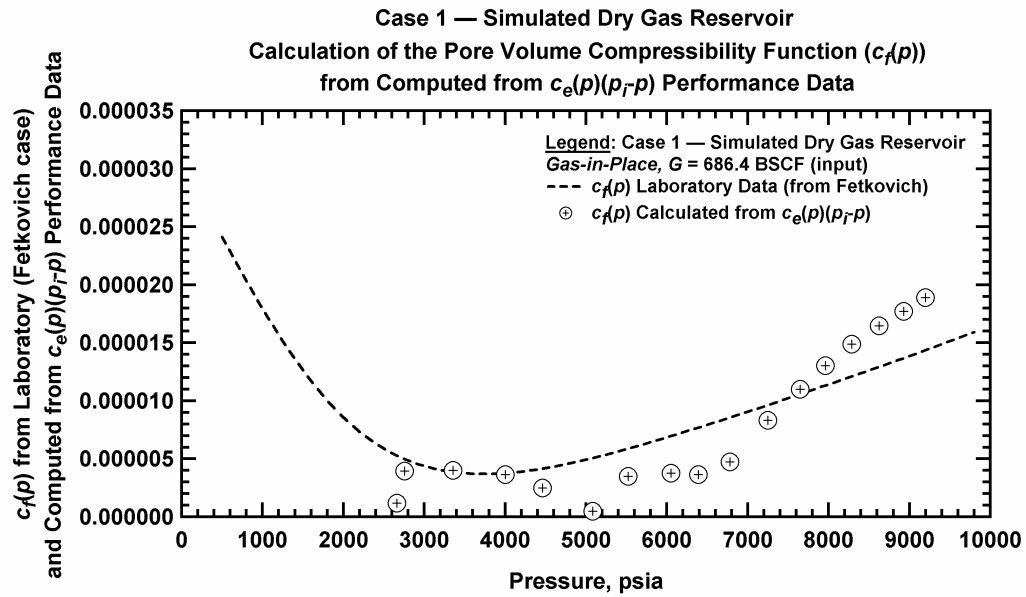


Figure D.2.q — Plot of Pore Volume Compressibility computed using Fetkovich, *et al.* approach and compared to laboratory data — Case 1.

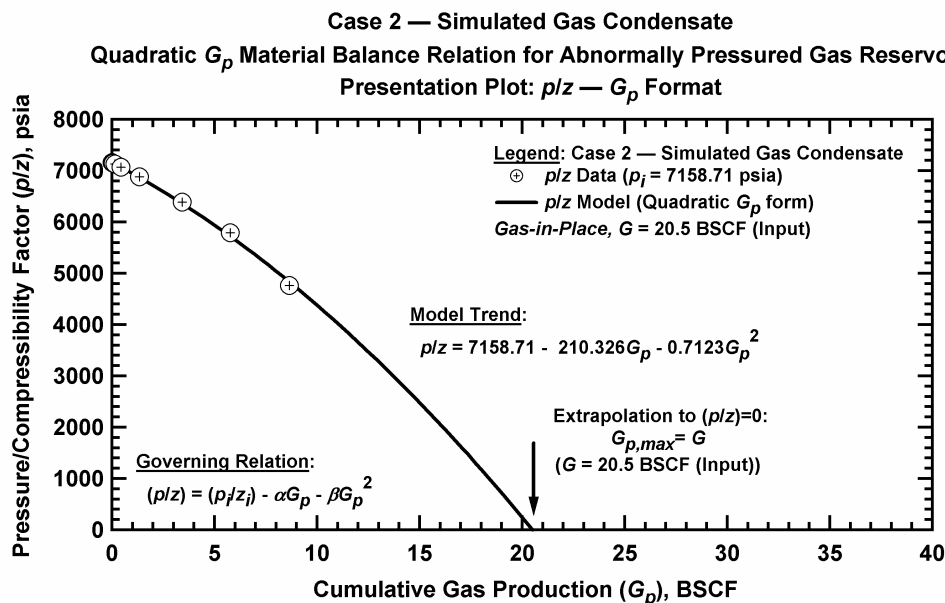


Figure D.3.a — Base plot of p/z vs. G_p — Case 2.

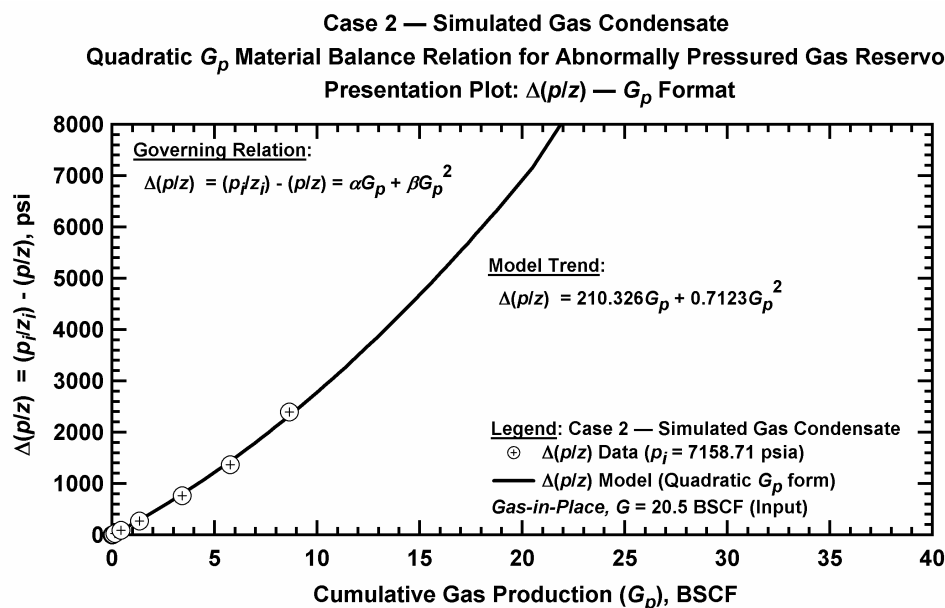


Figure D.3.b — Plot of $\Delta(p/z)$ vs. G_p — Case2.

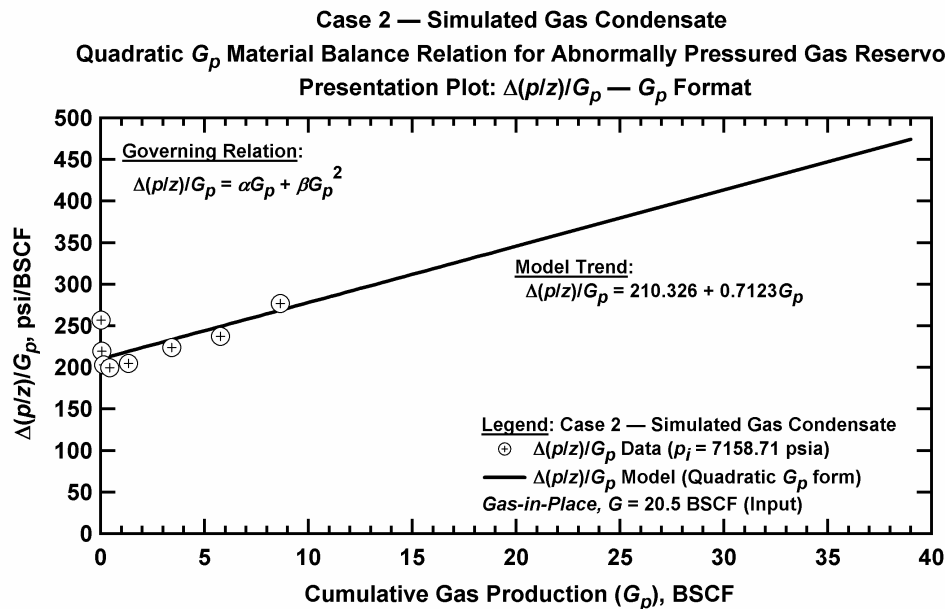


Figure D.3.c — Plot of $\Delta(p/z)/G_p$ vs. G_p — Case 2.

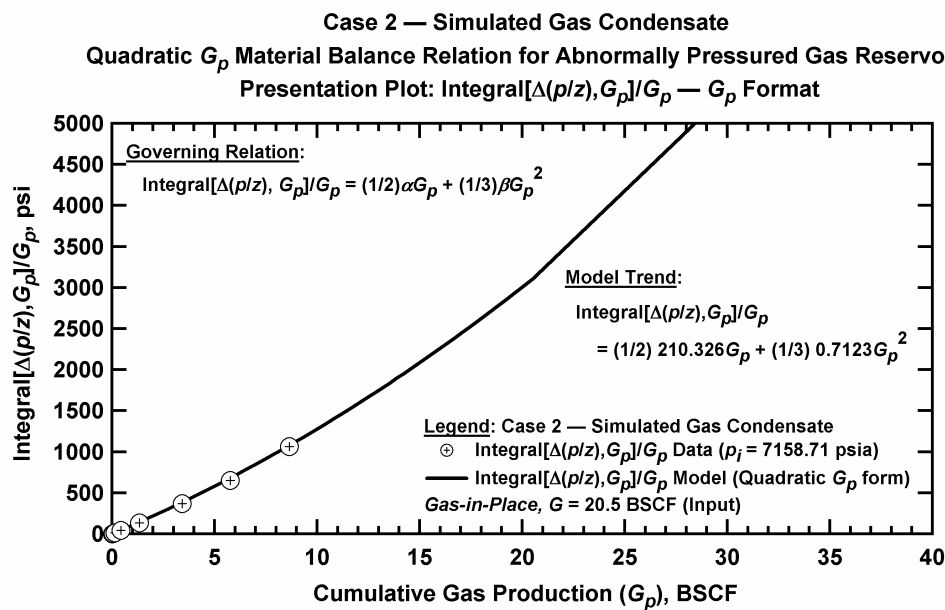


Figure D.3.d — Plot of $\frac{1}{G_p} \int_0^{G_p} \Delta(p/z) dG_p$ vs. G_p — Case 2.

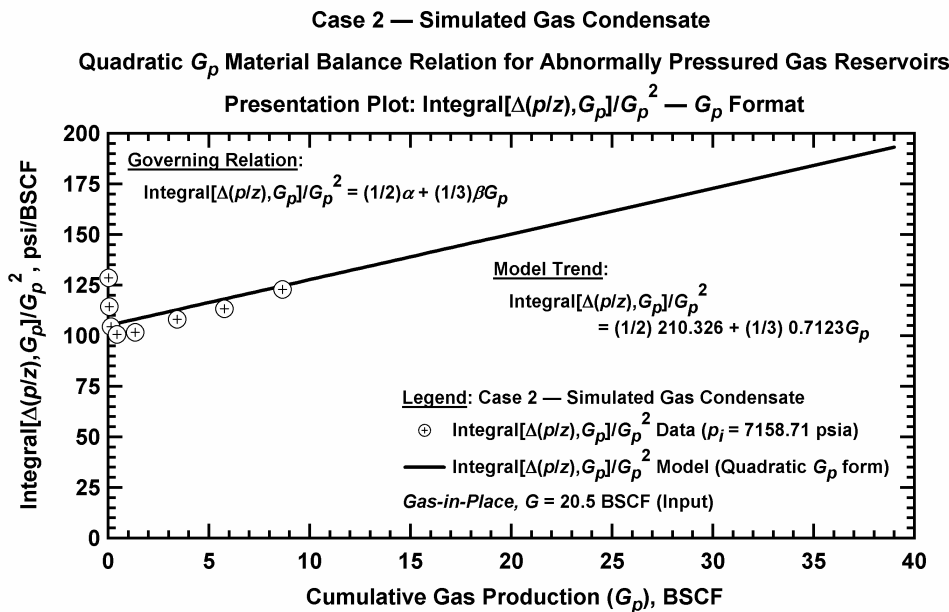


Figure D.3.e — Plot of $\frac{1}{G_p^2} \int_0^{G_p} \Delta(p/z) dG_p$ vs. G_p — Case 2.

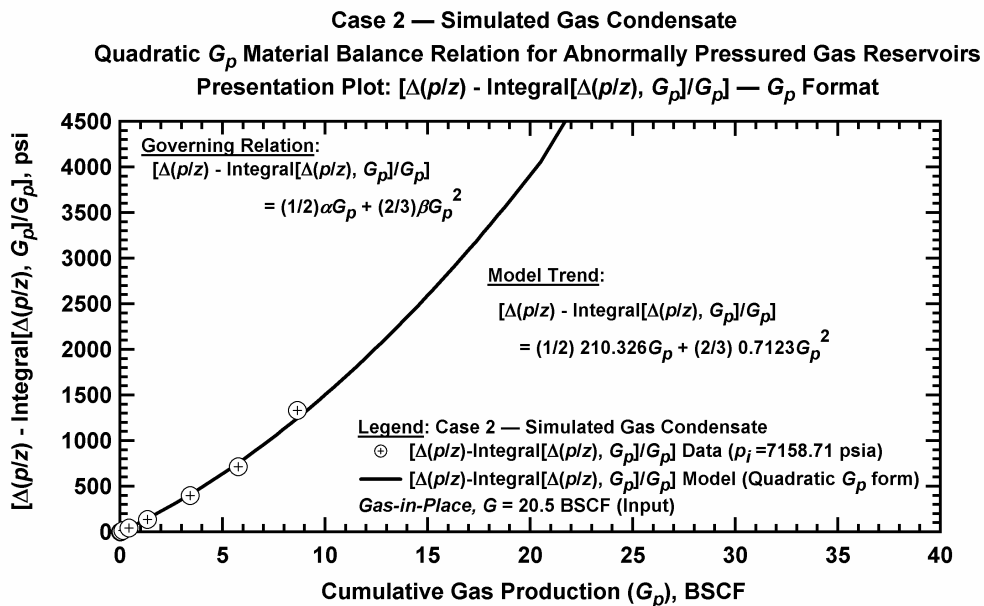


Figure D.3.f — Plot of $[\Delta(p/z) - \frac{1}{G_p} \int_0^{G_p} \Delta(p/z) dG_p] - G_p$ vs. G_p — Case 2.

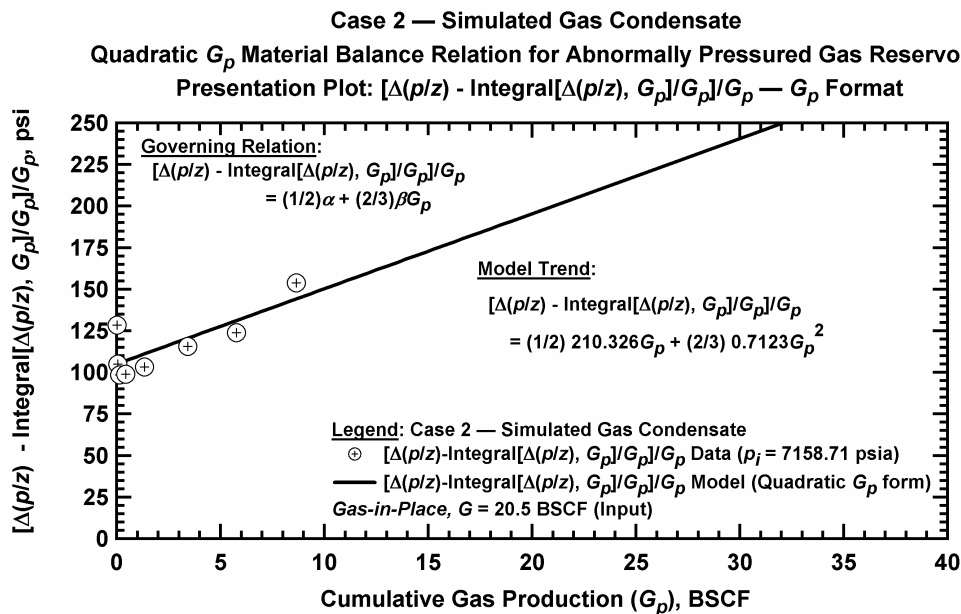


Figure D.3.g — Plot of $\frac{1}{G_p} \left[\Delta(p/z) - \frac{1}{G_p} \int_0^{G_p} \Delta(p/z) dG_p \right]$ vs. G_p — Case 2.

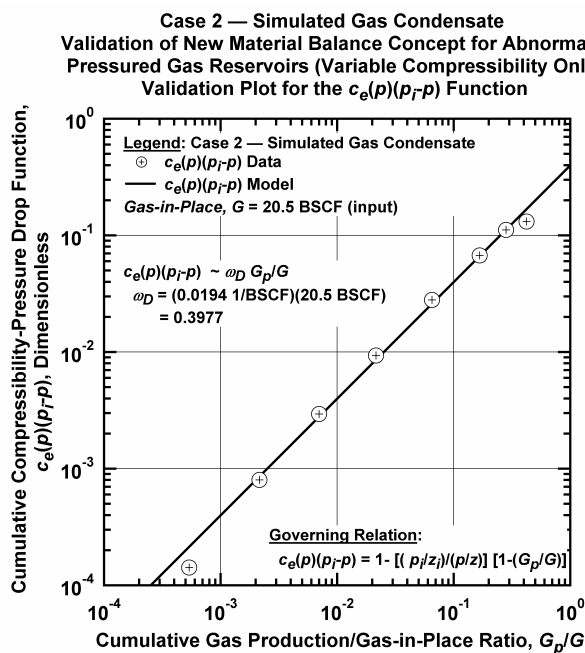


Figure D.3.h — Plot of $\bar{c}_e(p)(p_i - p)$ vs. G_p/G — Case 2.

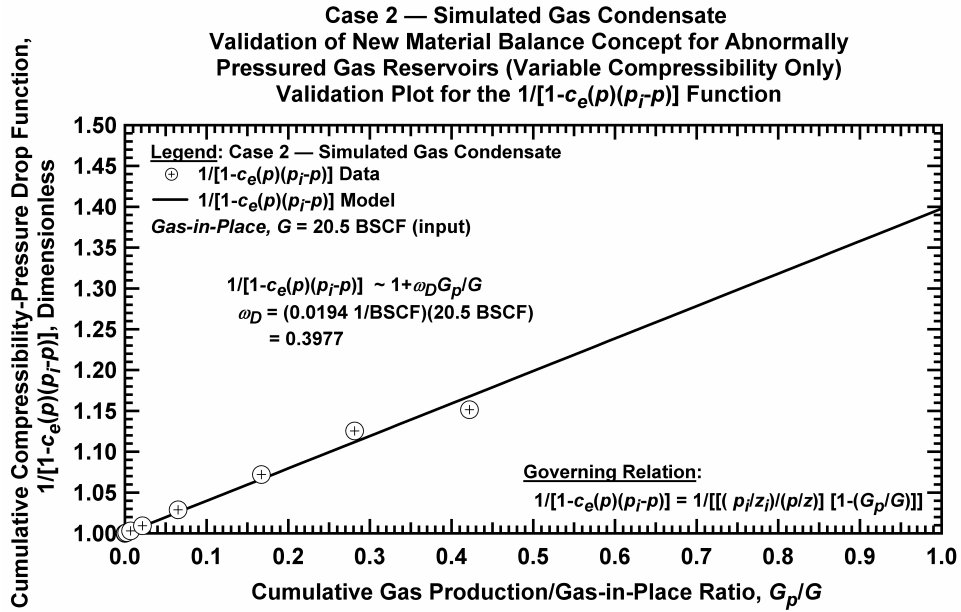


Figure D.3.i — Plot of $1/[1-\bar{c}_e(p)(p_i - p)]$ vs. G_p/G — Case 2.

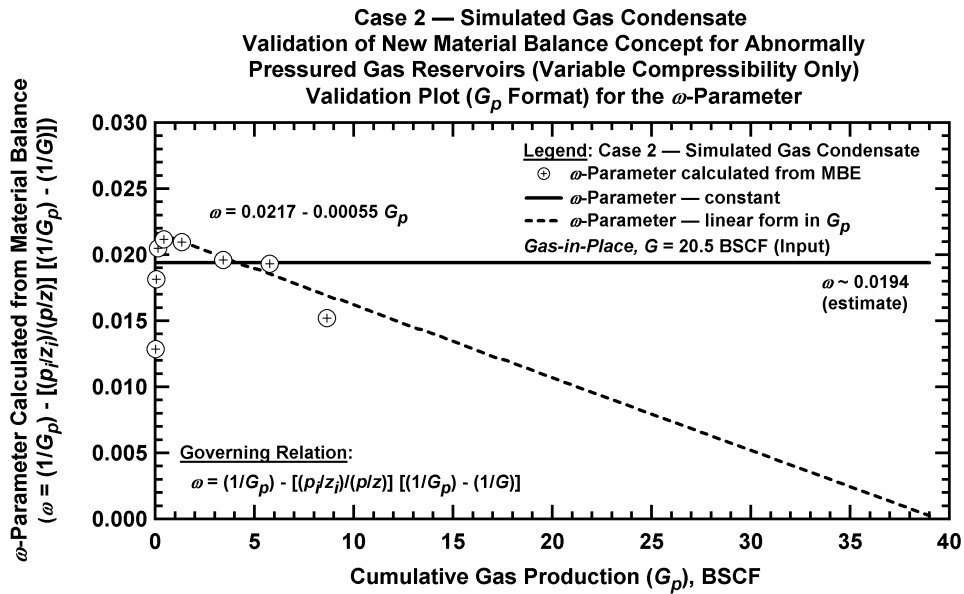


Figure D.3.j — Plot of ω vs. G_p — Case 2.

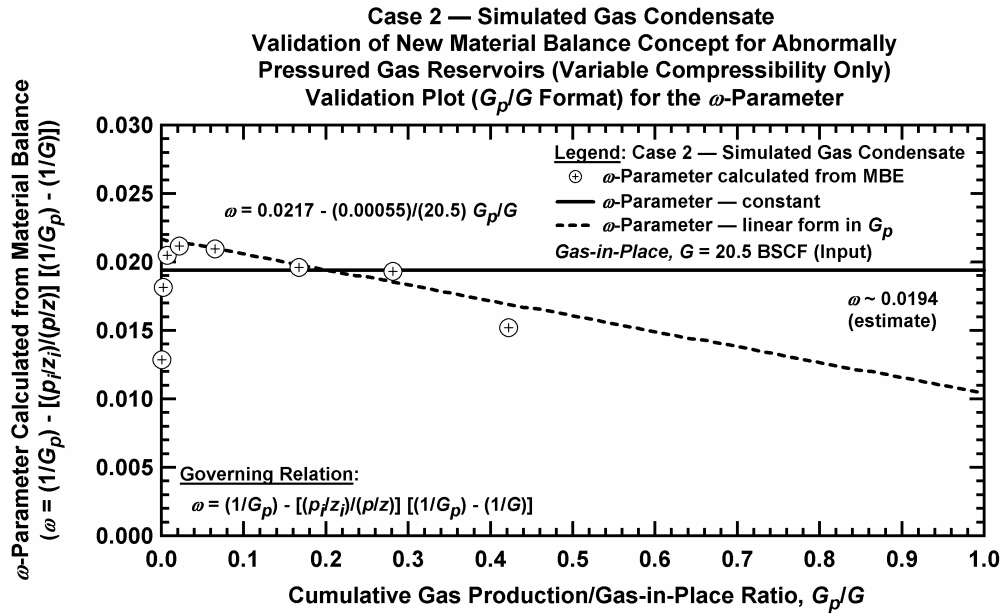


Figure D.3.k — Plot of ω vs. G_p/G — Case 2.

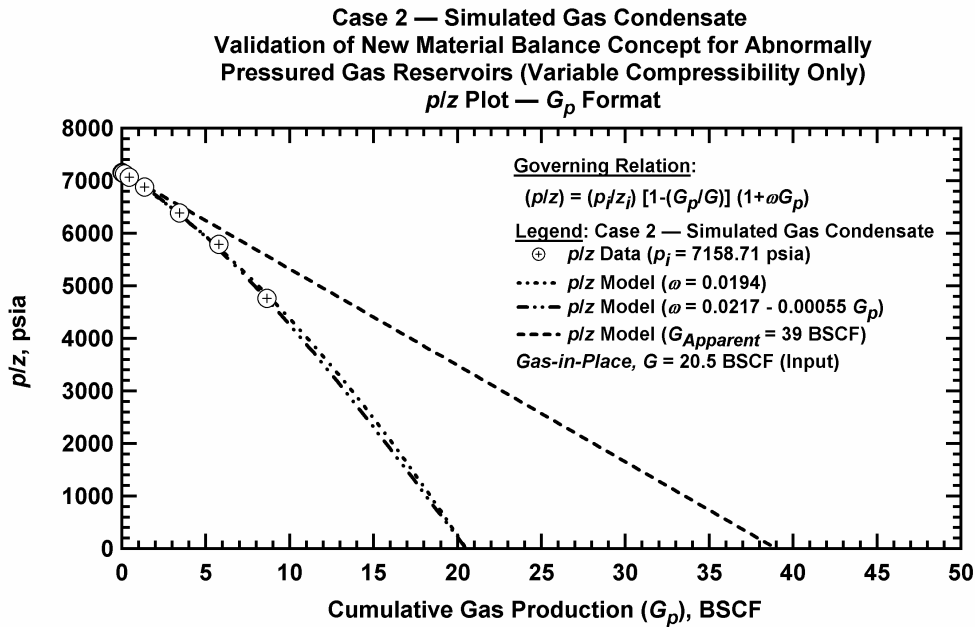


Figure D.3.l — Comparison plot of p/z vs. G_p — Case 2.

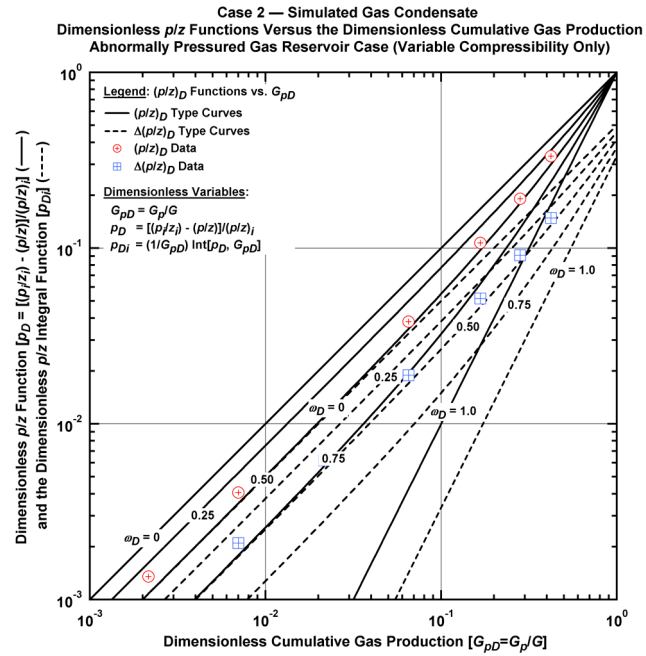


Figure D.3.m — Plot of dimensionless p/z functions vs. G_{pD} — Case 2.

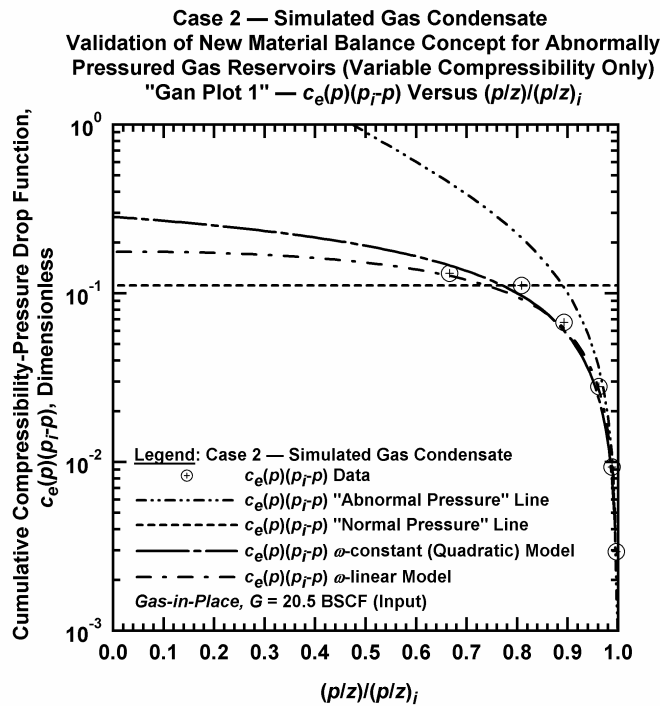


Figure D.3.n — Plot of $\bar{c}_e(p)(p_i - p)$ vs. $(p/z)/(p/z)_i$ — Case 2/

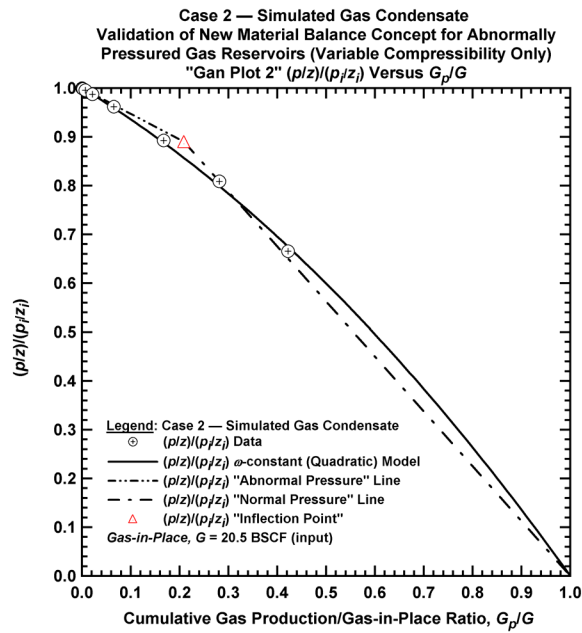


Figure D.3.o — Plot of $(p/z)/(p/z_i)$ vs. G_p/G — Case 2.

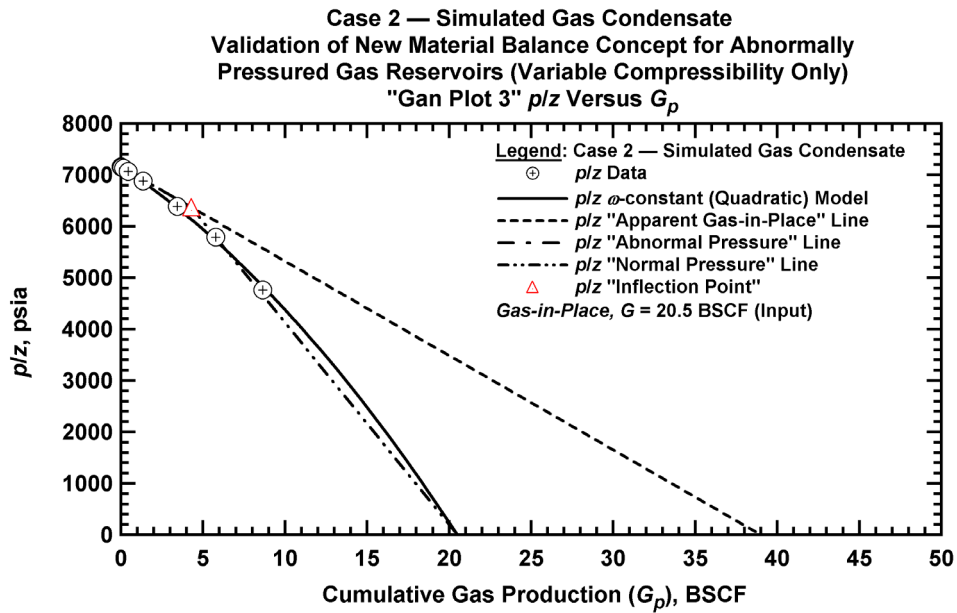


Figure D.3.p — Summary plot of p/z vs. G_p — Case 2.

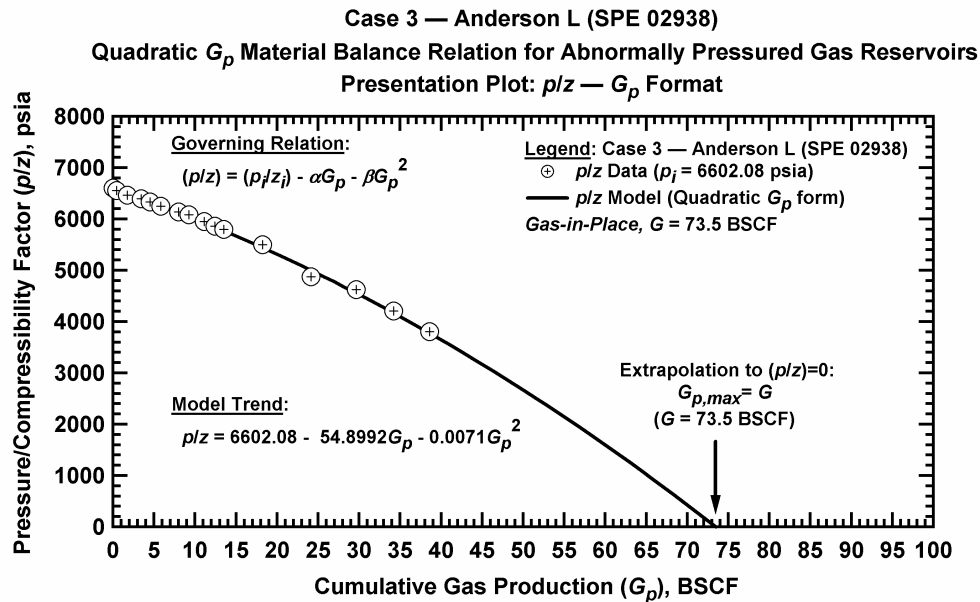


Figure D.4.a — Base plot of p/z vs. G_p — Case 3.

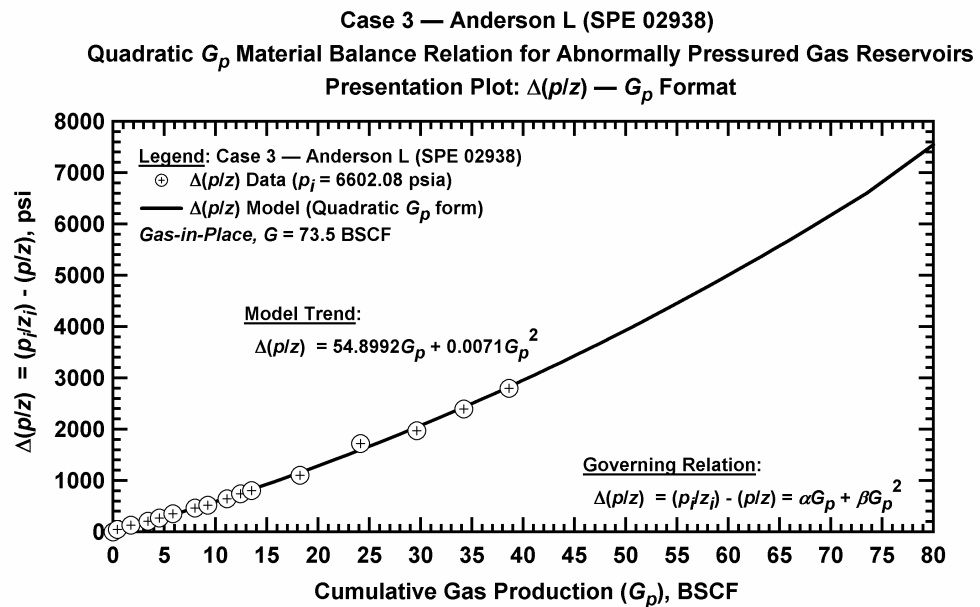
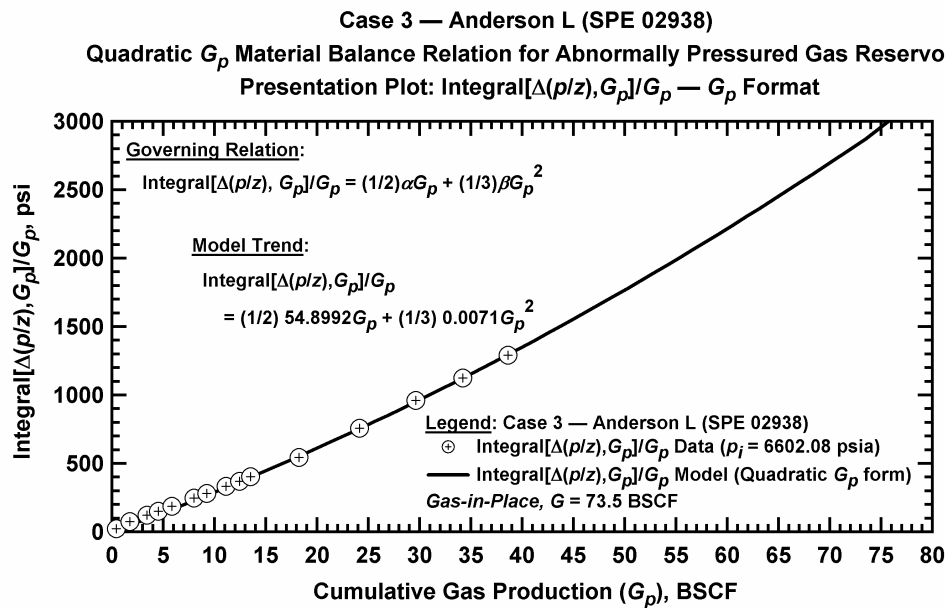
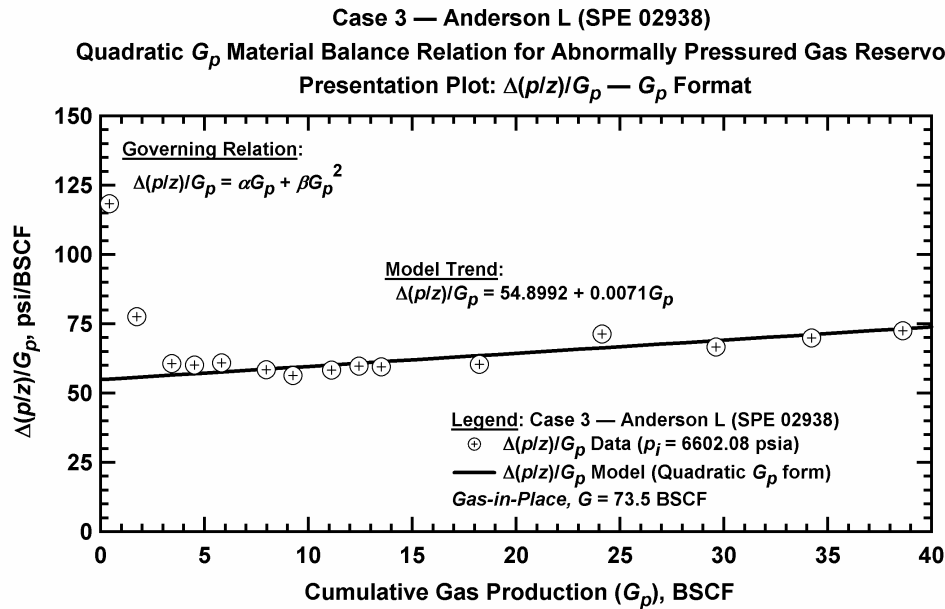


Figure D.4.b — Plot of $\Delta(p/z)$ vs. G_p — Case 3.



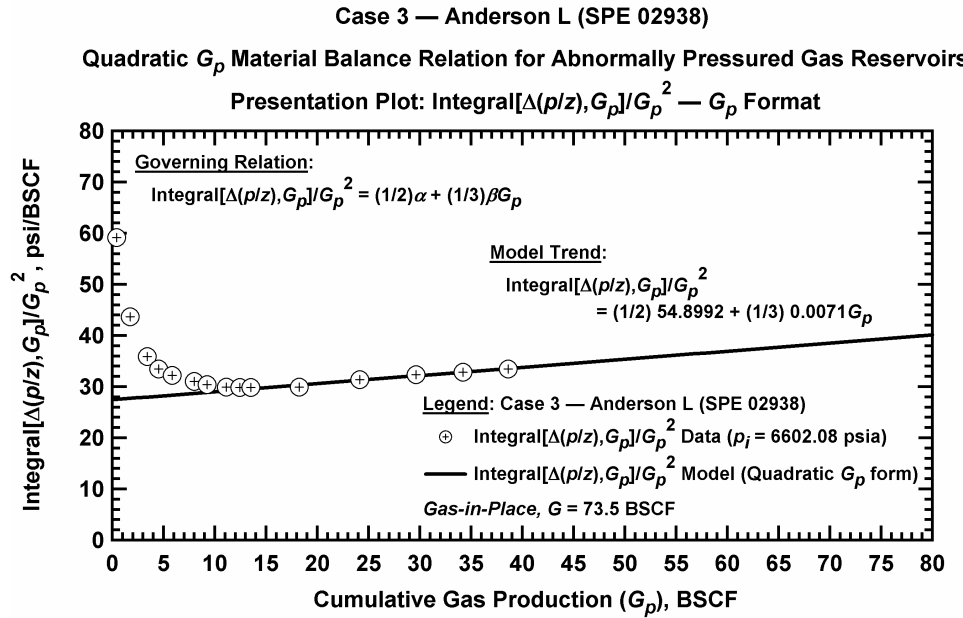


Figure D.4.e — Plot of $\frac{1}{G_p^2} \int_0^{G_p} \Delta(p/z) dG_p$ vs. G_p — Case 3.

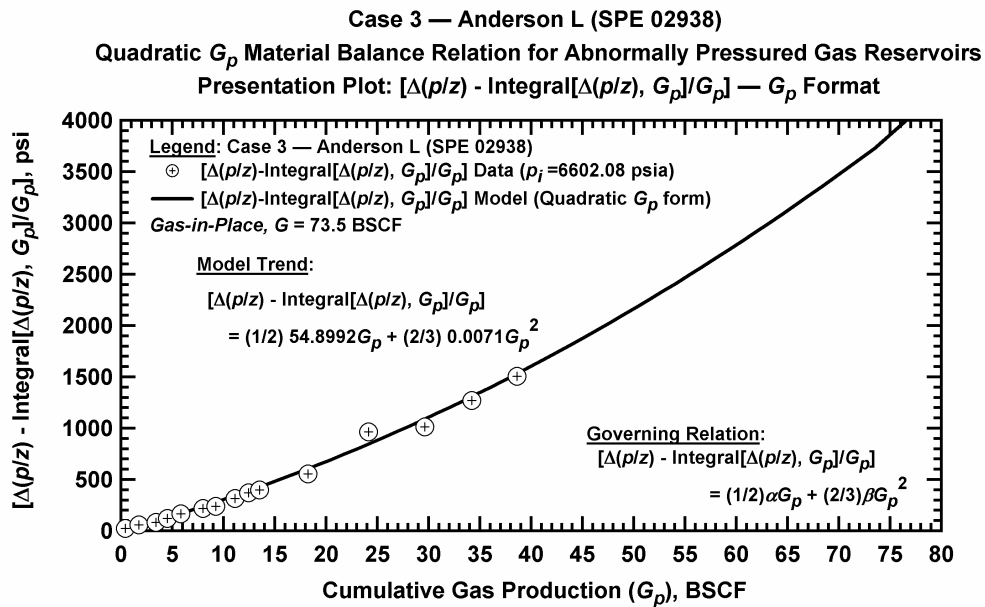


Figure D.4.f — Plot of $\Delta(p/z) - \frac{1}{G_p} \int_0^{G_p} \Delta(p/z) dG_p$ vs. G_p — Case 3.

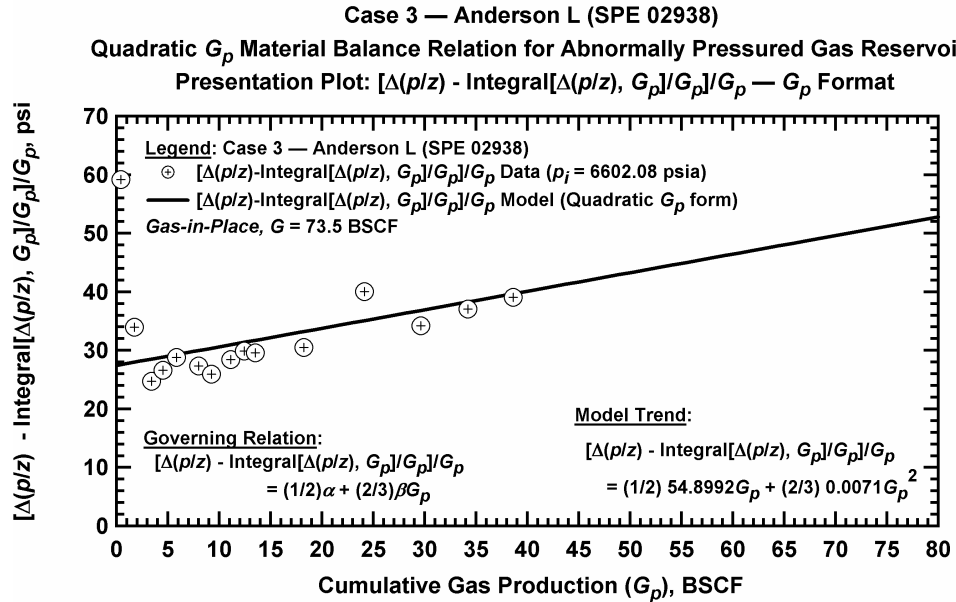


Figure D.4.g — Plot of $\frac{1}{G_p} \left[\Delta(p/z) - \frac{1}{G_p} \int_0^{G_p} \Delta(p/z) dG_p \right]$ vs. G_p — Case 3.

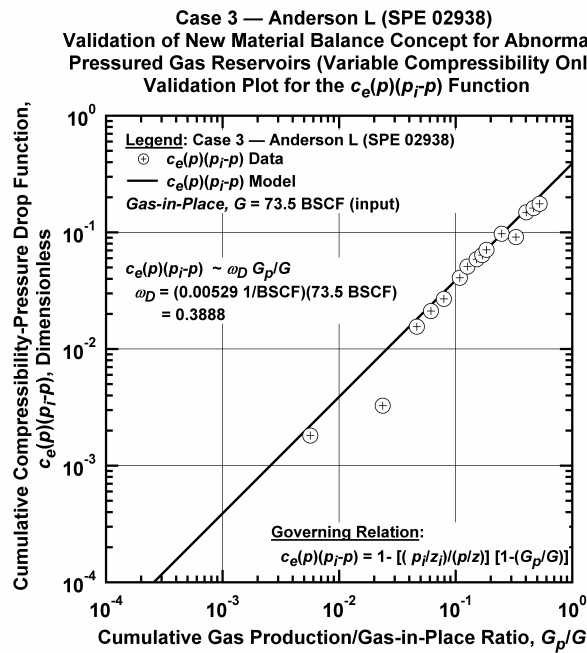


Figure D.4.h — Plot of $\bar{c}_e(p)(p_i - p)$ vs. G_p/G — Case 3.

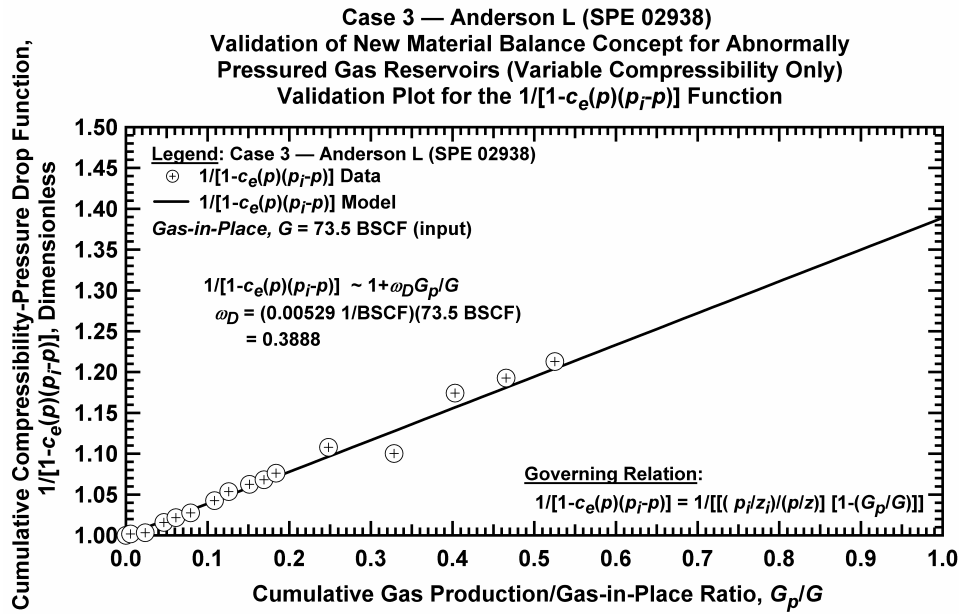


Figure D.4.i — Plot of $1/[1-\bar{c}_e(p)(p_i - p)]$ vs. G_p/G — Case 3.

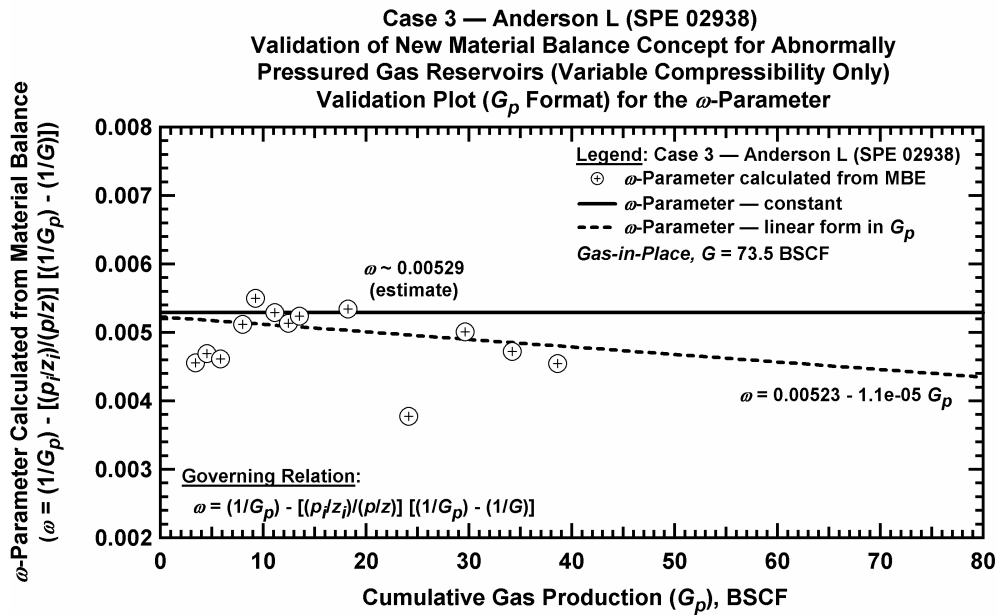


Figure D.4.j — Plot of ω vs. G_p — Case 3.

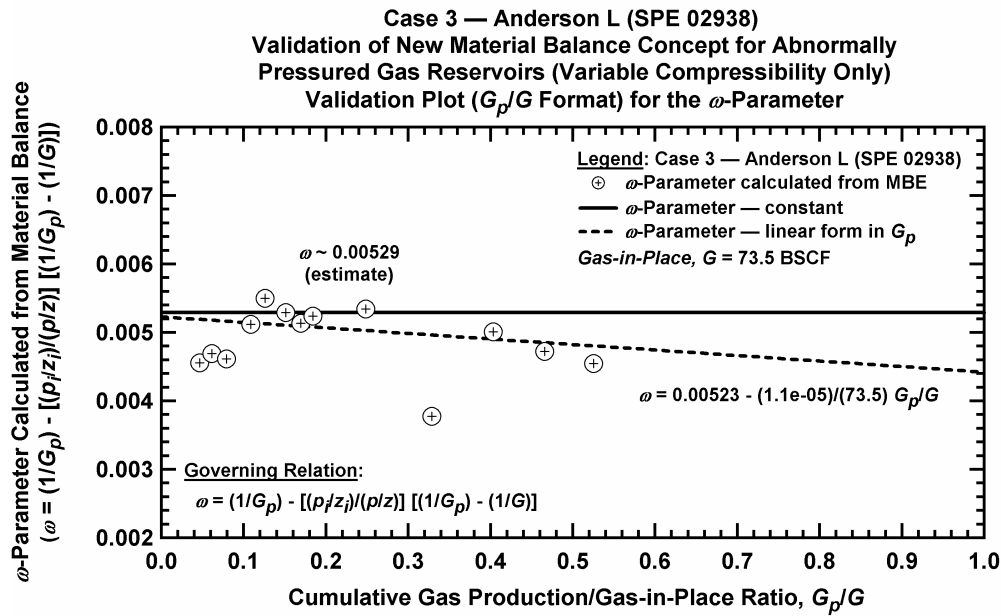


Figure D.4.k — Plot of ω vs. G_p/G — Case 3.

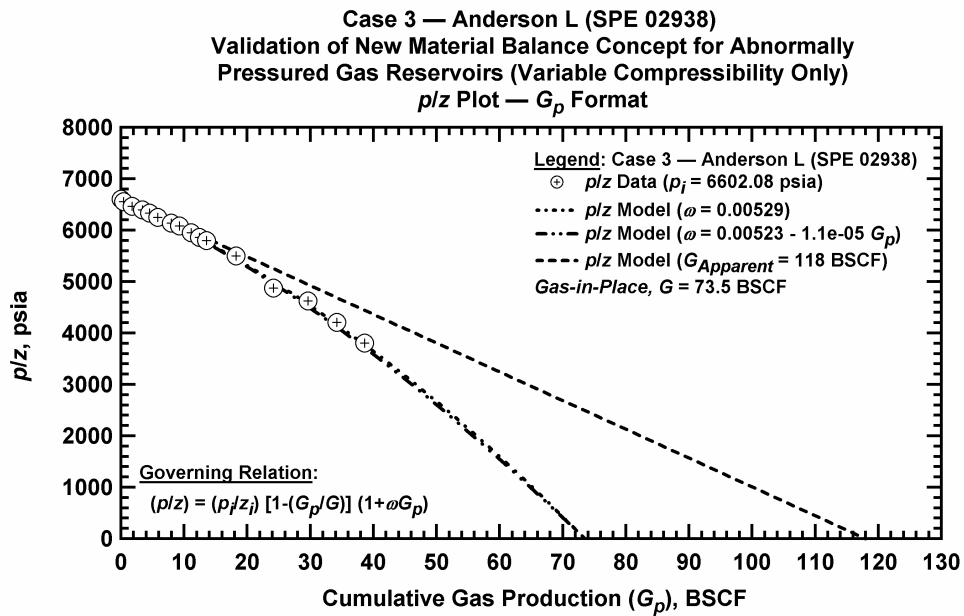


Figure D.4.l — Comparison plot of p/z vs. G_p — Case 3.

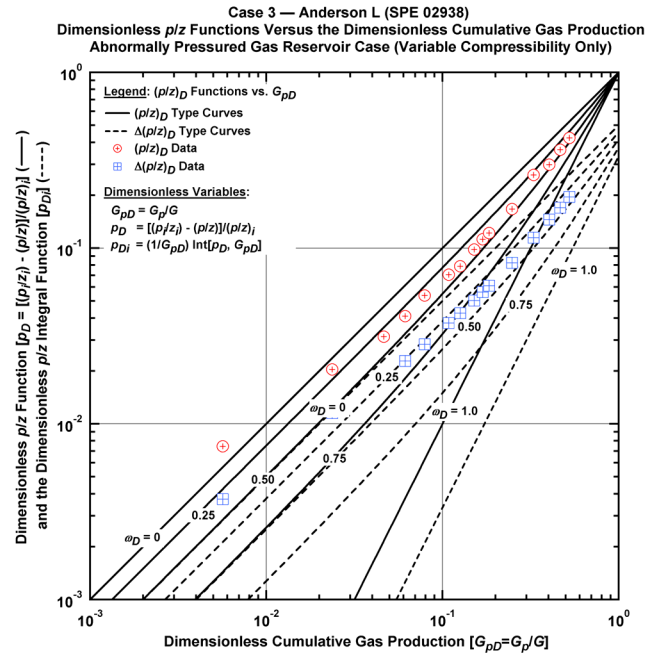


Figure D.4.m — Plot of dimensionless p/z functions vs. G_{pD} — Case 3.

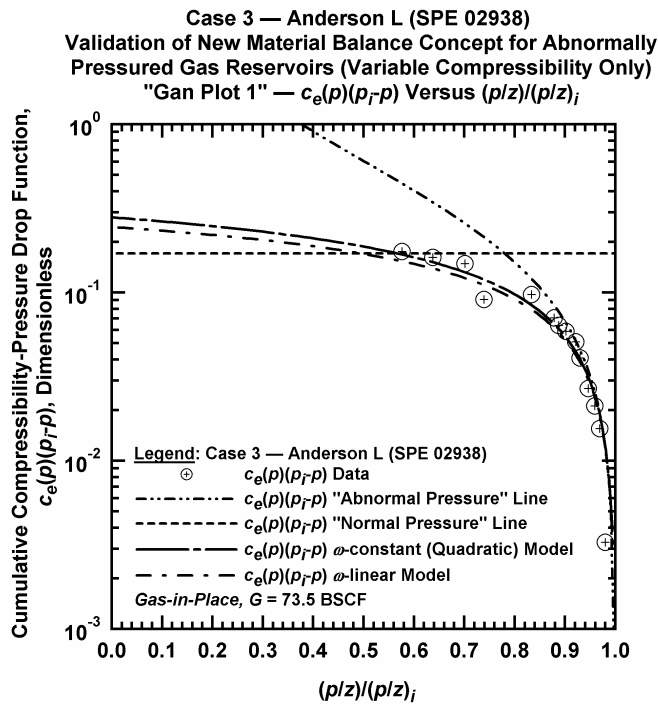


Figure D.4.n — Plot of $\bar{c}_e(p)(p_i - p)$ vs. $(p/z)/(p/z)_i$ — Case 3.

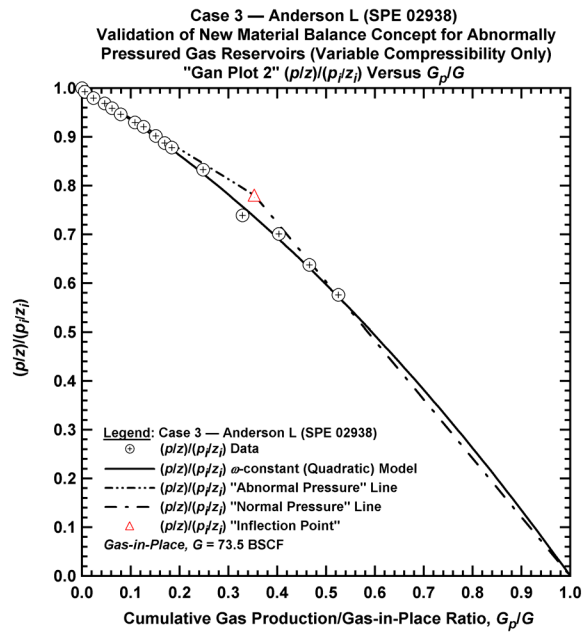


Figure D.4.o — Plot of $(p/z)/(p_i/z_i)$ vs. G_p/G — Case 3.

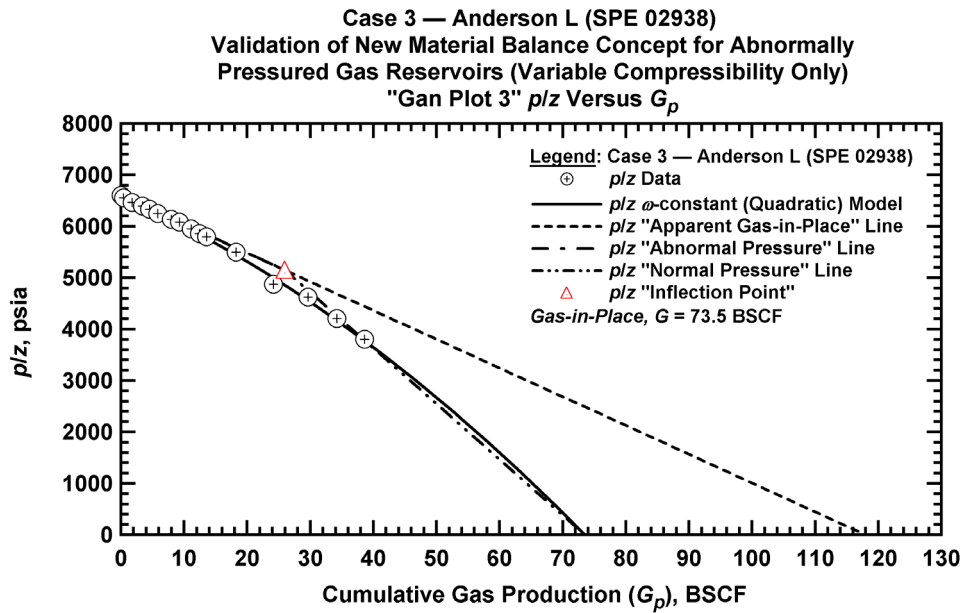


Figure D.4.p — Summary plot of p/z vs. G_p — Case 3.

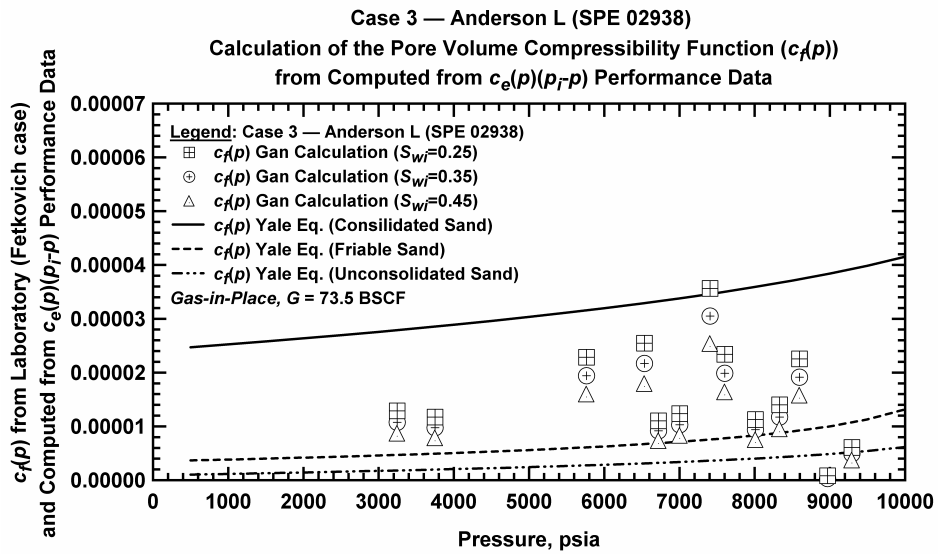


Figure D.4.q — Plot of Pore Volume Compressibility computed using Fetkovich, *et al.* approach and compared to laboratory data — Case 3 (Anderson L Reservoir (assumed $S_{wi}=0.25$)).

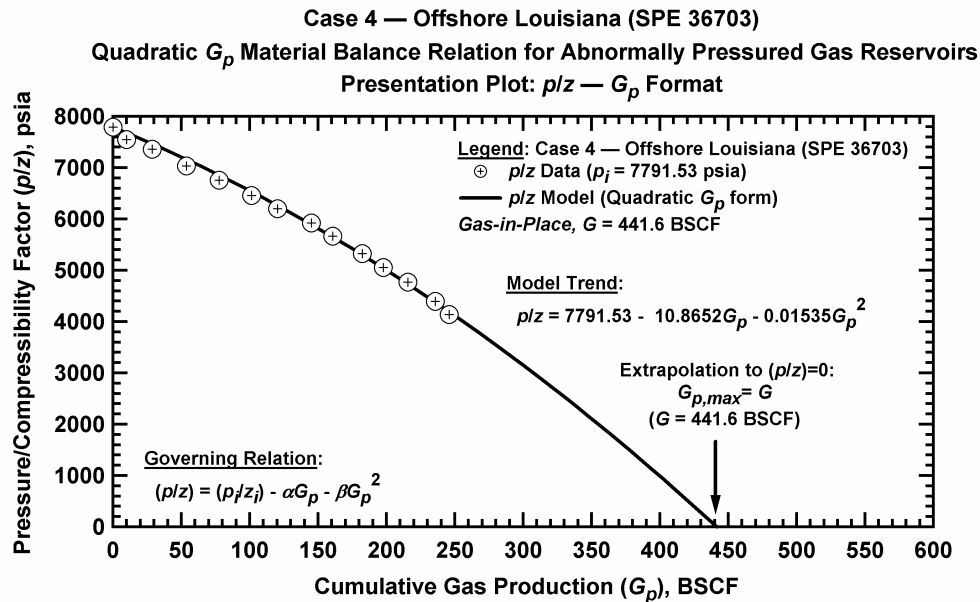


Figure D.5.a — Base plot of p/z vs. G_p — Case 4.

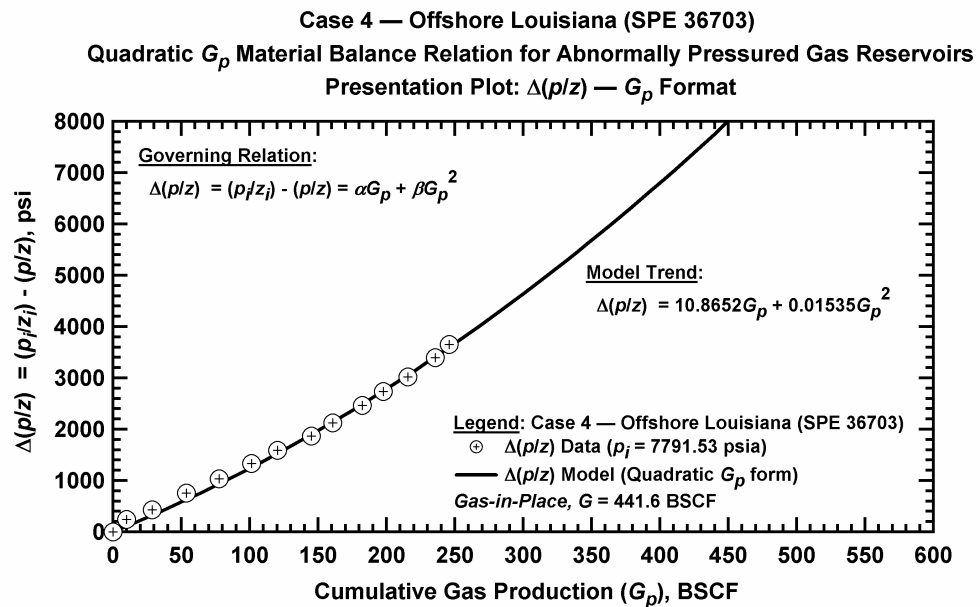


Figure D.5.b — Plot of $\Delta(p/z)$ vs. G_p — Case 4.

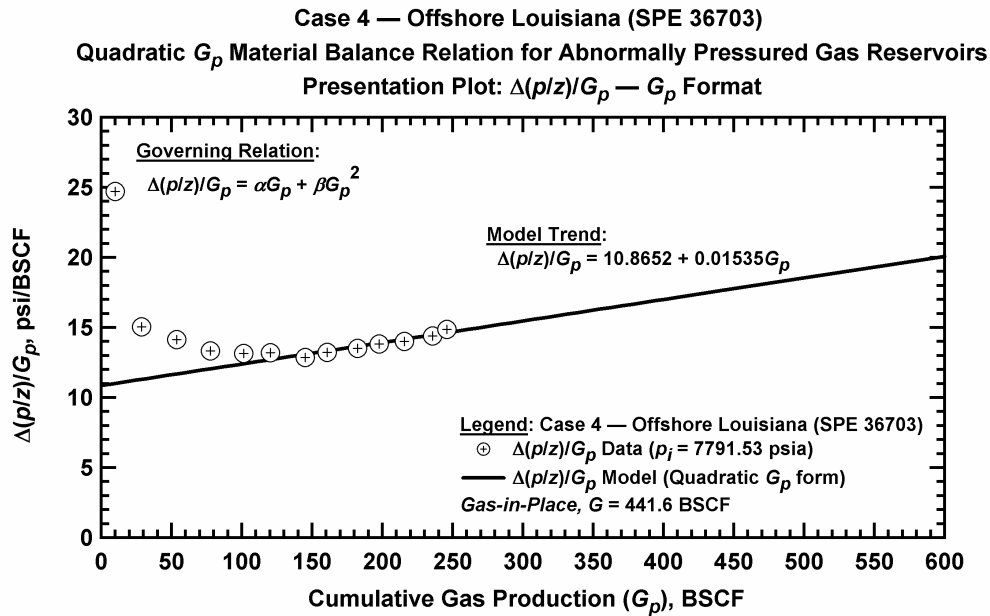


Figure D.5.c — Plot of $\Delta(p/z)/G_p$ vs. G_p — Case 4.

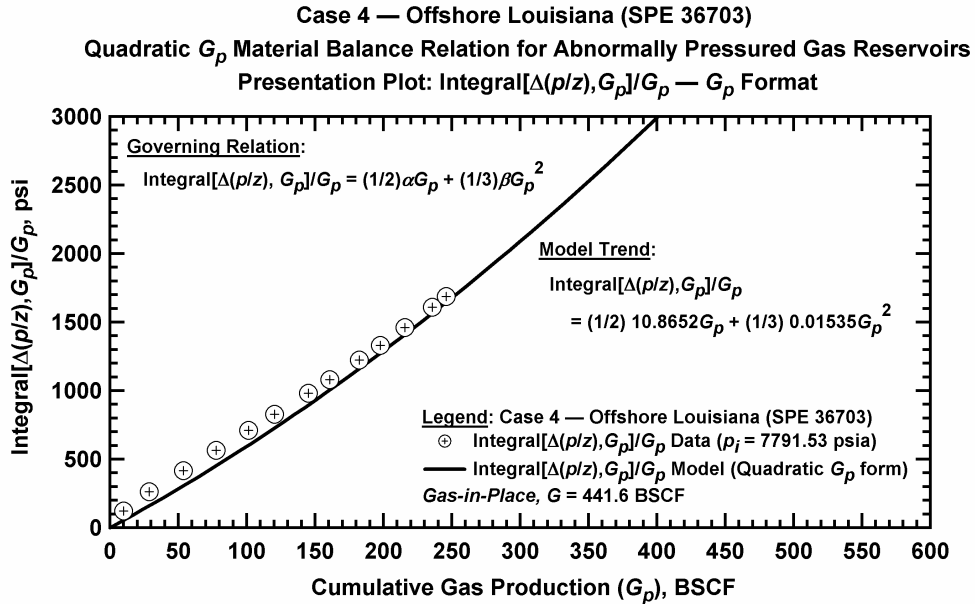


Figure D.5.d — Plot of $\frac{1}{G_p} \int_0^{G_p} \Delta(p/z) dG_p$ vs. G_p — Case 4.

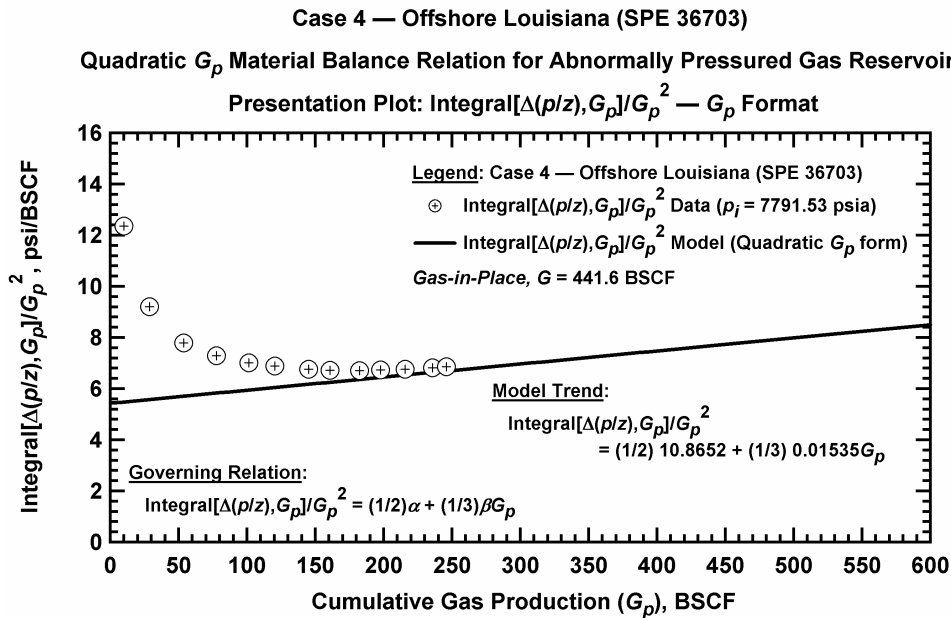


Figure D.5.e — Plot of $\frac{1}{G_p^2} \int_0^{G_p} \Delta(p/z) dG_p$ vs. G_p — Case 4.

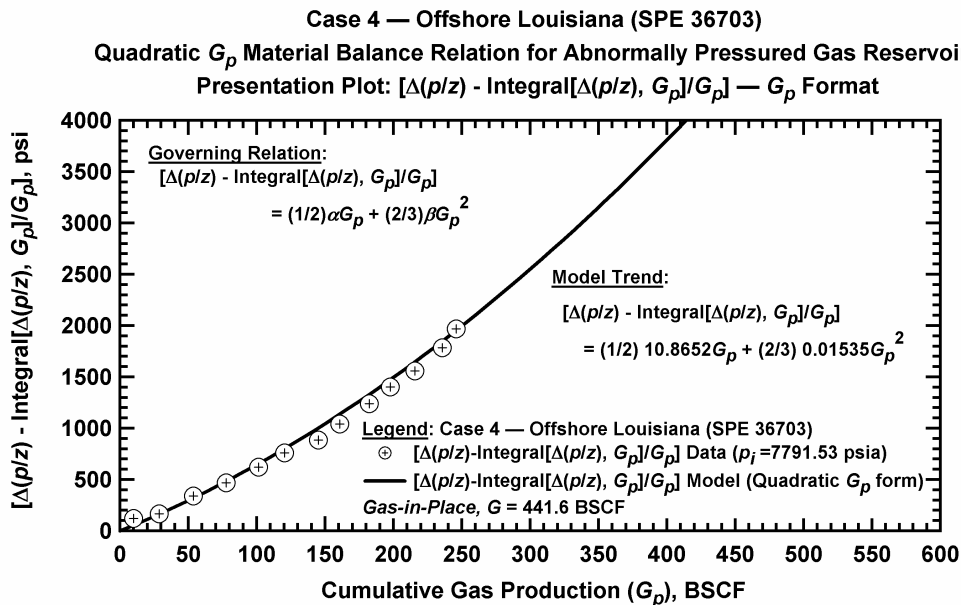


Figure D.5.f — Plot of $\Delta(p/z) - \frac{1}{G_p} \int_0^{G_p} \Delta(p/z) dG_p$ vs. G_p — Case 4.

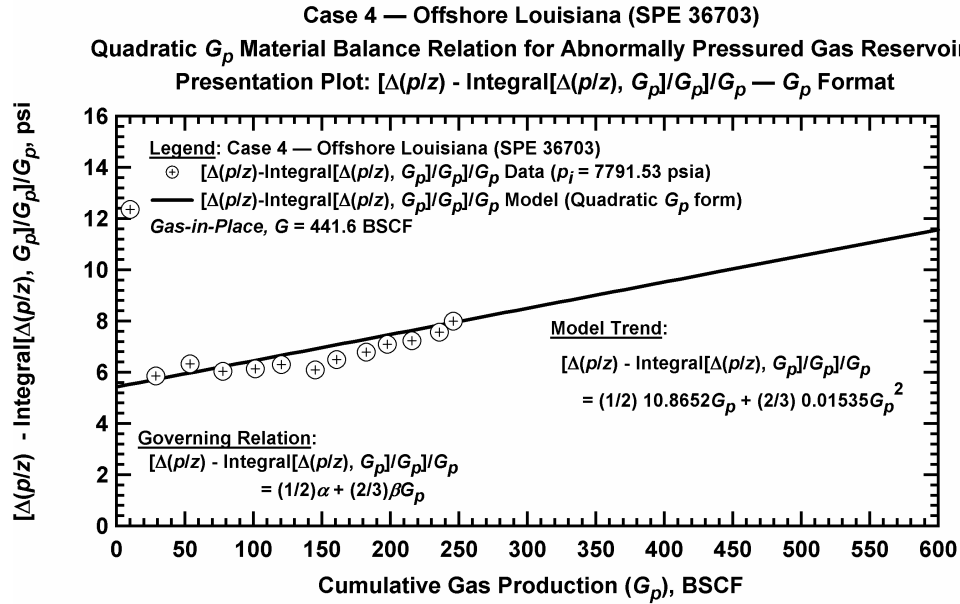


Figure D.5.g — Plot of $\frac{1}{G_p} \left[\Delta(p/z) - \frac{1}{G_p} \int_0^{G_p} \Delta(p/z) dG_p \right]$ vs. G_p — Case 4.

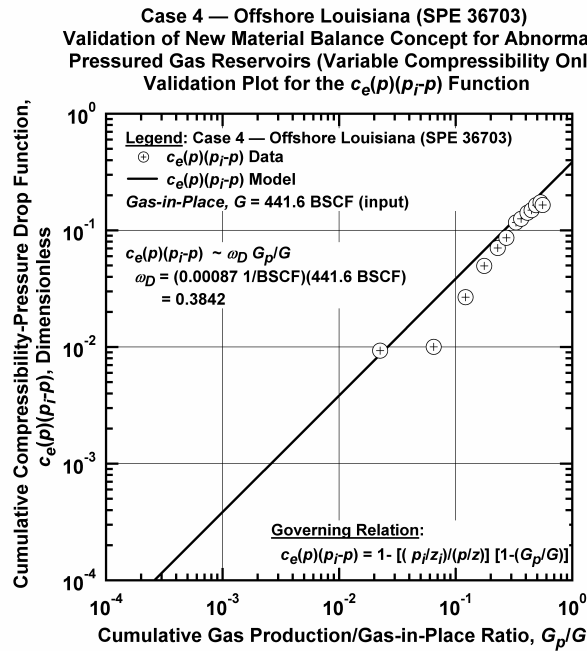


Figure D.5.h — Plot of $\bar{c}_e(p)(p_i - p)$ vs. G_p/G — Case 4.

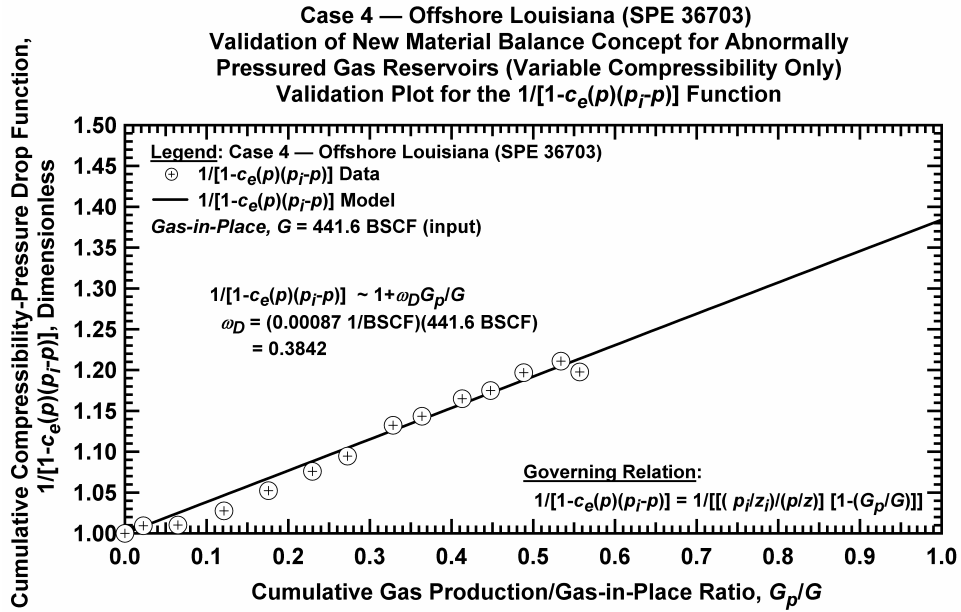


Figure D.5.i — Plot of $1/[1-\bar{c}_e(p)(p_i - p)]$ vs. G_p/G — Case 4.

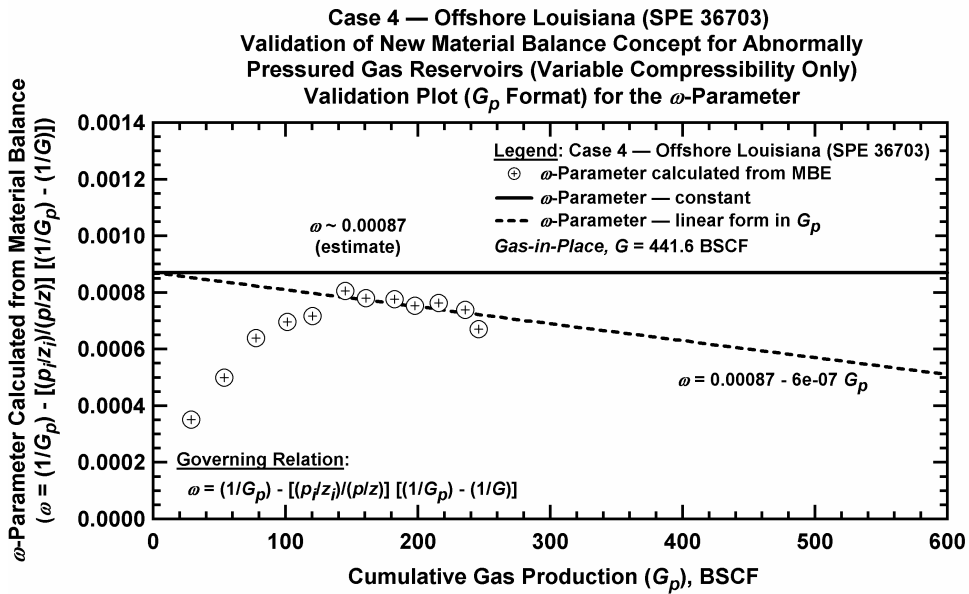


Figure D.5.j — Plot of ω vs. G_p — Case 4.

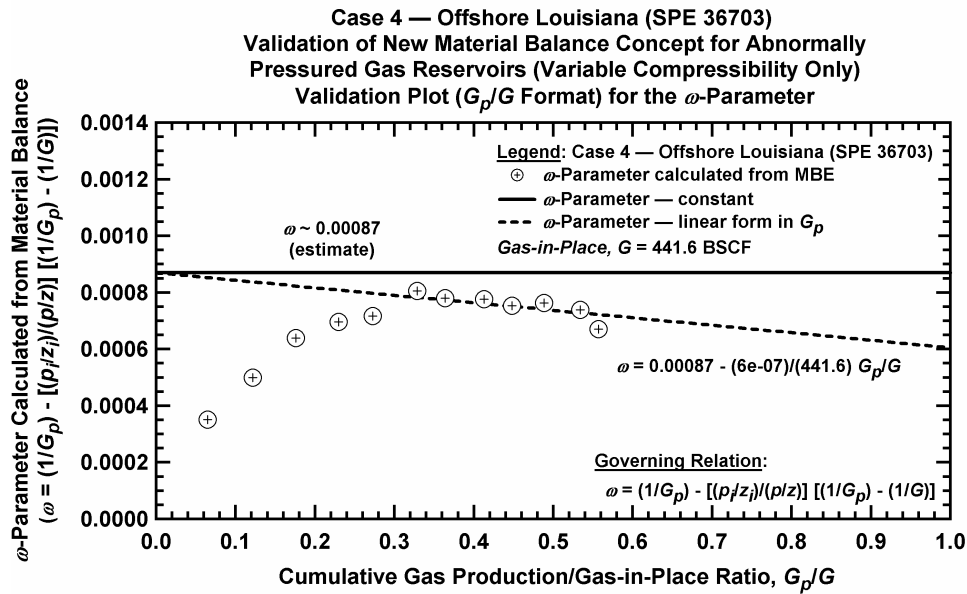


Figure D.5.k — Plot of ω vs. G_p/G — Case 4.

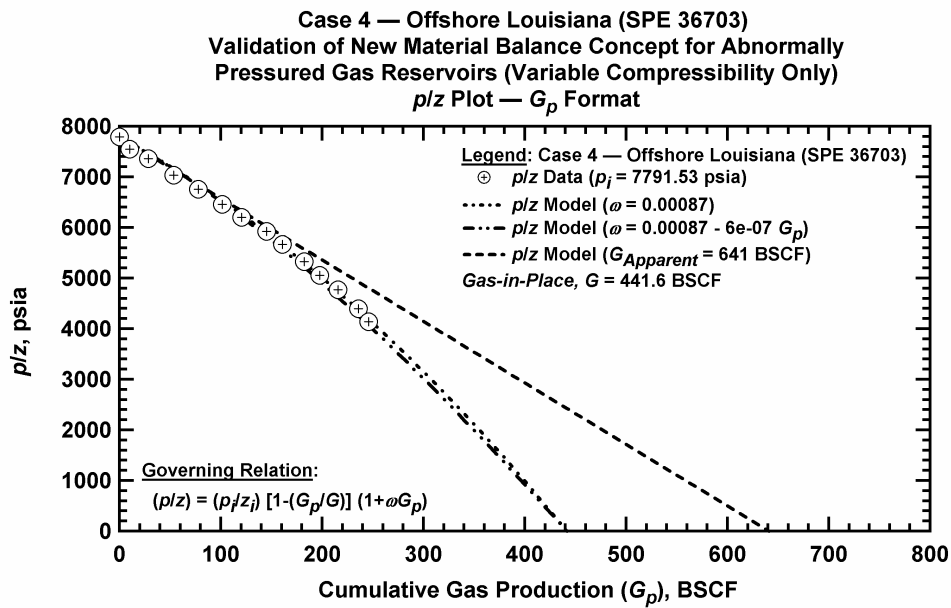


Figure D.5.l — Comparison plot of p/z vs. G_p — Case 4.

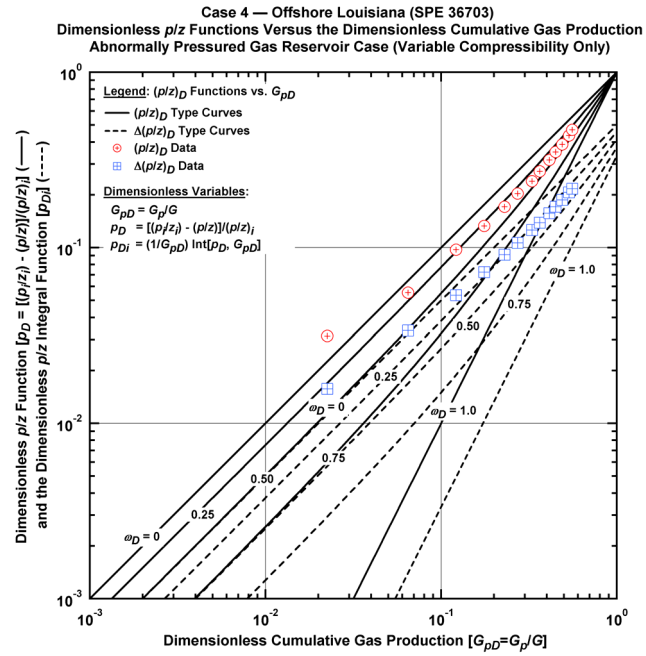


Figure D.5.m — Plot of dimensionless p/z functions vs. G_{pD} — Case 4.

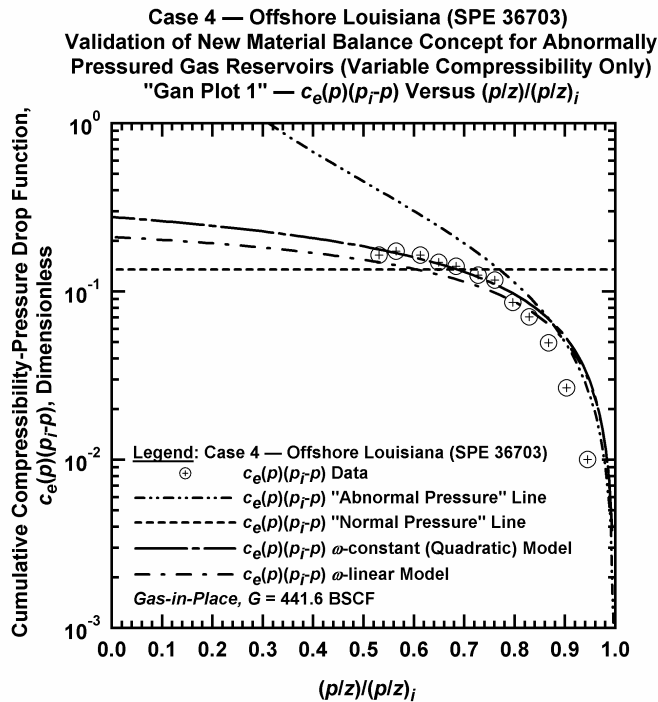


Figure D.5.n — Plot of $\bar{c}_e(p)(p_i - p)$ vs. $(p/z)/(p/z)_i$ — Case 4.

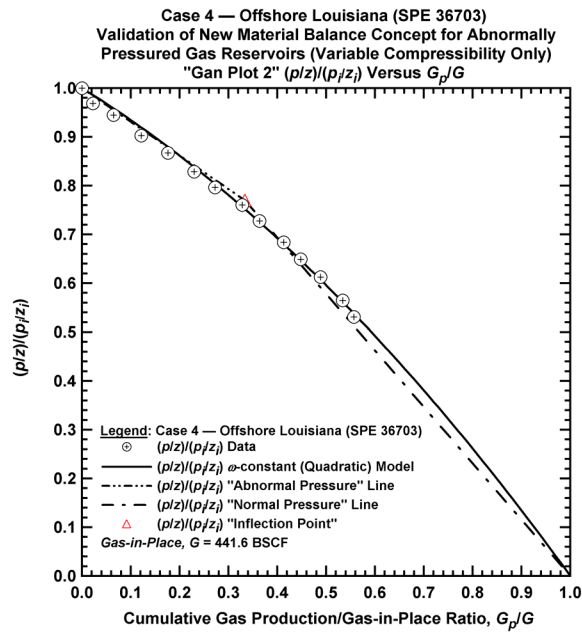


Figure D.5.o — Plot of $(p/z)/(p_i/z_i)$ vs. G_p/G — Case 4.

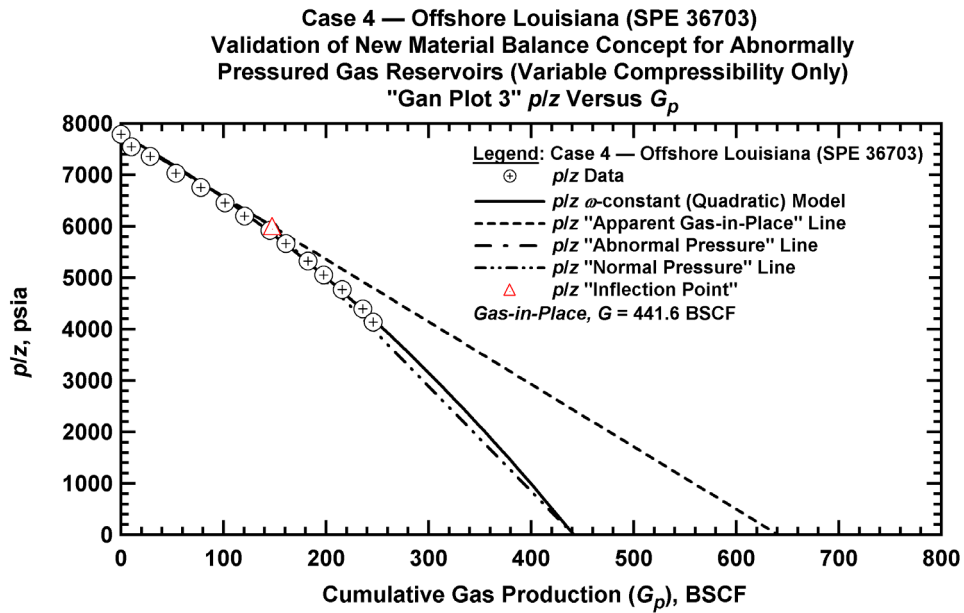


Figure D.5.p — Summary plot of p/z vs. G_p — Case 4.

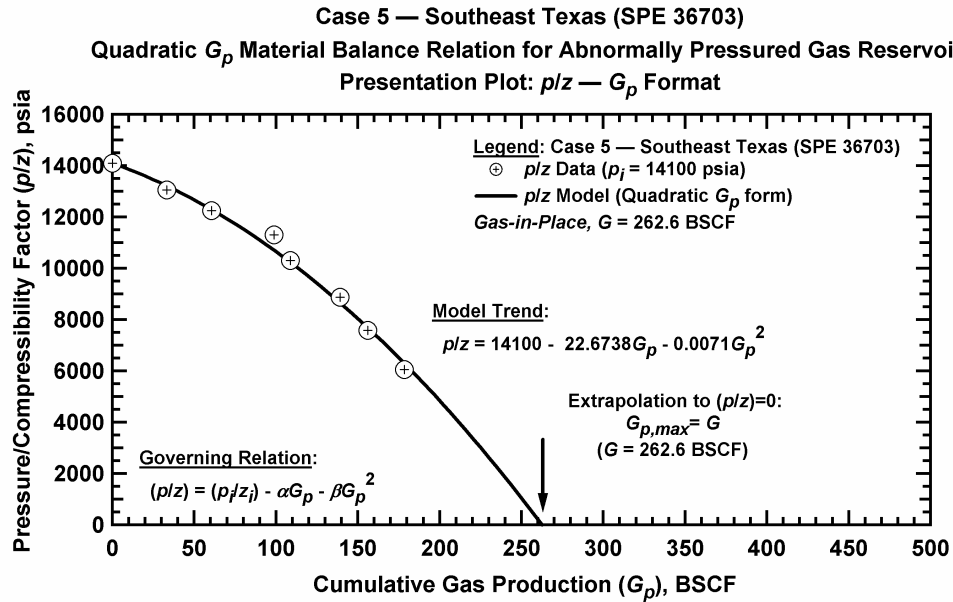


Figure D.6.a — Plot of p/z vs. G_p — Case 5.

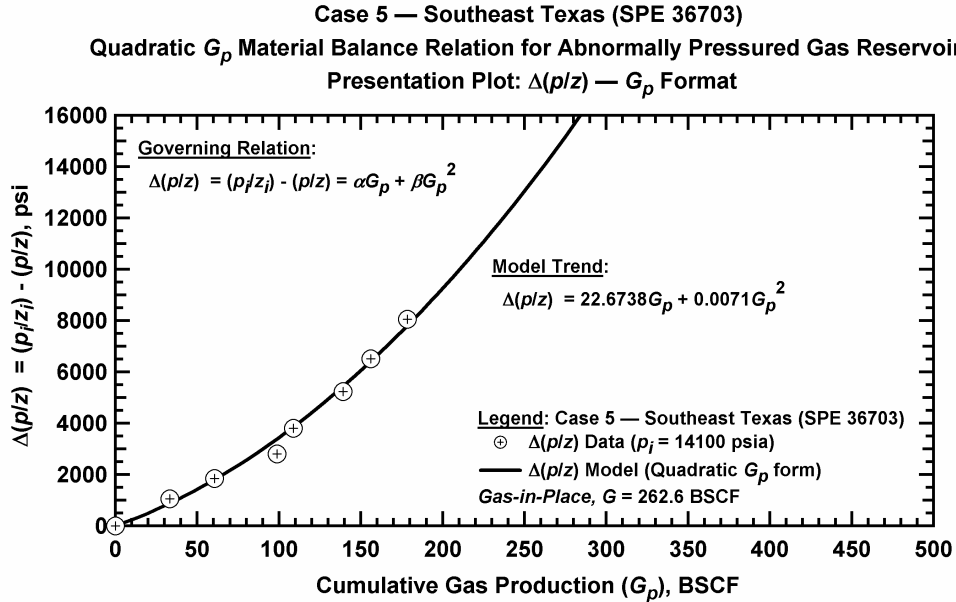


Figure D.6.b — Plot of $\Delta(p/z)$ vs. G_p — Case 5.

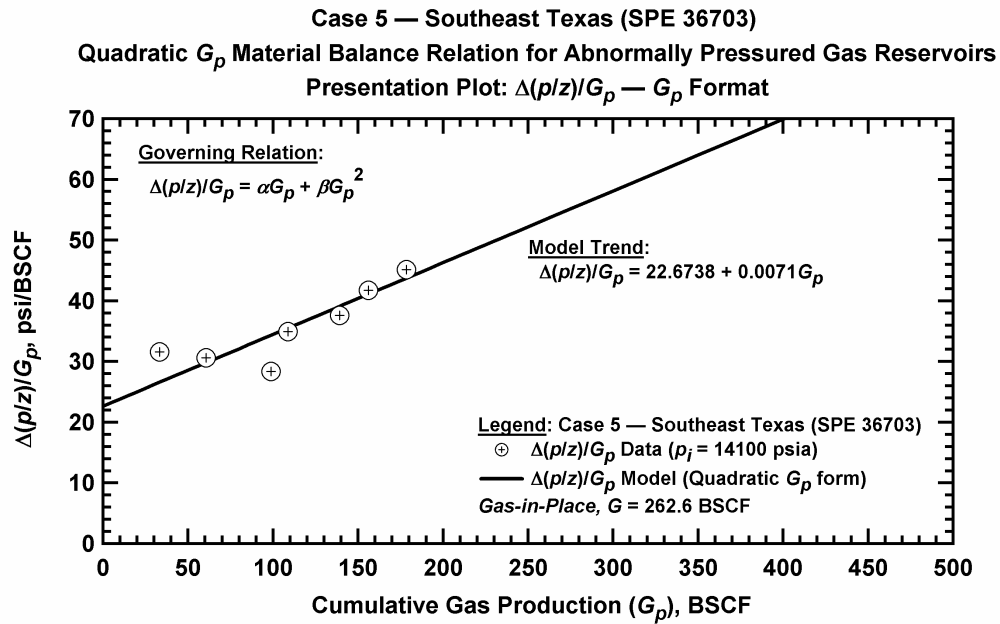


Figure D.6.c — Plot of $\Delta(p/z)/G_p$ vs. G_p — Case 5.

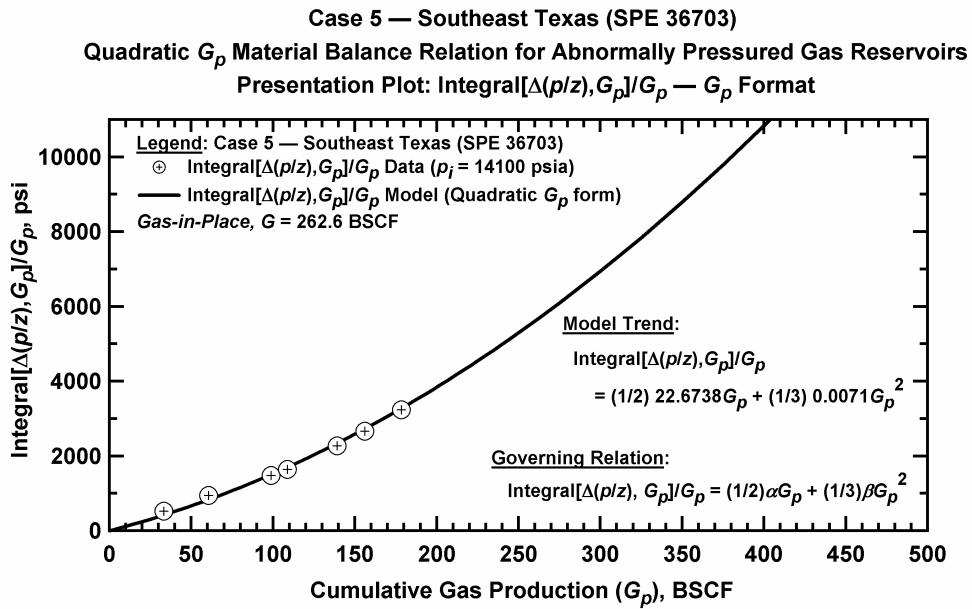


Figure D.6.d — Plot of $\frac{1}{G_p} \int_0^{G_p} \Delta(p/z) dG_p$ vs. G_p — Case 5.

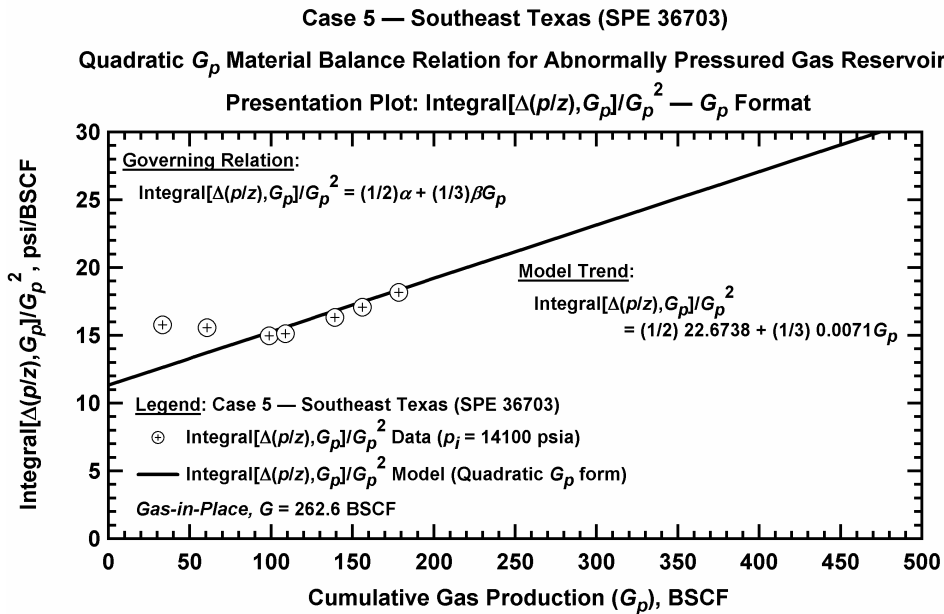


Figure D.6.e — Plot of $\frac{1}{G_p^2} \int_0^{G_p} \Delta(p/z) dG_p$ vs. G_p — Case 5.

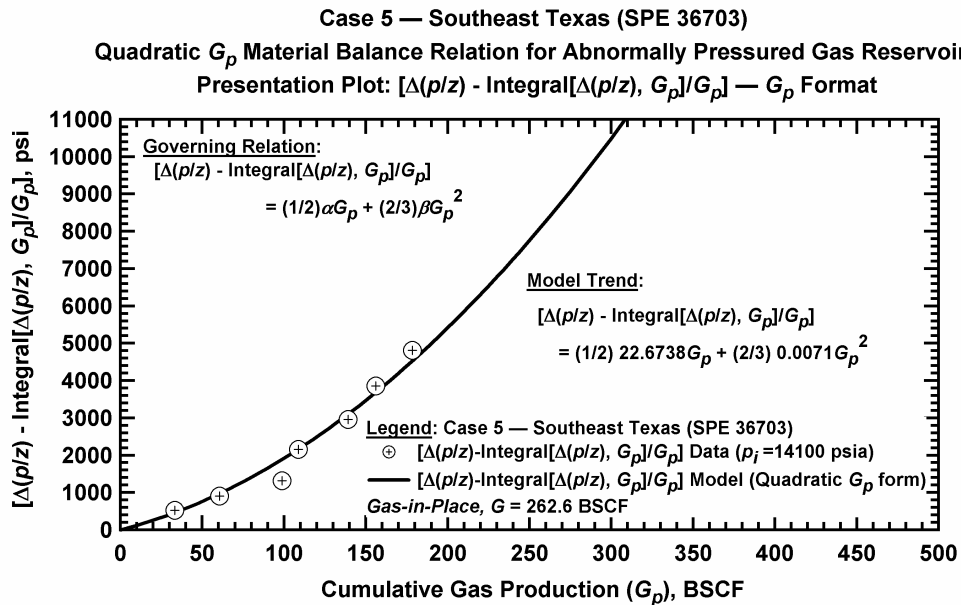


Figure D.6.f — Plot of $\Delta(p/z) - \frac{1}{G_p} \int_0^{G_p} \Delta(p/z) dG_p$ vs. G_p — Case 5.

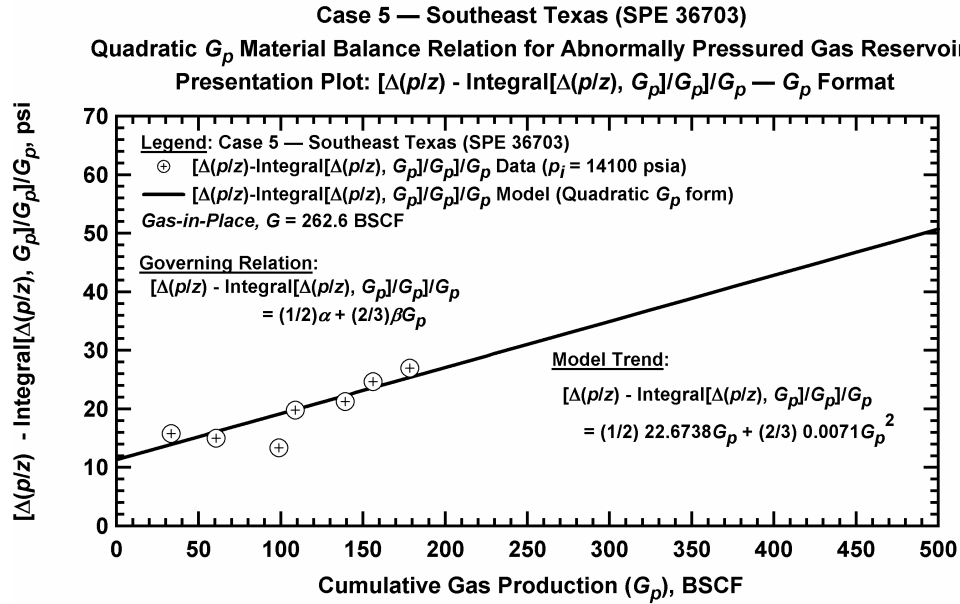


Figure D.6.g — Plot of $\frac{1}{G_p} \left[\Delta(p/z) - \frac{1}{G_p} \int_0^{G_p} \Delta(p/z) dG_p \right]$ vs. G_p — Case 5.

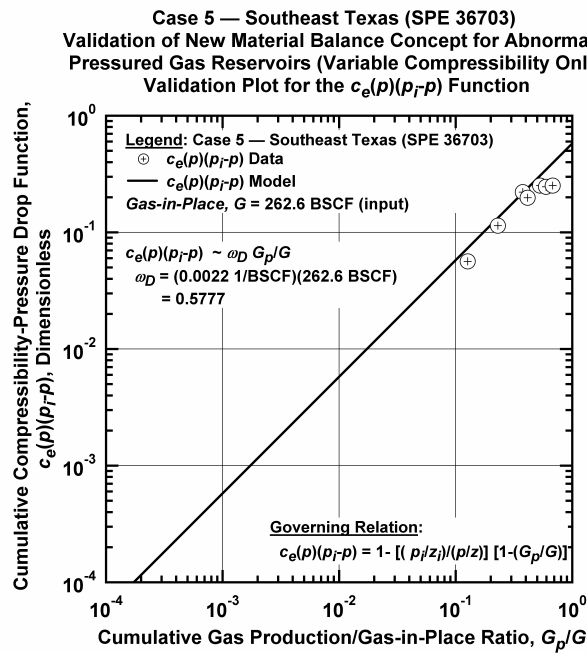


Figure D.6.h — Plot of $\bar{c}_e(p)(p_i - p)$ vs. G_p/G — Case 5.

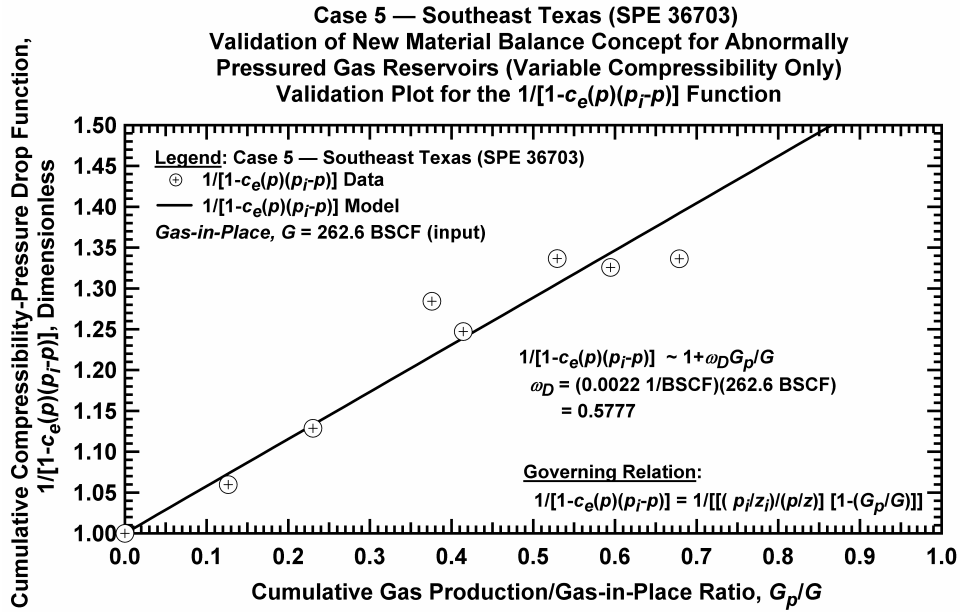


Figure D.6.i — Plot of $1/[1-\bar{c}_e(p)(p_i-p)]$ vs. G_p/G — Case 5.

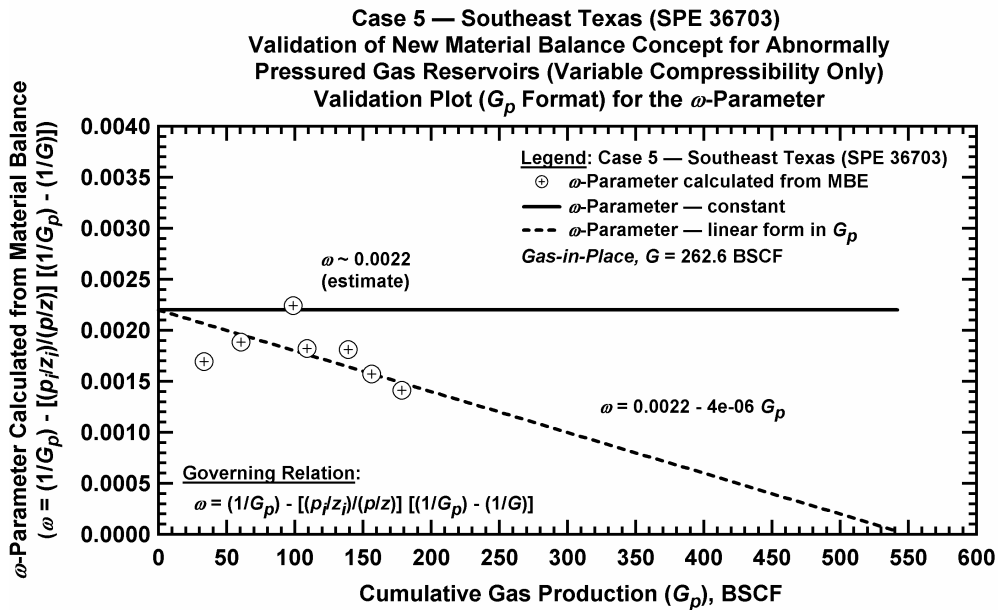


Figure D.6.j — Plot of ω vs. G_p — Case 5.

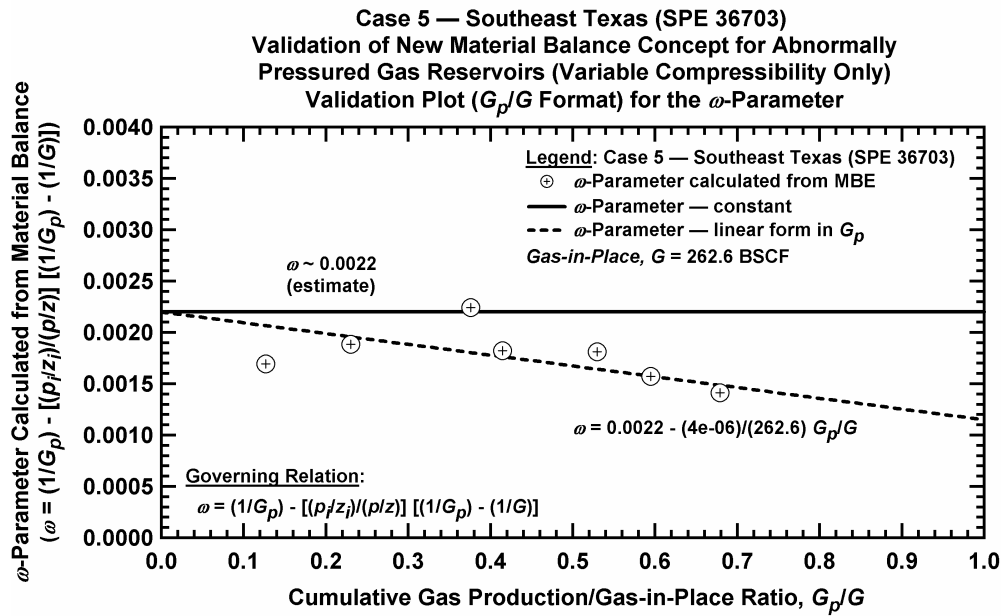


Figure D.6.k — Plot of ω vs. G_p/G — Case 5.

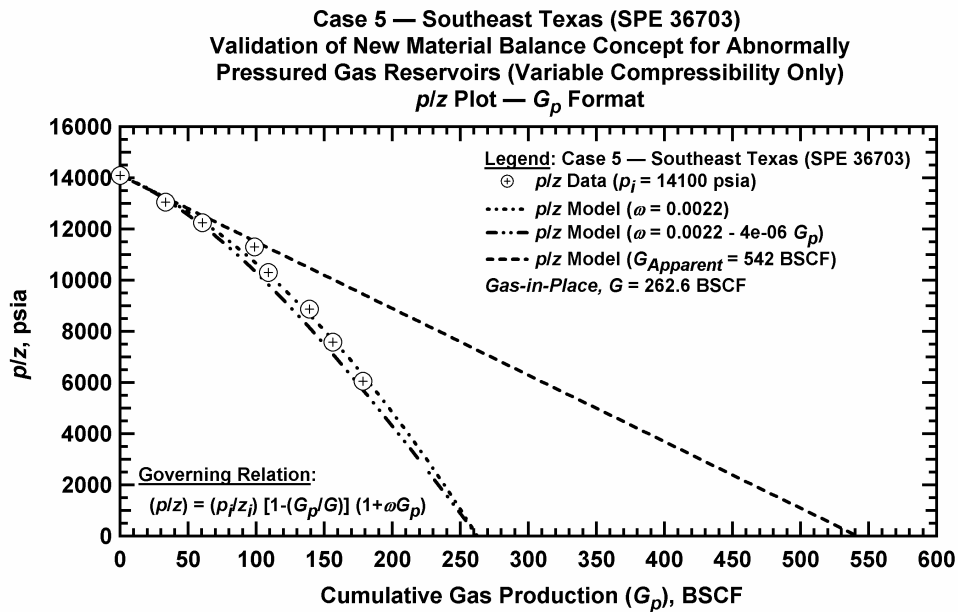


Figure D.6.l — Comparison plot of p/z vs. G_p — Case 5.

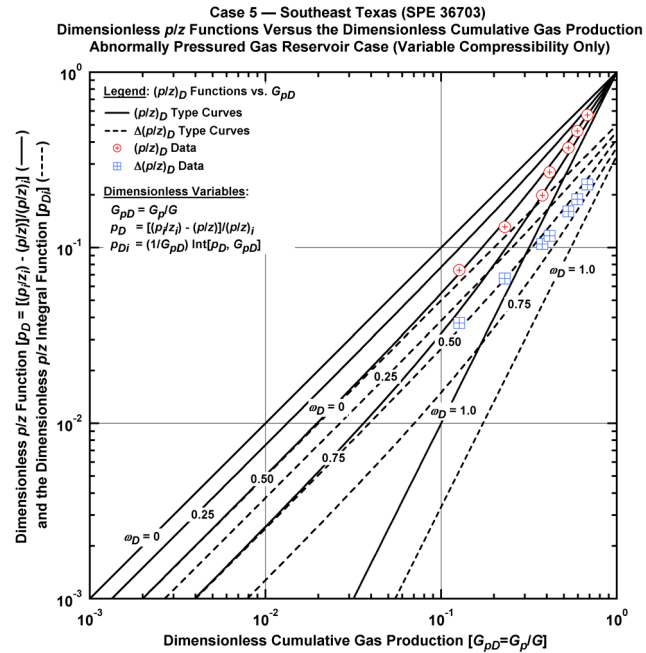


Figure D.6.m — Plot of dimensionless p/z functions vs. G_{pD} — Case 5.

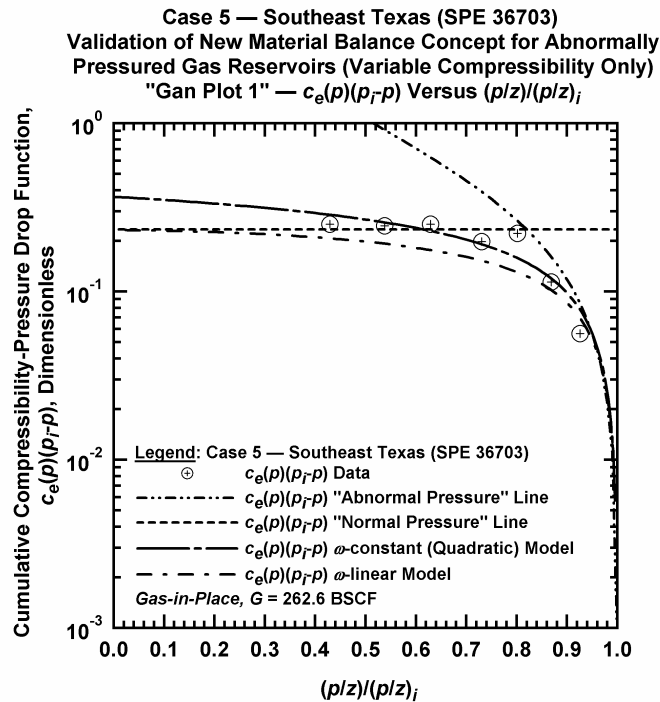


Figure D.6.n — Plot of $\bar{c}_e(p)(p_i - p)$ vs. $(p/z)/(p/z)_i$ — Case 5.

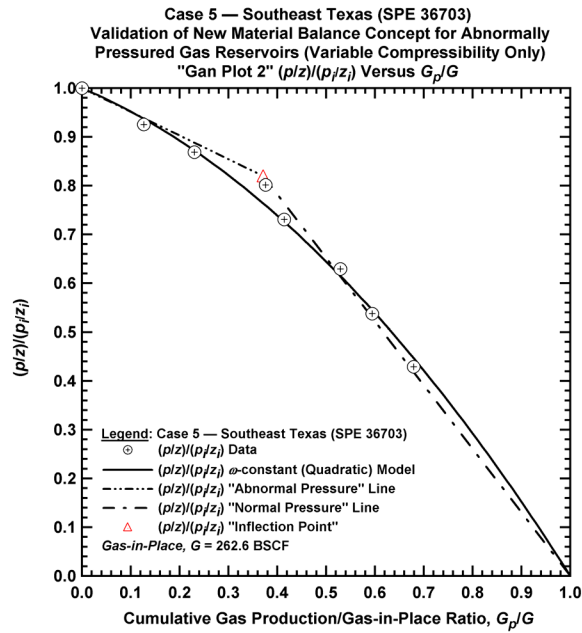


Figure D.6.o — Plot of $(p/z)/(p/z_i)$ vs. G_p/G — Case 5.

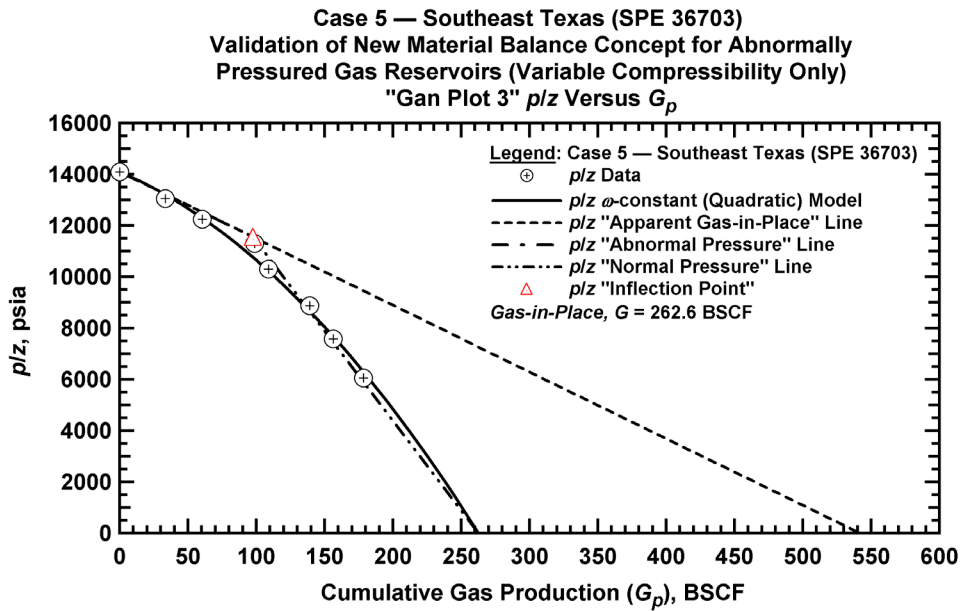


Figure D.6.p — Summary plot of p/z vs. G_p — Case 5.

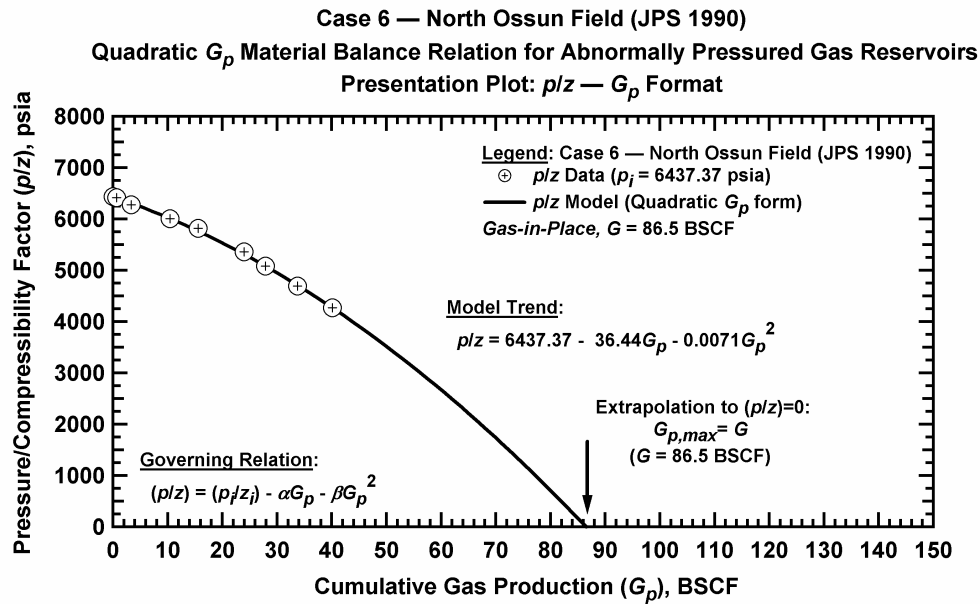


Figure D.7.a — Plot of p/z vs. G_p — Case 6

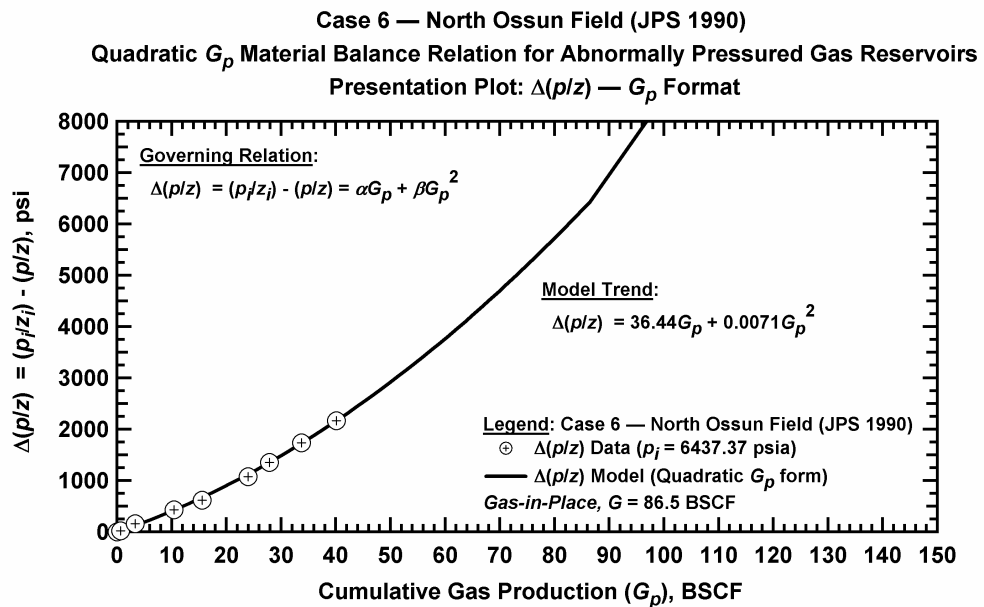


Figure D.7.b — Plot of $\Delta(p/z)$ vs. G_p — Case 6.

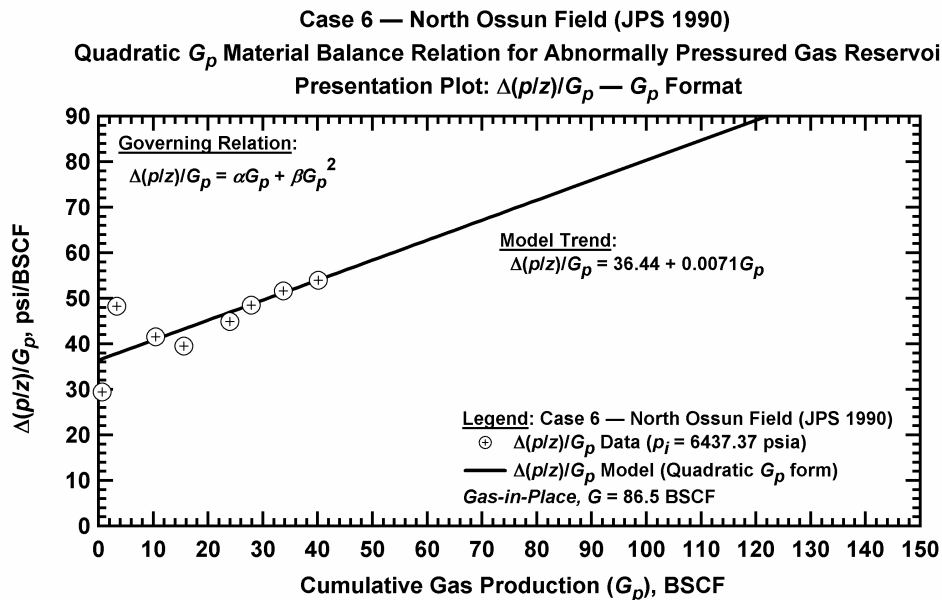


Figure D.7.c — Plot of $\Delta(p/z)/G_p$ vs. G_p — Case 6.

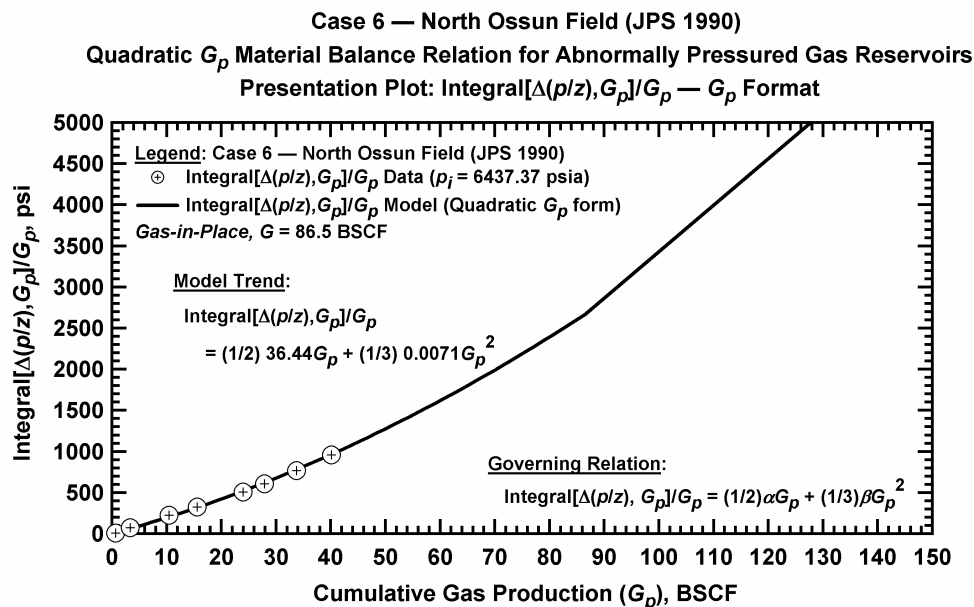


Figure D.7.d — Plot of $\frac{1}{G_p} \int_0^{G_p} \Delta(p/z) dG_p$ vs. G_p — Case 6.

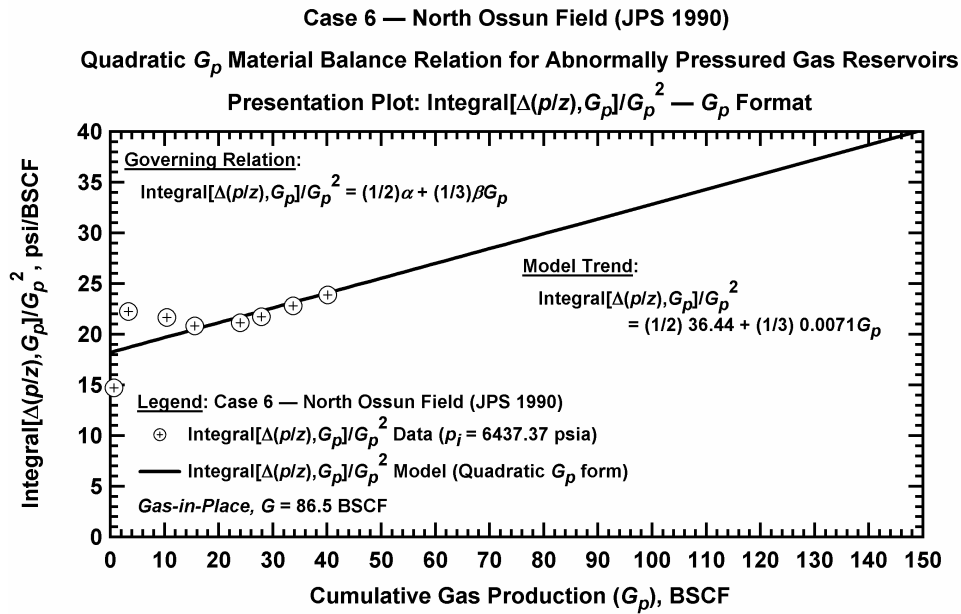


Figure D.7.e — Plot of $\frac{1}{G_p^2} \int_0^{G_p} \Delta(p/z) dG_p$ vs. G_p — Case 6.

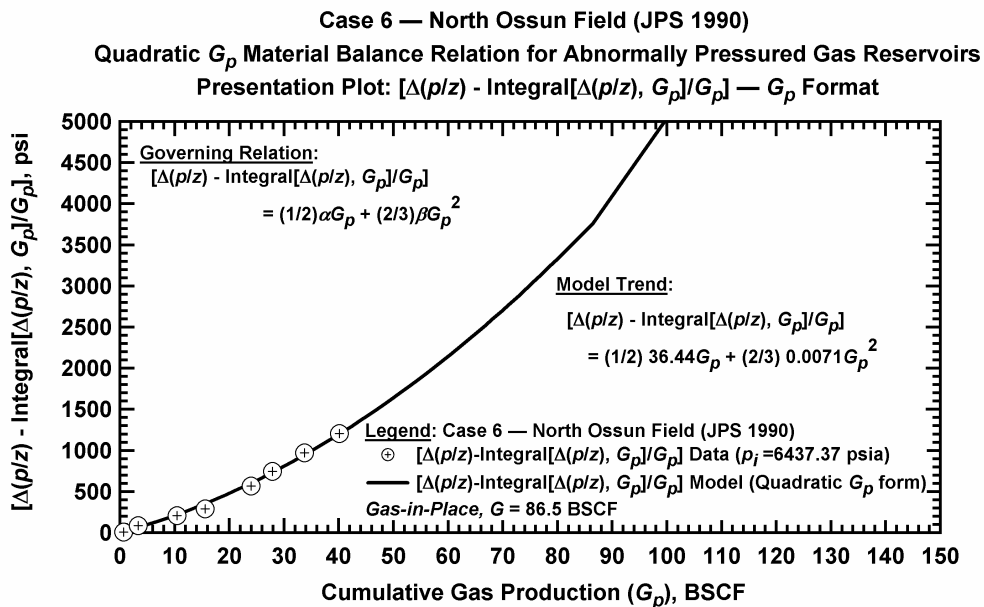


Figure D.7.f — Plot of $\Delta(p/z) - \frac{1}{G_p} \int_0^{G_p} \Delta(p/z) dG_p$ vs. G_p — Case 6.

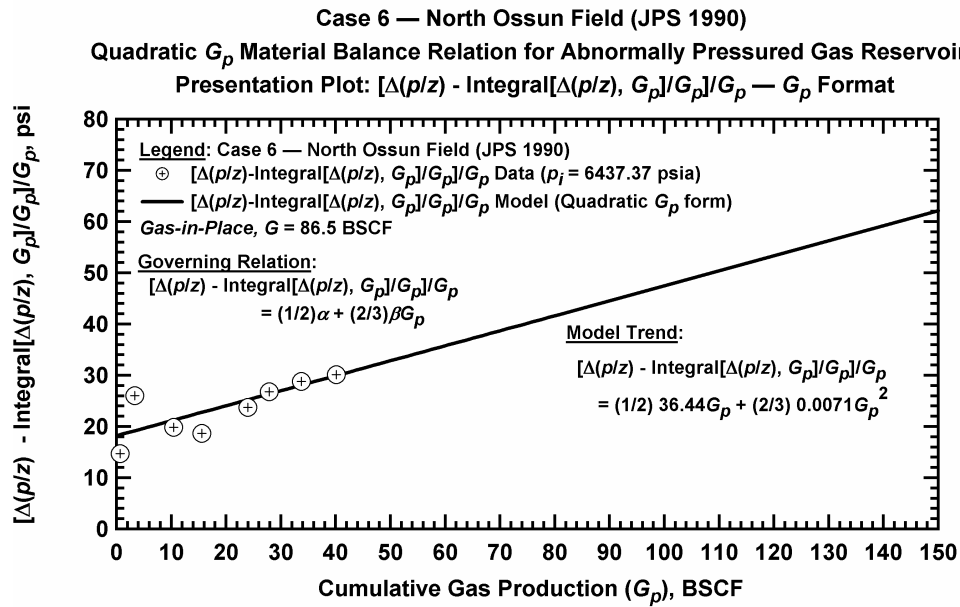


Figure D.7.g — Plot of $\frac{1}{G_p} \left[\Delta(p/z) - \frac{1}{G_p} \int_0^{G_p} \Delta(p/z) dG_p \right]$ vs. G_p — Case 6.

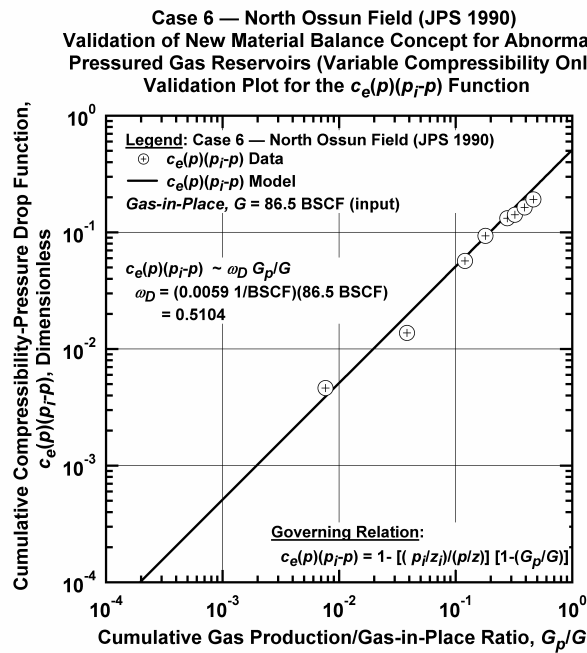


Figure D.7.h — Plot of $\bar{c}_e(p)(p_i - p)$ vs. G_p/G — Case 6.

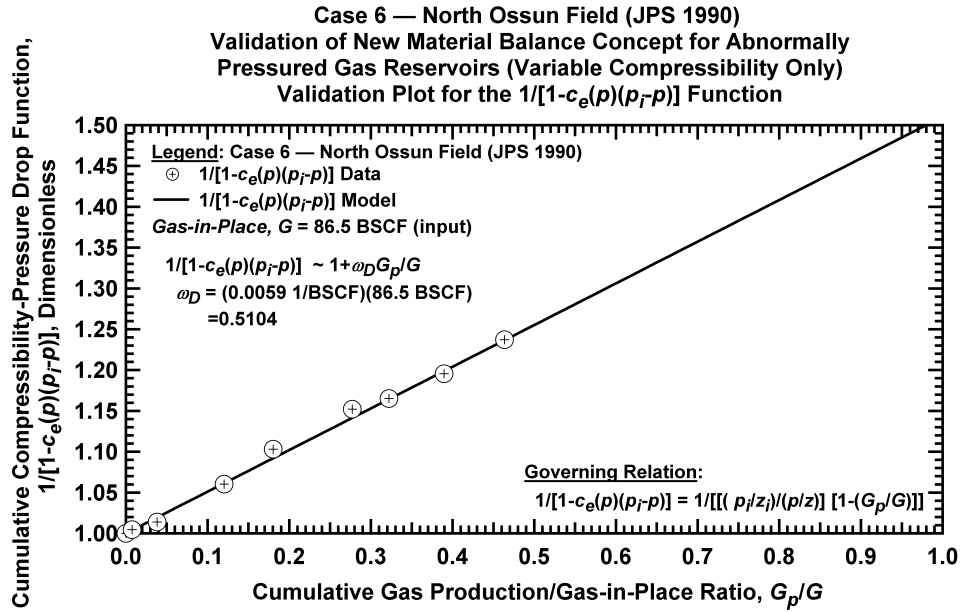


Figure D.7.i — Plot of $1/[1-\bar{c}_e(p)(p_i-p)]$ vs. G_p/G — Case 6.

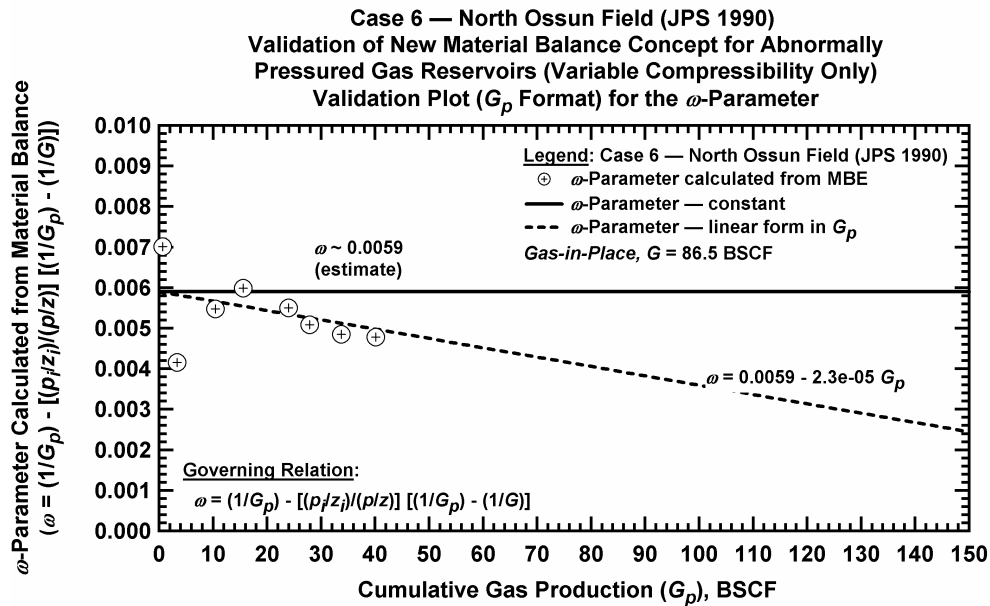


Figure D.7.j — Plot of ω vs. G_p — Case 6.

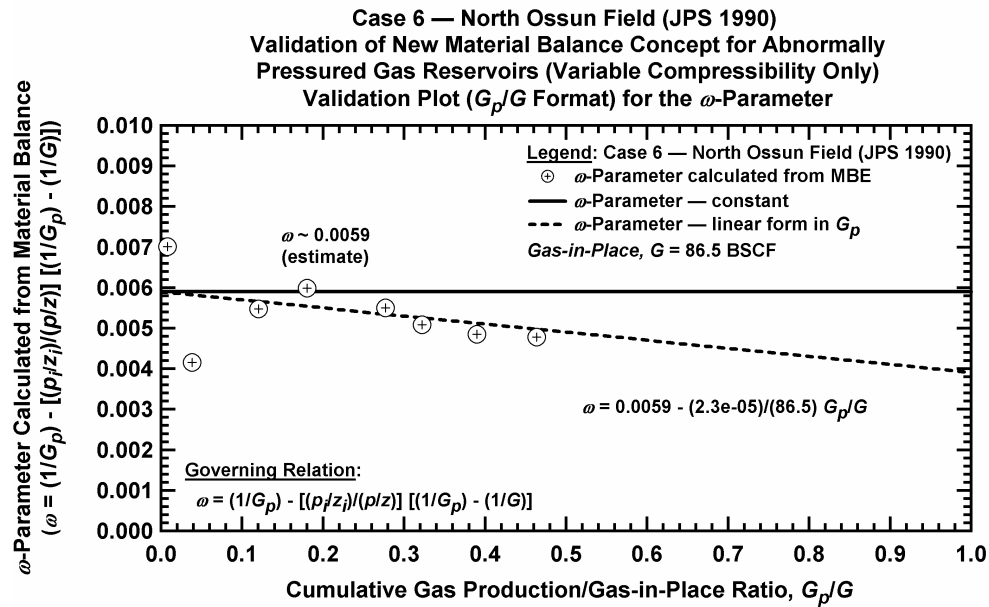


Figure D.7.k — Plot of ω vs. G_p/G — Case 6.

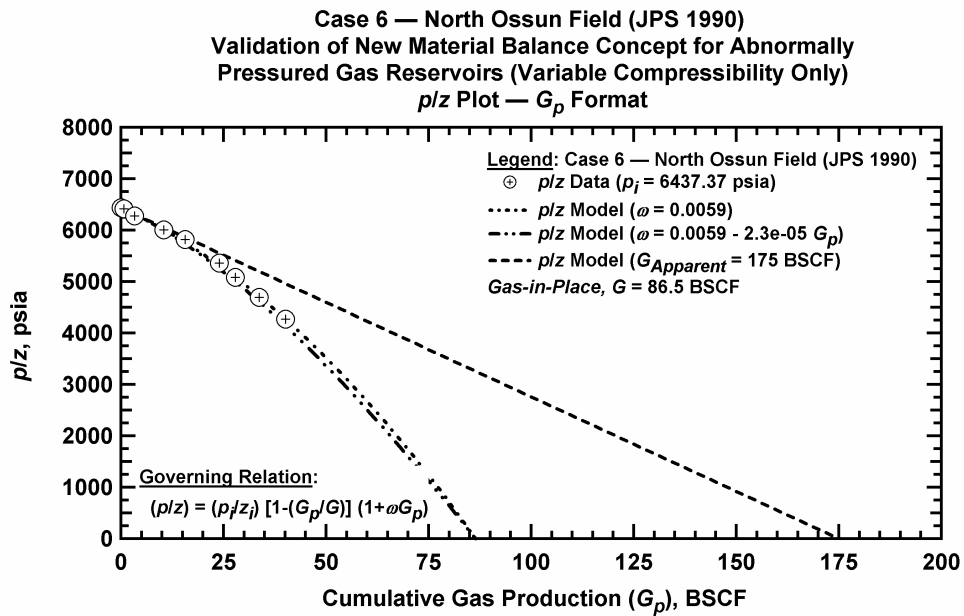


Figure D.7.l — Comparison plot of p/z vs. G_p — Case 6.

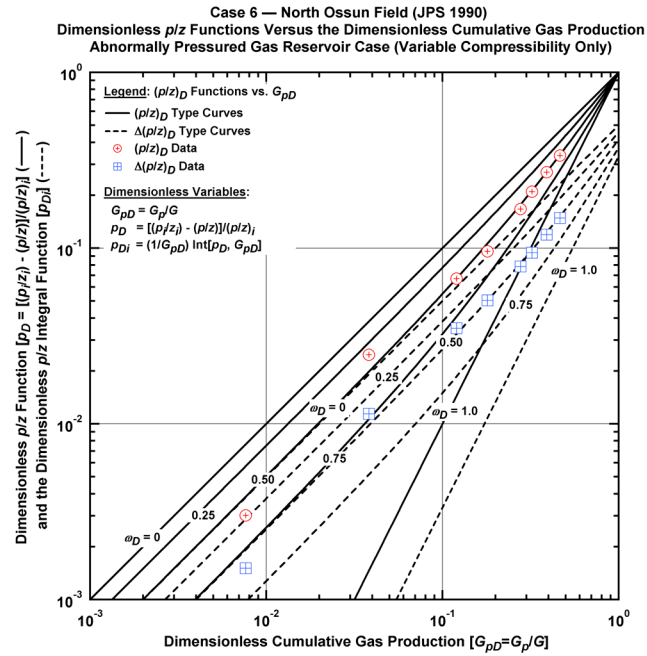


Figure D.7.m — Plot of dimensionless p/z functions vs. G_{pD} — Case 6.

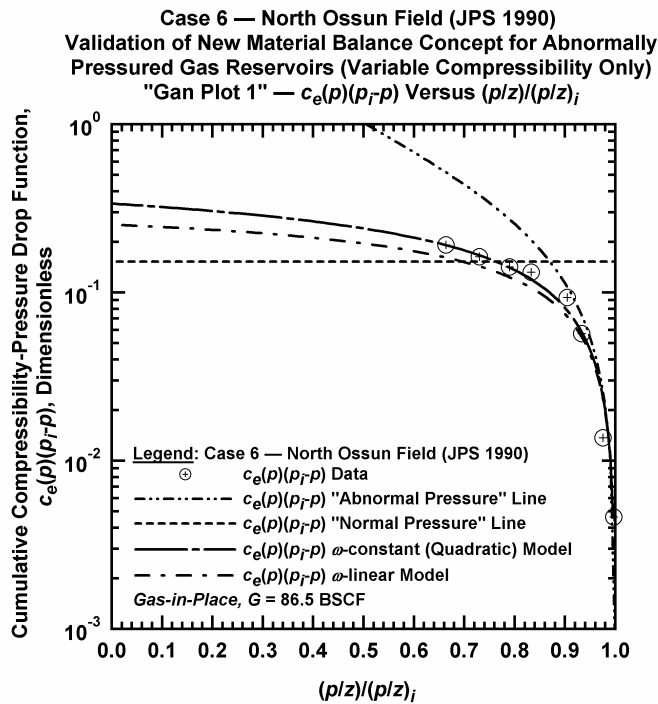


Figure D.7.n — Plot of $\bar{c}_e(p)(p_i - p)$ vs. $(p/z)/(p/z)_i$ — Case 6.

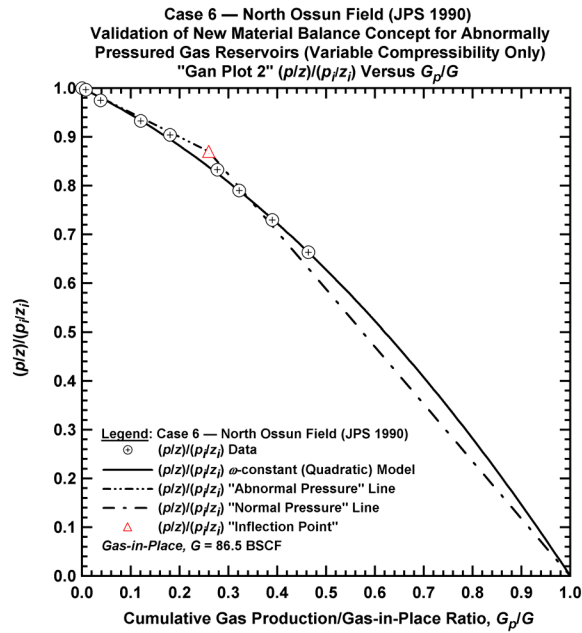


Figure D.7.o — Plot of $(p/z)/(p/z_i)$ vs. G_p/G — Case 6.

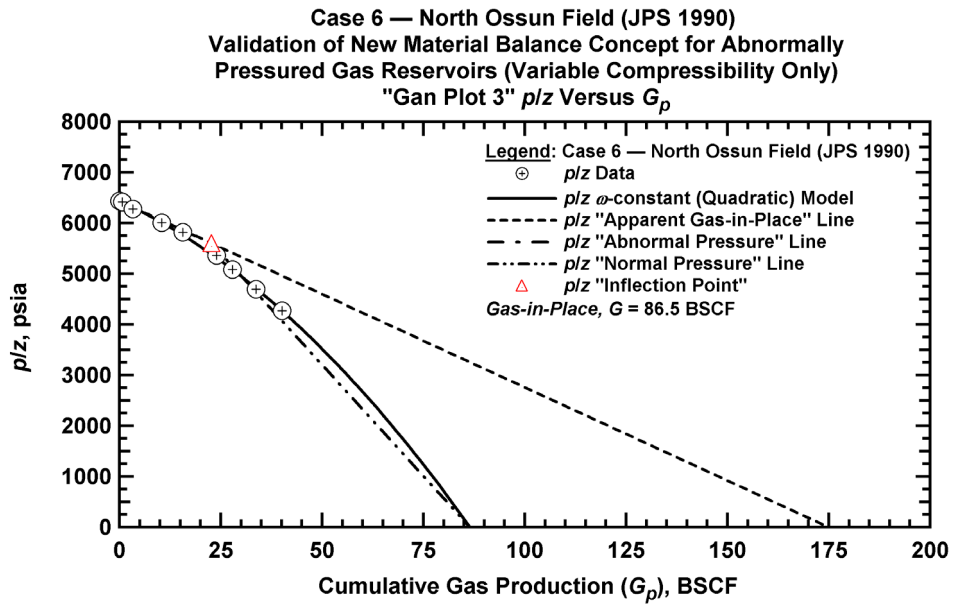


Figure D.7.p — Summary plot of p/z vs. G_p — Case 6.

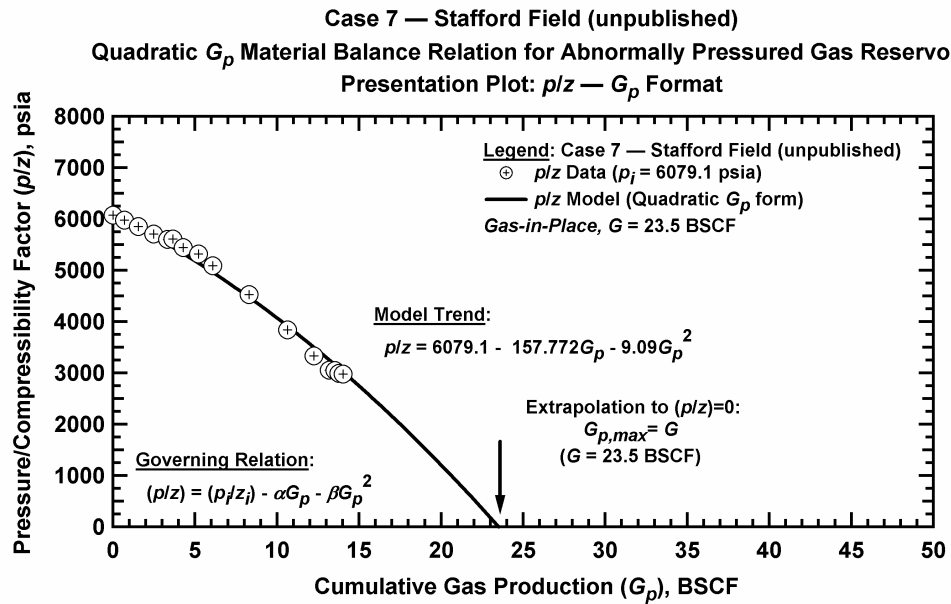


Figure D.8.a — Base plot of p/z vs. G_p — Case 7.

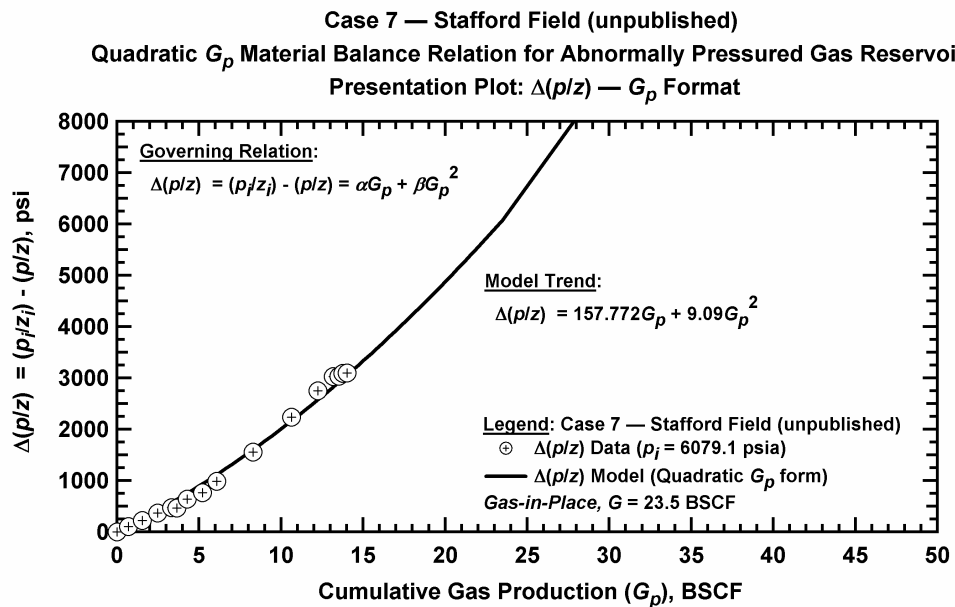


Figure D.8.b — Plot of $\Delta(p/z)$ vs. G_p — Case 7.

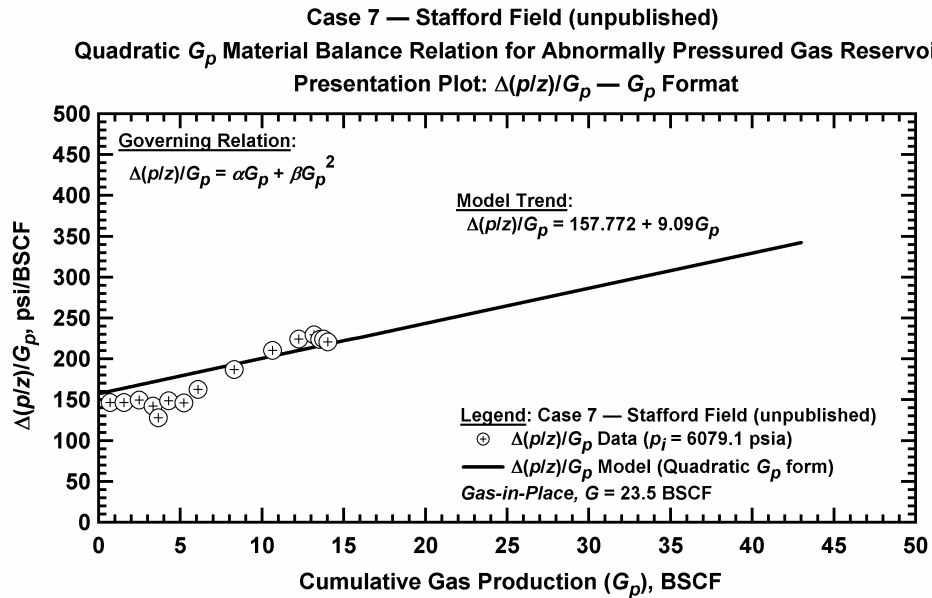


Figure D.8.c — Plot of $\Delta(p/z)/G_p$ vs. G_p — Case 7.

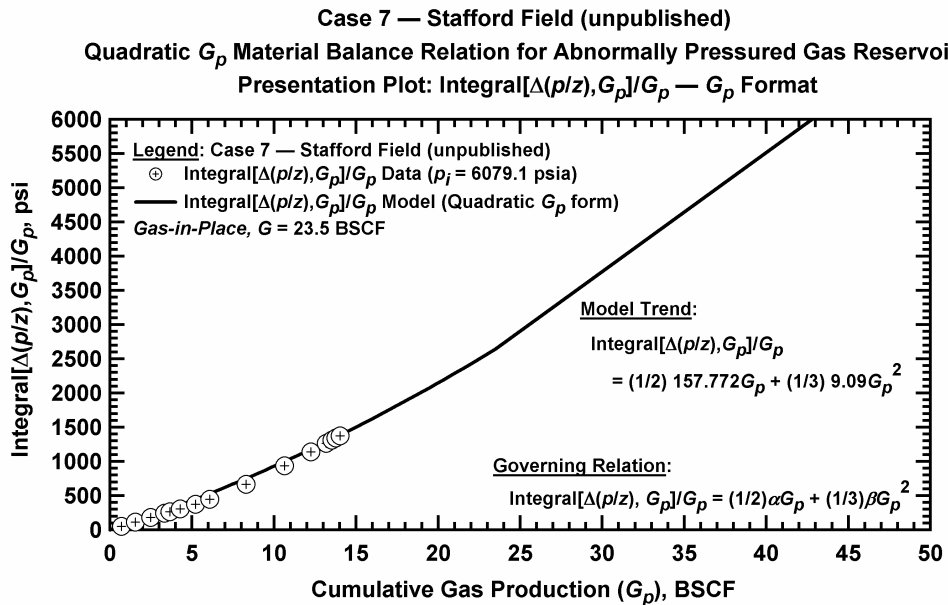


Figure D.8.d — Plot of $\frac{1}{G_p} \int_0^{G_p} \Delta(p/z) dG_p$ vs. G_p — Case 7.

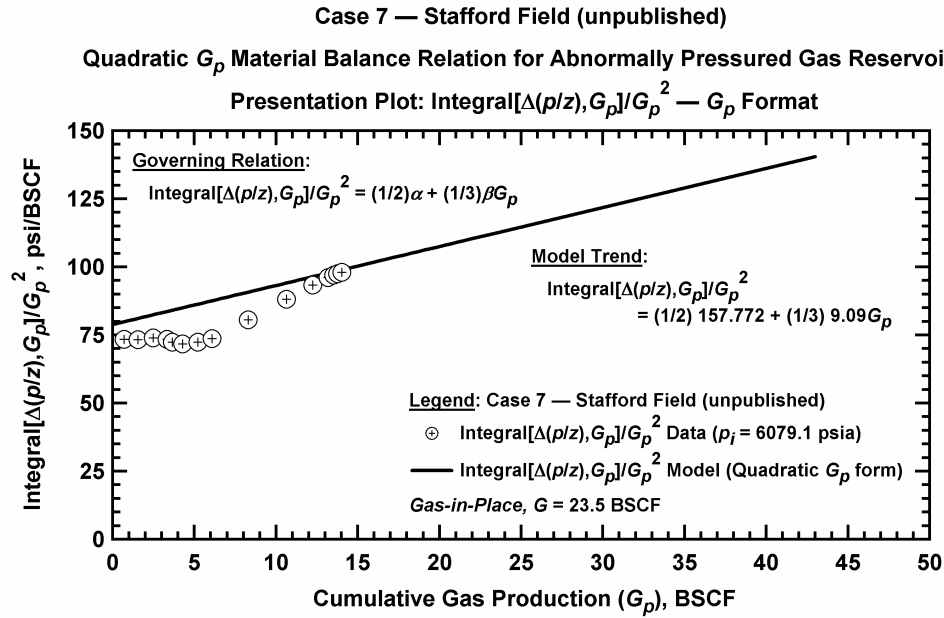


Figure D.8.e — Plot of $\frac{1}{G_p^2} \int_0^{G_p} \Delta(p/z) dG_p$ vs. G_p — Case 7.

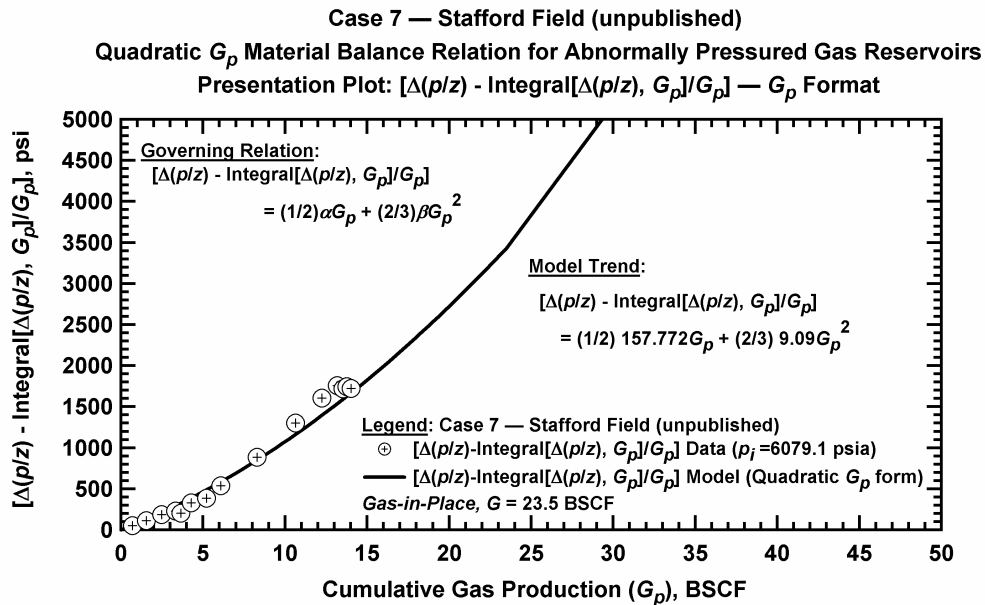


Figure D.8.f — Plot of $\Delta(p/z) - \frac{1}{G_p} \int_0^{G_p} \Delta(p/z) dG_p$ vs. G_p — Case 7.

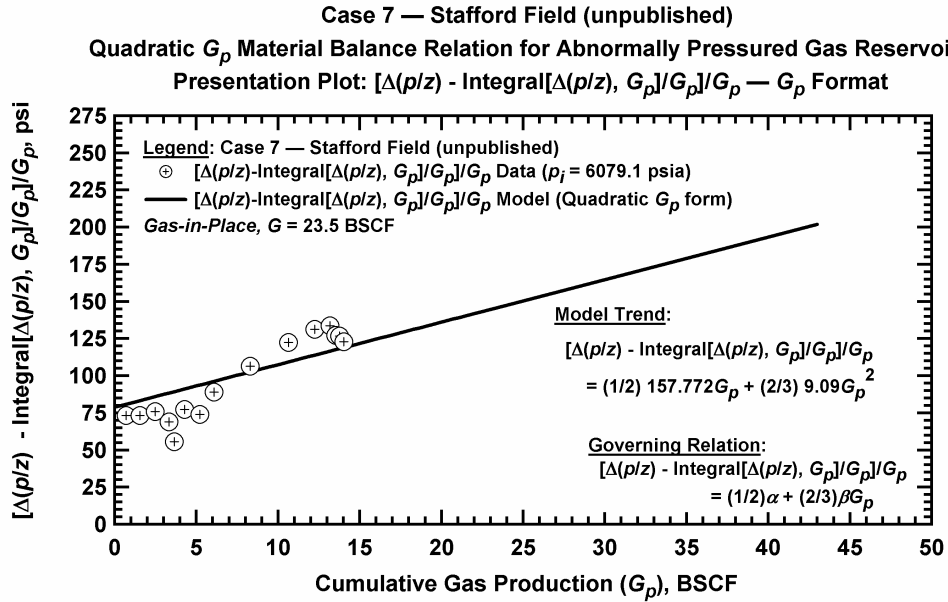


Figure D.8.g — Plot of $\frac{1}{G_p} \left[\Delta(p/z) - \frac{1}{G_p} \int_0^{G_p} \Delta(p/z) dG_p \right]$ vs. G_p — Case 7.

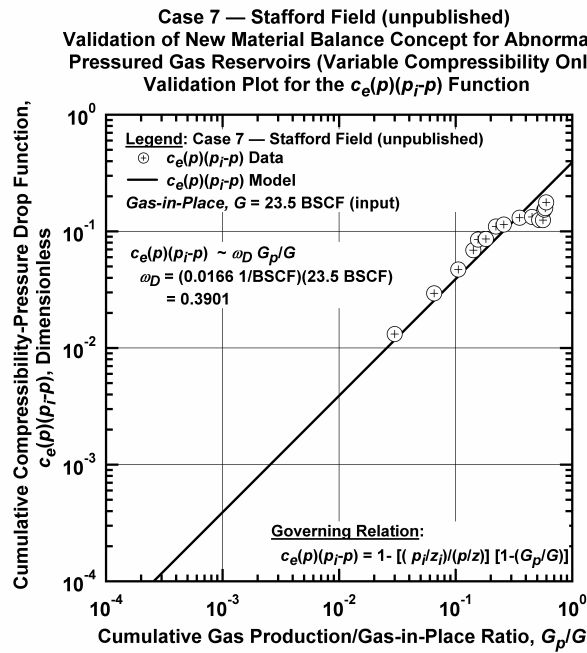


Figure D.8.h — Plot of $\bar{c}_e(p)(p_i - p)$ vs. G_p/G — Case 7.

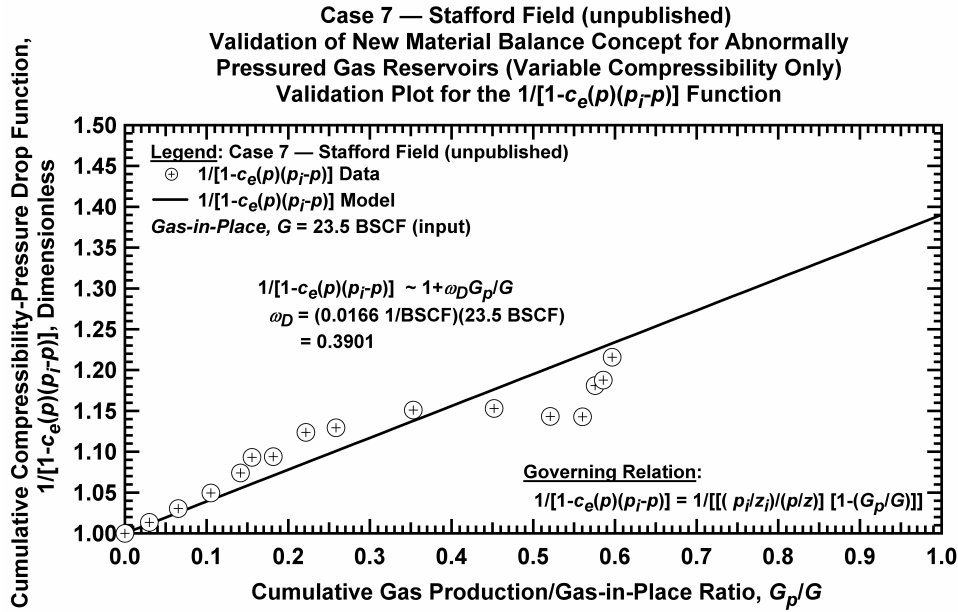


Figure D.8.i — Plot of $1/[1-\bar{c}_e(p)(p_i - p)]$ vs. G_p/G — Case 7.

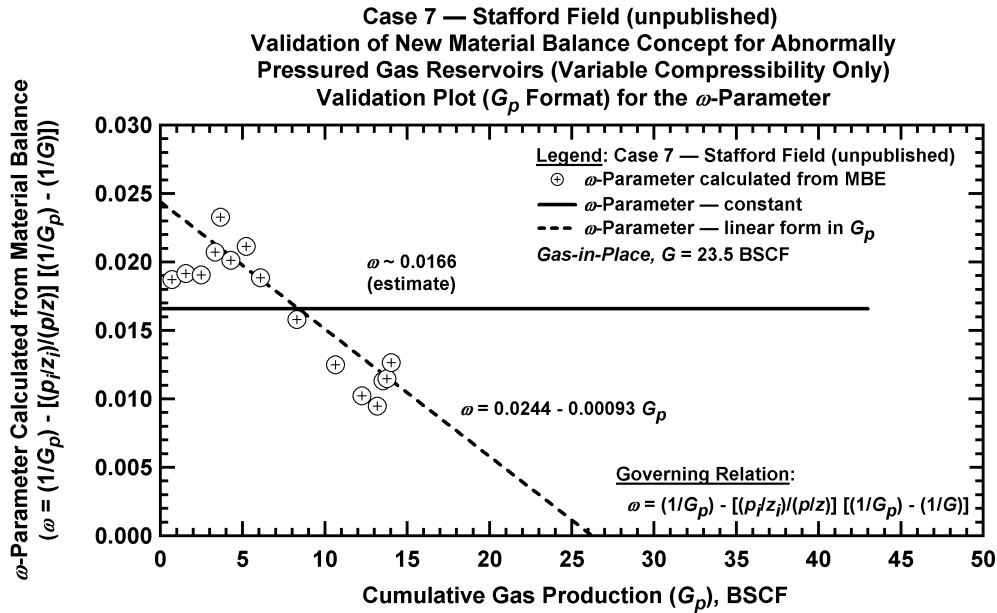


Figure D.8.j — Plot of ω vs. G_p — Case 7.

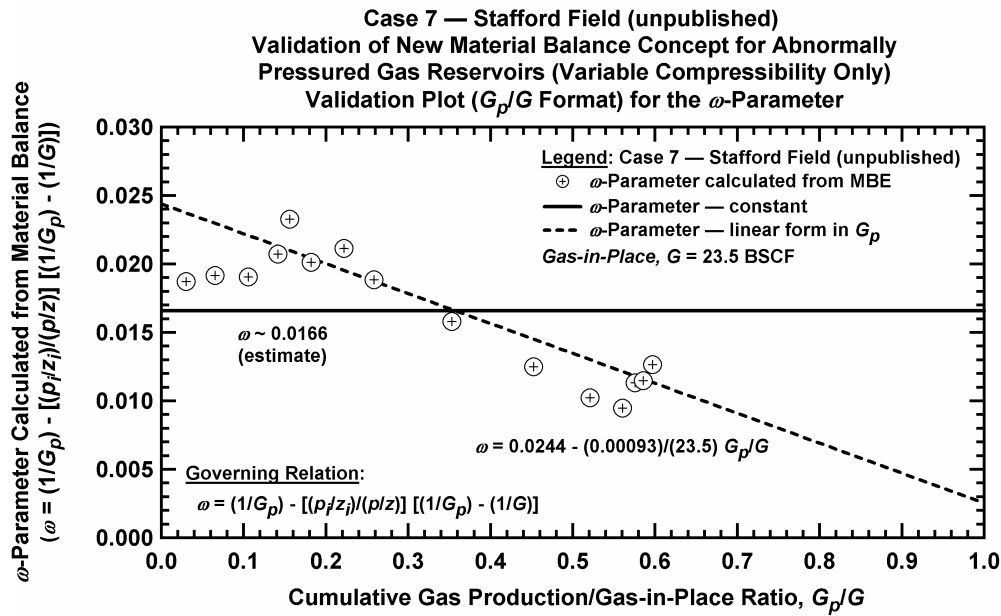


Figure D.8.k — Plot of ω vs. G_p/G — Case 7.

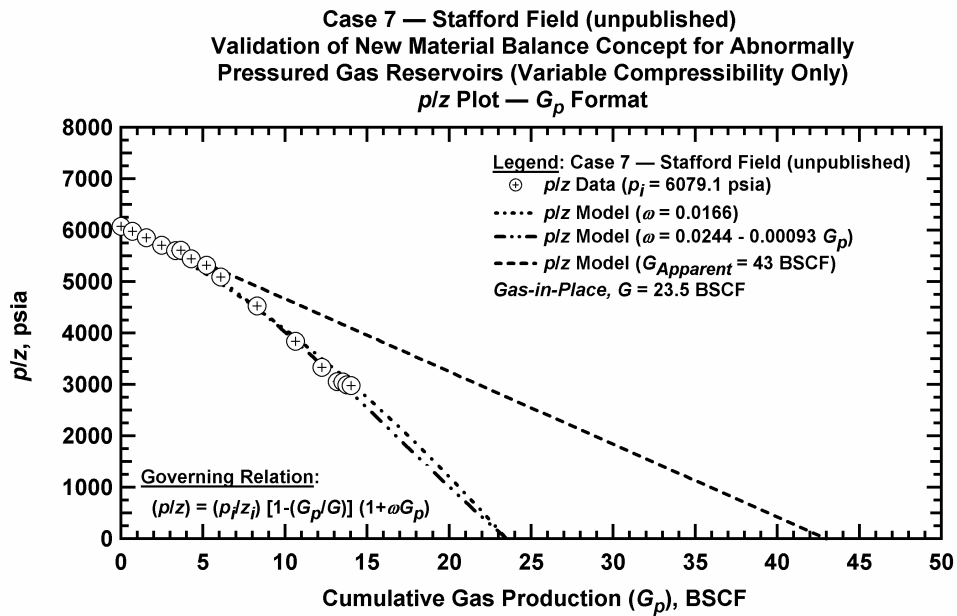


Figure D.8.l — Comparison plot of p/z vs. G_p — Case 7.

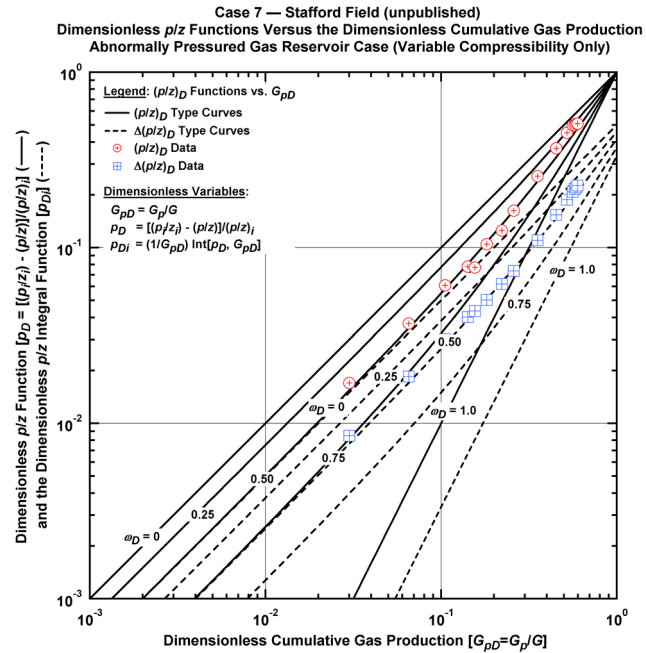


Figure D.8.m — Plot of dimensionless p/z functions vs. G_{pD} — Case 7.

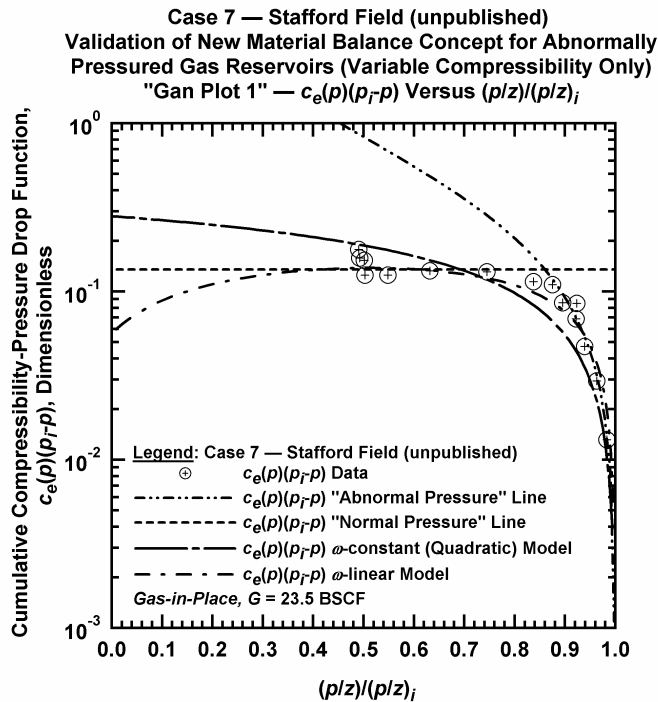


Figure D.8.n — Plot of $\bar{c}_e(p)(p_i - p)$ vs. $(p/z)/(p/z)_i$ — Case 7.

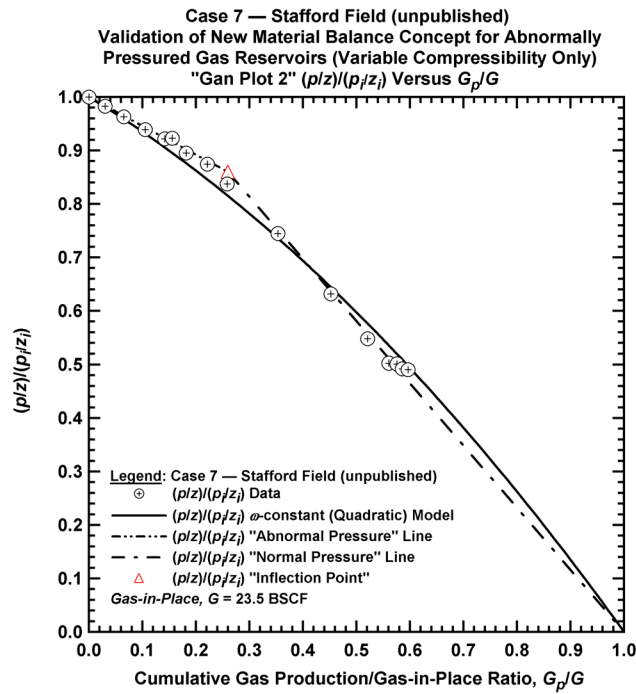


Figure D.8.o — Plot of $(p/z)/(p/z_i)$ vs. G_p/G — Case 7.

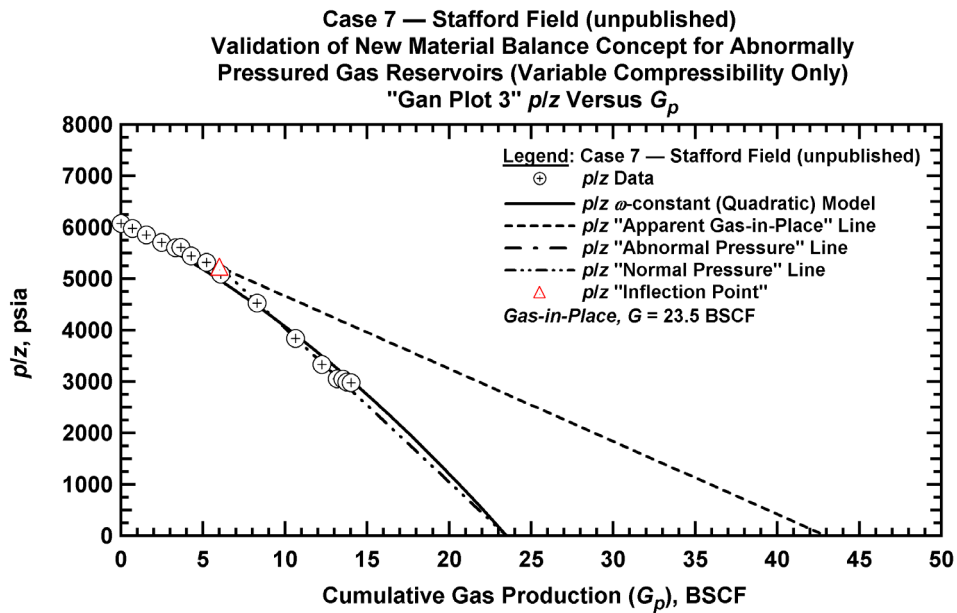


Figure D.8.p — Summary plot of p/z vs. G_p — Case 7.

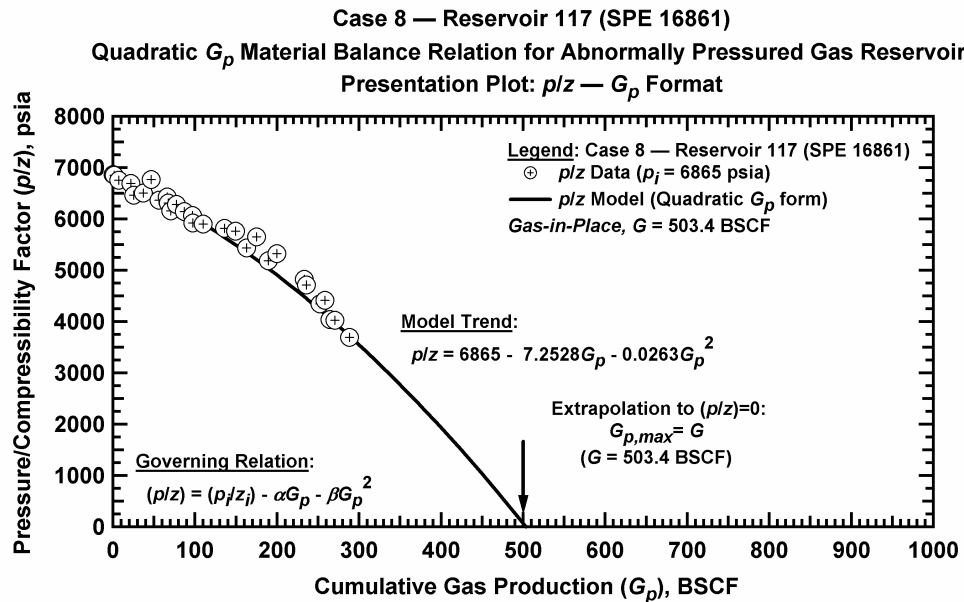


Figure D.9.a — Base plot of p/z vs. G_p — Case 8.

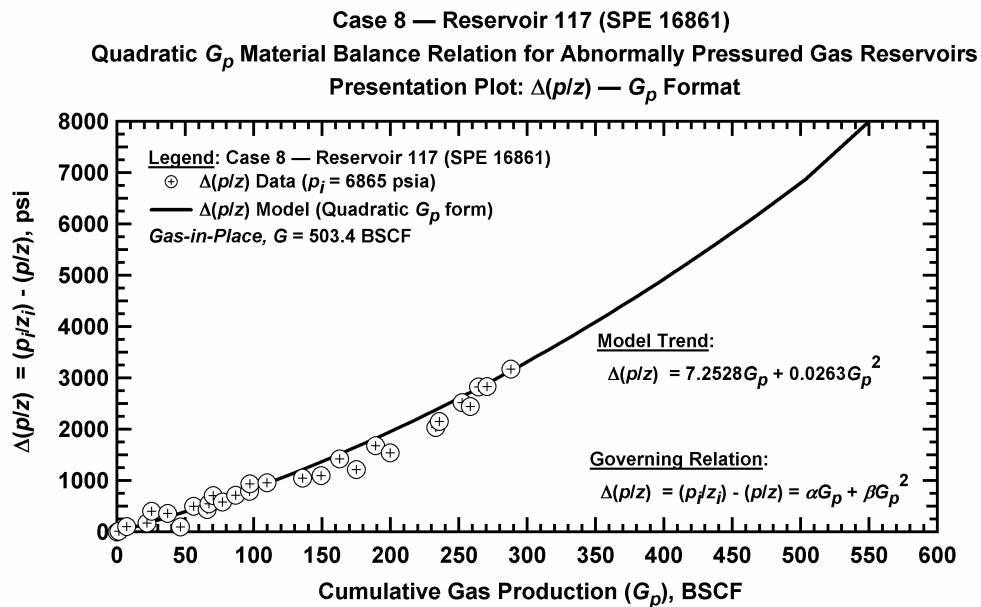


Figure D.9.b — Plot of $\Delta(p/z)$ vs. G_p — Case 8.

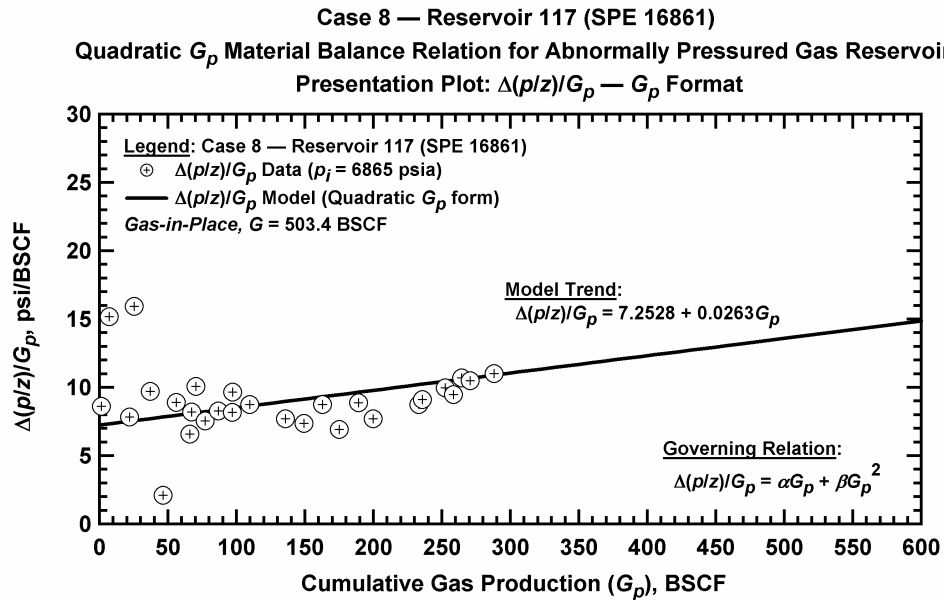


Figure D.9.c — Plot of $\Delta(p/z)/G_p$ vs. G_p — Case 8.

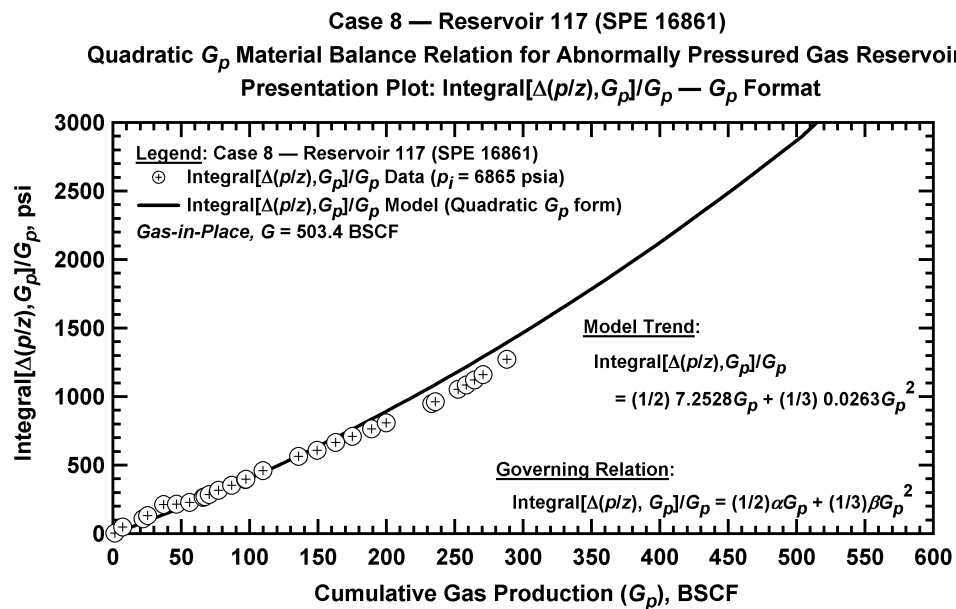


Figure D.9.d — Plot of $\frac{1}{G_p} \int_0^{G_p} \Delta(p/z) dG_p$ vs. G_p — Case 8.

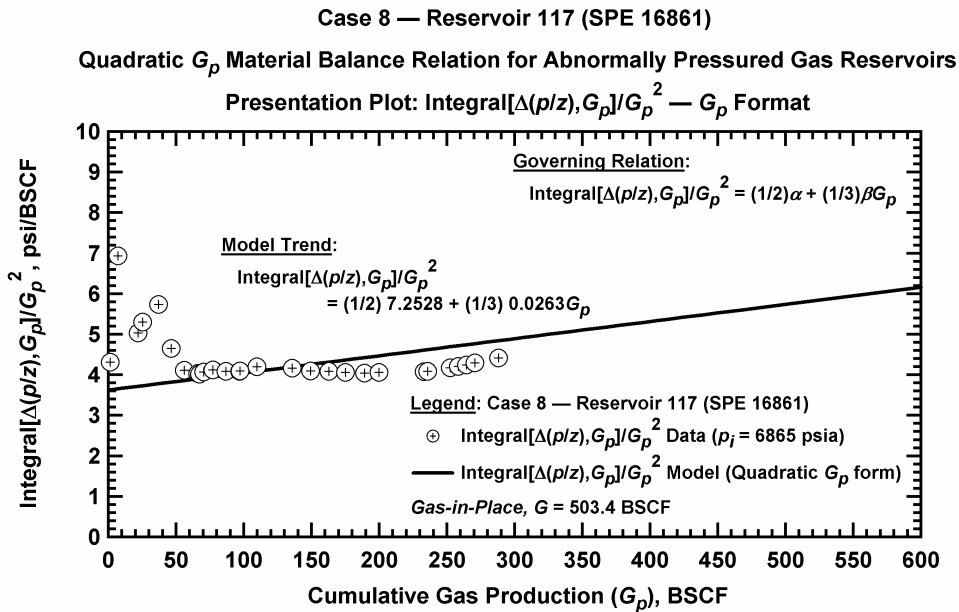


Figure D.9.e — Plot of $\frac{1}{G_p^2} \int_0^{G_p} \Delta(p/z) dG_p$ vs. G_p — Case 8.

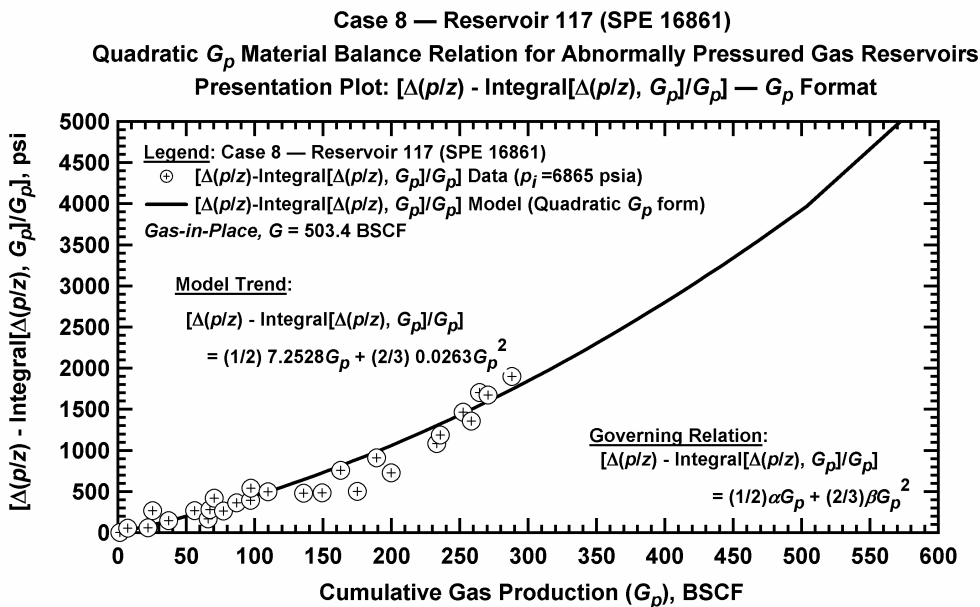


Figure D.9.f — Plot of $[\Delta(p/z) - \frac{1}{G_p} \int_0^{G_p} \Delta(p/z) dG_p] - G_p$ vs. G_p — Case 8.

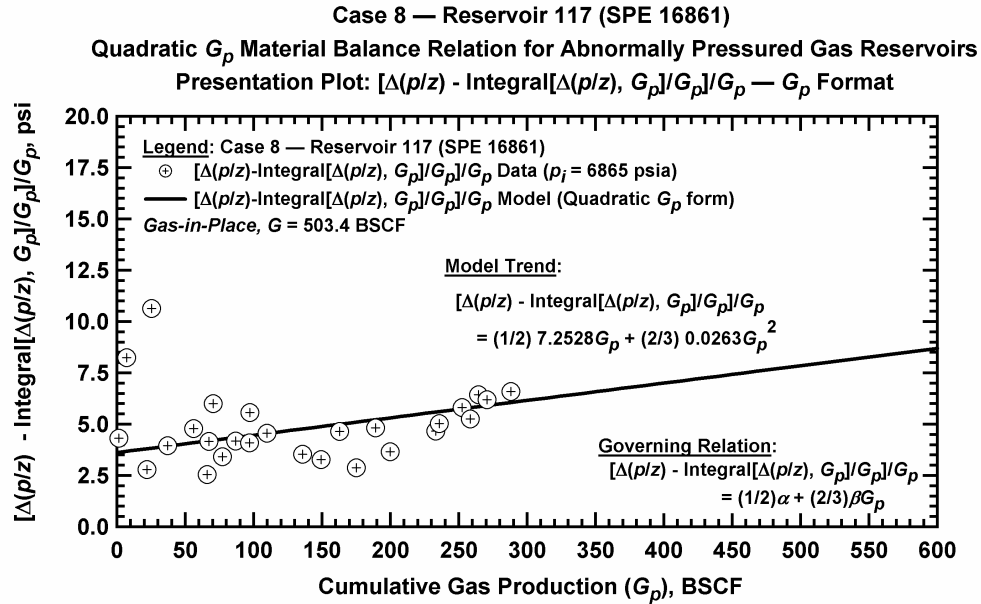


Figure D.9.g — Plot of $\frac{1}{G_p} \left[\Delta(p/z) - \frac{1}{G_p} \int_0^{G_p} \Delta(p/z) dG_p \right]$ vs. G_p — Case 8.

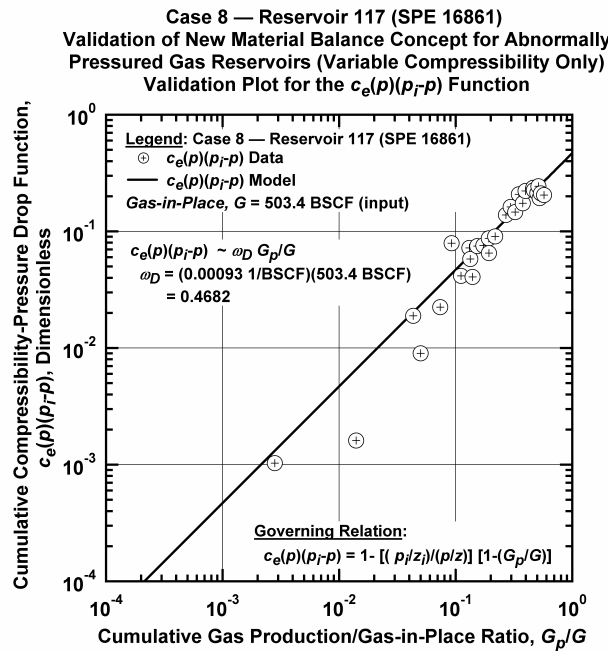


Figure D.9.h — Plot of $\bar{c}_e(p)(p_i - p)$ vs. G_p/G — Case 8.

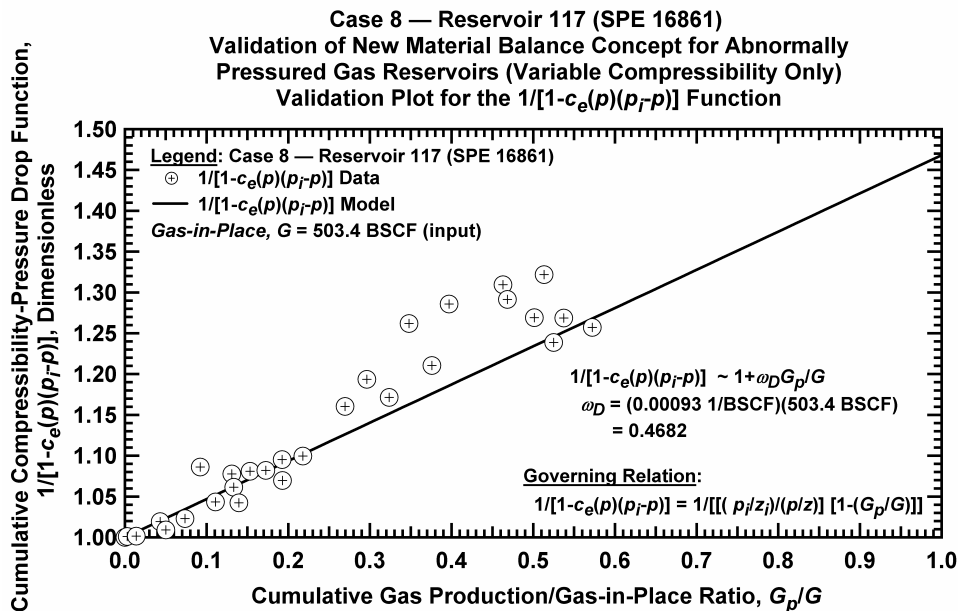


Figure D.9.i — Plot of $1/[1-\bar{c}_e(p)(p_i - p)]$ vs. G_p/G — Case 8.

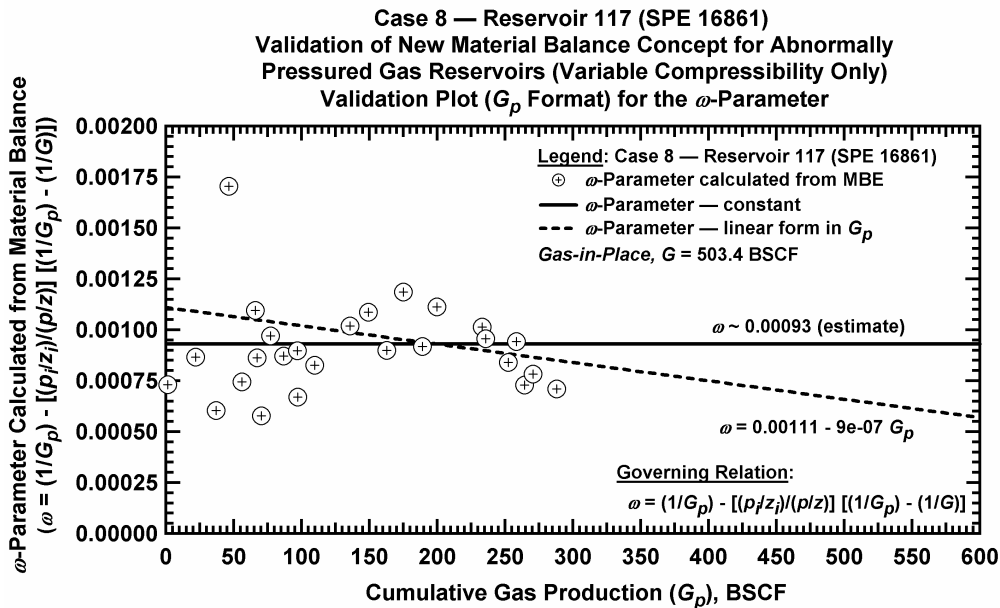


Figure D.9.j — Plot of ω vs. G_p — Case 8.

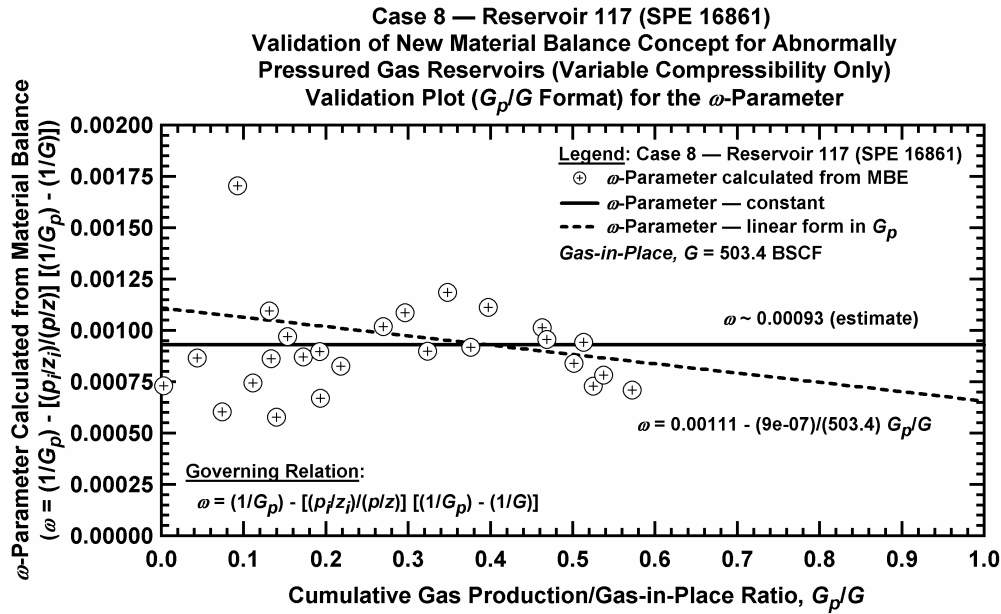


Figure D.9.k — Plot of ω vs. G_p/G — Case 8.

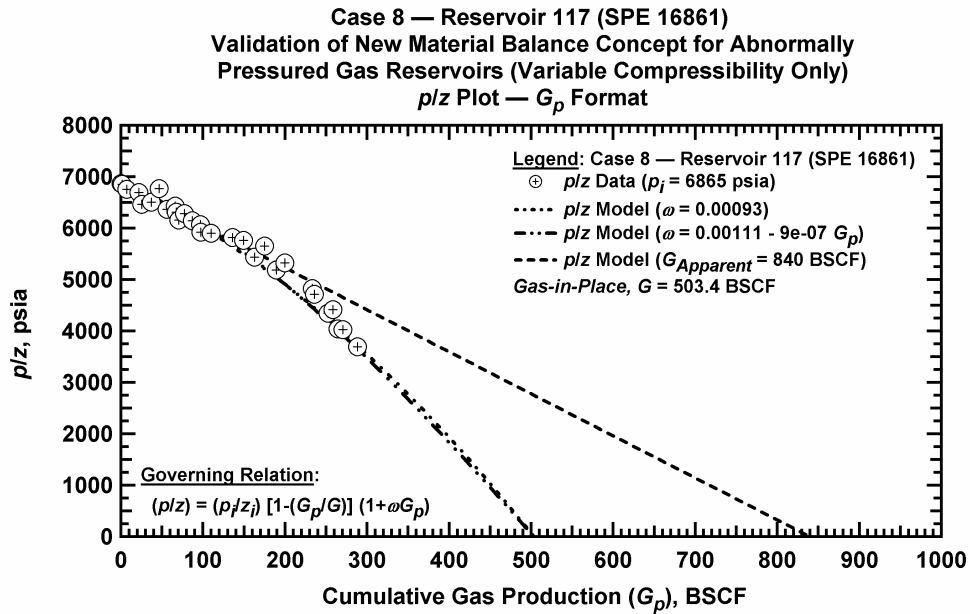
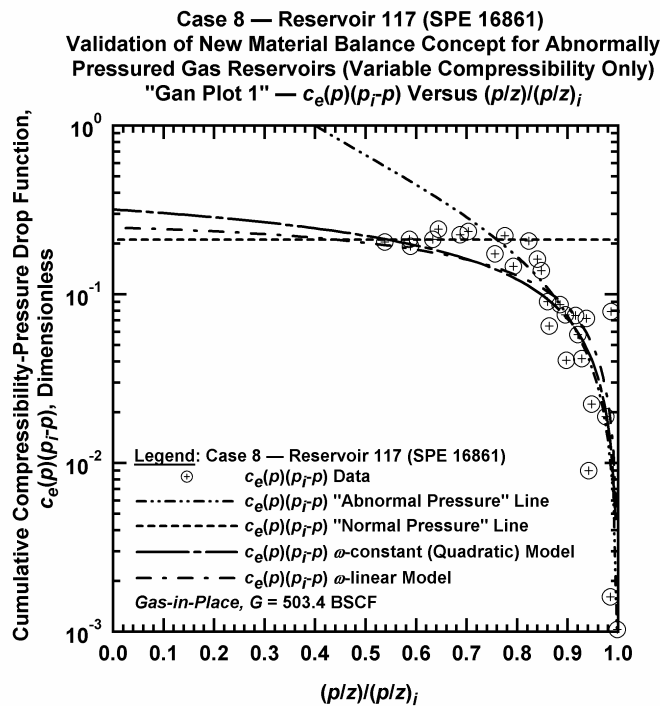
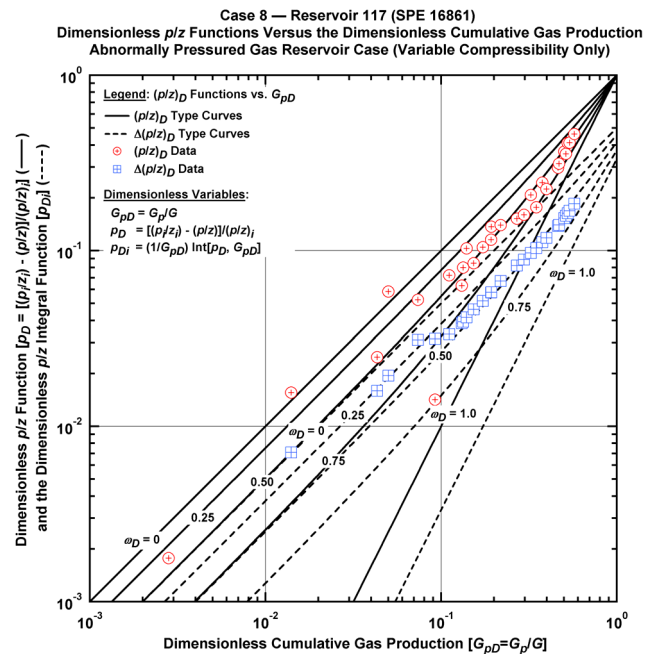


Figure D.9.l — Comparison plot of p/z vs. G_p — Case 8.



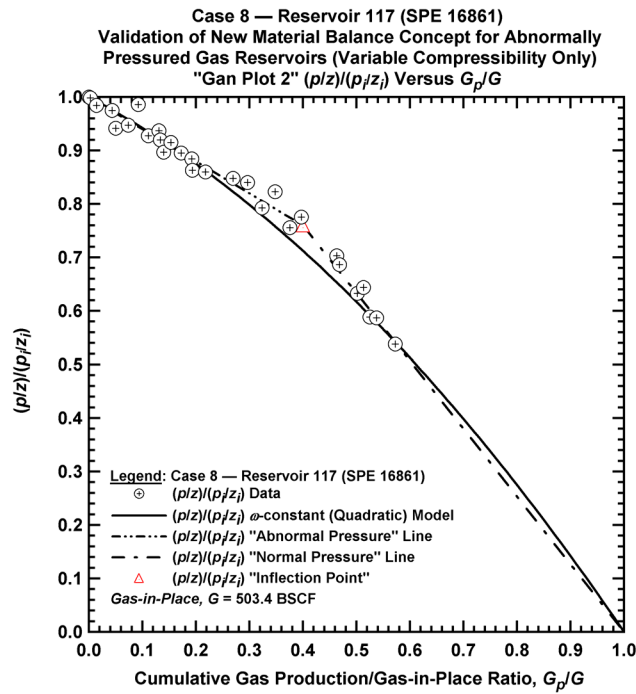


Figure D.9.o — Plot of $(p/z)/(p/z_i)$ vs. G_p/G — Case 8.

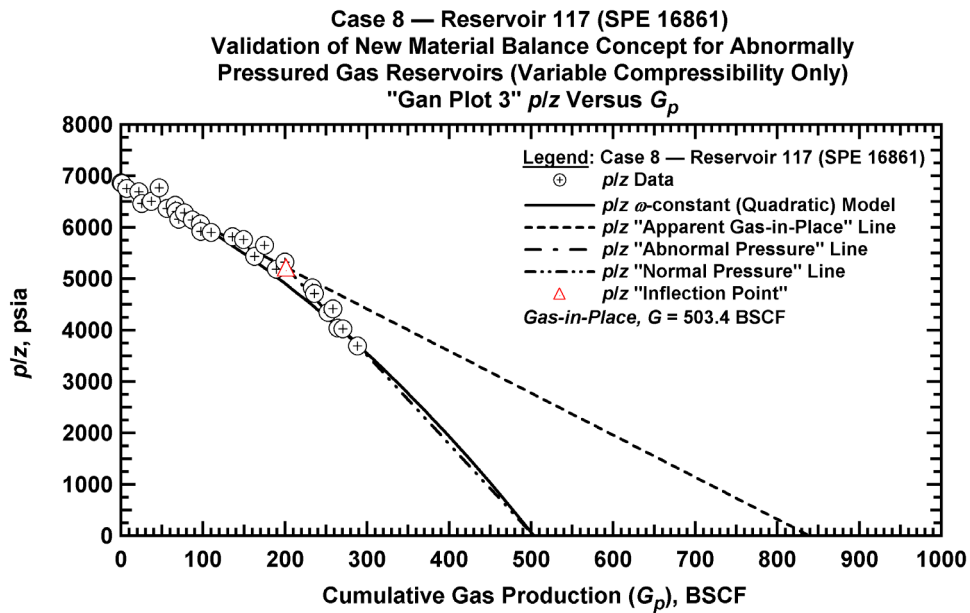


Figure D.9.p — Summary plot of p/z vs. G_p — Case 8.

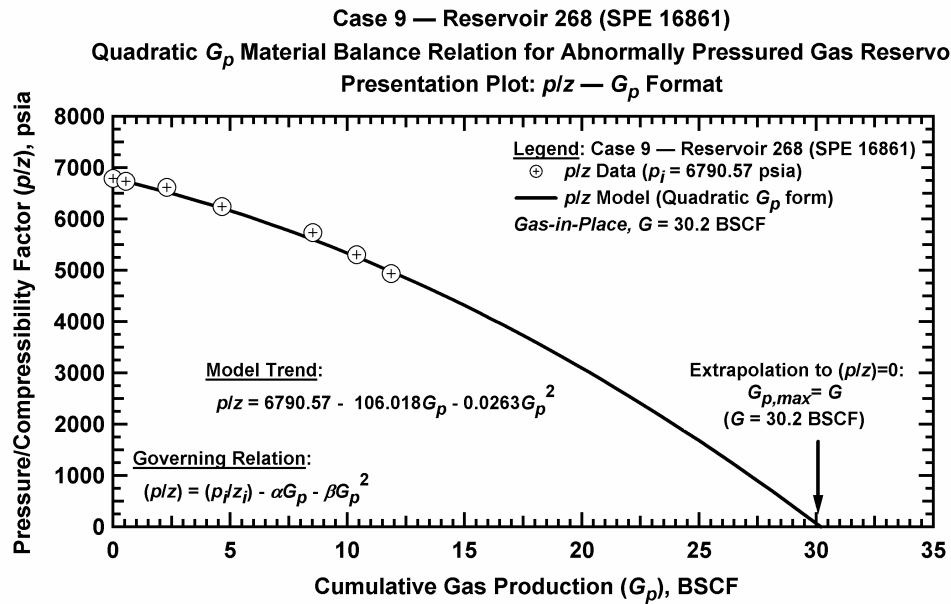


Figure D.10.a — Plot of p/z vs. G_p — Case 9.

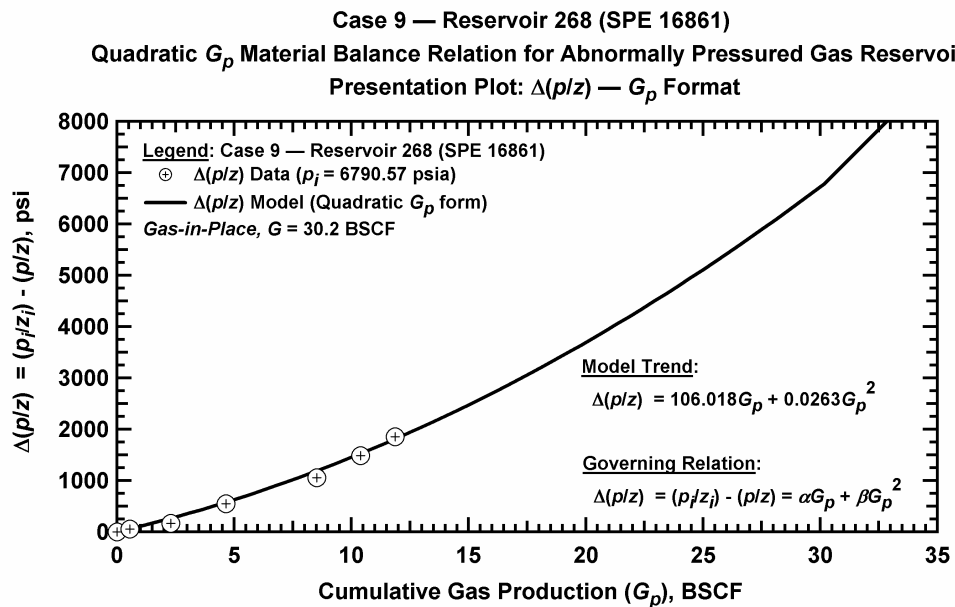


Figure D.10.b — Plot of $\Delta(p/z)$ vs. G_p — Case 9.

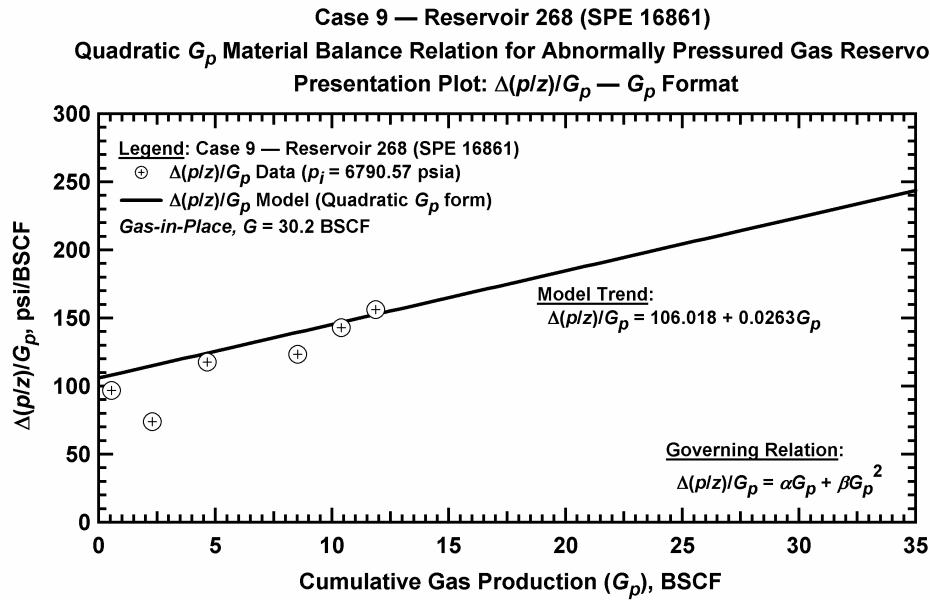


Figure D.10.c — Plot of $\Delta(p/z)/G_p$ vs. G_p — Case 9.

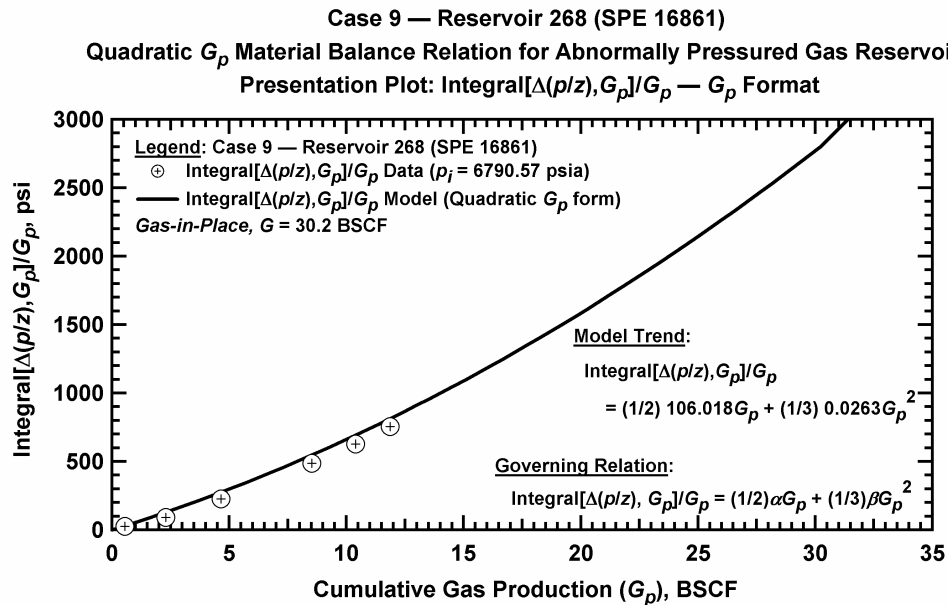


Figure D.10.d — Plot of $\frac{1}{G_p} \int_0^{G_p} \Delta(p/z) dG_p$ vs. G_p — Case 9.

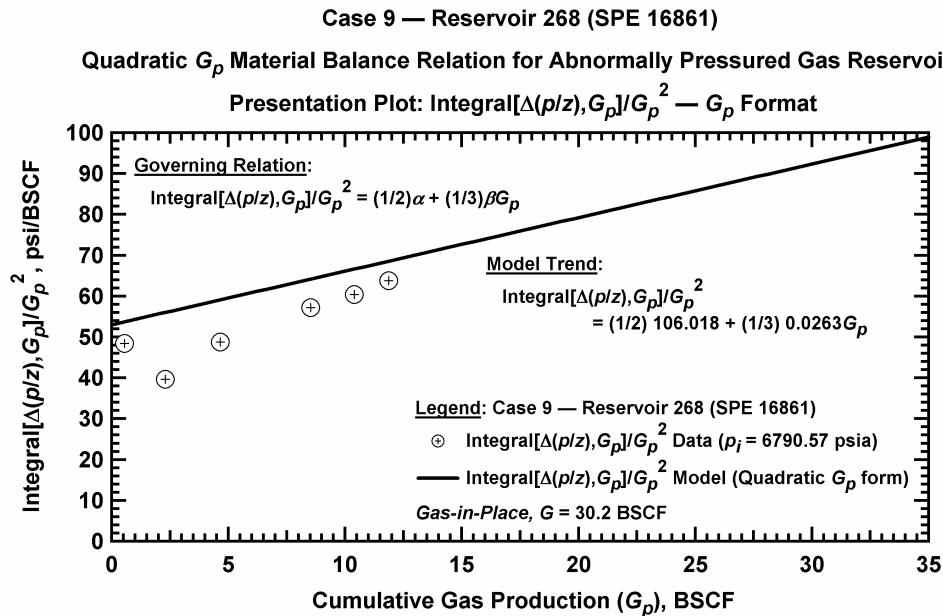


Figure D.10.e — Plot of $\frac{1}{G_p^2} \int_0^{G_p} \Delta(p/z) dG_p$ vs. G_p — Case 9.

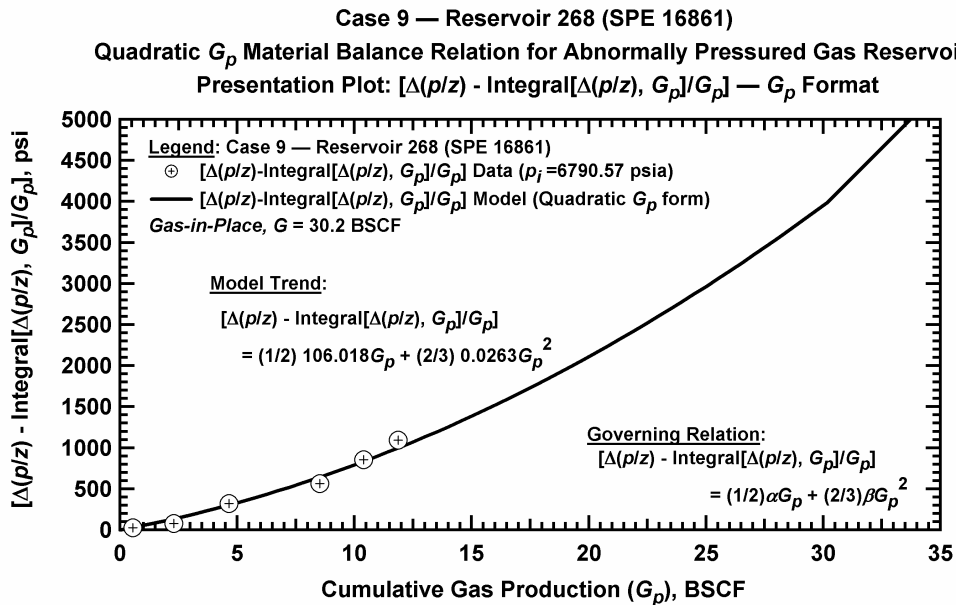


Figure D.10.f — Plot of $\Delta(p/z) - \frac{1}{G_p} \int_0^{G_p} \Delta(p/z) dG_p$ vs. G_p — Case 9.

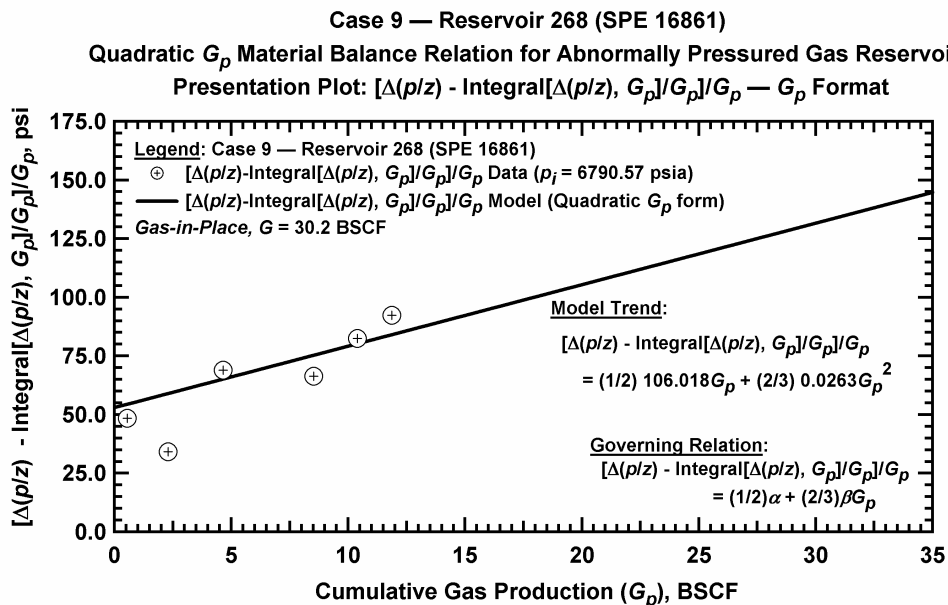


Figure D.10.g — Plot of $\frac{1}{G_p} \left[\Delta(p/z) - \frac{1}{G_p} \int_0^{G_p} \Delta(p/z) dG_p \right]$ vs. G_p — Case 9.

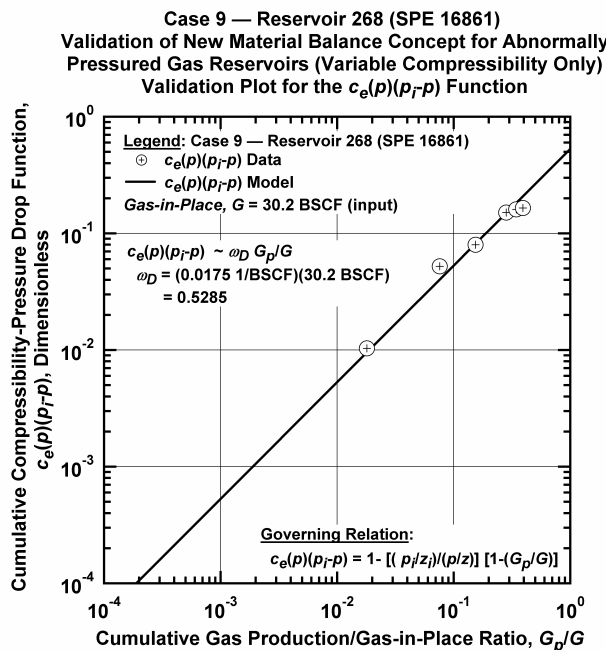


Figure D.10.h — Plot of $\bar{c}_e(p)(p_i - p)$ vs. G_p/G — Case 9.

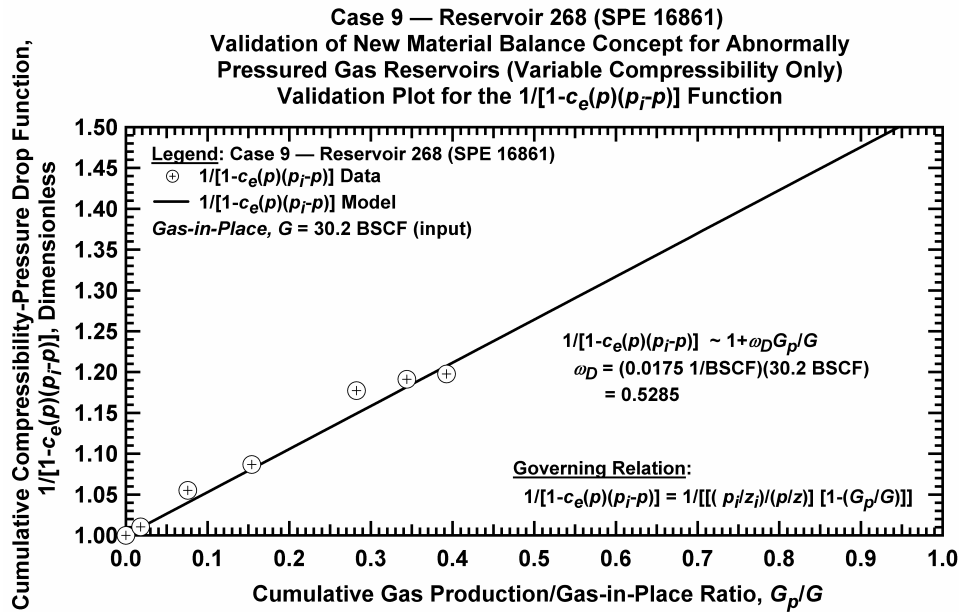


Figure D.10.i — Plot of $1/[1-\bar{c}_e(p)(p_i - p)]$ vs. G_p/G — Case 9.

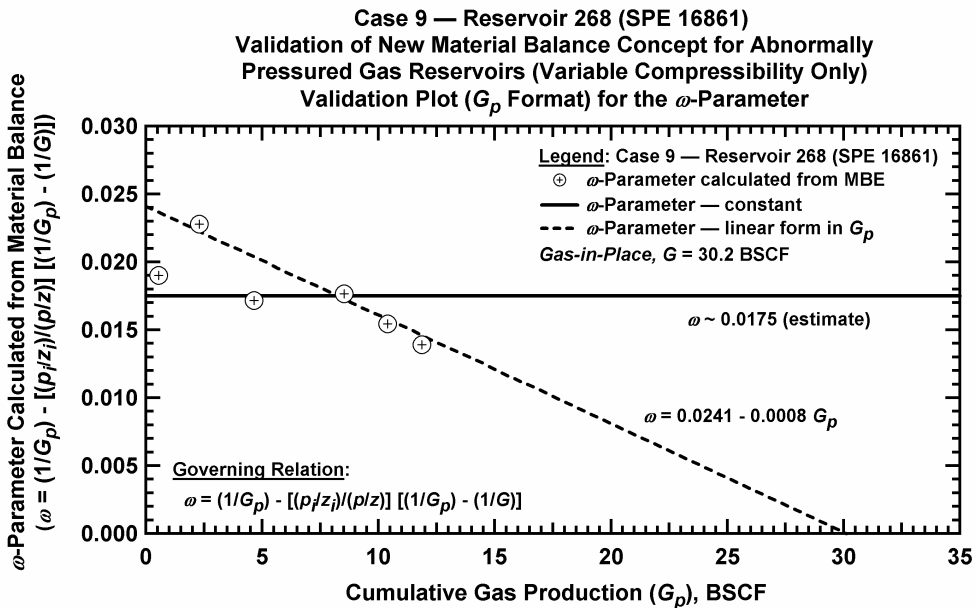


Figure D.10.j — Plot of ω vs. G_p — Case 9.

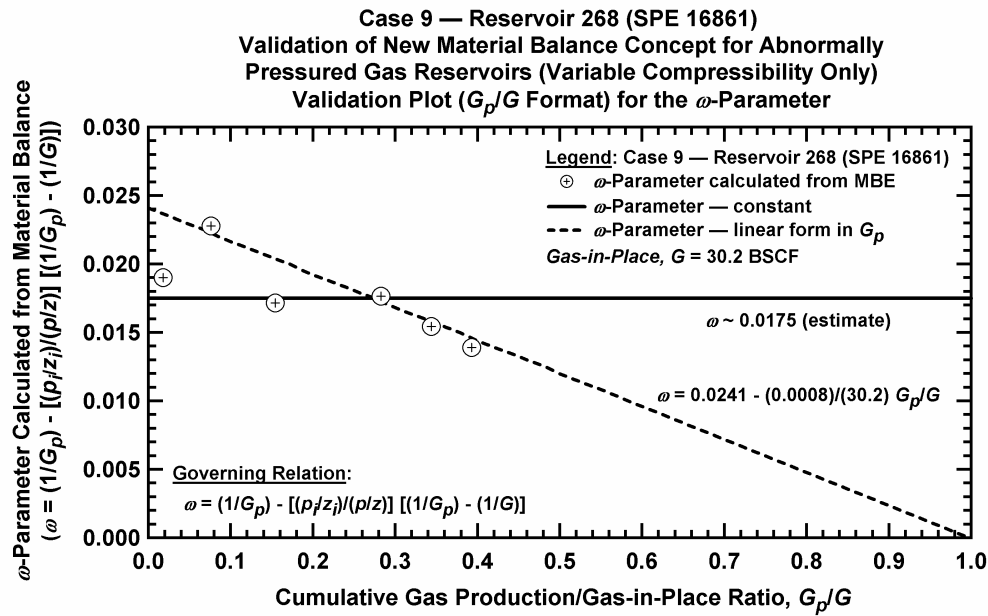


Figure D.10.k — Plot of ω vs. G_p/G — Case 9.

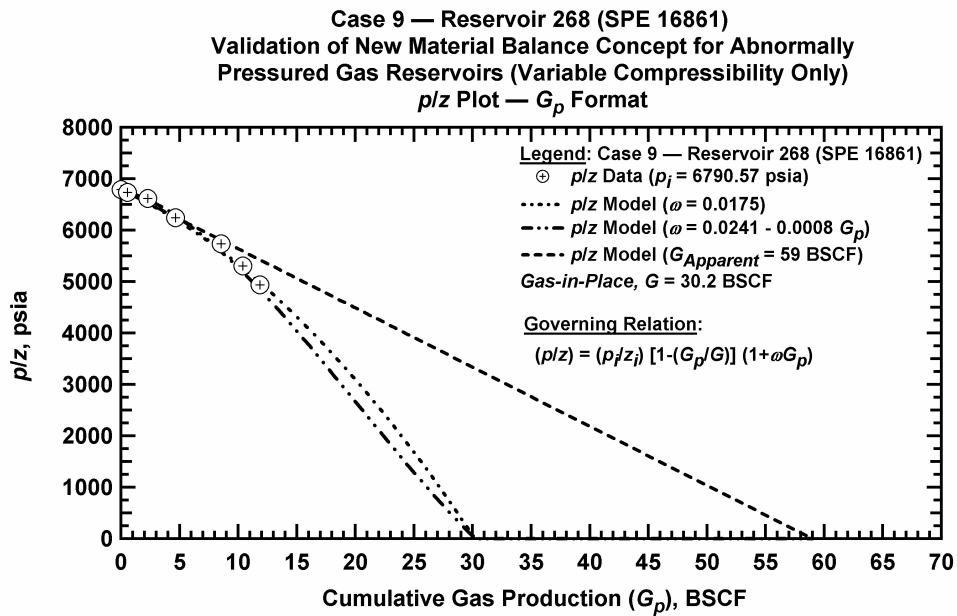


Figure D.10.l — Comparison plot of p/z vs. G_p — Case 9.

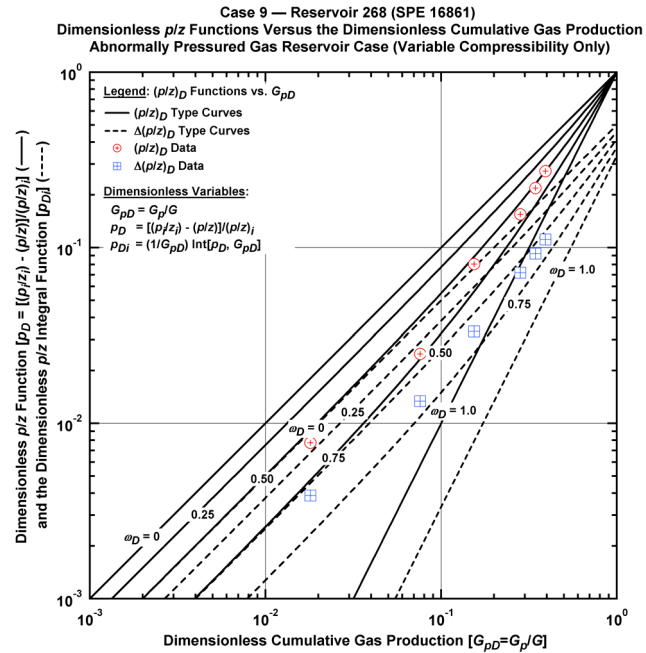


Figure D.10.m — Plot of dimensionless p/z functions vs. G_{pD} — Case 9.

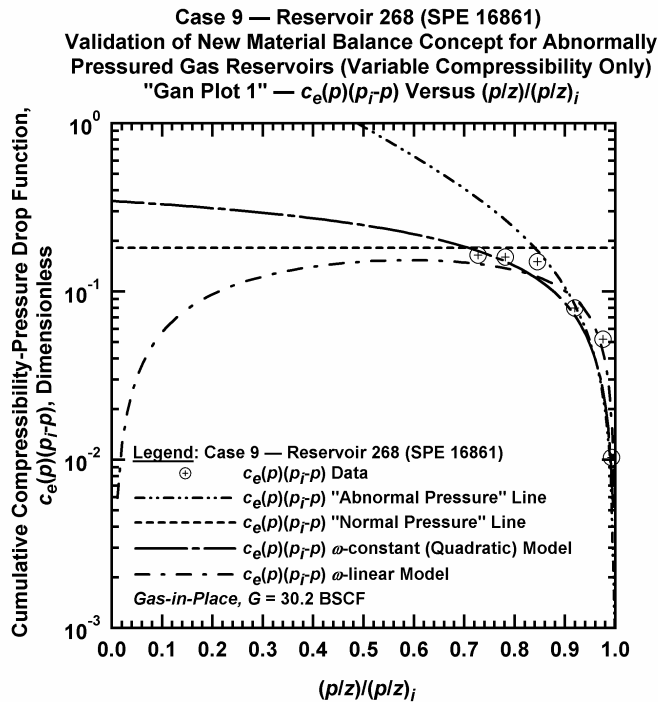


Figure D.10.n — Plot of $\bar{c}_e(p)(p_i - p)$ vs. $(p/z)/(p/z)_i$ — Case 9.

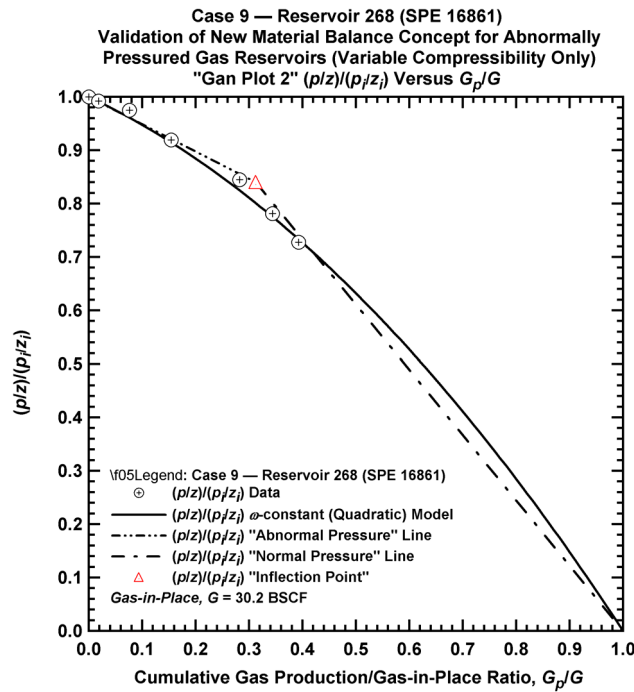


Figure D.10.o — Plot of $(p/z)/(p/z_i)$ vs. G_p/G — Case 9.

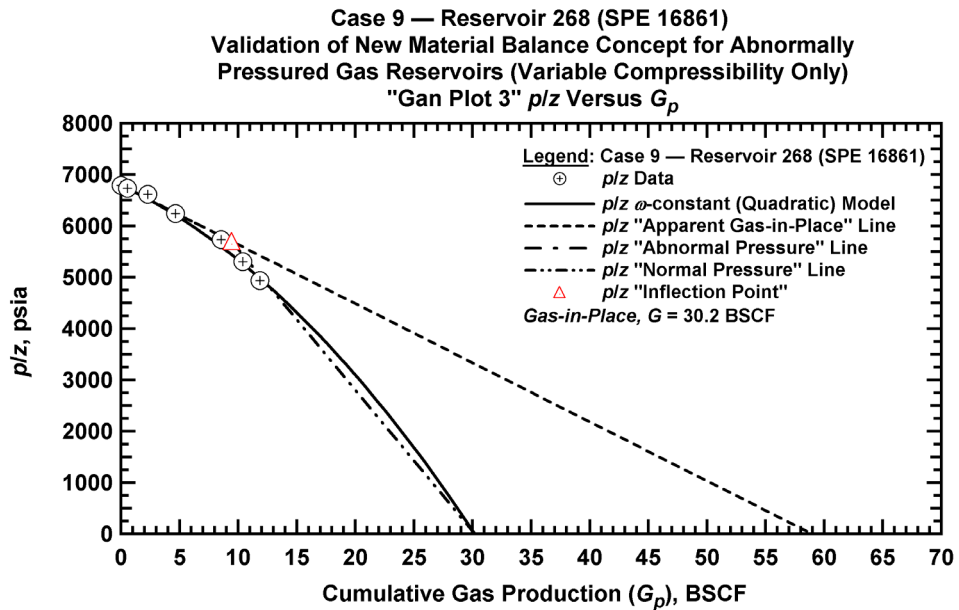


Figure D.10.p — Summary plot of p/z vs. G_p — Case 9.

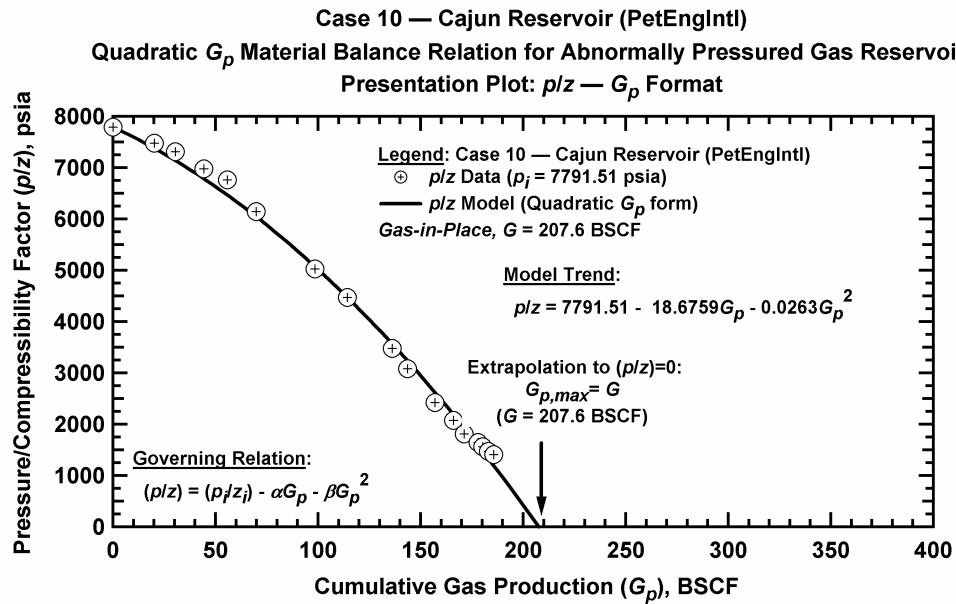


Figure D.11.a — Plot of p/z vs. G_p — Case 10.

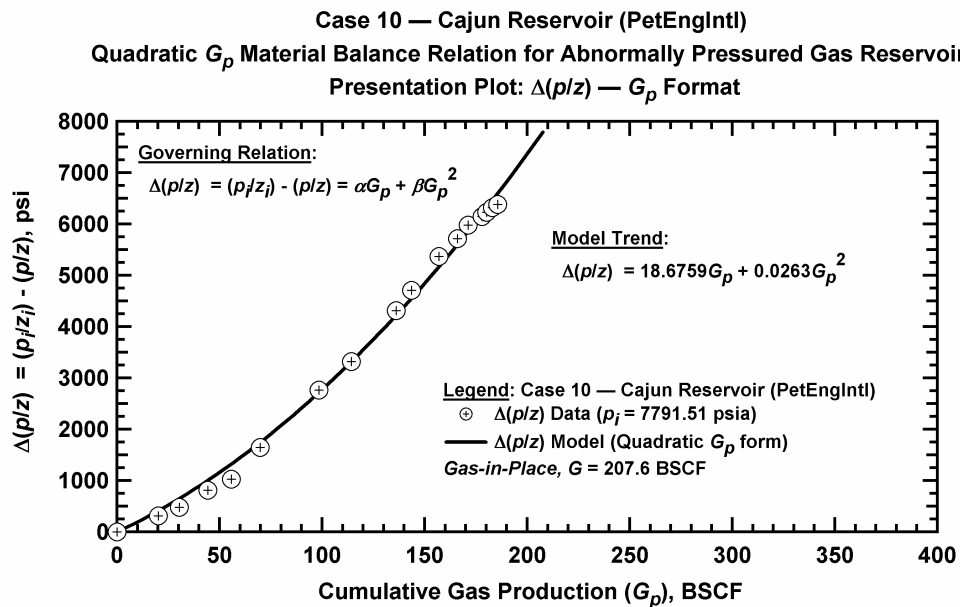


Figure D.11.b — Plot of $\Delta(p/z)$ vs. G_p — Case 10.

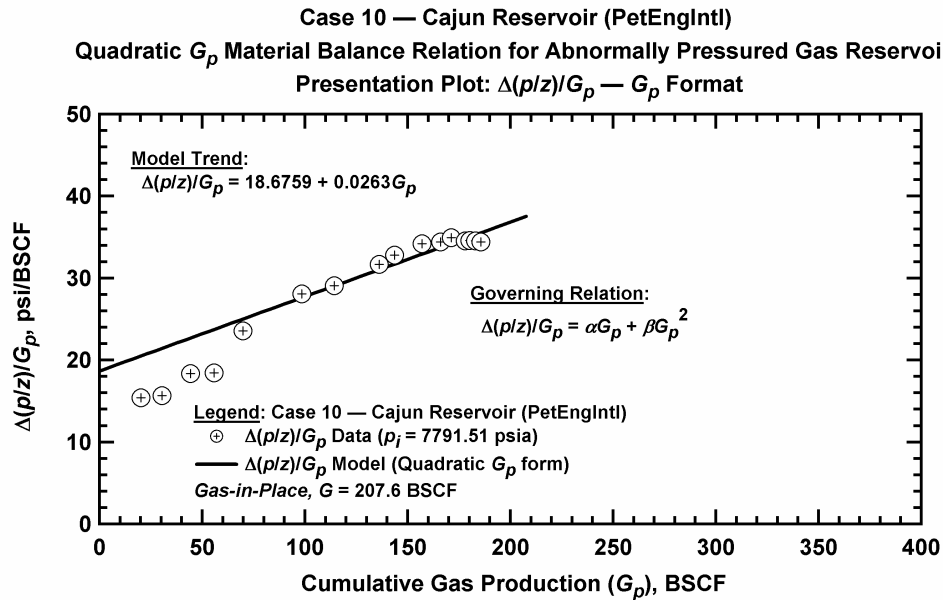


Figure D.11.c — Plot of $\Delta(p/z)/G_p$ vs. G_p — Case 10.

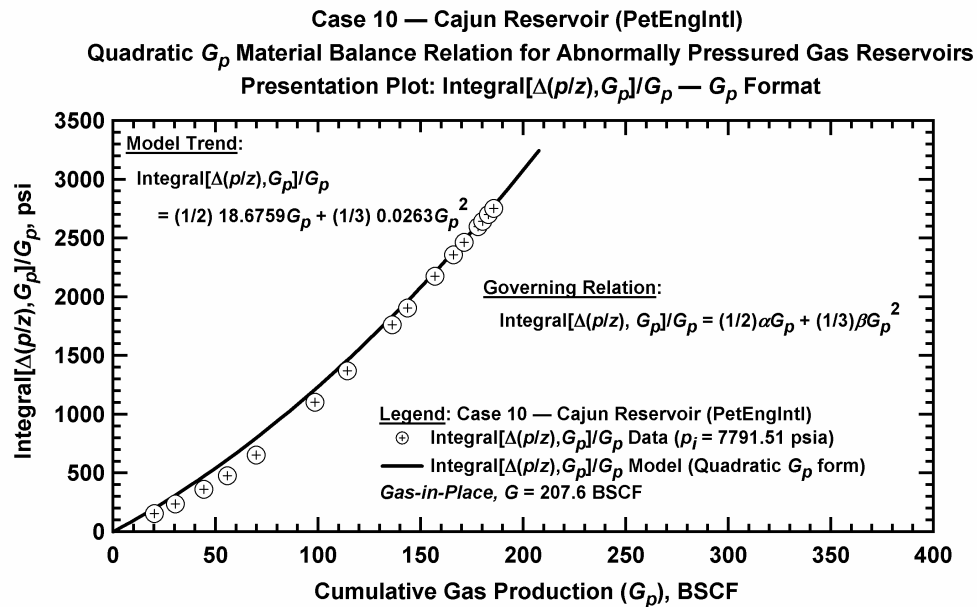


Figure D.11.d — Plot of $\frac{1}{G_p} \int_0^{G_p} \Delta(p/z) dG_p$ vs. G_p — Case 10.

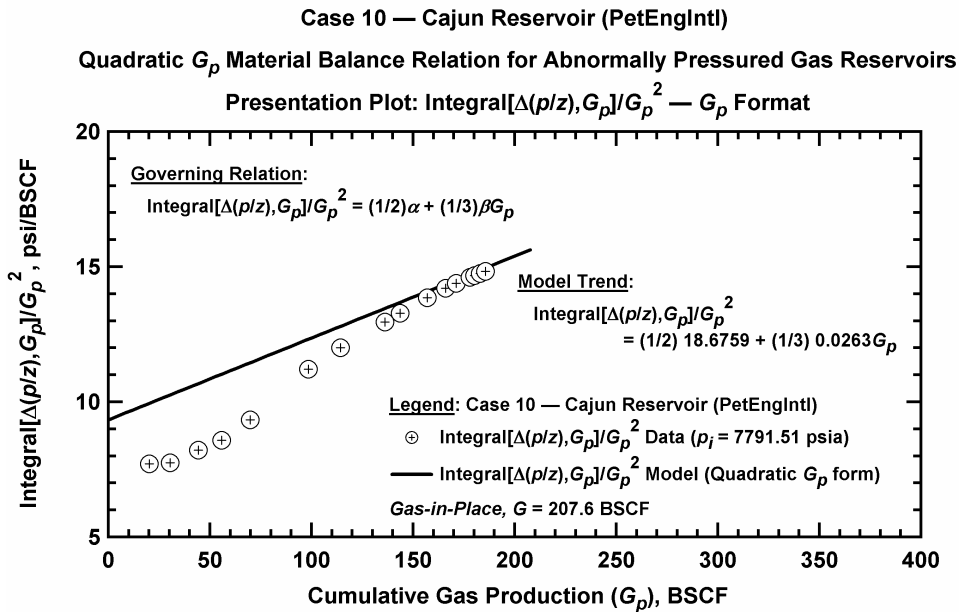


Figure D.11.e — Plot of $\frac{1}{G_p^2} \int_0^{G_p} \Delta(p/z) dG_p$ vs. G_p — Case 10.

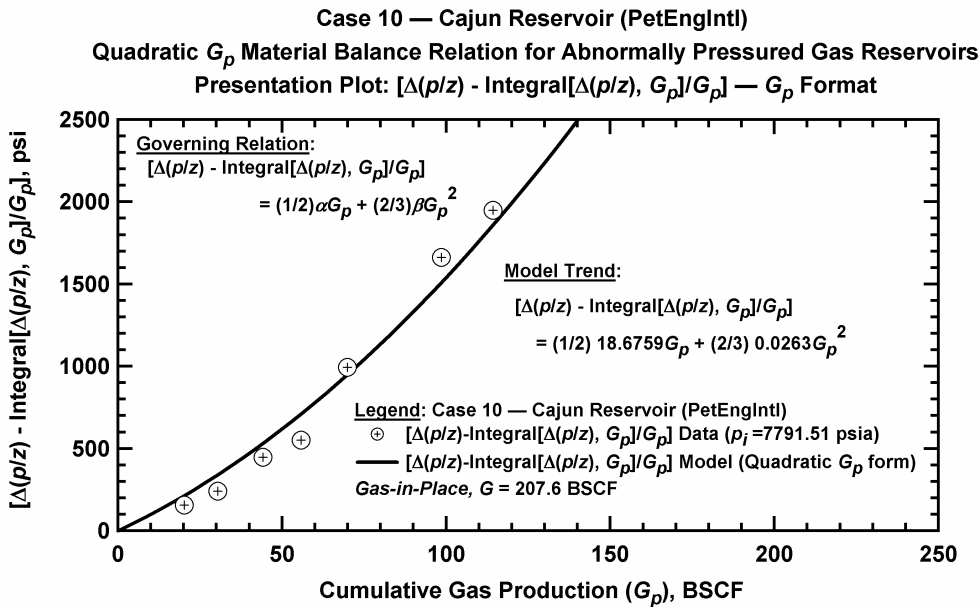


Figure D.11.f — Plot of $\Delta(p/z) - \frac{1}{G_p} \int_0^{G_p} \Delta(p/z) dG_p$ vs. G_p — Case 10.

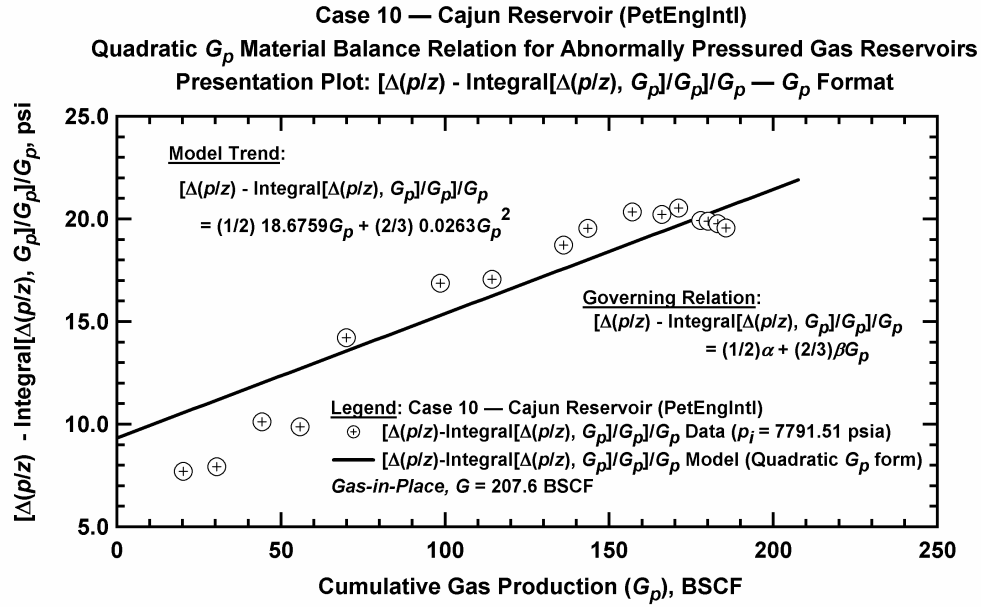


Figure D.11.g — Plot of $\frac{1}{G_p} \left[\Delta(p/z) - \frac{1}{G_p} \int_0^{G_p} \Delta(p/z) dG_p \right]$ vs. G_p — Case 10.

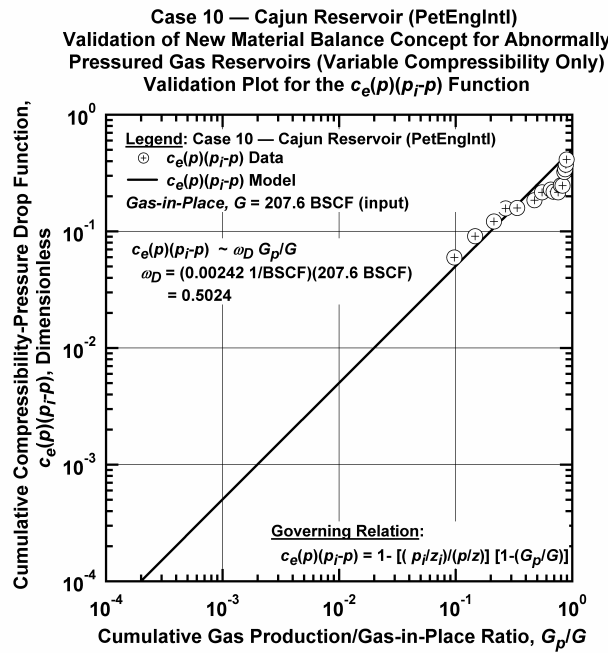


Figure D.11.h — Plot of $\bar{c}_e(p)(p_i - p)$ vs. G_p/G — Case 10.

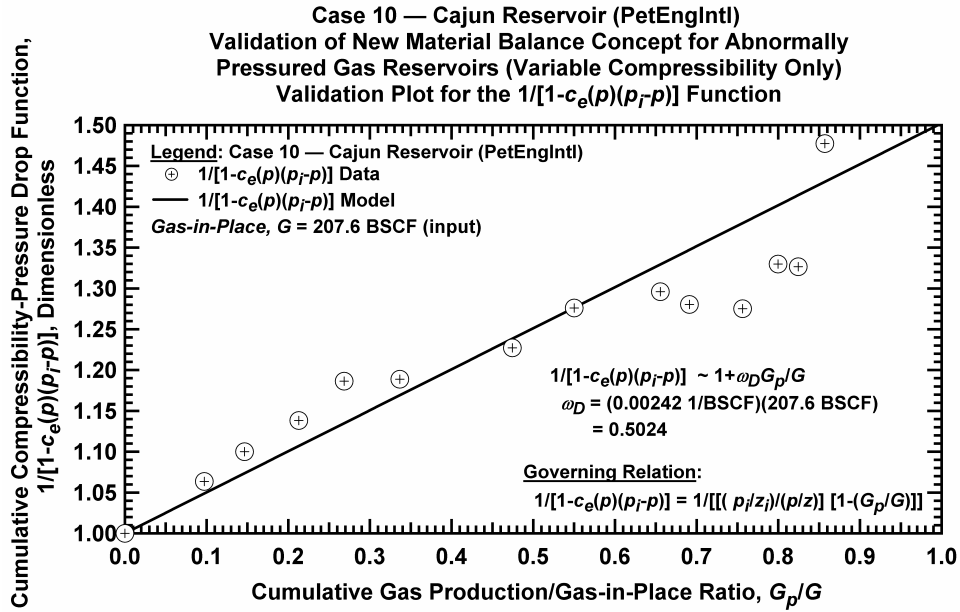


Figure D.11.i — Plot of $1/[1-\bar{c}_e(p)(p_i-p)]$ vs. G_p/G — Case 10.

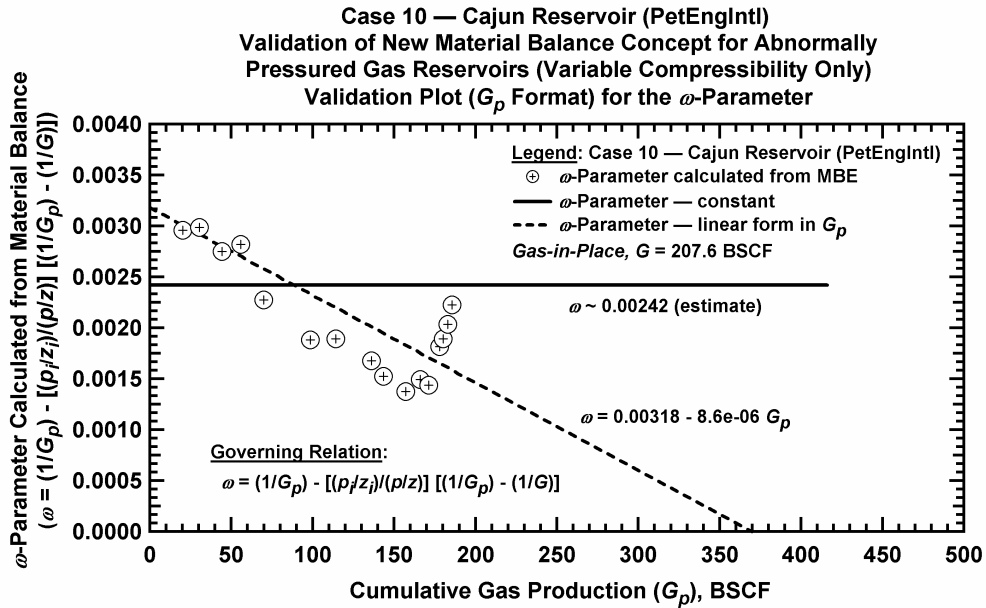


Figure D.11.j — Plot of ω vs. G_p — Case 10.

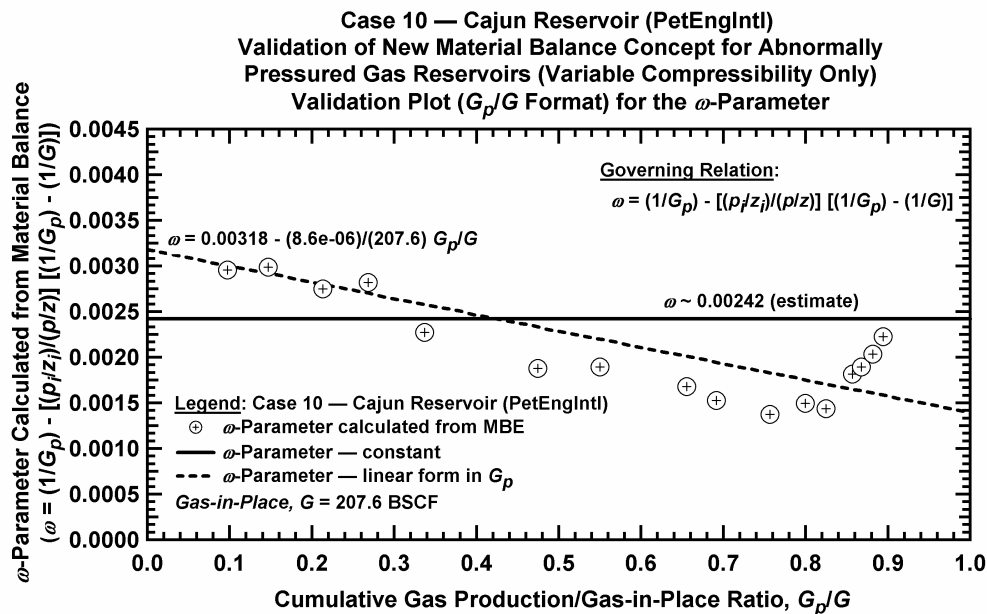


Figure D.11.k — Plot of ω vs. G_p/G — Case 10.

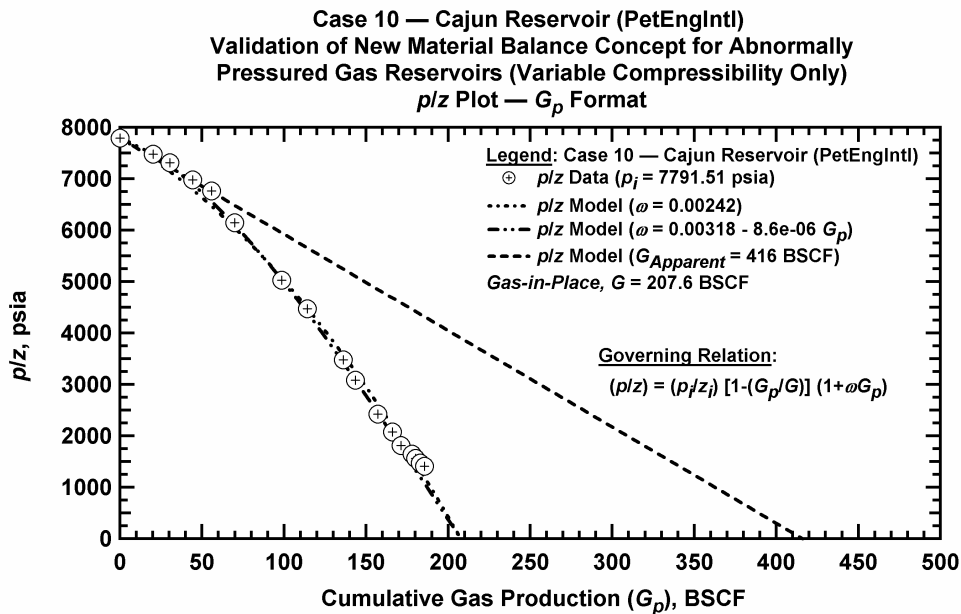


Figure D.11.l — Comparison plot of p/z vs. G_p — Case 10.

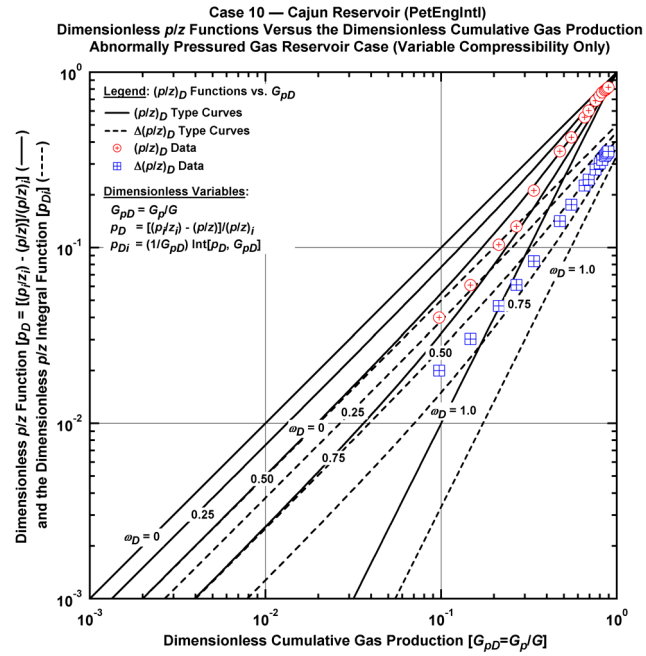


Figure D.11.m — Plot of dimensionless p/z functions vs. G_{pD} — Case 10.

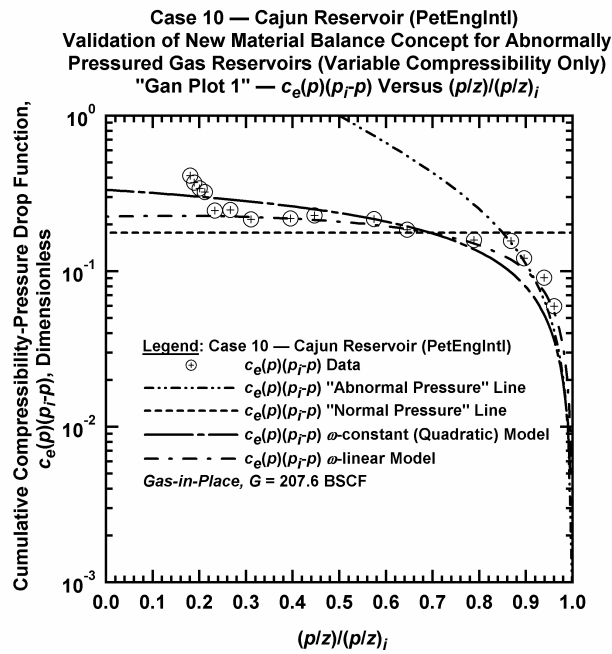


Figure D.11.n — Plot of $\bar{c}_e(p)(p_i - p)$ vs. $(p/z)/(p/z)_i$ — Case 10.

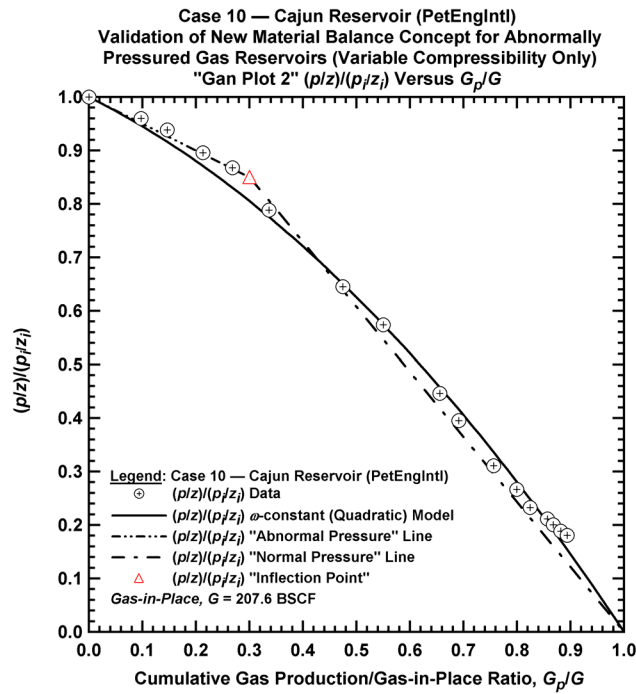


Figure D.11.o — Plot of $(p/z)/(p/z_i)$ vs. G_p/G — Case 10.

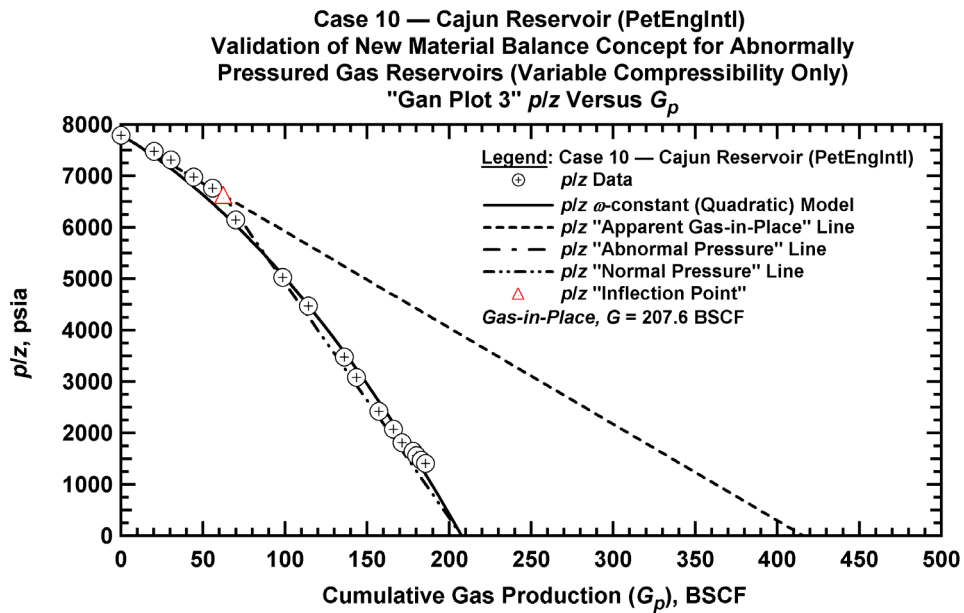


Figure D.11.p — Summary plot of p/z vs. G_p — Case 10.

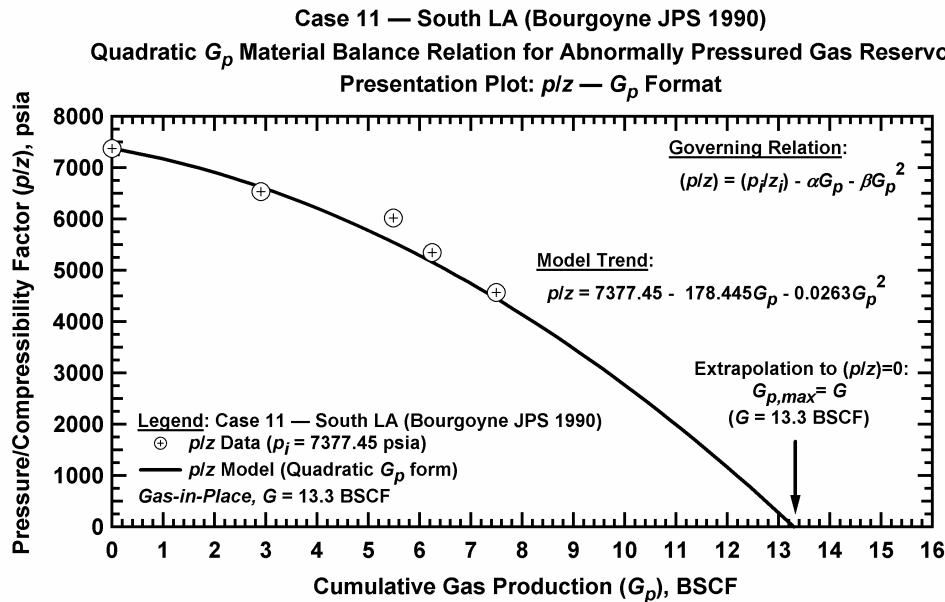


Figure D.12.a — Plot of p/z vs. G_p — Case 11.

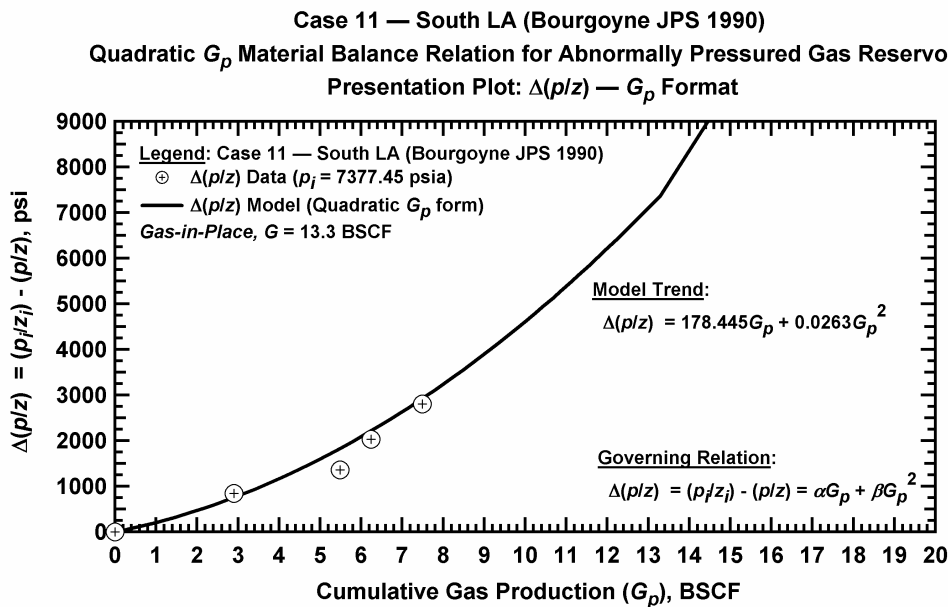


Figure D.12.b — Plot of $\Delta(p/z)$ vs. G_p — Case 11.

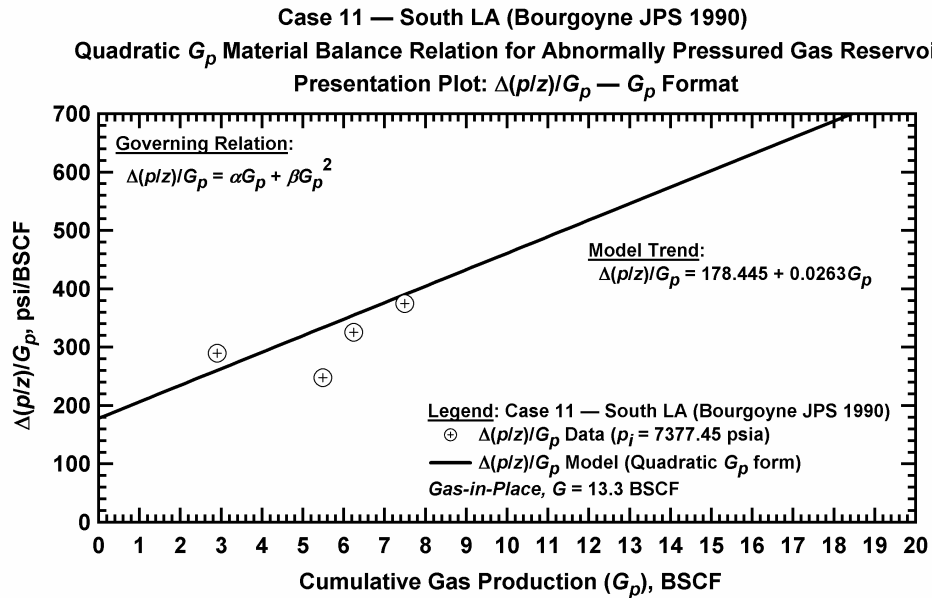


Figure D.12.c — Plot of $\Delta(p/z)/G_p$ vs. G_p — Case 11.

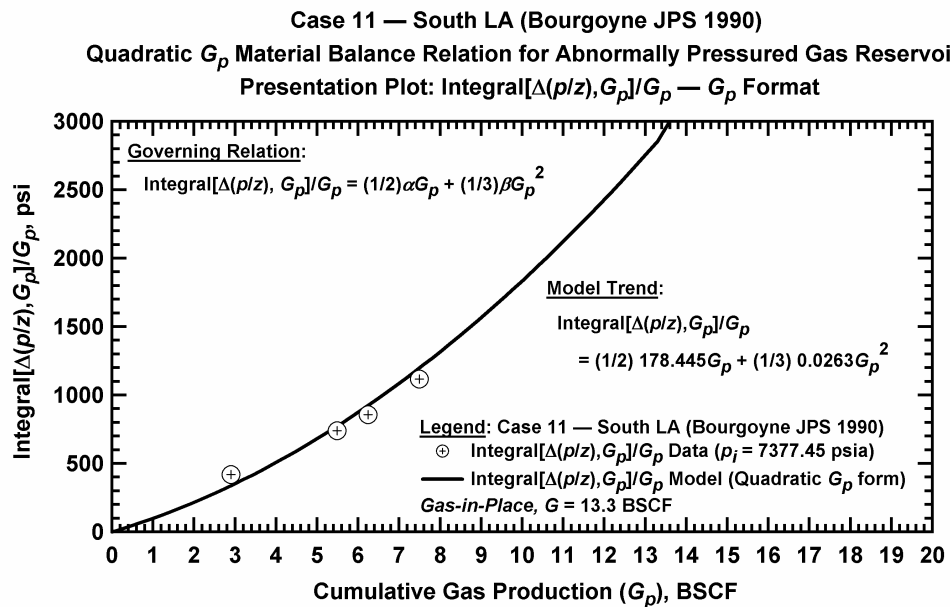


Figure D.12.d — Plot of $\frac{1}{G_p} \int_0^{G_p} \Delta(p/z) dG_p$ vs. G_p — Case 11.

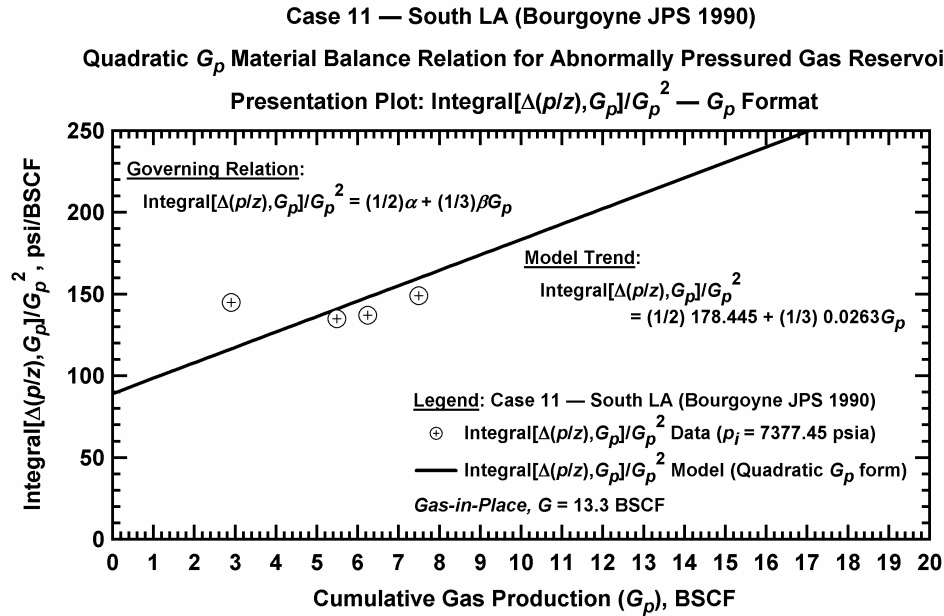


Figure D.12.e — Plot of $\frac{1}{G_p^2} \int_0^{G_p} \Delta(p/z) dG_p$ vs. G_p — Case 11.

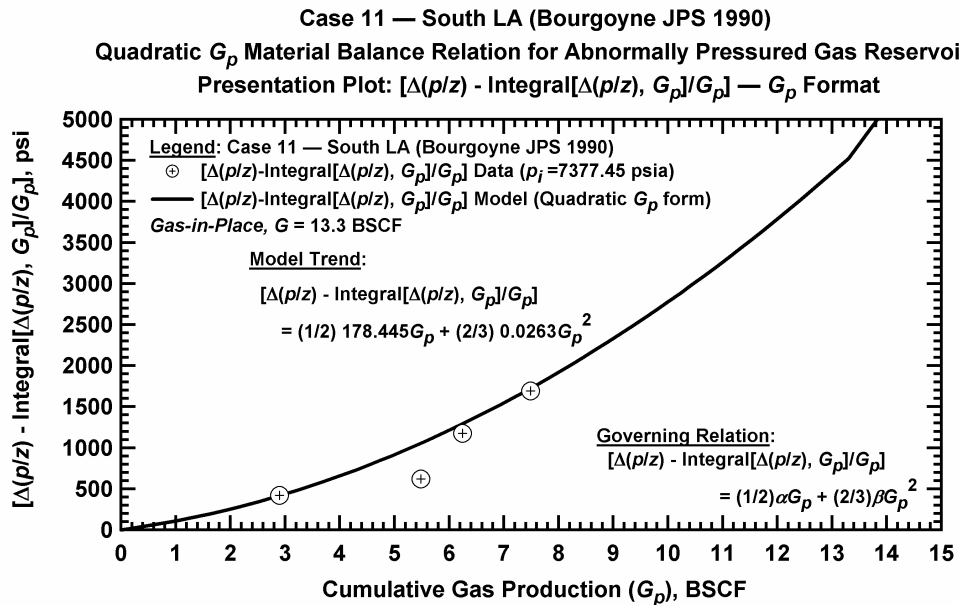


Figure D.12.f — Plot of $\Delta(p/z) - \frac{1}{G_p} \int_0^{G_p} \Delta(p/z) dG_p$ vs. G_p — Case 11.

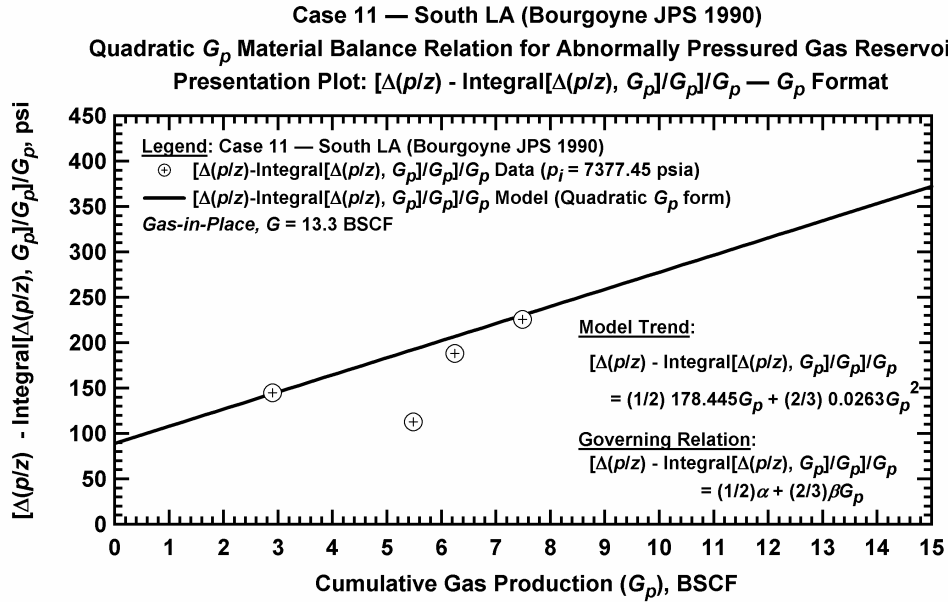


Figure D.12.g — Plot of $\frac{1}{G_p} \left[\Delta(p/z) - \frac{1}{G_p} \int_0^{G_p} \Delta(p/z) dG_p \right]$ vs. G_p — Case 11.

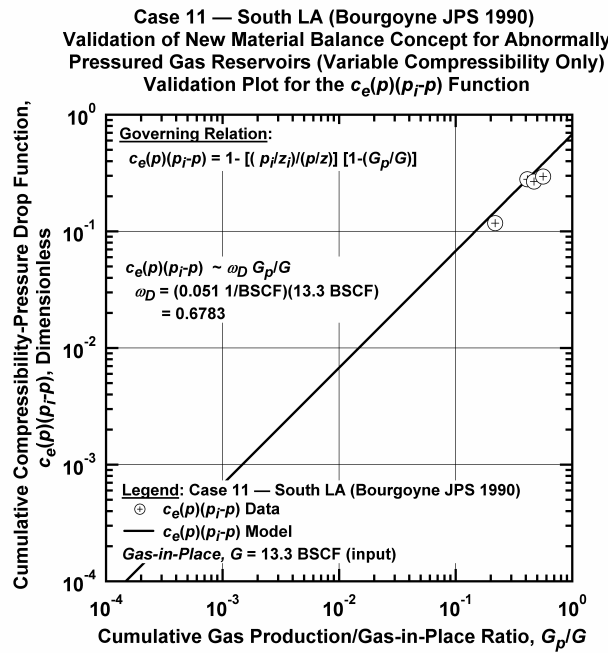


Figure D.12.h — Plot of $\bar{c}_e(p)(p_i - p)$ vs. G_p/G — Base Simulation Case 11.

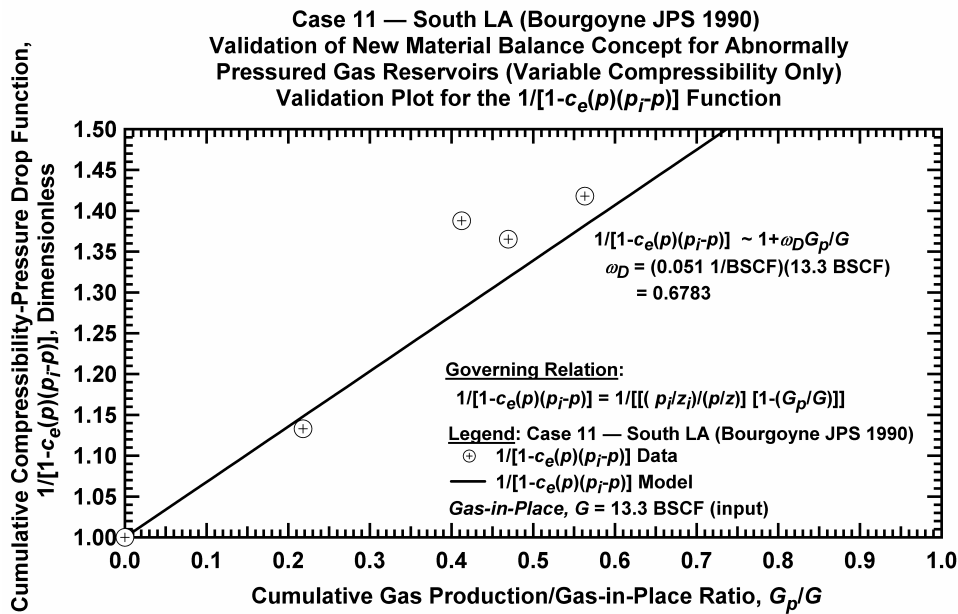


Figure D.12.i — Plot of $1/[1-\bar{c}_e(p)(p_i - p)]$ vs. G_p/G — Case 11.

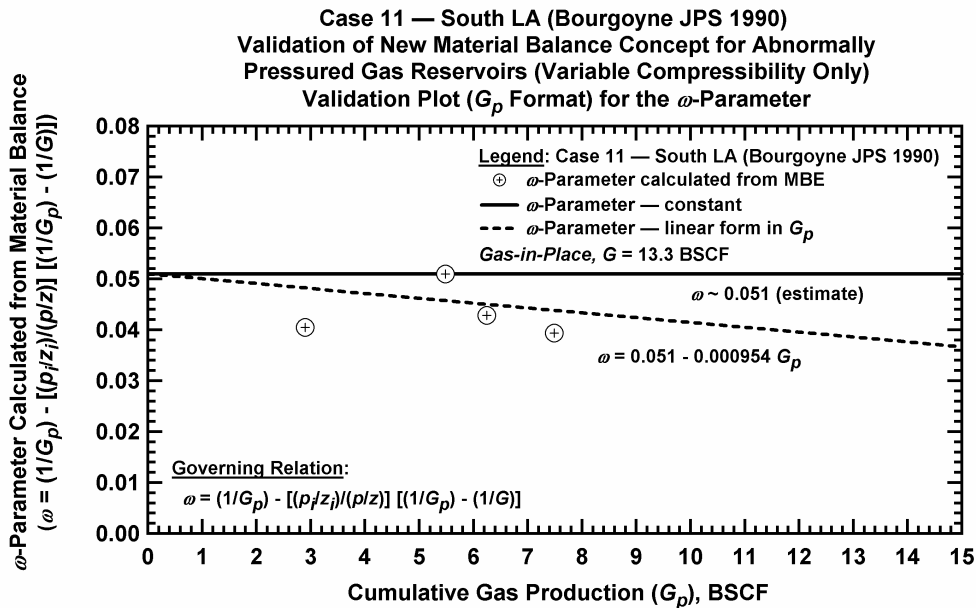


Figure D.12.j — Plot of ω vs. G_p — Base Simulation Case 11.

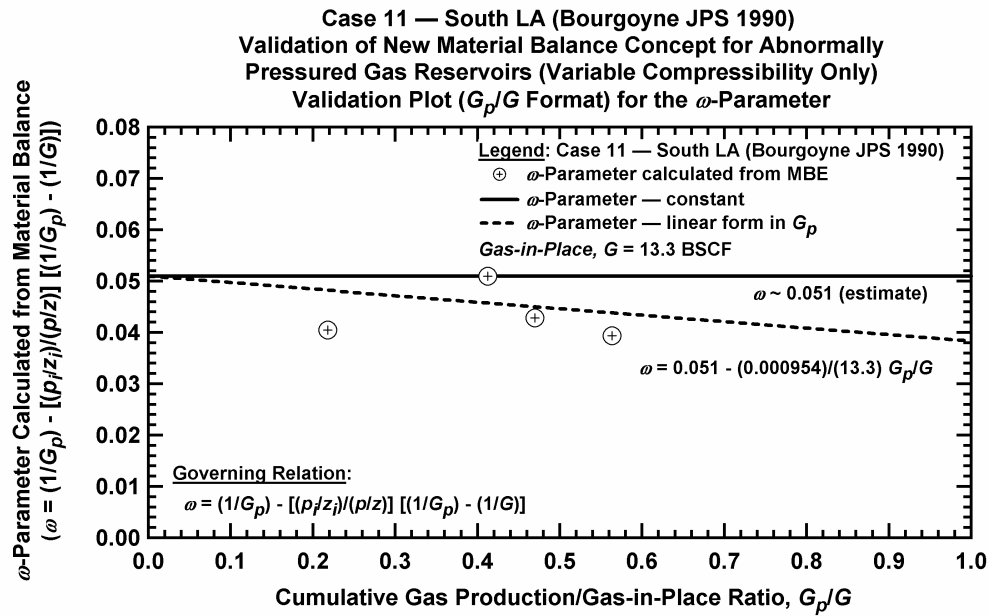


Figure D.12.k — Plot of ω vs. G_p/G — Case 11.

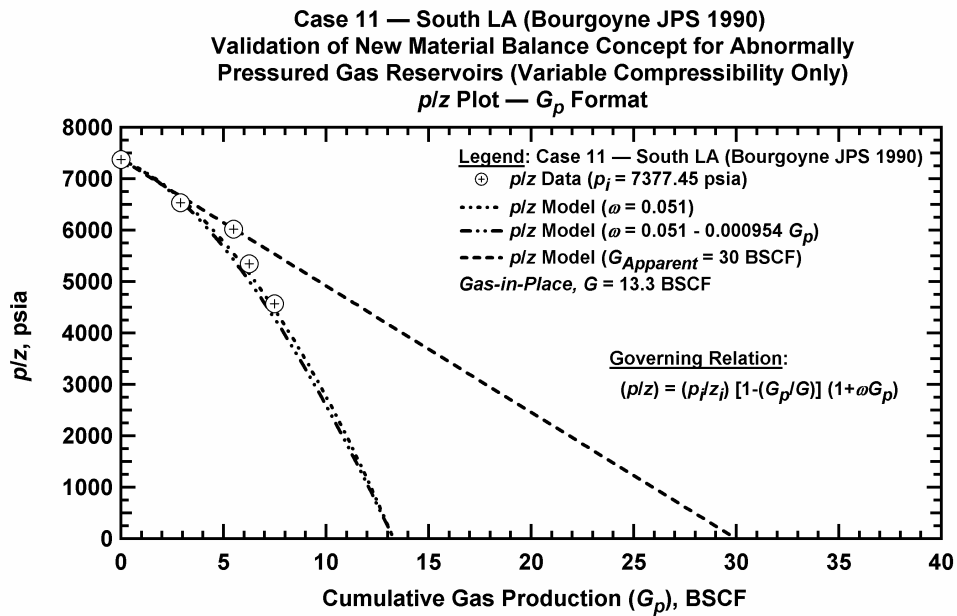


Figure D.12.l — Comparison plot of p/z vs. G_p — Case 11.

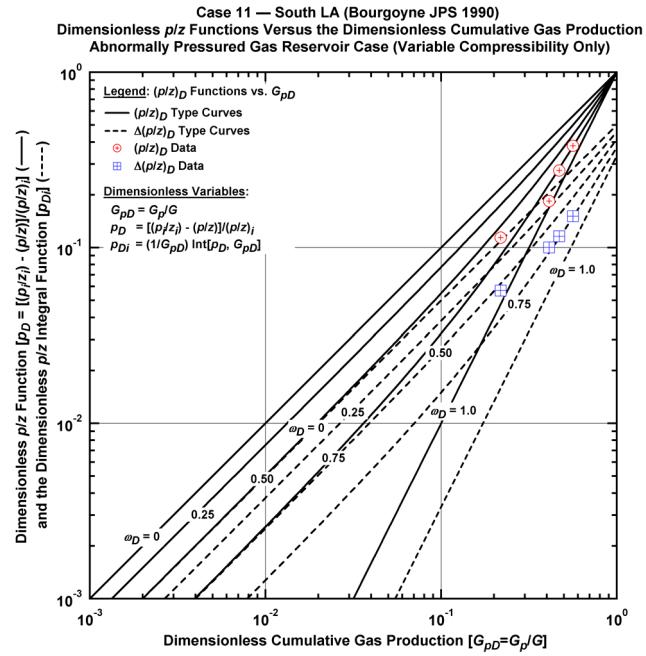


Figure D.12.m — Plot of dimensionless p/z functions vs. G_{pD} — Case 11.

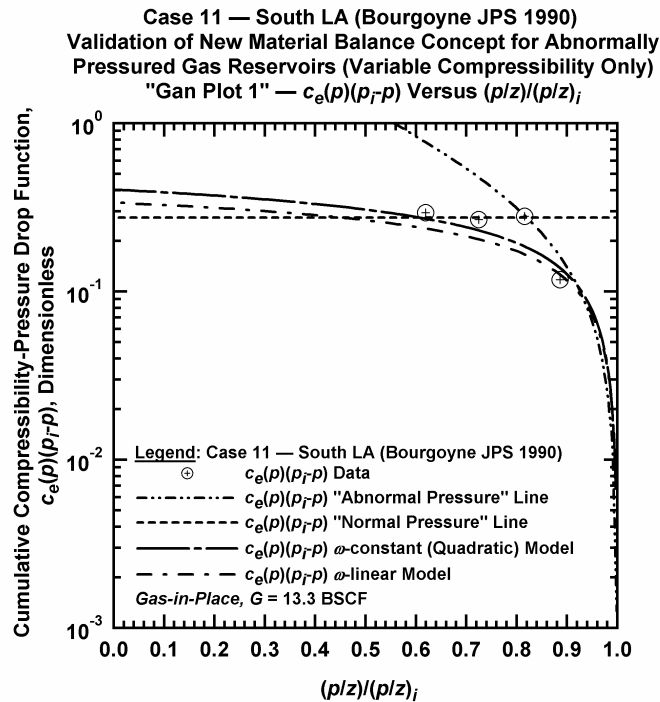


Figure D.12.n — Plot of $\bar{c}_e(p)(p_i - p)$ vs. $(p/z)/(p/z)_i$ — Case 11.

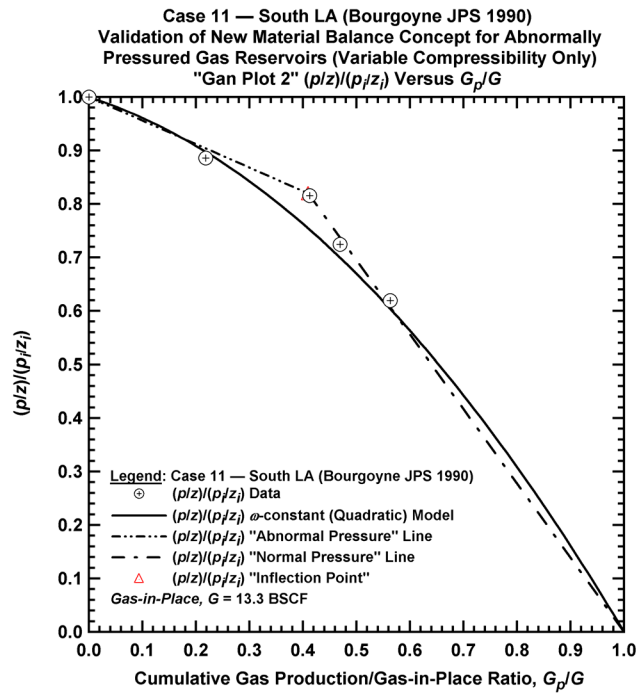


Figure D.12.o — Plot of $(p/z)/(p/z_i)$ vs. G_p/G — Case 11.

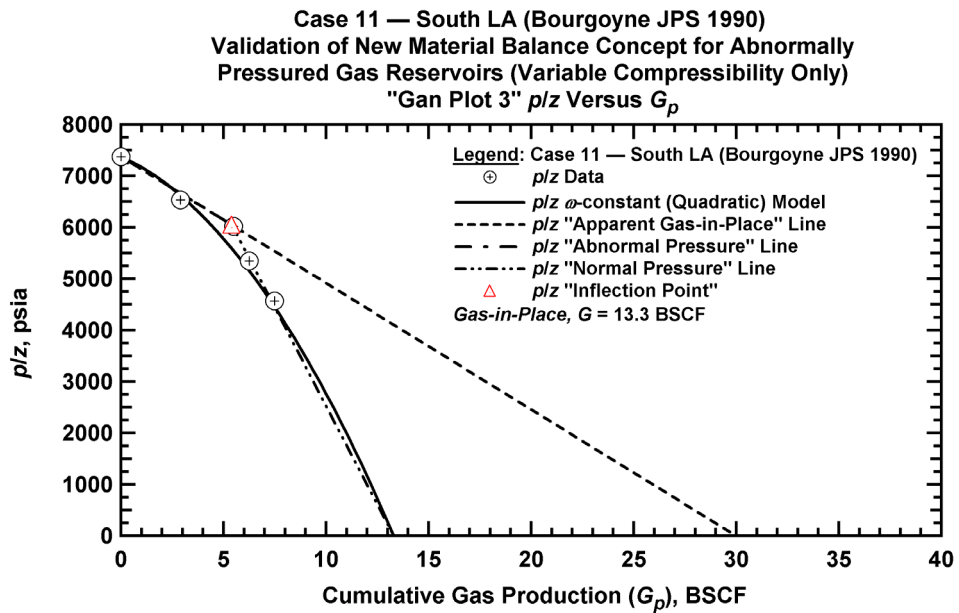


Figure D.12.p — Summary plot of p/z vs. G_p — Case 11.

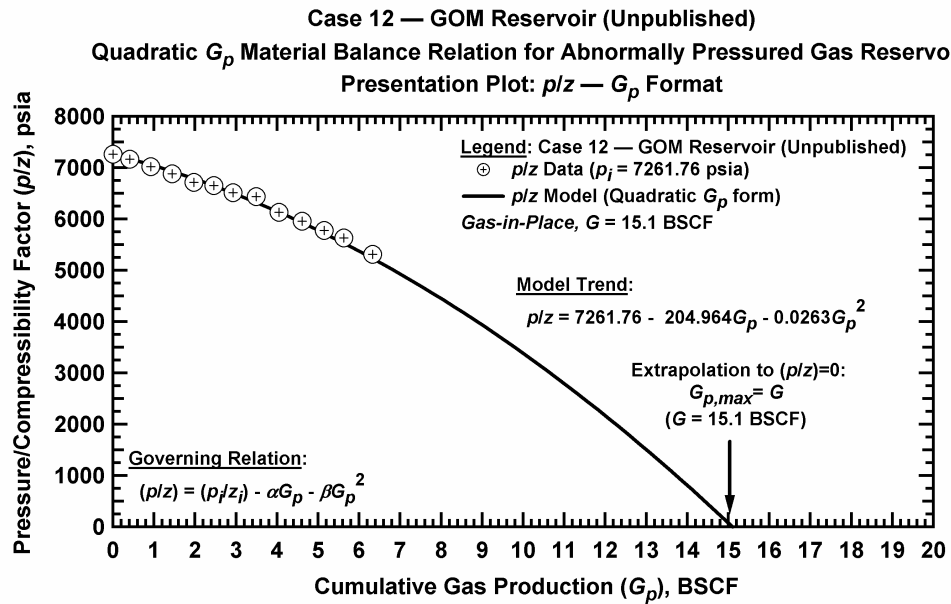


Figure D.13.a — Plot of p/z vs. G_p — Case 12.

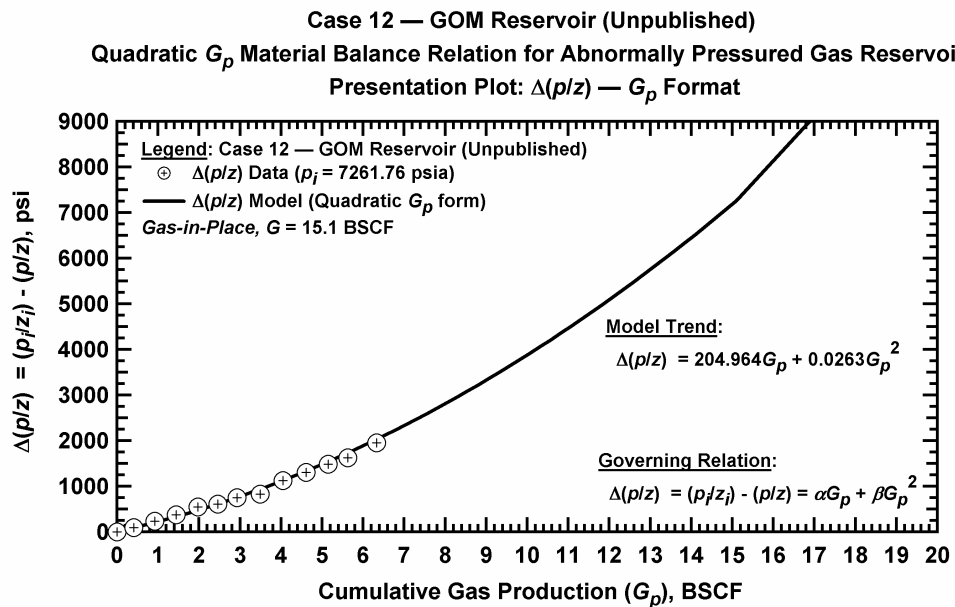


Figure D.13.b — Plot of $\Delta(p/z)$ vs. G_p — Case 12.

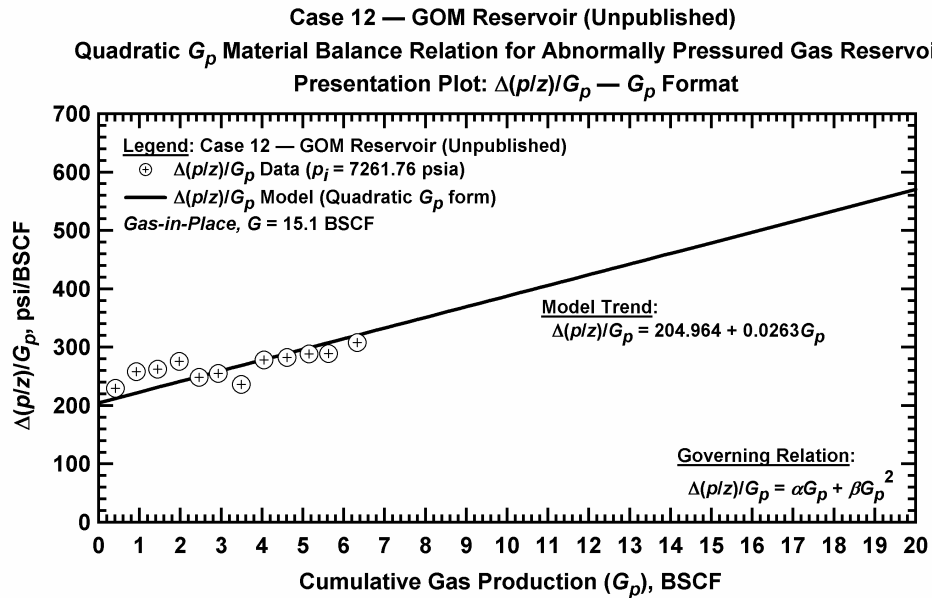


Figure D.13.c — Plot of $\Delta(p/z)/G_p$ vs. G_p — Case 12.

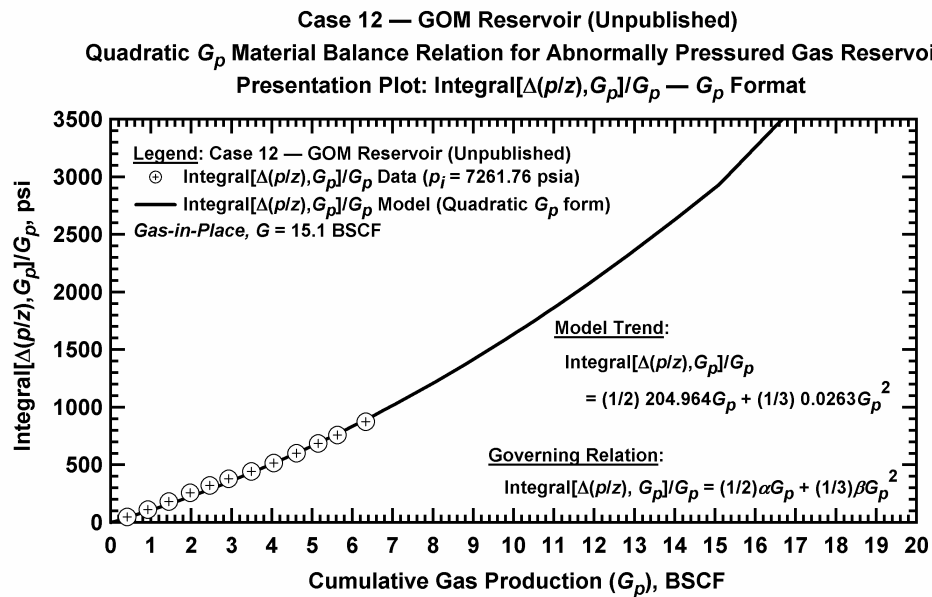


Figure D.13.d — Plot of $\frac{1}{G_p} \int_0^{G_p} \Delta(p/z) dG_p$ vs. G_p — Case 12.

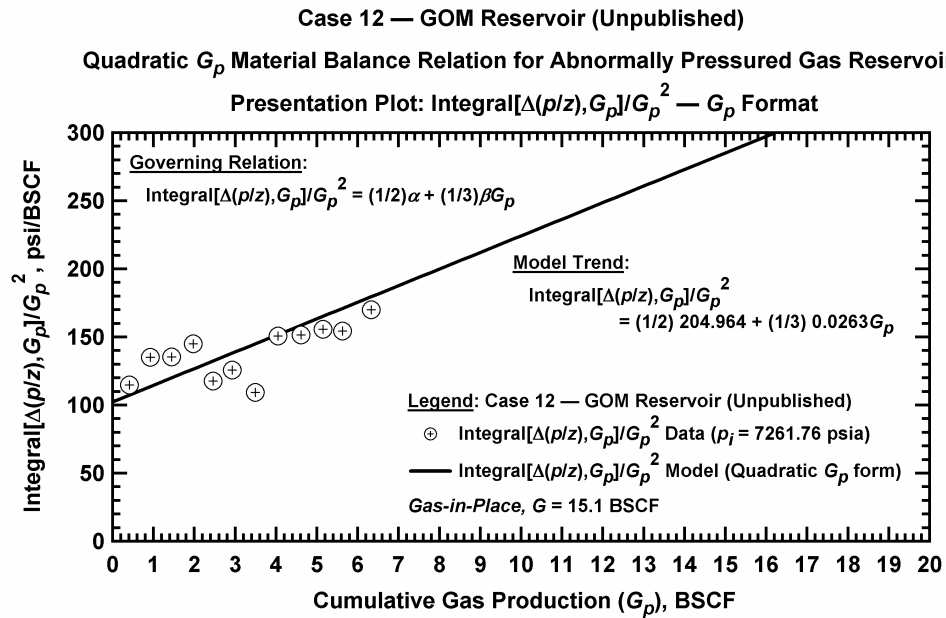


Figure D.13.e — Plot of $\frac{1}{G_p^2} \int_0^{G_p} \Delta(p/z) dG_p$ vs. G_p — Case 12.

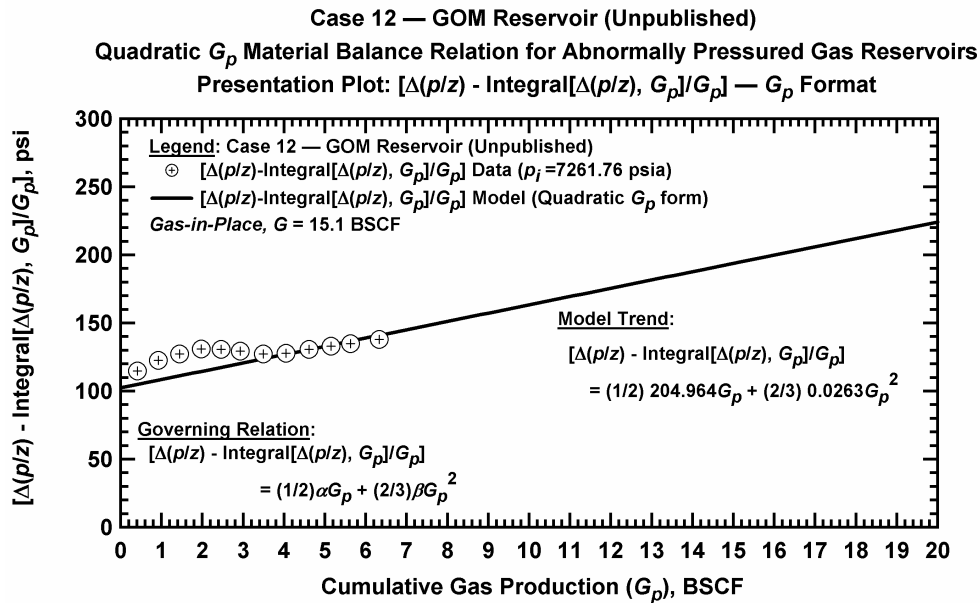


Figure D.13.f — Plot of $\Delta(p/z) - \frac{1}{G_p} \int_0^{G_p} \Delta(p/z) dG_p$ vs. G_p — Case 12.

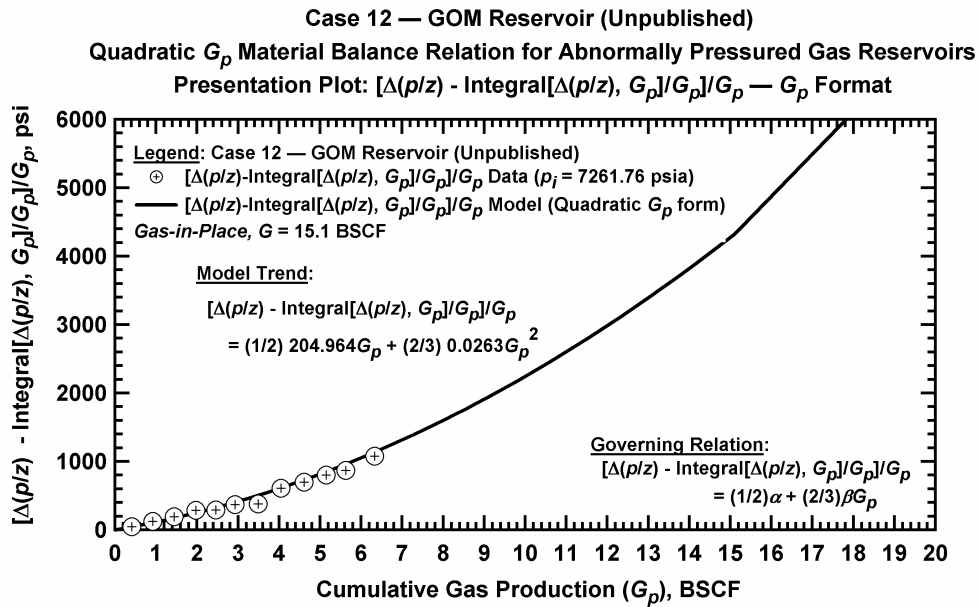


Figure D.13.g — Plot of $\frac{1}{G_p} \left[\Delta(p/z) - \frac{1}{G_p} \int_0^{G_p} \Delta(p/z) dG_p \right]$ vs. G_p — Case 12.

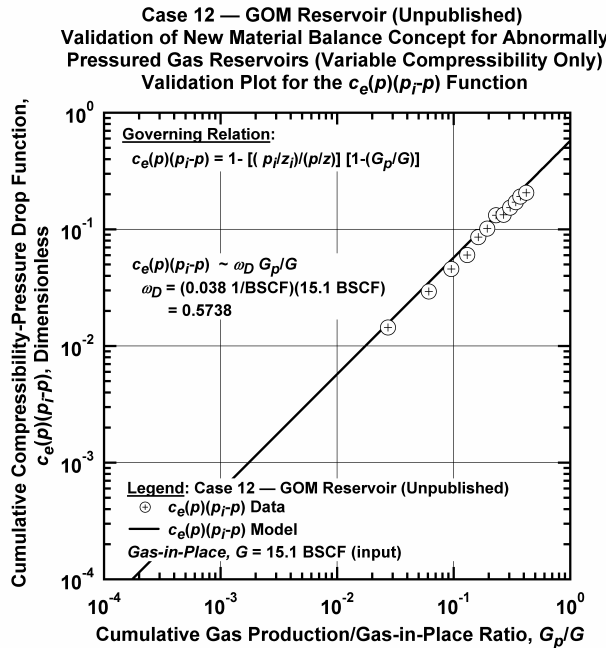


Figure D.13.h — Plot of $\bar{c}_e(p)(p_i - p)$ vs. G_p/G — Base Simulation Case 12.

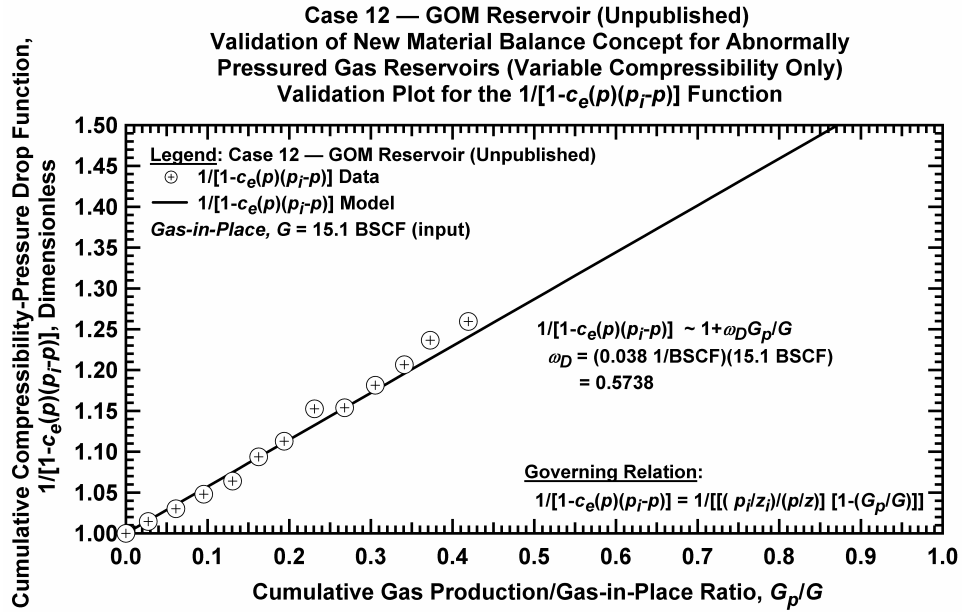


Figure D.13.i — Plot of $1/[1-\bar{c}_e(p)(p_i - p)]$ vs. G_p/G — Case 12.

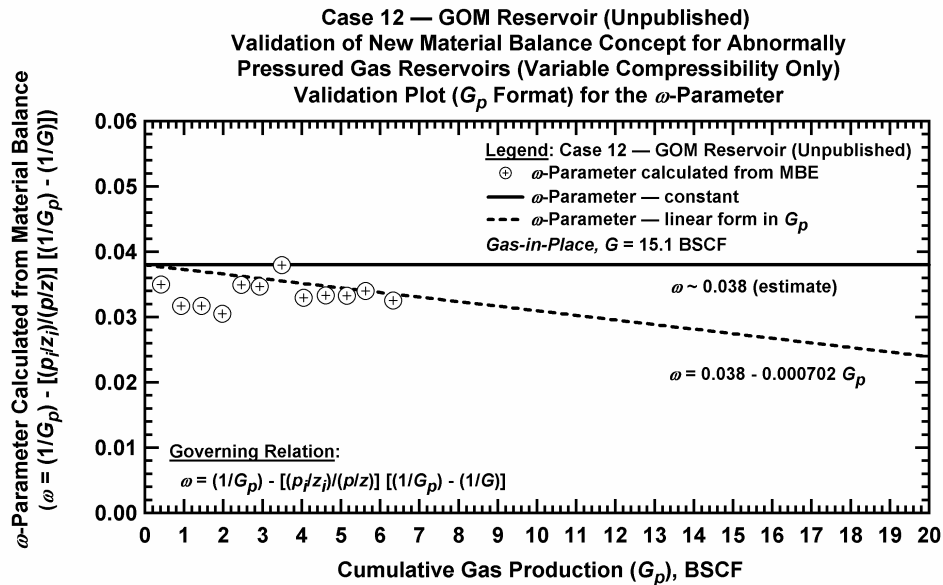


Figure D.13.j — Plot of ω vs. G_p — Base Simulation Case 12.

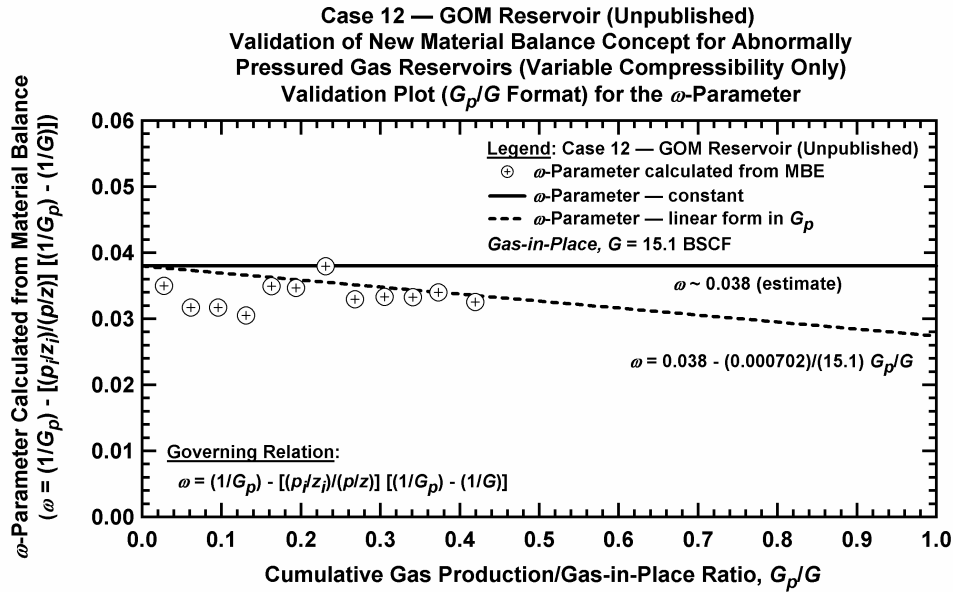


Figure D.13.k — Plot of ω vs. G_p/G — Case 12.

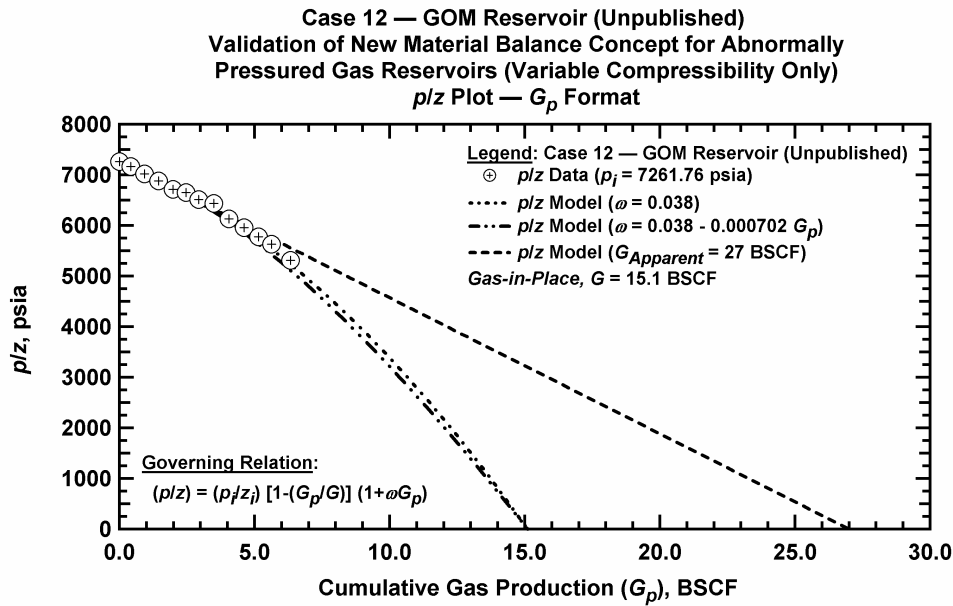


Figure D.13.l — Comparison plot of p/z vs. G_p — Case 12.

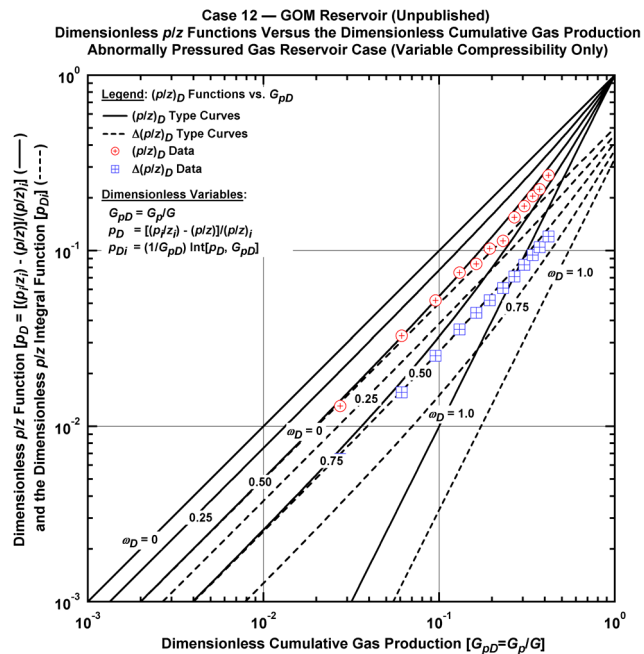


Figure D.13.m — Plot of dimensionless p/z functions vs. G_{pD} — Case 12.

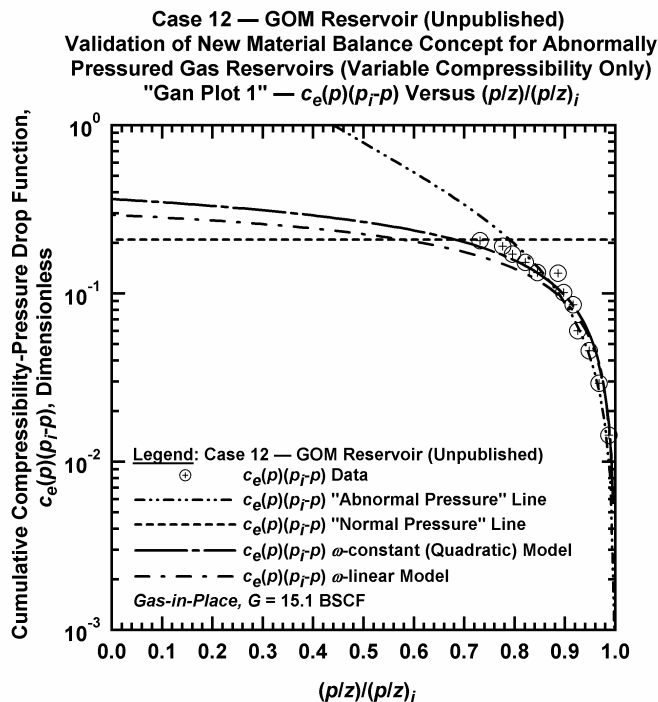


Figure D.13.n — Plot of $\bar{c}_e(p)(p_i - p)$ vs. $(p/z)/(p/z)_i$ — Case 12.

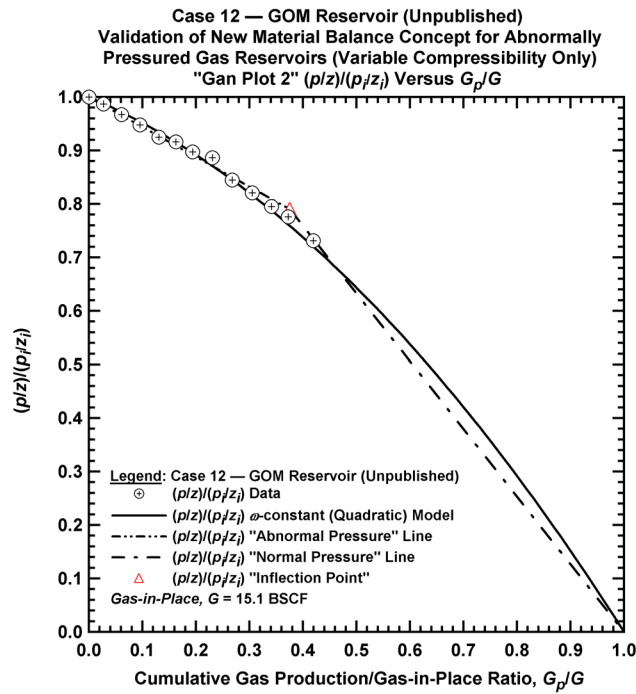


Figure D.13.o — Plot of $(p/z)/(p/z_i)$ vs. G_p/G — Case 12.

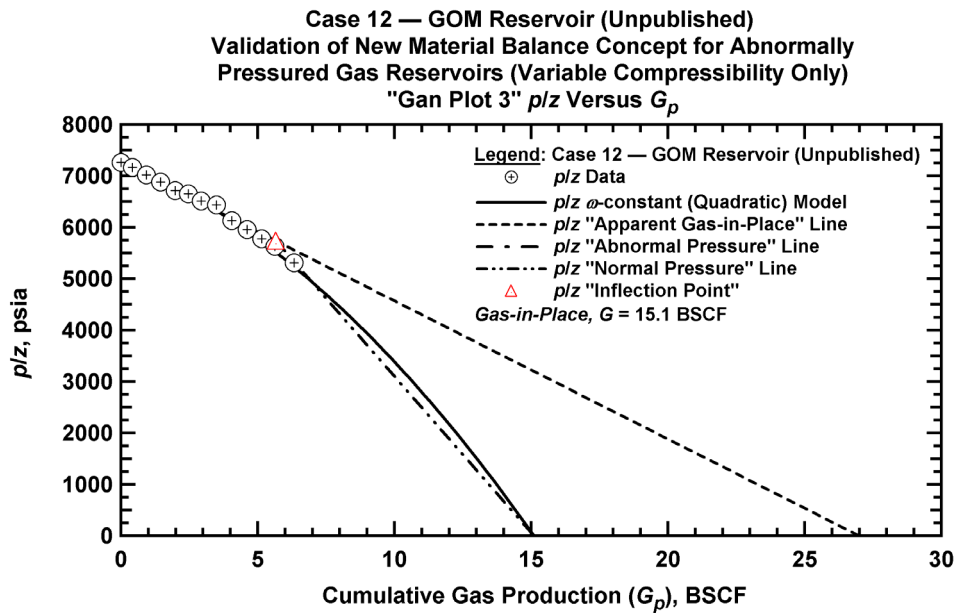


Figure D.13.p — Summary plot of p/z vs. G_p — Case 12.

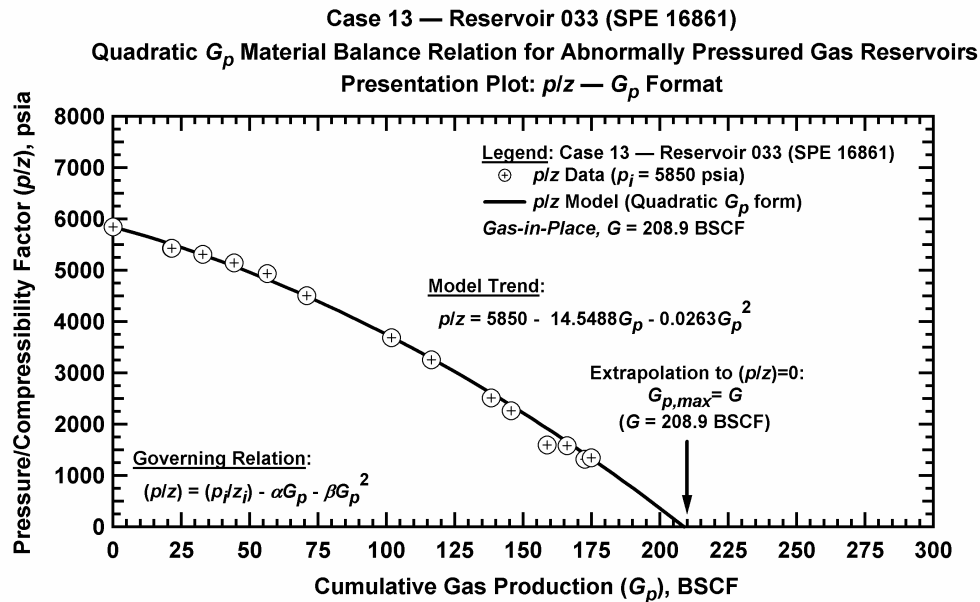


Figure D.14.a — Plot of p/z vs. G_p — Case 13.

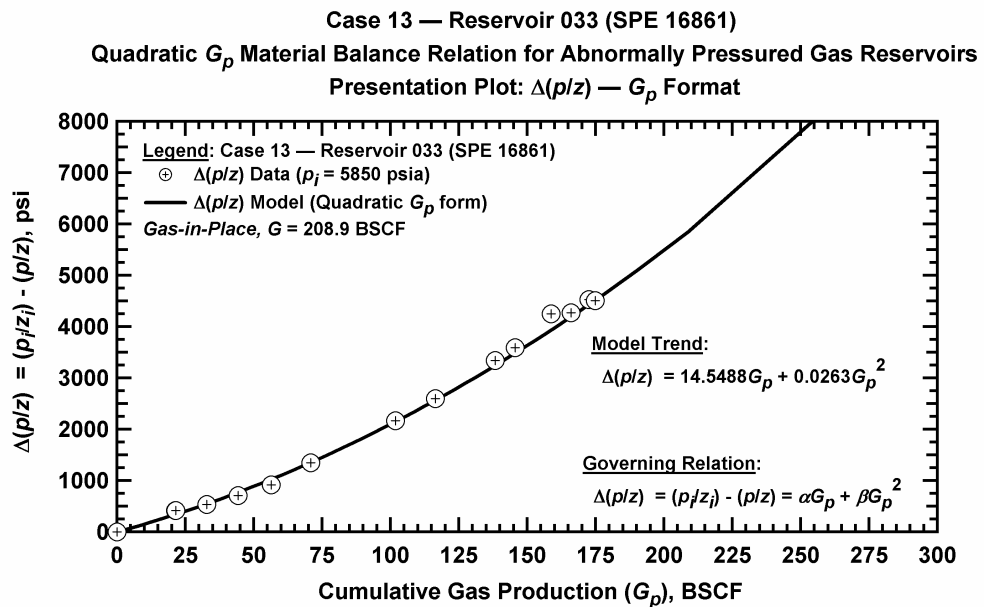


Figure D.14.b — Plot of $\Delta(p/z)$ vs. G_p — Case 13.

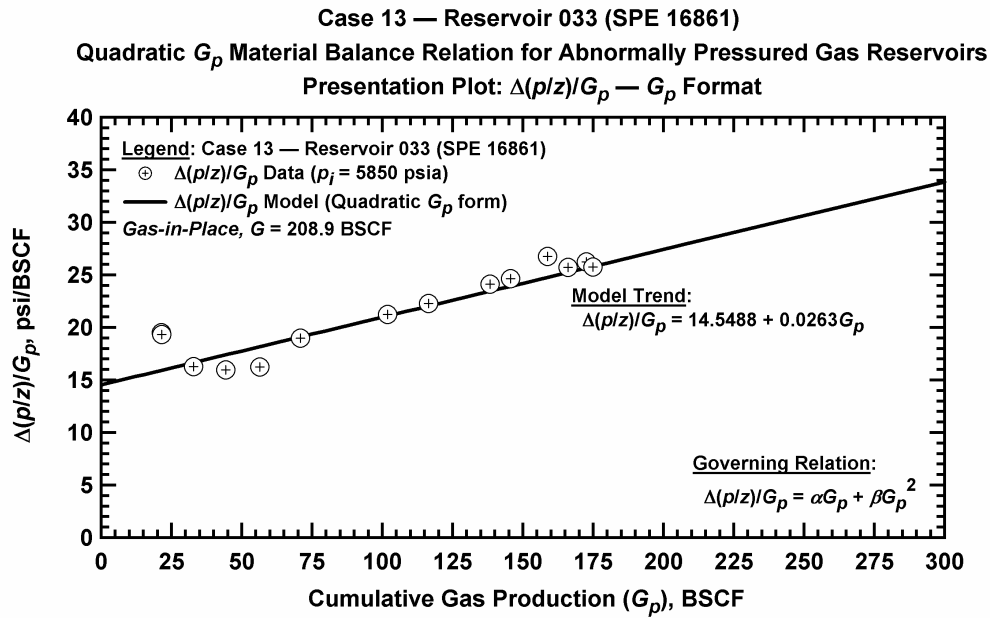


Figure D.14.c — Plot of $\Delta(p/z)/G_p$ vs. G_p — Case 13.

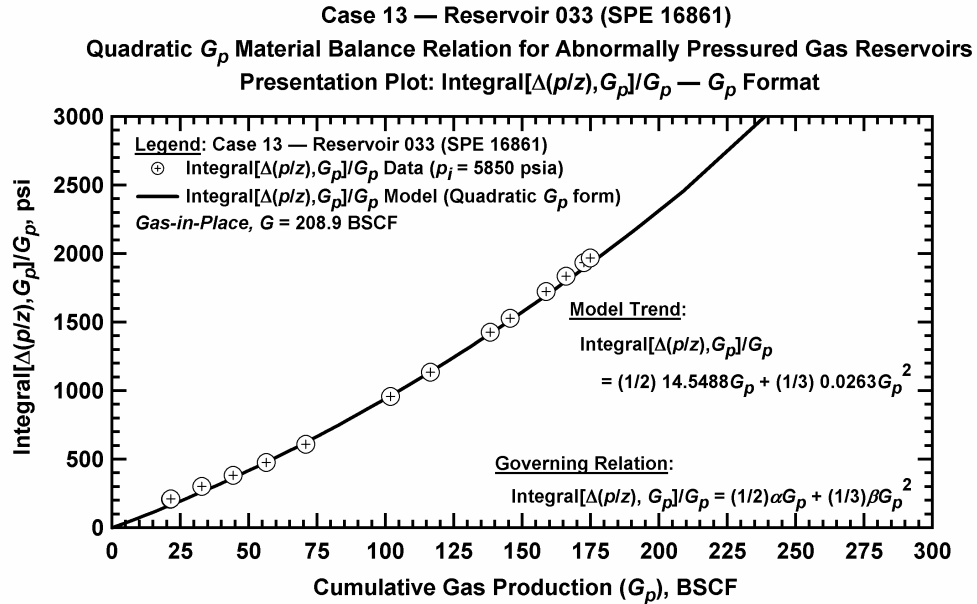


Figure D.14.d — Plot of $\frac{1}{G_p} \int_0^{G_p} \Delta(p/z) dG_p$ vs. G_p — Case 13.

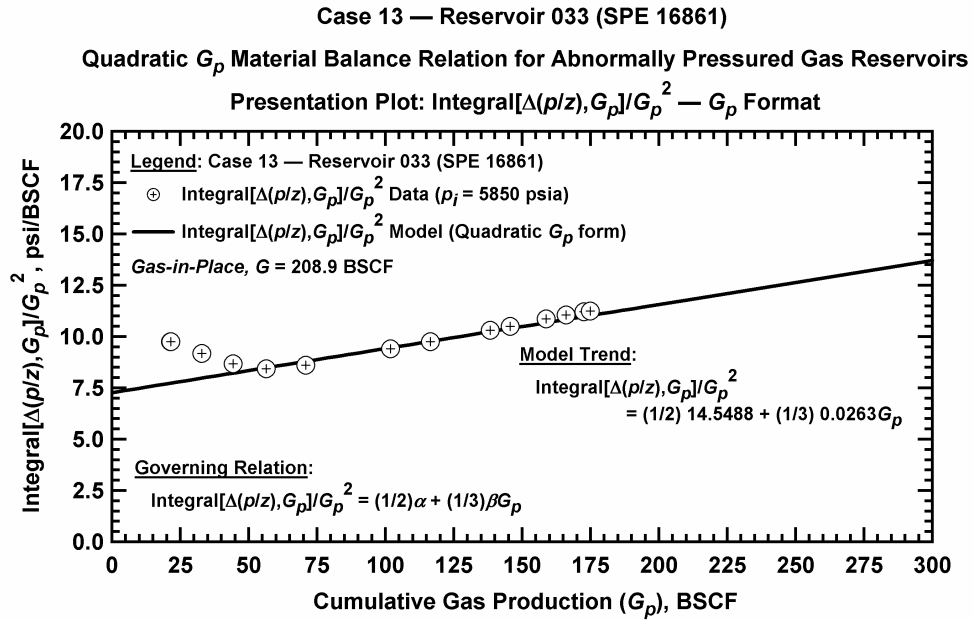


Figure D.14.e — Plot of $\frac{1}{G_p^2} \int_0^{G_p} \Delta(p/z) dG_p$ vs. G_p — Case 13.

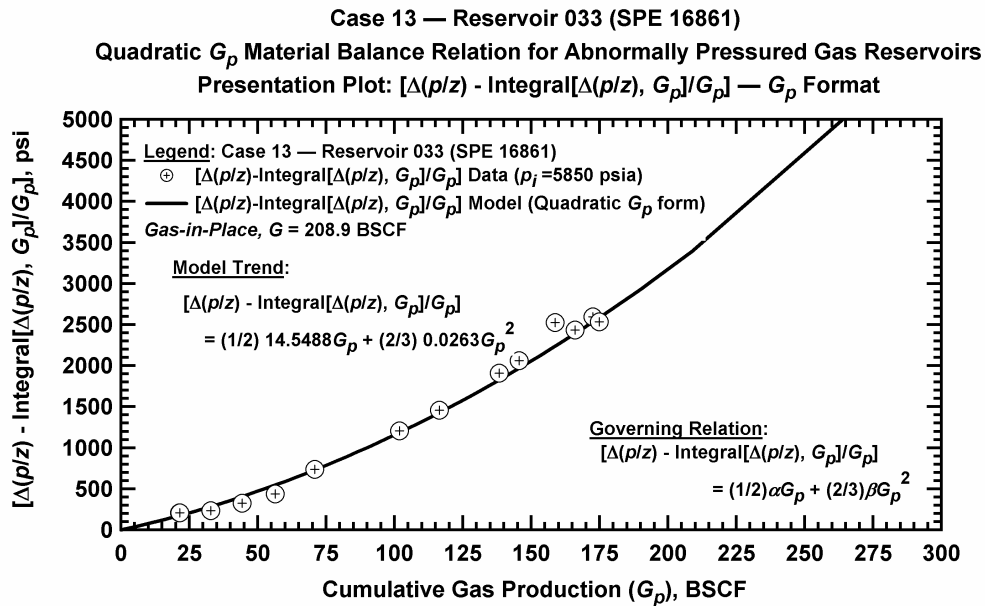


Figure D.14.f — Plot of $\Delta(p/z) - \frac{1}{G_p} \int_0^{G_p} \Delta(p/z) dG_p$ vs. G_p — Case 13.

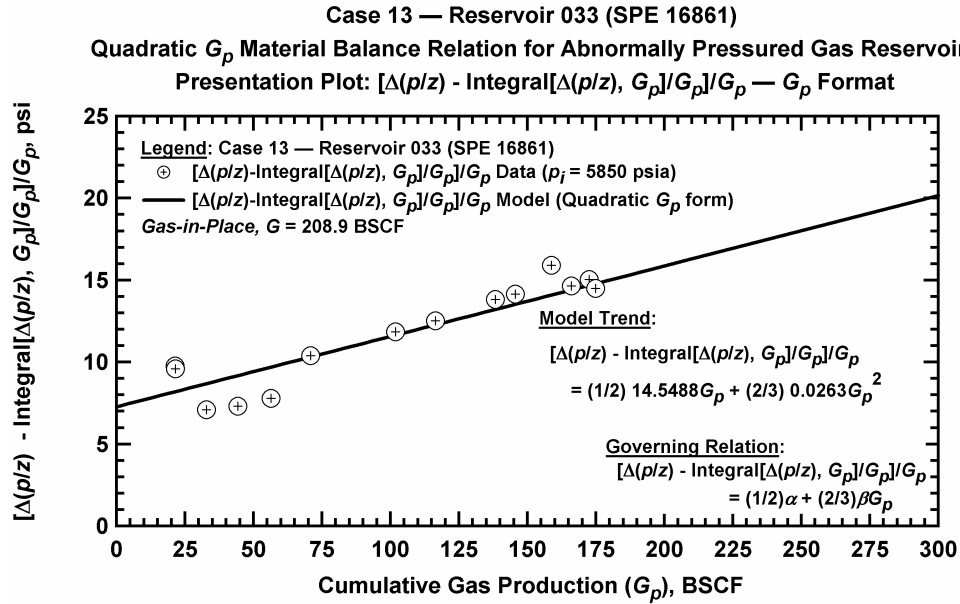


Figure D.14.g — Plot of $\frac{1}{G_p} \left[\Delta(p/z) - \frac{1}{G_p} \int_0^{G_p} \Delta(p/z) dG_p \right]$ vs. G_p — Case 13.

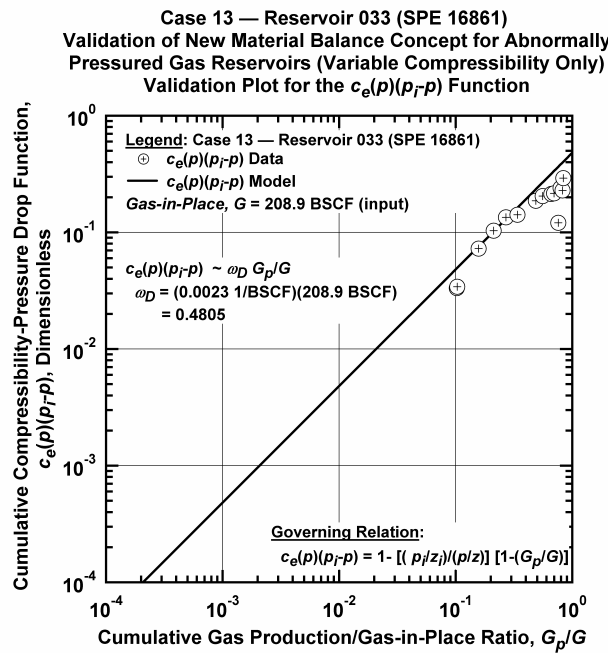


Figure D.14.h — Plot of $\bar{c}_e(p)(p_i - p)$ vs. G_p/G — Base Simulation Case 13.

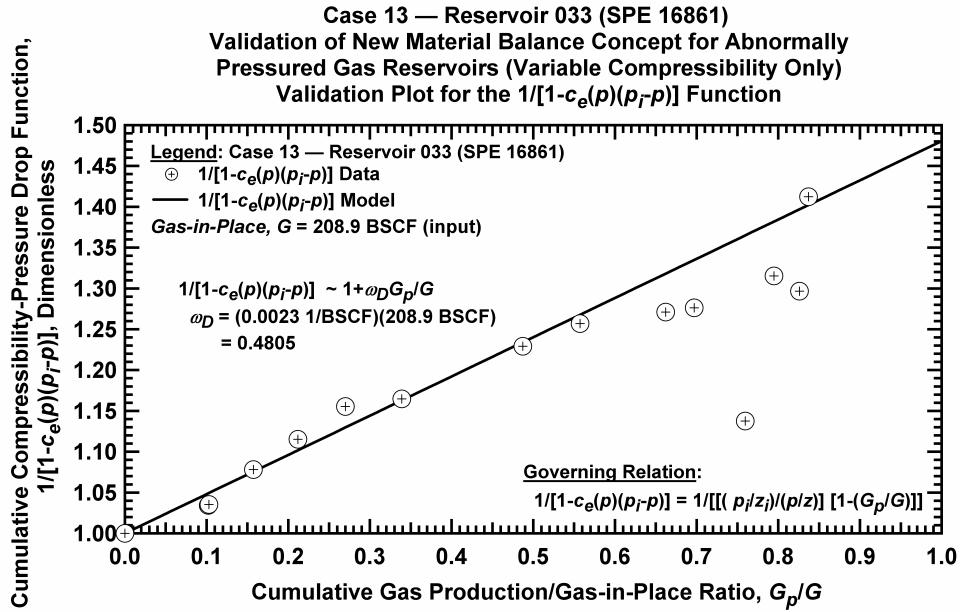


Figure D.14.i — Plot of $1/[1-\bar{c}_e(p)(p_i - p)]$ vs. G_p/G — Case 13.

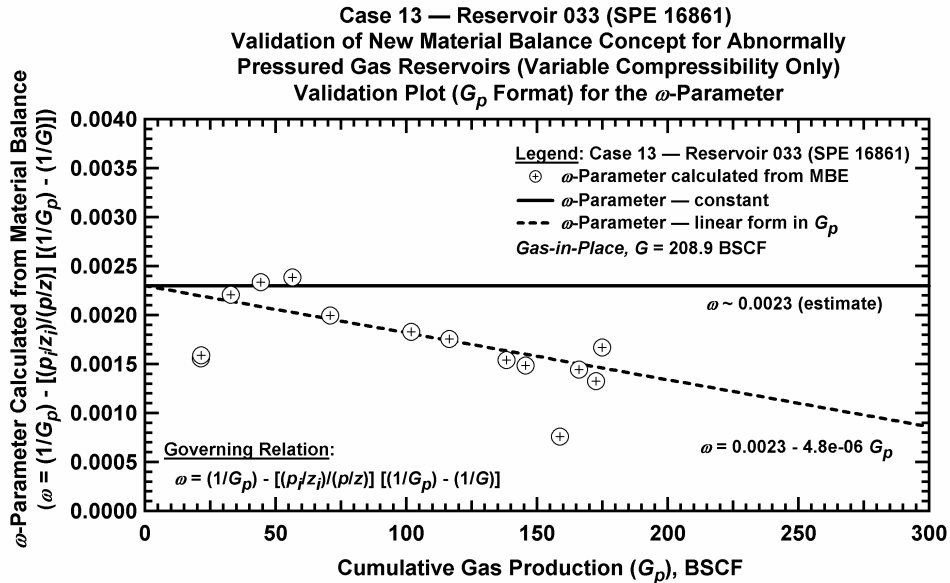


Figure D.14.j — Plot of ω vs. G_p — Base Simulation Case 13.

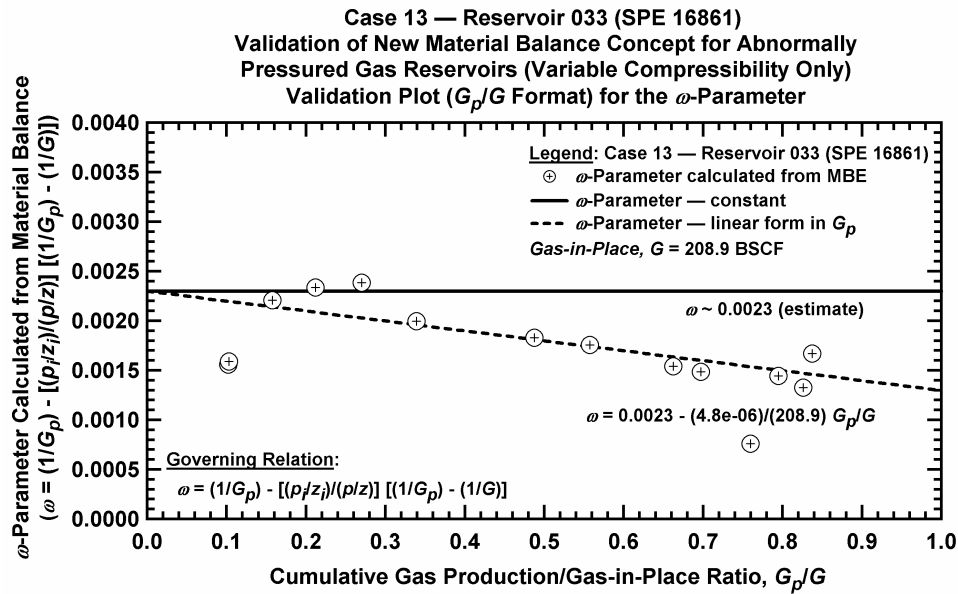


Figure D.14.k — Plot of ω vs. G_p/G — Case 13.

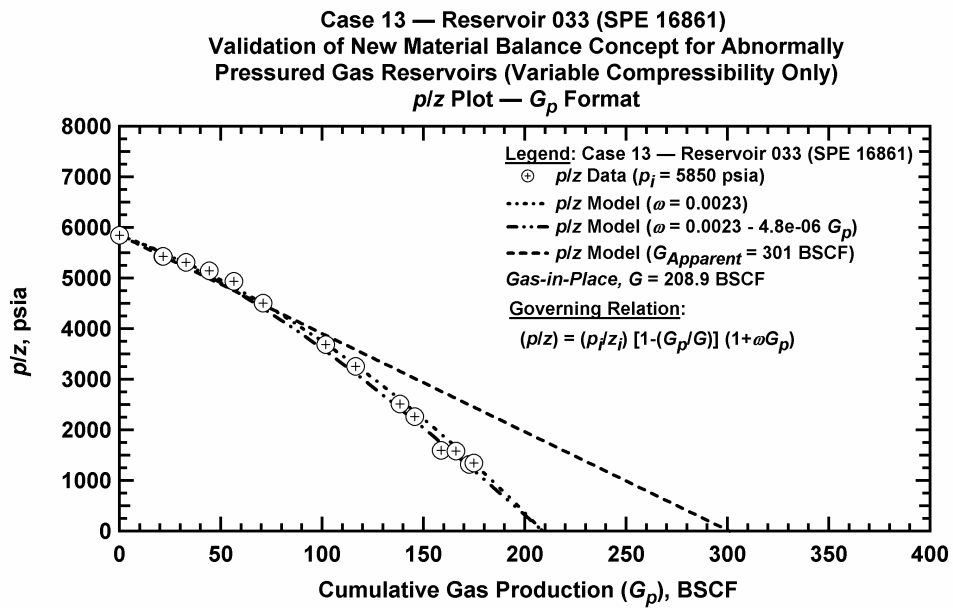


Figure D.14.l — Comparison plot of p/z vs. G_p — Case 13.

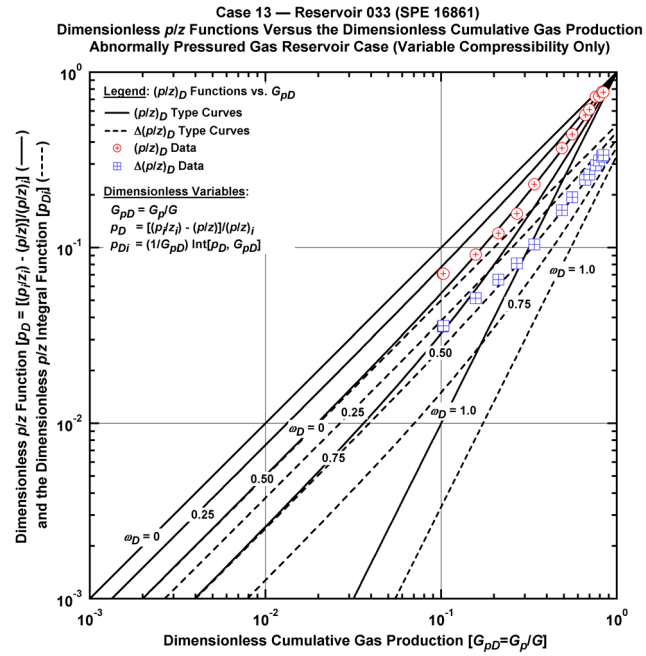


Figure D.14.m — Plot of dimensionless p/z functions vs. G_{pD} — Case 13.

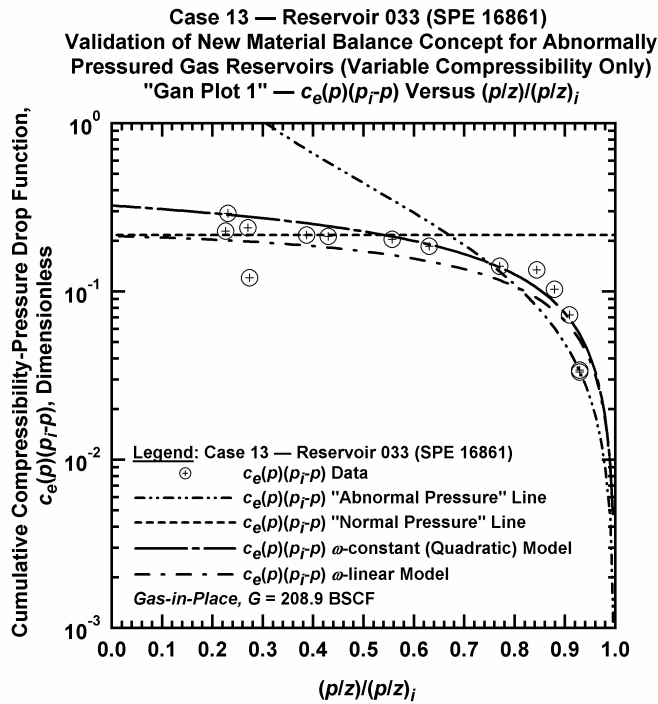


Figure D.14.n — Plot of $\bar{c}_e(p)(p_i - p)$ vs. $(p/z)/(p_i/z_i)$ — Case 13.

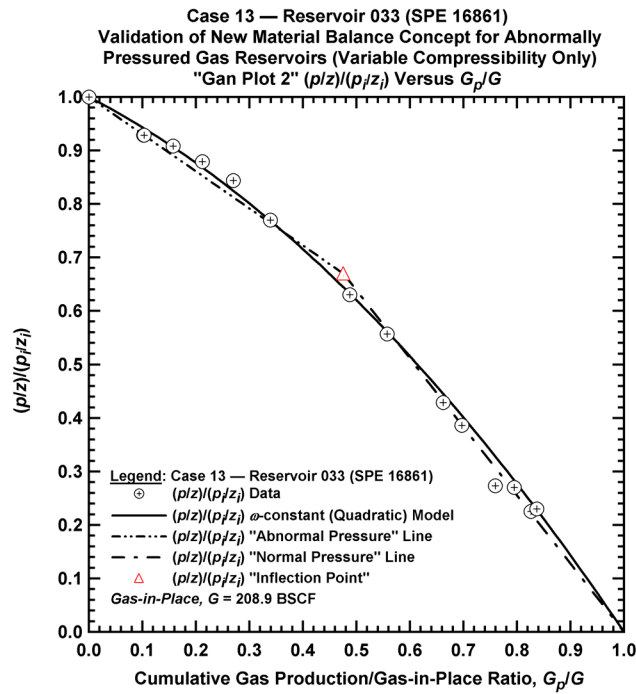


Figure D.14.o Plot of $(p/z)/(p/z_i)$ vs. G_p/G — Case 13.

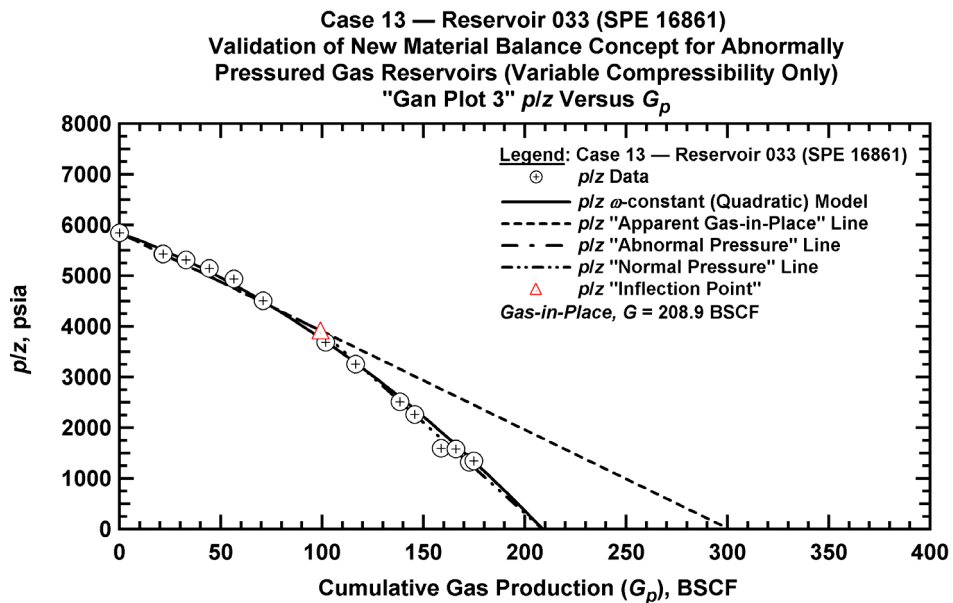


Figure D.14.p— Summary plot of p/z vs. G_p — Case 13.

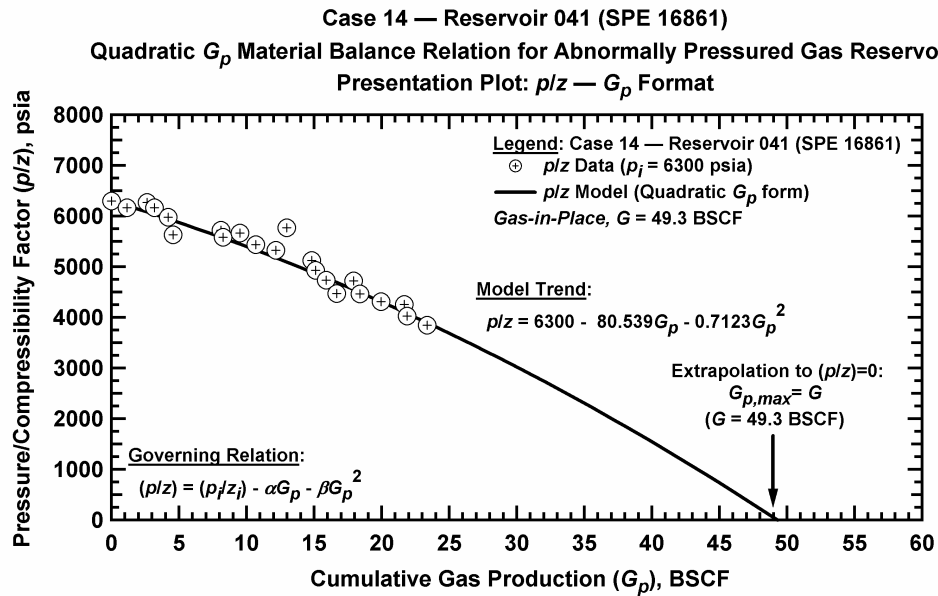


Figure D.15.a — Plot of p/z vs. G_p — Case 14.

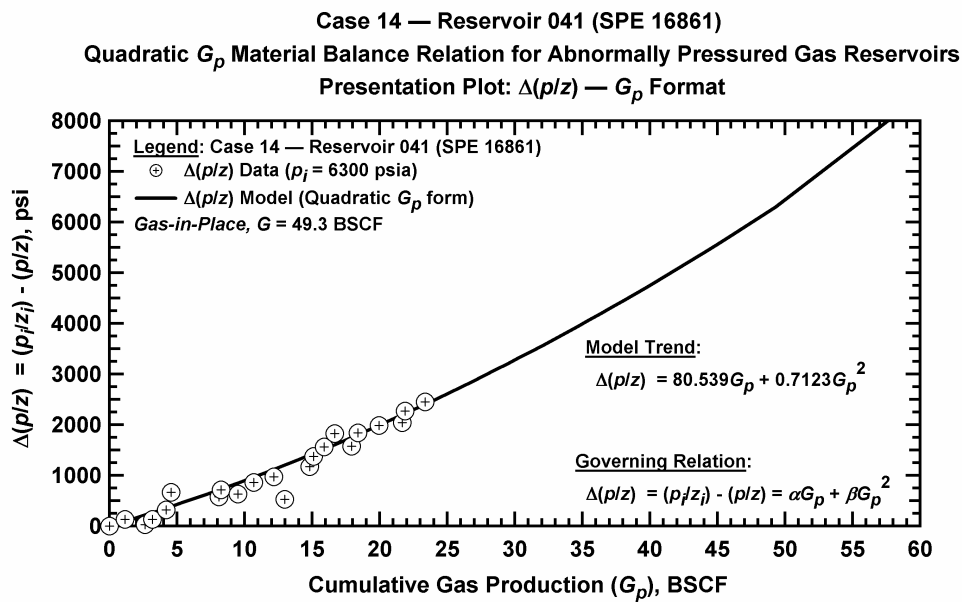


Figure D.15.b — Plot of $\Delta(p/z)$ vs. G_p — Case 14.

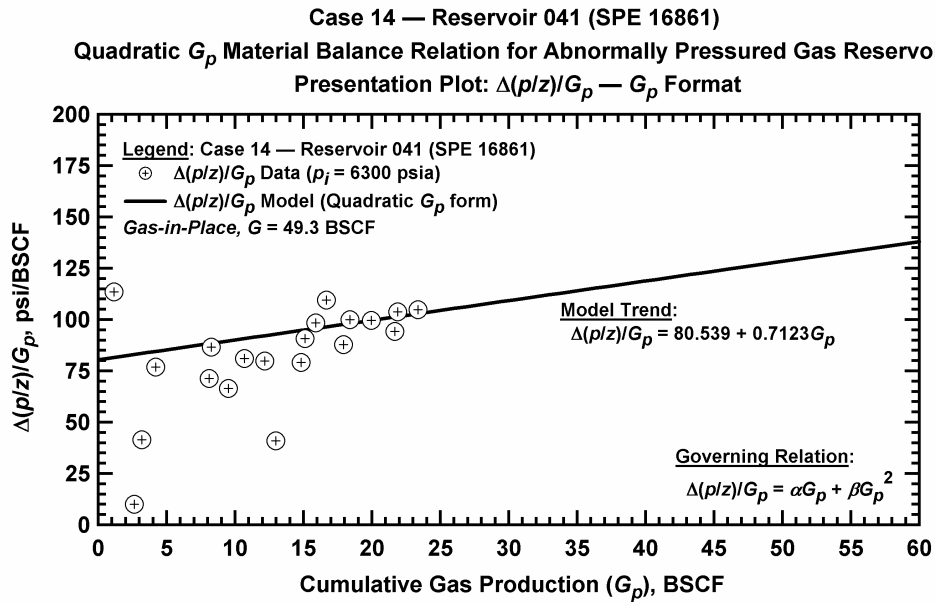


Figure D.15.c — Plot of $\Delta(p/z)/G_p$ vs. G_p — Case 14.

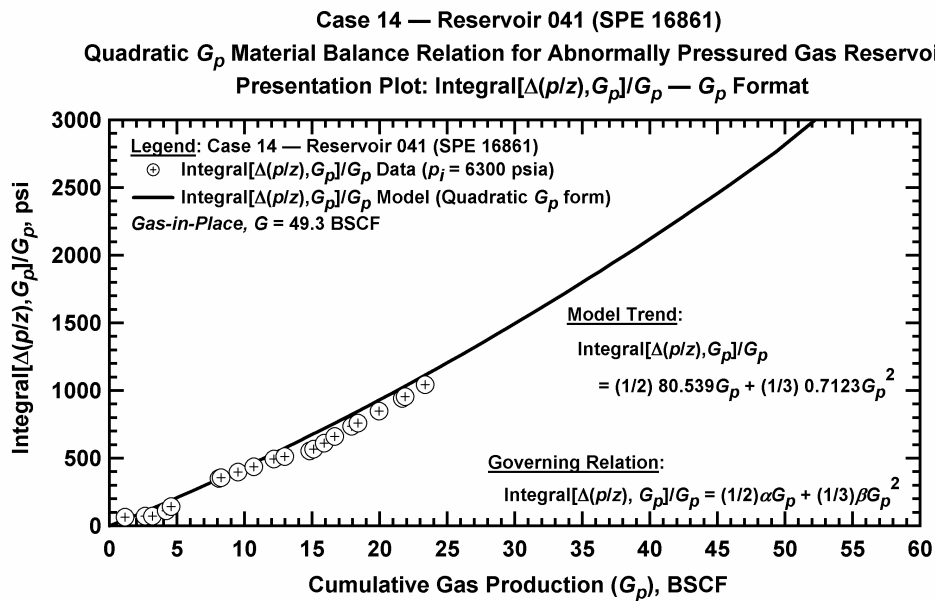
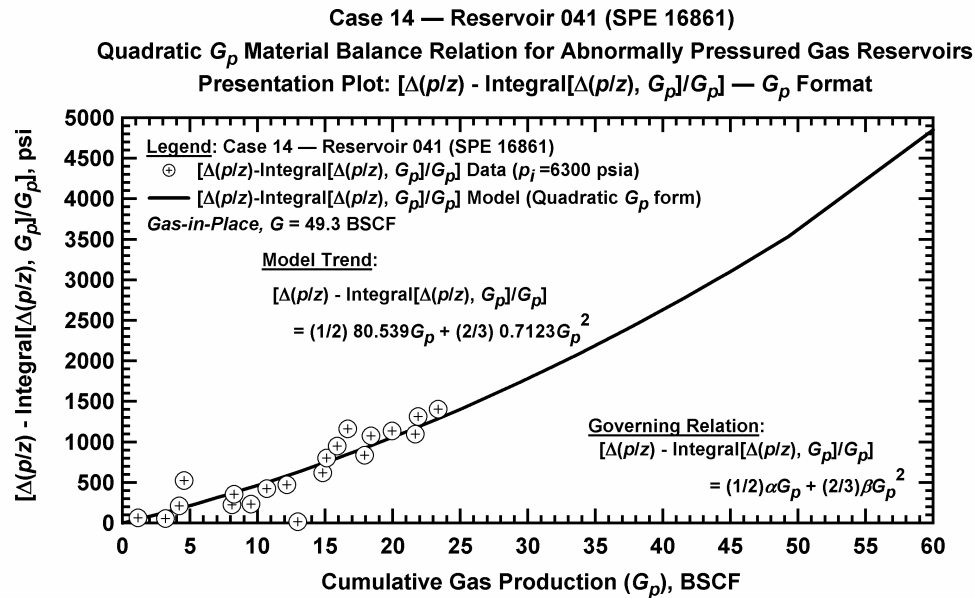
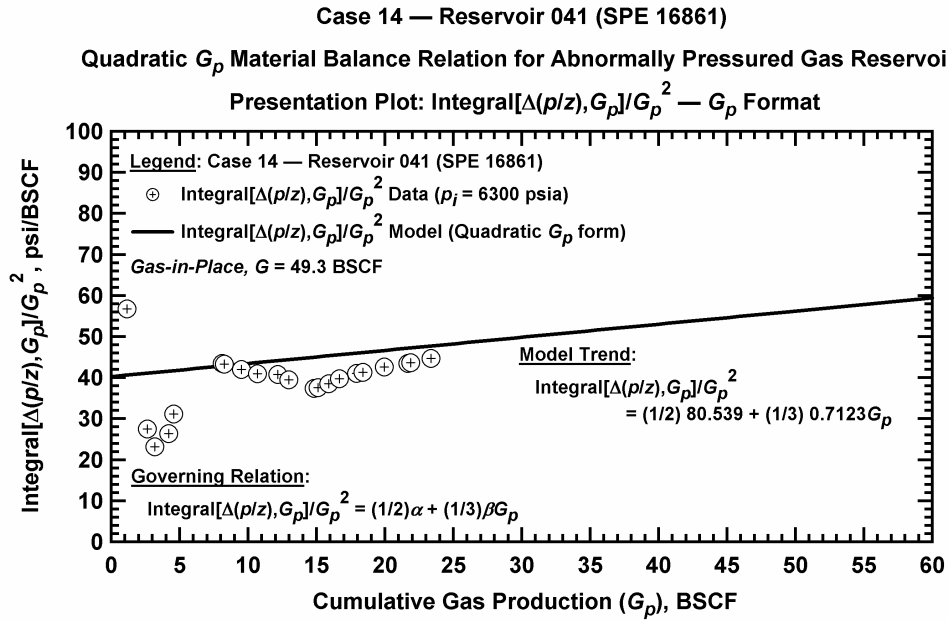


Figure D.15.d — Plot of $\frac{1}{G_p} \int_0^{G_p} \Delta(p/z) dG_p$ vs. G_p — Case 14.



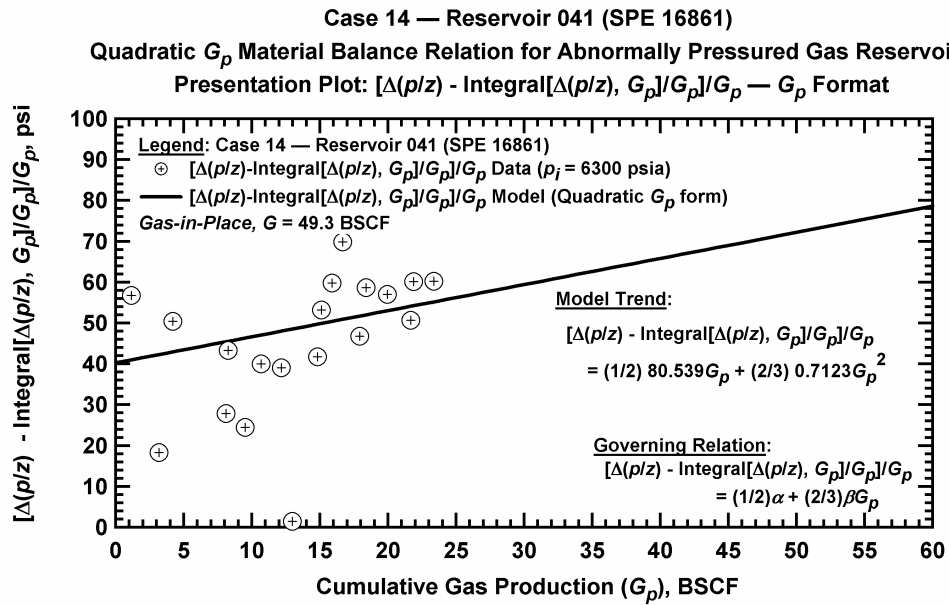


Figure D.15.g — Plot of $\frac{1}{G_p} \left[\Delta(p/z) - \frac{1}{G_p} \int_0^{G_p} \Delta(p/z) dG_p \right]$ vs. G_p — Case 14.

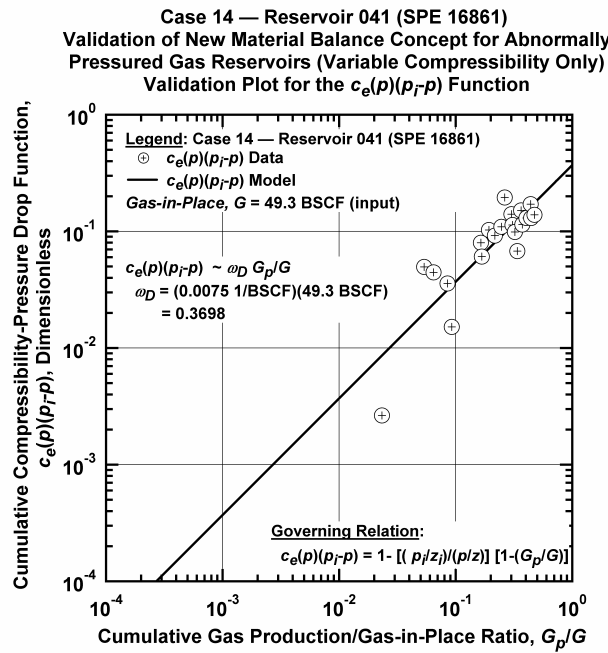


Figure D.15.h — Plot of $\bar{c}_e(p)(p_i - p)$ vs. G_p/G — Base Simulation Case 14.

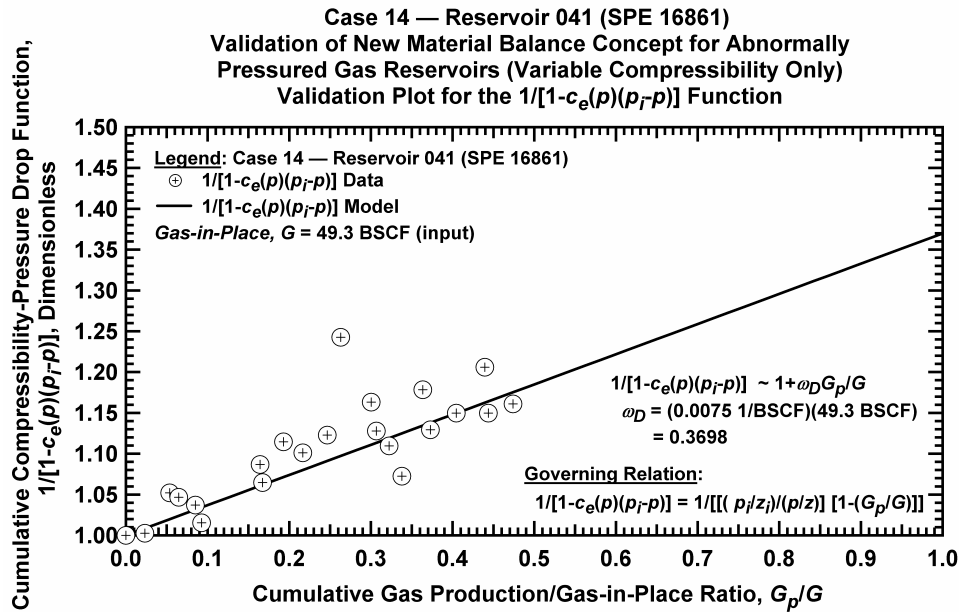


Figure D.15.i — Plot of $1/[1-\bar{c}_e(p)(p_i - p)]$ vs. G_p/G — Case 14.

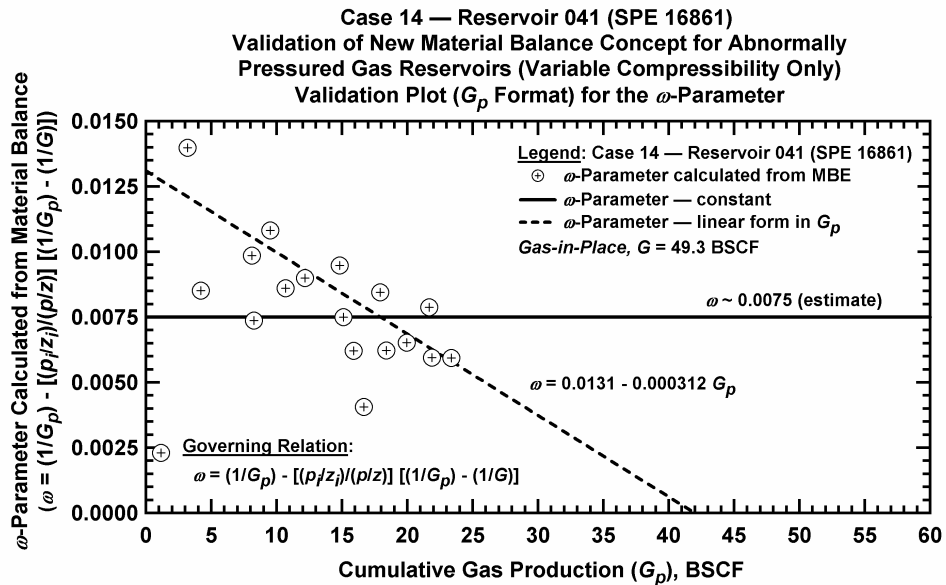


Figure D.15.j — Plot of w vs. G_p — Base Simulation Case 14.

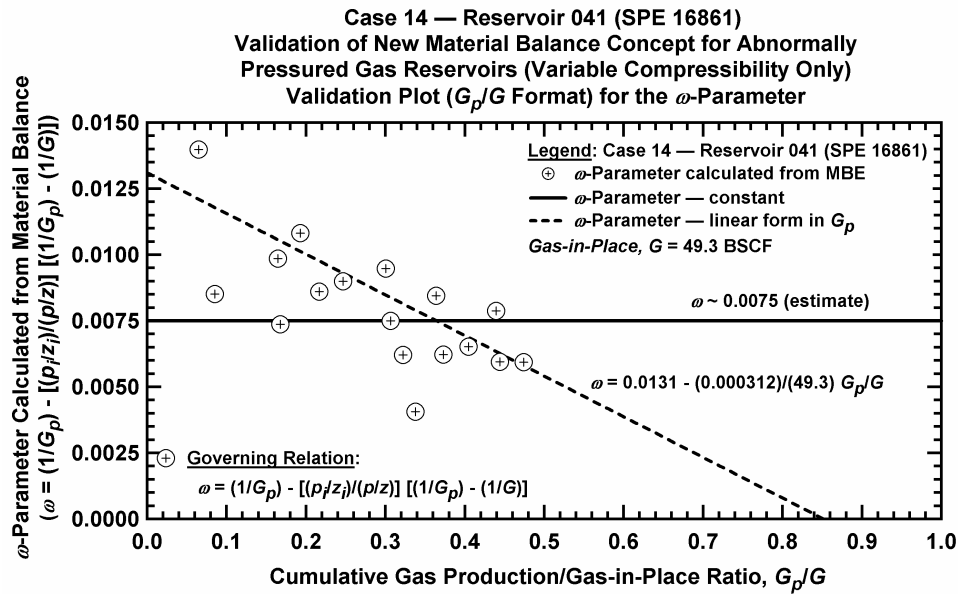


Figure D.15.k — Plot of ω vs. G_p/G — Case 14.

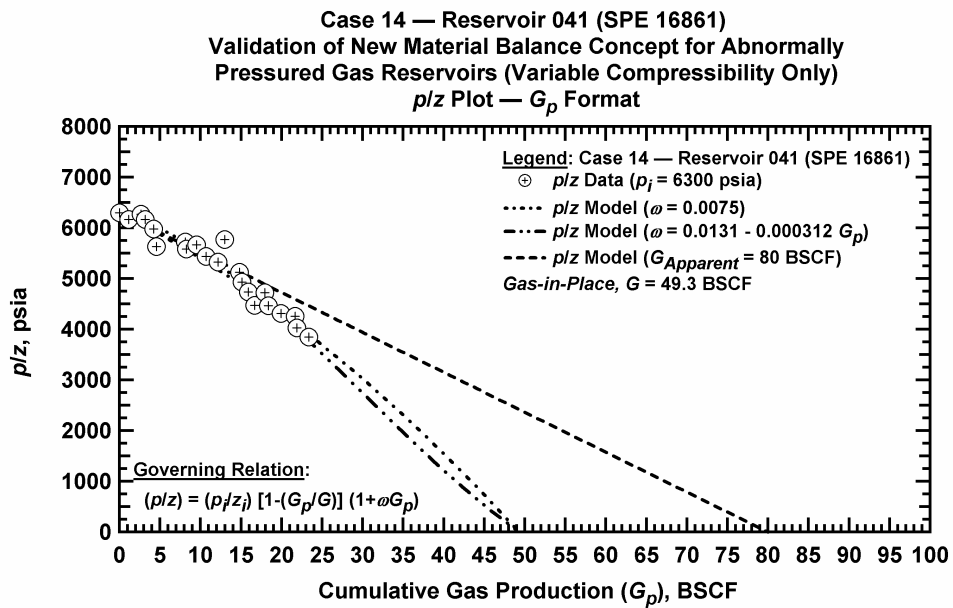


Figure D.15.l — Comparison plot of p/z vs. G_p — Case 14.

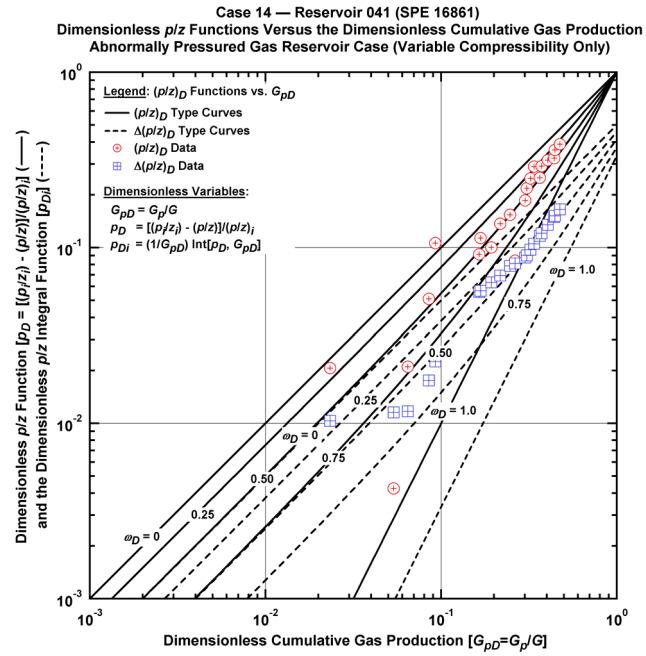


Figure D.15.m — Plot of dimensionless p/z functions vs. G_{pD} — Case 14.

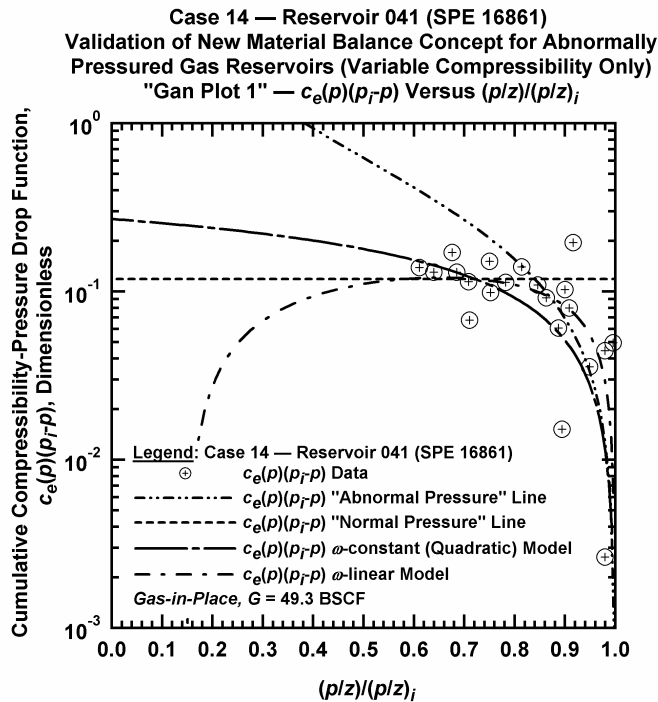


Figure D.15.n — Plot of $\bar{c}_e(p)(p_i - p)$ vs. $(p/z)/(p_i/z_i)$ — Case 14.

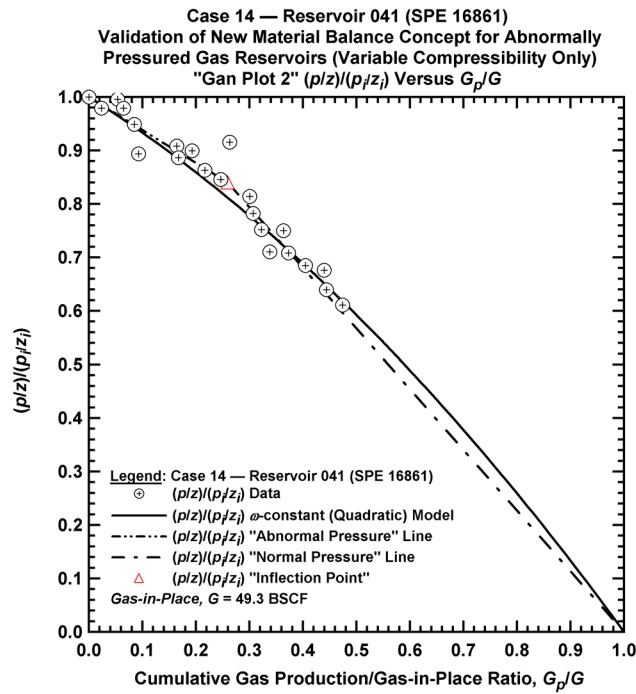


Figure D.15.o — Plot of $(p/z)/(p/z_i)$ vs. G_p/G — Case 14.

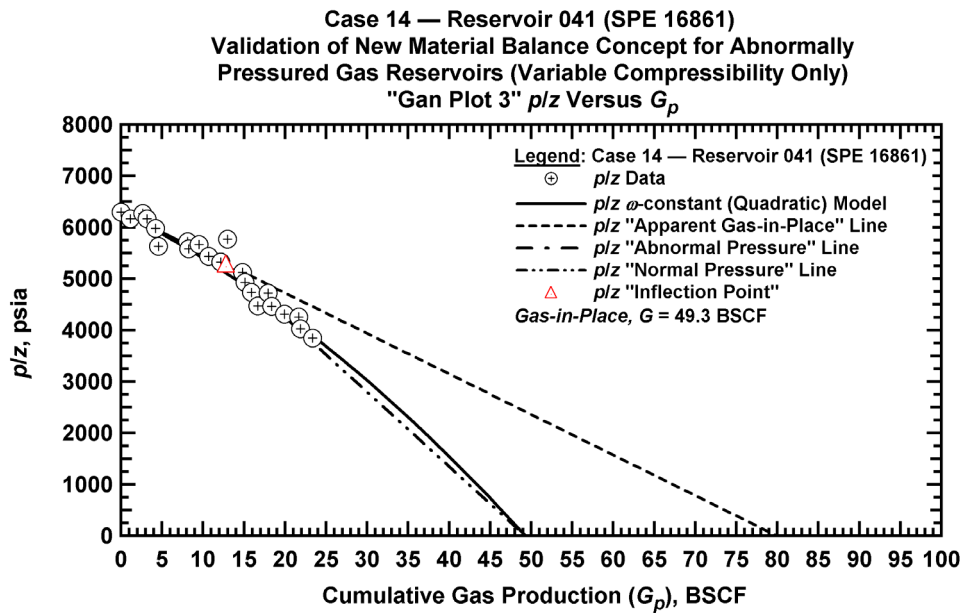


Figure D.15.p — Summary plot of p/z vs. G_p — Case 14.

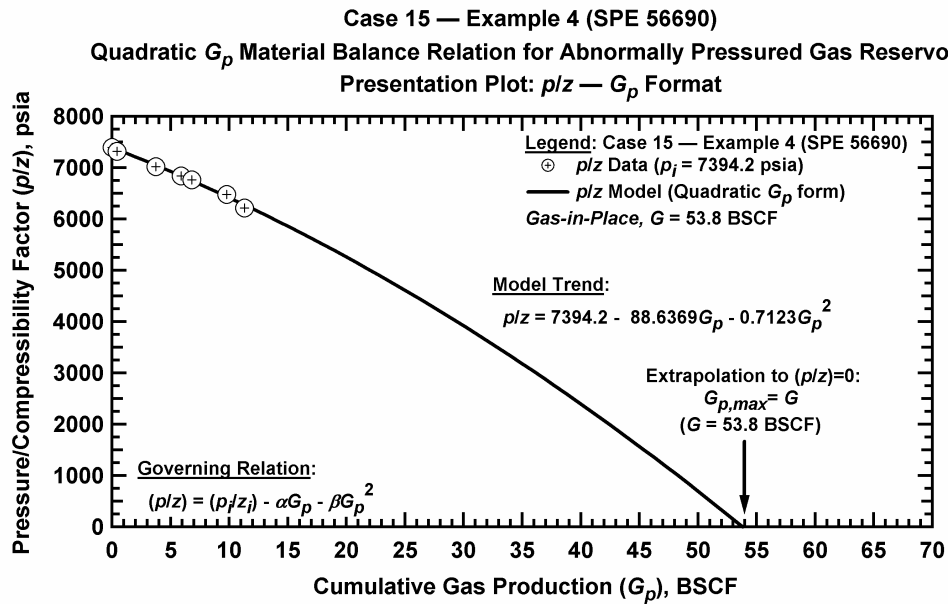


Figure D.16.a — Plot of p/z vs. G_p — Case 15.

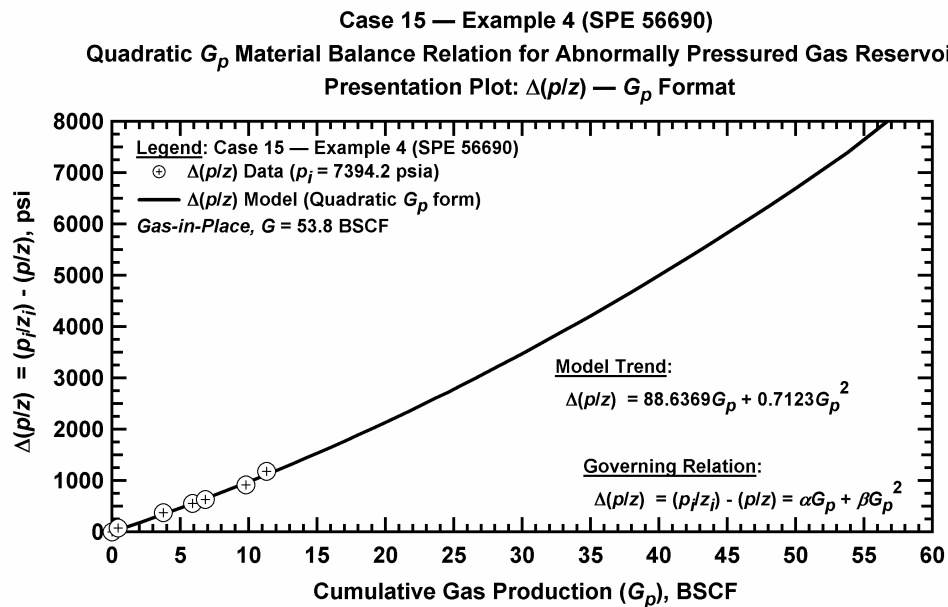


Figure D.16.b — Plot of $\Delta(p/z)$ vs. G_p — Case 15.

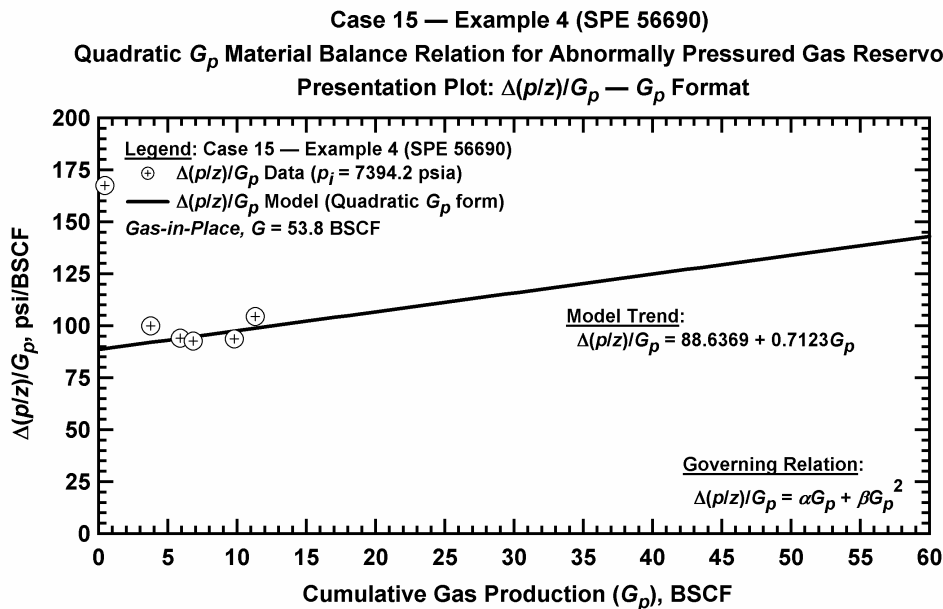


Figure D.16.c — Plot of $\Delta(p/z)/G_p$ vs. G_p — Case 15.

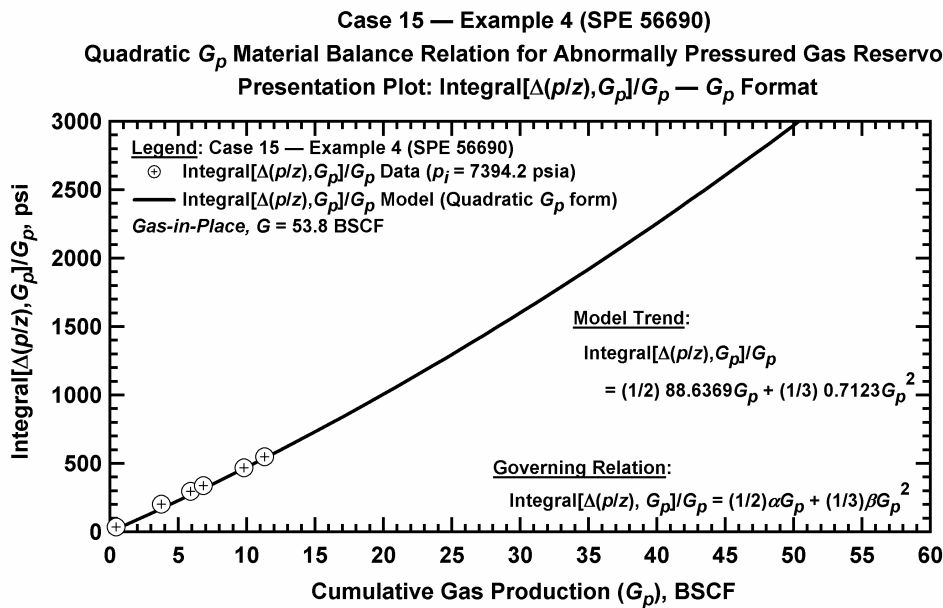


Figure D.16.d — Plot of $\frac{1}{G_p} \int_0^{G_p} \Delta(p/z) dG_p$ vs. G_p — Case 15.

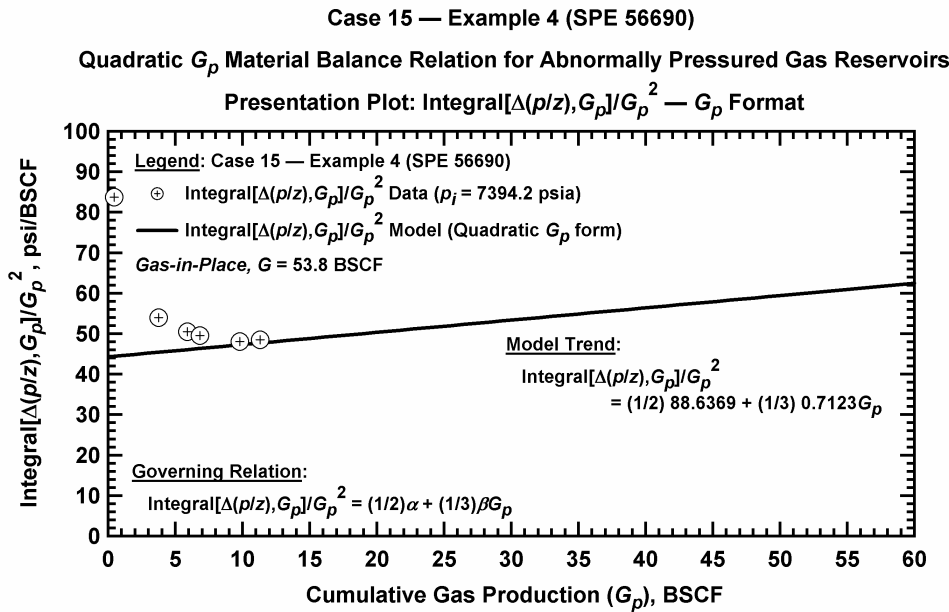


Figure D.16.e — Plot of $\frac{1}{G_p^2} \int_0^{G_p} \Delta(p/z) dG_p$ vs. G_p — Case 15.

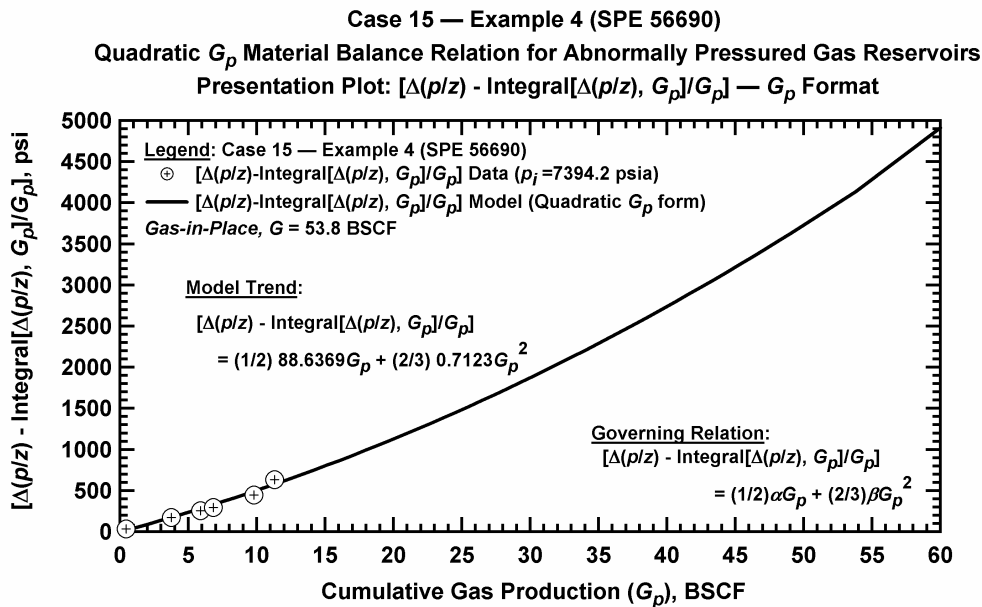


Figure D.16.f — Plot of $\Delta(p/z) - \frac{1}{G_p} \int_0^{G_p} \Delta(p/z) dG_p$ vs. G_p — Case 15.

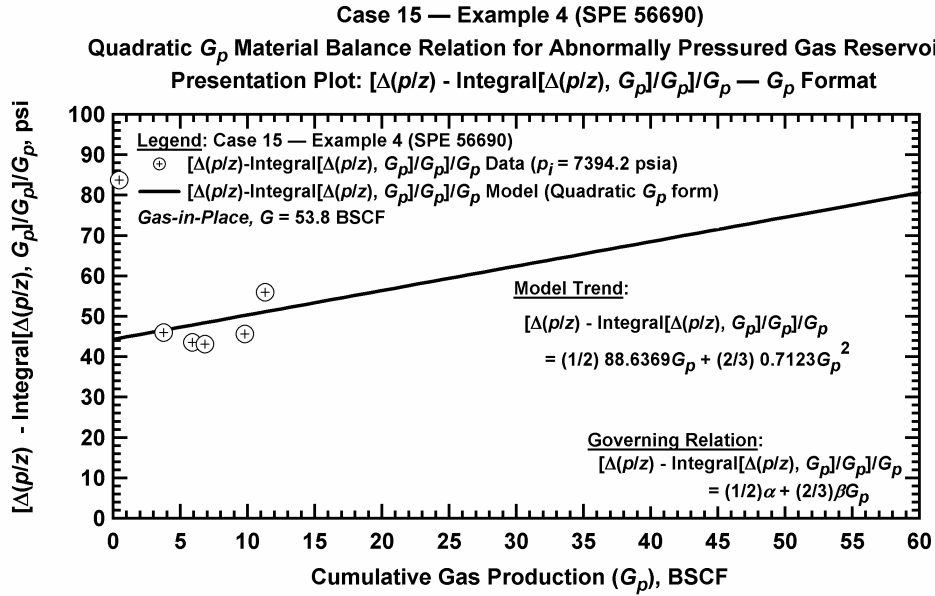


Figure D.16.g — Plot of $\frac{1}{G_p} \left[\Delta(p/z) - \frac{1}{G_p} \int_0^{G_p} \Delta(p/z) dG_p \right]$ vs. G_p — Case 15.

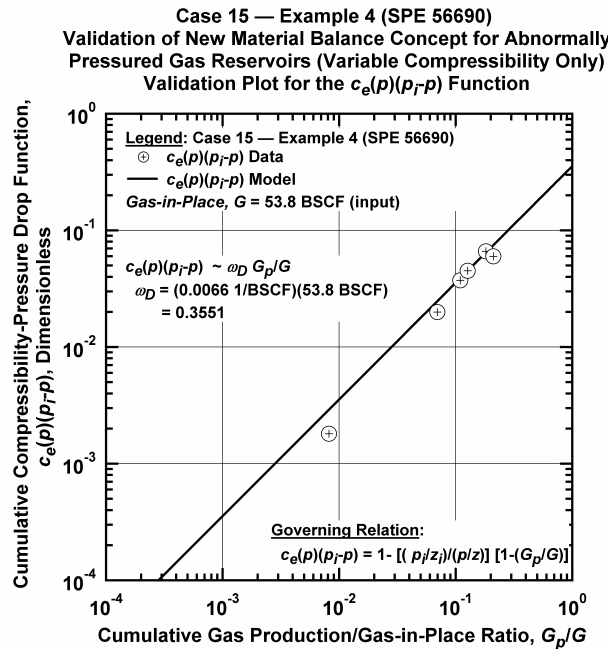


Figure D.16.h — Plot of $\bar{c}_e(p)(p_i - p)$ vs. G_p/G — Base Simulation Case 15.

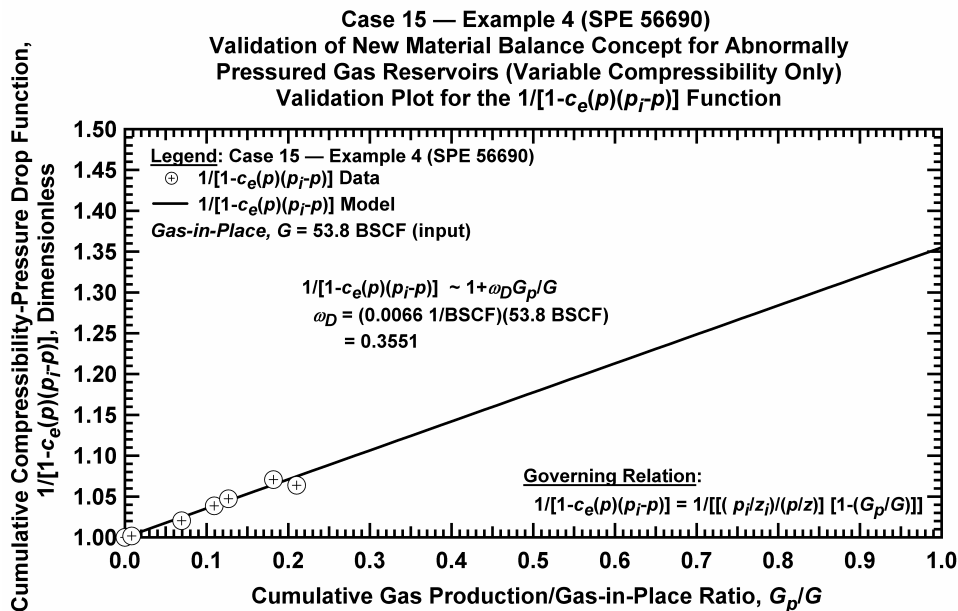


Figure D.16.i — Plot of $1/[1-\bar{c}_e(p)(p_i - p)]$ vs. G_p/G — Case 15.

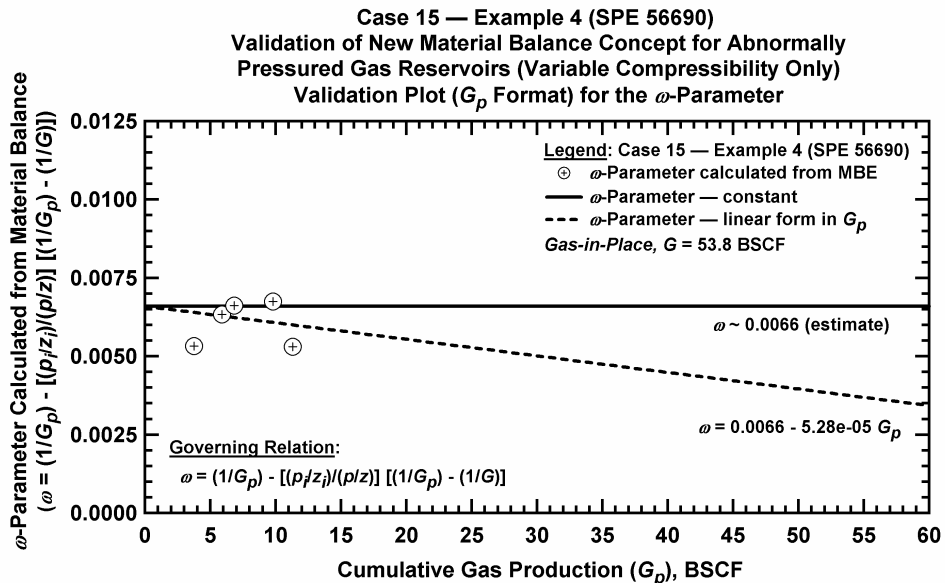
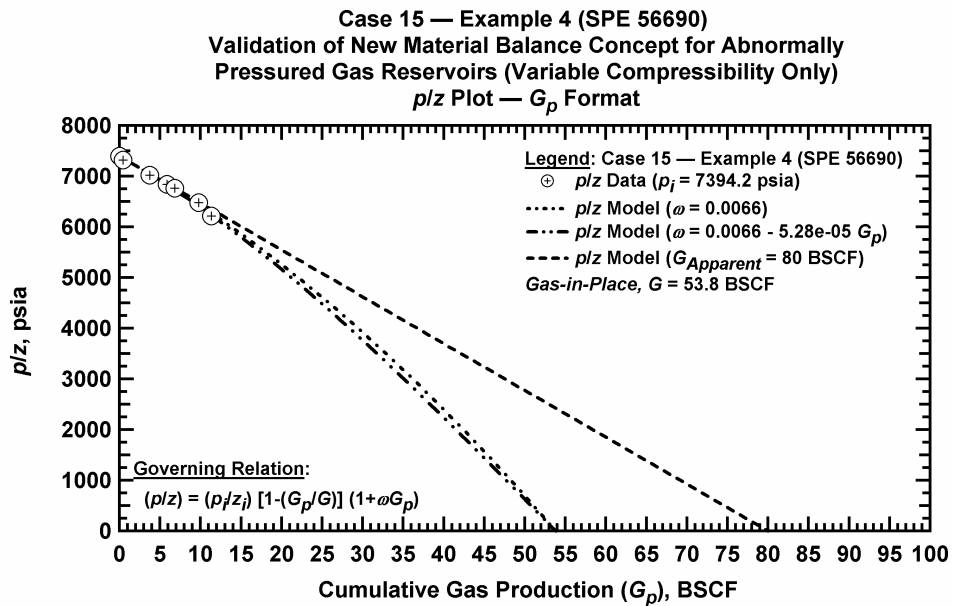
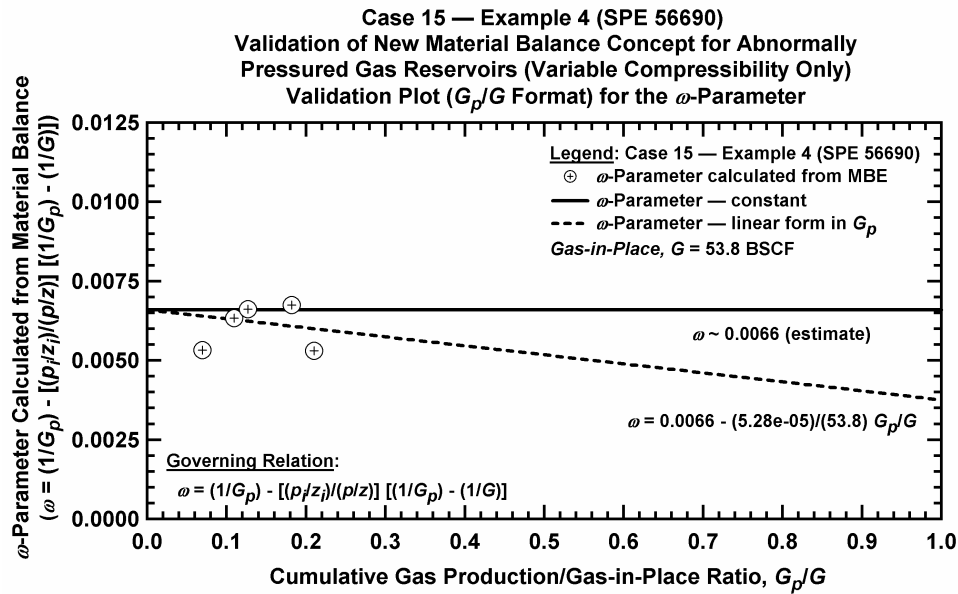


Figure D.16.j — Plot of ω vs. G_p — Base Simulation Case 15.



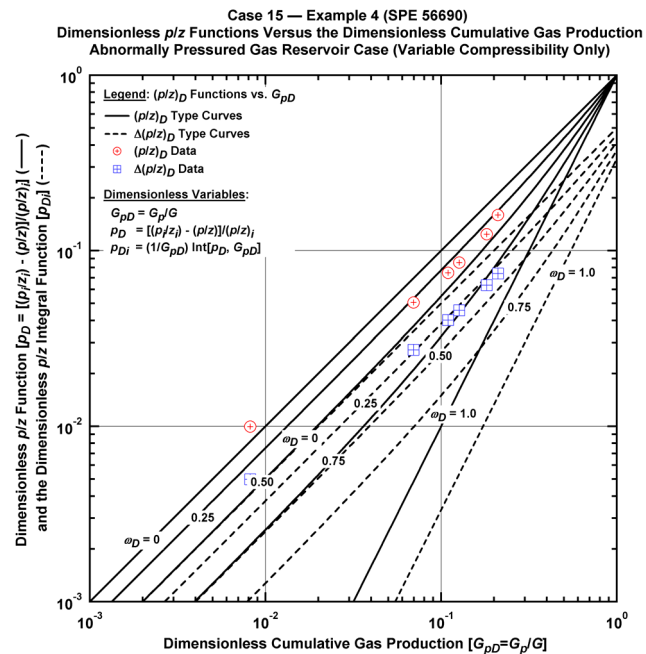


Figure D.16.m — Plot of dimensionless p/z functions vs. G_{pD} — Case 15.

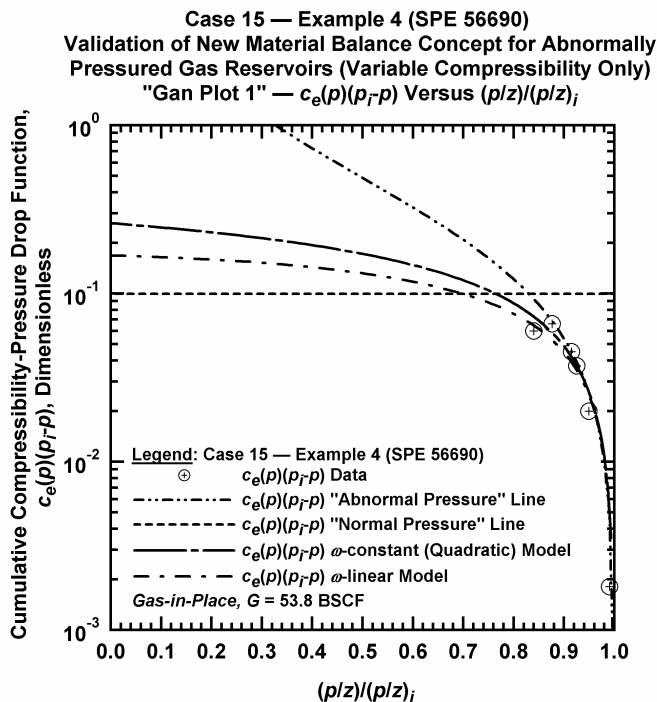


Figure D.16.n — Plot of $\bar{c}_e(p)(p_i - p)$ vs. $(p/z)/(p/z)_i$ — Case 15.

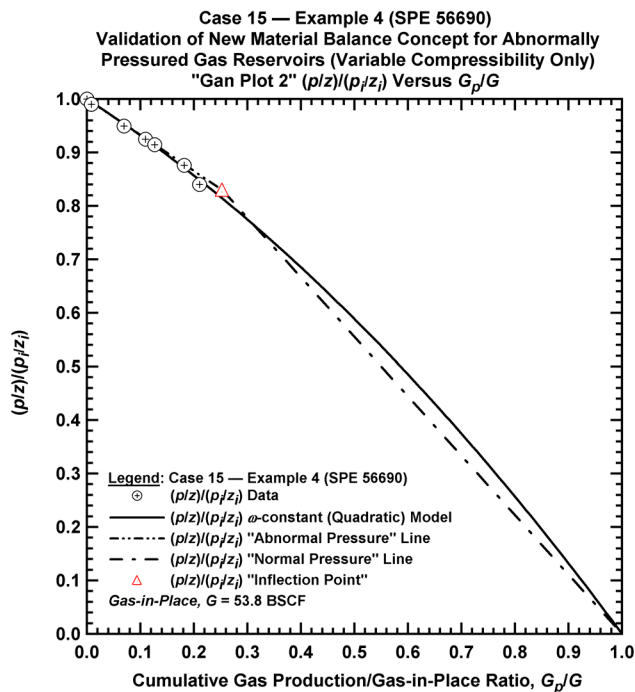


Figure D.16.o — Plot of $(p/z)/(p/z_i)$ vs. G_p/G — Case 15.

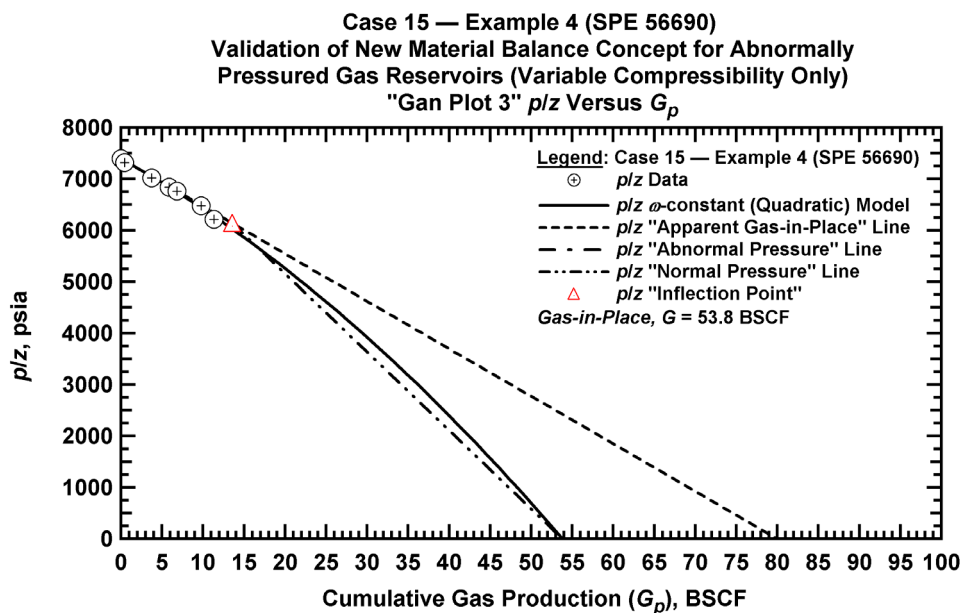


Figure D.16.p — Summary plot of p/z vs. G_p — Case 15.

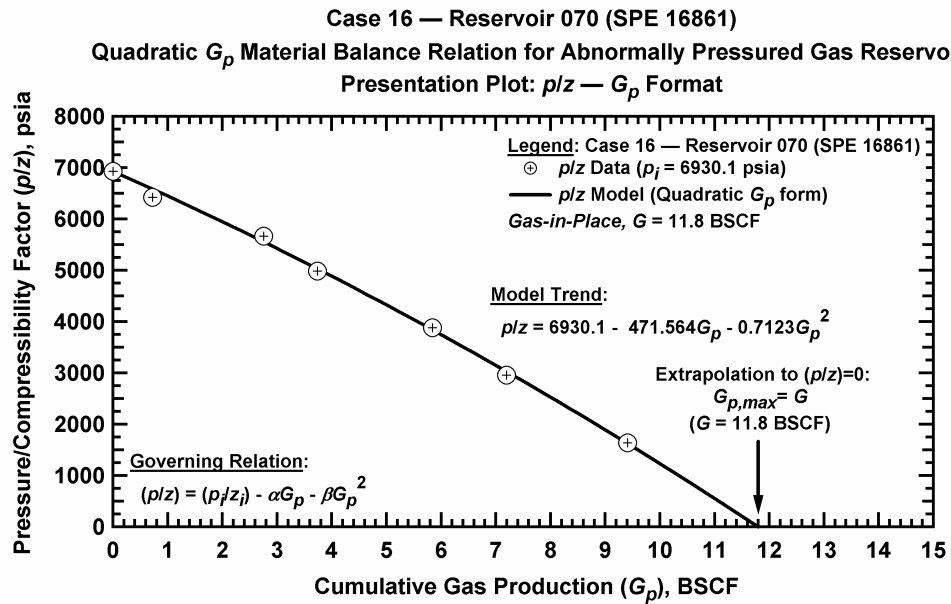


Figure D.17.a — Plot of p/z vs. G_p — Case 16.

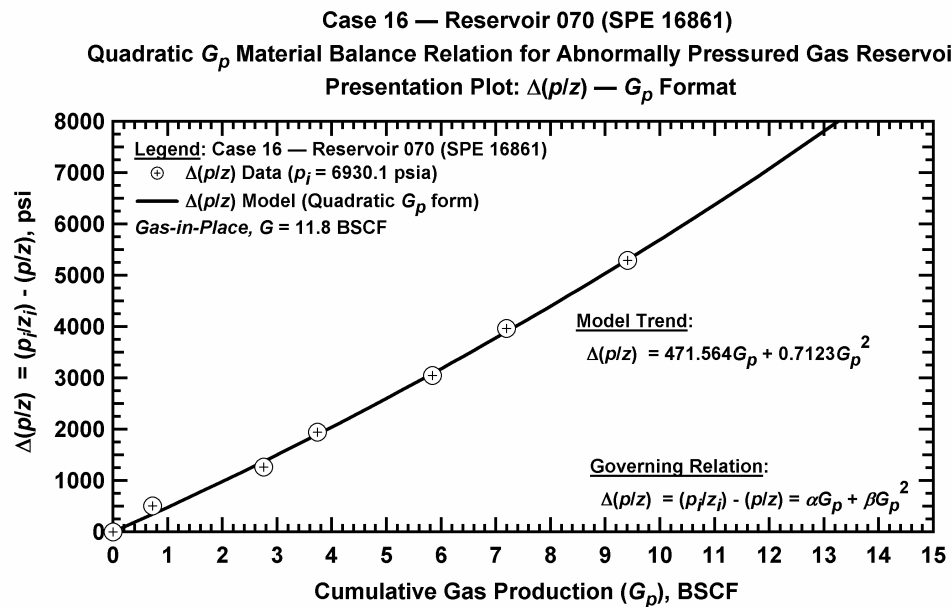


Figure D.17.b — Plot of $\Delta(p/z)$ vs. G_p — Case 16.

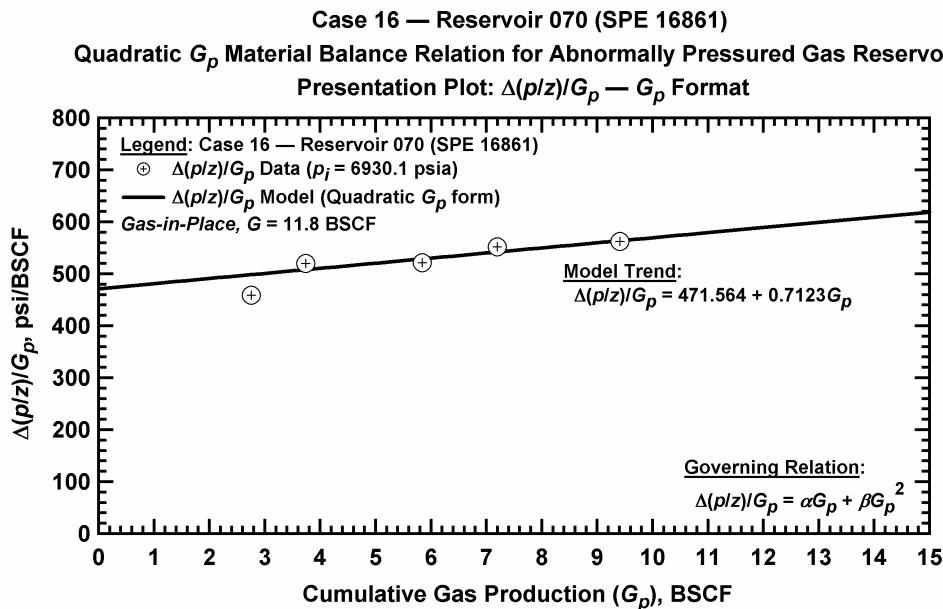


Figure D.17.c — Plot of $\Delta(p/z)/G_p$ vs. G_p — Case 16.

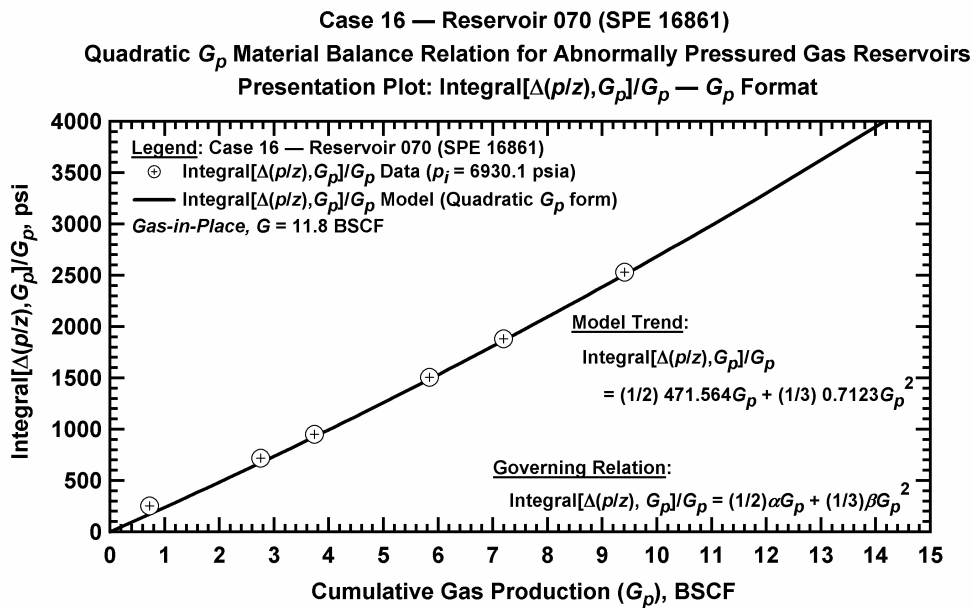


Figure D.17.d — Plot of $\frac{1}{G_p} \int_0^{G_p} \Delta(p/z) dG_p$ vs. G_p — Case 16.

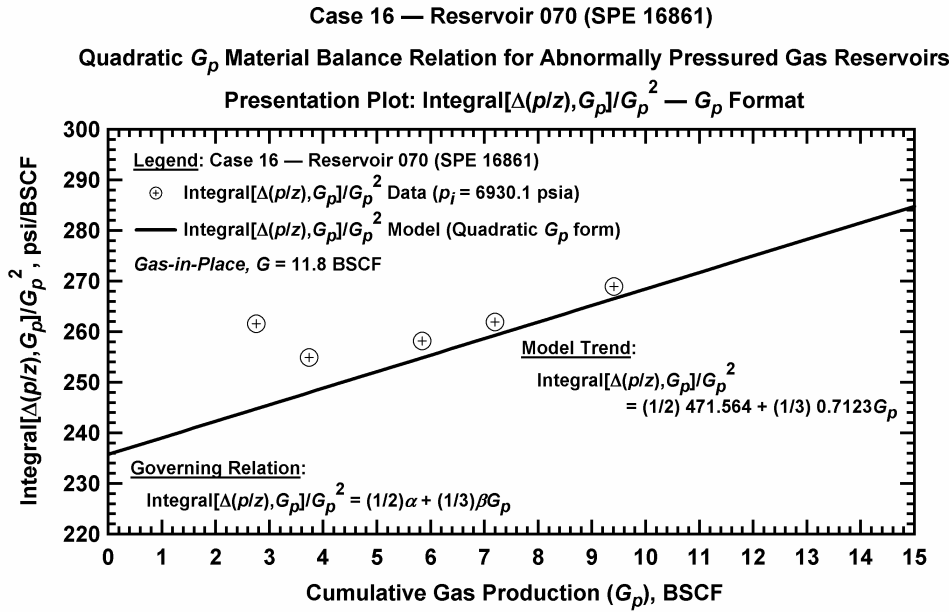


Figure D.17.e — Plot of $\frac{1}{G_p^2} \int_0^{G_p} \Delta(p/z) dG_p$ vs. G_p — Case 16.

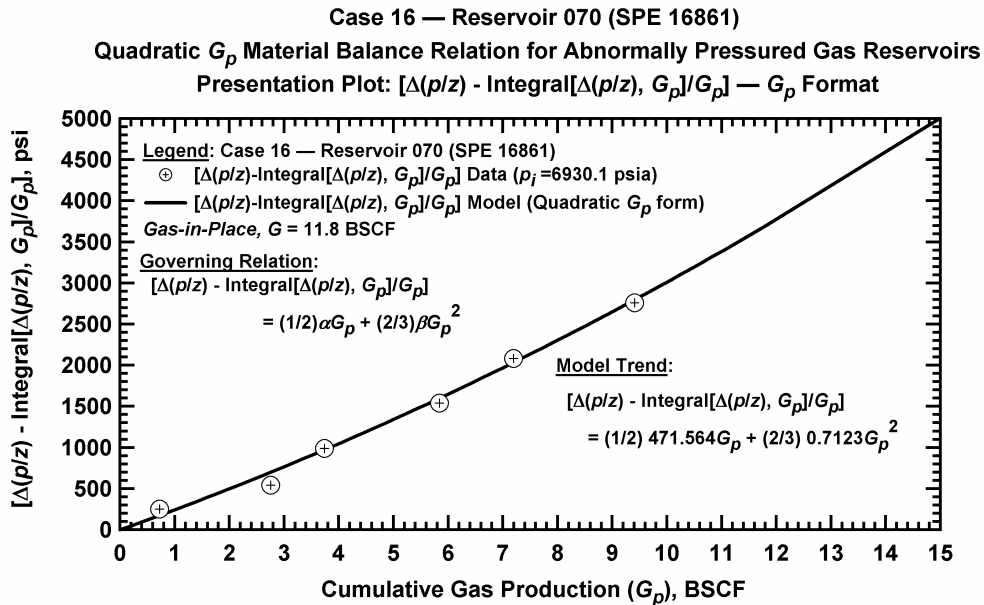


Figure D.17.f — Plot of $\Delta(p/z) - \frac{1}{G_p} \int_0^{G_p} \Delta(p/z) dG_p$ vs. G_p — Case 16.

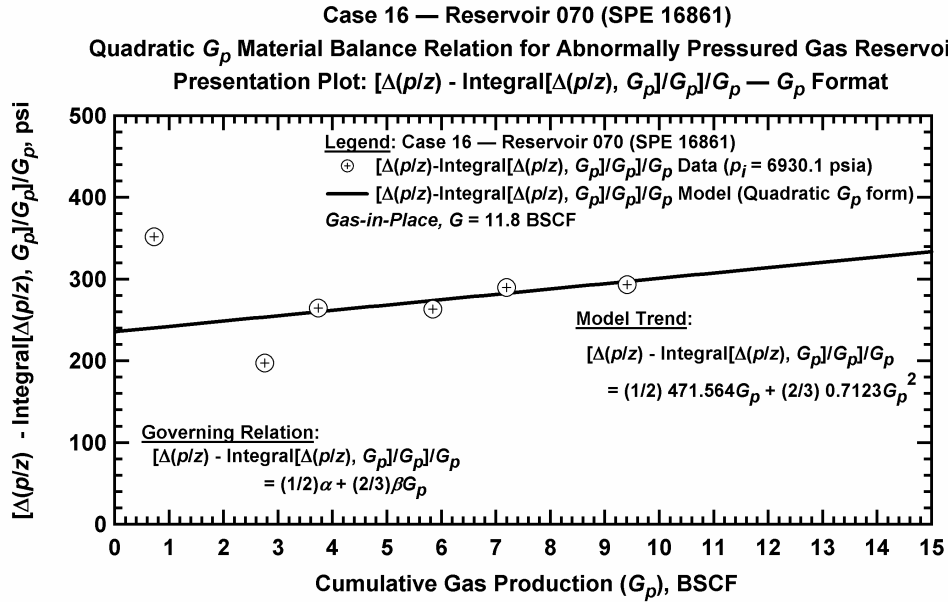


Figure D.17.g — Plot of $\frac{1}{G_p} \left[\Delta(p/z) - \frac{1}{G_p} \int_0^{G_p} \Delta(p/z) dG_p \right]$ vs. G_p — Case 16.

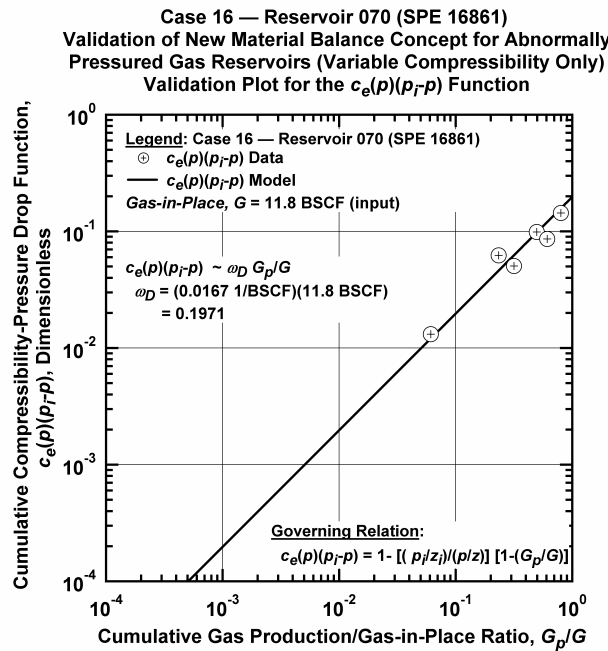


Figure D.17.h — Plot of $\bar{c}_e(p)(p_i - p)$ vs. G_p/G — Base Simulation Case 16.

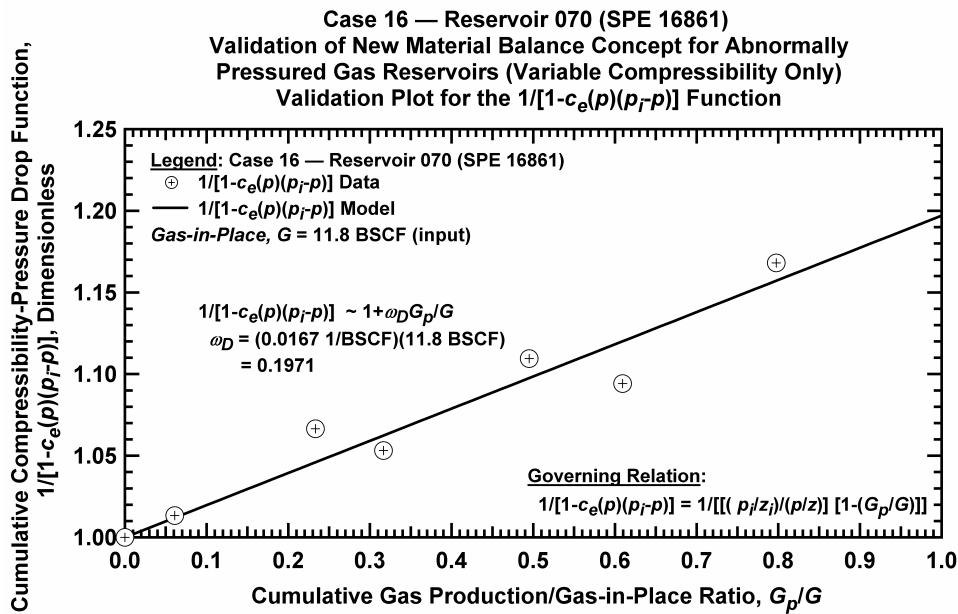


Figure D.17.i — Plot of $1/[1-\bar{c}_e(p)(p_i - p)]$ vs. G_p/G — Case 16.

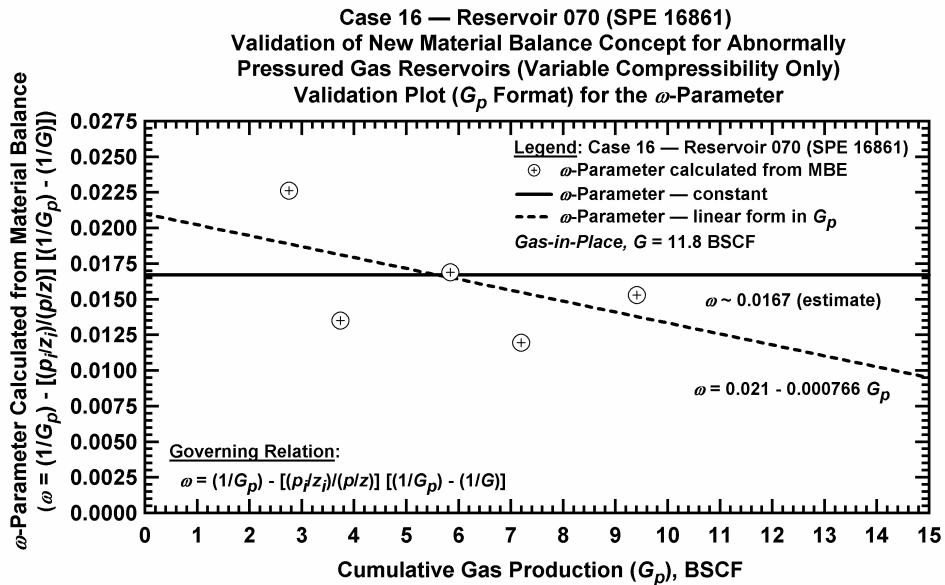


Figure D.17.j — Plot of ω vs. G_p — Base Simulation Case 16.

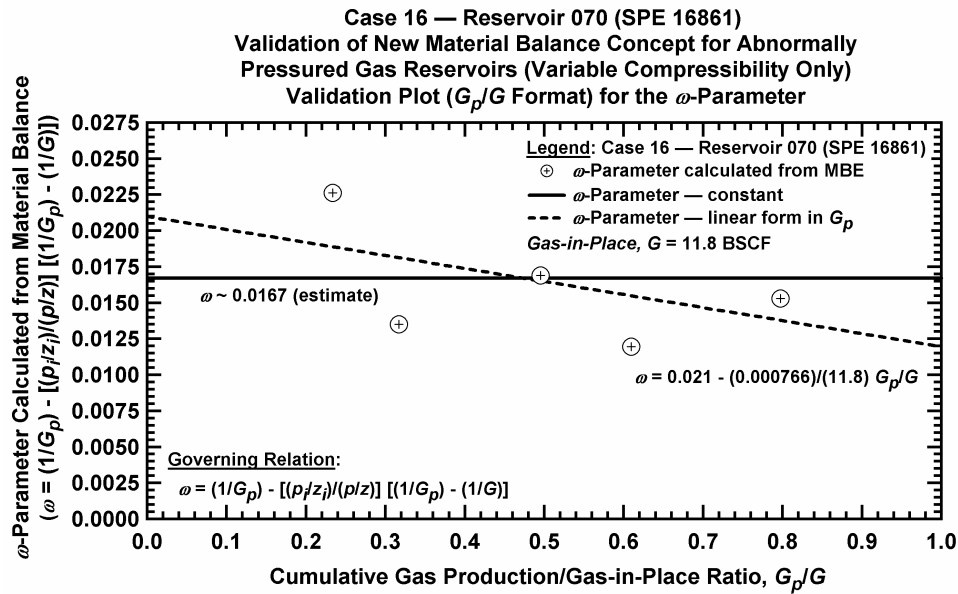


Figure D.17.k — Plot of ω vs. G_p/G — Case 16.

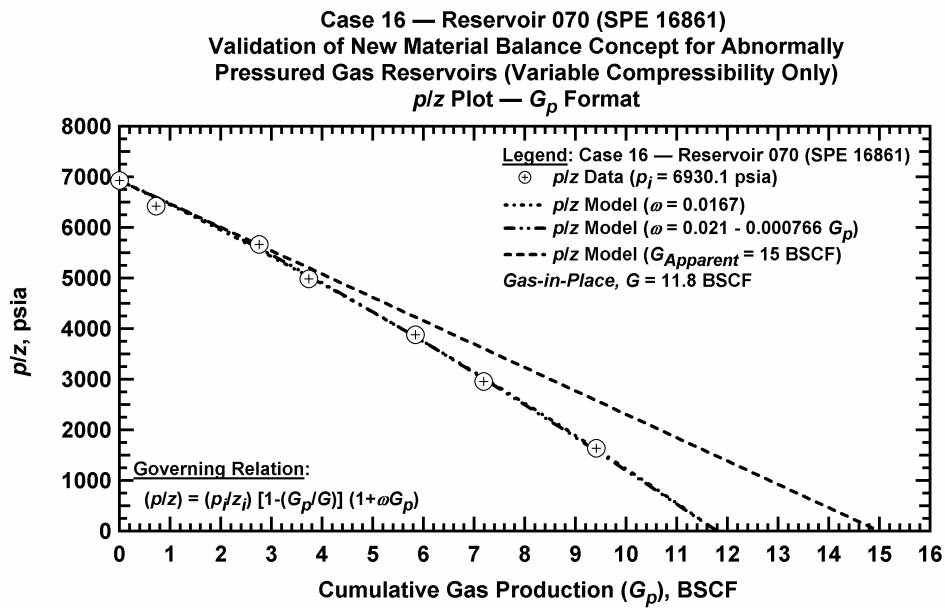


Figure D.17.l — Comparison plot of p/z vs. G_p — Case 16.

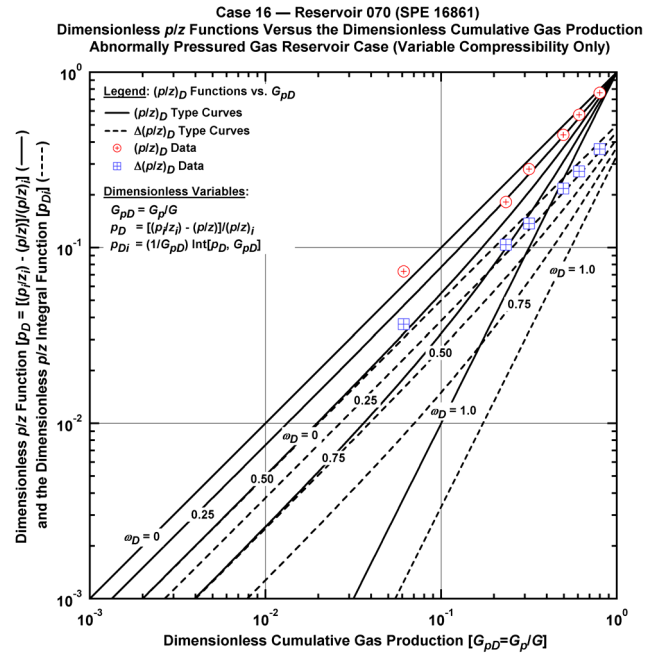


Figure D.17.m — Plot of dimensionless p/z functions vs. G_{pD} — Case 16.

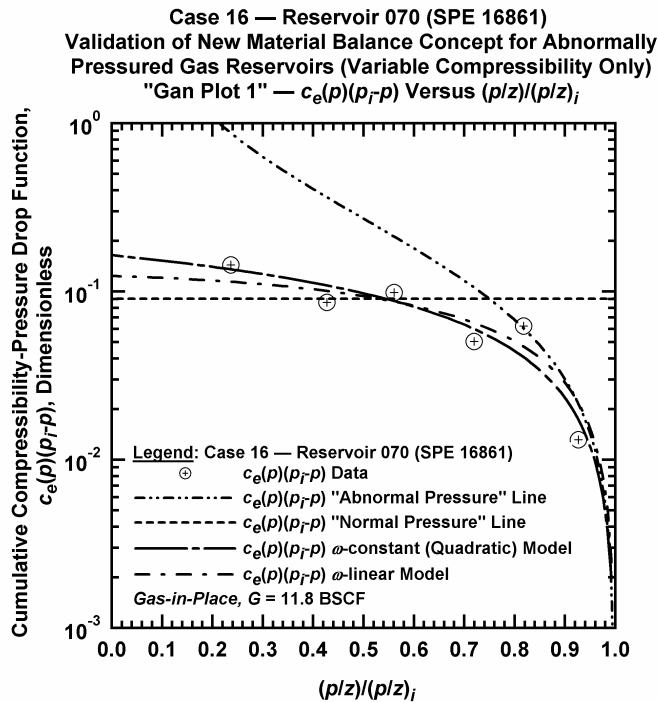


Figure D.17.n — Plot of $\bar{c}_e(p)(p_i - p)$ vs. $(p/z)/(p_i/z_i)$ — Case 16.

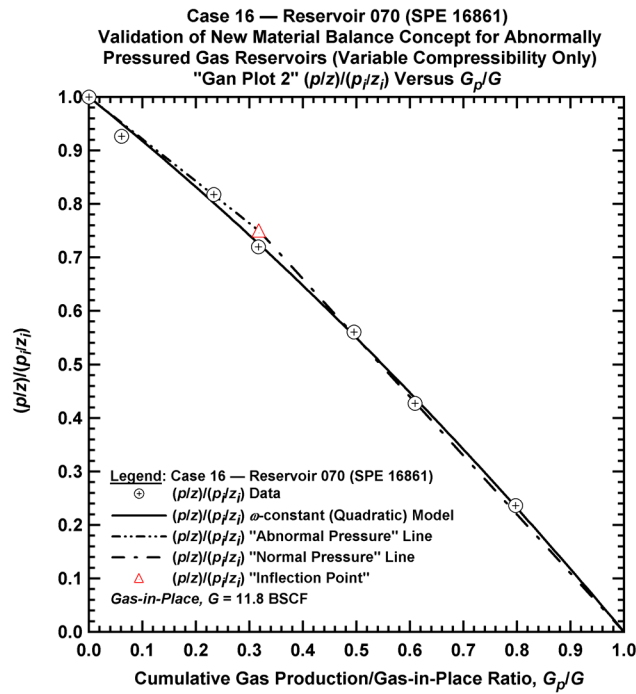


Figure D.17.o — Plot of $(p/z)/(p/z_i)$ vs. G_p/G — Case 16.

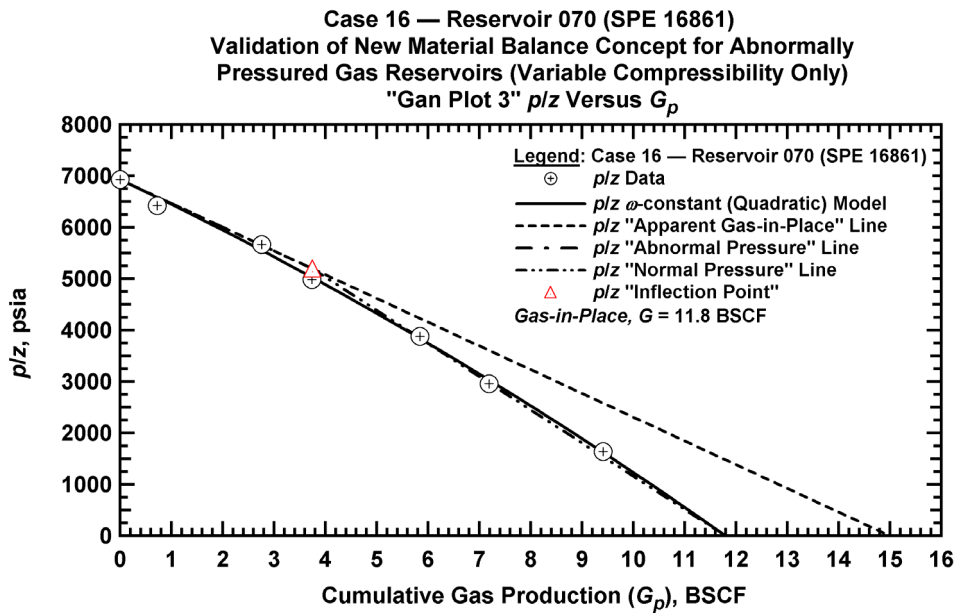


Figure D.17.p — Summary plot of p/z vs. G_p — Case 16.

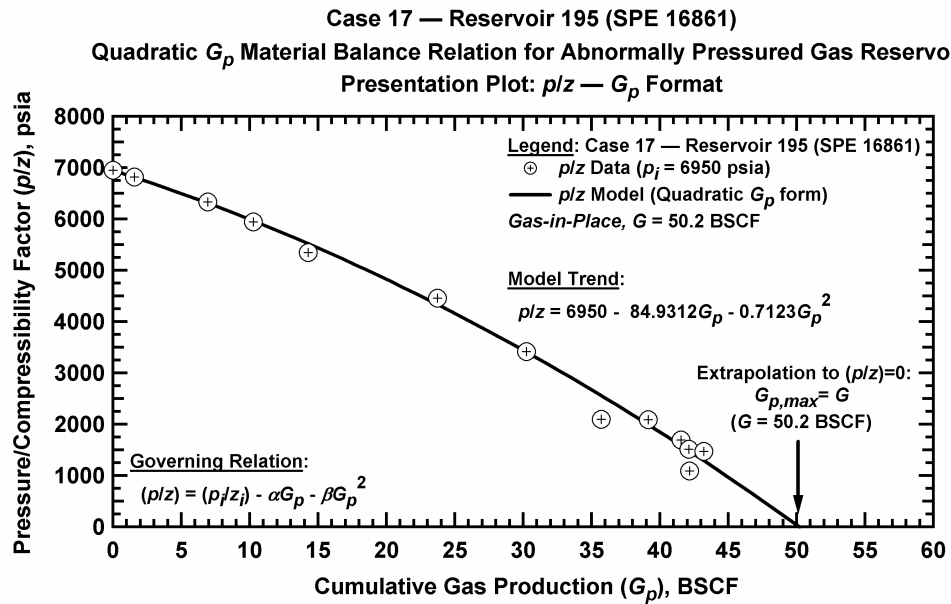


Figure D.18.a — Plot of p/z vs. G_p — Case 17.

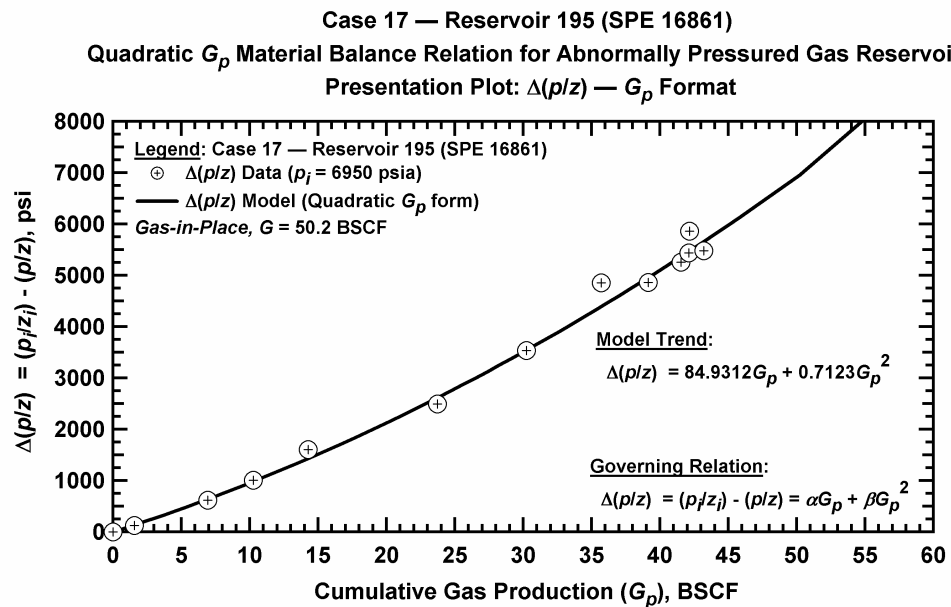


Figure D.18.b — Plot of $\Delta(p/z)$ vs. G_p — Case 17.

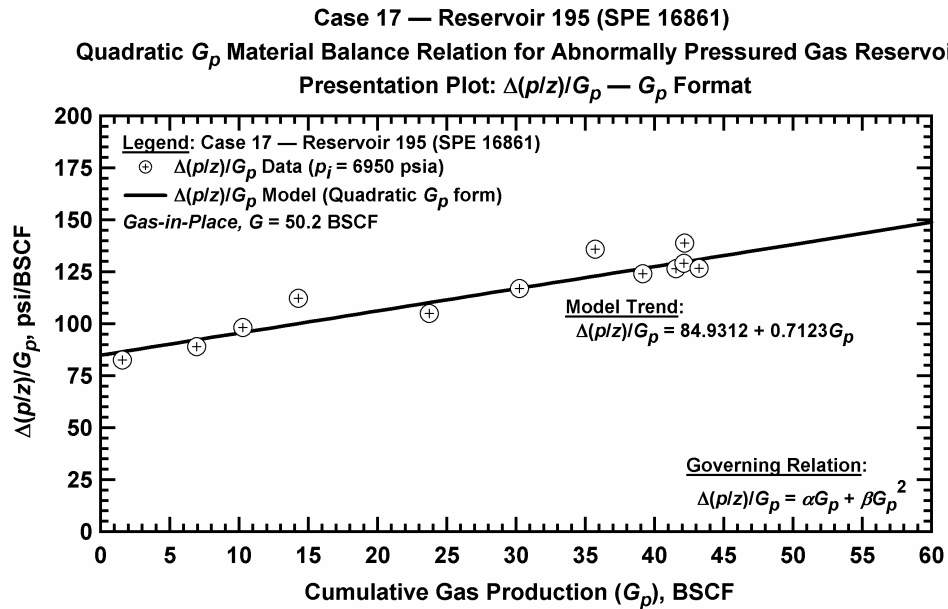


Figure D.18.c — Plot of $\Delta(p/z)/G_p$ vs. G_p — Case 17.

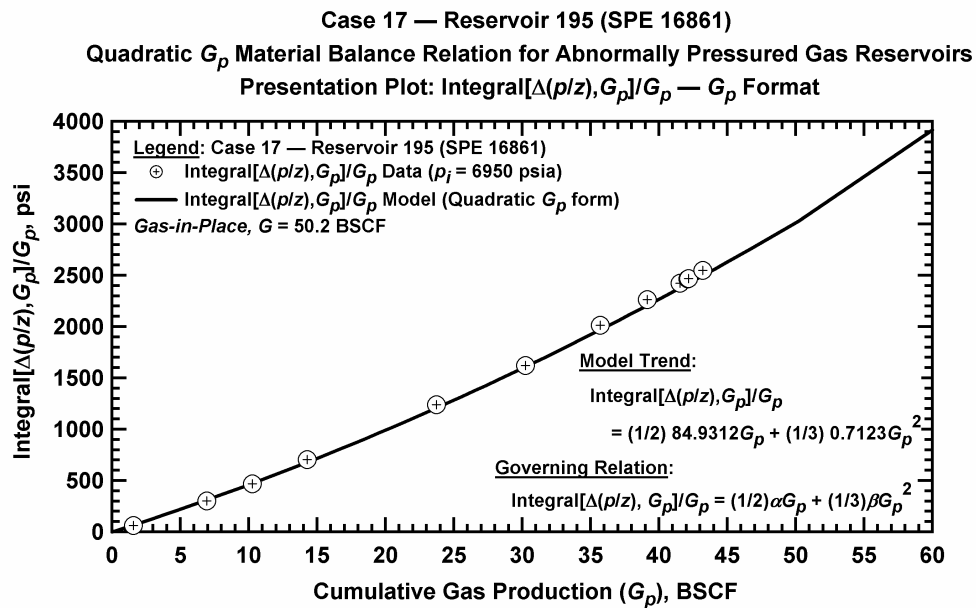


Figure D.18.d — Plot of $\frac{1}{G_p} \int_0^{G_p} \Delta(p/z) dG_p$ vs. G_p — Case 17.

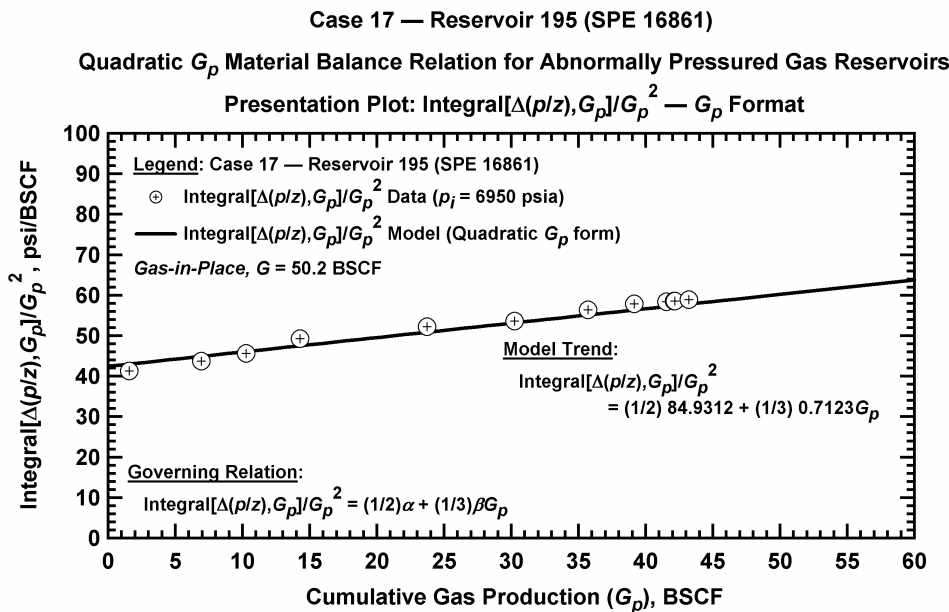


Figure D.18.e — Plot of $\frac{1}{G_p^2} \int_0^{G_p} \Delta(p/z) dG_p$ vs. G_p — Case 17.

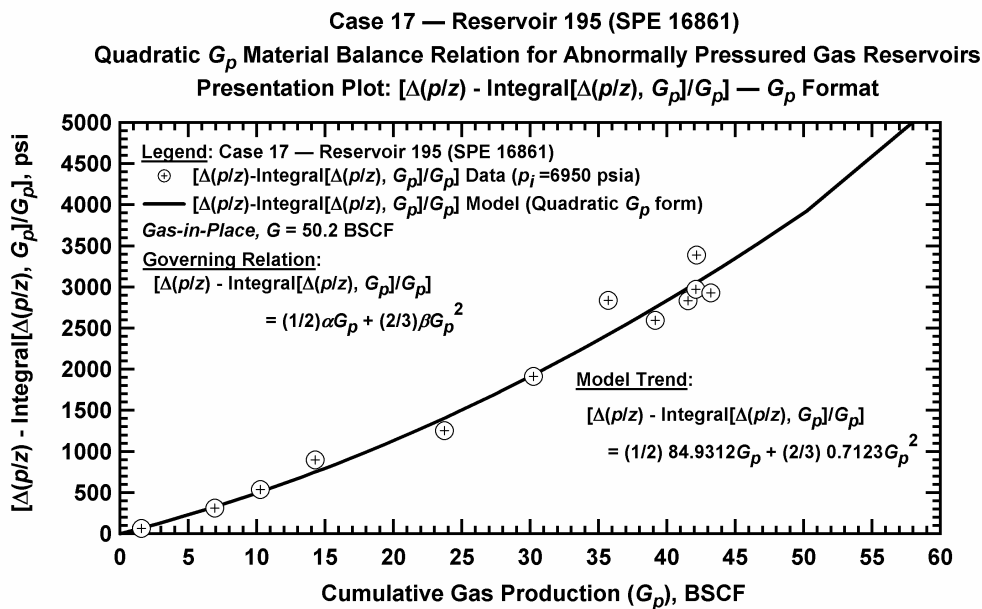


Figure D.18.f — Plot of $\Delta(p/z) - \frac{1}{G_p} \int_0^{G_p} \Delta(p/z) dG_p$ vs. G_p — Case 17.

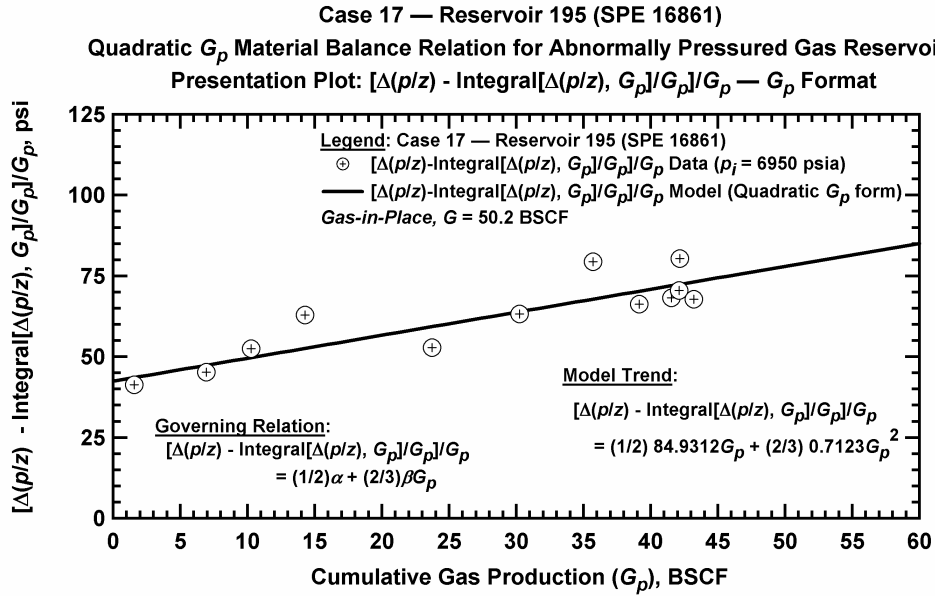


Figure D.18.g — Plot of $\frac{1}{G_p} \left[\Delta(p/z) - \frac{1}{G_p} \int_0^{G_p} \Delta(p/z) dG_p \right]$ vs. G_p — Case 17.

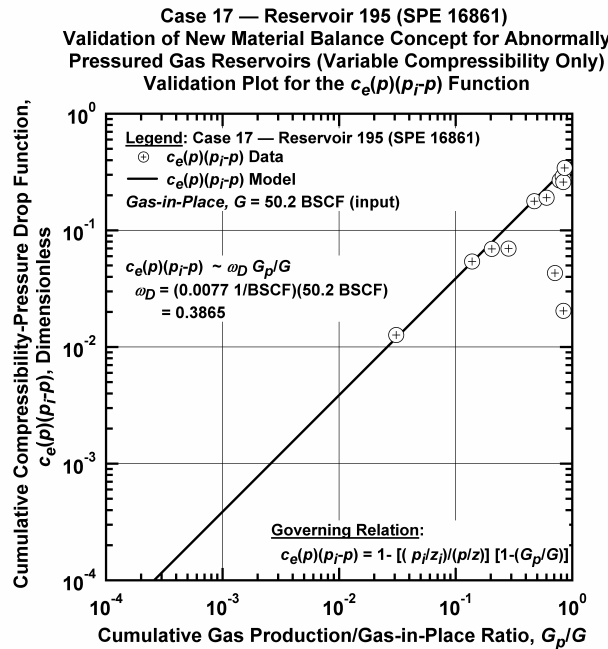


Figure D.18.h — Plot of $\bar{c}_e(p)(p_i - p)$ vs. G_p/G — Base Simulation Case 17.

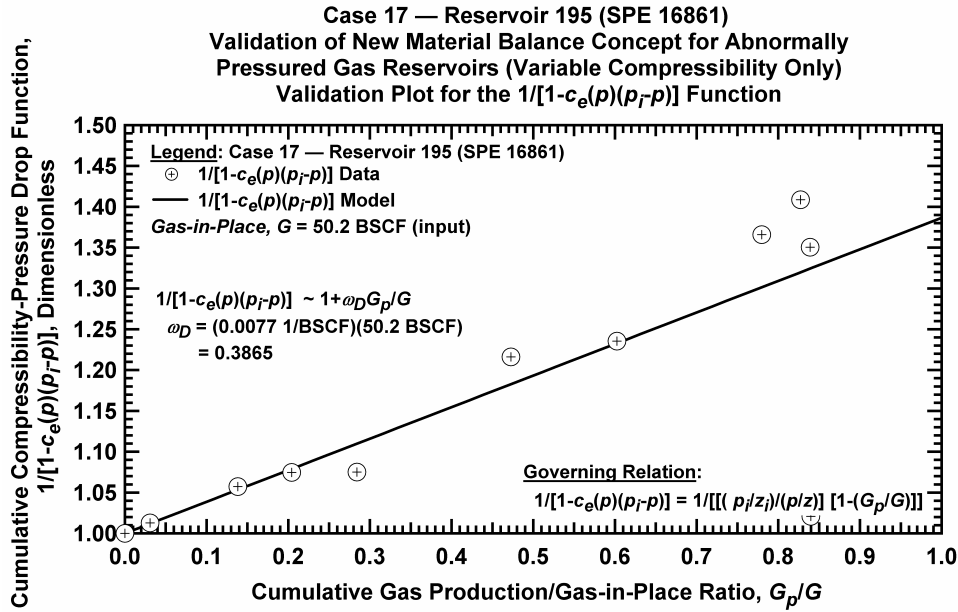


Figure D.18.i — Plot of $1/[1-\bar{c}_e(p)(p_i - p)]$ vs. G_p/G — Case 17.

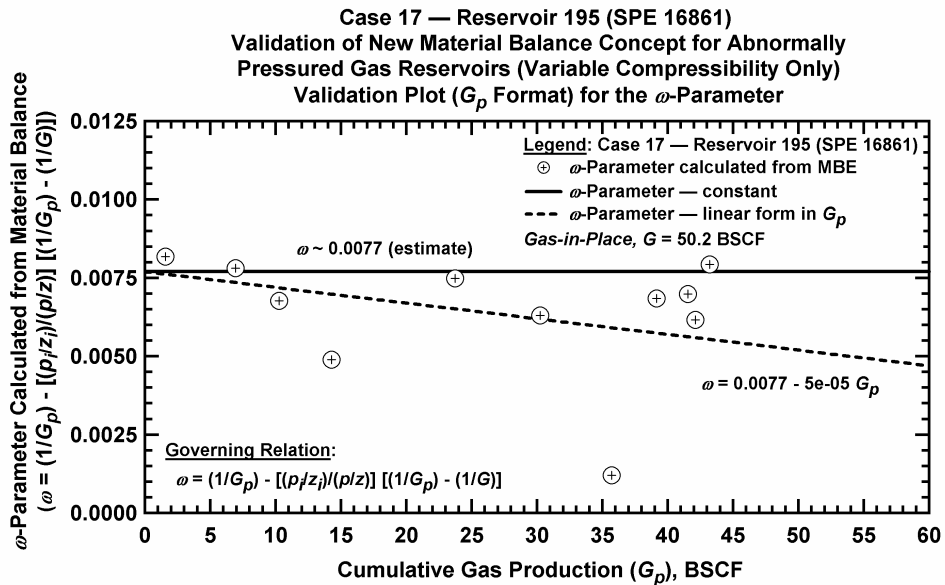


Figure D.18.j — Plot of ω vs. G_p — Base Simulation Case 17.

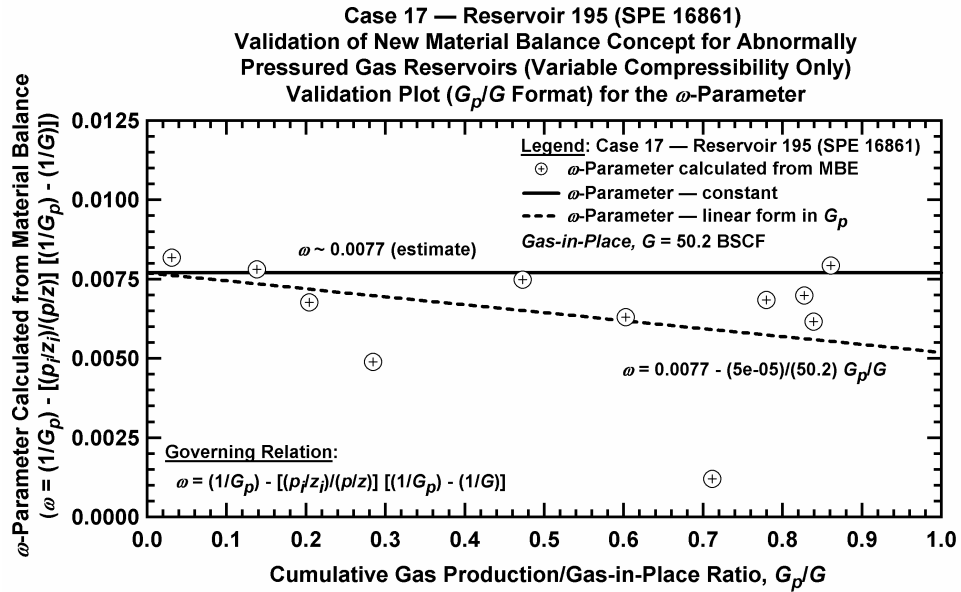


Figure D.18.k — Plot of ω vs. G_p/G — Case 17.

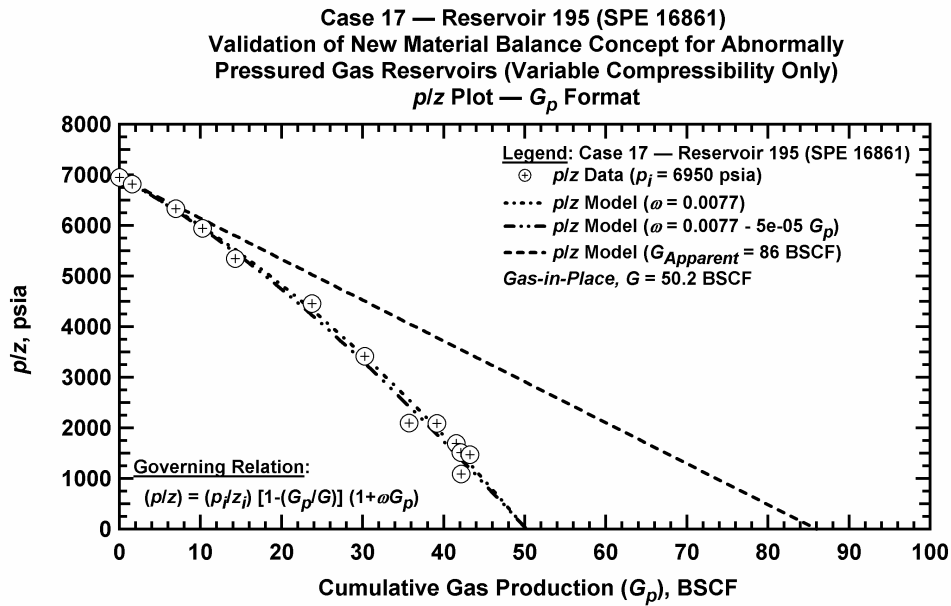
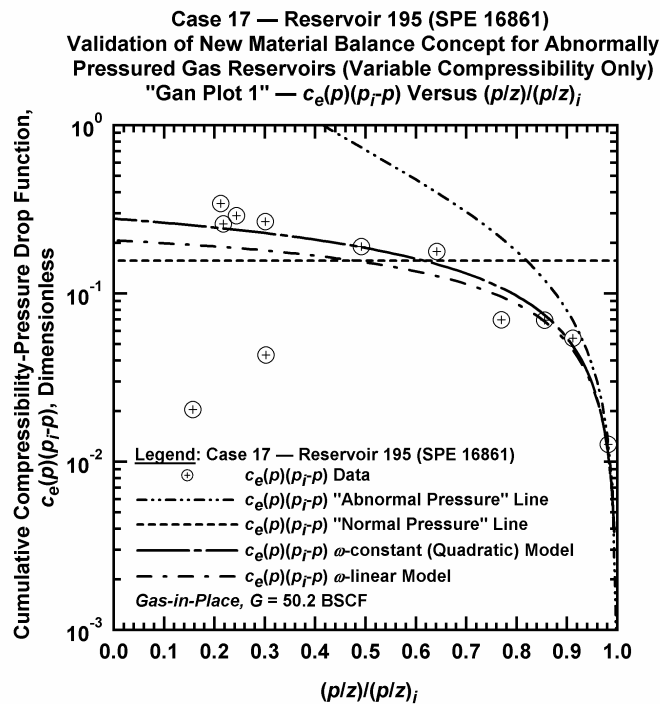
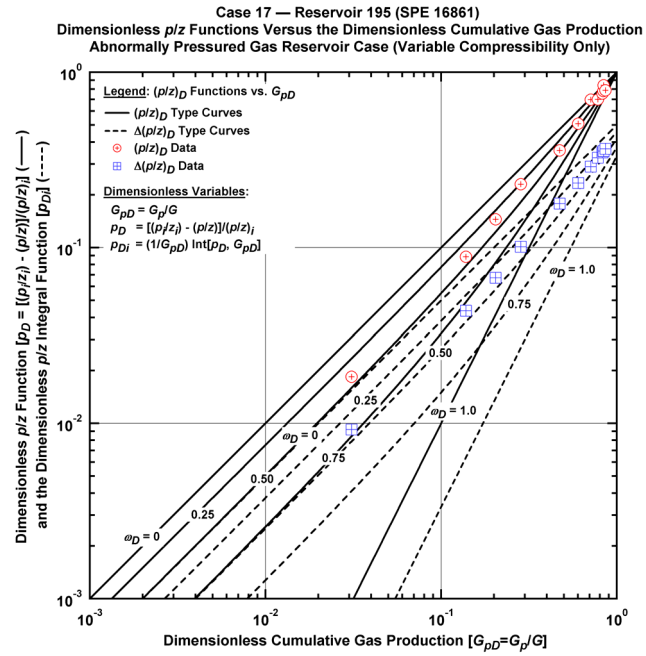


Figure D.18.l — Comparison plot of p/z vs. G_p — Case 17.



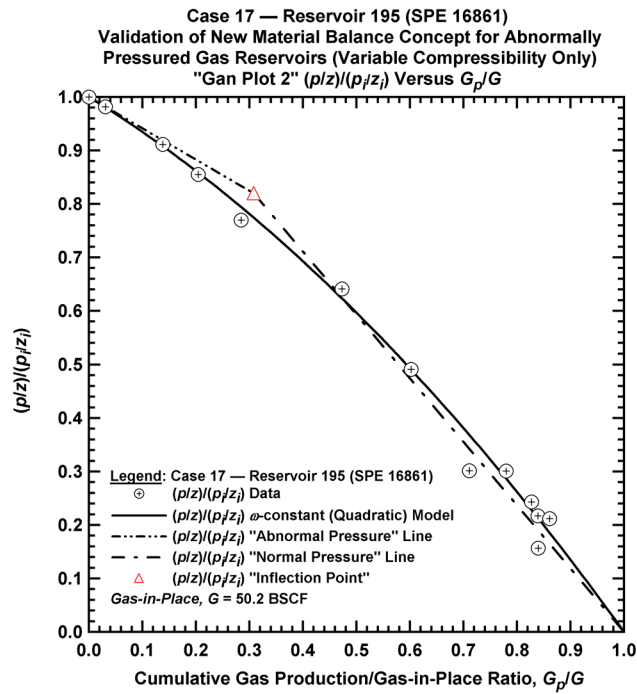


Figure D.18.o — Plot of $(p/z)/(p/z_i)$ vs. G_p/G — Case 17.

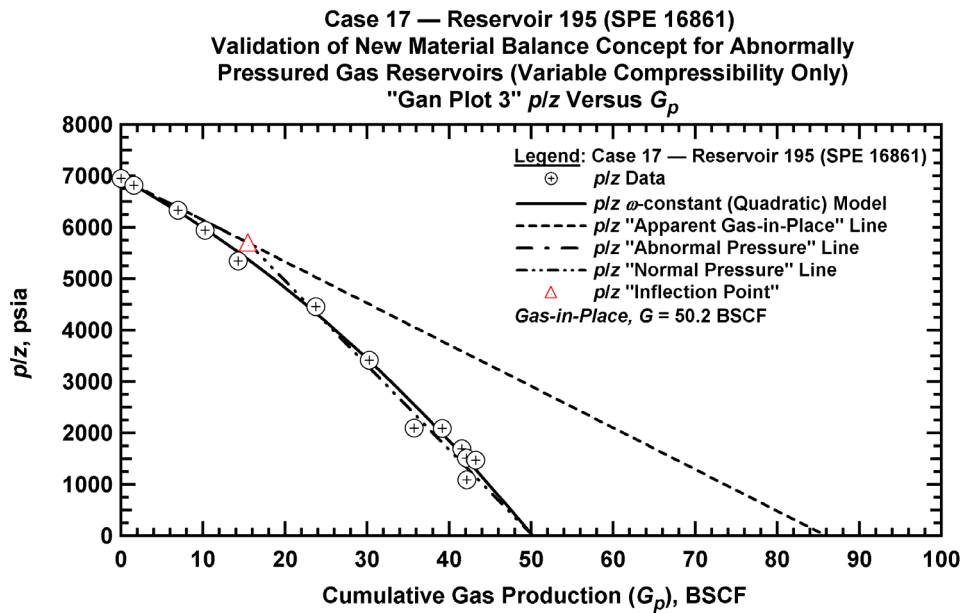


Figure D.18.p — Summary plot of p/z vs. G_p — Case 17.

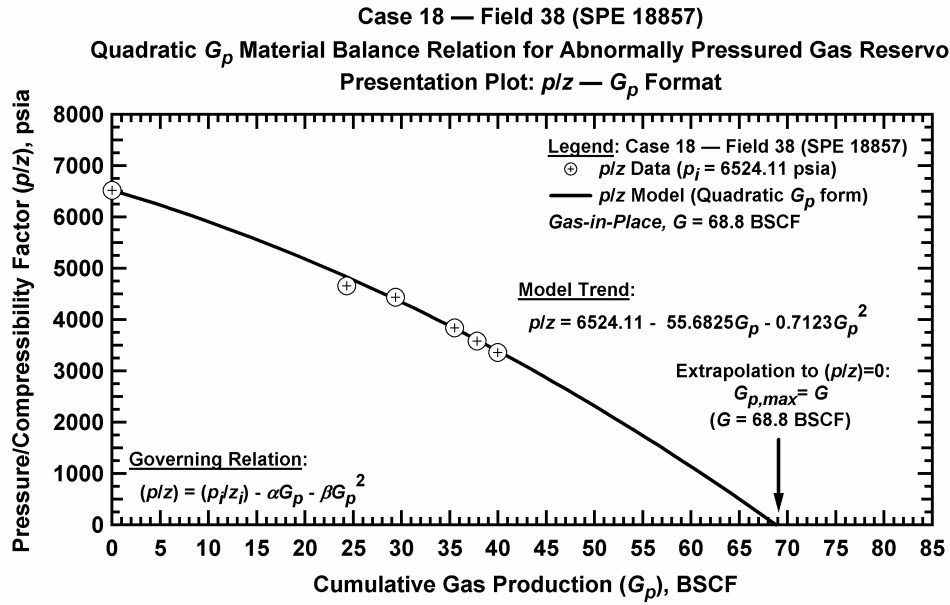


Figure D.19.a — Plot of p/z vs. G_p — Case 18.

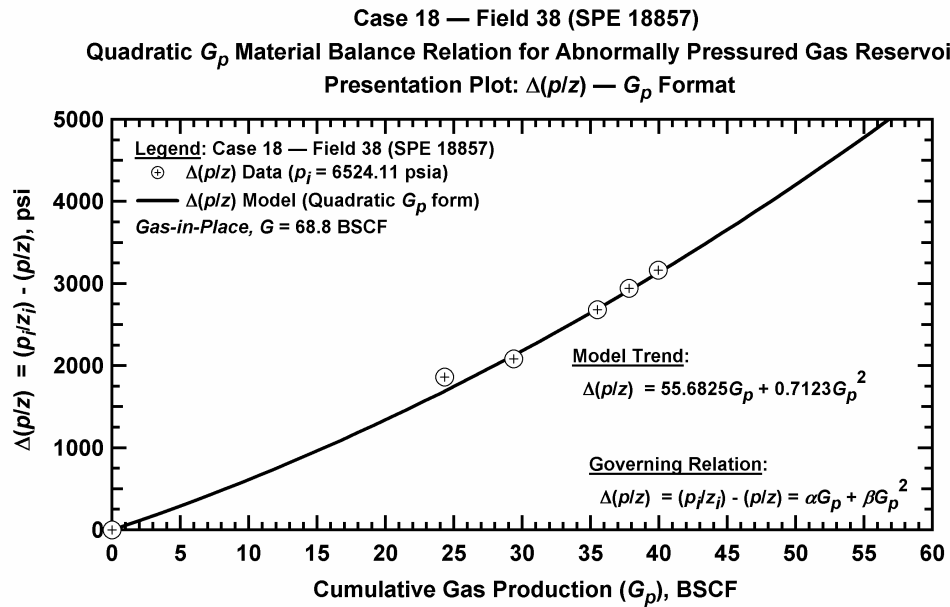


Figure D.19.b — Plot of $\Delta(p/z)$ vs. G_p — Case 18.

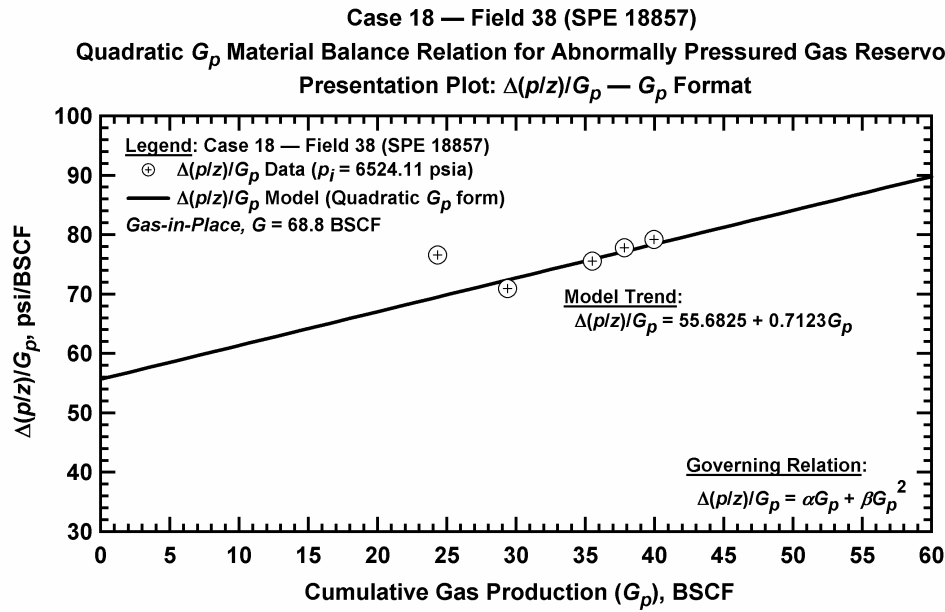


Figure D.19.c — Plot of $\Delta(p/z)/G_p$ vs. G_p — Case 18.

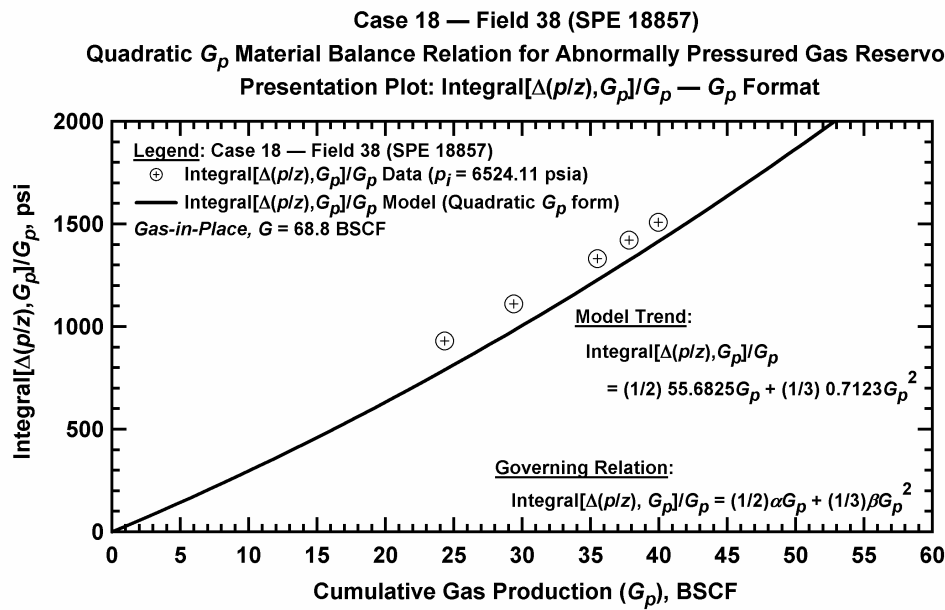


Figure D.19.d — Plot of $\frac{1}{G_p} \int_0^{G_p} \Delta(p/z) dG_p$ vs. G_p — Case 18.

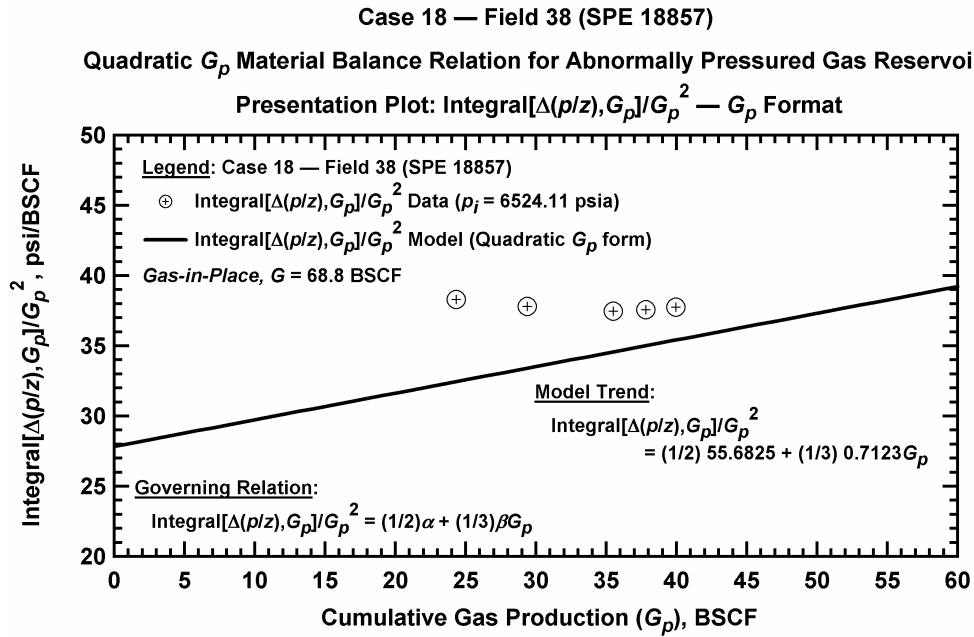


Figure D.19.e — Plot of $\frac{1}{G_p^2} \int_0^{G_p} \Delta(p/z) dG_p$ vs. G_p — Case 18.

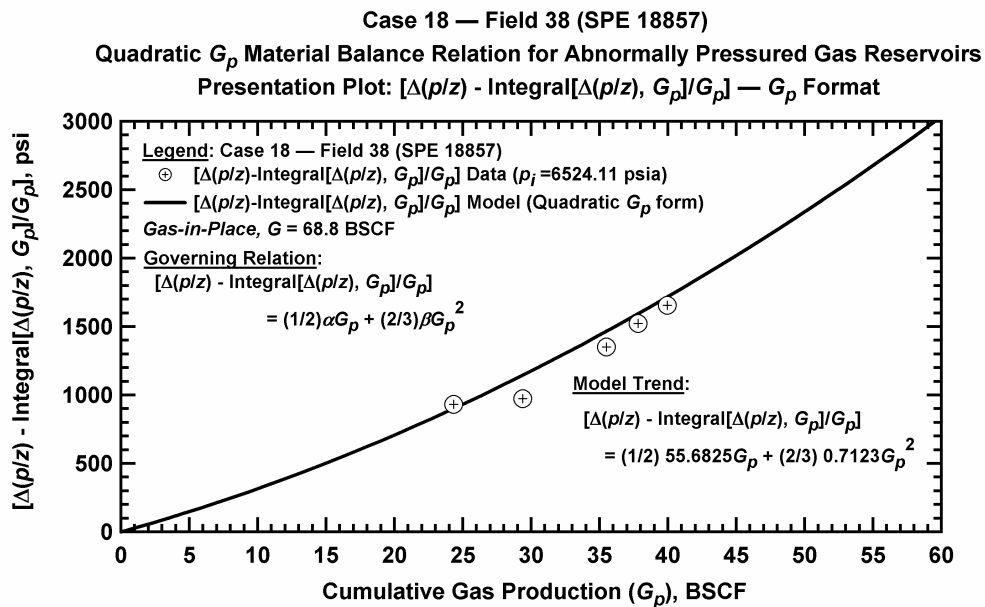


Figure D.19.f — Plot of $\Delta(p/z) - \frac{1}{G_p} \int_0^{G_p} \Delta(p/z) dG_p$ vs. G_p — Case 18.

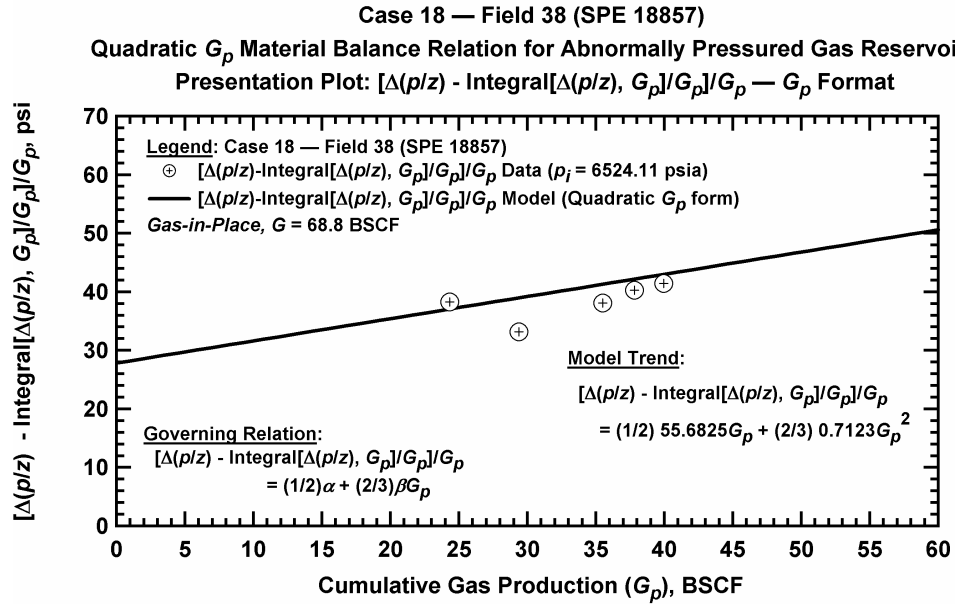


Figure D.19.g — Plot of $\frac{1}{G_p} \left[\Delta(p/z) - \frac{1}{G_p} \int_0^{G_p} \Delta(p/z) dG_p \right]$ vs. G_p — Case 18.

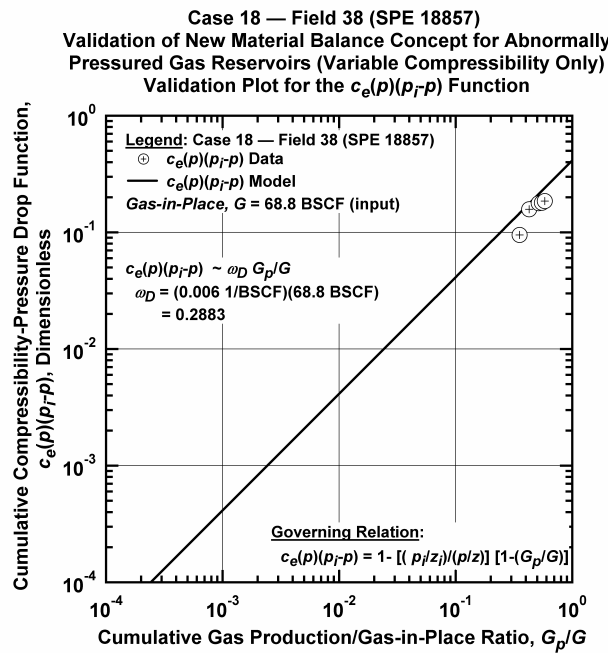


Figure D.19.h — Plot of $\bar{c}_e(p)(p_i - p)$ vs. G_p/G — Base Simulation Case 18.

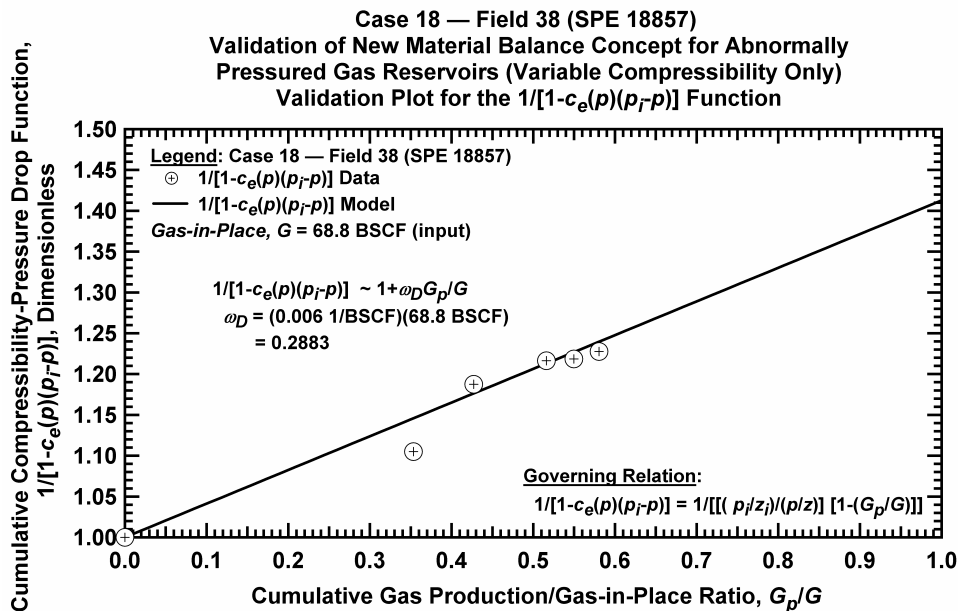


Figure D.19.i — Plot of $1/[1-\bar{c}_e(p)(p_i - p)]$ vs. G_p/G — Case 18.

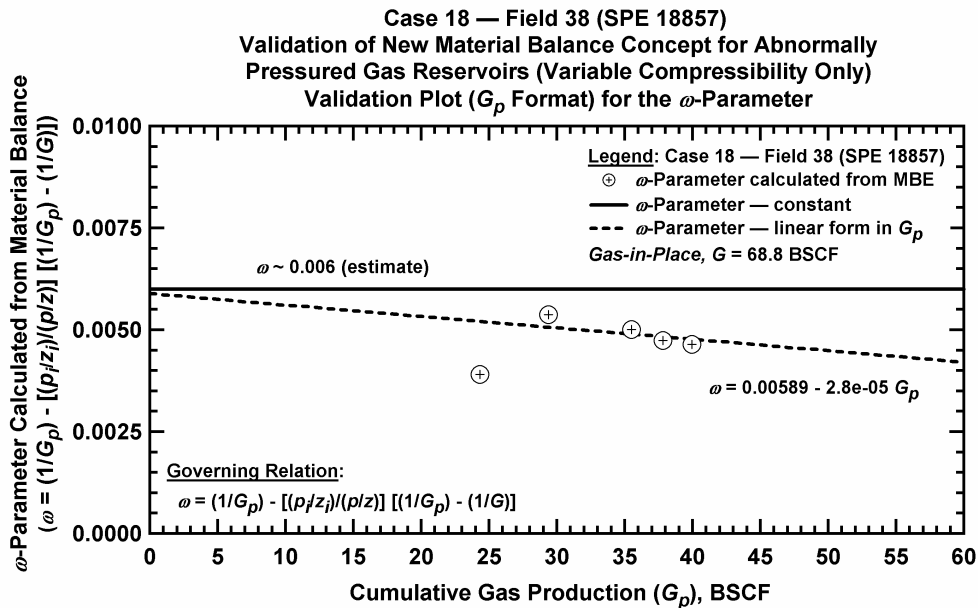


Figure D.19.j — Plot of ω vs. G_p — Base Simulation Case 18.

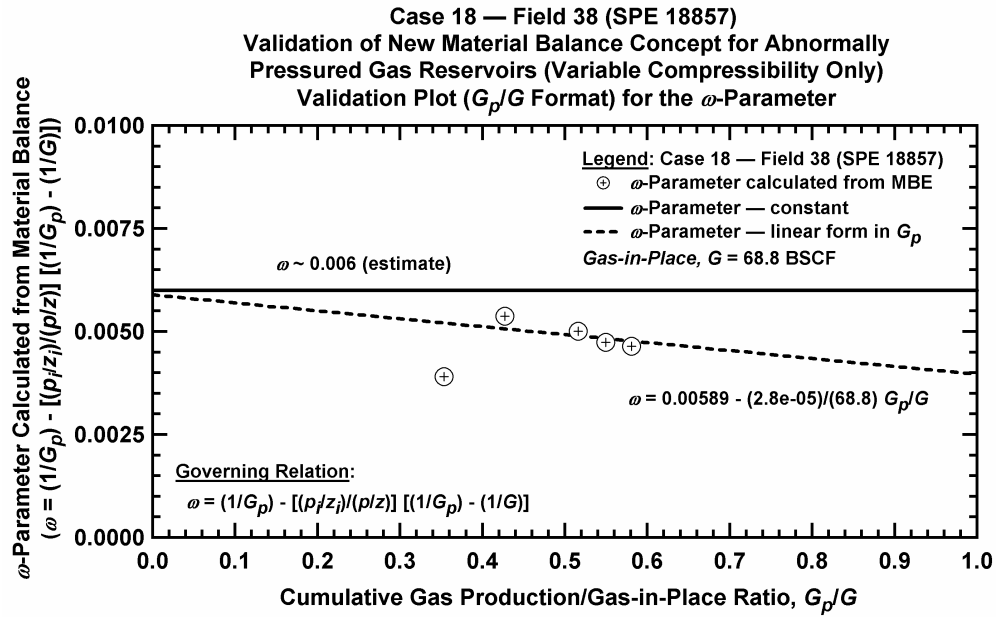


Figure D.19.k — Plot of ω vs. G_p/G — Case 18.

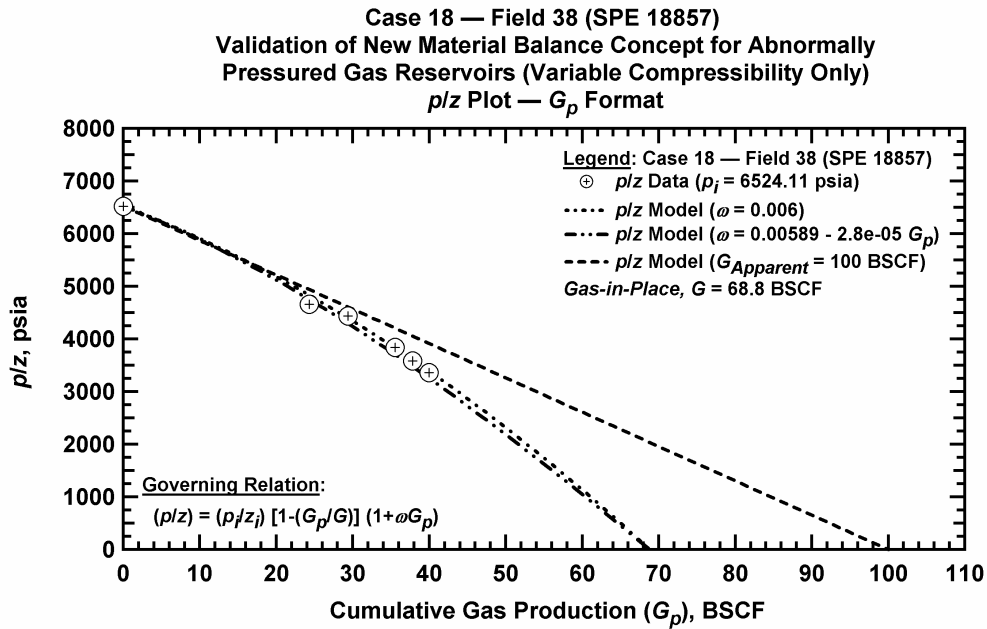


Figure D.19.l — Comparison plot of p/z vs. G_p — Case 18.

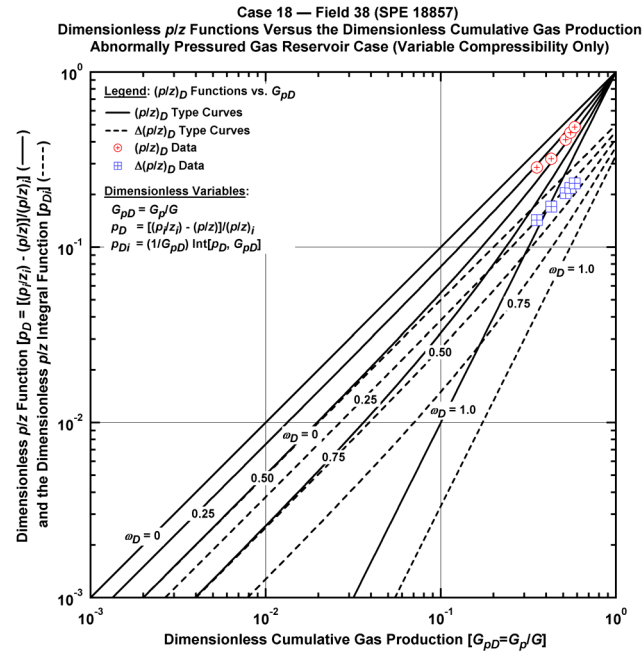


Figure D.19.m — Plot of dimensionless p/z functions vs. G_{pD} — Case 18.

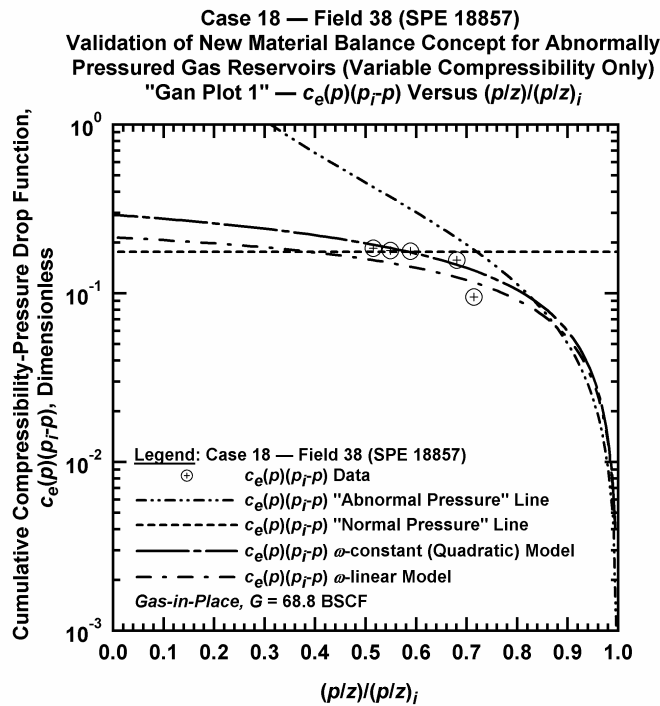


Figure D.19.n — Plot of $\bar{c}_e(p)(p_i - p)$ vs. $(p/z)/(p/z)_i$ — Case 18.

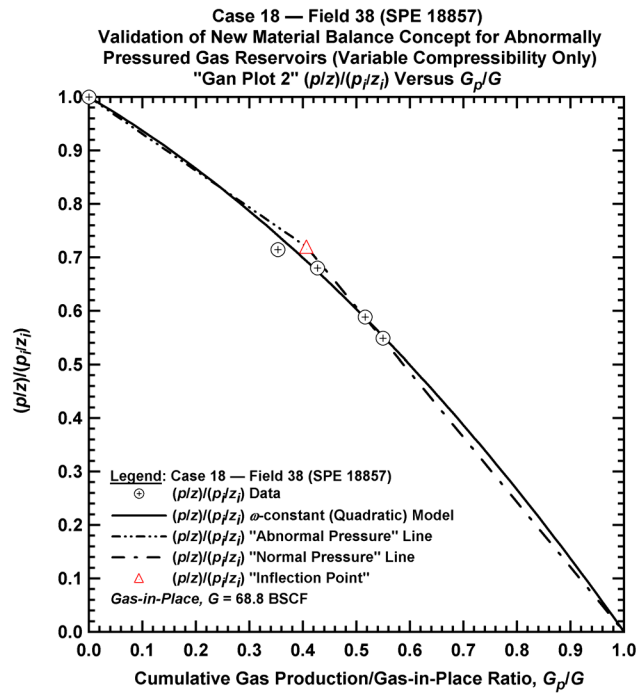


Figure D.19.o — Plot of $(p/z)/(p/z_i)$ vs. G_p/G — Case 18.

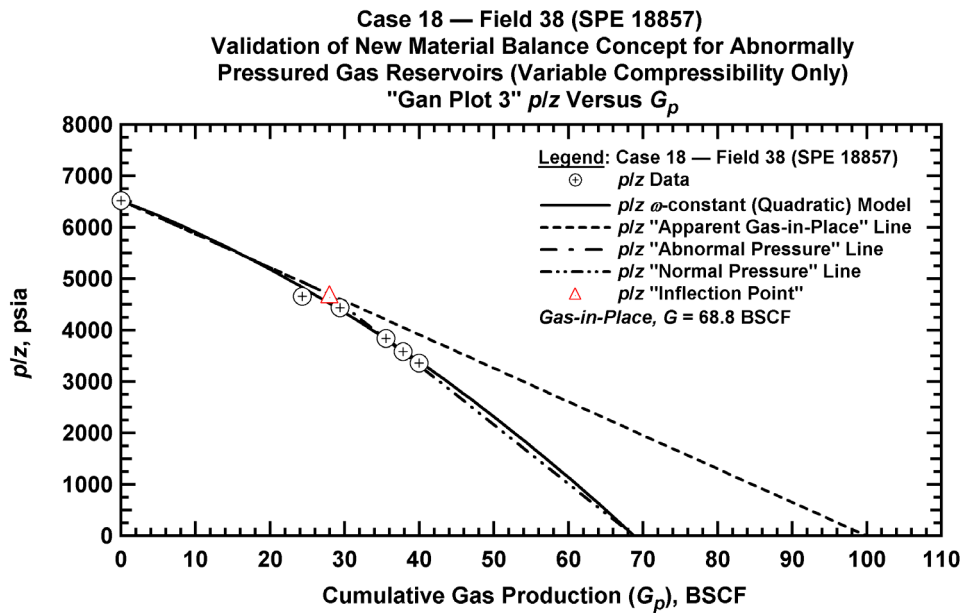


Figure D.19.p — Summary plot of p/z vs. G_p — Case 18.

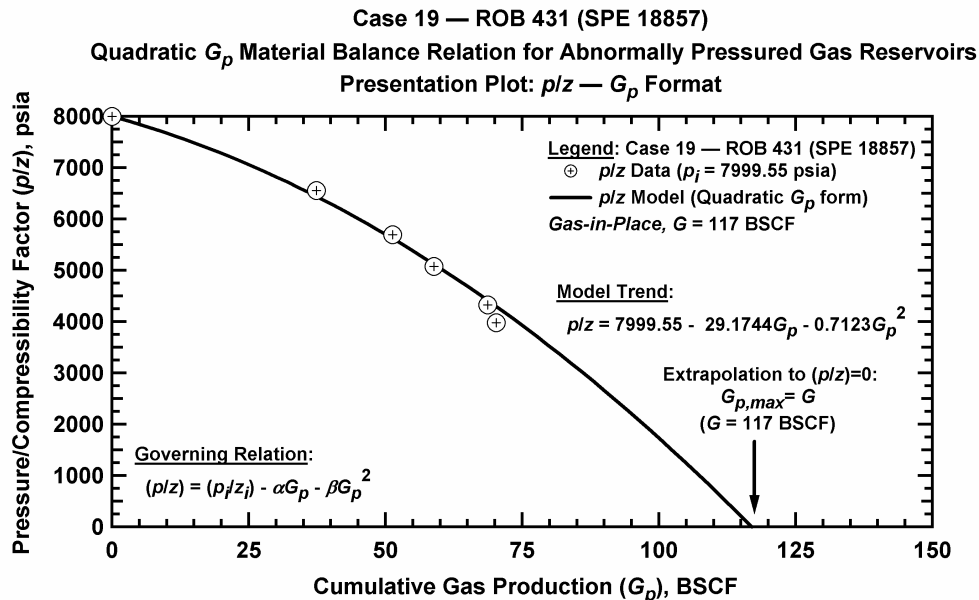


Figure D.20.a — Plot of p/z vs. G_p — Case 19.

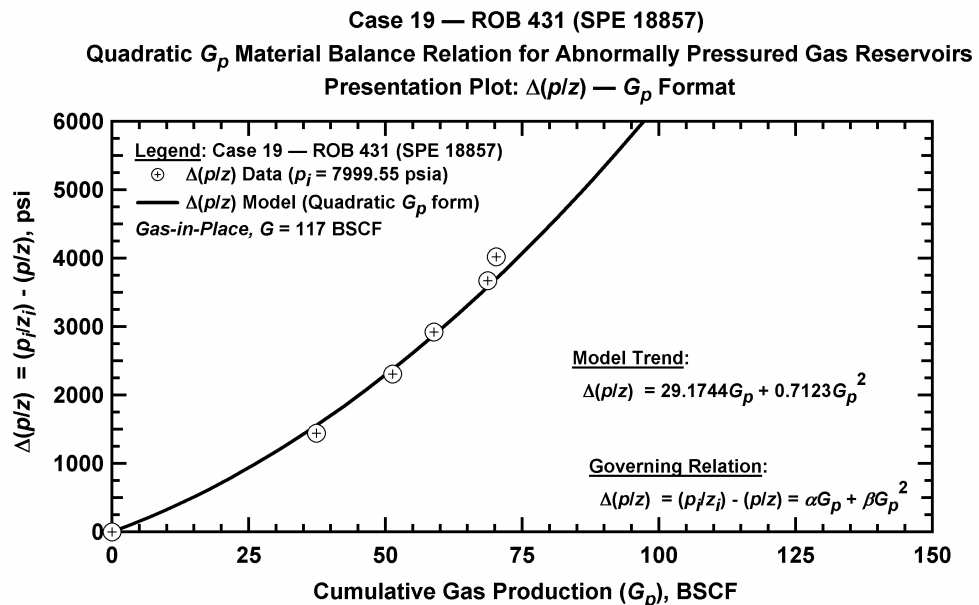


Figure D.20.b — Plot of $\Delta(p/z)$ vs. G_p — Case 19.

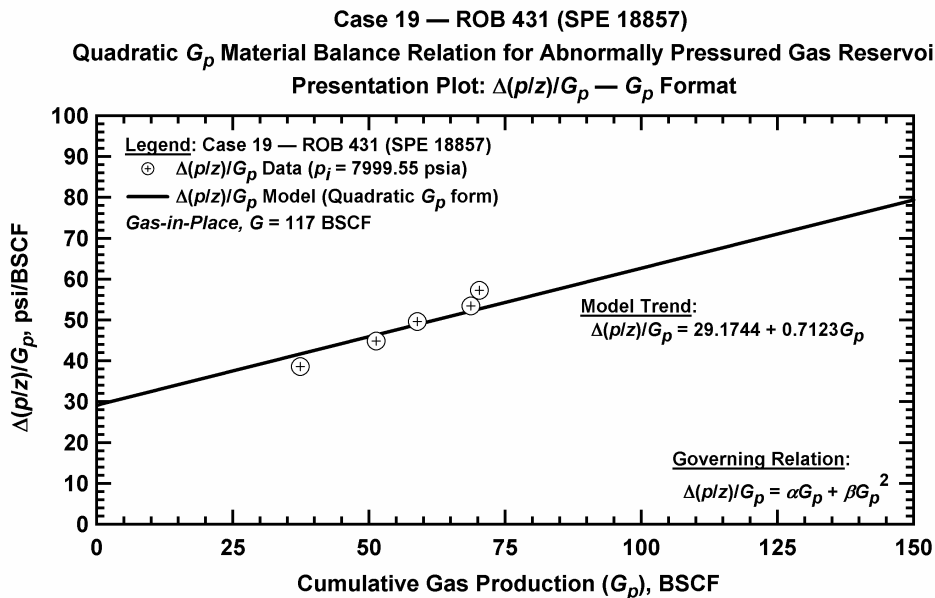


Figure D.20.c — Plot of $\Delta(p/z)/G_p$ vs. G_p — Case 19.

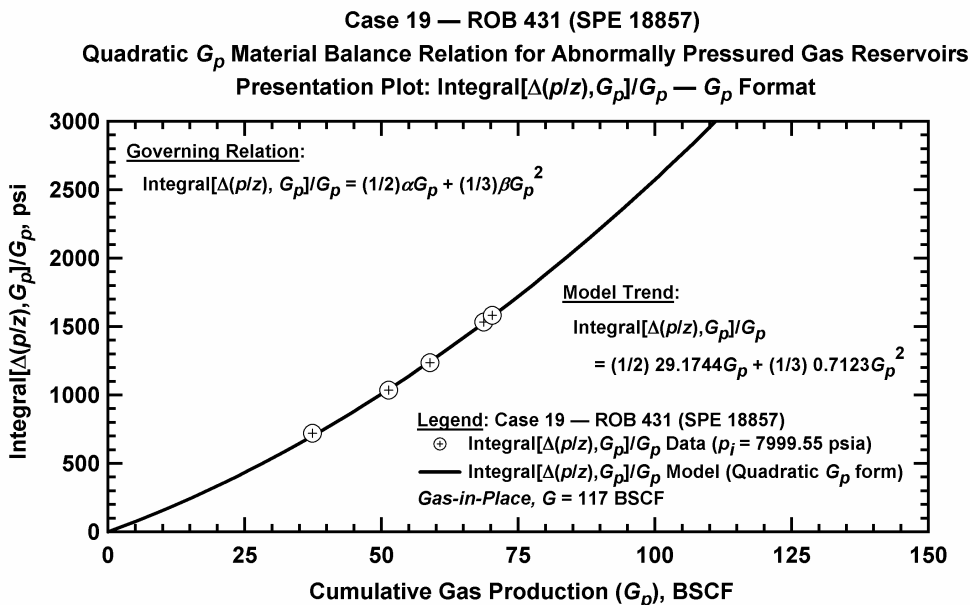


Figure D.20.d — Plot of $\frac{1}{G_p} \int_0^{G_p} \Delta(p/z) dG_p$ vs. G_p — Case 19.

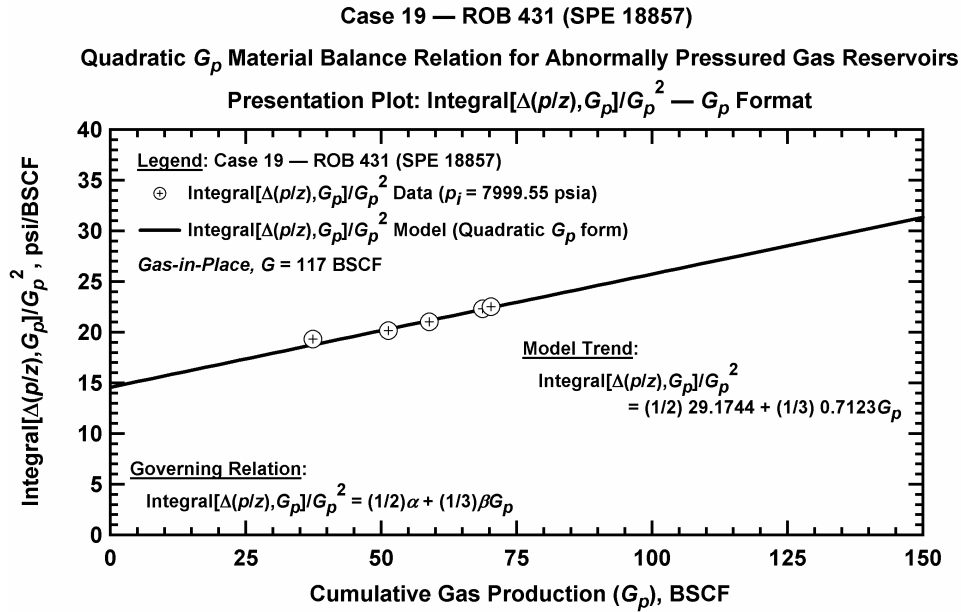


Figure D.20.e — Plot of $\frac{1}{G_p^2} \int_0^{G_p} \Delta(p/z) dG_p$ vs. G_p — Case 19.

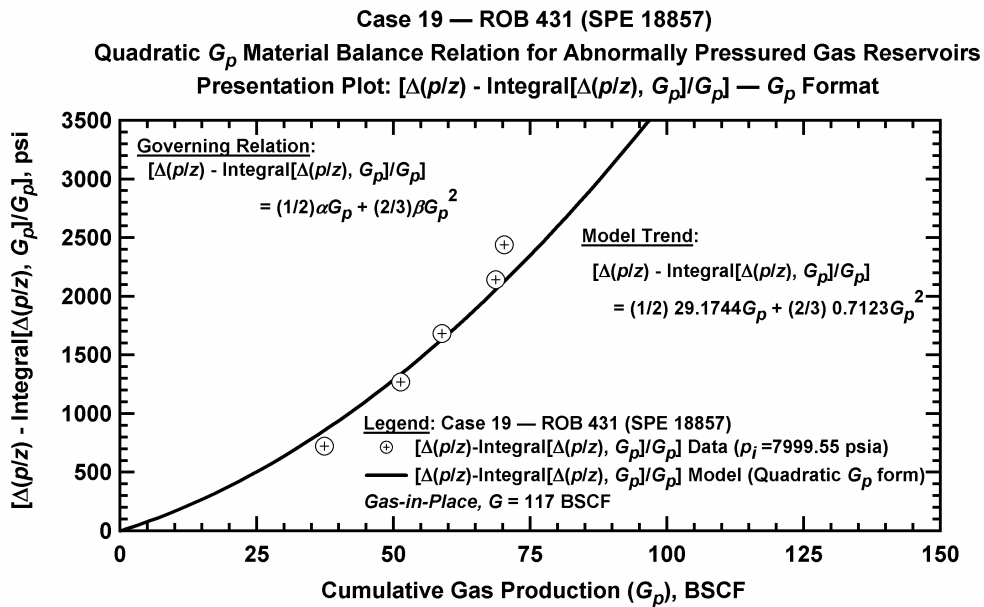


Figure D.20.f — Plot of $\Delta(p/z) - \frac{1}{G_p} \int_0^{G_p} \Delta(p/z) dG_p$ vs. G_p — Case 19.

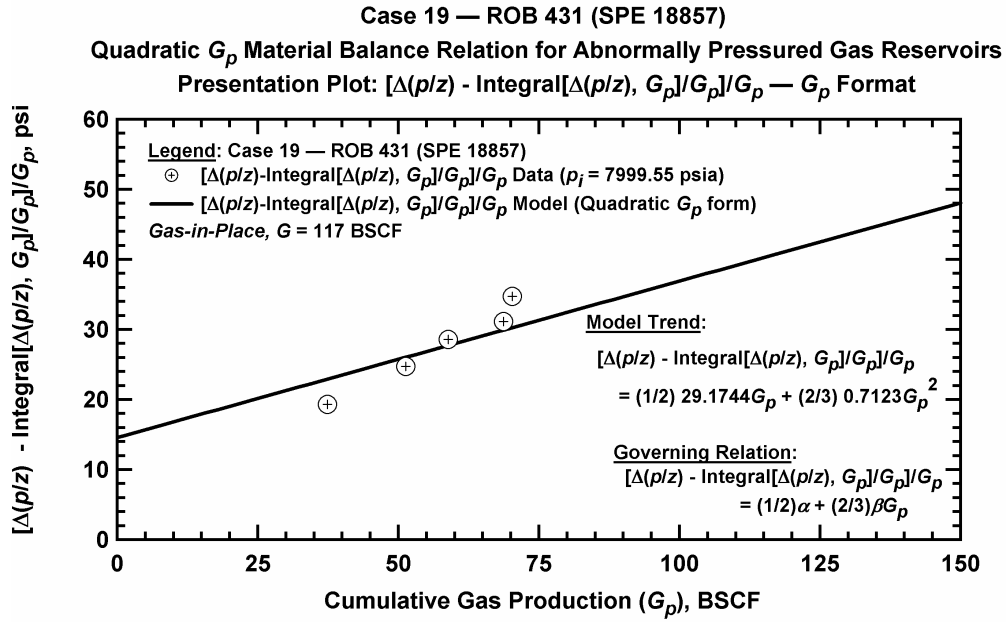


Figure D.20.g — Plot of $\frac{1}{G_p} \left[\Delta(p/z) - \frac{1}{G_p} \int_0^{G_p} \Delta(p/z) dG_p \right]$ vs. G_p — Case 19.

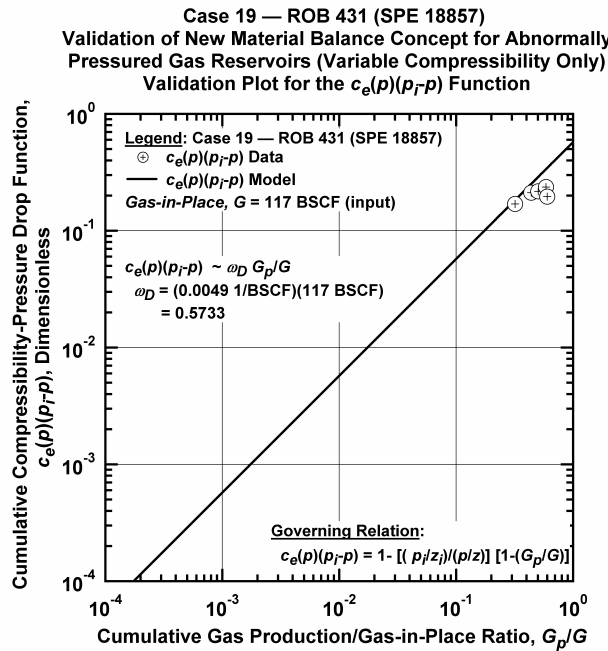


Figure D.20.h — Plot of $\bar{c}_e(p)(p_i - p)$ vs. G_p/G — Base Simulation Case 19.

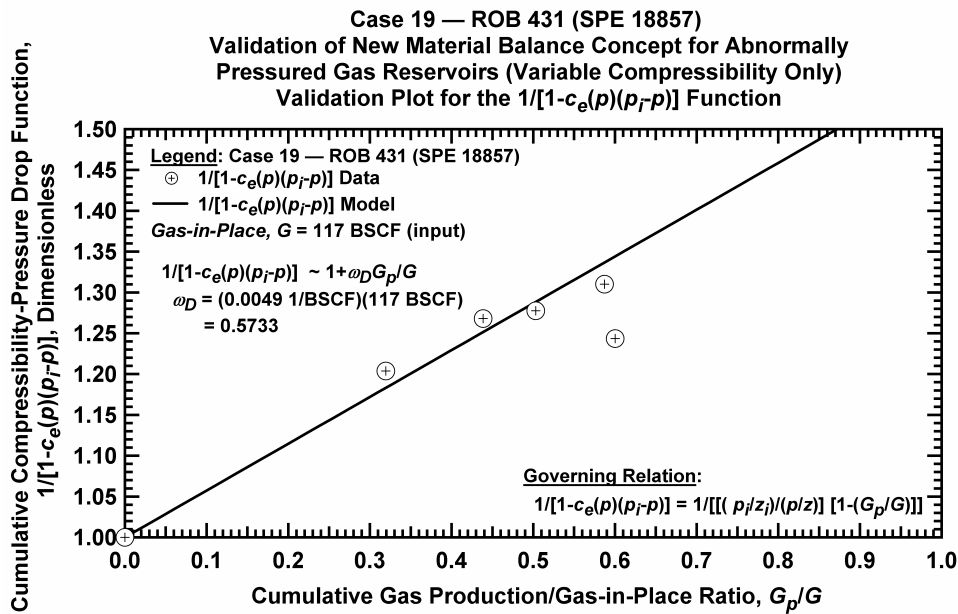


Figure D.20.i — Plot of $1/[1-\bar{c}_e(p)(p_i-p)]$ vs. G_p/G — Case 19.

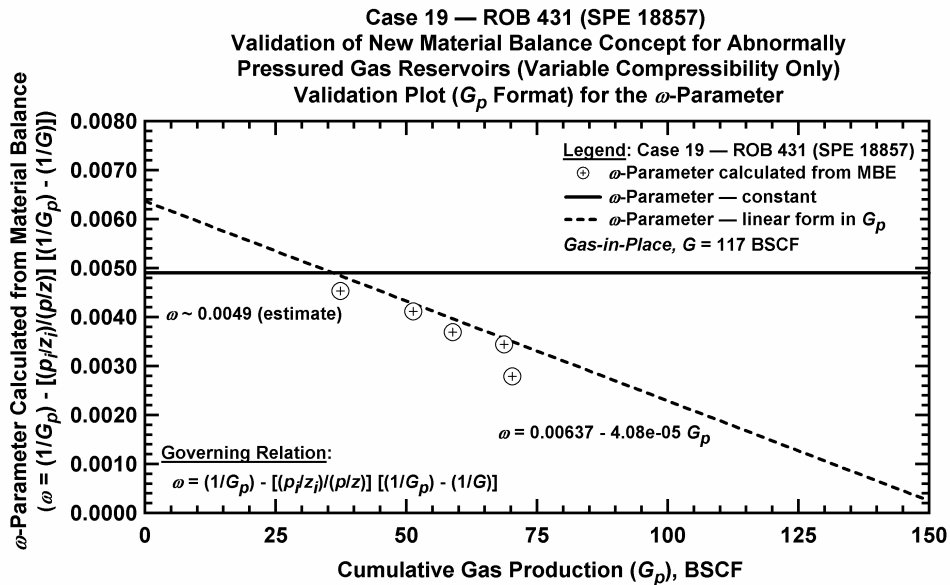


Figure D.20.j — Plot of ω vs. G_p — Base Simulation Case 19.

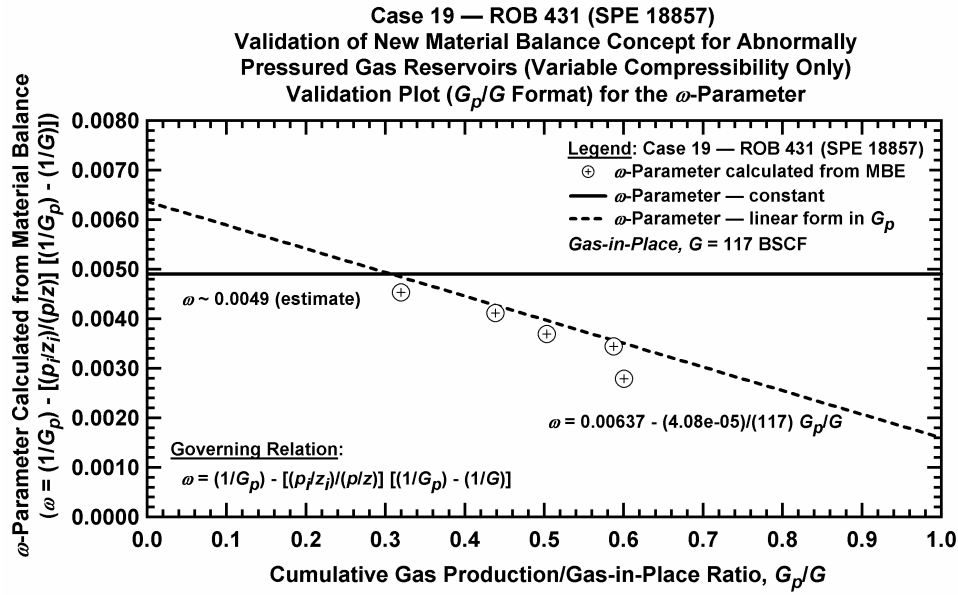


Figure D.20.k — Plot of ω vs. G_p/G — Case 19.

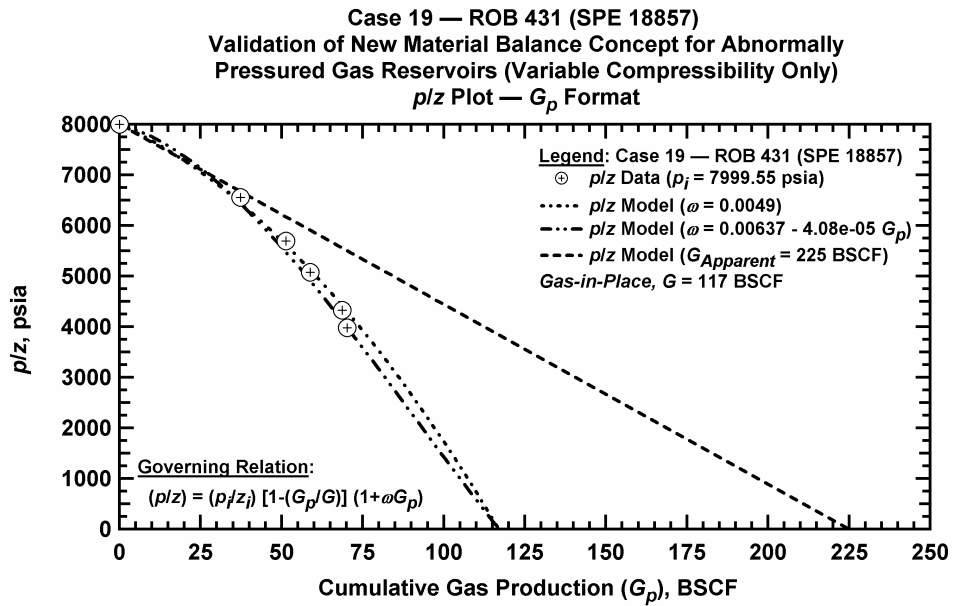


Figure D.20.l — Comparison plot of p/z vs. G_p — Case 19.

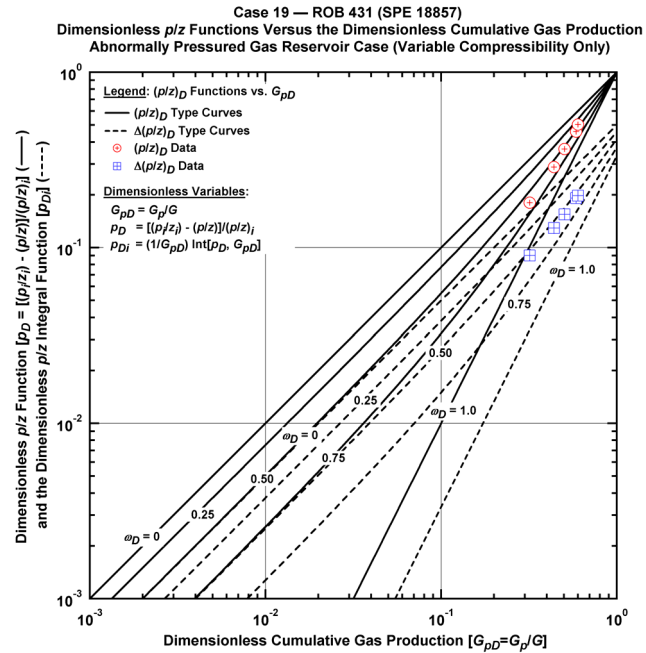


Figure D.20.m — Plot of dimensionless p/z functions vs. G_{pD} — Case 19.

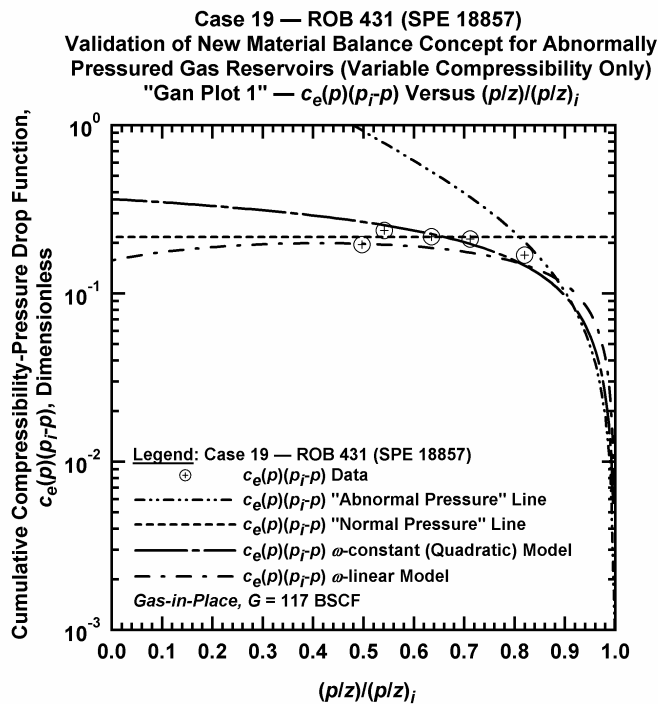


Figure D.20.n — Plot of $\bar{c}_e(p)(p_i - p)$ vs. $(p/z)/(p_i/z_i)$ — Case 19.

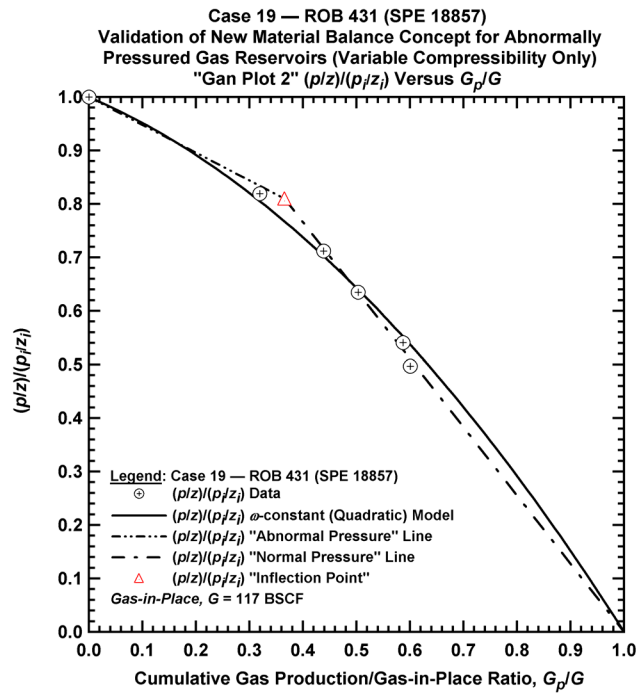


Figure D.20.o — Plot of $(p/z)/(p/z_i)$ vs. G_p/G — Case 19.

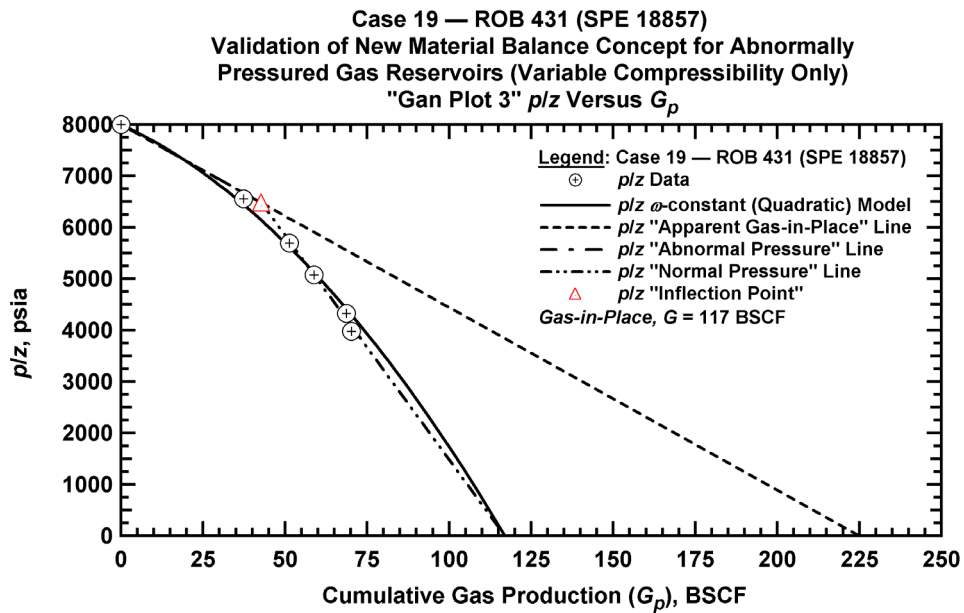


Figure D.20.p — Summary plot of p/z vs. G_p — Case 19.

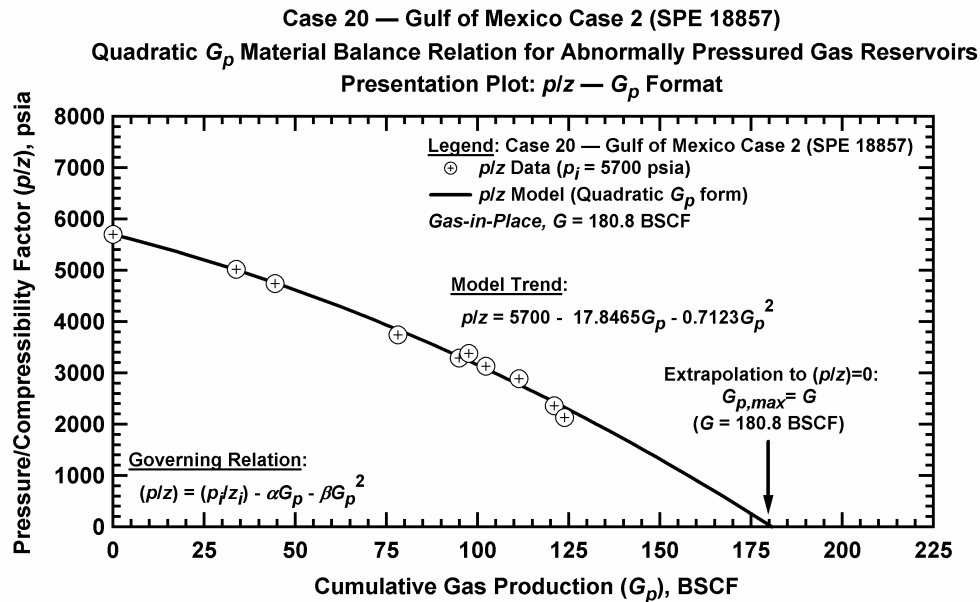


Figure D.21.a — Plot of p/z vs. G_p — Case 20.

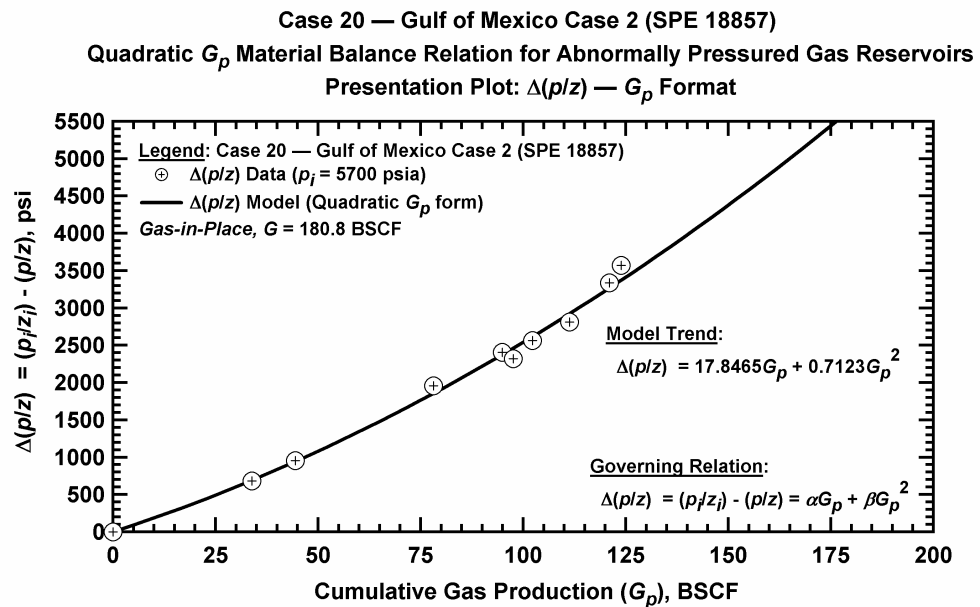


Figure D.21.b — Plot of $\Delta(p/z)$ vs. G_p — Case 20.

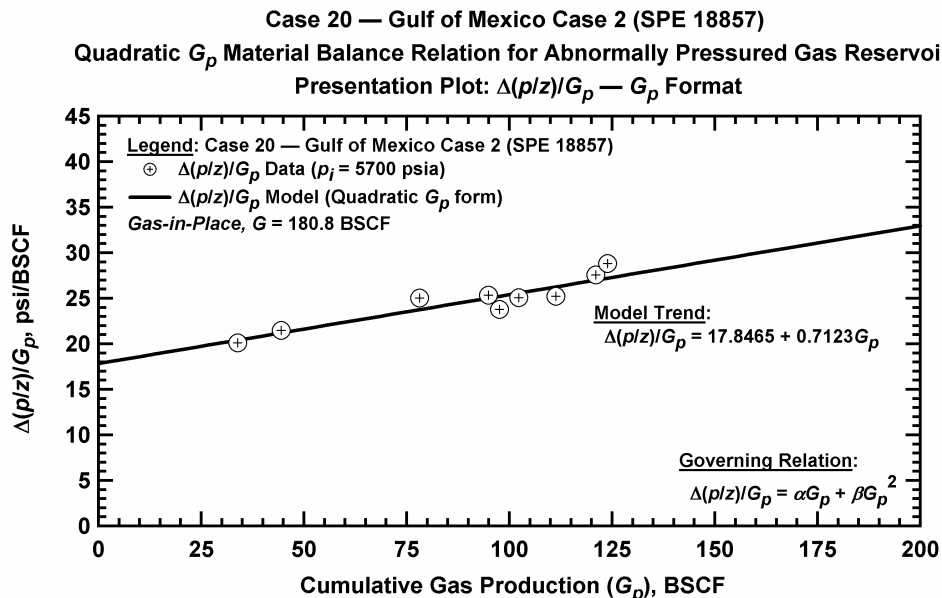


Figure D.21.c — Plot of $\Delta(p/z)/G_p$ vs. G_p — Case 20.

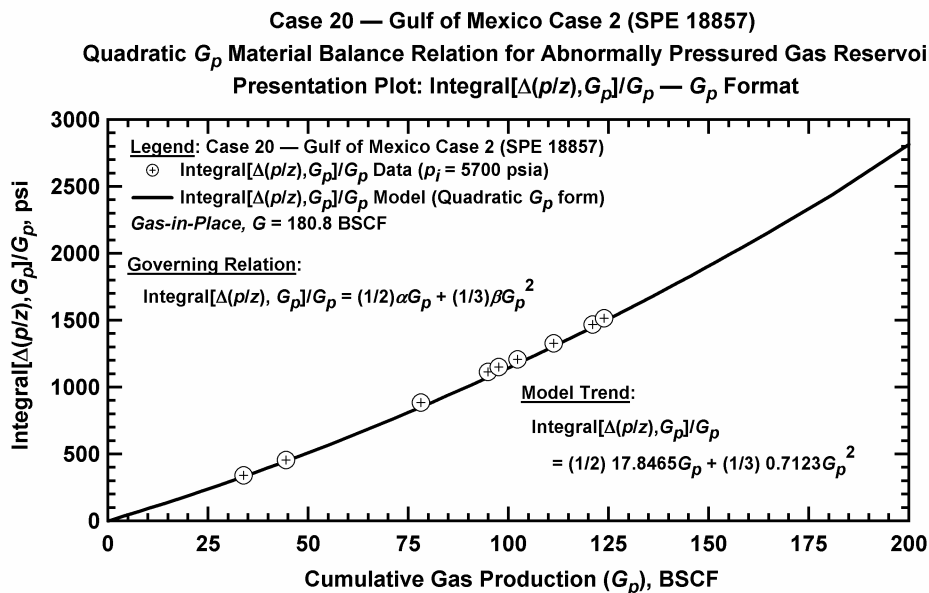
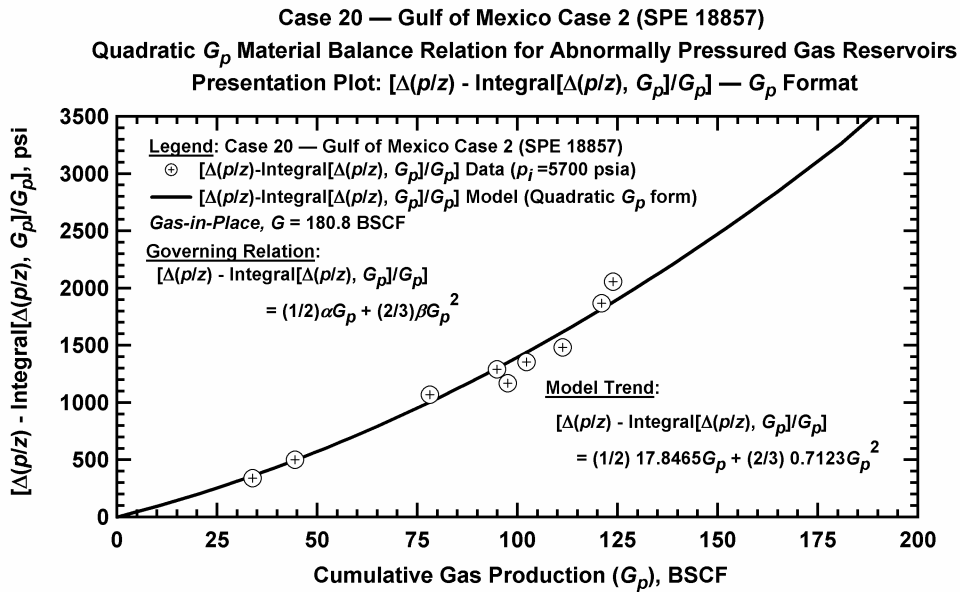
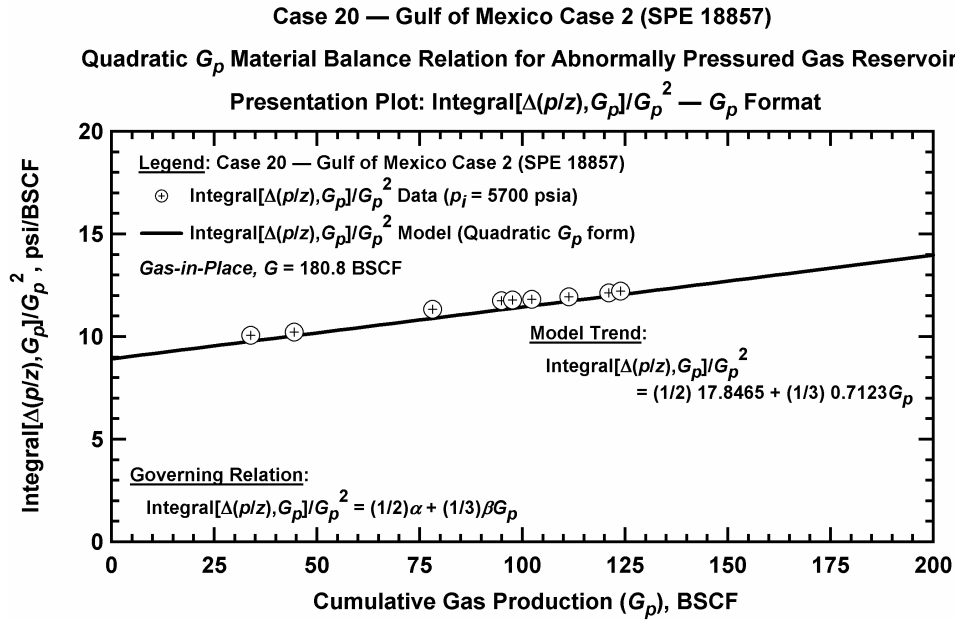


Figure D.21.d — Plot of $\frac{1}{G_p} \int_0^{G_p} \Delta(p/z) dG_p$ vs. G_p — Case 20.



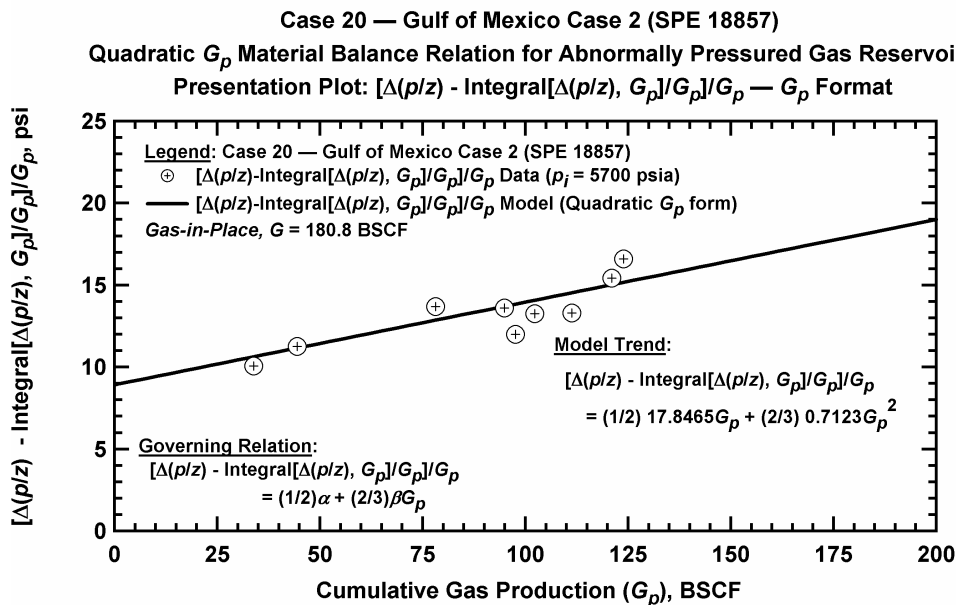


Figure D.21.g — Plot of $\frac{1}{G_p} \left[\Delta(p/z) - \frac{1}{G_p} \int_0^{G_p} \Delta(p/z) dG_p \right]$ vs. G_p — Case 20.

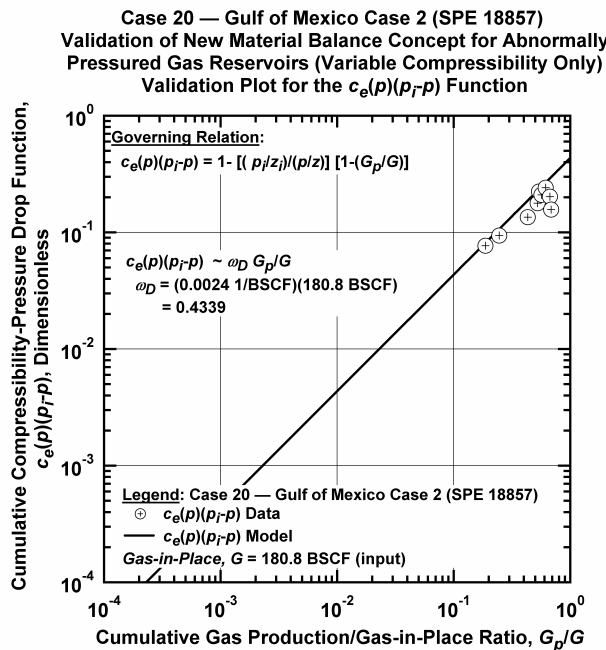


Figure D.21.h — Plot of $\bar{c}_e(p)(p_i - p)$ vs. G_p/G — Base Simulation Case 20.

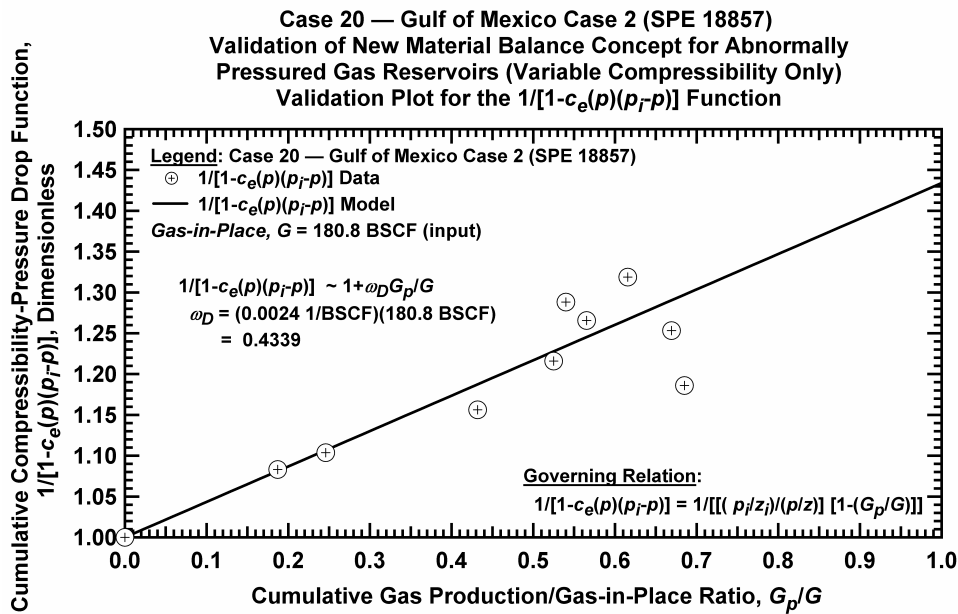


Figure D.21.i — Plot of $1/[1-\bar{c}_e(p)(p_i-p)]$ vs. G_p/G — Case 20.

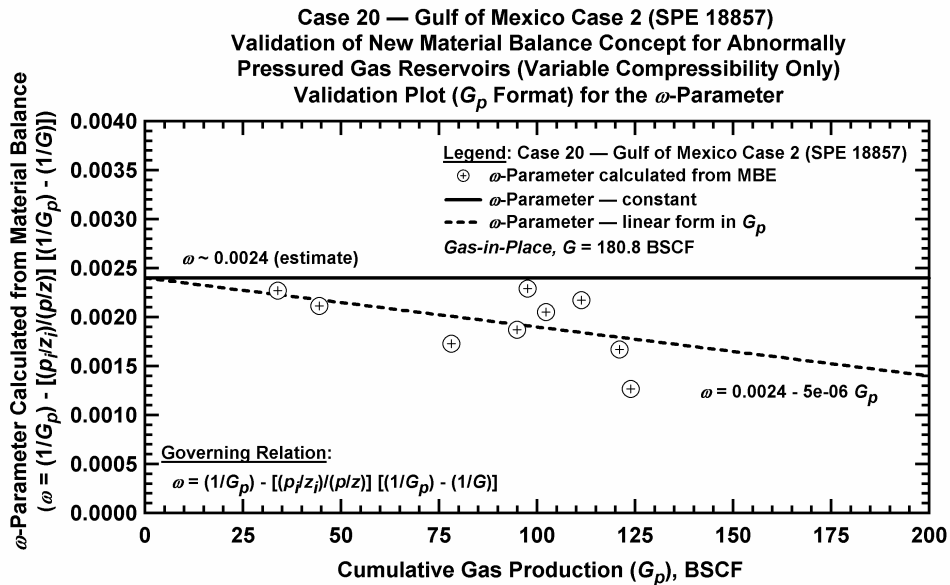


Figure D.21.j — Plot of ω vs. G_p — Base Simulation Case 20.

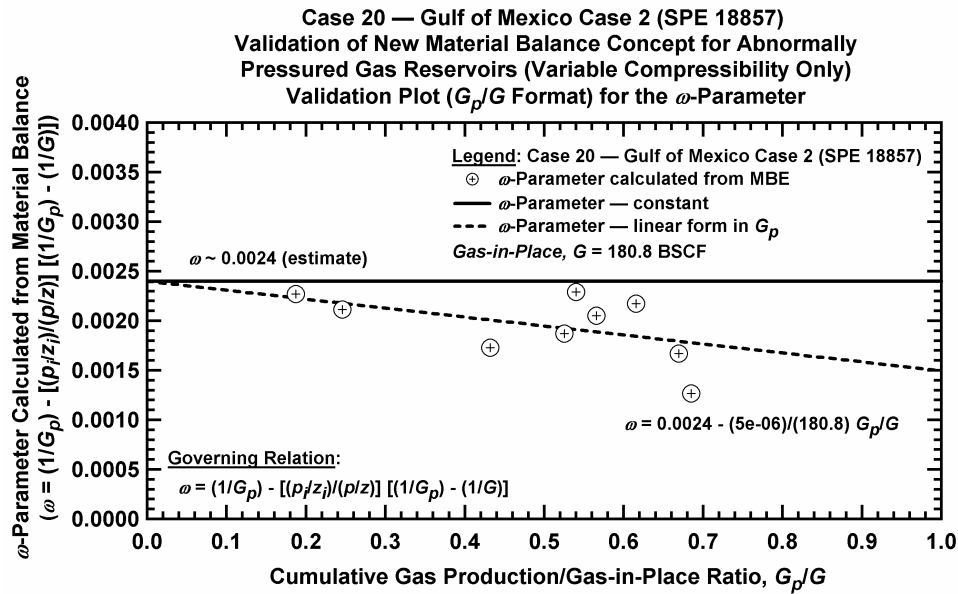


Figure D.21.k — Plot of ω vs. G_p/G — Case 20.

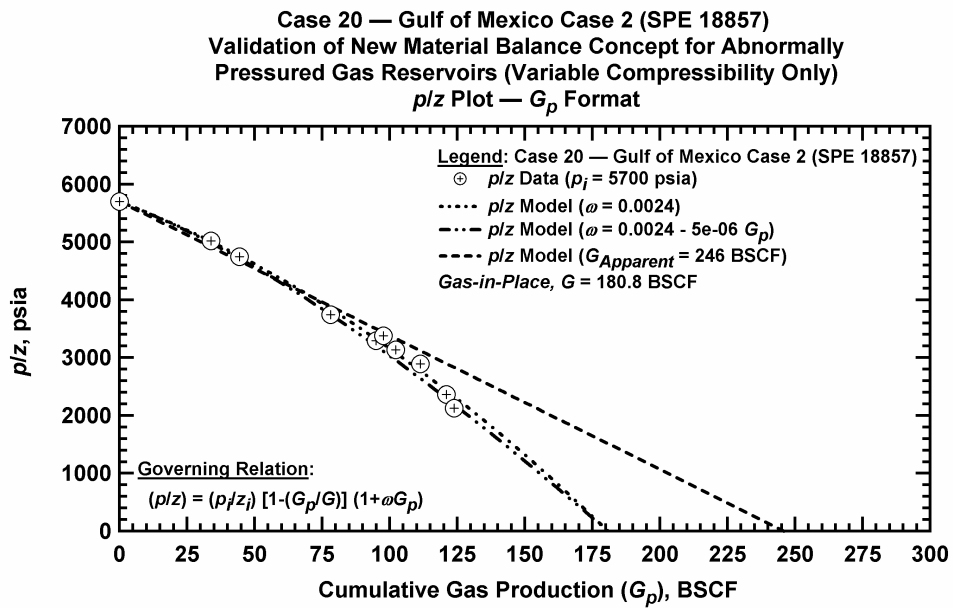


Figure D.21.l — Comparison plot of p/z vs. G_p — Case 20.

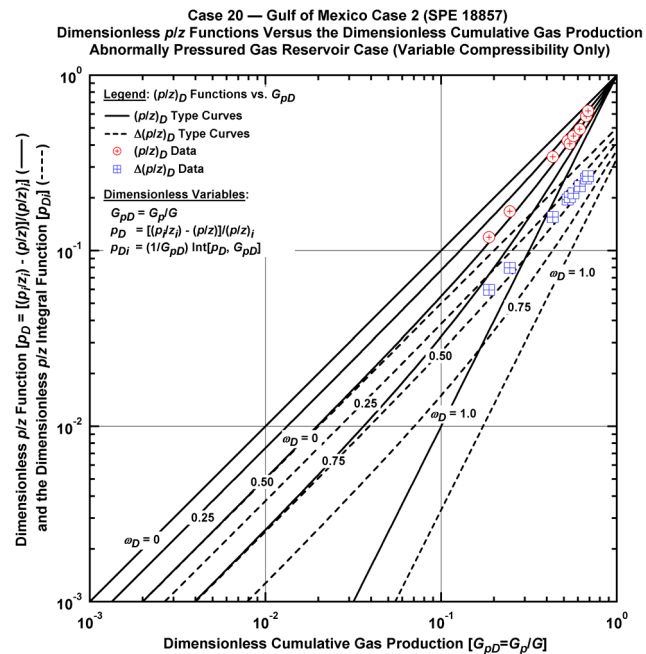


Figure D.21.m — Plot of dimensionless p/z functions vs. G_{pD} — Case 20.

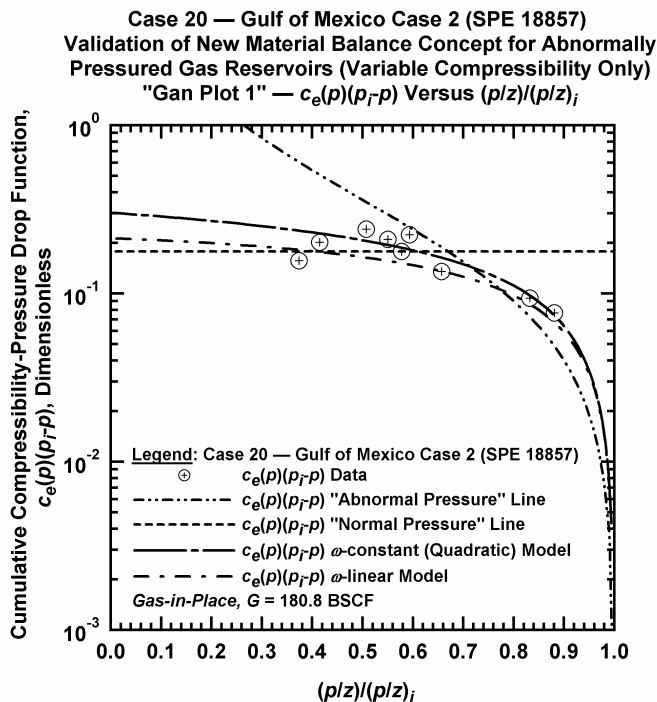


Figure D.21.n — Plot of $\bar{c}_e(p)(p_i - p)$ vs. $(p/z)/(p_i/z_i)$ — Case 20.

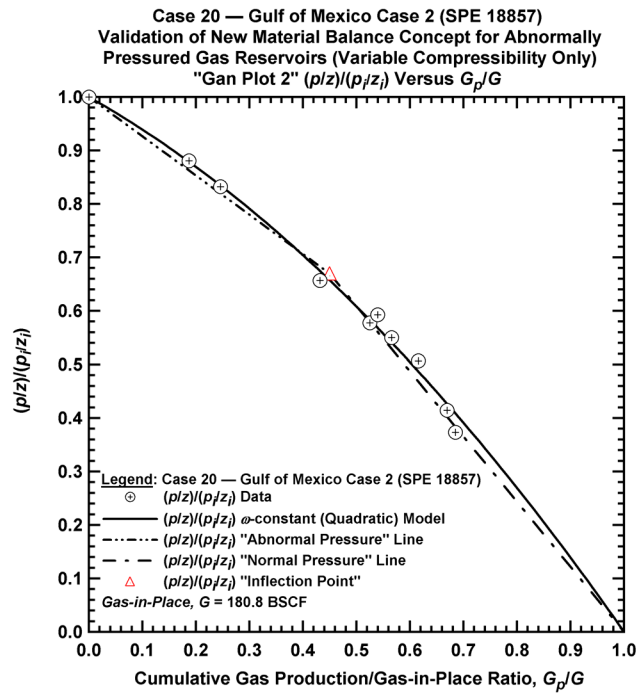


Figure D.21.o — Plot of $(p/z)/(p/z_i)$ vs. G_p/G — Case 20.

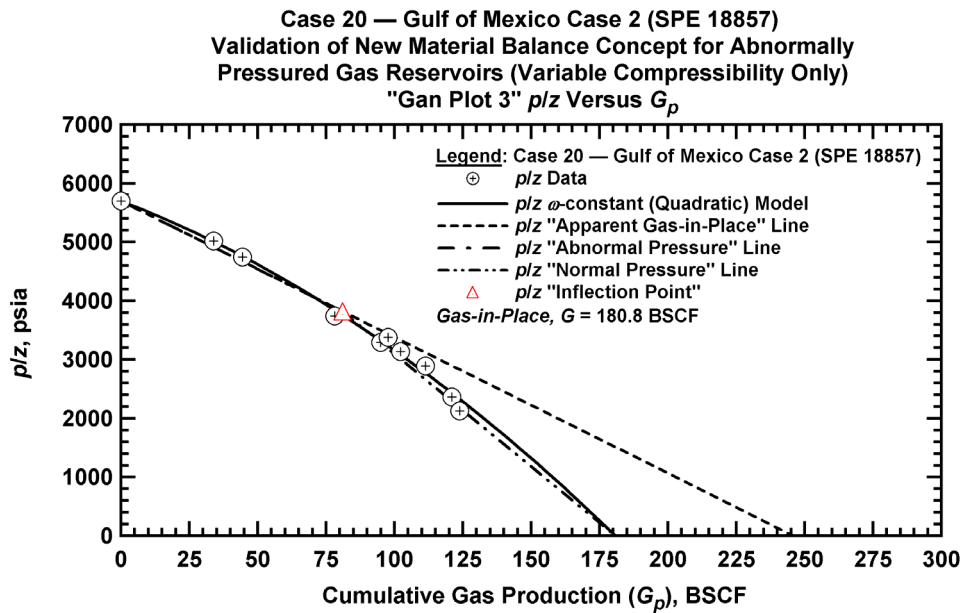


Figure D.21.p — Summary plot of p/z vs. G_p — Case 20.

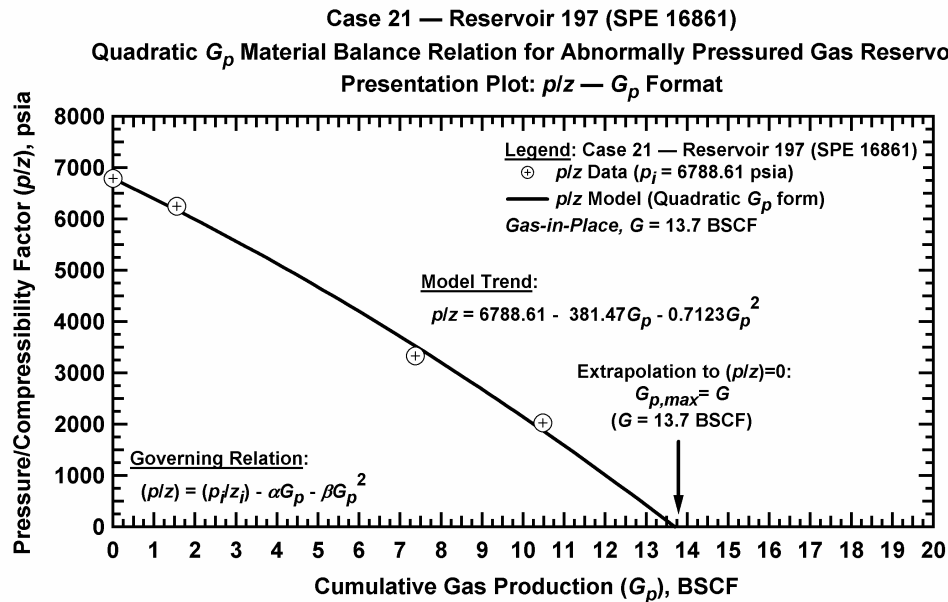


Figure D.22.a — Plot of p/z vs. G_p — Case 21.

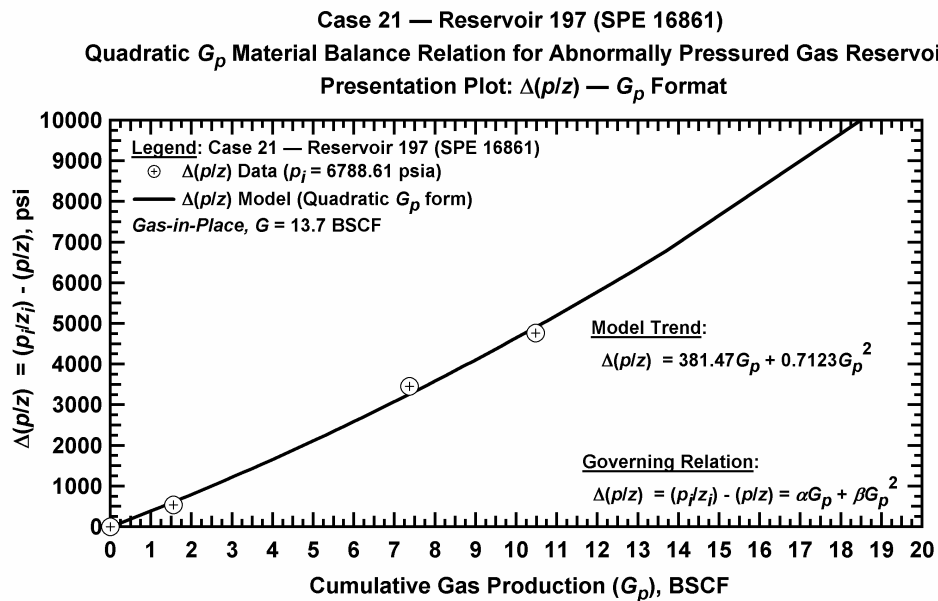


Figure D.22.b — Plot of $\Delta(p/z)$ vs. G_p — Case 21.

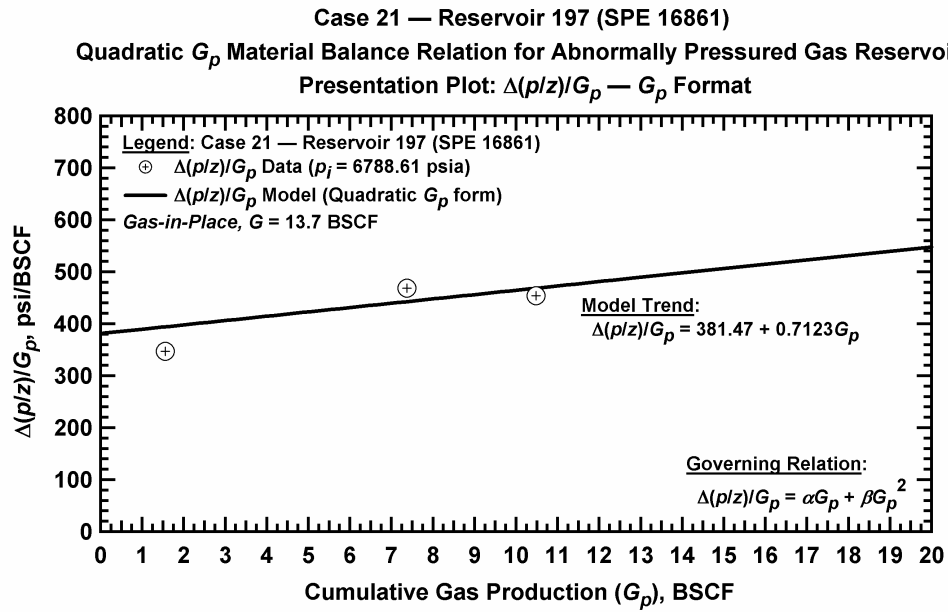


Figure D.22.c — Plot of $\Delta(p/z)/G_p$ vs. G_p — Case 21.

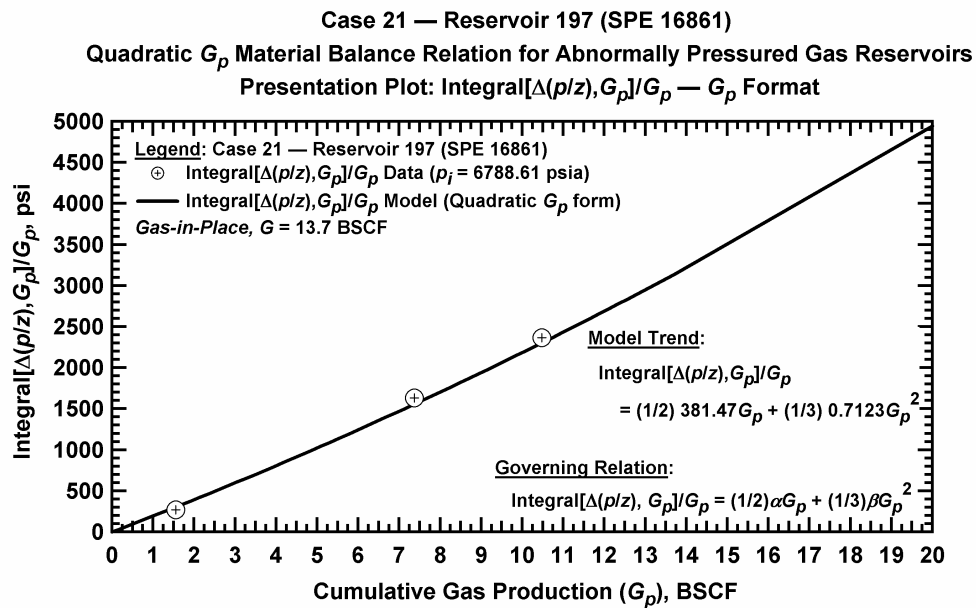


Figure D.22.d — Plot of $\frac{1}{G_p} \int_0^{G_p} \Delta(p/z) dG_p$ vs. G_p — Case 21.

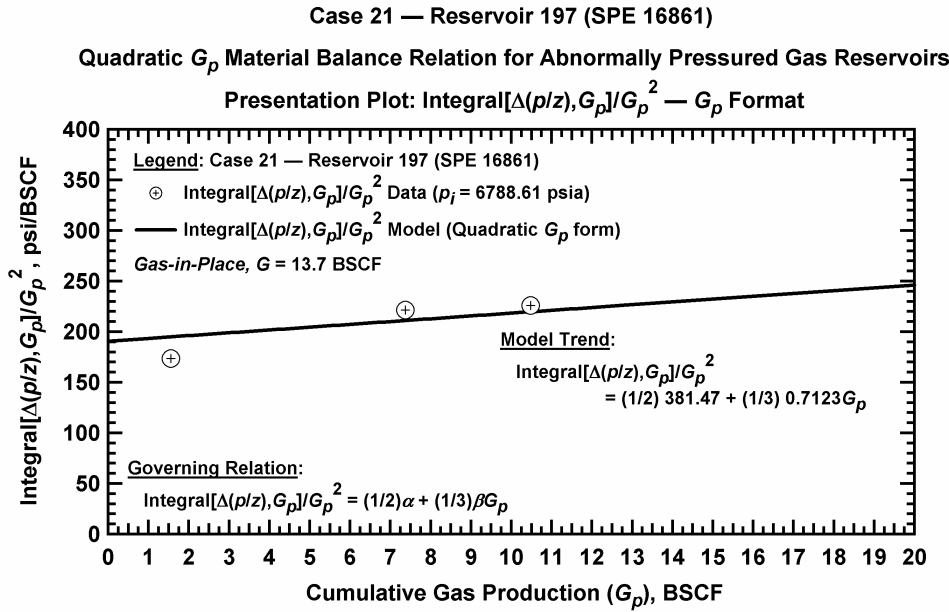


Figure D.22.e — Plot of $\frac{1}{G_p^2} \int_0^{G_p} \Delta(p/z) dG_p$ vs. G_p — Case 21.

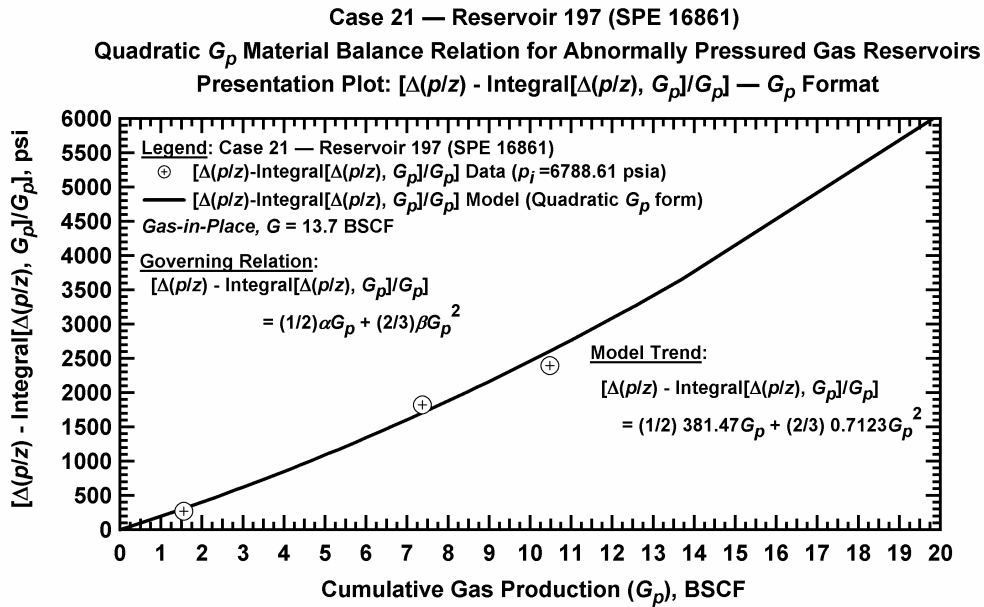


Figure D.22.f — Plot of $\Delta(p/z) - \frac{1}{G_p} \int_0^{G_p} \Delta(p/z) dG_p$ vs. G_p — Case 21.

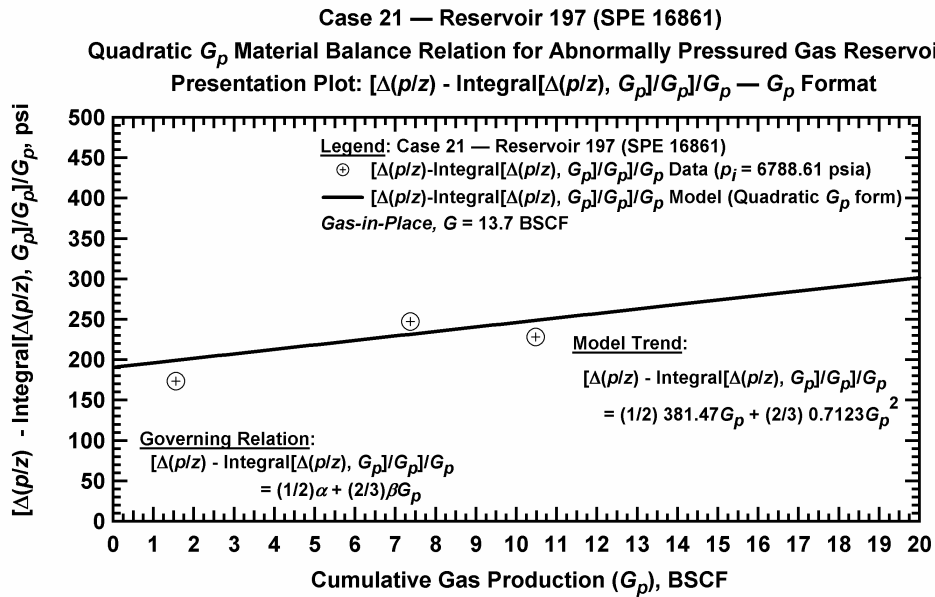


Figure D.22.g — Plot of $\frac{1}{G_p} \left[\Delta(p/z) - \frac{1}{G_p} \int_0^{G_p} \Delta(p/z) dG_p \right]$ vs. G_p — Case 21.

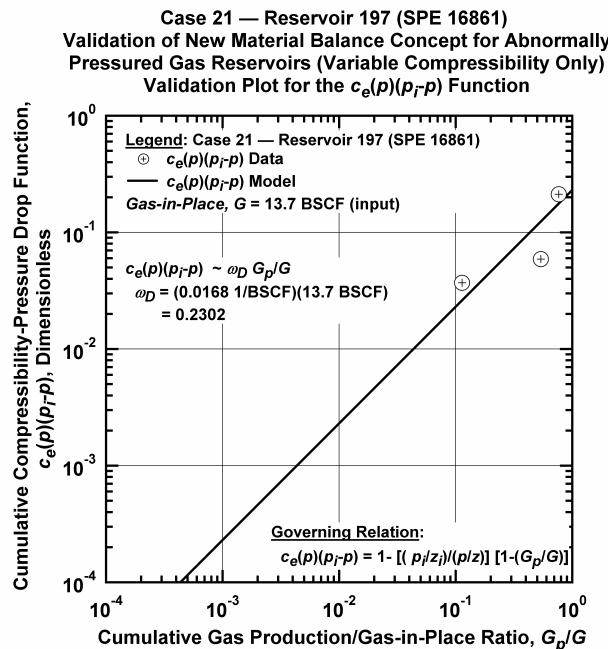
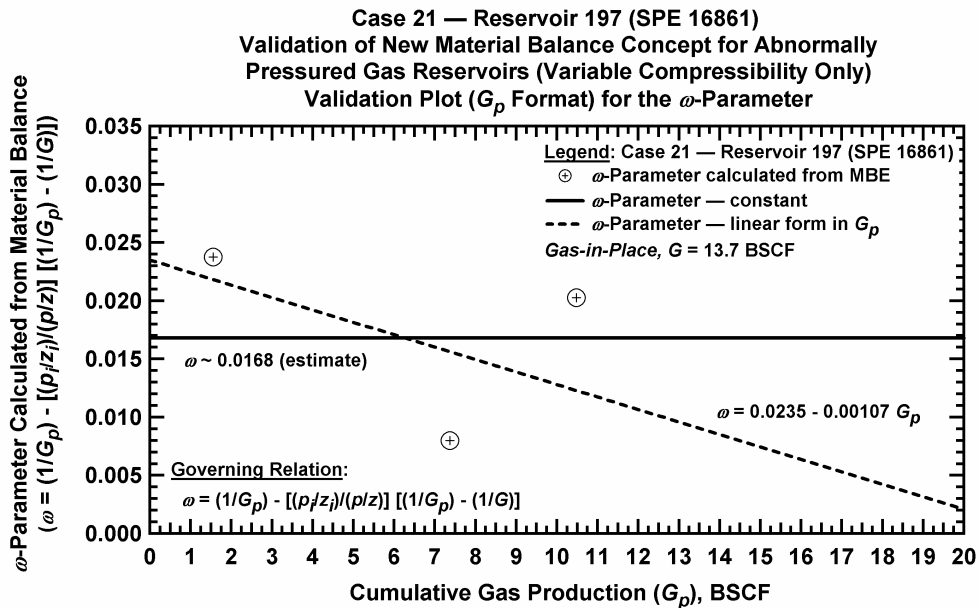
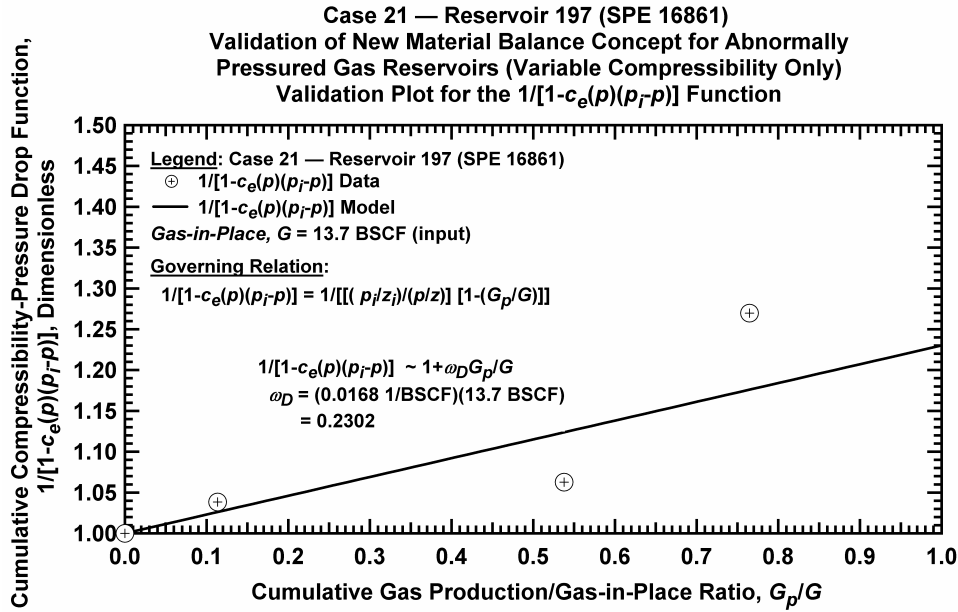


Figure D.22.h — Plot of $\bar{c}_e(p)(p_i - p)$ vs. G_p/G — Base Simulation Case 21.



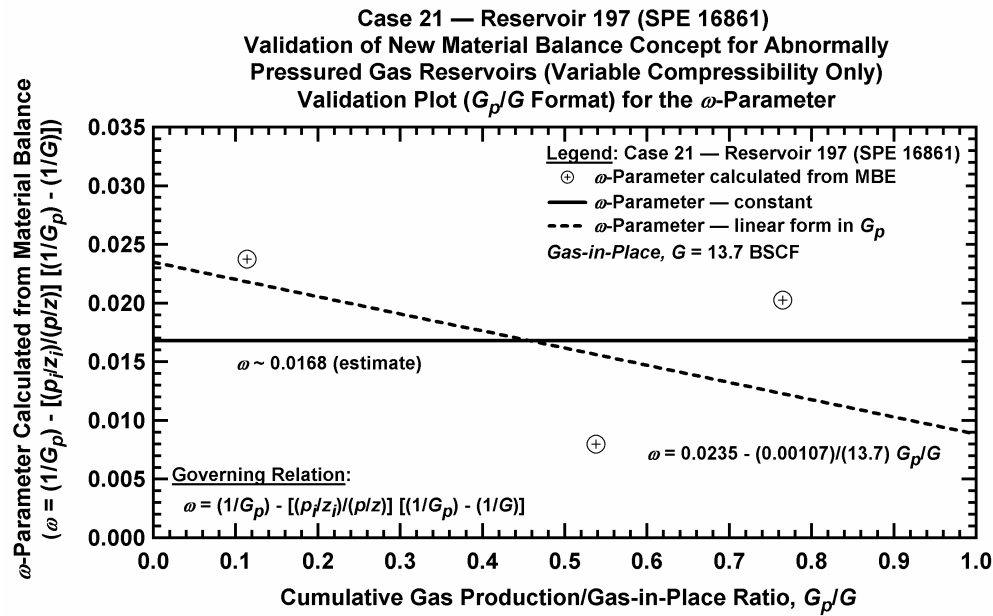


Figure D.22.k — Plot of ω vs. G_p/G — Case 21.

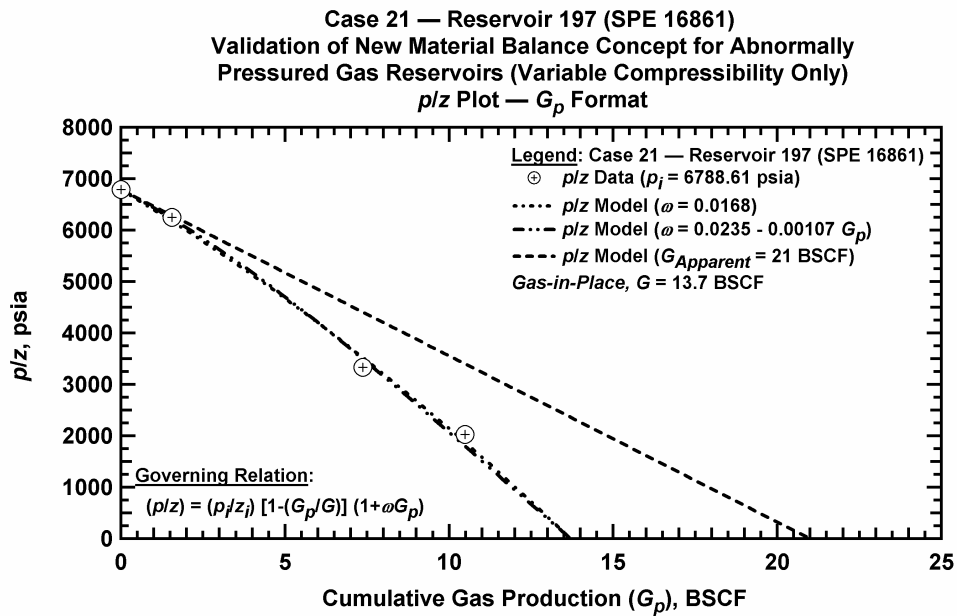
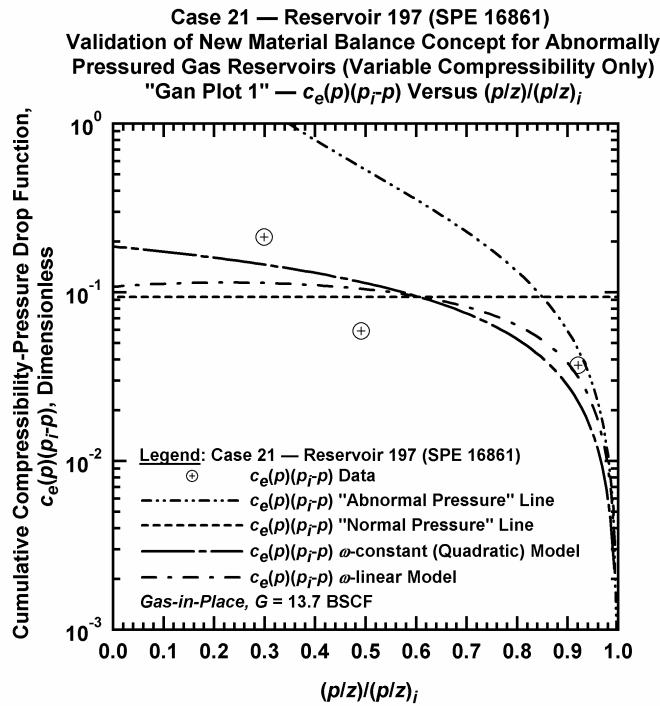
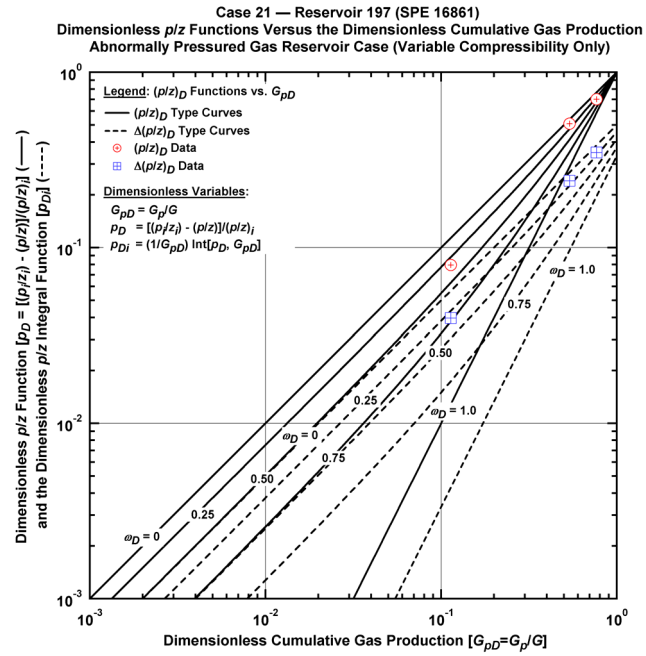


Figure D.22.l — Comparison plot of p/z vs. G_p — Case 21.



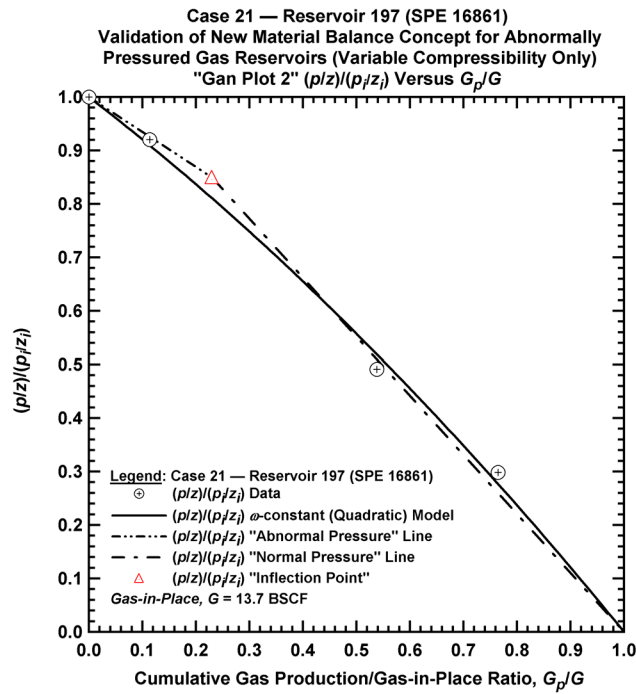


Figure D.22.o — Plot of $(p/z)/(p/z_i)$ vs. G_p/G — Case 21.

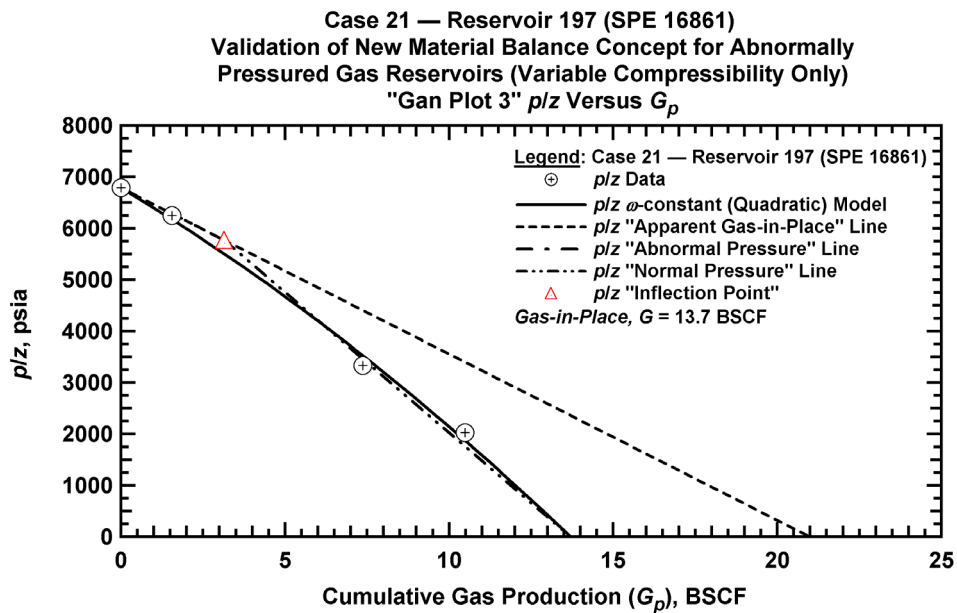


Figure D.22.p — Summary plot of p/z vs. G_p — Case 21.

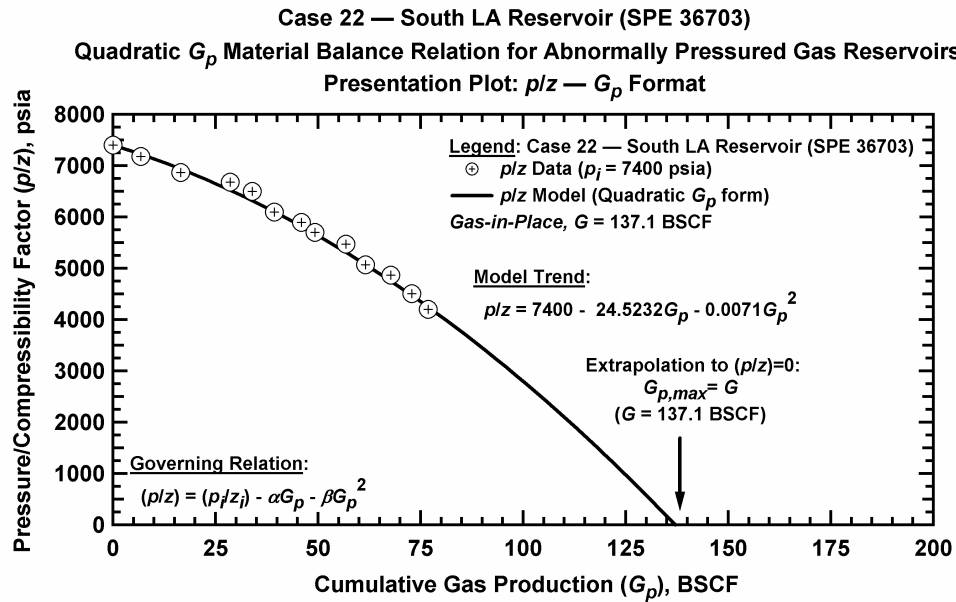


Figure D.23.a — Plot of p/z vs. G_p — Case 22.

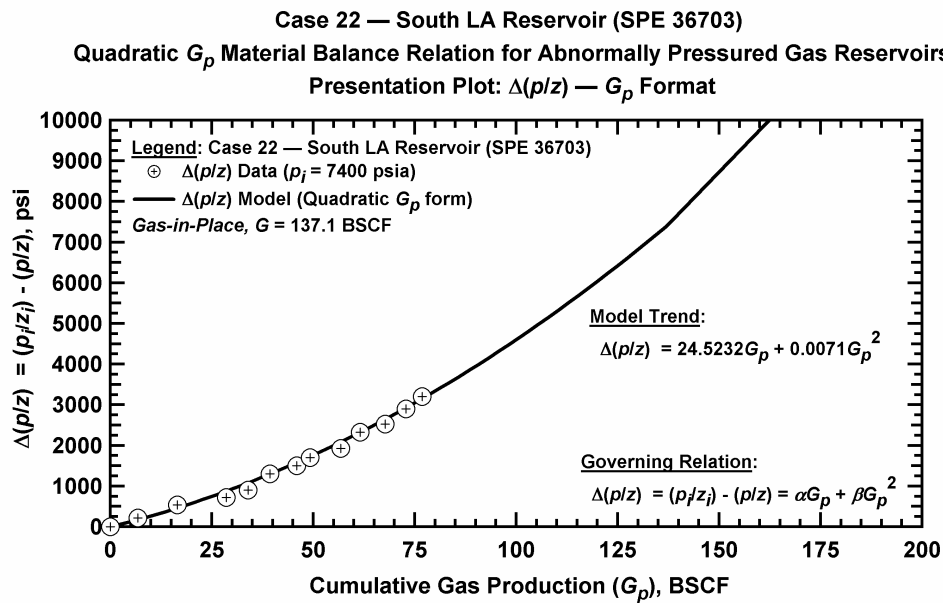


Figure D.23.b — Plot of $\Delta(p/z)$ vs. G_p — Case 22.

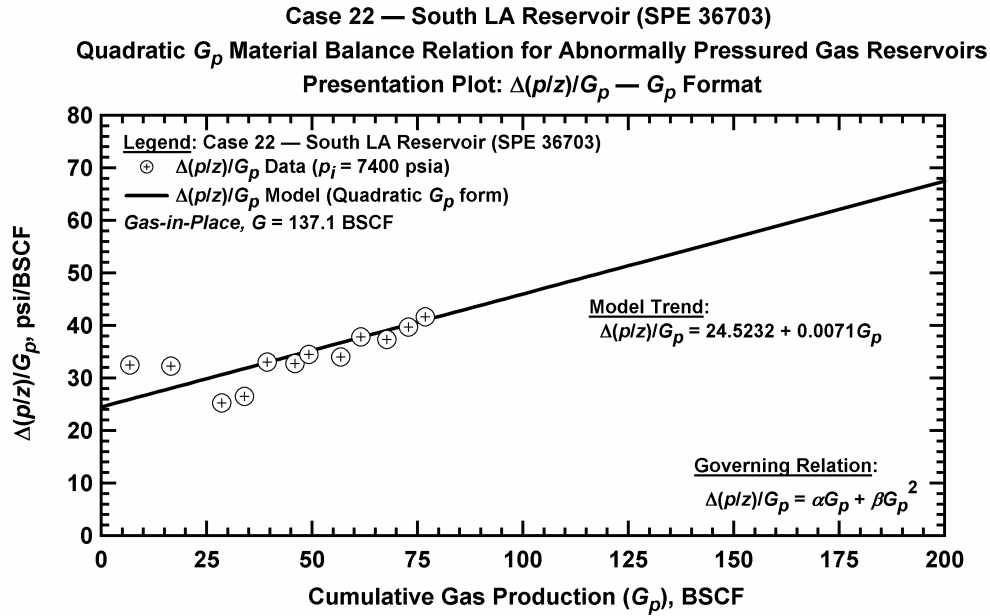


Figure D.23.c — Plot of $\Delta(p/z)/G_p$ vs. G_p — Case 22.

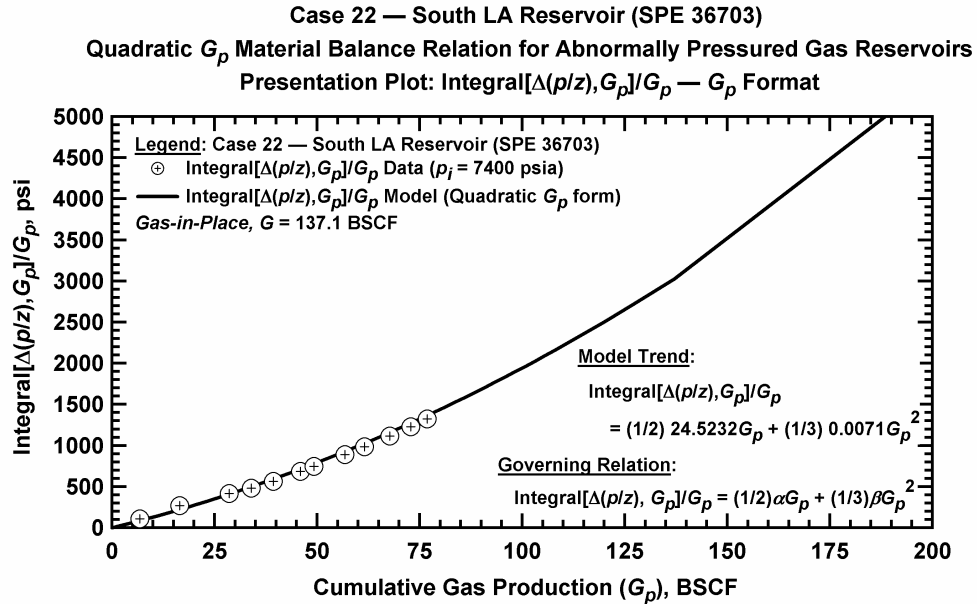


Figure D.23.d — Plot of $\frac{1}{G_p} \int_0^{G_p} \Delta(p/z) dG_p$ vs. G_p — Case 22.

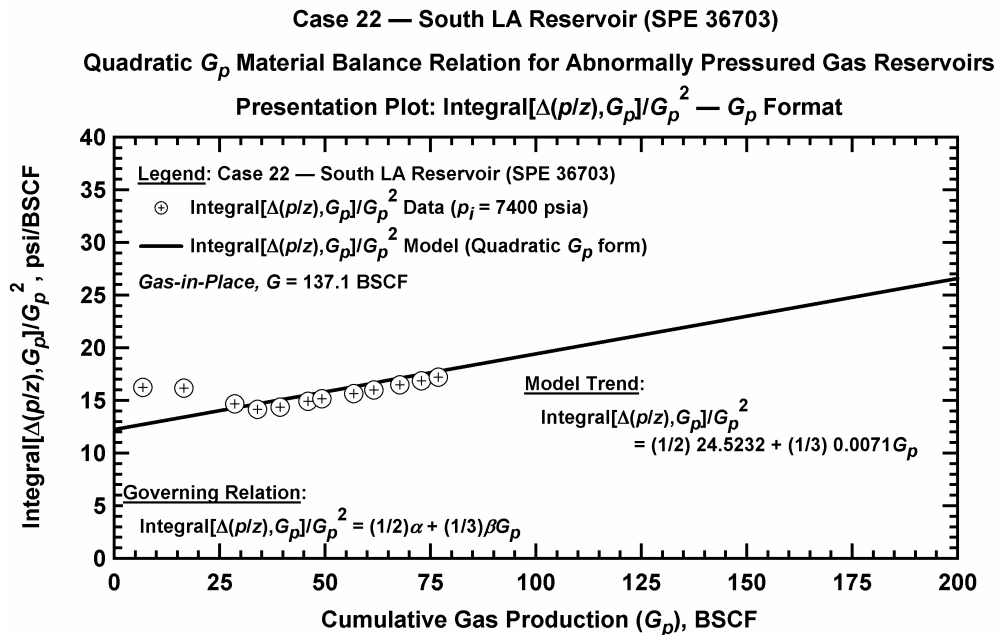


Figure D.23.e — Plot of $\frac{1}{G_p^2} \int_0^{G_p} \Delta(p/z) dG_p$ vs. G_p — Case 22.

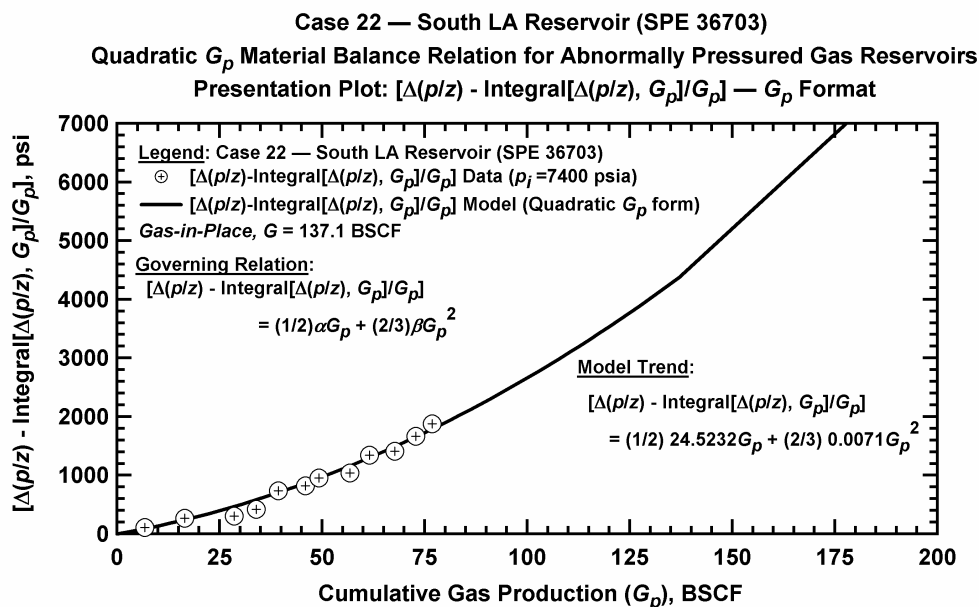


Figure D.23.f — Plot of $\Delta(p/z) - \frac{1}{G_p} \int_0^{G_p} \Delta(p/z) dG_p$ vs. G_p — Case 22.

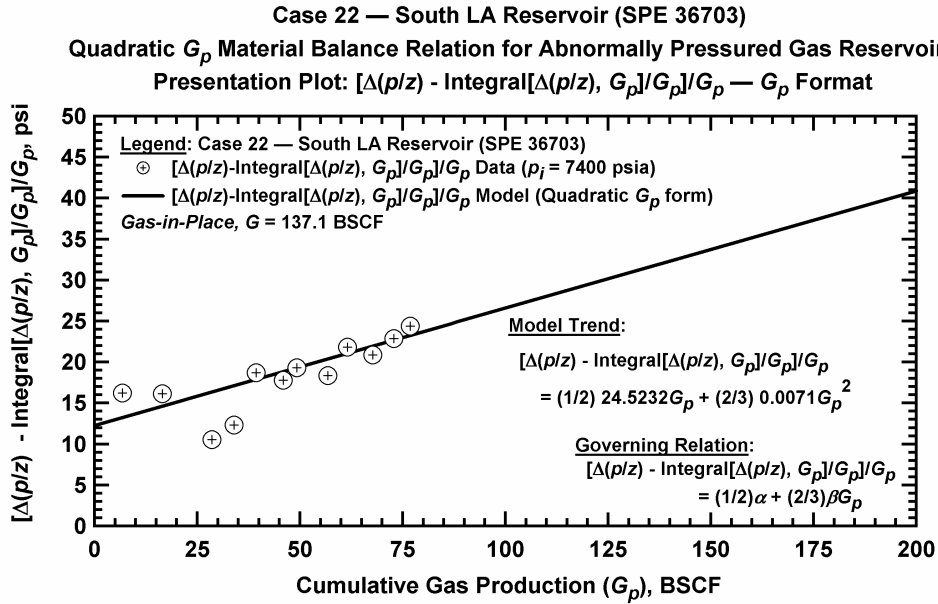


Figure D.23.g — Plot of $\frac{1}{G_p} \left[\Delta(p/z) - \frac{1}{G_p} \int_0^{G_p} \Delta(p/z) dG_p \right]$ vs. G_p — Case 22.

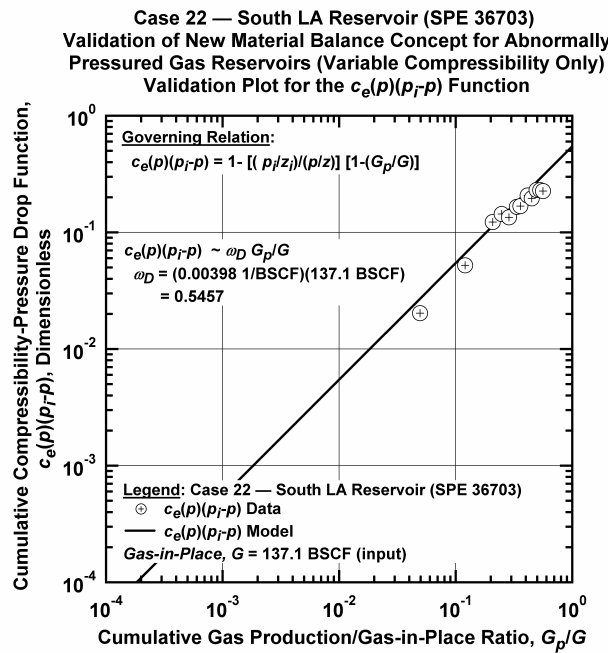
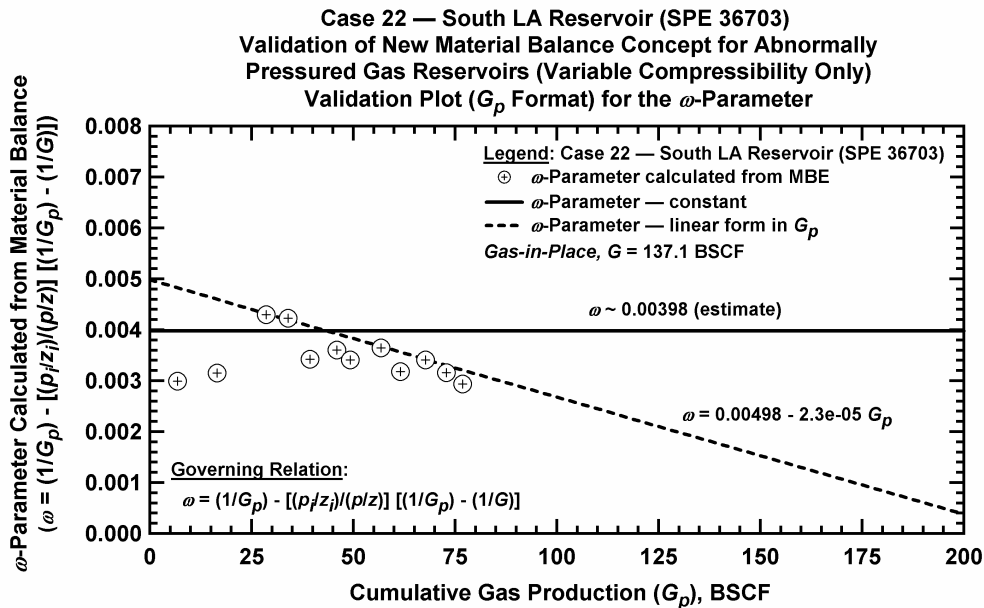
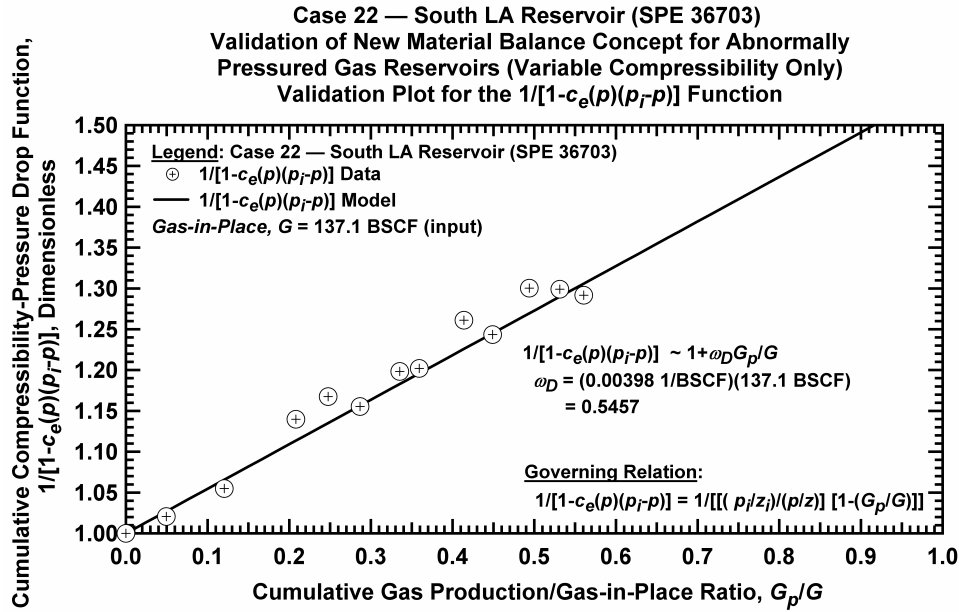


Figure D.23.h — Plot of $\bar{c}_e(p)(p_i - p)$ vs. G_p/G — Base Simulation Case 22.



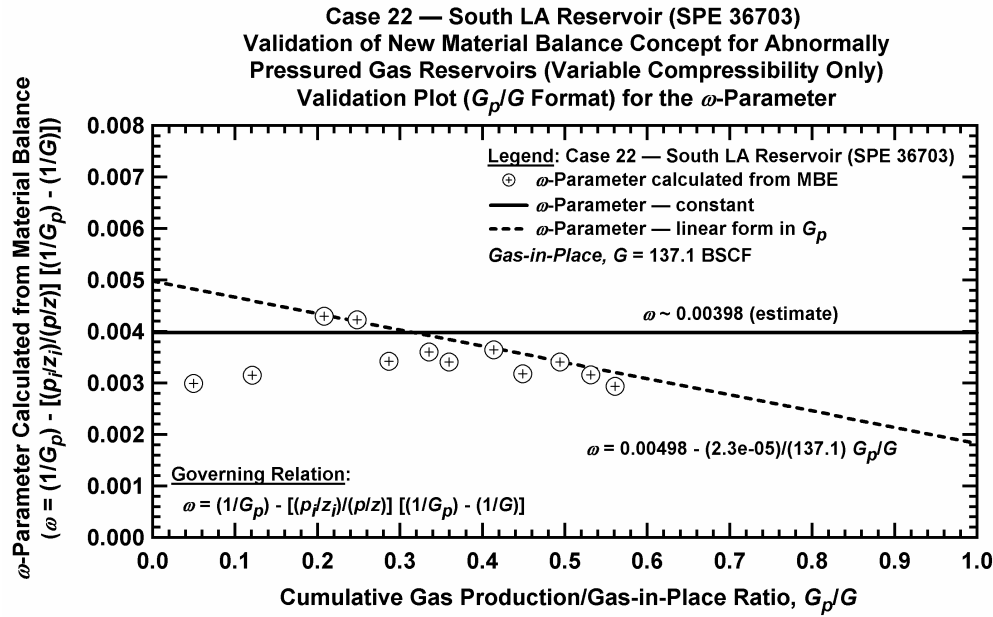


Figure D.23.k — Plot of ω vs. G_p/G — Case 22.

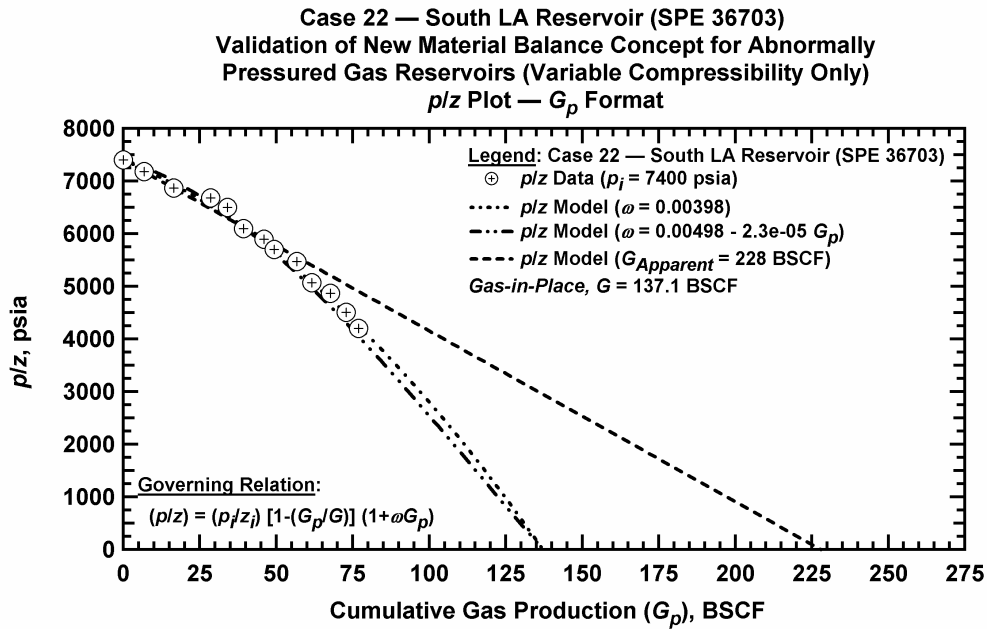


Figure D.23.l — Comparison plot of p/z vs. G_p — Case 22.

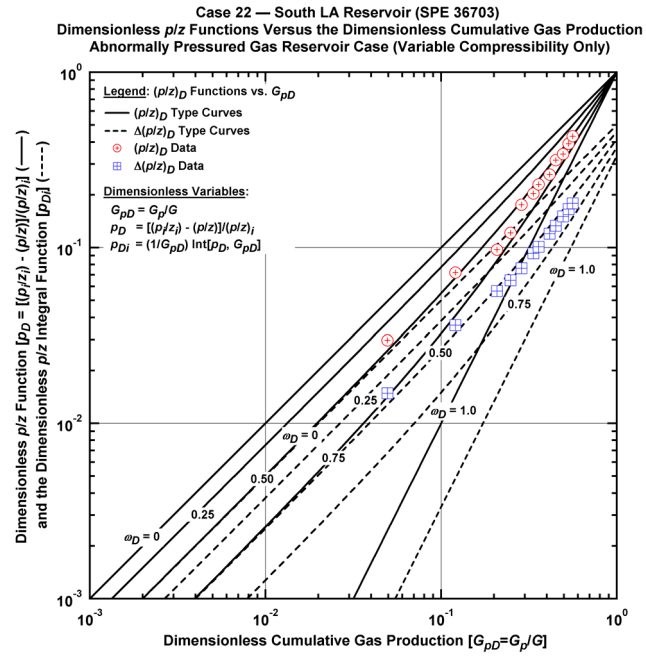


Figure D.23.m — Plot of dimensionless p/z functions vs. G_{pD} — Case 22.

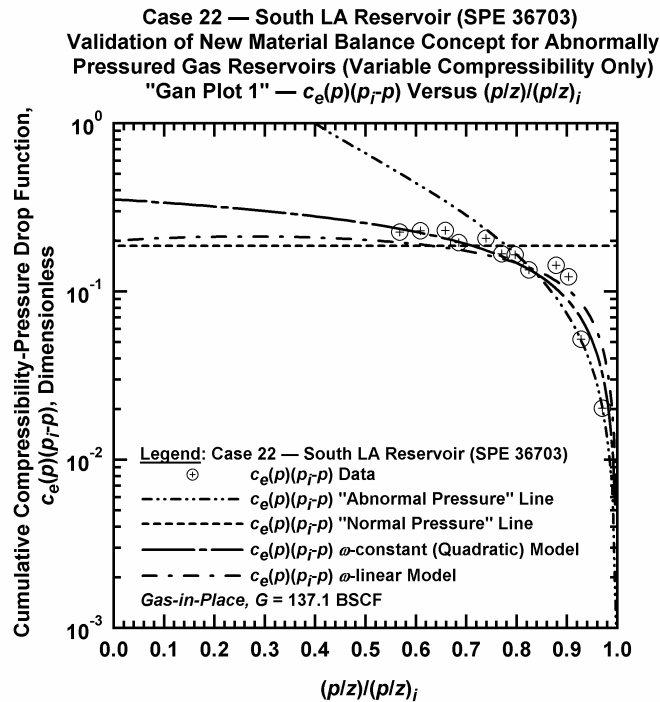


Figure D.23.n — Plot of $\bar{c}_e(p)(p_i - p)$ vs. $(p/z)/(p/z)_i$ — Case 22.

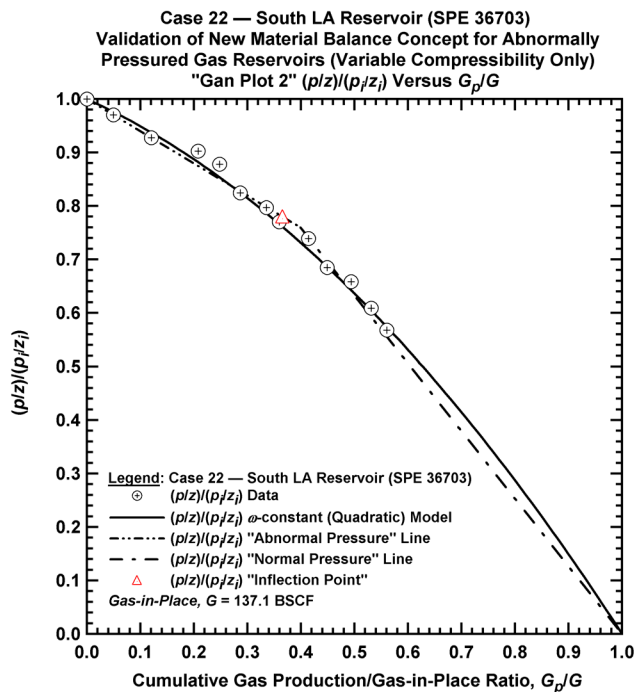


Figure D.23.o — Plot of $(p/z)/(p/z_i)$ vs. G_p/G — Case 22.

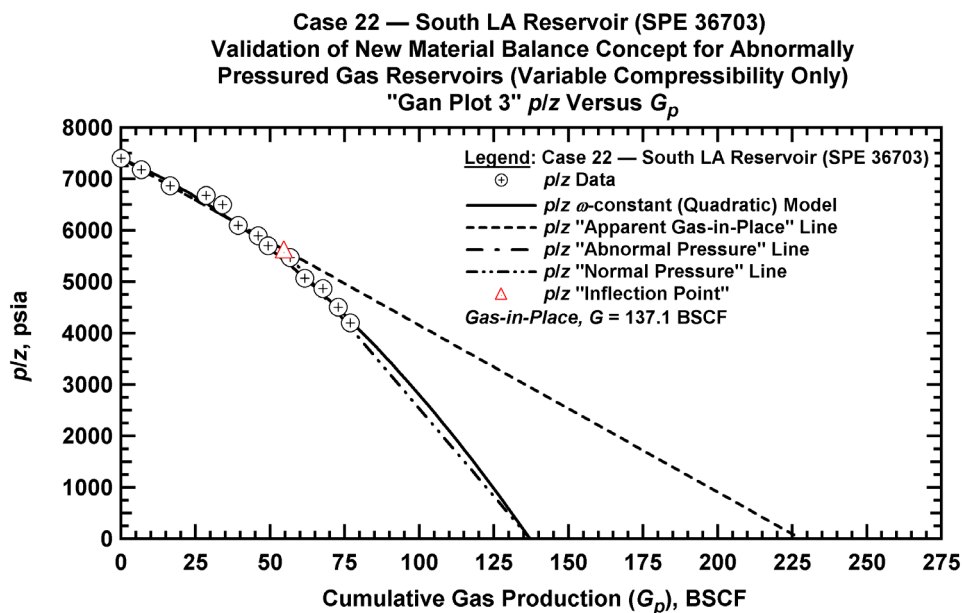


Figure D.23.p — Summary plot of p/z vs. G_p — Case 22.

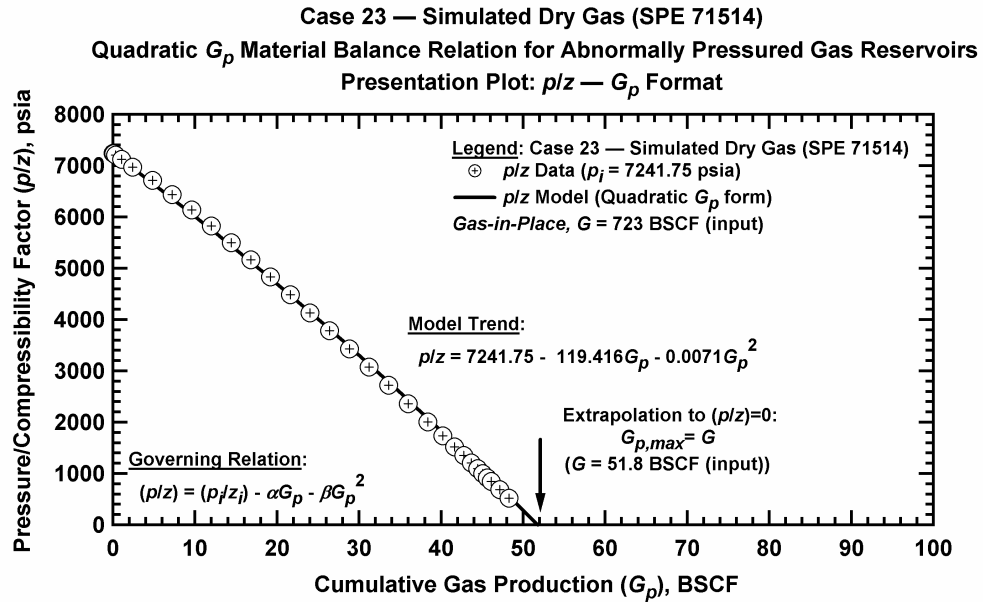


Figure D.24.a — Plot of p/z vs. G_p — Case 23.

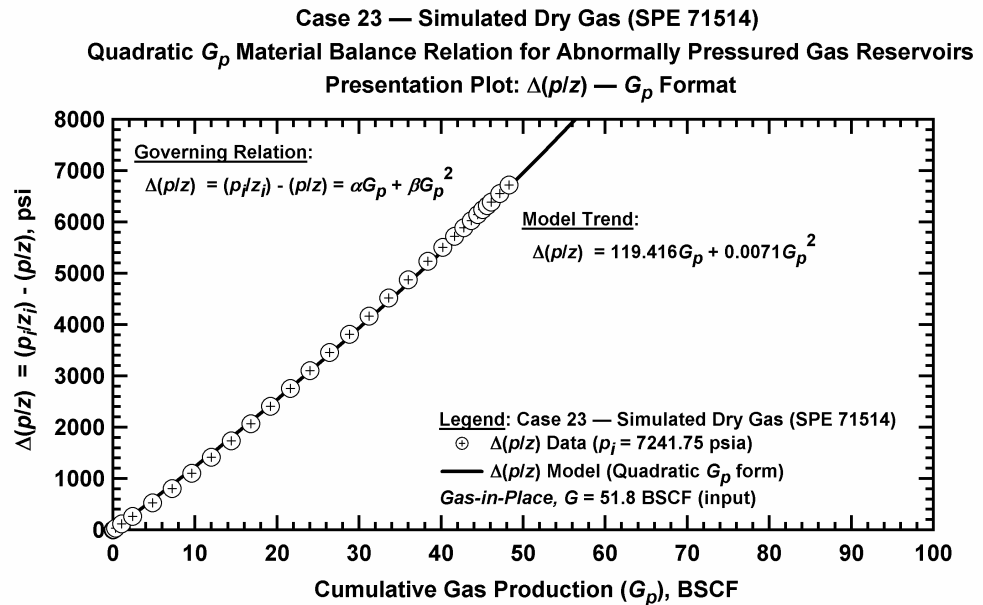


Figure D.24.b — Plot of $\Delta(p/z)$ vs. G_p — Case 23.

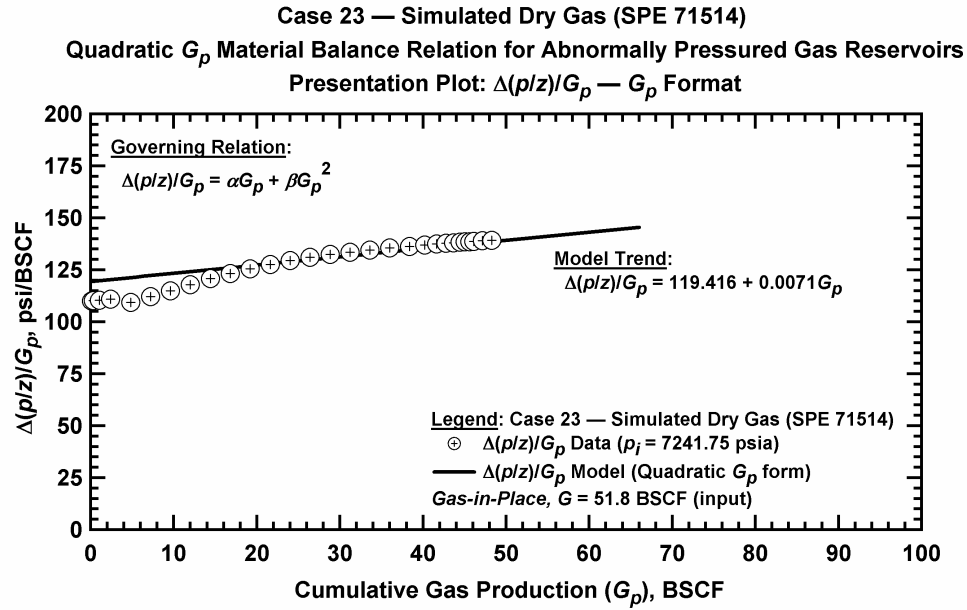


Figure D.24.c — Plot of $\Delta(p/z)/G_p$ vs. G_p — Case 23.

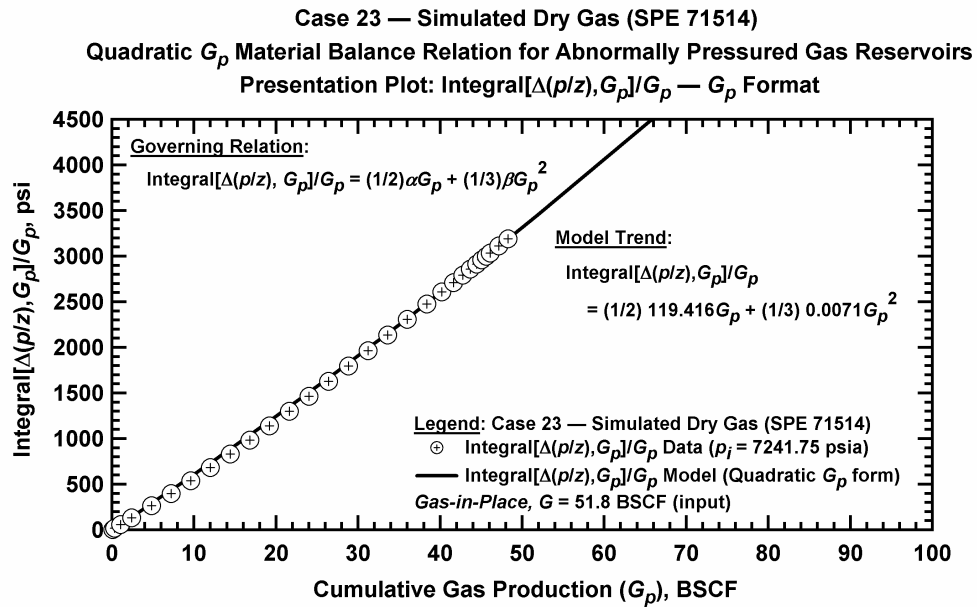


Figure D.24.d — Plot of $\frac{1}{G_p} \int_0^{G_p} \Delta(p/z) dG_p$ vs. G_p — Case 23.

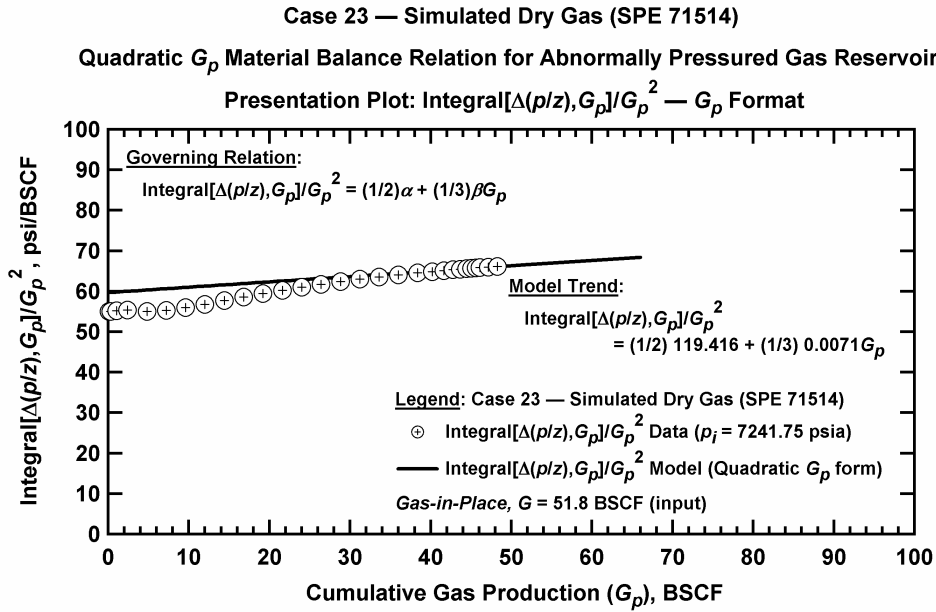


Figure D.24.e — Plot of $\frac{1}{G_p^2} \int_0^{G_p} \Delta(p/z) dG_p$ vs. G_p — Case 23.

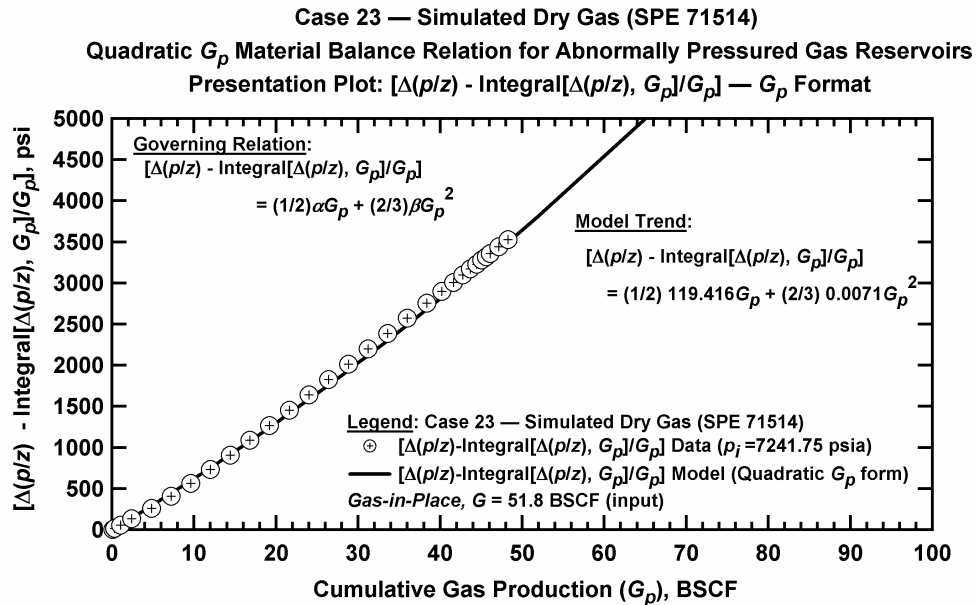


Figure D.24.f — Plot of $\Delta(p/z) - \frac{1}{G_p} \int_0^{G_p} \Delta(p/z) dG_p$ vs. G_p — Case 23.

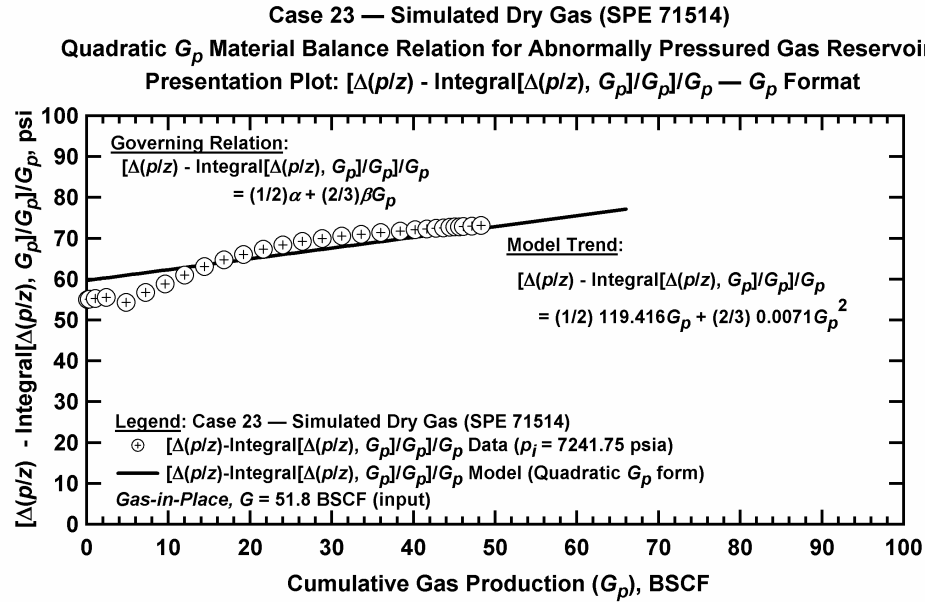


Figure D.24.g — Plot of $\frac{1}{G_p} \left[\Delta(p/z) - \frac{1}{G_p} \int_0^{G_p} \Delta(p/z) dG_p \right]$ vs. G_p — Case 23.

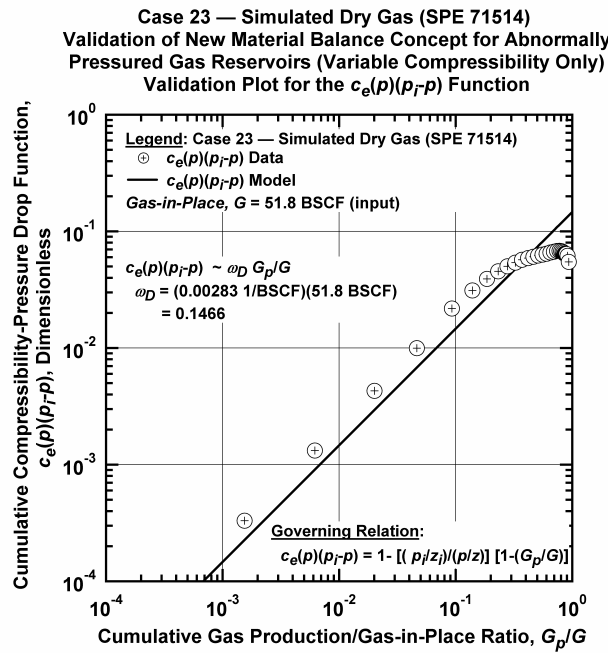
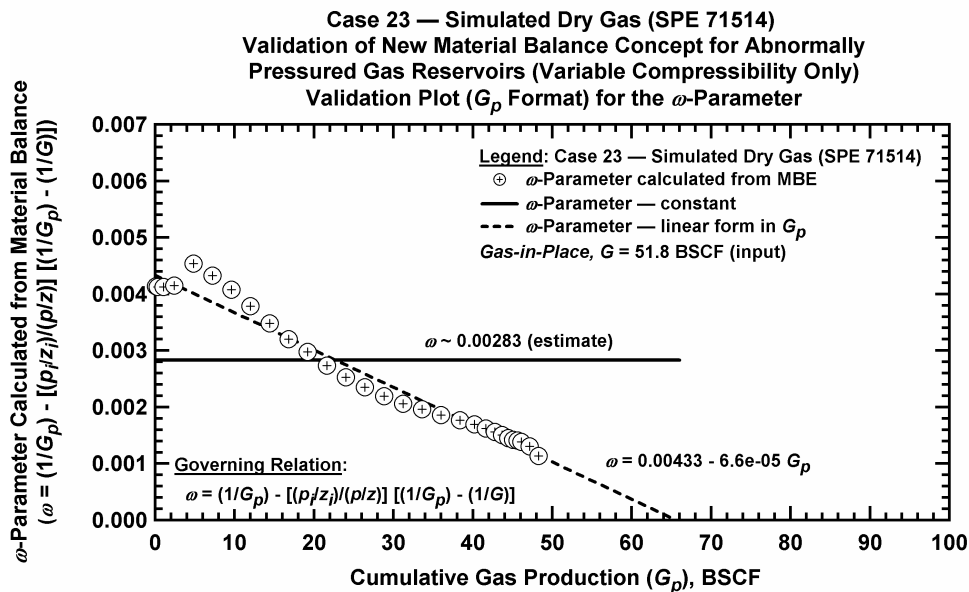
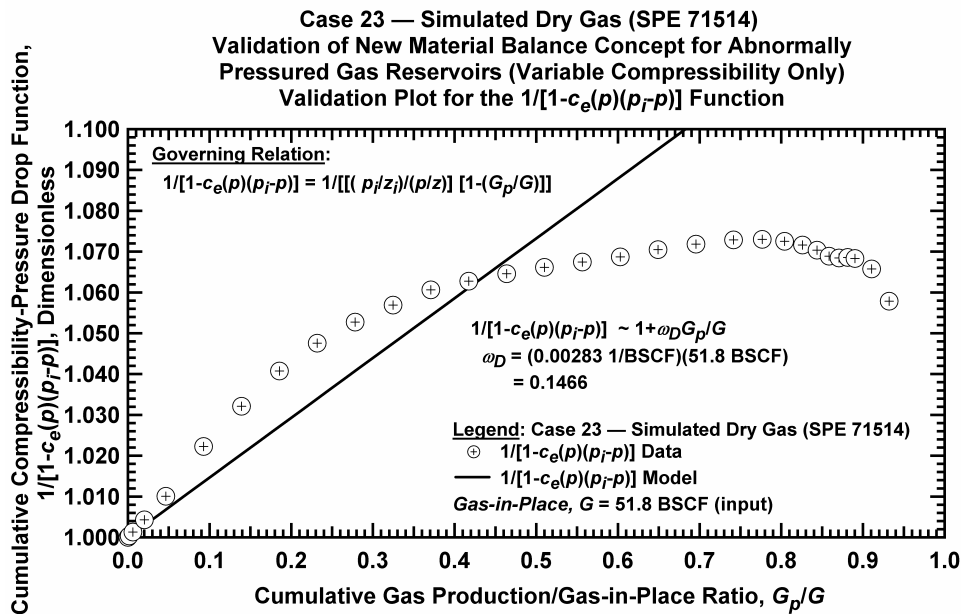


Figure D.24.h — Plot of $\bar{c}_e(p)(p_i - p)$ vs. G_p/G — Base Simulation Case 23.



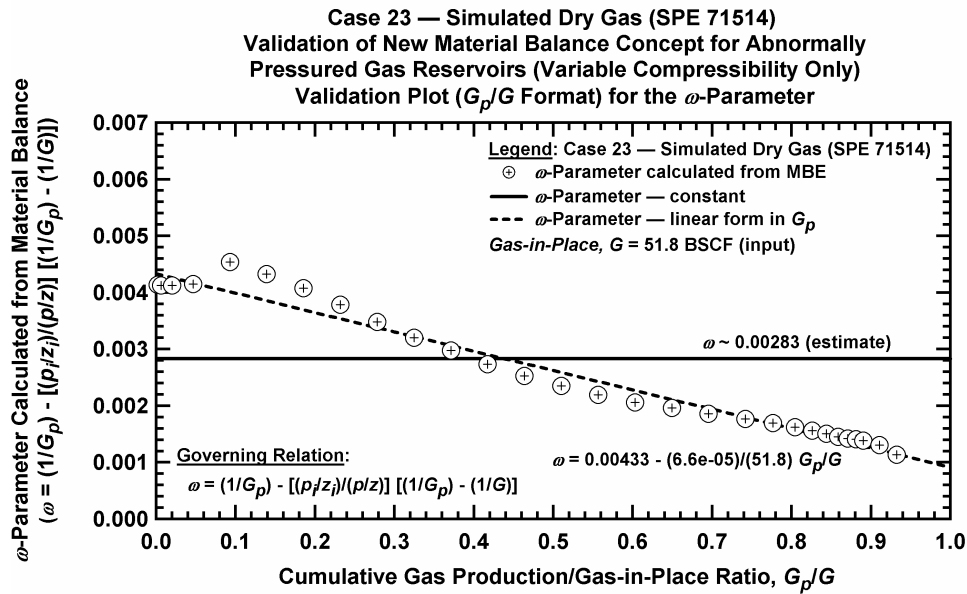


Figure D.24.k — Plot of ω vs. G_p/G — Case 23.

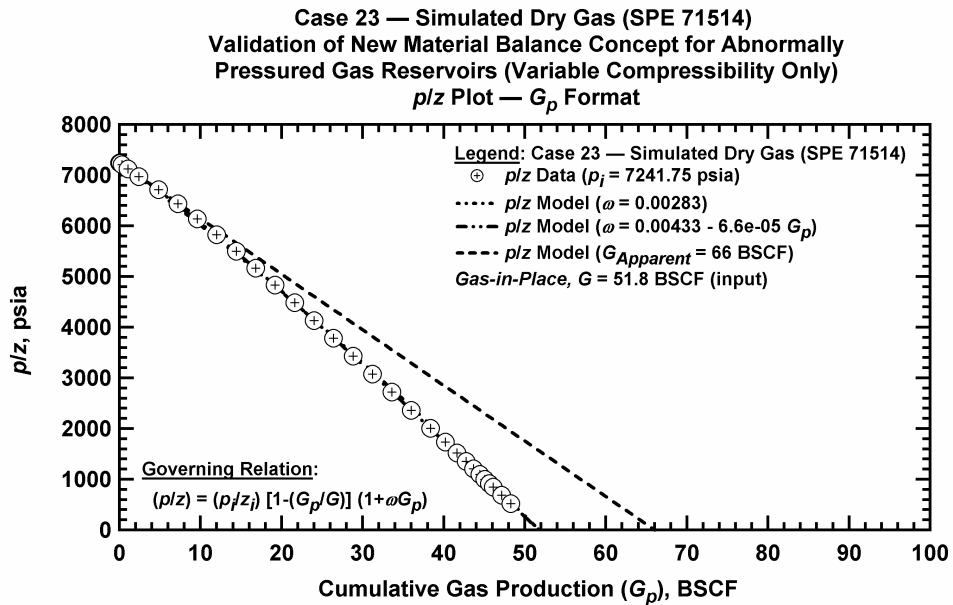
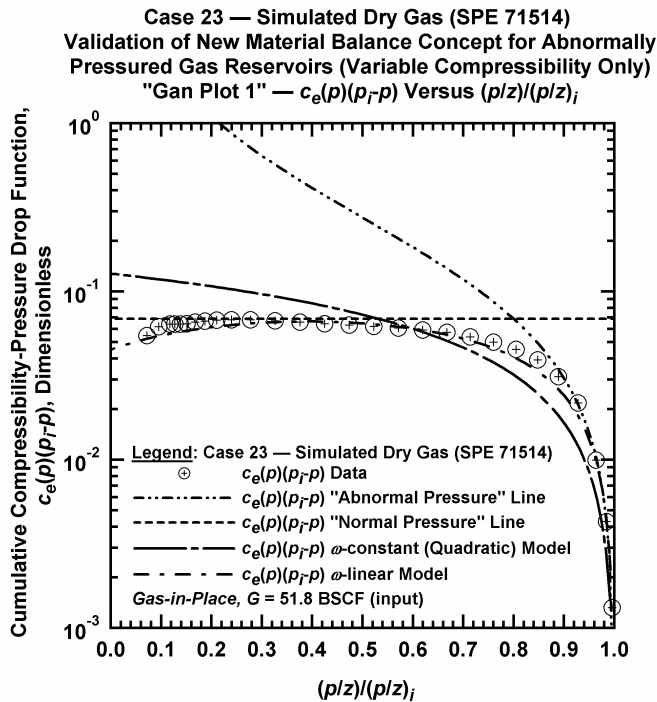
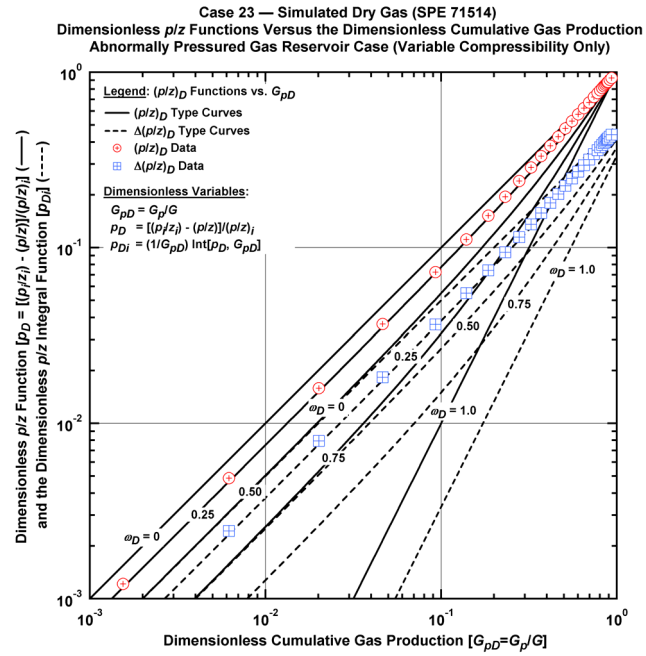


Figure D.24.l — Comparison plot of p/z vs. G_p — Case 23.



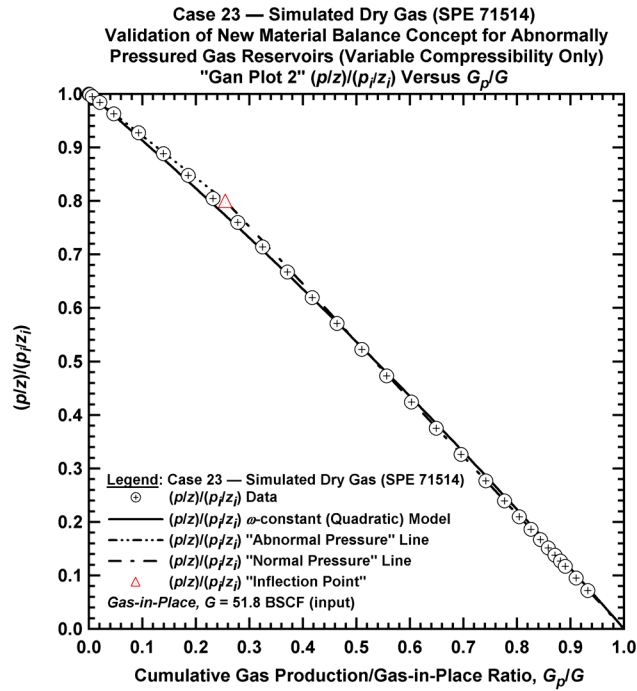


Figure D.24.o — Plot of $(p/z)/(p/z_i)$ vs. G_p/G — Case 23.

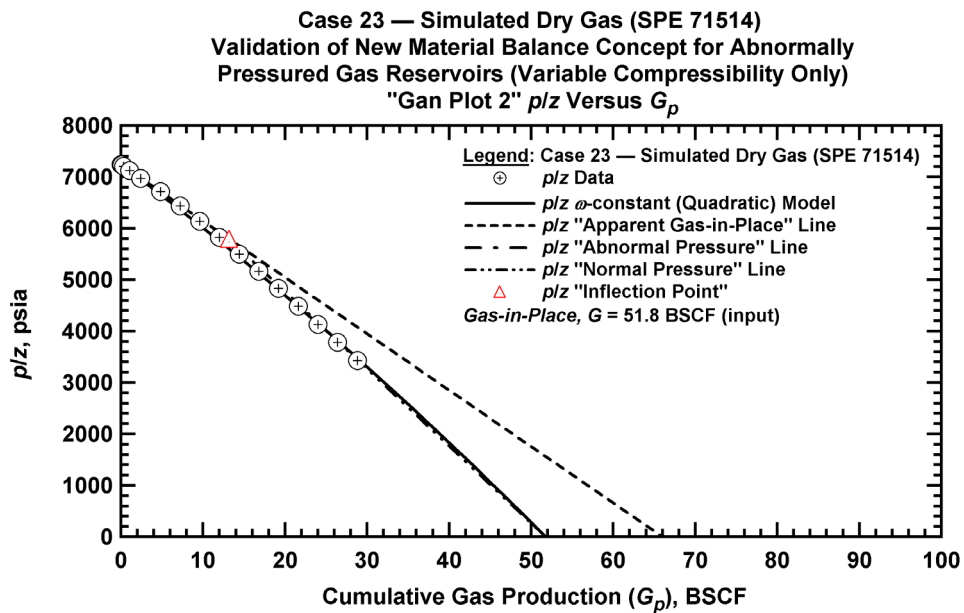


Figure D.24.p — Summary plot of p/z vs. G_p — Case 23.

VITA

Name: Felix E. Gonzalez Romero

Born: January 24, 1967
Maracaibo, Zulia, Venezuela

Permanent Address: Resd "Los Helechos," Torre "E", piso 5, Apt 52
Calle Pumarrosa, Sector El Sitio, San Antonio de los Altos,
Edo-Miranda, Venezuela.

Phone: 058-212-5779374
058-212-5776920

E-mail Address: felixgonzalezr@hotmail.com
felixgonzalezr@yahoo.com

Education: Texas A&M University, College Station, Texas, USA
Master of Science Degree in Petroleum Engineering
December 2003

Universidad Simon Bolivar, Caracas, Venezuela
Specialization in Reservoir Management
March 2000

Universidad Central de Venezuela, Caracas, Venezuela
Bachelor of Science Degree in Petroleum Engineering
July 1996

Professional Experience: 1995.....Halliburton Laboratory-Cabimas, Venezuela
1996-2001 PDVSA-INTEVEP-Los Teques, Venezuela

Affiliations: Society of Petroleum Engineers
Society of Venezuelan Engineers
Venezuelan Student Association